The Synthesis, Post-polymerization Functionalization and Applications of Oxygenated Polymers

Thomas Tai Dung Chen



Wolfson College
Department of Inorganic Chemistry
University of Oxford
January 2020

A thesis submitted in partial fulfilment of the requirements for the degree of Doctor of Philosophy in Chemistry

To my mother and grandmother

Declaration

The work described in this thesis was conducted between October 2016 and January 2020 at the University of Oxford. This is the work of the author unless otherwise stated.

The copyright of this thesis rests with the author and is made available under a Creative Commons Attribution Non-Commercial No Derivatives licence. Researchers are free to copy, distribute or transmit the thesis on the condition that they attribute it, that they do not use it for commercial purposes and that they do not alter, transform or build-upon it. For any reuse or distribution, researchers must make clear to others the licence terms of this work.



Thomas Chen

Abstract

This thesis focuses on the synthesis and properties of block polyesters and polycarbonates, proposed as sustainable alternatives to existing petrochemicals. The polymers are prepared using efficient catalysed reactions, including the ring opening copolymerization (ROCOP) of epoxide/anhydride or CO_2 and lactone ring opening polymerization (ROP). The thesis comprises an introduction, providing a review of the literature and setting out the thesis aims, followed by three related research chapters which examine different aspects of these block polymers.

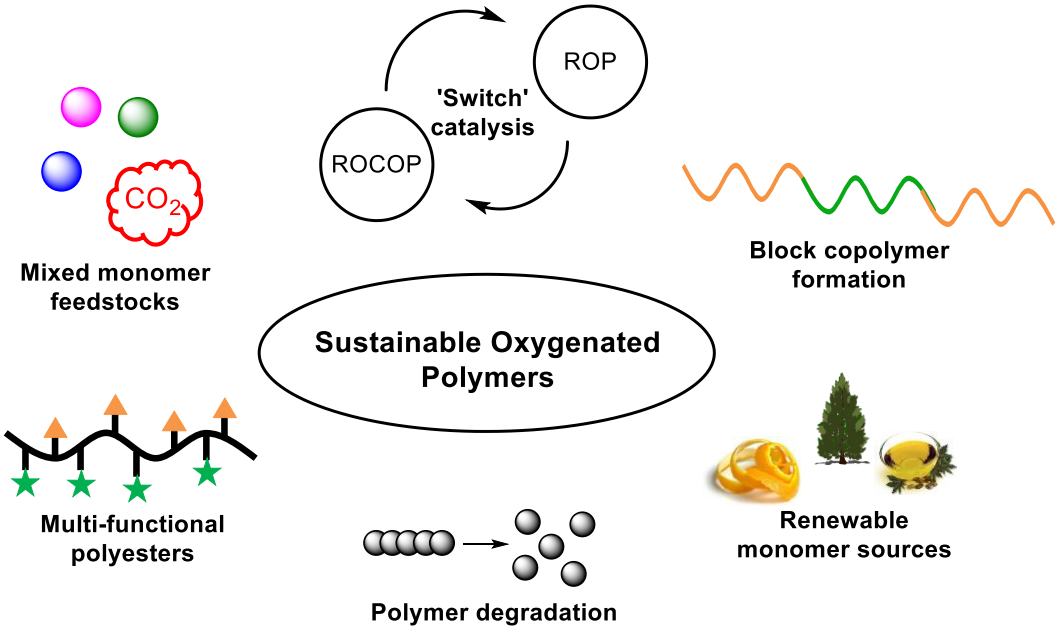
Chapter 2 describes the use of 'Switch catalysis' to prepare pentablock copolymers from mixtures of four different monomers: epoxide, anhydride, CO_2 and lactone. Using the highly selective catalysis, the monomer mixture is transformed into only one product and into a single block polymer sequence. The block polymers produced are characterized using a range of nuclear magnetic resonance (NMR) spectroscopies, size exclusion chromatography (SEC), *in-situ* ATR-IR spectroscopy and differential scanning calorimetry (DSC).

Chapter 3 describes the development of a new post-polymerization functionalization that is applied to alternating polyesters, prepared by epoxide/anhydride ROCOP, to install pendant hydroxyl groups onto polyester backbones. The method exploits a highly selective alkene hydroboration-oxidation reaction whereby different alkene groups react at different rates. This allows for the 'patterning' of polyesters so as to install a hydroxyl functionality on every other repeat unit. The method may also be extended to prepare dual functionalised polyesters, by combining the thiol-ene coupling with the hydroboration-oxidation reaction. The

chapter presents the method using an exemplar polymer structure and also provides evidence of its ability to be generalized to a range of different polymer, prepared from various epoxides and anhydrides. The properties of the resulting functionalized polyesters are presented, including preliminary assessment of their ability to self-assemble from aqueous solutions.

Chapter 4 describes the application of epoxide/anhydride ROCOP to prepare polyesters derived fully or partially from renewable resources. In particular, limonene oxide and tricyclic anhydrides are copolymerized to yield block polyesters with a high renewable content. The polymers properties are presented with a preliminary assessment of their potential as pressure sensitive adhesives.

Chapter 5 provides an overall conclusion and outlook to the research in the thesis and Chapter 6 presents the experimental methods and techniques. An appendix to the thesis provides access to all the data used to characterize compounds and to further specialized experimental protocols.



Acknowledgments

First and foremost, I would like to thank my supervisor, Professor Charlotte Williams, for granting me the opportunity to carry out my DPhil in her research group. I am grateful for your continuous guidance and encouragement.

I have been very fortunate to be able to work with some very talented and knowledgeable post-docs who have taught me a lot. I would like to express my thanks to Dr. Frank Zhu, Dr. Leticia Peña Carrodeguas and Dr. Georgina Gregory for not only being fantastic mentors but also great friends. A special thanks goes to Arron, Alice and Greg for the breaks and 'interesting' chats as well as Frank and Ni for the lunch time outings, you have all made my time in Oxford very enjoyable and memorable.

I would like to thank the Williams group, past and present, for the pleasant and supportive working environment. Thank you to all the post docs (Sumesh, Andrés, Giulia, Frank, Chris, Leti, Duncan, Patrick, Caroline, George, Ryan and Andy) and students (Alice, Arnaud, Charlie, Gemma, Ni, Arron, Tim, Peck, Greg, Saïd, Natalia, Wilf, Lisa, Gloria and Wouter).

To Qirong, thank you so much for enjoying the good times with me and supporting me through the tough times. You have made Oxford a very special place for me. Finally, I would like to thank my parents who have supported me, especially my mother and grandmother who have sacrificed so much to get me to where I am today – I will forever be in your debt, this is for you.

List of Publications

'Switch' catalysis: from monomer mixtures to sequence-controlled block copolymers

T. Stößer,* T. T. D. Chen,* Y. Zhu and C. K. Williams, *Phil. Trans., R. Soc. A.*, **2017**, *376*, 20170066.

Pentablock Copolymer from Tetracomponent Monomer Mixture Using a Switchable Dizinc Catalyst

T. T. D. Chen, Y. Q. Zhu and C. K. Williams, Macromolecules, **2018**, *51*, 5346–5351

Orthogonal functionalization of alternating polyesters: selective patterning of $(AB)_n$ sequences

N. Yi,* T. T. D. Chen,* J.Unruangsri, Y. Zhu and C. K. William, *Chem. Sci*., **2019**, *10*, 9974-9980

Bio-derived and degradable block copolymers as pressure sensitive adhesives

T. T. D. Chen, L. P. Carrodeguas, G. Sulley, G. Gregory and C. K. Williams*, manuscript in preparation*

List of Abbreviations

AGE	Ally Glycidyl Ether
Anhy.	Anhydride
ATR	Attenuated Total Reflactance
ATRP	Atom Transfer Radical Polymerization
BDI	β-Diiminate
BPA	Bisphenol-A
BDM	1,4-benzenedimethano
BL	β-butyrolactone
$CHCl_3$	Chloroform
χ	Flory-Huggins Interaction Parameter
CHD	*Trans*-cyclohexane-1,2-diol
CHO	Cyclohexene Oxide
CL	ε-caprolactone
COSY	Homonuclear Correlation Spectroscopy
CTA	Chain Transfer Agent
CuAAC	Copper (I) catalysed azide-alkyne cycloaddition
$Đ$	Dispersity
DBU	1,8-Diazabicyclo[5.4.0]undec-7-ene
DCM	Dichloromethane
DFT	Density Functional Theory
D_h	Hydrodynamic Diameter
DLS	Dynamic Light Scattering
DMA	Dynamic Mechanical Analysis
DOSY	Diffusion Ordered NMR Spectroscopy
DMSO	Dimethyl Sulfoxide
DMPA	2,2-Dimethoxy-2-phenylacetophenone
DP	Degree of Polymerization
DSC	Differential Scanning Calorimetry
HSQC	Heteronuclear Single Quantum Coherence

IR	Infrared
L	Ligand
LA	Lactide
LO	Limonene Oxide
M	Mol L^{-1}
MA	Maleic anhydride
MALDI	Matrix Assisted Laser Desorption Ionisation
mCPBA	3-Chloroperoxybenzoic acid
MeOH	Methanol
min	Minute
M_n	Number Averaged Molar Mass
MS	Mass Spectrometry
NA	Norbornene Anhydride
NMR	Nuclear Magnetic Resonance
OAc	Acetate
PA	Phthalic Anhydride
PBL	Poly(β-butyrolactone)
PC	Polycarbonate
PCHC	Poly(Cyclohexene carbonate)
PCHNBE	Poly(Cyclohexene norbornene ester)
PCHPE	Poly(Cyclohexene phthalate)
PCL	Poly(ε-caprolactone)
PDL	Poly(ε-decalactone)
PE	Polyester
Ph	Phenyl
PLA	Polylactide
PO	Propylene Oxide
PPNCl	Bis(triphenylphosphine)iminium Chloride
PS	Polystyrene
PSA	Pressure Sensitive Adhesive
ROCOP	Ring Opening Copolymerization

ROP	Ring Opening Polymerization
SEC	Size Exclusion Chromatography
TBD	1,5,7-Triazabicyclo[4.4.0]dec-5-ene
TCA	Tricyclic anhydride
TCE	1,1,2,2-Tetrachloroethane
TEM	Transmission Electron Microscopy
TFA	Trifluroacetate
T_g	Glass Transition Temperature
THF	Tetrahydrofuran
THPA	1,2,3,6-Tetrahydrophthalic anhydride
TMC	Trimethylene Carbonate
ToF	Time of Flight
TOF	Turn Over Frequency
TON	Turn Over Number
VCHO	4-Vinyl-1-Cyclohexene 1,2-Epoxide
VPO	2-Vinyl Oxirane
X	Co-ligand

List of Figures, Schemes and Tables

Chapter 1: Introduction

Figure 1.1 Global plastic production from 1975 to 2015 (note: CAGR refers to the compound annual growth rate).

Figure 1.2 Coordination-insertion mechanism for the ROP of lactide ([M] denotes a Lewis acidic metal in a ROP catalyst).

Figure 1.3 Selected examples of cyclic esters and carbonates used in ROCOP.

Figure 1.4 Characteristic changes in ΔG_p for different monomer ring sizes in ROP

Figure 1.5 ROCOP of epoxide/CO_2 or anhydride for the synthesis of polyesters and polycarbonates, respectively.

Figure 1.6 Illustration of the elementary steps for epoxide/CO_2 ROCOP.

Figure 1.7 Dinuclear mechanism for the ROCOP of epoxide/CO_2.

Figure 1.8 Selected examples epoxide and anhydride used in ROCOP.

Figure 1.9 'Switch' catalysis and proposed mechanism for CHO/CO_2/CL using diphenolate macrocyclic Zn catalysts.

Figure 1.10 Computation analysis for 'Switch' catalysis using CHO/PA/CO_2/CL. (Not: TS denotes transition state barriers).

Figure 1.11 'Switch' catalysis for CHO(LO)/CO_2/BL using (BDI)-based Zn catalyst.

Figure 1.12 'Switch' catalysis for epoxide/anhydride/lactone using [SalcyCr(III)Cl].

Figure 1.13 'Switch' catalysis for PO/PA/LA using [SalphenAlCl].

Figure 1.14 'Switch' catalysis for epoxides/anhydrides/LA using $^{t}BuP_1$.

Table 1.1 Comparison of 'Switch' catalysts

Figure 1.15 Exemplar In-situ ATR-IR spectrum demonstrating the 'Switch' mechanism for PA/CHO/DL polymerization.

Figure 1.16 Exemplar SEC traces for (A) block polymer formation and (B) mixture of homopolymers or block polymer with homopolymer contamination.

Figure 1.17 End group analysis using ^{31}P {^{1}H} NMR spectroscopy (note: R denotes polymer chain end).

Figure 1.18 End group analysis using $^{31}P\{^{1}H\}$ NMR spectroscopy illustrating a change in the end group signals indicating block polymer formation (in a homopolymer blend, two end group signals would be observed0 (Bisphenol A used as internal standard).

Figure 1.19 ^{1}H DOSY NMR of block polymer and homopolymer blend with one and two diffusion coefficient, respectively.

Figure 1.20 Selected post-polymerization methods for polyesters and polycarbonates.

Chapter 2: Pentablock Copolymer from Tetra-Component Monomer Mixture Using a Switchable Dizinc Catalyst

Scheme 2.1 Synthesis of pentablock copolymer from a dizinc catalyst, **1**, using four monomers *via* Switchable catalysis.

Scheme 2.2 Attempted 4 monomer polymerization using switch catalysis. Molar ratio: [**1**]/[CHD]/[PA]/[DL]/[CHO] = 1/4/100/200/1000, 100 °C, (**A**, **B**) CO_2 and (**C**) N_2, 1 bar; **A** (anhydride/epoxide ROCOP), **B** (epoxide/CO_2 ROCOP) and **C** (failed lactone ROP).

Figure 2.1 Selected region of ^{1}H NMR spectra illustrating changes in various resonances during an initial failed attempt to form pentablock copolymers using CO_2 as the gas atmosphere first before switching to N_2. No PDL formation was observed after 30 h, but the cyclic carbonate (4.0 ppm) signal can be seen to increase over time (in $CDCl_3$).

Figure 2.2 Illustration of the back-biting side reaction (formation of trans-cyclic carbonate) being favoured over the ROP of lactone (i.e. $k_2 > k_1$) from the zinc-alkoxide chain end formed at the end of the ROCOP of epoxide/CO_2. 'P' indicates polymer chain.

Figure 2.3 SEC traces illustrating a decrease in molar mass and increase in $Đ$ towards the end of the 4 monomer polymerization progresses; **A** (anhydride/epoxide ROCOP), **B** (epoxide/CO_2 ROCOP) and **C** (failed ROP of DL) (calibrated with narrow dispersity polystyrene standards).

Scheme 2.3 Polymerization of tetra-component monomer mixture: PA/VCHO/DL/CO_2.

Figure 2.4 Conversion vs. time plot illustrating block formation; **A** (anhydride/epoxide ROCOP), **B** (lactone ROP) and **C** (epoxide/CO_2 ROCOP).

Figure 2.5 Selected region of ^{1}H NMR spectra illustrating changes in various resonances during different stages of the polymerization using PA/VCHO/DL/CO_2 as monomer feedstock (in $CDCl_3$).

Figure 2.6 Selected region of ^{1}H NMR spectrum of pentablock copolymer from the 4 monomer polymerization of PA/VCHO/CO_2/DL

Figure 2.7 SEC traces illustrating the increase in M_n and retention of $Đ$ during a successful 3 stage pentablock copolymer formation; **A** (anhydride/epoxide ROCOP), **B** (lactone ROP) and **C**

(epoxide/CO_2 ROCOP) (calibrated with narrow dispersity polystyrene standards).

Figure 2.8 $^{31}P\{^1H\}$ NMR spectra of end group analysis on the polymerization of PA/VCHO/DL/CO_2. PE, PDL and PC end groups can be observed at 146.7-146.9, 147.1 and 146.5-146.9 ppm respectively. Bisphenol A (BPA) is added as an internal standard (in $CDCl_3$).

Figure 2.9 (a)^1H DOSY NMR spectra of pentablock copolymer from the polymerization of PA/VCHO/DL/CO_2 showing a single diffusion coefficient (bottom) homopolymer blend of PVCHPE, PDL and PVCHC with similar MW to the respective blocks showing three different coefficients (in $CDCl_3$).

Figure 2.10 Carbonyl region of $^{13}C\{^1H\}4$ NMR spectra of pentablock copolymer from the polymerization of PA/VCHO/DL/CO_2 and PE, PDL and PC homopolymers. Carbonyl resonances for PE, PDL and PC blocks can be seen at 166.6-166.4 ppm,173.4 ppm and 153.5-153.3 ppm respectively (in $CDCl_3$).

Table 2.1 Four monomer polymerizations using anhydride, epoxide, lactone and CO_2

Figure 2.11 Polymerization of tetra-component monomer mixture, PA/CHO/DL/CO_2.

Figure 2.12 Polymerization of tetra-component monomer mixture, NA/CHO/DL/CO_2.

Figure 2.13 Polymerization of tetra-component monomer mixture, NA/VCHO/DL/CO_2.

Figure 2.14 ^1H DOSY NMR spectrum of (top) pentablock copolymer from the polymerization of PA/CHO/DL/CO_2 (middle) pentablock copolymer from the polymerization of NA/CHO/DL/CO_2

(bottom) pentablock copolymer from the polymerization of NA/VCHO/DL/CO_2 (in $CDCl_3$).

Figure 2.15 Selected region of $^{31}P\{^1H\}$ NMR spectra of hydroxyl polymer end analysis of (top) pentablock copolymer from the polymerization of PA/CHO/DL/CO_2 (middle) pentablock copolymer from the polymerization of NA/CHO/DL/CO_2 (bottom) pentablock copolymer from the polymerization of NA/VCHO/DL/CO_2. The hydroxyl end group assessed is highlighted in red. (in $CDCl_3$)

Scheme 2.4 Four monomer selective polymerization, using [LZn_2Ph_2] (**1**)/1,2-cyclohexanediol (CHD) catalytic system.

Figure 2.16 Proposed mechanisms occurring during polymerization of anhydride, epoxide, lactone and CO_2, highlighting the central role for the zinc alkoxide intermediate

Scheme 2.5 Thiol-ene functionalization of the pentablock copolymers

Figure 2.17 ^1H NMR spectra showing the changes in NMR resonances on the pentablock copolymer before and after thiol-ene post-polymerization functionalization. New resonances after functionalization is displayed in blue and green (in $CDCl_3$).

Figure 2.18 SEC analyses of the thiol-ene functionalization of the pentablock copolymer. Dashed red and solid blue lines illustrate the molar mass distributions before and after reaction, respectively.

Figure 2.19 DSC thermograph of the original block copolymer (Black) and functionalised polymers using 1-butanethiol (blue) and 2-mercaptoethanol (green).

Scheme 2.6 ROP of L-LA using [LZn_2Ph_2]/CHD catalyst system (CHO used as the solvent).

Table 2.2 ROP of L-LA using **1**/CHD

Scheme 2.7 Intermolecular and intramolecular transesterification of PLA.

Scheme 2.8 Terpolymerization of PA/CHO/L-LA.

Table 2.3 Terpolymerization of PA/CHO/L-LA.

Figure 2.20 Selected region of ^{1}H NMR spectra illustrating changes in various resonances during stages **A** (ROCOP of anhydride/epoxide) and **B** (ROP of lactide) of the terpolymerization using PA/L-LA/CHO as monomer feedstock (in $CDCl_3$).

Figure 2.21 SEC traces illustrating the changes in M_n and $Đ$ as the polymerization progresses through stages A (ROCOP of anhydride/epoxide) and B (ROP of lactide) of the terpolymerization using PA/L-LA/CHO as monomer feedstock (calibrated using narrow dispersity polystyrene standards).

Scheme 2.9 Terpolymerization of CHO/L-LA/CO_2.

Table 2.4 Terpolymerization of L-LA/CHO/CO_2

Figure 2.22 Selected region of ^{1}H NMR spectra illustrating changes in various resonances during stages A (ROP of Lactide) and B (ROCOP of epoxide/CO_2) of the terpolymerization using L-LA/CHO/CO2 as monomer feedstock (in $CDCl_3$)

Figure 2.23 SEC traces illustrating the decrease of M_n and increase in $Đ$ as the polymerization progresses through stages **A** (ROP of lactide) and **B** (ROCOP of CO_2/epoxide) in the terpolymerization of L-LA/CO_2/CHO (calibrated using narrow dispersity polystyrene standards).

Chapter 3: Orthogonal Functionalization of Alternating Polyesters: Selective Patterning of $(AB)_n$ Sequences

Scheme 3.1 Dual-functionalized polyester synthesis through sequential hydroboration-oxidation and thiol-ene coupling reactions.

Scheme 3.2 Selective synthesis of orthogonal functionalization of dual-functional alternating polyesters

Figure 3.1 Structures of the alternating polyesters **P5** – **P13**, all featuring internal and terminal alkene functionalities.

Table 3.1 Composition and Properties of **P5**-**P13**.

Scheme 3.3 ROCOP of epoxide/anhydride using [SalcyCrCl] and PPNCl.

Figure 3.2 ^{1}H NMR spectrum of polymer **P5** ($CDCl_3$, 500.0 MHz, 298 K).

Figure 3.3 ^{1}H-^{1}H COSY NMR spectrum of polymer **P5**. ($CDCl_3$, 500.0 MHz, 298 K). Important chemical shifts are listed in brackets.

Figure 3.4 ^{13}C{^{1}H} NMR spectrum of **P5** ($CDCl_3$, 500.0 MHz, 298 K).

Figure 3.5 ^{13}C-^{1}H HSQC NMR spectrum of **P5** ($CDCl_3$, 500.0 MHz, 298 K).

Scheme 3.4 Hydroboration of polyetsers monitored *in-situ* ^{1}H NMR spectroscopy to investigate the internal/terminal alkene selectivity.

Figure 3.6 A) Percentage conversion of the two different alkene groups (internal = blue circles and terminal = red squares) vs. time during the hydroboration reaction of **P5** (B) stacked NMR spectra (in $CDCl_3$, mesitylene as internal standard).

Figure 3.7 Plot of $\ln([C=C]_0/[C=C]_t)$ vs time of terminal alkene groups. Rate = $k[C=C]^1[9\text{-BBN}]^x$, $k_{obs} = k[9\text{-BBN}]^x$.

Figure 3.8 Percentage conversion of the two different alkene groups (internal = blue circles and terminal = red squares) vs. time during the hydroboration reaction of **P7**.

Scheme 3.5 One-pot hydroboration-oxidation reaction to convert the polyester **P1** terminal alkenes to alternating hydroxyl groups.

Figure 3.9 ^{1}H NMR spectrum of **P5(a)** ($CDCl_3$, 500 MHz, 298 K).

Table 3.2 Characterization Data for Hydroxyl-functionalized polyesters **P5(a)** – **P13(a)**.

Scheme 3.6 Photo-initiated thiol-ene reactions to transform the hydroxyl-functionalized alternating polyesters into orthogonally functionalized (AB)n Polyesters

Figure 3.10 ^{1}H NMR spectrum of **P5(b)** ($CDCl_3$, 500.0 MHz, 298 K).

Figure 3.11 Selected regions of the ^{1}H NMR spectra showing the changes in proton resonances of (purified) polymers after functionalization steps (in $CDCl_3$).

Table 3.3 SEC characterization data (in THF and DMF) for **P5** and **P6**.

Figure 3.12 SEC (in DMF) showing an increase in molar mass after functionalization, in each case with retention of monomodal distributions and narrow dispersity.

Scheme 3.7 Thiol-ene control reaction using polyester from the ROCOP of MA and VCHO

Figure 3.13 SEC traces (in THF) illustrating a successful coupling in the control reaction.

Figure 3.14 ^{1}H NMR data illustrating the unselective UV-initiated thiol-ene reactions. (Bottom) before application of thiol-ene reaction. (Top) after the thiol-ene reaction (mesitylene as internal standard).

Table 3.4 Glass transition temperatures for dual-functionalized polyesters

Table 3.5 Glass transition temperatures for hydroxyl-functionalized polyesters

Figure 3.15 DSC thermograms of **P5**, **P5(a)** and **P5(b)** showing an increase in T_g after the hydroboration-oxidation and a decrease after the further instalment of butyl thiolether groups.

Figure 3.16 (A) DLS data collected from an aqueous solution of **P5(b)** (A) and **P6(b)** (B) (10 mgmL-1).

Figure 3.17 TEM images for the structure of the homopolymer micelle from **P5(b)**.

Figure 3.18 TEM images for the structure of the homopolymer micelle from **P6(b).**

Scheme 3.8 Block copolyester synthesis *via* switchable catalysis and sites for selective functionalization.

Scheme 3.9 Block copolymer formation to include 3 post-polymerization functionalization sites *via* sequential ROCOP.

Scheme 3.10 *In-situ* ^{1}H NMR studies of iEDDA using **P2** and **P3** with 3,6-Diphenyl-1,2,4,5-tetrazine (in $CDCl_3$ and Mesitylene used as internal standard).

Figure 3.19 Percentage conversion of the two different alkene groups (internal = blue circles and terminal = red squaers) vs. time during the iEDDA reaction with tetrazine of **P6** (A) and **P7**(B).

Chapter 4: Bio-derived Degradable Block Copolymers as Presure-Sensitive Adhesives

Figure 4.1 Literature examples of polyesters synthesised hrough ROCOP utilizing either renewable anhydrides (TOP) or epoxides (Bottom).

Figure 4.2 One post synthesis for triblock copolymers using a combination of LO, DL and TCA with a 'switch' catalyst and bifunctional initiator.

Scheme 4.1 ROCOP of LO with TCA 1 using various dinuclear catalysts **1**, **2**, and **3**

Table 4.1 ROCOP of LO with TCA 1 using various dinuclear catalysts **1**, **2**, and **3**.

Figure 4.3 SEC curve comparison between the polymer product made using catalyst **2** and **3**.

Table 4.2 ROCOP of LO and TCAs

Figure 4.4 M_n and $Đ$ vs. conversion for the ROCOP of LO/TCA 1

Figure 4.5 SEC traces of aliquots obtained in thee ROCOP of LO/TCA 1 (between 5% and 90% conv.)

Figure 4.6 Conversion % vs. time for the ROCOP of LO/TCA 1.

Figure 4.7 ^{1}H NMR of the polyester from the ROCOP of LO/TCA 1 ($CDCl_3$, 500.0 MHz, 298K).

Figure 4.8 ^{1}H-^{13}C HSQC NMR spectrum of the polyester from the ROCOP of LO/TCA 1 in $CDCl_3$.

Figure 4.9 Representative MALDI-ToF of the polyester from the ROCOP of LO/TCA 1

Figure 4.10 SEC trace comparison between before and after deliberate heating at 140 °C for 7 days for the ROCOP of LO/TCA 1.

Figure 4.11 Assessed theoretical renewable content of polyesters from different epoxide/anhydride ROCOP

Table 4.3 ROP of DL

Figure 4.12 Illustration of the DL ROP and transesterification mechanisms.

Scheme 4.2 Selectivity study using **2**/BDM catalyst system

Figure 4.13 Conversion vs. time plot for the ROP of DL and ROCOP of LO/TCA1.

Figure 4.14 Proposed mechanism for ROCOP of LO/TCA and ROP of DL using a single catalyst

Scheme 4.3 ABA-triblock polymer synthesis *via* a sequential addition strategy using **2**/BDM catalyst system with DL, LO and TCA 1-4 as monomers

Table 4.4 One pot ABA-triblock copolymer

Figure 4.15 ^{1}H NMR spectrum of **P16.**

Figure 4.16 ^{1}H NMR spectrum of a block polymer illustrating junction units signals

Figure 4.17 COSY NMR spectrum of **P16**

Figure 4.18 Selected region of $^{31}P\{^{1}H\}$ NMR spectra of **P16**, PE from LO/TCA 1 ROCOP and PDL hydroxyl polymers

Figure 4.19 Illustration of the reactions to form different LO end groups

Figure 4.20 ^{1}H DOSY NMR spectra of **P16** with a single diffusion coefficient (Top) and the homopolymer blend, at equivalent molar masses, showing two diffusion coefficients (Bottom)

Figure 4.21 SEC traces illustrating an increase molar mass with retention of very narrow Đ (in THF at 30 °C, calibrated using polystyrene standards) for **P16**.

Figure 4.22 TGA curve of **P16** showing a two-step thermal degradation process.

Figure 4.23 First derivative TGA curve for of **P16**.

Figure 4.24 DSC thermograph of **P16** (third cycle).

Figure 4.25 Storage and loss modulus and tan(δ) vs. temperature plot of **P16**.

Figure 4.26 Plot of storage and loss moduli vs. frequency for **P16**.

Figure 4.27 Schematic diagram illustrating the 180 ° Peel test apparatus.

Figure 4.28 180° Peel adhesion test results comparison between DL/LO/TCA 1 triblock samples (~40 kg mol^{-1}) of varying hard block weight %.and commercial samples.

Figure 4.29 Stainless steel substrate photograph post-peel test show the difference between (A) an adhesive mode of failure with no polymer residue left over and (B) a cohesive mode of failure with visible polymer residue on the substrate.

Figure 4.30 180° Peel adhesion test results for the series of polymers from DL/LO and TCA 1-4 (~40 kg mol^{-1} and ~40% weight hard block, **P16** and **P18 – P20**) and literature renewable triblock polymer systems.

Figure 4.31 Schematic of *G'* vs. *G''* plot used for illustrating an adhesive's potential application.

Figure 4.32 Viscoelastic windows for DL/LO/TCA 1 triblock polymer with 41 and 30 $wt\%_{Hard}$.

Figure 4.33 Acid degradation of DL/LO/TCA 1 triblock polymer with (41 $wt\%_{Hard}$), using *p*-toluenesulfonic acid (1M in THF at 60 °C).

Figure 4.34 Stacked SEC traces for the acid degradation test on trblock polymer from DL/LO/TCA 1 with 41 $wt\%_{Hard}$ (1M in THF, 60 °C).

Figure 4.35 Bio-based epoxides for use in the synthesis of renewable polyesters.

Figure 4.36 Possible candidates for use as monomer for the *soft* block

Figure 4.37 Post-polymerization functionalization to install functional groups on to the triblock copolymer to improve properties.

Figure 4.38 Possible multi-arm initiators to use for different polymer architectures.

Chapter 5: Perspective and Future work

Figure 5.1 Three layered view of 'Switch' catalysis research.

Figure 5.2 Selection of possible candidate monomers for 'Switch' catalysis

Figure 5.3 Proposed selectivity mechanism for a 5 monomer (epoxide, anhydride, lactide, CO_2 and lactone) 'Switch' polymerization.

Figure 5.4 Potential new sequential post-polymerization modification methods.

Figure 5.5 Potential procedure for preparing PLA with interspersed hydroxyl functionalized polyesters.

Table of Contents

	Declaration	3
	Abstract	4
	Acknowledgements	6
	List of Publications	7
	List of Abbreviations	8
	List of Figures, Schemes and Tables	11
Chapter 1: Introduction		
1.1	Sustainable Polymers – Polyesters and Polycarbonates	28
1.2	Ring opening copolymerization (ROCOP) and ring-opening polymerization (ROP)	30
1.3	Block polymers	39
1.4	Switch Catalysis: A new route to block polymers	40
1.5	Switch catalysis: guide to block polymer formation	52
1.6	Post-polymerization modification	61
1.7	References	63
Chapter 2: Pentablock Copolymer from Tetra-Component Monomer Mixture Using a Switchable Dizinc Catalyst		
2.1	Introduction	70
2.2	Aims	71
2.3	Four monomer Switch Catalysis: One-pot strategy	72
2.4	Four monomer Switch Catalysis: Sequential addition of CO_2	76
2.5	Mechanistic hypothesis	91
2.6	Post-polymerization modification	93

2.7 Initial studies using lactide 97

2.8 Summary & Future work 105

2.9 References 107

Chapter 3: Orthogonal Functionalization of Alternating Polyesters: Selective Patterning of $(AB)_n$ Sequences

3.1 Introduction 111

3.2 Aims 113

3.3 Polyester synthesis 115

3.4 Hydroboration-oxidation of polyesters 124

3.5 Dual-functionalization of alternating polyesters 131

3.6 Thermal properties of dual-functional polyesters 138

3.7 Alternating homopolymer self-assembly 140

3.8 Summary & Future work 144

3.9 References 149

Chapter 4: Bio-Derived Degradable Block Copolymers as Pressure-Sensitive Adhesive

4.1 Introduction 153

4.2 Aims 156

4.3 Hard block polyester through ROCOP 158

4.4 Soft block polyester through ROP 172

4.5 Triblock copolymer formation: Selectivity study 174

4.6 Triblock copolymer formation: Material preparation 177

4.7 Adhesion property testing 193

4.8 Triblock polymer degradation 199

4.9 Summary & Future work 201

4.10 References 205

Chapter 5: Perspective and Future Work

5.1 'Switch' catalysis and sustainable polymers 210

5.2 Post-polymerization modification and applications 216

5.3 References 219

Chapter 6: Experimental

6.1 General Comments 223

6.2 Techniques 225

6.3 Experimental Procedures 228

6.4 References 234

Chapter 7: Appendices

7.1 Chapter 2 236

7.2 Chapter 3 254

7.3 Chapter 4 270

Chapter 1

Introduction

1.1. Sustainable Polymers – Polyesters and Polycarbonates

The manufacturing efficiency and property improvements of synthetic polymers have increased exponentially over the past 50 years.[1] These technological developments, as well as favorable economics, have resulted in polymers becoming ubiquitous in society. Their uses span sectors such as transport, energy storage, clothing, construction, electronics, medical products and packaging.[2]

Whilst polymers bring many benefits including being light weight, substitution of high embedded energy materials and resource efficiency, they also have sustainability issues, in particular, ~8 % of the total annual oil production is used for polymer synthesis.[3] Today, the global production is estimated to be around 380 Mt and it is set to grow at around 8.4 %.[4] Furthermore, many of these commodity plastics are non-degradable. Between 1950 and 2015, the estimated total plastic waste reached 6300 Mt and 79 % of it has ended up in landfill with a meagre 9 % being recycled (with the majority of the remaining being incinerated).[4] These factors contribute to enormous societal and environmental costs and burdens for disposal and end-of-life options (Fig. 1.1).

Current research is focused on improving polymer sustainability and a plethora of options are being investigated. This thesis focusses on investigating polyester (PE) and polycarbonate (PC) materials as future options in the polymer palette. These polymers are selected because they contain backbone chemistries which can be more easily broken than hydrocarbons.[5-6] Both polyesters and polycarbonates can undergo hydrolysis or alcoholysis reactions which could allow for future chemical recycling (recycling to monomers) and might improve upon sustainability options at the end-of-

life.[7-8] The thesis also examines how petrochemicals may be partly or even fully substituted with bio-based monomers in the synthesis of PE and PC. Although detailed sustainability assessment is beyond the scope of this work, using bio-based monomers, especially as co-products from other industries (e.g. agriculture, forestry of food waste) could allow for reductions to greenhouse gas emissions associated with polymer production.

Currently, the most widely used examples include poly(ethylene terephthalate) (PET) and polycarbonate (PC) (from bisphenol A and phosgene). These materials display useful thermal and mechanical properties and have been employed in industries such as packaging and electronics.[6] These commodity materials are derived from fossil fuels.[5] Currently, only around 1.7 Mt of plastics produced every year are biorenewable polymers, where one of the leading examples is polylactide (PLA).[9]

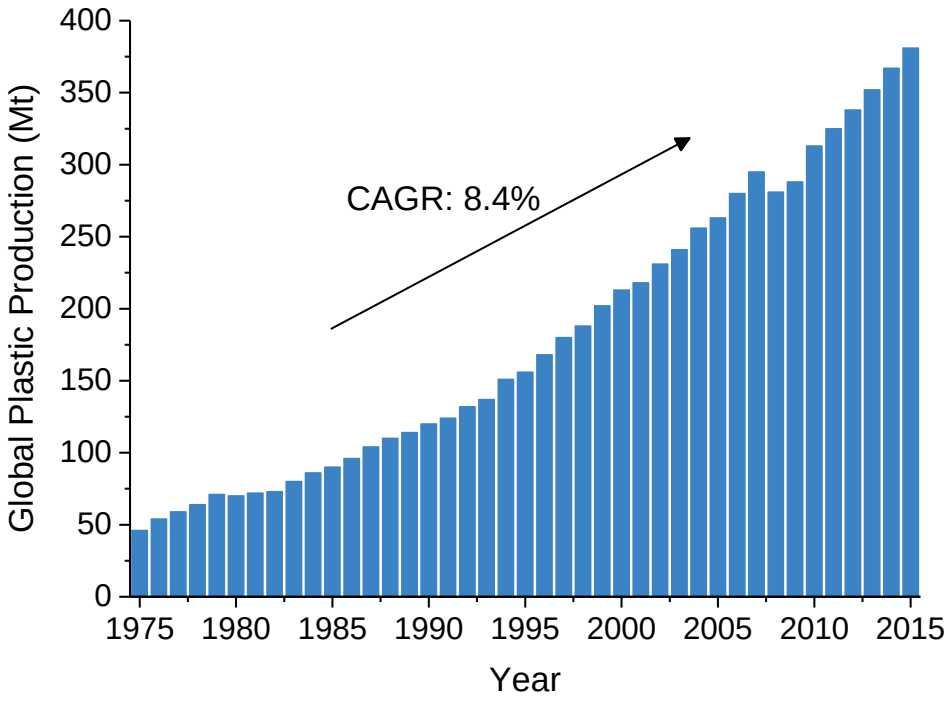


Figure 1.1 Global plastic production from 1975 to 2015 (note: CAGR refers to the compound annual growth rate).[4]

1.2. Ring opening copolymerization (ROCOP) and ring-opening polymerization (ROP)

PE and PC are synthesized using step-growth polymerization, but this method is not so well suited to new polymer development and especially copolymer investigations. Step-growth reactions are hard to apply at small scale especially as high conversion must deliver appreciable polymer molecular weight. Furthermore, the resulting PE and PC show broad molecular weight distribution and cannot be used to make block polymers. To investigate the potential of PE and PC, it would be preferable to use a chain growth method and to apply living polymerization. Living polymerization (i.e. polymerization where the termination is removed) by Szwarc in 1956 has enabled precise control over the polymer composition and polydispersity.[10] Two particularly useful living polymerizations for the synthesis of PE and PC are lactone ring opening polymerization (ROP) and epoxide/anhydride (or CO_2) ring opening copolymerization (ROCOP).[6, 11]

The ring opening polymerization (ROP) of cyclic esters or carbonates is a well-developed area of polymer chemistry that allows for the controlled synthesis of PE and PC.[12-16] This thesis concerns metal catalyzed living polymerizations and so it is relevant to discuss the mechanism for metal-catalysts for ROP. ROP can be catalyzed by metal-based complexes through a coordination-insertion mechanism.[17] For instance, in the ROP of lactide, the carbonyl group of the lactide is activated by the metal resulting in a more electrophilic carbon centre that is susceptible to attack from the metal bound alkoxide species. This is followed by rearrangement of the metal complex that places it in close proximity to the oxygen in the ester group. Finally, ring-opening of the cyclic

ester occurs and the metal alkoxide species is reformed. A subsequent monomer unit can then insert again and allow for polymer propagation (Fig. 1.2).

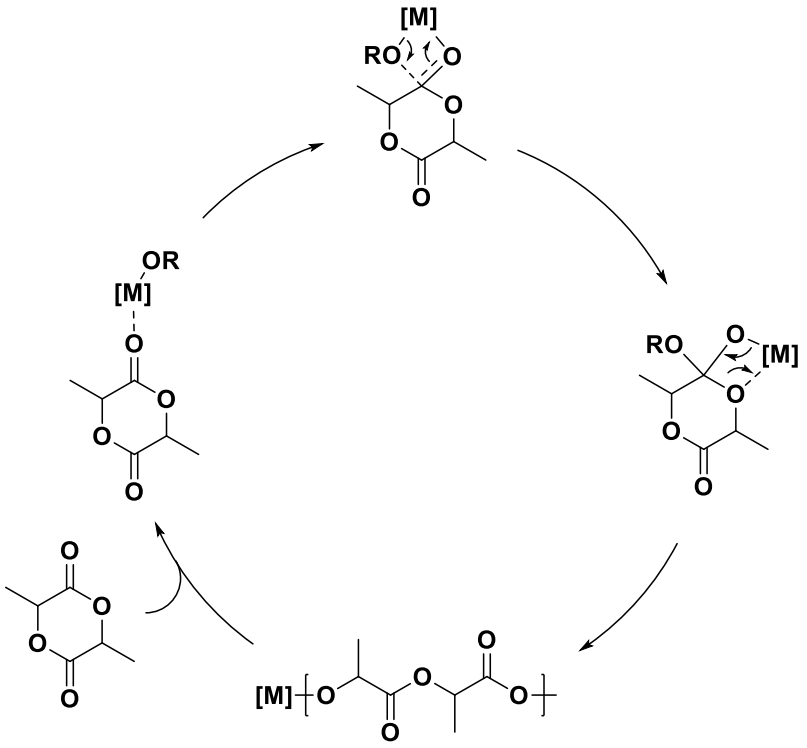


Figure 1.2 Coordination-insertion mechanism for the ROP of lactide ([M] denotes a Lewis acidic metal in a ROP catalyst).

Whilst ROP is an excellent method for the preparation of aliphatic polyesters, its available monomer pool is rather limited. The most commonly used monomers in ROP include various lactones (such as ε-caprolactone (CL), ε-decalactone (DL), β-butyrolactone (BL) and lactide (LA)) or cyclic carbonates (not discussed in this thesis) (Fig. 1.3). Furthermore, the thermodynamics of polymerization (ΔG_p) are highly dependent upon the lactone ring size and substituents.[18] In polymerizations, entropy (ΔS_p) typically decreases and so for smaller ring sizes, reactions are driven by enthalpy

(ΔH_p) . As such, for ROP to occur at a given temperature, it is important that the enthalpy contribution (ΔH_p) is sufficient in compensating the loss in entropy (i.e. ΔG_p should be < 0 for polymerization to occur).

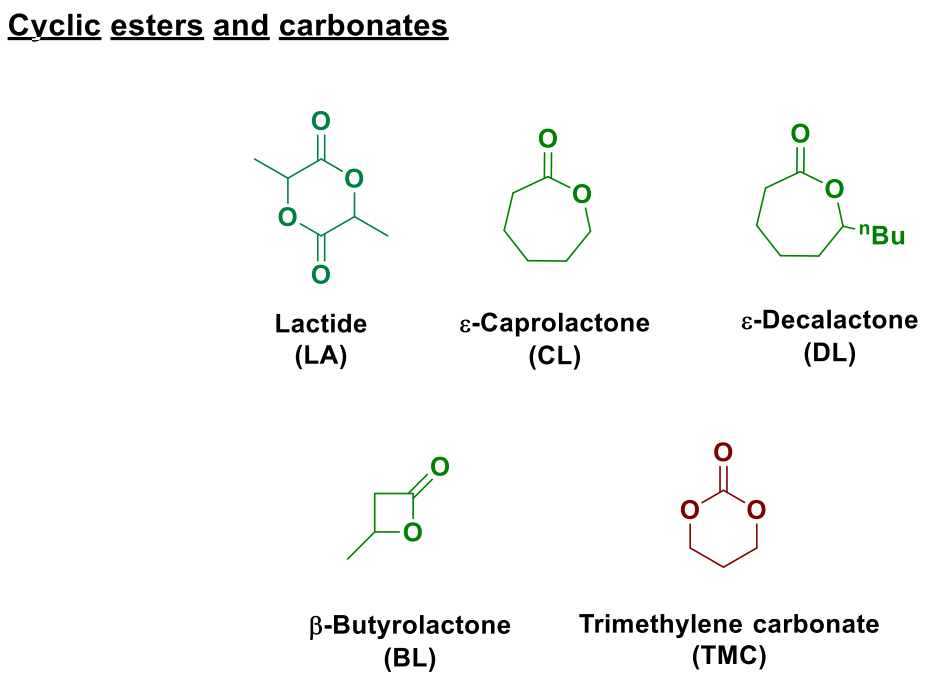


Figure 1.3 Selected examples of cyclic esters and carbonates used in ROCOP.

The polymerization enthalpy is highly dependent on the monomer ring size (n) and the resulting ring strain.[19] For instance, highly strained four or seven membered rings are readily polymerized by a variety of catalysts,[20-22] whereas five membered rings are sufficiently stable as to give rise to very high equilibrium monomer concentrations (Fig. 1.4).[23]

It is important to emphasise that ROP is a reversible process where the monomer-polymer equilibrium can be dictated by external factors including the reaction temperature and monomer concentration.[18] As the reaction temperature

increases, polymerization conversion decreases, eventually reaching a point where no conversion occurred. The temperature in which no monomer conversion is observed and the reverse depolymerisation process is thermodynamically feasible is known as the ceiling temperature.[24]

On the other hand, epoxide/anhydride (CO_2) ROCOP has received less attention but is nonetheless an effective method for the production of PE and PC.[6, 11] For instance, by combining epoxide and CO_2, polycarbonates can be formed in a much more renewable fashion compared to the conventional condensation of bisphenol A and phosgene, where the latter is highly toxic.[25] Furthermore, polyesters can also be prepared through coupling epoxide/anhydride ROCOP (Fig. 1.5).

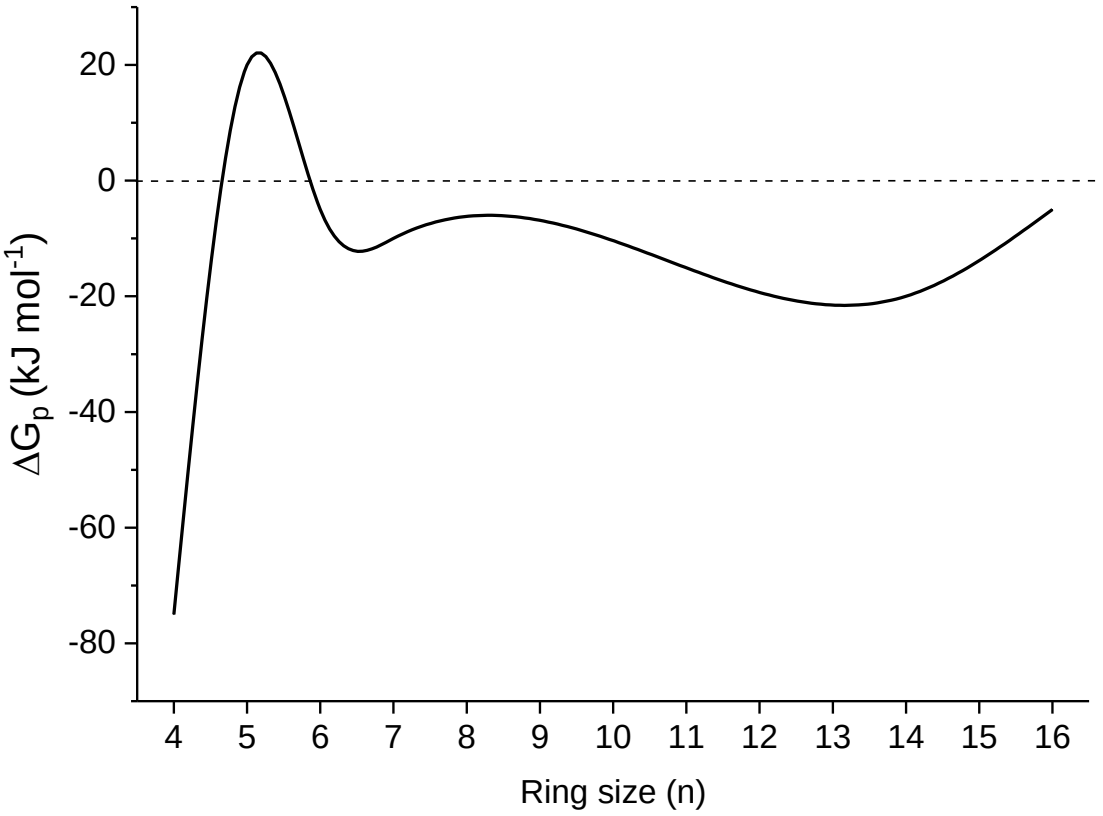


Figure 1.4 Characteristic changes in ΔG_p for different monomer ring sizes in ROP.[19]

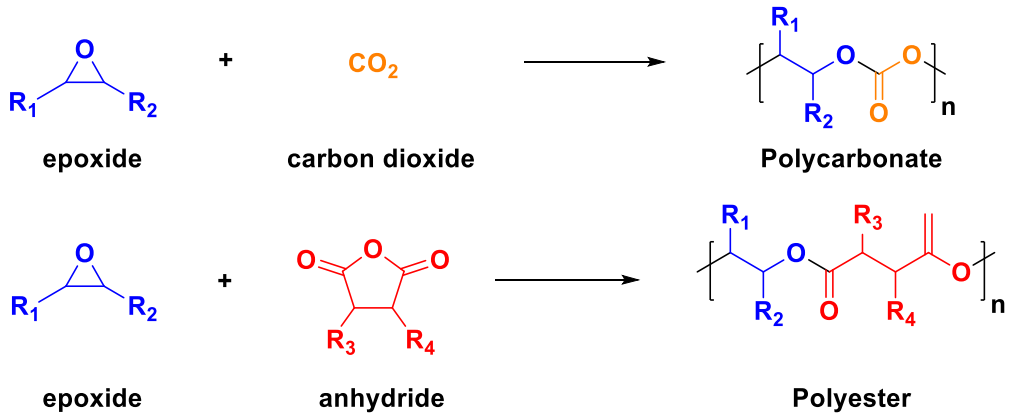


Figure 1.5 ROCOP of epoxide/CO_2 or anhydride for the synthesis of polyesters and polycarbonates, respectively.

In general, ROCOP is catalyzed using a metal complex, [M], with an initiating group, X, such as halide, alkoxide or acetate. The polymerization mechanism involves a series of different steps (Fig. 1.6). Initiation entails the insertion of the epoxide monomer into the [M]-X bond to generate a metal alkoxide species. Thus, the initiating group typically becomes the end group of a polymer chain. Subsequently, the metal alkoxide attacks a CO_2 (or anhydride) monomer to generate a metal carbonate (or carboxylate) which consequently ring opens an epoxide monomer to re-generate the metal alkoxide species. Side reactions can also occur. For instance, double insertion of epoxide monomers can lead to formation of undesired ether linkages (as opposed to ester or carbonate linkages) which are non-degradable and affect polymer properties.

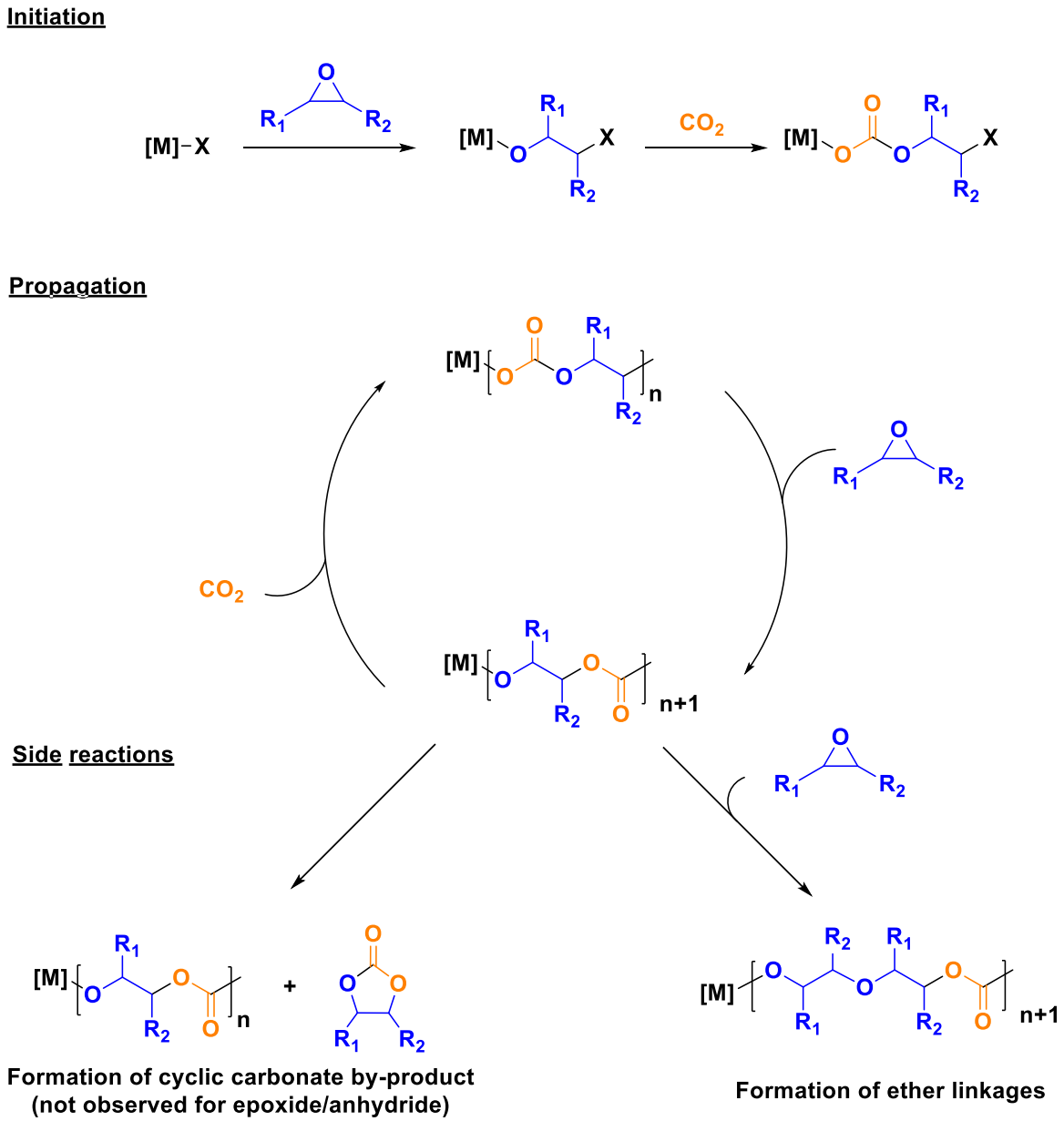


Figure 1.6 Illustration of the elementary steps for epoxide/CO_2 ROCOP.

For epoxide/CO_2 ROCOP, backbiting of the polymer chain would result in formation of cyclic carbonate by-products and reduce the molar mass of the polymer. As such, ROCOP reactions are typically optimized in order to minimize these side reactions. During chain transfer reactions, the metal bound polymer chains are in constant and rapid exchange with hydroxyl terminated polymer chains. Under normal conditions, the chain transfer reactions occur much faster than propagation. As such, a chain transfer agent (CTA) can be deliberately added to control the polymer molar mass and dispersity. CTAs are usually hydroxyl containing compounds including water and alcohols.

ROCOP catalysts usually comprise two components either in the form of a dinuclear metal complex[26-27] or bicomponent systems such as a metal catalyst with a ionic co-catalyst.[28] Dinuclear catalysts are favoured in this thesis as these do not require co-catalysts. In dinuclear catalysts, the complex must feature a co-ligand (e.g. acetate). In a similar fashion to the general ROCOP scheme, the initiation step involves binding of the epoxide by one of the metal centres. The other metal centre then delivers the nucleophile which attacks the bound monomer to form a metal-alkoxide. In the presence of CO_2 (or anhydride), the second monomer rapidly inserts into the metal-alkoxide bond to form a metal carbonate (or carboxylate) species. Subsequent epoxide and CO_2 (or anhydride) insertion propagates the polymerization, with the epoxide opening being the rate-determining step (Fig. 1.7).[29] As each of the metals carry out a specific role, the use of two distinct metals, tailored to their roles, can lead to synergistic effects.[30] This method is particularly effective as the wide scope of commercially available epoxides and anhydrides allows access to a wide variety of materials with differing properties (Fig. 1.8).[6, 11]

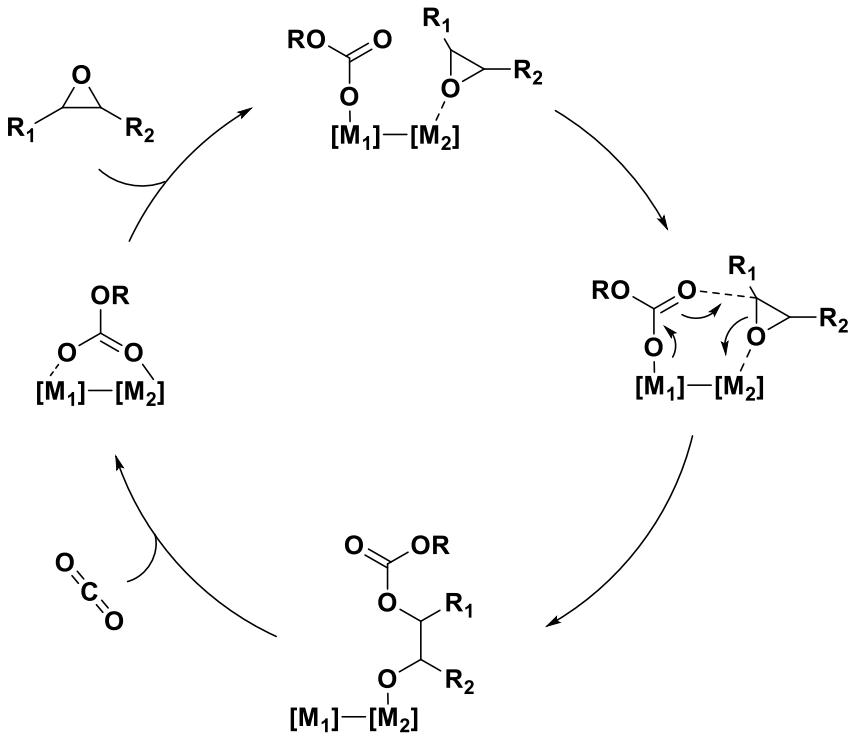
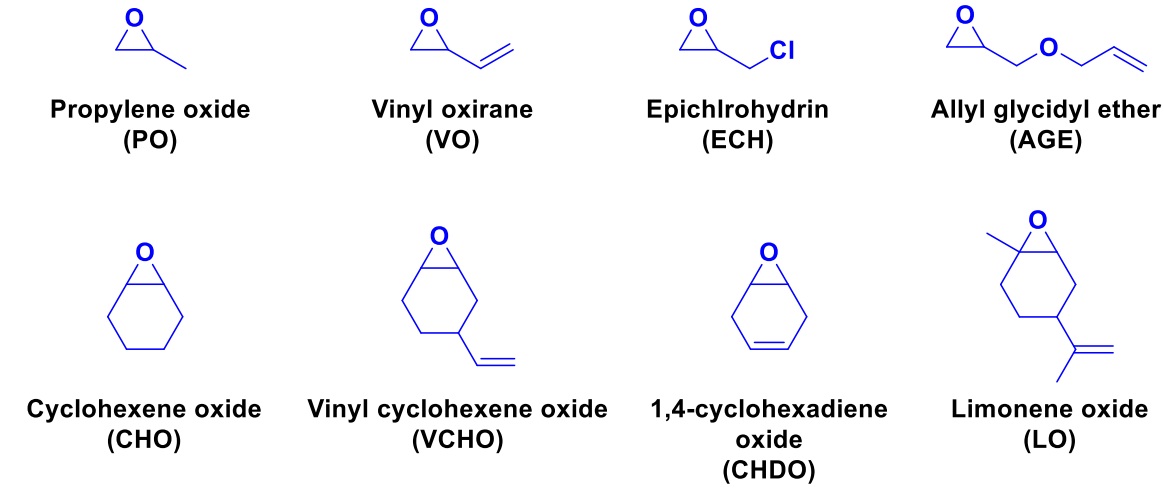


Figure 1.7 Dinuclear mechanism for the ROCOP of epoxide/CO_2 ([M] denotes the two metals in a dinuclear complex).

Epoxides



Anhydrides

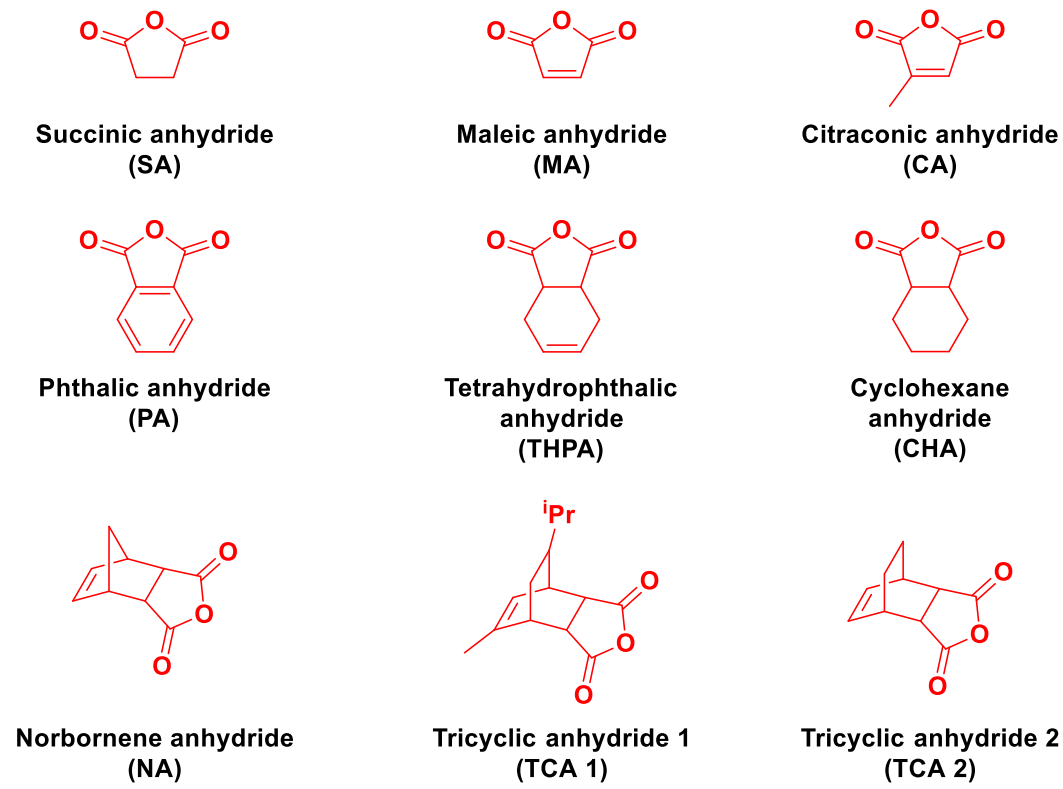


Figure 1.8 Selected examples epoxide and anhydride used in ROCOP.

1.3. **Block polymers**

Block polymers are macromolecules that can be formed by covalently joining two different polymer chains.[31] These materials are particularly interesting as they have the ability to display microphase separation that brings about the properties of the constituting blocks in a synergistic manner. The most well-known block copolymer are based on poly(styrene) and poly(butadiene) (or poly(isoprene)). The block polymer is composed in a ABA arrangement with the 'A' being the *hard* polystyrene with high glass transition temperatures (typically > 50 °C) and 'B' being the *soft* polybutadiene with low glass transition temperature (typically < 0 °C). Today, these blocks are commercially available and have applications in many sectors including adhesives, lithography, electronics, photonics and elastomers.[32-34]

Traditionally, there are two main methods of synthesizing block polymers. The first type of methods relies on carefully timed monomer additions or through selection of monomers that provide the correct 'reactivity ratios'.[35-38] Whilst these may be convenient, the available monomer pool is limited due to the need for compatibility between the different monomer/catalyst systems. The other method is through the use of macroinitiators after intermediate isolation and purification steps.[32, 39-42] These methods suffer from a lack of efficiency and can be very time-consuming. As such, further research in developing more effective block polymer synthetic procedures is warranted.

1.4. **Switch Catalysis: A new route to block polymers**

The term 'Switch' catalysis has been widely used to describe a change in the chemical reactivity of the catalyst system in response to an external stimulus.[43-44] Initial usage of the term referred to an 'On/Off switch', where a particular polymerization cycle would propagate or halt based on the stimulus applied. These 'On/Off' type switches utilized different stimulus mechanisms including redox,[45] photochemical,[46] chemical[47-48] and electrochemical reactions.[49] Whilst modulation of the polymerization activity is novel, it can be argued that its application is limited. Control over the *selectivity* of the polymerization would offer greater benefits in terms of material preparation. As such, there had been an insurgence of work based on monomer discrimination for a single polymerization cycle. For instance, Coates and co-workers first demonstrated selectivity between the epoxide/anhydride and epoxide/CO_2 ROCOP cycles using a zinc β-diiminate (BDI)catalyst.[50] The researchers used three different monomers, namely epoxide, anhydride and CO_2 to form diblock copolymers and this method is termed terpolymerization. This work was followed by similar concepts demonstrated using other metal catalysts.[51-54]

More recently, research has been conducted to combine different polymerization cycles, namely ROCOP and ROP and this switching between polymerization mechanism is referred to here as 'Switch catalysis'. In this context, it is important to note that 'Switch' catalysis is distinct from terpolymerization, where the latter simply refers to monomer discrimination and entails no switch in mechanism (i.e. the synthesis is based on the same polymerization mechanism and the selectivity is controlled through reactivity ratios).[55] In 2014, Williams and co-workers introduced the first example of

a homogenous catalyst, [LZn$_2$(OAc)$_2$] (**I**), that accessed both ROP and ROCOP cycles using a mixture of epoxide/CO_2/lactone (Fig. 1.9).[56] In a reaction mixture containing CHO and CL, the diphenolate macrocyclic catalyst selectively underwent the ROCOP cycle under the presence of a CO_2 atmosphere. When CO_2 was removed, only the ROP cycle was accessed. As such, CO_2 acted as an exogenous 'switch' reagent. The proposed mechanism suggests that the insertion of CO_2 into the common metal-alkoxide intermediate (k_1) was much faster than that of CL (k_3). Once CO_2 was inserted, the polymer chain end becomes a metal-carbonate, which selectively attacks the epoxide (k_2).[56] Overall, the metal chain end controls the chemoselectivity of the catalysis and CO_2 acts as an exogenous 'switch' reagent.

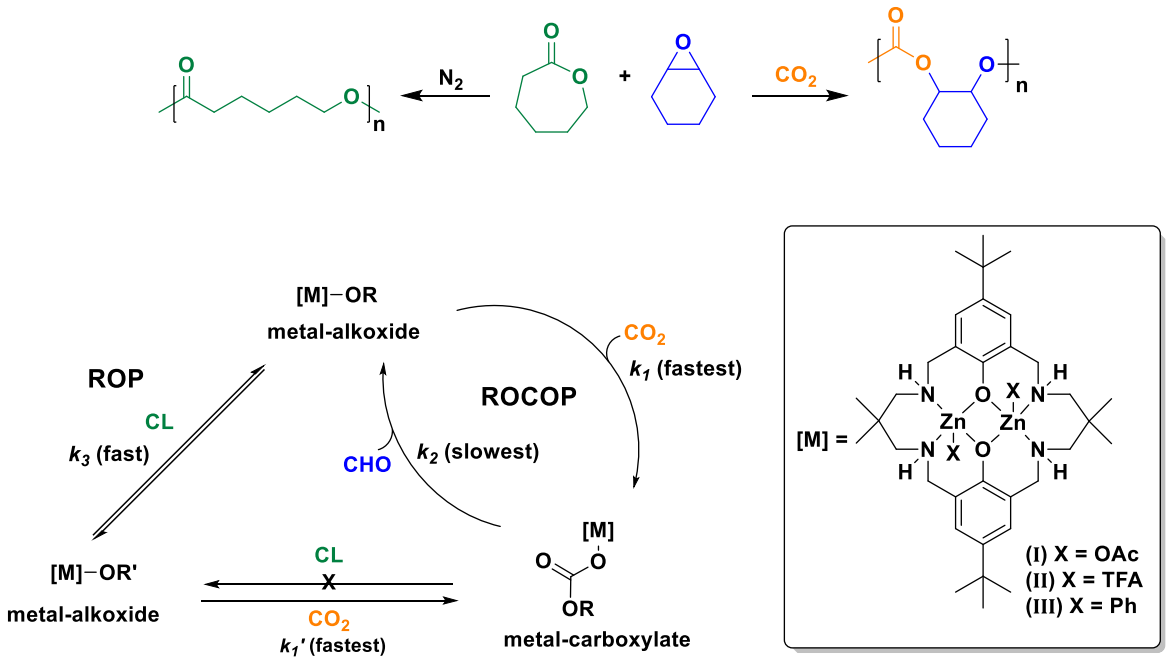


Figure 1.9 'Switch' catalysis and proposed mechanism for CHO/CO_2/CL using diphenolate macrocyclic Zn catalysts (rate: $k_1 \approx k_1' > k_3 >> k_2$).[56]

The 'Switch' catalysis methodology was utilized to synthesise block poly(ester-*b*-carbonates).[56] However, the mixture of acetate co-ligands and residual adventitious 1,2-cyclohexane diol (CHD) (a bifunctional initiator, present in the CHO) resulted in a mixture of AB and ABA blocks. It is worth mentioning that the presence of CHD in CHO is a common problem reported by different researchers in the epoxide/CO_2 ROCOP field.[29, 57-59] In the pursuit of obtaining well-defined block copolymers, a new catalyst [$LZn_2(TFA)_2$] (**II**) (note: TFA = trifluoracetate), was synthesised and employed. Whilst the TFA ligands also initiated the polymerization, its susceptibility to hydrolysis resulted in the formation of mainly ABA-type block copoly(ester-*b*-carbonate-*b*-ester).[60] In 2015, a third iteration was presented in the form of [LZn_2Ph_2] (**III**) featuring an organometallic co-ligand. This catalyst was used in 'Switch' catalysis between CHO/PA ROCOP and DL ROP.[61] The benefit of **III** lies in the fact that the phenyl co-ligands do not initiate the polymerization and rather efficiently reacts with diol to eliminate benzene in the presence of protic reagents. Similar to the epoxide/CO_2/lactone reaction, the ROCOP of epoxide/anhydride was shown to be preferred over the ROP of lactone and the latter only occurred once the anhydride was fully depleted. Thus, through careful choice of initiator design (such as CHD), well-defined ABA-type triblock copolyesters can be accessed.

The pathways accessible during 'Switch' catalysis were further investigated using DFT calculations.[62] Using **I** as the catalyst, the reaction pathways for CHO/PA ROCOP and CHO/CO_2 ROCOP as well as CL ROP were analysed in detail (Fig. 1.10). The theoretical investigation illustrated that both the kinetic barriers and the thermodynamic stability of the linkages help govern the unusual catalyst selectivity. For instance, CHO and PA insertion into the Zn alkoxide intermediate had similar

energy barriers and both are lower than the equivalent insertion of CL. Furthermore, the ester linkage from CHO/PA ROCOP was shown to be the most thermodynamically stable followed by the carbonate linkage from the ROCOP of CHO/CO_2. The ester linkage from the ROP of CL was revealed to be the least stable. Overall, the computational investigation suggests that the dizinc catalyst has a preference for epoxide/anhydride ROCOP, followed by epoxide/CO_2 ROCOP with lactone ROP being the least preferred exactly as observed experimentally.

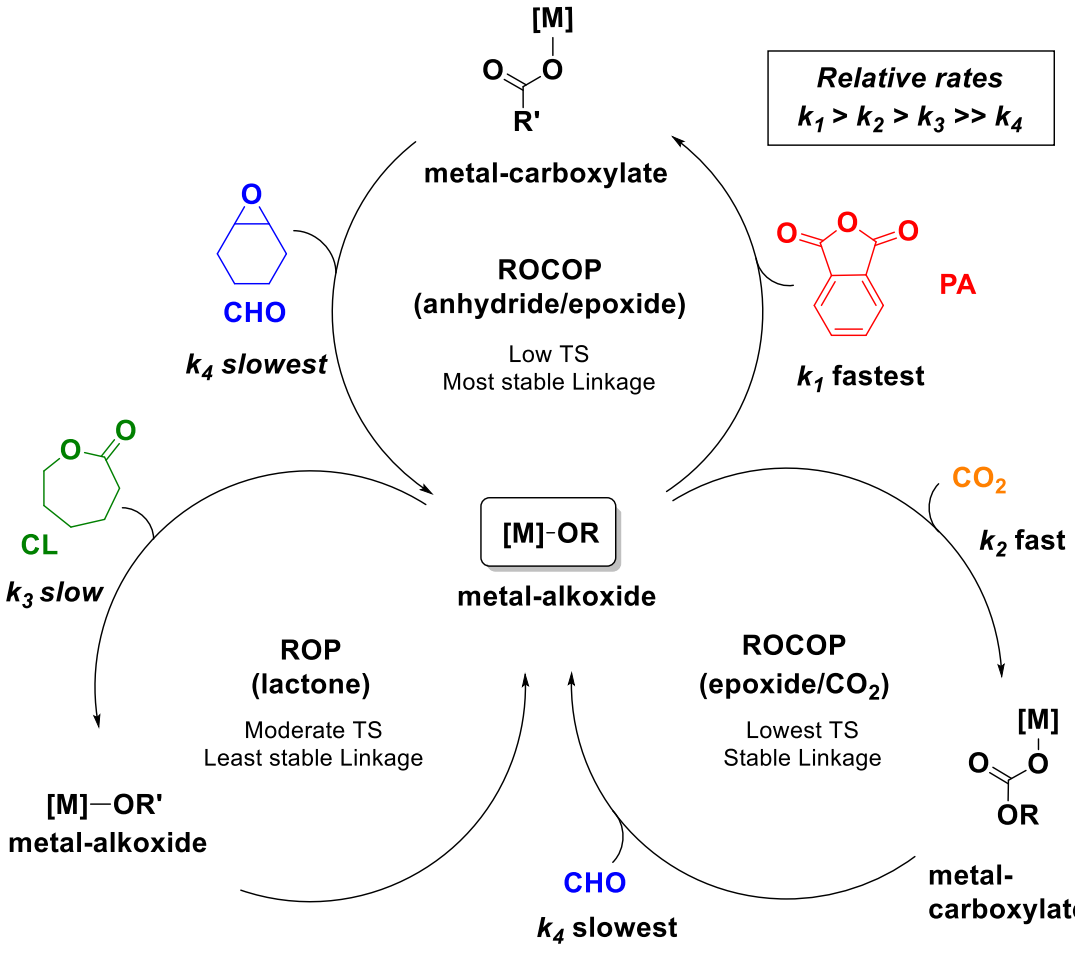


Figure 1.10 Computation analysis for 'Switch' catalysis using CHO/PA/CO_2/CL. (Not: TS denotes transition state barriers).[62]

Next, Williams and co-workers employed **I** to selectively polymerize a mixture of epoxide and *O*-carboxyanhydride (OCA) to form block poly(lactide-*b*-carbonate).[63] This monomer mixture exploits the ability of the dizinc catalyst to carry out epoxide/CO_2 ROCOP at 1 bar CO_2 pressure and allows for the recycling of the waste CO_2 from the OCA ROP into a new block polymer.

In 2017, Rieger and co-workers applied the same 'Switch' catalysis using a BDI-based Zn catalyst (**IV**) (Fig. 1.11).[64] Using a mixture of CHO (or CPO)/CO_2/BL, different CO_2 gas pressures produced different polymer microstructures. For instance, at high CO_2 pressures (40 bars), only the polycarbonate from the ROCOP of CHO/CO_2 was observed. Subsequent release of CO_2 led to formation of block poly(carbonate-*b*-ester). Under low CO_2 pressures (3 bars), a statistical polymer was produced. In the absence of CO_2, only the polyester from BL ROP was observed. The same group later applied the same principle to mixtures featuring BL, CO_2 and limonene oxide (LO), where the latter is a renewable epoxide.[65] In this case, the statistical copolymer could not be produced as low pressure environments lead to depolymerisation of the LO/CO_2 block.

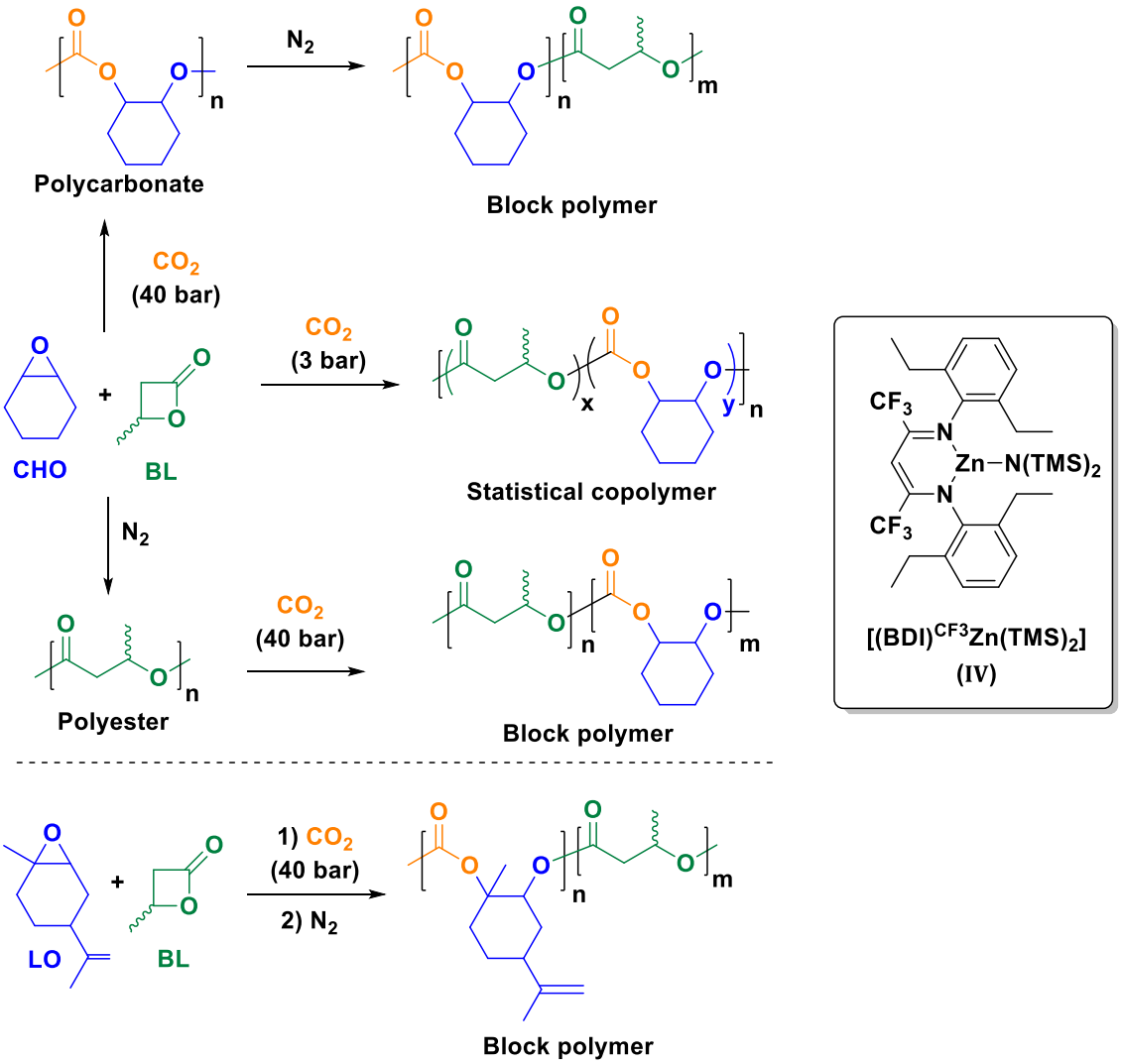


Figure 1.11 'Switch' catalysis for CHO(LO)/CO_2/BL using (BDI)-based Zn catalyst.[64-65]

Investigation of 'Switch' catalysis accelerated in 2018/2019, where multiple groups showed the concept is generally applicable to other catalysts systems. For instance, the commercially available Cr(III) catalyst, [SalcyCr(III)Cl] (**V**), was shown to selectively catalyze 'Switch' polymerization using mixture of CHO/NA/DL (Fig. 1.12).[66] Furthermore, the concept was demonstrated with a range of different bicyclic and tricyclic anhydrides to prepare block polyesters. It is worth noting that a drawback of this system is the requirement of a co-catalyst to reach acceptable rates. Due to the

multiple initiators, including the chloride from the catalyst and co-catalyst as well as the residual diol residues, the molar mass of the block copolymers was limited to ~5 kg mol^{-1}. Upon switching the epoxide from CHO to PO (and its derivatives), a third polymerization cycle, the epoxide ROP, was accessed (Fig. 1.12).[67] This addition allowed for polyether to be incorporated into the block polymers prepared *via* 'Switch' catalysis.

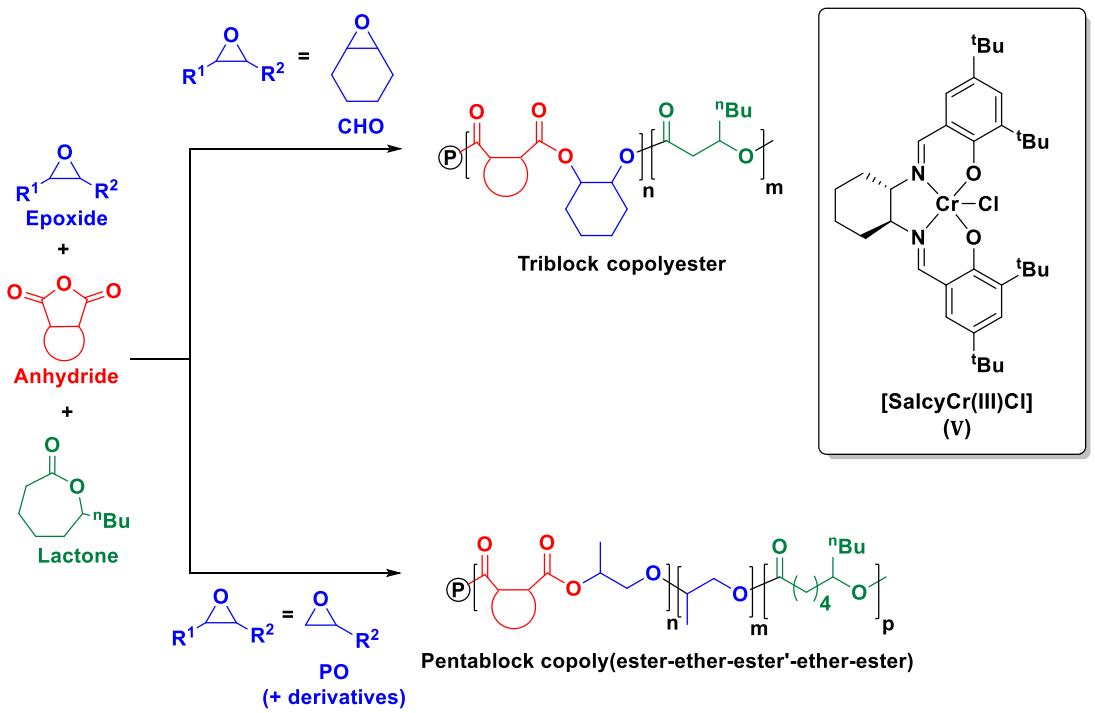


Figure 1.12 'Switch' catalysis for epoxide/anhydride/lactone using [SalcyCr(III)Cl].[66-67]

Up until this point, only a limited number of ROP monomers had been utilised in 'Switch' catalysis. LA is a promising candidate as it is commercially produced and used at large scale (~1Mt/annual production).[9] Furthermore, it is fully bio-based and

delivers degradable polylactide (PLA).[68-69] Whilst LA is active in ROP, it is also susceptible to possible transesterification.[70] As such, a modified Al-salphen catalyst featuring electron-withdrawing fluorine substituents, [Salphen^{F}AlCl] (**VI**), was employed in 'Switch' catalysis with PO/PA/LA to form triblock copolyesters featuring PLA blocks (Fig. 1.13).[71]

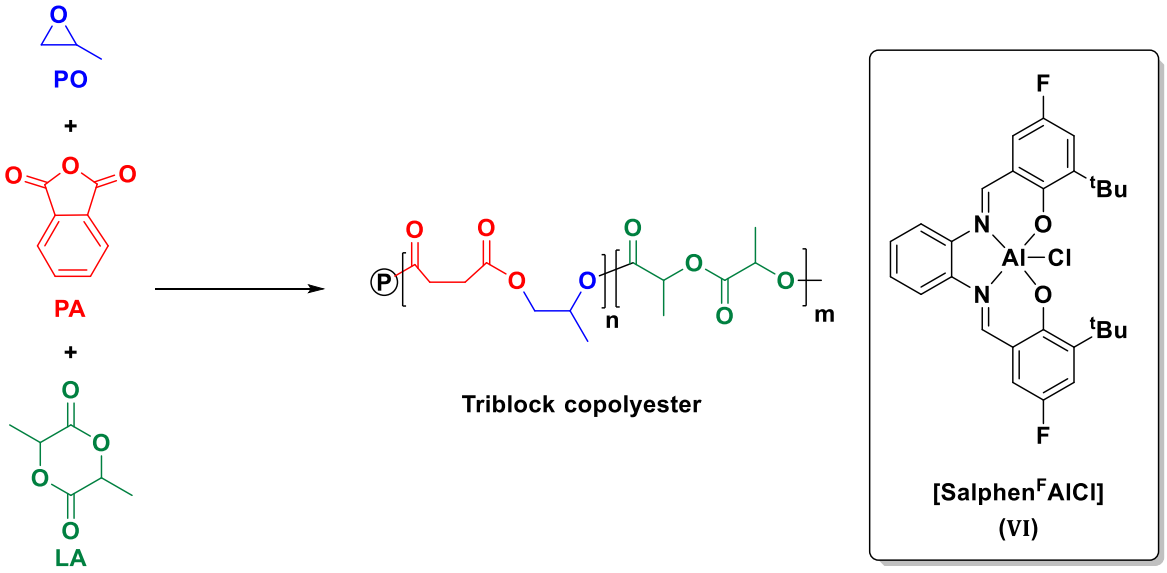


Figure 1.13 'Switch' catalysis for PO/PA/LA using [SalphenAlCl].[71]

Recently, the concept of 'Switch' catalysis has also been applied to metal-free organocatalysts.[72-73] For instance, Ji *et al.* have utilized the commercially available phosphazene, ^{t}BuP$_1$ (**VII**), as a catalyst in the polymerization of various epoxides, anhydrides and LA to prepare different block polymers including diblocks, triblocks and star shaped polymers (Fig. 1.14).

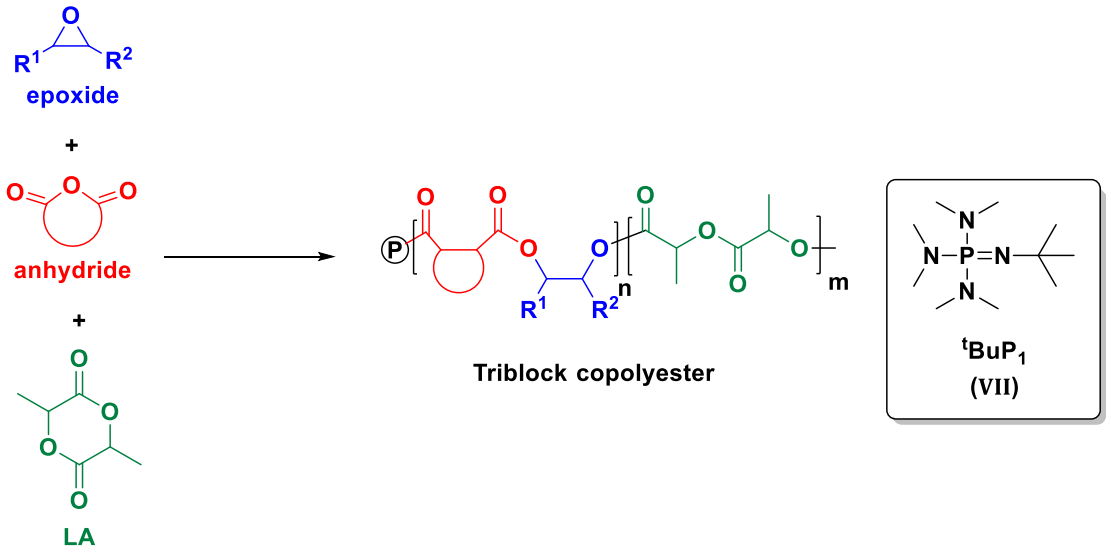
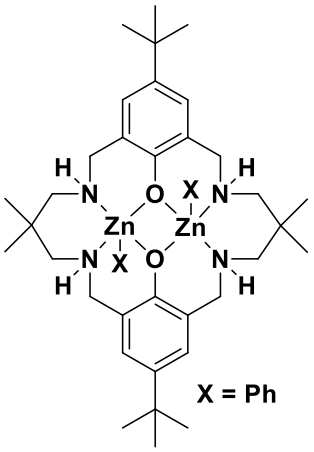


Figure 1.14 'Switch' catalysis for epoxides/anhydrides/LA using $^{t}BuP_1$.[72-73]

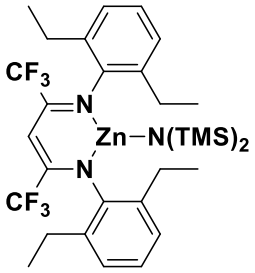
Whilst many different catalysts have been shown to demonstrate the ability to switch between epoxide/CO_2(anhydride) ROCOP and lactone/lactide ROP, they each come with different advantages and drawbacks. Some of the important factors to consider when comparing the different 'Switch' catalysts include the complexity of the catalyst preparation, the need of co-catalysts and available monomer scope (Table 1.1). For instance, the diphenolate macrocyclic catalysts,(**I**, **II**, **III**) (Figure 1.9) are unusual in allowing for 'Switch' catalysis with low pressure CO_2 pressure (1 bar).

Table 1.1 Comparison of 'Switch' catalysts

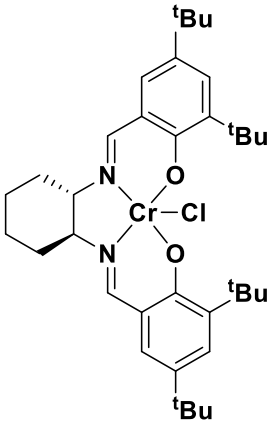
Factors \ Catalyst		**I/II/III**	**IV**	**V**	**VI**	**VII**
Catalyst Features	Synthesis	4 steps (~7 days)	2 steps (~6 days)	*Not Applicable*	3 steps (~6 days)	*Not Applicable*
	Commercial	No	No	Yes	No	Yes
	Colour	White	White	Coloured	Coloured	White
Switch Catalysis	Co-catalyst	No	No	Yes	Yes	No
	Monomer Scope (as shown in 'Switch' catalysis)	**ROCOP:** Epoxide/CO_2 (1 bar) Epoxide/anhy. ---------- *Epoxide: CHO & deriv. Anhy.: bi/tricyclics*	**ROCOP:** Epoxide/CO_2 (40 bar) ---------- *Epoxide: CHO, CPO & LO*	**ROCOP:** Epoxide/anhy. ---------- *Epoxide: wide scope (CHO & PO deriv.) Anhy.: wide scope Mono/bi/tricyclics*	**ROCOP:** Epoxide/anhy. ---------- *Epoxide: PO Anhy.: PA, TCA1*	**ROCOP:** Epoxide/anhy. ---------- *Epoxide: wide scope CHO & PO derivatives Anhy.: wide scope Mono/bi/tricyclics*
		ROP: Lactone (CL, DL) *O*-carboxyanhydride (OCA)	**ROP:** Lactone (BL)	**ROP:** Lactone (CL, DL) Epoxide (PO)	**ROP:** Lactide (LA)	**ROP:** Lactide (LA)
	Temp. window	80 °C – 100 °C	50 °C – 60 °C	100 °C	60 °C	100 °C
	Block Selectivity	Fully selective	Fully selective at high press.; not selective at low press.	Mostly selective	Mostly selective	Fully selective
Triblock polymer	Reported M_n (kg mol^{-1}) [$Đ$]	**I**: 2 – 5 [1.28 – 1.49] **II**: 2 – 14 [1.33 – 1.43] **III**: 12 – 16 [1.15 – 1.29]	70 - 146 [1.23 – 1.33]	4 – 7 [1.20 – 1.32]	3 - 14 [1.21 – 1.22]	4 – 31 [1.07 – 1.20]
Reference		56, 60-61, 63	64-65	66	71	72-73



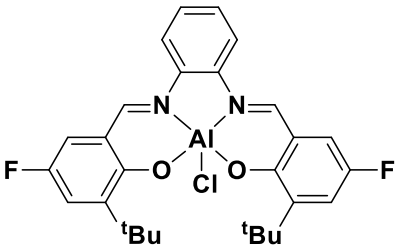
$[LZn_2Ph_2]$
(III)



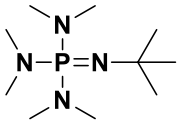
$[(BDI)^{CF3}Zn(TMS)_2]$
(IV)



[SalcyCr(III)Cl]
(V)



$[Salphen^{F}AlCl]$
(VI)



$^{t}BuP_1$
(VII)

This is especially useful from a practically perspective as no high pressure equipment are needed. However, a particular drawback of these di-zinc catalysts is their inability to carry out ROCOP with industrially relevant monomers such as PO or LA. Whilst **4** needed 40 bar of CO_2 pressure to be fully selective in its 'Switch' catalysis operations, this catalyst system is able to produce triblock polymers with molar masses >140 kg mol^{-1}.

Although **5** and **6**, have been demonstrated to carry out 'Switch' catalysis for a wide range of monomers, including a wide range of epoxides, anhydrides as well as lactone and lactide, the chloride co-ligand and need for a co-catalyst limits the overall

molar mass of the block polymer. Furthermore, the highly coloured nature of these catalysts results in unattractive coloured polymers. Finally, the exemplar metal-free organocatalyst, **7**, is applicable with a wide range of monomers, gives access to block polymers of moderate molar mass (~30 kg mol^{-1}) and do not need the assistance of a co-catalyst. However, its application in 'Switch' catalysis involving CO_2 remains to be investigated. Thus, selection of the appropriate 'Switch' catalysis for the desired product is paramount.

1.5. **Switch catalysis: guide to block polymer formation**

'Switch' catalysis is a powerful method to prepare block polymers from a mixture of different monomers through a one-pot process. Once a candidate catalyst demonstrates the ability to carry out ROP and ROCOP separately, it has the potential to operate as a 'Switch' catalyst for producing polyesters/carbonates. When assessing a new catalyst for its applicability in performing 'Switch' catalysis, there are two main challenges it needs to overcome.[55] First, the catalyst needs to demonstrate monomer discrimination (i.e. the catalyst needs to perform either ROP or ROCOP selectively in the presence of a monomer mixture). Second, the product should be examined to ensure formation of block polymer rather than a mixture of homopolymers.

To demonstrate monomer discrimination and selectivity between ROP and ROCOP there are two main techniques that can be employed. *In-situ* ATR-IR monitoring is a non-intrusive and sensitive method of examining the reaction. By selecting the appropriate wavenumbers to observe, both the monomer consumption and the polymer formation can be monitored. For instance, the 'Switch' polymerization between PA/CHO/DL can be monitored through *in-situ* ATR-IR by following the PA and DL consumption at 1790 cm^{-1} and 1735 cm^{-1}, respectively (Fig. 1.15). Similarly, the polyester formation from the ROCOP of PA/CHO (PE) and ROP of DL (PDL), at 1065-1068 cm^{-1} and 1190 cm^{-1}, respectively, can be followed and should be the inverse of the trend observed for the respective monomer consumption.

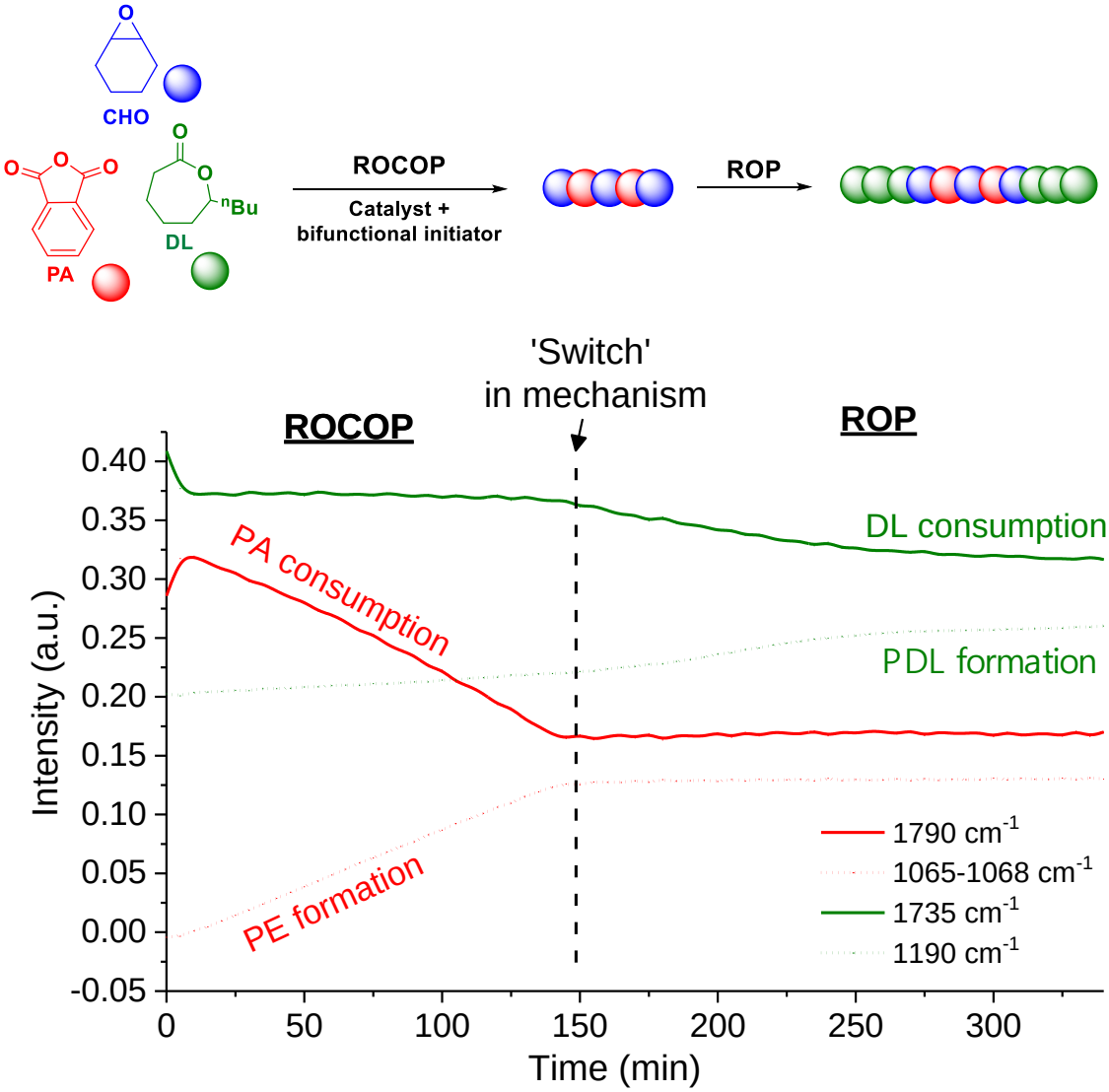


Figure 1.15 Exemplar In-situ ATR-IR spectrum demonstrating the 'Switch' mechanism for PA/CHO/DL polymerization. Adopted from [55].

During the first 2.5 h, the *in-situ* ATR-IR trace suggests only the PA is consumed (and PE is formed). The intensity of DL or PDL remained constant. At around the 150 min mark, DL starts to decrease in intensity with concurrent increase in the intensity of PDL. The intensity of PA and PE both remained constant. This indicates a 'Switch' in mechanism. Moreover, ^{1}H NMR spectroscopy experiments of aliquots taken at key intervals can be conducted to accompany the *in-situ* monitoring and further support the selectivity of the catalyst. This can be achieved by comparing the integrations of the monomers (PA and DL) and polymers (PE and PDL).

The selectivity assessment can ascertain whether the catalyst is able to discriminate monomers. However, whether the product is a block polymer (or mixture of homopolymers) still needs to be identified. Furthermore, side-reactions such as transesterification and back-biting are also possible. As such, the block composition also needs to be examined. There are seven main methods to investigate whether the product is a well-defined block polymer:

1) Monitoring by size exclusion chromatography (SEC): A major piece of evidence for block polymer formation is the observation of a continuous increase in molar mass with retention of narrow dispersity between the enchainment of sequential blocks (Fig. 1.16(A)). In practice, this can be achieved by running SEC analysis of aliquots taken before and after the 'Switch' in mechanism. On the other hand, a mixture of homopolymer (or block polymer with homopolymer contamination) would lead to two peaks in the SEC plot (Fig. 1.16(B).

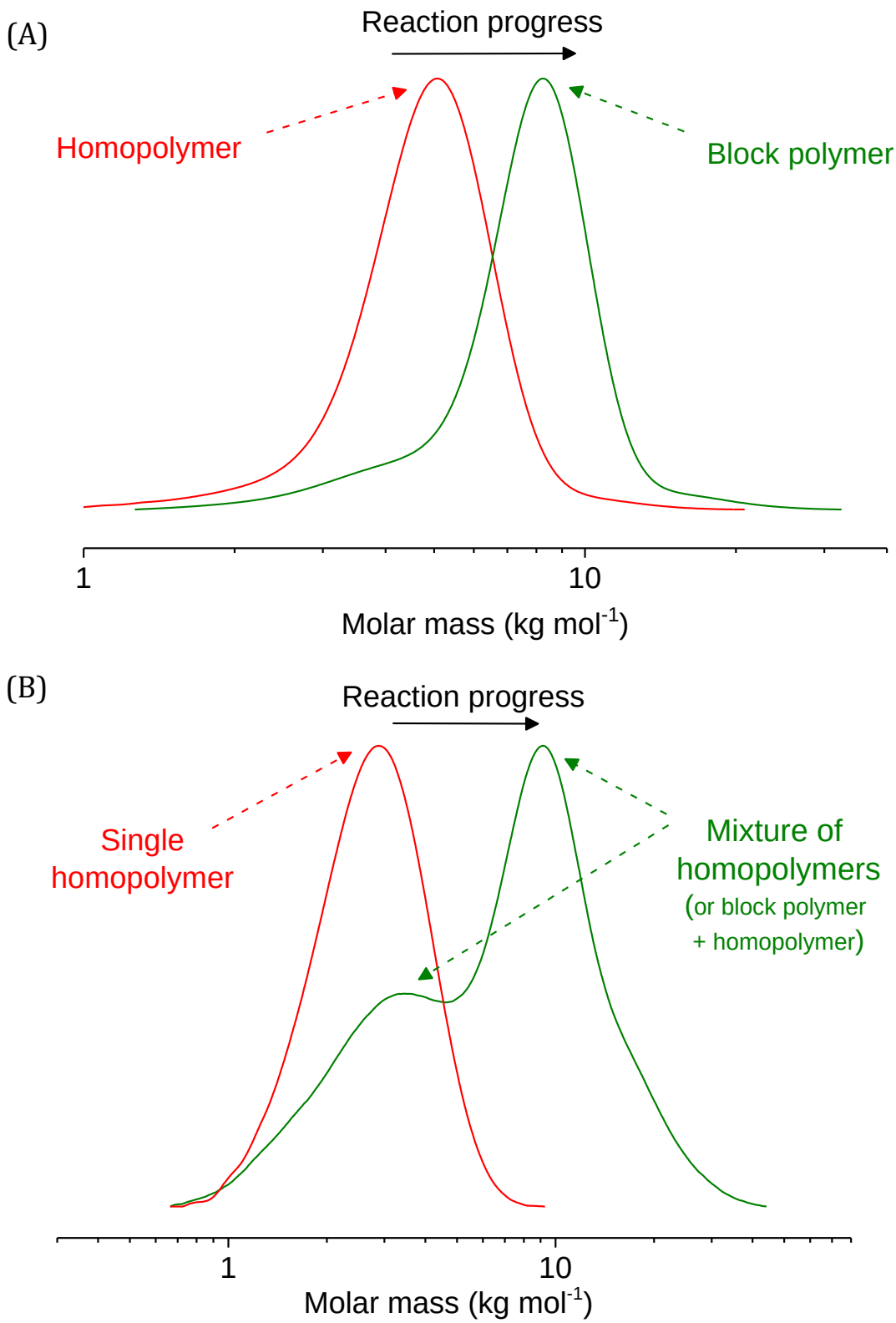


Figure 1.16 Exemplar SEC traces for (A) block polymer formation and (B) mixture of homopolymers or block polymer with homopolymer contamination.

2) End group analysis: Block polymer formation necessitates extension from the chain end. Therefore, the end group of the inner block should not be present after addition of the outer block. This feature can be investigated by looking for the polymer end groups in ^{1}H NMR spectroscopy.[21] Alternatively, the hydroxyl chain ends can be reacted with a phosphorus-containing reagent (e.g. 4,4,5,5-tetramethyl dioxaphospholane) (Fig. 1.17). The resulting sample can be examined using $^{31}P\{^{1}H\}$ NMR spectroscopy (using Bisphenol A as an internal standard), where a change in end group signals should be observed for block polymer formation (Fig. 1. 18).[61, 74]

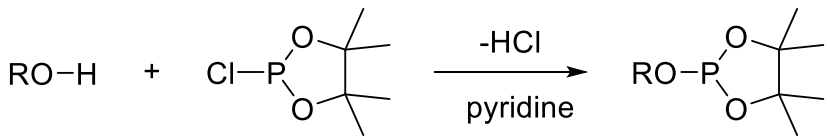


Figure 1.17. End group analysis using $^{31}P\ \{^{1}H\}$ NMR spectroscopy (note: R denotes polymer chain end).

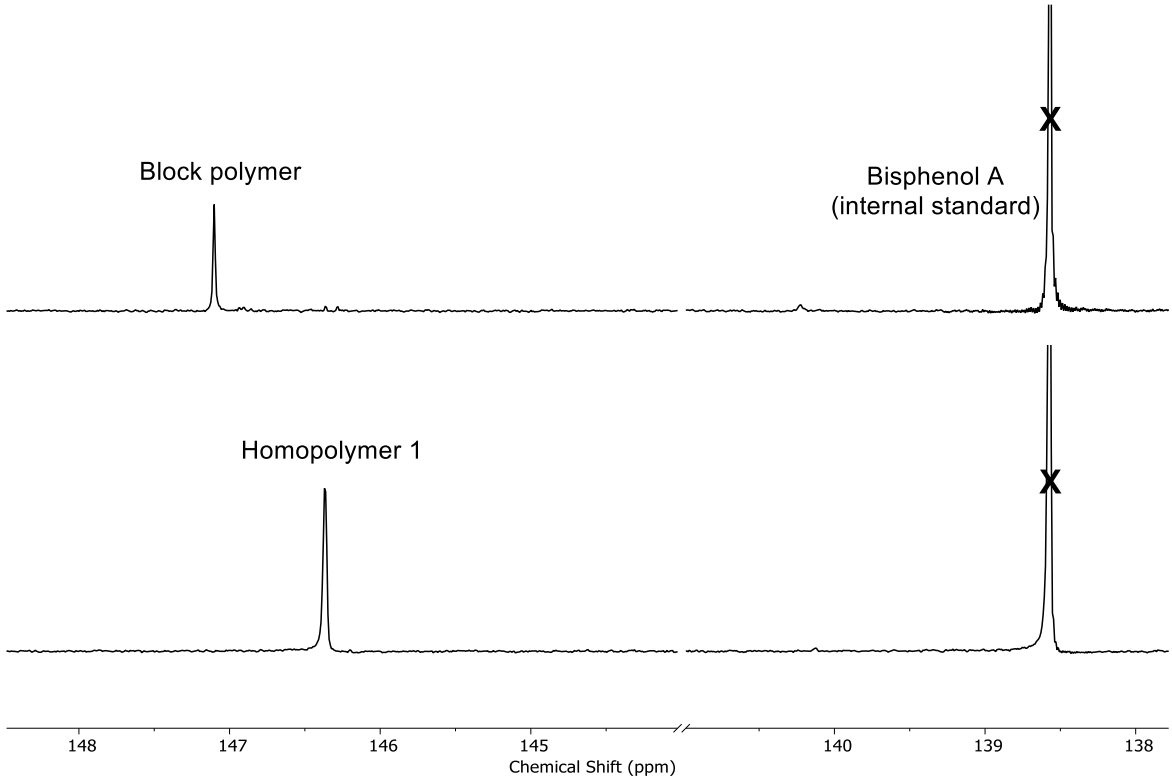


Figure 1.18 End group analysis using $^{31}P\{^{1}H\}$ NMR spectroscopy illustrating a change in the end group signals indicating block polymer formation (in a homopolymer blend, two end group signals would be observed0 (Bisphenol A used as internal standard).

3) DOSY NMR spectroscopy (diffusion-ordered spectroscopy): DOSY is a 2D NMR technique that depicts the diffusion coefficient of resonances in NMR spectra.[75] This technique can be employed to differentiate the number of different polymer distributions present in a sample based on the number of diffusion coefficients present. For instance, well-defined block copolymers should only exhibit one diffusion coefficient, as all the proton signals should diffuse at the same rate. In a mixture of homopolymers, if the chains diffuse at different rates, more than one diffusion coefficient would be observed (Fig. 1.19).[61]

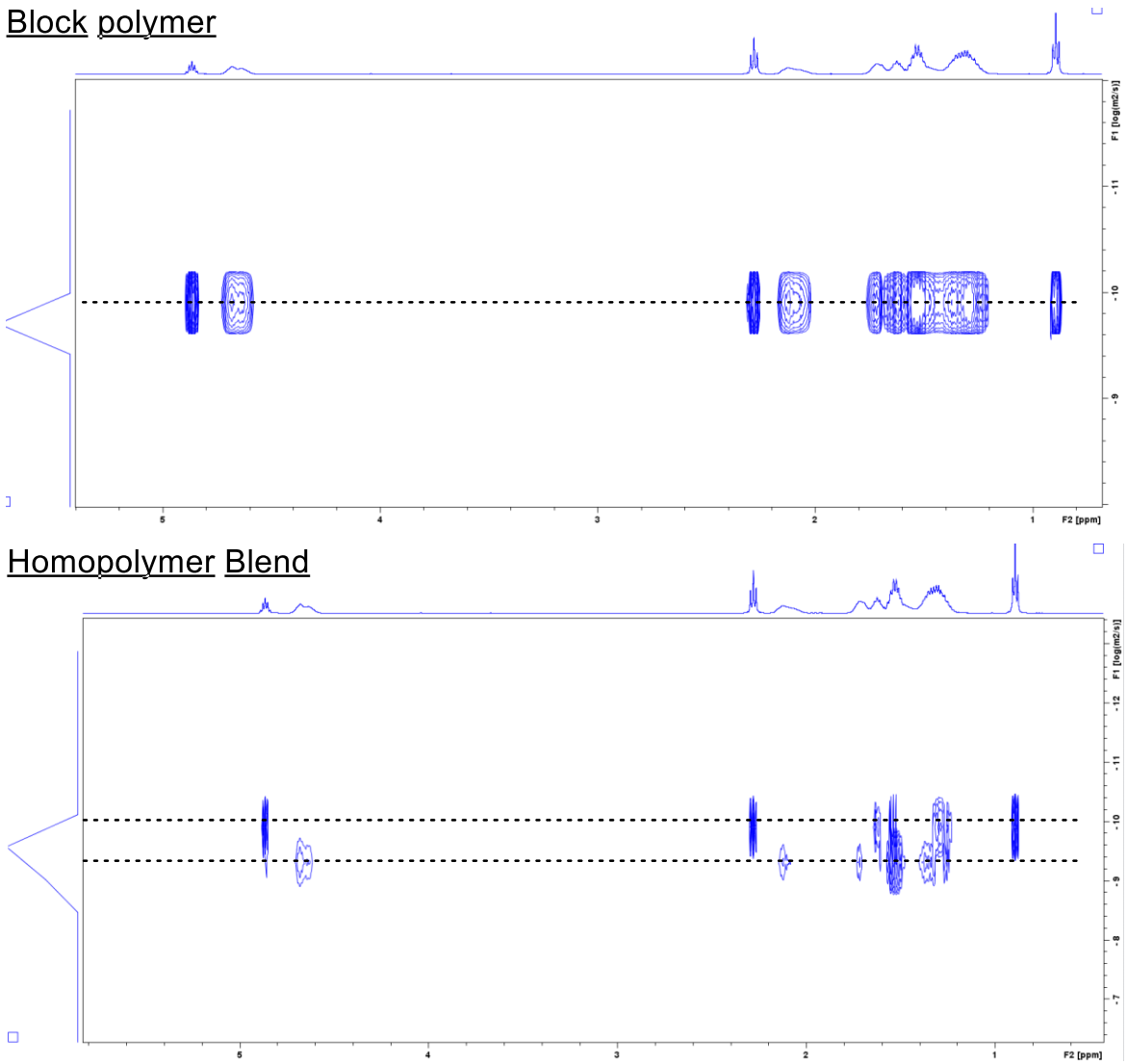


Figure 1.19 ^{1}H DOSY NMR of block polymer and homopolymer blend with one and two diffusion coefficient, respectively.

4) Junction units: In a block polymer, the monomer unit that forms the junction between blocks is in a slightly different chemical environment compared to the main chain repeating units. As a result, the junction units have marginally different chemical shifts. Junction unit signals may be observed in the ^{1}H NMR spectrum and assigned using 2D COSY NMR.[60] It should be noted that this necessitates that the junction units are of sufficient intensity and the chemical

shift does not overlap with the main chain signals. Nevertheless, junction units can prove to be an effective way of proving block polymer formation as this feature is unique to block polymers and not present in a mixture of homopolymers (see Chapter 4 for examples).

5) $^{13}C\{^{1}H\}$ NMR spectroscopy: In well-defined block polymers, the only signals that should appear in the carbonyl region (160-180 ppm) should be those belonging to the constituting homopolymers. In the case of transesterification (scrambling of the blocks), additional carbonyl signals would appear. However, as junction units and end group signals may also lead to separate carbonyl resonances, deliberate transesterification using specific catalysts (e.g. 1,5,7-triazabicyclo[4.4.0]dec-5-ene (TBD)) should be performed as control reactions.

6) Material properties: A unique property of block polymers is their ability to phase separate on the microscale. Blends of homopolymers would phase separate on the macroscale. Micro-phase separation leads to changes in the material's thermal and mechanical properties. Thus, comparison of the material's macroscopic properties (e.g. glass transition temperature) may be another method to distinguish between block polymers and mixtures of homopolymers.

7) Physical separation: A simple method to illustrate block polymer formation is to investigate whether the block composition changes upon fractionation. These experiments include washing the sample with solvents that are selective

for a particular homopolymer or repeated precipitation of the polymer solution from an anti-solvent. The polymer composition for a well-defined block polymer should not change, whereas a mixture of homopolymers would lead to changes in composition (see chapter 2 for examples).

1.6. **Post-polymerization modification**

The design and synthesis of highly functional polymers remains a significant goal as it offers avenues towards advanced applications in materials science.[76-77] Functional polymers are usually prepared *via* two approaches: (1) the polymerization of monomers containing specific functional groups or (2) the post-polymerization modification of reactive groups on a polymer precursor. Due to the difficulties in functional monomer synthesis and possible functional group incompatibilities with the polymerization conditions, the post-polymerization modification approach is arguably more attractive as it allows the preparation of a range of functional polymers with greater ease.[78-81]

Different post-polymerization modification techniques, including coupling, addition and deprotection reactions, have been reported by researchers.[76, 82-83] Due to the compatibility of unsaturated moieties with ROP and ROCOP, the most common post-polymerization modifications for polyesters and polycarbonates entail addition reactions across the carbon-carbon double/triple bonds. Examples of these reactions include thiol-ene/thiol-yne addition reactions,[84-87] Michael additions,[85, 88] epoxidation,[89-90] Copper (I) catalysed azide-alkyne cycloaddition (CuAAC),[91-93] and Diels-Alder reactions (Fig. 1.20).[94]

The most prominent modification technique is arguably the thiol-ene addition reaction due to the highly versatile nature of the method with myriad of thiol reagents commercially available. Furthermore, the addition reaction is highly atom efficient. Through thiol-ene addition, various functionalities can be installed on to the polymer chain including simple functional groups such as alkyl chains, carboxylic acids, amines,

esters to more complex functionalities such as PEG chains and quaternary ammonium salts.[84, 95]

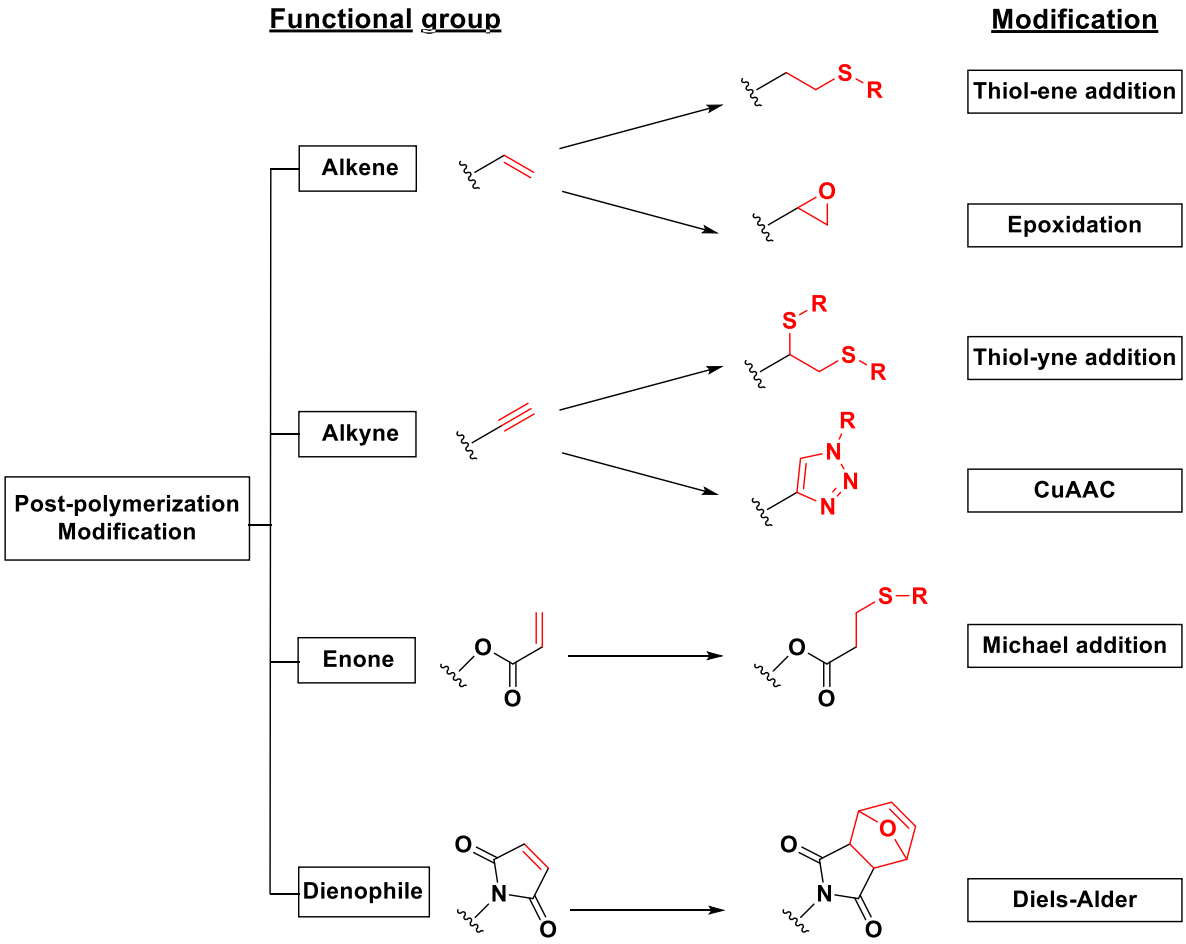


Figure 1.20 Selected post-polymerization methods for polyesters and polycarbonates. [84-94]

1.7. References

1. Grubbs, R. B.; Grubbs, R. H., 50th Anniversary Perspective: Living Polymerization-Emphasizing the Molecule in Macromolecules. *Macromolecules* **2017,** *50*, 6979-6997.
2. Schneiderman, D. K.; Hillmyer, M. A., 50th Anniversary Perspective: There Is a Great Future in Sustainable Polymers. *Macromolecules* **2017,** *50*, 3733-3749.
3. Hopewell, J.; Dvorak, R.; Kosior, E., Plastics recycling: challenges and opportunities. *Philos. Trans. Royal Soc. B* **2009,** *364*, 2115-2126.
4. Geyer, R.; Jambeck, J. R.; Law, K. L., Production, use, and fate of all plastics ever made. *Sci. Adv.* **2017,** *3*.
5. Williams, C. K., Synthesis of functionalized biodegradable polyesters. *Chem. Soc. Rev.* **2007,** *36*, 1573-1580.
6. Paul, S.; Zhu, Y. Q.; Romain, C.; Brooks, R.; Saini, P. K.; Williams, C. K., Ring-opening copolymerization (ROCOP): synthesis and properties of polyesters and polycarbonates. *Chem. Commun.* **2015,** *51*, 6459-6479.
7. Krause, M. J.; Townsend, T. G., Life-Cycle Assumptions of Landfilled Polylactic Acid Underpredict Methane Generation. *Environ. Sci. Technol. Lett.* **2016,** *3*, 166-169.
8. Hedir, G. G.; Bell, C. A.; Ieong, N. S.; Chapman, E.; Collins, I. R.; O'Reilly, R. K.; Dove, A. P., Functional Degradable Polymers by Xanthate-Mediated Polymerization. *Macromolecules* **2014,** *47*, 2847-2852.
9. Shen, L.; Worrell, E.; Patel, M., Present and future development in plastics from biomass. *Biofuel. Bioprod. Bior.* **2010,** *4*, 25-40.
10. Szwarc, M., 'Living' Polymers. *Nature* **1956,** *178*, 1168-1169.
11. Longo, J. M.; Sanford, M. J.; Coates, G. W., Ring-Opening Copolymerization of Epoxides and Cyclic Anhydrides with Discrete Metal Complexes: Structure-Property Relationships. *Chem. Rev.* **2016,** *116*, 15167-15197.
12. Yasuda, T.; Aida, T.; Inoue, S., Synthesis of Polyester Polyether Block Copolymer with Controlled Chain-Length from Beta-Lactone and Epoxide by Aluminum Porphyrin Catalyst. *Macromolecules* **1984,** *17*, 2217-2222.
13. Chamberlain, B. M.; Cheng, M.; Moore, D. R.; Ovitt, T. M.; Lobkovsky, E. B.; Coates, G. W., Polymerization of lactide with zinc and magnesium beta-diiminate complexes: Stereocontrol and mechanism. *J. Am. Chem. Soc.* **2001,** *123*, 3229-3238.
14. Rieth, L. R.; Moore, D. R.; Lobkovsky, E. B.; Coates, G. W., Single-site beta-diiminate zinc catalysts for the ring-opening polymerization of beta-butyrolactone and beta-valerolactone to poly(3-hydroxyalkanoates). *J. Am. Chem. Soc.* **2002,** *124*, 15239-15248.
15. Williams, C. K.; Breyfogle, L. E.; Choi, S. K.; Nam, W.; Young, V. G.; Hillmyer, M. A.; Tolman, W. B., A highly active zinc catalyst for the controlled polymerization of lactide. *J. Am. Chem. Soc.* **2003,** *125*, 11350-11359.
16. Chen, X. H.; Gross, R. A., Versatile copolymers from [L]-lactide and [D]-xylofuranose. *Macromolecules* **1999,** *32*, 308-314.
17. Dechy-Cabaret, O.; Martin-Vaca, B.; Bourissou, D., Controlled Ring-Opening Polymerization of Lactide and Glycolide. *Chem. Rev.* **2004,** *104*, 6147-6176.
18. Snow, R. D.; Frey, F. E., The Reaction of Sulfur Dioxide with Olefins: the Ceiling Temperature Phenomenon. *J. Am. Chem. Soc.* **1943,** *65*, 2417-2418.
19. Dubois, P.; Coulembier, O.; Raquez, J.-M., *Handbook of Ring-Opening Polymerization*. Wiley-VCH: 2009.
20. Rieth, L. R.; Moore, D. R.; Lobkovsky, E. B.; Coates, G. W., Single-Site β-Diiminate Zinc Catalysts for the Ring-Opening Polymerization of β-Butyrolactone and β-Valerolactone to Poly(3-hydroxyalkanoates). *J. Am. Chem. Soc.* **2002,** *124*, 15239-15248.

21. Zhu, Y. Q.; Romain, C.; Poirier, V.; Williams, C. K., Influences of a Dizinc Catalyst and Bifunctional Chain Transfer Agents on the Polymer Architecture in the Ring-Opening Polymerization of epsilon-Caprolactone. *Macromolecules* **2015,** *48*, 2407-2416.
22. Zhuo, Z. X.; Zhang, C.; Luo, Y. J.; Wang, Y. R.; Yao, Y. M.; Yuan, D.; Cui, D. M., Stereoselectivity switchable ROP of rac-beta-butyrolactone initiated by salan-ligated rare-earth metal amide complexes: the key role of the substituents on ligand frameworks. *Chem. Commun.* **2018,** *54*.
23. Myers, D.; Cyriac, A.; Williams, C. K., To react the impossible ring. *Nat. Chem.* **2016,** *8*, 3-4.
24. Olsén, P.; Odelius, K.; Albertsson, A.-C., Thermodynamic Presynthetic Considerations for Ring-Opening Polymerization. *Biomacromolecules* **2016,** *17*, 699-709.
25. WSchneider, W.; Diller, W., *Ullmann's Encyclopedia of Industrial Chemistry*. Wiley-VCH: 2005.
26. Kember, M. R.; Knight, P. D.; Reung, P. T. R.; Williams, C. K., Highly Active Dizinc Catalyst for the Copolymerization of Carbon Dioxide and Cyclohexene Oxide at One Atmosphere Pressure. *Angew. Chem. Int. Ed.* **2009,** *48*, 931-933.
27. Nagae, H.; Aoki, R.; Akutagawa, S.-n.; Kleemann, J.; Tagawa, R.; Schindler, T.; Choi, G.; Spaniol, T. P.; Tsurugi, H.; Okuda, J.; Mashima, K., Lanthanide Complexes Supported by a Trizinc Crown Ether as Catalysts for Alternating Copolymerization of Epoxide and CO2: Telomerization Controlled by Carboxylate Anions. *Angew. Chem. Int. Ed.* **2018,** *57*, 2492-2496.
28. Klaus, S.; Lehenmeier, M. W.; Anderson, C. E.; Rieger, B., Recent advances in CO2/epoxide copolymerization-New strategies and cooperative mechanisms. *Coord. Chem. Rev.* **2011,** *255*, 1460-1479.
29. Jutz, F.; Buchard, A.; Kember, M. R.; Fredriksen, S. B.; Williams, C. K., Mechanistic Investigation and Reaction Kinetics of the Low-Pressure Copolymerization of Cyclohexene Oxide and Carbon Dioxide Catalyzed by a Dizinc Complex. *J. Am. Chem. Soc.* **2011,** *133*, 17395-17405.
30. Garden, J. A.; Saini, P. K.; Williams, C. K., Greater than the Sum of Its Parts: A Heterodinuclear Polymerization Catalyst. *J. Am. Chem. Soc.* **2015,** *137*, 15078-15081.
31. Bates, C. M.; Bates, F. S., 50th Anniversary Perspective: Block Polymers-Pure Potential. *Macromolecules* **2017,** *50*, 3-22.
32. Hillmyer, M. A.; Tolman, W. B., Aliphatic Polyester Block Polymers: Renewable, Degradable, and Sustainable. *Acc. Chem. Res.* **2014,** *47*, 2390-2396.
33. Wang, Z. K.; Yuan, L.; Tang, C. B., Sustainable Elastomers from Renewable Biomass. *Acc. Chem. Res.* **2017,** *50*, 1762-1773.
34. Park, C.; Yoon, J.; Thomas, E. L., Enabling nanotechnology with self assembled block copolymer patterns. *Polymer* **2003,** *44*, 6725-6760.
35. Fineman, M.; Ross, S. D., Linear Method for Determining Monomer Reactivity Ratios in Copolymerization. *J. Polym. Sci.* **1950,** *5*, 259-262.
36. Hirao, A.; Goseki, R.; Ishizone, T., Advances in Living Anionic Polymerization: From Functional Monomers, Polymerization Systems, to Macromolecular Architectures. *Macromolecules* **2014,** *47*, 1883-1905.
37. Szwarc, M.; Levy, M.; Milkovich, R., Polymerization Initiated by Electron Transfer to Monomer - a New Method of Formation of Block Polymers. *J. Am. Chem. Soc.* **1956,** *78*, 2656-2657.
38. Anastasaki, A.; Waldron, C.; Wilson, P.; Boyer, C.; Zetterlund, P. B.; Whittaker, M. R.; Haddleton, D., High Molecular Weight Block Copolymers by Sequential Monomer Addition via Cu(0)-Mediated Living Radical Polymerization (SET-LRP): An Optimized Approach. *ACS Macro Lett.* **2013,** *2*, 896-900.

39. Ouchi, M.; Terashima, T.; Sawamoto, M., Transition Metal-Catalyzed Living Radical Polymerization: Toward Perfection in Catalysis and Precision Polymer Synthesis. *Chem. Rev.* **2009,** *109*, 4963-5050.
40. Matyjaszewski, K.; Tsarevsky, N. V., Nanostructured functional materials prepared by atom transfer radical polymerization. *Nat. Chem.* **2009,** *1*, 276-288.
41. Moad, G., RAFT polymerization to form stimuli-responsive polymers. *Polym. Chem.* **2017,** *8*, 177-219.
42. Lutz, J. F.; Ouchi, M.; Liu, D. R.; Sawamoto, M., Sequence-Controlled Polymers. *Science* **2013,** *341*, 628.
43. Guillaume, S. M.; Kirillov, E.; Sarazin, Y.; Carpentier, J. F., Beyond Stereoselectivity, Switchable Catalysis: Some of the Last Frontier Challenges in Ring-Opening Polymerization of Cyclic Esters. *Chem. - Eur. J.* **2015,** *21*, 7988-8003.
44. Teator, A. J.; Lastovickova, D. N.; Bielawski, C. W., Switchable Polymerization Catalysts. *Chem. Rev.* **2016,** *116*, 1969-1992.
45. Gregson, C. K. A.; Gibson, V. C.; Long, N. J.; Marshall, E. L.; Oxford, P. J.; White, A. J. P., Redox control within single-site polymerization catalysts. *J. Am. Chem. Soc.* **2006,** *128*, 7410-7411.
46. Myers, D.; White, A. J. P.; Forsyth, C. M.; Bown, M.; Williams, C. K., Phosphasalen Indium Complexes Showing High Rates and Isoselectivities in rac-Lactide Polymerizations. *Angew. Chem. Int. Ed.* **2017,** *56*, 5277-5282.
47. Yoon, H. J.; Kuwabara, J.; Kim, J. H.; Mirkin, C. A., Allosteric Supramolecular Triple-Layer Catalysts. *Science* **2010,** *330*, 66-69.
48. Coulembier, O.; Moins, S.; Todd, R.; Dubois, P., External and Reversible CO2 Regulation of Ring-Opening Polymerizations Based on a Primary Alcohol Propagating Species. *Macromolecules* **2014,** *47*, 486-491.
49. Magenau, A. J. D.; Strandwitz, N. C.; Gennaro, A.; Matyjaszewski, K., Electrochemically Mediated Atom Transfer Radical Polymerization. *Science* **2011,** *332*, 81-84.
50. Jeske, R. C.; Rowley, J. M.; Coates, G. W., Pre-rate-determining selectivity in the terpolymerization of epoxides, cyclic anhydrides, and CO2: A one-step route to diblock copolymers. *Angew. Chem. Int. Ed.* **2008,** *47*, 6041-6044.
51. Ren, W. M.; Zhang, X.; Liu, Y.; Li, J. F.; Wang, H.; Lu, X. B., Highly Active, Bifunctional Co(III)-Salen Catalyst for Alternating Copolymerization of CO2 with Cyclohexene Oxide and Terpolymerization with Aliphatic Epoxides. *Macromolecules* **2010,** *43*, 1396-1402.
52. Darensbourg, D. J.; Poland, R. R.; Strickland, A. L., (Salan)CrCl, An Effective Catalyst for the Copolymerization and Terpolymerization of Epoxides and Carbon Dioxide. *J. Polym. Sci. Poly. Chem.* **2012,** *50*, 127-133.
53. Huijser, S.; HosseiniNejad, E.; Sablong, R.; de Jong, C.; Koning, C. E.; Duchateau, R., Ring-Opening Co- and Terpolymerization of an Alicyclic Oxirane with Carboxylic Acid Anhydrides and CO2 in the Presence of Chromium Porphyrinato and Salen Catalysts. *Macromolecules* **2011,** *44*, 1132-1139.
54. Darensbourg, D. J.; Poland, R. R.; Escobedo, C., Kinetic Studies of the Alternating Copolymerization of Cyclic Acid Anhydrides and Epoxides, and the Terpolymerization of Cyclic Acid Anhydrides, Epoxides, and CO2 Catalyzed by (salen)(CrCl)-Cl-III. *Macromolecules* **2012,** *45*, 2242-2248.
55. Stosser, T.; Chen, T. T. D.; Zhu, Y.; Williams, C. K., 'Switch' catalysis: from monomer mixtures to sequence-controlled block copolymers. *Philos. Trans. Royal Soc. A* **2018,** *376*.
56. Romain, C.; Williams, C. K., Chemoselective Polymerization Control: From Mixed-Monomer Feedstock to Copolymers. *Angew. Chem. Int. Ed.* **2014,** *53*, 1607-1610.
57. Nakano, K.; Hashimoto, S.; Nakamura, M.; Kamada, T.; Nozaki, K., Stereocomplex of Poly(propylene carbonate): Synthesis of Stereogradient Poly(propylene carbonate) by

Regio- and Enantioselective Copolymerization of Propylene Oxide with Carbon Dioxide. *Angew. Chem. Int. Ed.* **2011,** *50*, 4868-4871.

58. Chatterjee, C.; Chisholm, M. H., The Influence of the Metal (Al, Cr, and Co) and the Substituents of the Porphyrin in Controlling the Reactions Involved in the Copolymerization of Propylene Oxide and Carbon Dioxide by Porphyrin Metal(III) Complexes. 1. Aluminum Chemistry. *Inorg. Chem.* **2011,** *50*, 4481-4492.
59. Xiao, Y. L.; Wang, Z.; Ding, K. L., Intramolecularly dinuclear magnesium complex catalyzed copolymerization of cyclohexene oxide with CO2 under ambient CO2 pressure: Kinetics and mechanism. *Macromolecules* **2006,** *39*, 128-137.
60. Paul, S.; Romain, C.; Shaw, J.; Williams, C. K., Sequence Selective Polymerization Catalysis: A New Route to ABA Block Copoly(ester-b-carbonate-b-ester). *Macromolecules* **2015,** *48*, 6047-6056.
61. Zhu, Y.; Romain, C.; Williams, C. K., Selective Polymerization Catalysis: Controlling the Metal Chain End Group to Prepare Block Copolyesters. *J. Am. Chem. Soc.* **2015,** *137*, 12179-12182.
62. Romain, C.; Zhu, Y. Q.; Dingwall, P.; Paul, S.; Rzepa, H. S.; Buchard, A.; Williams, C. K., Chemoselective Polymerizations from Mixtures of Epoxide, Lactone, Anhydride, and Carbon Dioxide. *J. Am. Chem. Soc.* **2016,** *138*, 4120-4131.
63. Raman, S. K.; Raja, R.; Arnold, P. L.; Davidson, M. G.; Williams, C. K., Waste not, want not: CO2 (re)cycling into block polymers. *Chem. Commun.* **2019,** *55*, 7315-7318.
64. Kernbichl, S.; Reiter, M.; Adams, F.; Vagin, S.; Rieger, B., CO2-Controlled One-Pot Synthesis of AB, ABA Block, and Statistical Terpolymers from beta-Butyrolactone, Epoxides, and CO2. *J. Am. Chem. Soc.* **2017,** *139*, 6787-6790.
65. Kernbichl, S.; Reiter, M.; Mock, J.; Rieger, B., Terpolymerization of β-Butyrolactone, Epoxides, and CO2: Chemoselective CO2-Switch and Its Impact on Kinetics and Material Properties. *Macromolecules* **2019,** *52*, 8476-8483.
66. Stosser, T.; Williams, C. K., Selective Polymerization Catalysis from Monomer Mixtures: Using a Commercial Cr-Salen Catalyst To Access ABA Block Polyesters. *Angew. Chem. Int. Ed.* **2018,** *57*, 6337-6341.
67. Stosser, T.; Sulley, G. S.; Gregory, G. L.; Williams, C. K., Easy access to oxygenated block polymers via switchable catalysis. *Nat. Commun.* **2019,** *10*, 2668.
68. Tsuji, H.; Miyauchi, S., Enzymatic hydrolysis of poly(lactide)s: Effects of molecular weight, L-lactide content, and enantiomeric and diastereoisomeric polymer blending. *Biomacromolecules* **2001,** *2*, 597-604.
69. Haider, T. P.; Völker, C.; Kramm, J.; Landfester, K.; Wurm, F. R., Plastics of the Future? The Impact of Biodegradable Polymers on the Environment and on Society. *Angew. Chem. Int. Ed.* **2019,** *58*, 50-62.
70. Lipik, V. T.; Widjaja, L. K.; Liow, S. S.; Abadie, M. J. M.; Venkatraman, S. S., Effects of transesterification and degradation on properties and structure of polycaprolactone-polylactide copolymers. *Polym. Degrad. Stabil.* **2010,** *95*, 2596-2602.
71. Stößer, T.; Mulryan, D.; Williams, C. K., Switch Catalysis To Deliver Multi-Block Polyesters from Mixtures of Propene Oxide, Lactide, and Phthalic Anhydride. *Angew. Chem. Int. Ed.* **2018,** *57*, 16893-16897.
72. Ji, H.-Y.; Wang, B.; Pan, L.; Li, Y.-S., One-Step Access to Sequence-Controlled Block Copolymers by Self-Switchable Organocatalytic Multicomponent Polymerization. *Angew. Chem. Int. Ed.* **2018,** *57*, 16888-16892.
73. Li, H.; Luo, H.; Zhao, J.; Zhang, G., Sequence-Selective Terpolymerization from Monomer Mixtures Using a Simple Organocatalyst. *ACS Macro Lett.* **2018,** 1420-1425.
74. Spyros, A.; Argyropoulos, D. S.; Marchessault, R. H., A study of poly(hydroxyalkanoate)s by quantitative P-31 NMR spectroscopy: Molecular weight and chain cleavage. *Macromolecules* **1997,** *30*, 327-329.

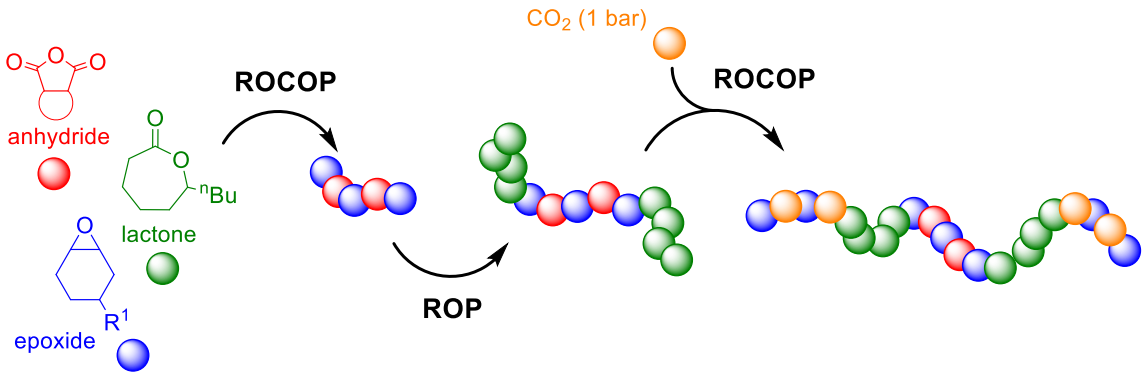
75. Groves, P., Diffusion ordered spectroscopy (DOSY) as applied to polymers. *Polym. Chem.* **2017,** *8*, 6700-6708.
76. Gauthier, M. A.; Gibson, M. I.; Klok, H.-A., Synthesis of Functional Polymers by Post-Polymerization Modification. *Angew. Chem. Int. Ed.* **2009,** *48*, 48-58.
77. Blasco, E.; Sims, M. B.; Goldmann, A. S.; Sumerlin, B. S.; Barner-Kowollik, C., 50th Anniversary Perspective: Polymer Functionalization. *Macromolecules* **2017,** *50*, 5215-5252.
78. Williams, R. J.; Barker, I. A.; O'Reilly, R. K.; Dove, A. P., Orthogonal Modification of Norbornene-Functional Degradable Polymers. *ACS Macro Lett.* **2012,** *1*, 1285-1290.
79. Li, Y. M.; Jiang, T.; Lv, Y.; Wu, Y.; He, F.; Zhuo, R. X., Amphiphilic copolymers with pendent carboxyl groups for high-efficiency loading and controlled release of doxorubicin. *Colloid Surface B* **2015,** *132*, 54-61.
80. Golas, P. L.; Matyjaszewski, K., Marrying click chemistry with polymerization: expanding the scope of polymeric materials. *Chem. Soc. Rev.* **2010,** *39*, 1338-1354.
81. Chin, W.; Yang, C. A.; Ng, V. W. L.; Huang, Y.; Cheng, J. C.; Tong, Y. W.; Coady, D. J.; Fan, W. M.; Hedrick, J. L.; Yang, Y. Y., Biodegradable Broad-Spectrum Antimicrobial Polycarbonates: Investigating the Role of Chemical Structure on Activity and Selectivity. *Macromolecules* **2013,** *46*, 8797-8807.
82. Günay, K. A.; Theato, P.; Klok, H.-A., Standing on the shoulders of Hermann Staudinger: Post-polymerization modification from past to present. *J. Polym. Sci., Part A: Polym. Chem.* **2013,** *51*, 1-28.
83. Thomas, A. W.; Dove, A. P., Postpolymerization Modifications of Alkene-Functional Polycarbonates for the Development of Advanced Materials Biomaterials. *Macromol. Biosci.* **2016,** *16*, 1762-1775.
84. Hoyle, C. E.; Bowman, C. N., Thiol–Ene Click Chemistry. *Angew. Chem. Int. Ed.* **2010,** *49*, 1540-1573.
85. Uysal, B. B.; Gunay, U. S.; Hizal, G.; Tunca, U., Orthogonal Multifunctionalization of Aliphatic Polycarbonate via Sequential Michael Addition and Radical-Thiol-Ene Click Reactions. *J. Polym. Sci. Poly. Chem.* **2014,** *52*, 1581-1587.
86. Darensbourg, D. J.; Tsai, F. T., Postpolymerization Functionalization of Copolymers Produced from Carbon Dioxide and 2-Vinyloxirane: Amphiphilic/Water-Soluble CO2-Based Polycarbonates. *Macromolecules* **2014,** *47*, 3806-3813.
87. Hauenstein, O.; Agarwal, S.; Greiner, A., Bio-based polycarbonate as synthetic toolbox. *Nat. Commun.* **2016,** *7*.
88. Chen, W.; Yang, H.; Wang, R.; Cheng, R.; Meng, F.; Wei, W.; Zhong, Z., Versatile Synthesis of Functional Biodegradable Polymers by Combining Ring-Opening Polymerization and Postpolymerization Modification via Michael-Type Addition Reaction. *Macromolecules* **2010,** *43*, 201-207.
89. Wang, C. F.; Lin, Y. X.; Jiang, T.; He, F.; Zhuo, R. X., Polyethylenimine-grafted polycarbonates as biodegradable polycations for gene delivery. *Biomaterials* **2009,** *30*, 4824-4832.
90. Jiang, T.; Li, Y. M.; Lv, Y.; Cheng, Y. J.; He, F.; Zhuo, R. X., Amphiphilic polycarbonate conjugates of doxorubicin with pH-sensitive hydrazone linker for controlled release. *Colloid Surface B* **2013,** *111*, 542-548.
91. Parrish, B.; Breitenkamp, R. B.; Emrick, T., PEG- and peptide-grafted aliphatic polyesters by click chemistry. *J. Am. Chem. Soc.* **2005,** *127*, 7404-7410.
92. Sisson, A. L.; Ekinci, D.; Lendlein, A., The contemporary role of epsilon-caprolactone chemistry to create advanced polymer architectures. *Polymer* **2013,** *54*, 4333-4350.
93. Sinnwell, S.; Inglis, A. J.; Stenzel, M. H.; Barner-Kowollik, C., Access to Three-Arm Star Block Copolymers by a Consecutive Combination of the Copper(I)-Catalyzed Azide–

Alkyne Cycloaddition and the RAFT Hetero Diels–Alder Concept. *Macromol. Rapid. Comm.* **2008,** *29*, 1090-1096.

94. Xiong, X. Q.; Xu, Y. H., A one-pot approach to dendritic star polymers via double click reactions. *Polym Bull* **2010,** *65*, 455-463.
95. Hoyle, C. E.; Lowe, A. B.; Bowman, C. N., Thiol-click chemistry: a multifaceted toolbox for small molecule and polymer synthesis. *Chem. Soc. Rev.* **2010,** *39*, 1355-1387.

Chapter 2

Pentablock Copolymer from Tetra-Component Monomer Mixture Using a Switchable Dizinc Catalyst



✓One pot 'switch' polymerisation ✓single catalyst ✓pentablock formation

Well-defined pentablock copolymers are prepared using a single catalyst, in one pot, from four different monomers: anhydride, epoxide, lactone and CO_2. The catalyst bridges three distinct polymerization cycles and performs a double switch in the polymerization mechanism to produce pentablock copolymers.

2.1. **Introduction**

Sustainable block copolymers featuring degradable ester/carbonate linkages may be prepared using lactone ring-opening polymerization (ROP) to form poly(lactones), epoxide/CO_2 ring-opening copolymerization (ROCOP) to form alternating polycarbonates (PC) or epoxide/anhydride ROCOP to form polyesters (PE).[1-4] While terpolymerizations using a single mechanism are well-known,[5,6] polymerizations applying both mechanisms are less investigated.[7-9] Tandem catalysis, applied by Darensbourg and Wu, enabled linking of the catalytic cycles to form ABA block polymers.[10-11]

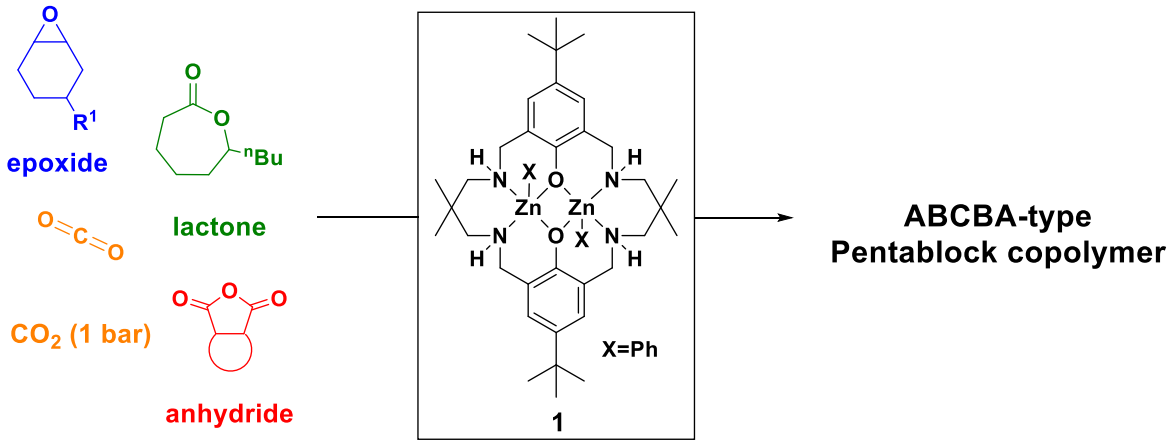
In 2014–2015, a single dizinc catalyst active using mixtures of epoxides/CO_2/lactones, switching between ROCOP and ROP, to produce block copolymers was reported by Williams and co-workers.[9, 12-13] The CO_2 monomer was later replaced for anhydrides to form ABA block copolyesters.[14, 15] It was suggested that a common zinc alkoxide intermediate linked together the ROCOP and ROP cycles and the insertion rate into this intermediate governed the selectivity.

Until now, all studies applied only *mixtures of three different monomers* limiting the resulting sequence to AB(A). To expand the capabilities of switch catalysis and prepare more complex materials, investigation into mixtures of four monomers containing epoxide/anhydride/CO_2/lactone is a clear target. In such mixtures, epoxide/anhydride ROCOP is expected to occur first, followed by epoxide/CO_2 ROCOP and lactone ROP is expected to occur last.

2.2. **Aims**

Following on from previous Switchable catalysis studies, the aim is to expand the capabilities of the switch mechanism and experimentally demonstrate a switch between *three* different polymerization cycles. Employing *four* different classes of monomers (epoxide, anhydride, lactone and CO_2), pentablock block polymers will be synthesized with a single dizinc catalyst, **1**, in one-pot (Scheme 2.1).

There are two important objectives to achieve: (1) To demonstrate high selectivity between the various polymerization cycles, which will be examined using *in-situ* ATR-IR and ^{1}H NMR spectroscopy. (2) Exclusive formation of pentablock copolymers will be shown and proven using SEC as well as $^{31}P\{^{1}H\}F$ NMR end group test, ^{1}H DOSY and $^{13}C\{^{1}H\}$ NMR spectroscopy.

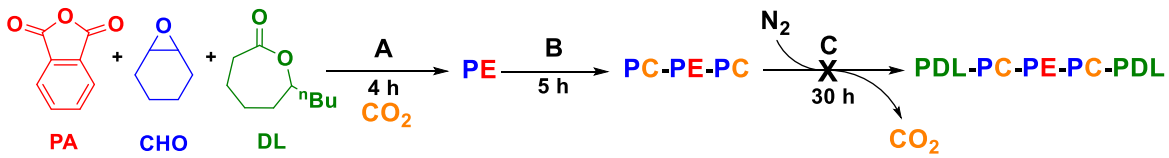


Scheme 2.1 Synthesis of pentablock copolymer from a dizinc catalyst, **1**, using four monomers *via* Switchable catalysis

2.3. **Four monomer Switch Catalysis: Full addition strategy**

Catalyst **1**, [LZn_2Ph_2], was activated using 1,2-cyclohexanediol (CHD) to form the zinc-alkoxide complex *in situ* (See scheme S1 for the activation of **1**, scheme S2 for ROP and ROCOP mechanisms and Figs. S1-S2 for ^{1}H and ^{13}C NMR spectrum of **1**).[16] This catalyst was selected because it has been shown to have high control for both ROP and ROCOP, yielding only hydroxyl-telechelic polymers with monomodal molar mass distributions in each separate polymerizations.[14, 16] The monomodal mass distribution is paramount since most other ROCOP catalysts result in bimodal molar mass distributions with differing end-groups.[10-12, 14, 17-18] Such bimodality prevents selective multi-block formation as it causes contamination by lower block sequences (i.e. AB/ABC/ABCB type).[19-20]

The **1**/CHD catalyst system was reacted with four monomers, namely phthalic anhydride (PA), cyclohexene oxide (CHO), ε-decalactone (DL) and CO_2, at 0.1 mol% catalyst loading, 100 °C under 1 bar pressure of CO_2 (Scheme 2.2).



Scheme 2.2 Attempted 4 monomer polymerization using switch catalysis. Molar ratio: [**1**]/[CHD]/[PA]/[DL]/[CHO] = 1/4/100/200/1000, 100 °C, (**A**, **B**) CO_2 and (**C**) N_2, 1 bar; **A** (anhydride/epoxide ROCOP), **B** (epoxide/CO_2 ROCOP) and **C** (failed lactone ROP).

DL was chosen as the model lactone as it affords a secondary metal alkoxide propagating species when ring-opened which results in well balanced kinetics (as the propagating species from both the epoxide and lactone would be secondary alkoxides) and resistance to transesterification; both features are expected to be important for good polymerization control.[21] From previous studies, the catalysis is expected to begin with epoxide/anhydride ROCOP, followed by epoxide/CO_2 ROCOP and finishing with lactone ROP.[13] However, the reaction yielded only the PC-PE-PC triblock formed by the ROCOP processes. To drive DL ROP, the CO_2 was completely removed, but the PDL block formation was not observed even after 30 h (Fig. 2.1).

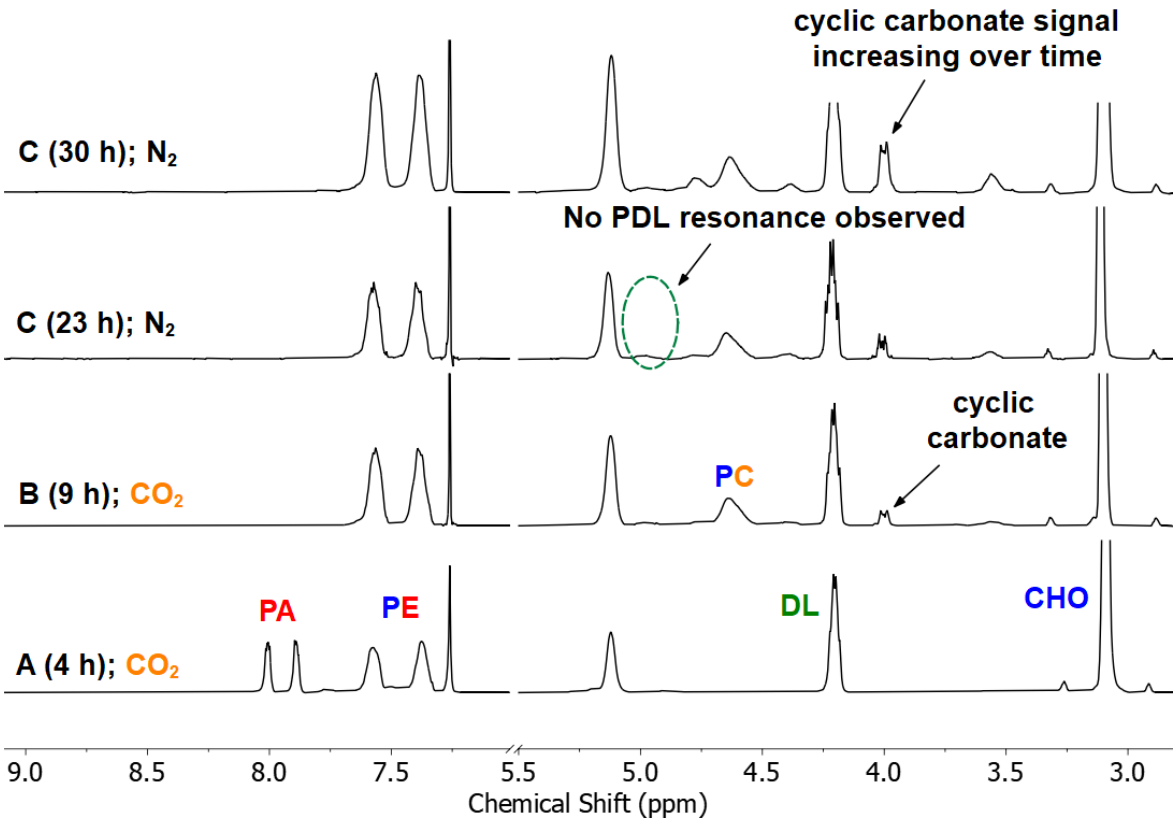


Figure 2.1 Selected region of ^{1}H NMR spectra illustrating changes in various resonances during an initial failed attempt to form pentablock copolymers using CO_2 as the gas

atmosphere first before switching to N_2. No PDL formation was observed after 30 h, but the cyclic carbonate (4.0 ppm) signal can be seen to increase over time (in $CDCl_3$).

Rather, the *trans*-cyclic carbonate by-product slowly evolved (a 20% drop in polycarbonate selectivity was observed between 9 h – 30 h). The formation of *trans*-cyclohexene carbonate indicates that chain back-biting occurred from the metal alkoxide intermediate.[20] Thus, whilst it is clear that the metal alkoxide intermediate is accessed, the rate of back-biting reaction appears to occur faster than the initiation of DL ROP (Fig. 2.2).

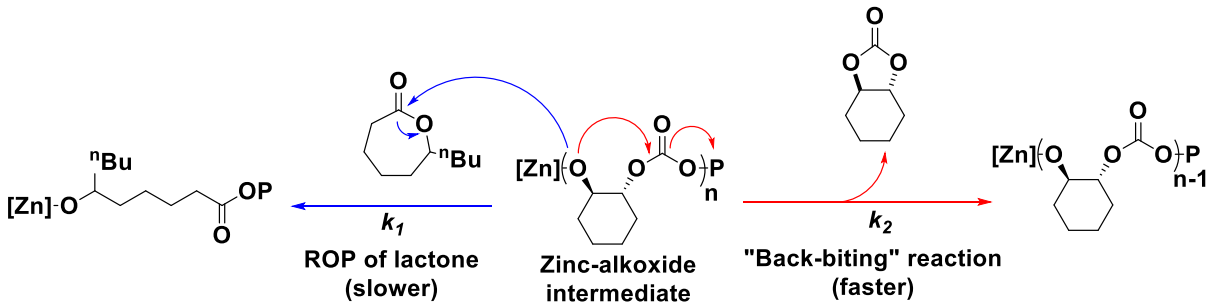


Figure 2.2 Illustration of the back-biting side reaction (formation of trans-cyclic carbonate) being favoured over the ROP of lactone (i.e. $k_2 > k_1$) from the zinc-alkoxide chain end formed at the end of the ROCOP of epoxide/CO_2. 'P' indicates polymer chain.

SEC analysis of the aliquots obtained at each stage of the reaction indicated an initial growth in molar mass from stage A to B and low dispersity ($Đ \leq 1.16$) (Fig. 2.3). However, in stage C (after removal of CO_2) a 50% decrease in molar mass and a major rise in $Đ$ are consistent with back biting reactions. It is worth mentioning that different reaction conditions, including lower temperature (80 °C) and higher DL concentration ([CHO]/[DL] = 1000/400) were examined in attempts to favour DL ROP over the back biting reaction. However, back-biting of the PC block and formation of the cyclic carbonate by product were observed in all cases. This suggests that a new synthesis strategy was needed to prepare pentablock copolymer from the 4 monomer mixture.

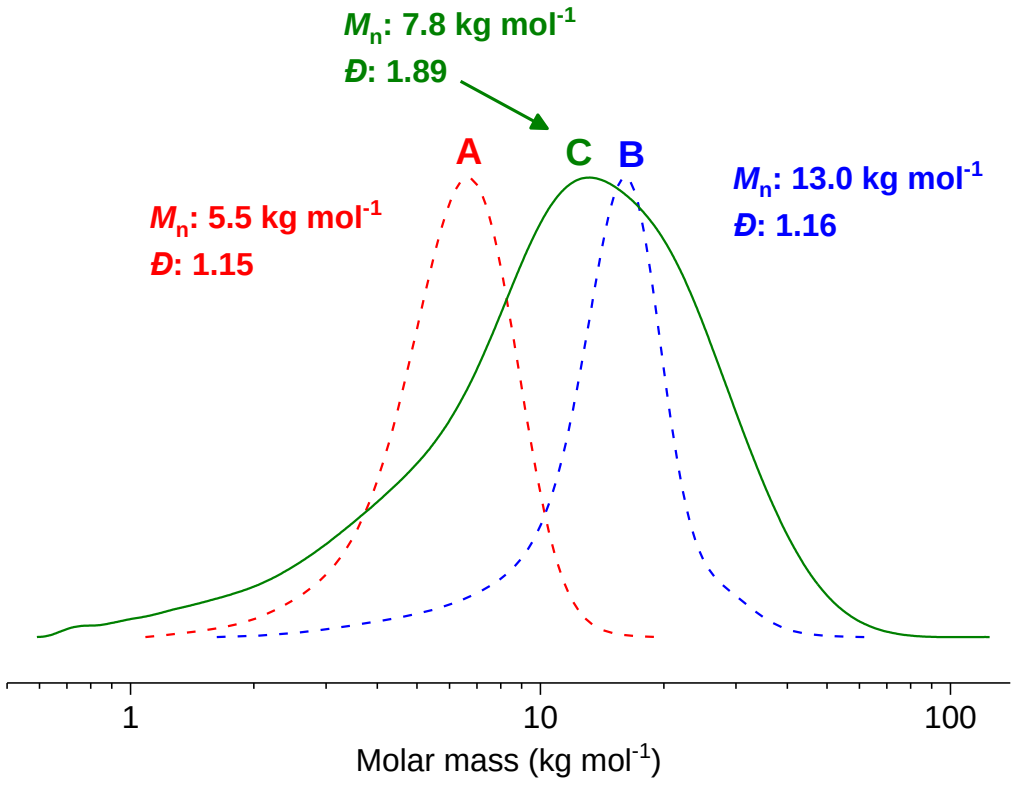
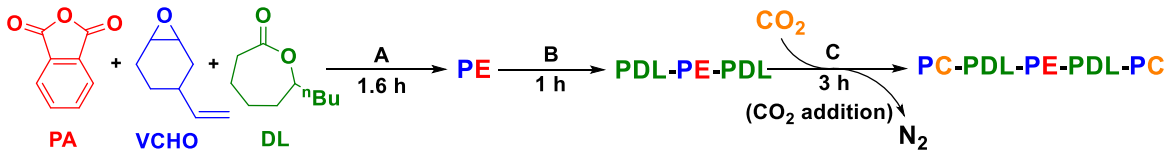


Figure 2.3. SEC traces illustrating a decrease in molar mass and increase in $Đ$ towards the end of the 4 monomer polymerization progresses; **A** (anhydride/epoxide ROCOP), **B** (epoxide/CO_2 ROCOP) and **C** (failed ROP of DL) (calibrated with narrow dispersity polystyrene standards).

2.4. **Four monomer Switch Catalysis: Sequential addition of CO_2**

The polycarbonate back-biting problem was overcome by a simple change in monomer addition order. First, the catalyst system was reacted with PA/CHO/DL forming the desired PDL-PE-PDL copolyester. Thereafter the N_2 atmosphere was replaced with 1 bar pressure of CO_2 resulting in selective PC-PDL-PE-PDL-PC pentablock formation (Scheme 2.3).



Scheme 2.3 Polymerization of tetra-component monomer mixture: PA/VCHO/DL/CO_2; molar ratio: [**1**]/[CHD]/[PA]/[DL]/[VCHO] = 1/4/50/200/1000, 100 °C, (**A**, **B**) N_2 and (**C**) CO_2, 1 bar; **A** (anhydride/epoxide ROCOP), **B** (lactone ROP) and **C** (epoxide/CO_2 ROCOP).

To demonstrate the generality of the switch catalysis, the tetra-component mixture polymerization was carried out using an epoxide containing a C=C double bond (vinyl-cyclohexene oxide, VCHO). The use of VCHO may offer further resistance to transesterification (from the presence of an additional side chain) and the double bond moiety would allow for post-polymerisation functionalization. The selectivity of the switch polymerization was first examined by *in situ* ATR-IR spectroscopy to follow the reaction progression. Sequential block formation was observed, where formation of PE (1065-1068 cm^{-1}) is followed by PDL (1190 cm^{-1}) (Figure 3.3 (a)). To demonstrate the high selectivity, CO_2 was added before full DL conversion and an immediate switch from DL ROP to VCHO/CO_2 ROCOP occurred, as evidenced by the PC formation (1246 cm^{-1}).

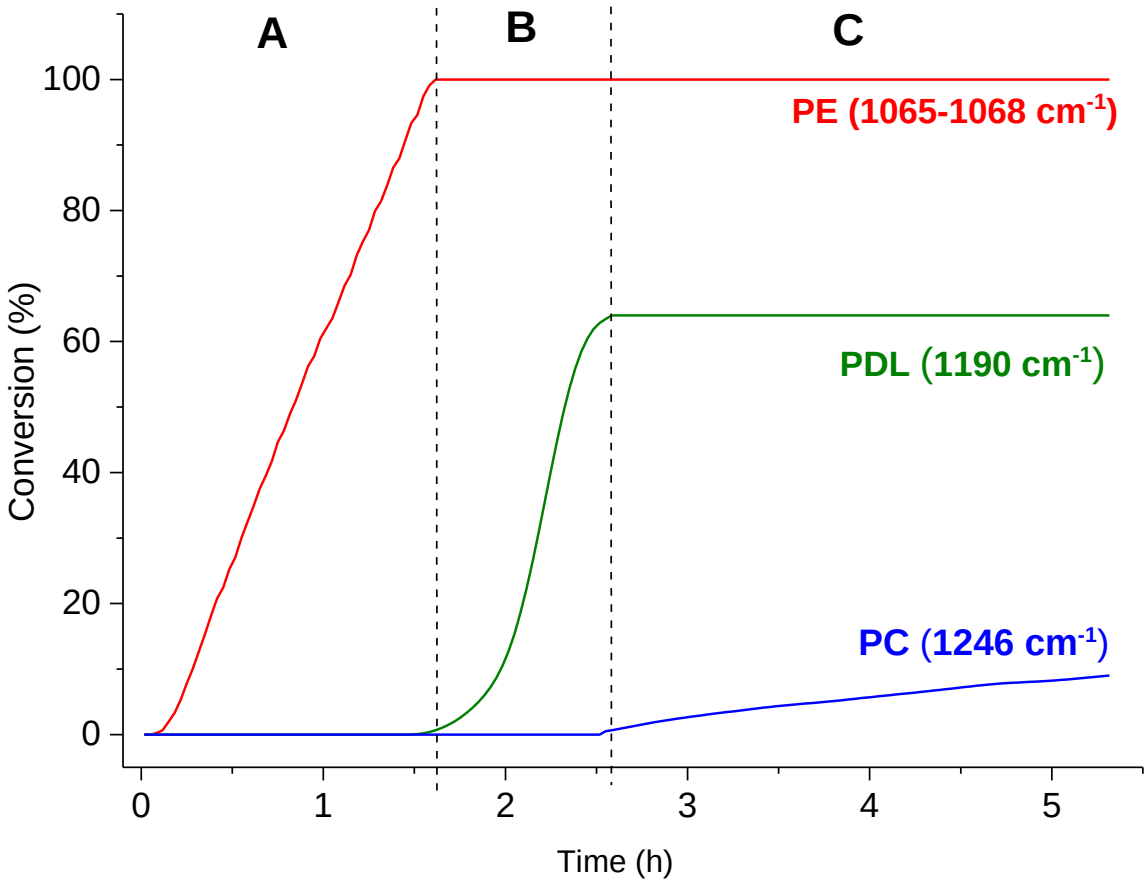


Figure 2.4. Conversion vs. time plot illustrating block formation; **A** (anhydride/epoxide ROCOP), **B** (lactone ROP) and **C** (epoxide/CO_2 ROCOP). Conversions calibrated using ^{1}H NMR spectroscopy (Fig. 2.5).

Furthermore, aliquots were taken at regular intervals and analyzed using ^{1}H NMR spectroscopy to quantify the monomer conversions against an internal standard (mesitylene) (Fig. 2.5). The initial ^{1}H NMR spectrum showed complete consumption of anhydride (8.02 and 7.90 ppm) and concurrent formation of polyester (7.66 and 7.50 ppm). The alternating copolymerization with VCHO was also confirmed (5.35 and 5.22 ppm). PDL blocks were only observed once all anhydride was consumed (4.84 ppm). The ^{1}H NMR spectrum at this stage also showed the growth of a signal at 4.76 ppm assigned to PC. All IR and ^{1}H NMR resonances were assigned by comparison with resonances observed in the constituent homopolymers (See Appendix, Figs. S5-S18).

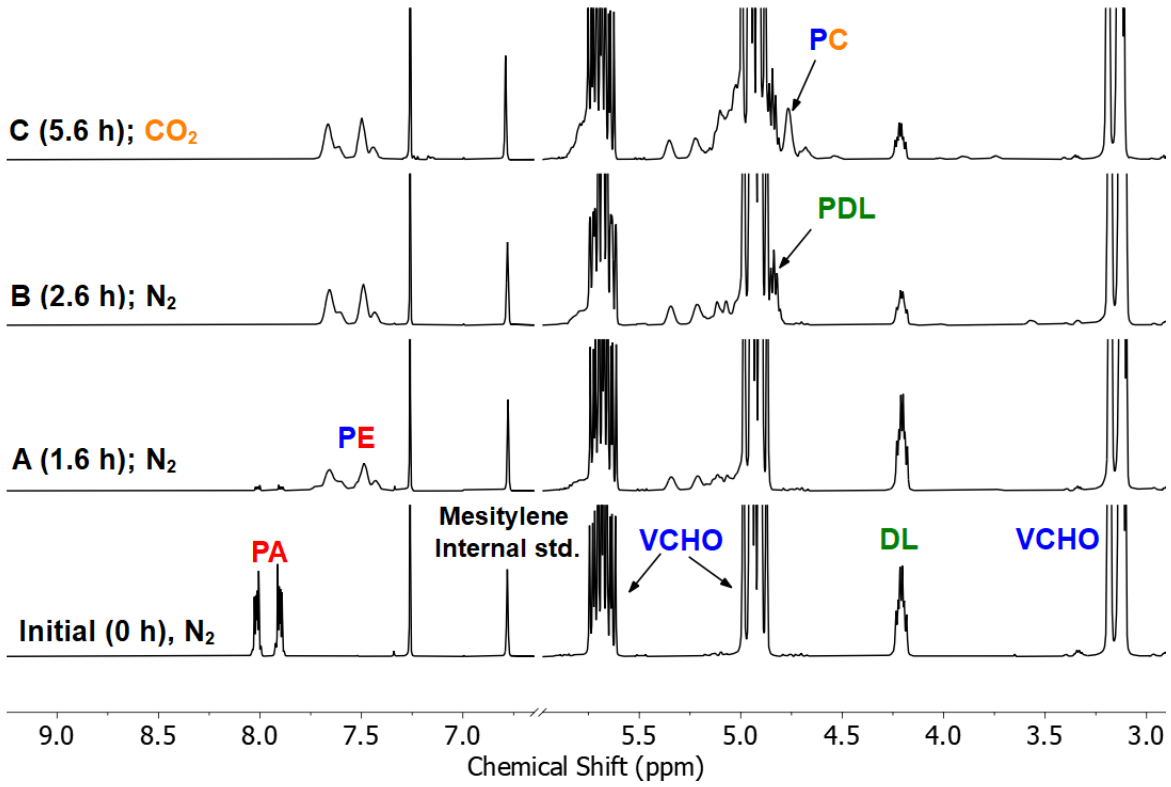


Figure 2.5 Selected region of ^{1}H NMR spectra illustrating changes in various resonances during different stages of the polymerization using PA/VCHO/DL/CO_2 as monomer feedstock (in $CDCl_3$).

It is important to note that high polymer conversions are achieved in each block but as the epoxide is applied as both reagent and solvent its conversion appears lower. Nonetheless, the epoxide conversion is fully consistent with the formation of perfectly alternating PE and PC blocks, where no polyether (3.3-3.5 ppm) was observed in the ^{1}H NMR spectrum. The catalyst maintains its activity throughout polymerization, with differing rates for each stage (TOFs for stage A, B and C were 32 h^{-1}, 128 h^{-1} and 30 h^{-1}, respectively).

The pentablock copolymer can be isolated from the crude mixture by precipitation of a DCM solution into methanol. By utilizing COSY NMR spectroscopy, the ^{1}H NMR spectrum of the purified polymer revealed characteristic peaks belonging to the PE, PC and PDL block segments (Fig. 2.6).

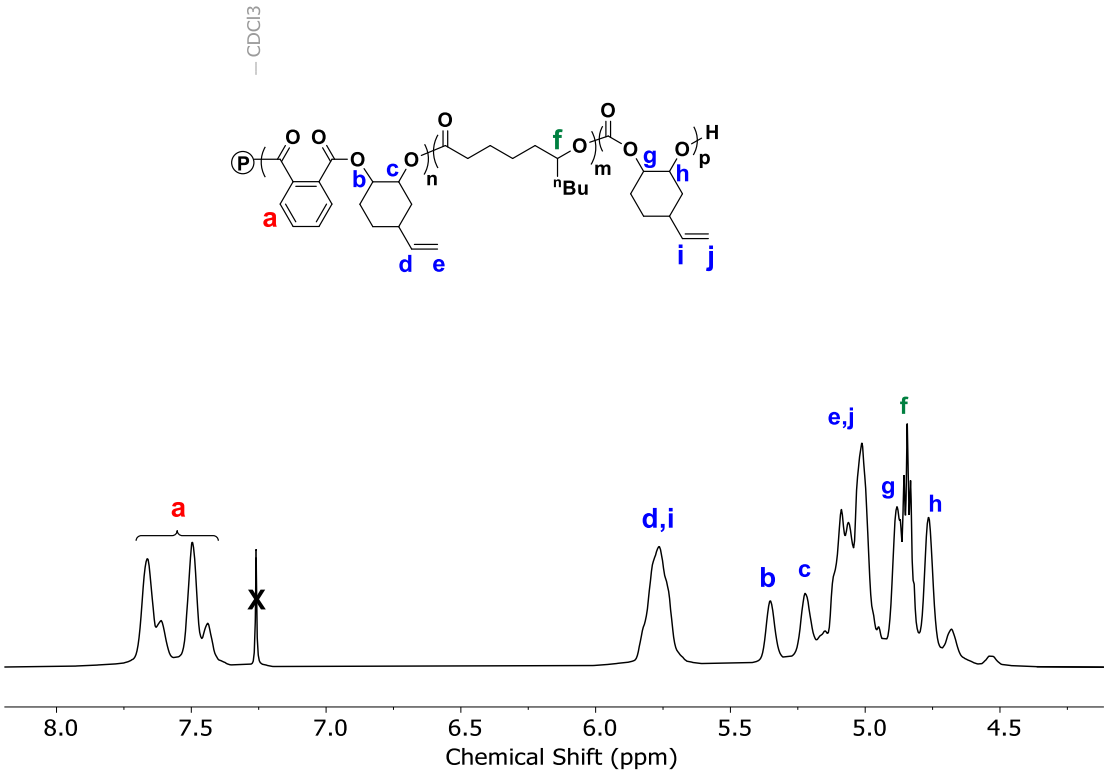


Figure 2.6 Selected region of ^{1}H NMR spectrum of pentablock copolymer from the 4 monomer polymerization of PA/VCHO/CO_2/DL (See Fig. S3 in the appendix for full spectrum).

Whilst the ^{1}H NMR spectrum can offer insight into the particular block segments present in the sample, such method cannot be used to establish the formation of block copolymers as a mixture of homopolymers would result in the same spectrum. As such, a variety of other characterization techniques were utilized to confirm block polymer formation. The SEC traces, obtained at each stage of the polymerization, illustrated a clear increase in molar mass with retention of narrow dispersity ($Đ$ < 1.17) (Fig. 2.7). This analysis is a strong indication of block polymer formation where each successive monomer addition is enchained onto the block polymer and not initiating additional polymer chains.

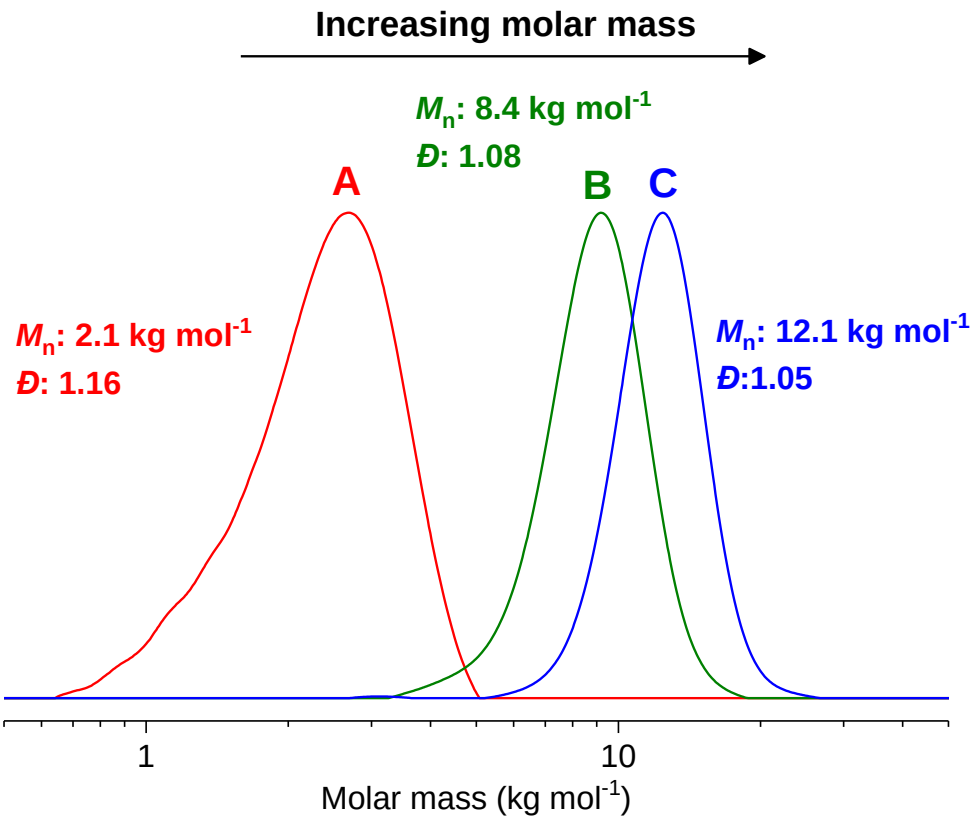


Figure 2.7 SEC traces illustrating the increase in M_n and retention of $Đ$ during a successful 3 stage pentablock copolymer formation; **A** (anhydride/epoxide ROCOP), **B** (lactone ROP) and **C** (epoxide/CO_2 ROCOP) (calibrated with narrow dispersity polystyrene standards).

$^{31}P\{^{1}H\}$ NMR spectroscopy enables characterization of chain end groups *via* reaction of the hydroxyl polymer chain ends with a phosphorus reagent (see section 1.5 for details).[14, 22] Analysis of the end group identity can be performed by acquiring aliquots after each stage (Fig. 2.8). During stage A peaks are observed at 146.7-146.8 ppm (assigned to PE) that shifted to a single peak for PDL (147.1 ppm) after stage B. Stage C revealed peaks consistent with PC formation (146.6-146.9 ppm). At all stages, hydroxyl end-group signals are observed. The appearance of multiplets in the $^{31}P\{^{1}H\}$ NMR spectra is due to the differing tacticity and regiochemistry of the neighbouring epoxide. The clear changes to the end group chemical shifts suggests the polymerization is consistently being initiated from the end of the polymer and further reinforces the idea of block copolymer formation.

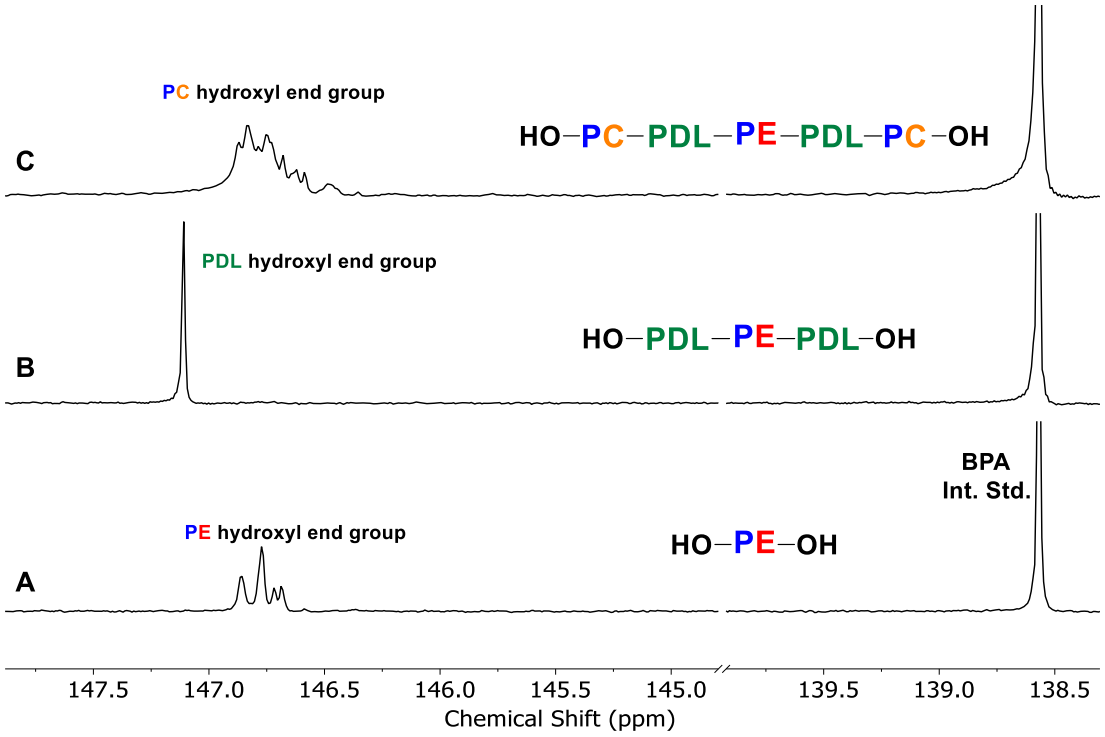


Figure 2.8 $^{31}P\{^{1}H\}$ NMR spectra of end group analysis on the polymerization of PA/VCHO/DL/CO_2. PE, PDL and PC end groups can be observed at 146.7-146.9, 147.1 and 146.5-146.9 ppm respectively. Bisphenol A (BPA) is added as an internal standard (in $CDCl_3$).

^{1}H DOSY NMR analysis of the pentablock shows a single diffusion coefficient for all resonances, suggesting all blocks are attached (Fig. 2.9, top). In contrast, a blend of the appropriate polymers, at similar molar masses, showed three different diffusion coefficients (Fig. 2.9, bottom).

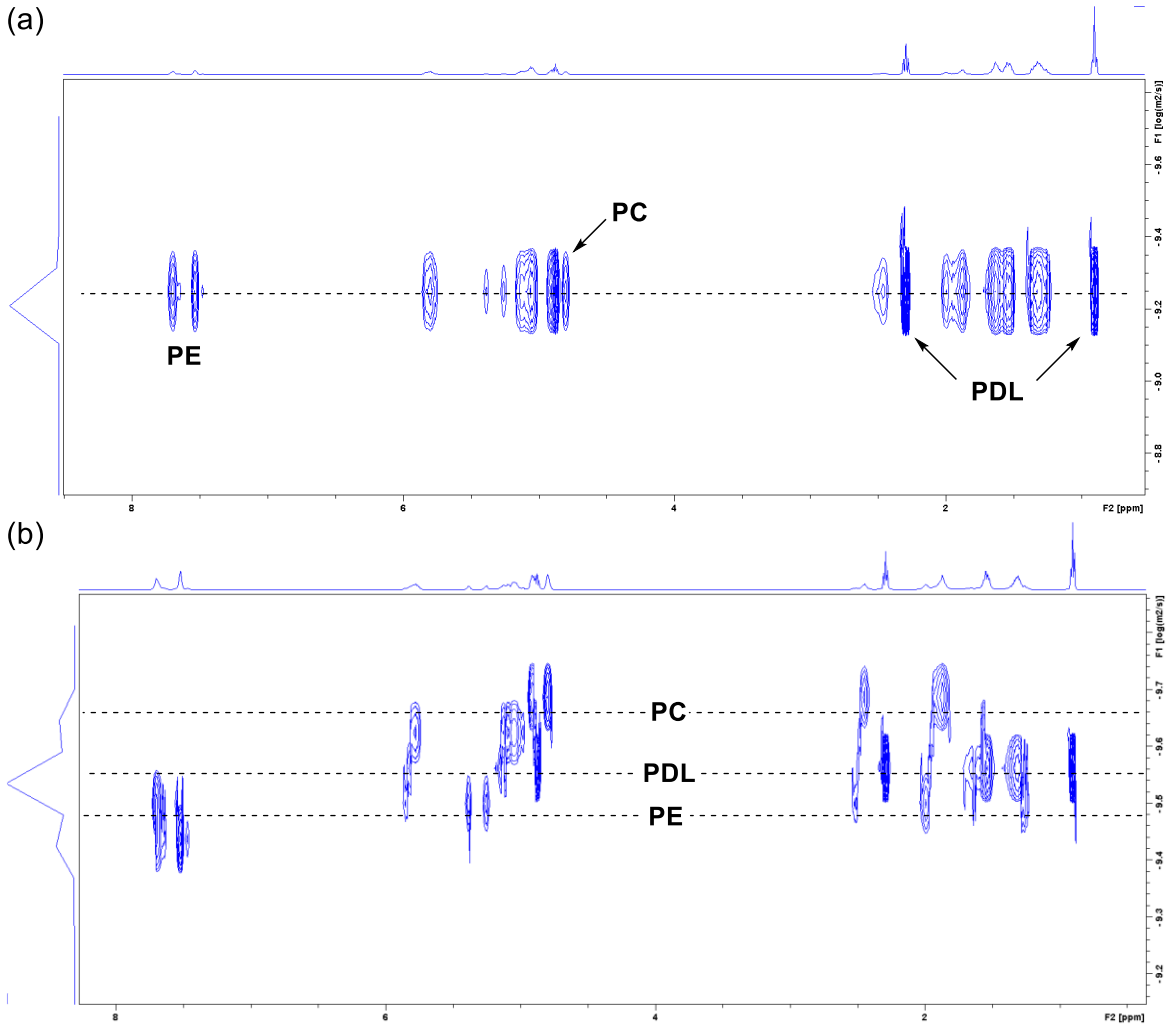


Figure 2.9 (a)^{1}H DOSY NMR spectra of pentablock copolymer from the polymerization of PA/VCHO/DL/CO_2 showing a single diffusion coefficient (bottom) homopolymer blend of PVCHPE, PDL and PVCHC with similar MW to the respective blocks showing three different coefficients (in $CDCl_3$).

The extent of transesterification must be understood since it could scramble block structure.[22] The ^{13}C NMR spectrum showed three major carbonyl peaks, corresponding to each of the three blocks, thus no transesterification or random incorporation of monomers were observed (Fig. 2.10). Furthermore SEC analysis reveals narrow dispersity values throughout the polymerization, which reinforces the lack of transesterification.

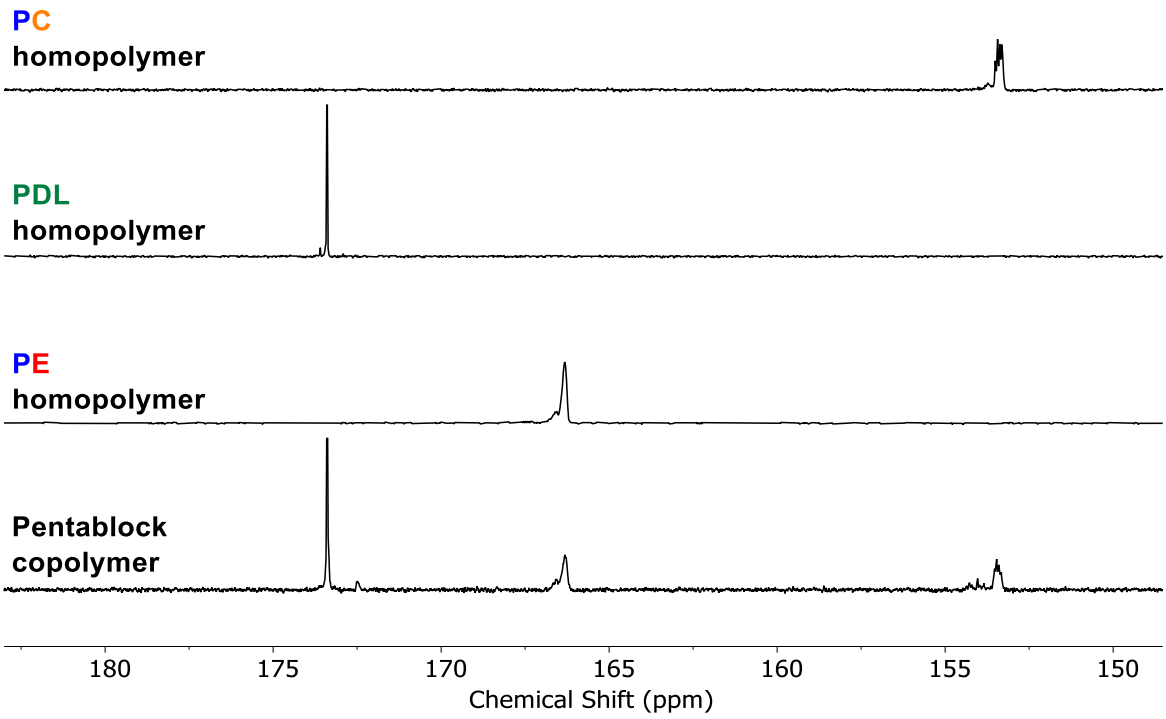


Figure 2.10 Carbonyl region of $^{13}C\{^{1}H\}4$ NMR spectra of pentablock copolymer from the polymerization of PA/VCHO/DL/CO_2 and PE, PDL and PC homopolymers. Carbonyl resonances for PE, PDL and PC blocks can be seen at 166.6-166.4 ppm,173.4 ppm and 153.5-153.3 ppm respectively (in $CDCl_3$).

Purification of the crude pentablocks did not change their composition, *i.e.* there is no significant homopolymer contamination (Fig. S4 in Appendix). Overall, the characterization data are consistent with selective pentablock copolymer formation.

The generality of the 4 monomer switchable catalysis was investigated using various anhydride/epoxide combinations (Table 2.1). High selectivity for pentablock formation was observed in all mixtures. For instance, the tetra-component polymerization produced narrowly dispersed PC-PDL-PE-PDL-PC pentablock copolymers with a mixture of PA/CHO/DL/CO_2 (Table 2.1, entry 1 & Fig. 2.11). *In-situ* ATR-IR spectroscopy confirmed the reaction first proceeded through the ROCOP of PA/CHO until full conversion before performing the DL ROP. Injection of CO_2 switched the catalysis to epoxide/CO_2 ROCOP (Fig. 2.11(a)). The SEC traces of aliquots obtained after each stage of the polymerization showed a constant increase in molar mass with narrow dispersities ($Đ$ = 1.11), suggesting successful formation of pentablock copolymers (Figure 2.11(b)). All IR and NMR resonances were assigned by comparison with the constituent homopolymers (See Appendix, Fig. S5-S19).

Table 2.1 Four monomer polymerizations using anhydride, epoxide, lactone and CO_2[a]

#	Monomer Combination	M_n (kg mol^{-1}) [$Đ$][b]			TOF (h^{-1})[c]		
		A	B	C	PE ROCOP	PDL ROP	PC ROCOP
P1	PA/CHO/DL/CO_2	1.7 [1.12]	7.5 [1.15]	8.8 [1.11]	27	160	6
P2	PA/VCHO/DL/CO_2	2.1 [1.16]	8.4 [1.08]	12.1 [1.05]	32	128	30
P3	NA/CHO/DL/CO_2	1.4 [1.15]	6.5 [1.12]	8.4 [1.08]	4	126	9
P4	NA/VCHO/DL/CO_2	1.5 [1.15]	7.1 [1.11]	10.2 [1.14]	8	160	44

[a][**1**]/[CHD]/[anhydride]/[lactone]/[epoxide] = 1/4/50/200/1000, 100 °C, (**A**, **B**) N_2 and (**C**) CO_2, 1 bar. PA, NA, DL, CHO and VCHO denote phthalic anhydride, *cis*-5-norbornene-*endo*-2,3-dicarboxylic anhydride, ε-decalactone, cyclohexene oxide and 4-vinyl-1-cyclohexene 1,2-epoxide, respectively. Conversion: anhydride > 99%, DL ≥ 64%, epoxide ≥ 11 (the apparently low conversions for epoxide are due to its dual use as monomer and solvent.) [b]Obtained from ^{1}H NMR spectroscopy. [b]M_n and $Đ$ measured by SEC (calibrated using polystyrene standards) . [c]Calculated from molar monomer conversion per mole of catalyst per hour.

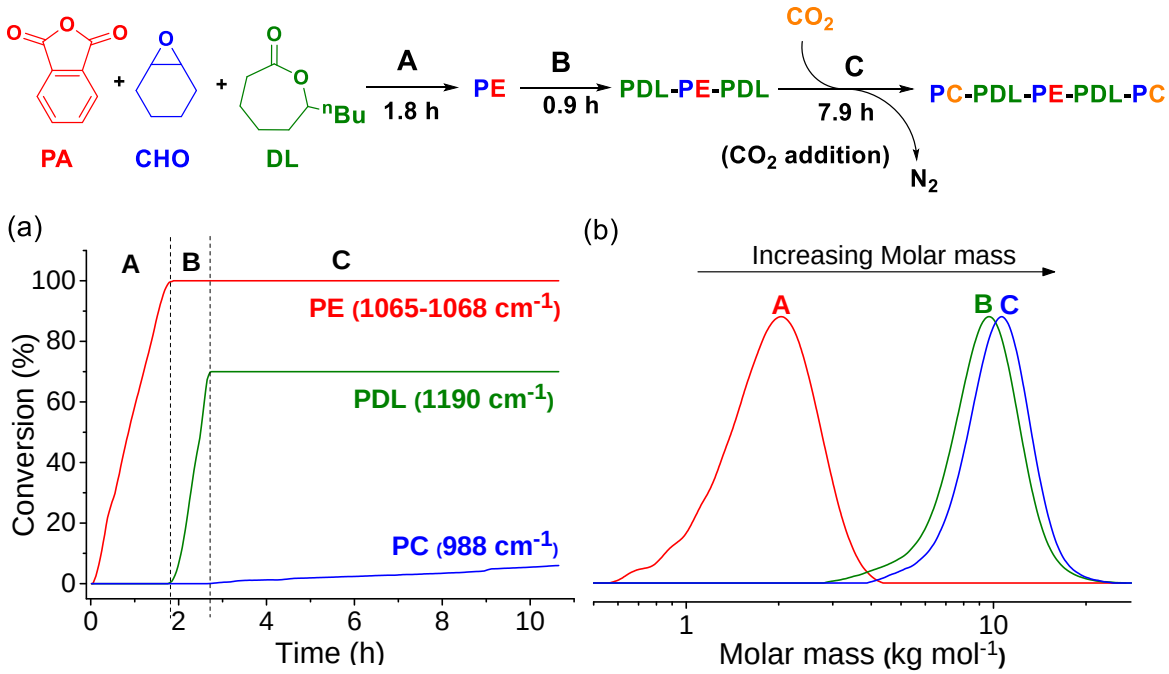


Figure 2.11 Polymerization of tetra-component monomer mixture, PA/CHO/DL/CO_2; reaction conditions: molar ratio of **1**/CHD/PA/DL/CHO = 1/4/50/200/1000, 100 °C under (**A**, **B**) N_2 and (**C**) CO_2, 1 bar. (a) Conv. vs. time plot illustrating the formation of different blocks during stages **A** (ROCOP of anhydride/epoxide), **B** (ROP of lactone) and **C** (ROCOP of epoxide/CO_2). Conversion data obtained using in situ ATR-IR spectroscopy and calibrated using ^{1}H NMR spectroscopy; (b) SEC traces illustrating the increase in M_n and retention of $Đ$ as the polymerization progresses (calibrated using narrow dispersity polystyrene standards).

A tricyclic anhydride variant was investigated using *cis*-5-norbornene-*endo*-2,3-dicarboxylic anhydride (NA) (Table 2.1, entry 3 & 4). Both reactions occurred firstly through NA/epoxide ROCOP (A), followed by DL ROP (B) and finally by epoxide/CO_2 ROCOP (C), as confirmed using *in-situ* ATR-IR spectroscopy (Fig. 2.12(a), 2.13(a)). The SEC analyses showed molar mass increases and narrow dispersity in all samples ($Đ \leq$ 1.15) (Fig. 2.12(b), 2.13(b)).

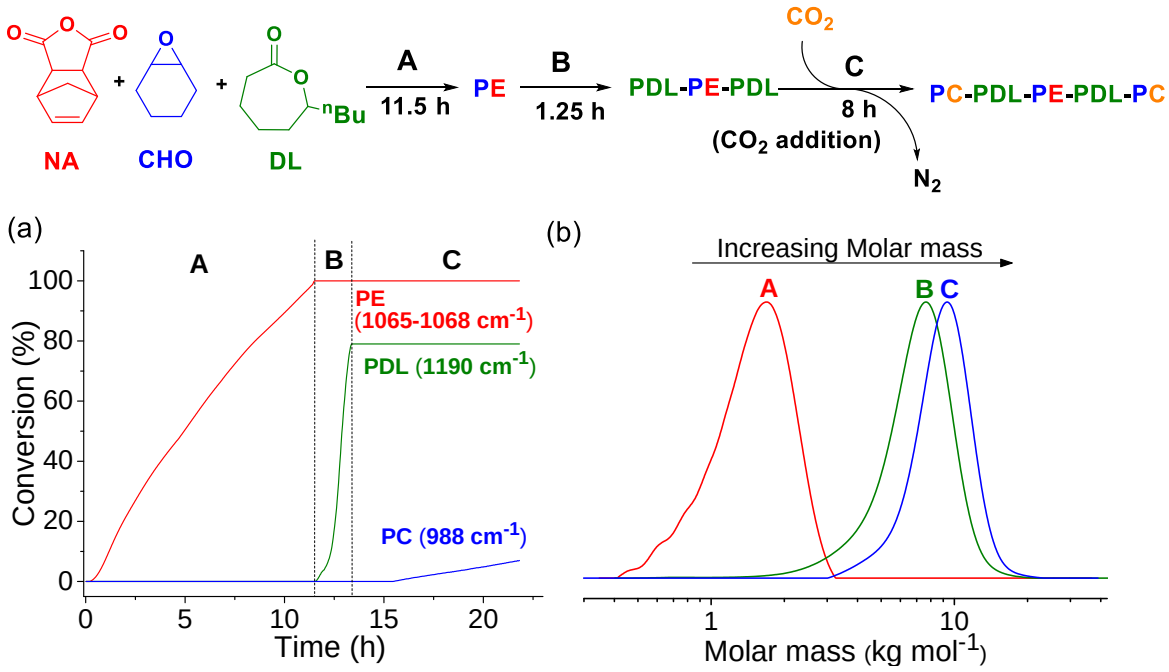


Figure 2.12 Polymerization of tetra-component monomer mixture, NA/CHO/DL/CO_2; reaction conditions: molar ratio of **1**/CHD/NA/DL/CHO = 1/4/50/200/1000, 100 °C under (A, B) N_2 and (C) CO_2, 1 bar. (a) Conv. vs. time plot illustrating the formation of different blocks during stages A (ROCOP of anhydride/epoxide), B (ROP of lactone) and C (ROCOP of epoxide/CO_2). Conversion data obtained using in situ ATR-IR spectroscopy and calibrated using ^{1}H NMR spectroscopy; (b) SEC traces illustrating the increase in M_n and retention of $Đ$ as the polymerization progresses (calibrated using narrow dispersity polystyrene standards).

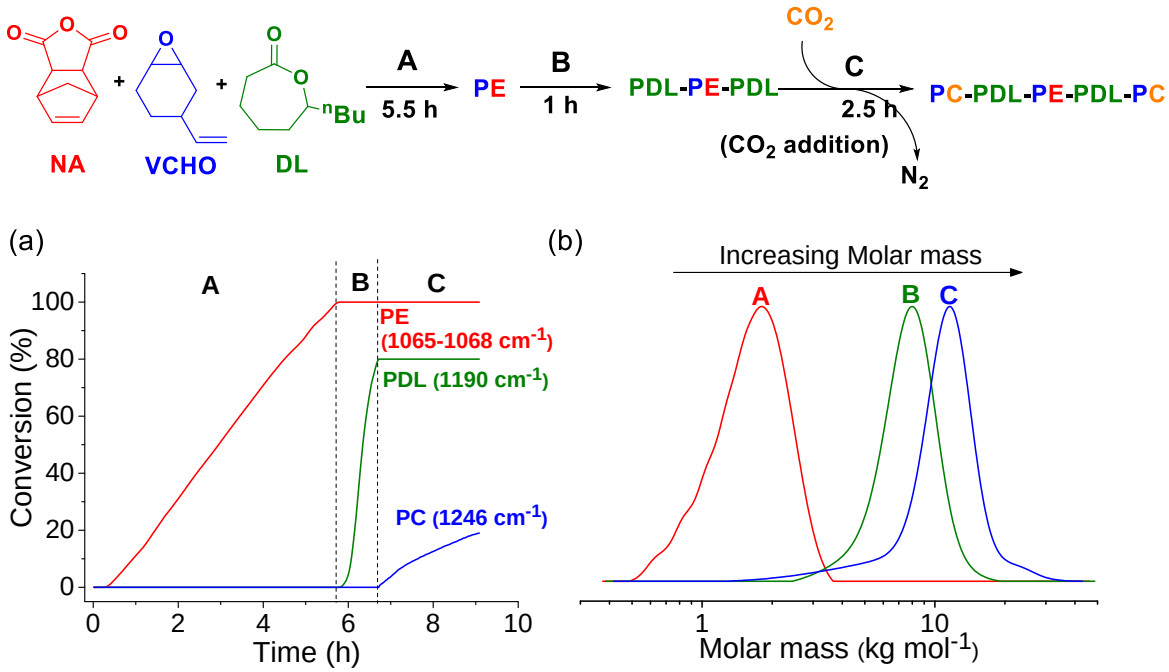


Figure 2.13 Polymerization of tetra-component monomer mixture, NA/VCHO/DL/CO_2; reaction conditions: molar ratio of **1**/CHD/NA/DL/VCHO = 1/4/50/200/1000, 100 °C under (A, B) N_2 and (C) CO_2, 1 bar. (a) Conv. vs. time plot illustrating the formation of different blocks during stages A (ROCOP of anhydride/epoxide), B (ROP of lactone) and C (ROCOP of epoxide/CO_2). Conversion data obtained using in situ ATR-IR spectroscopy and calibrated using ^{1}H NMR spectroscopy; (b) SEC traces illustrating the increase in M_n and retention of $Đ$ as the polymerization progresses (calibrated using narrow dispersity polystyrene standards).

The pentablock structures were further confirmed using a combination of ^{1}H, $^{13}C\{^{1}H\}$, ^{1}H DOSY NMR spectroscopy, $^{31}P\{^{1}H\}$ end group test (*vide supra*). For instance, the ^{1}H DOSY NMR revealed one diffusion coefficient for all pentablock copolymers **P1**, **P3** and **P4**, suggesting full chain attachment (Fig. 2.14).

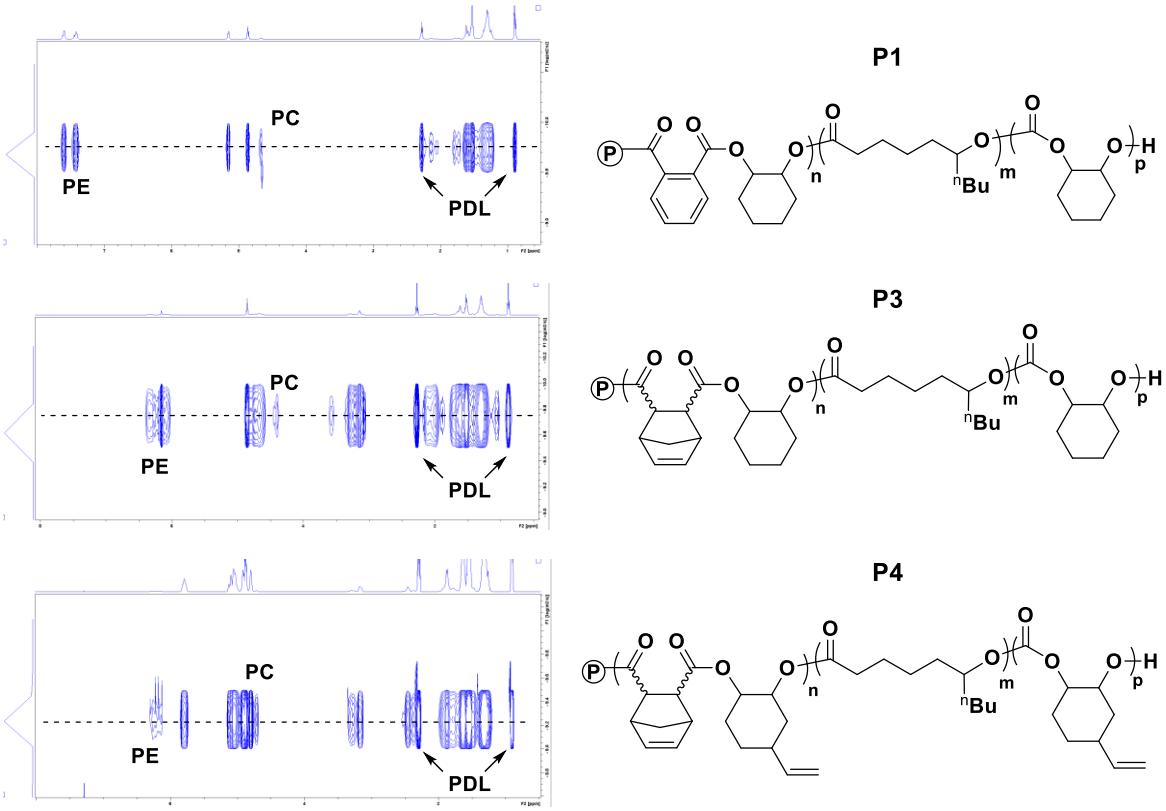


Figure 2.14 ^{1}H DOSY NMR spectrum of (top) pentablock copolymer from the polymerization of PA/CHO/DL/CO_2 (middle) pentablock copolymer from the polymerization of NA/CHO/DL/CO_2 (bottom) pentablock copolymer from the polymerization of NA/VCHO/DL/CO_2 (in $CDCl_3$).

The $^{31}P\{^{1}H\}$ NMR spectroscopy end group assessment of the final pentablock copolymer **P1**, **P3** and **P4** all exhibited end group resonances belonging to the PC hydroxyl end group (Fig. 2.15). No PDL were observed, which suggests all formation of the final PC block initiated from the PDL block ($^{31}P\{^{1}H\}$ NMR spectra of all stages can be found in Fig. S20-22 in the Appendix).

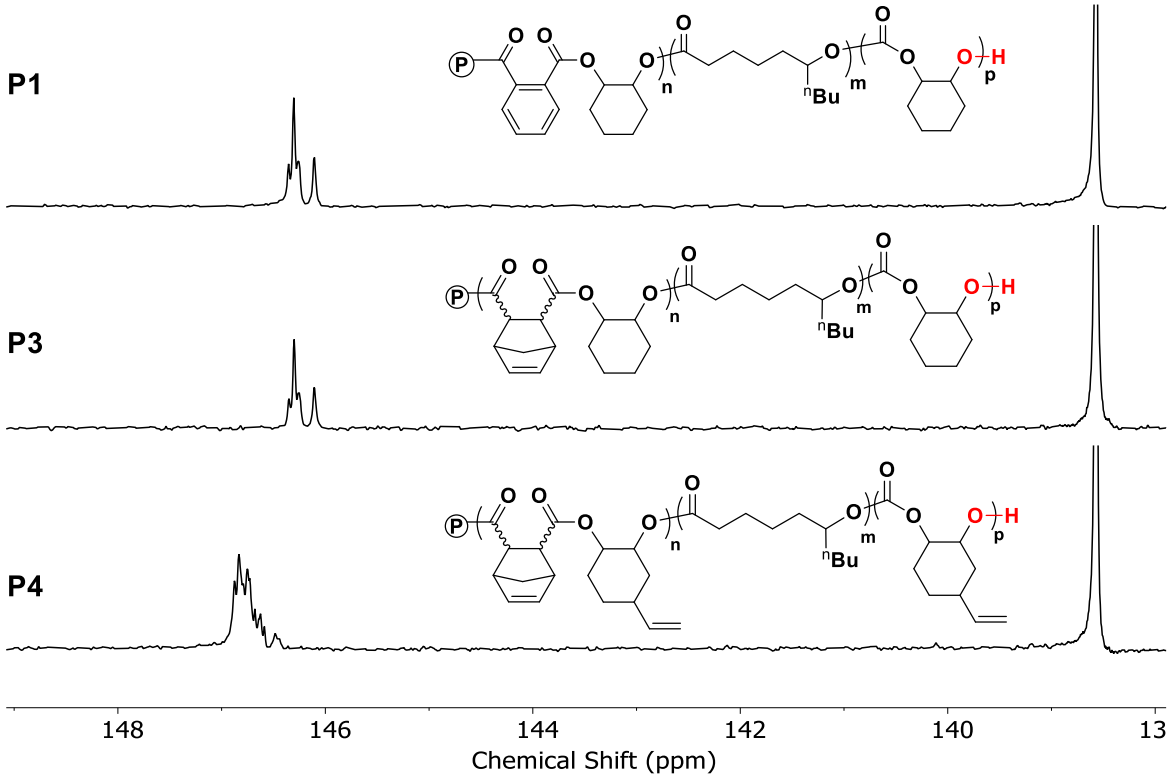
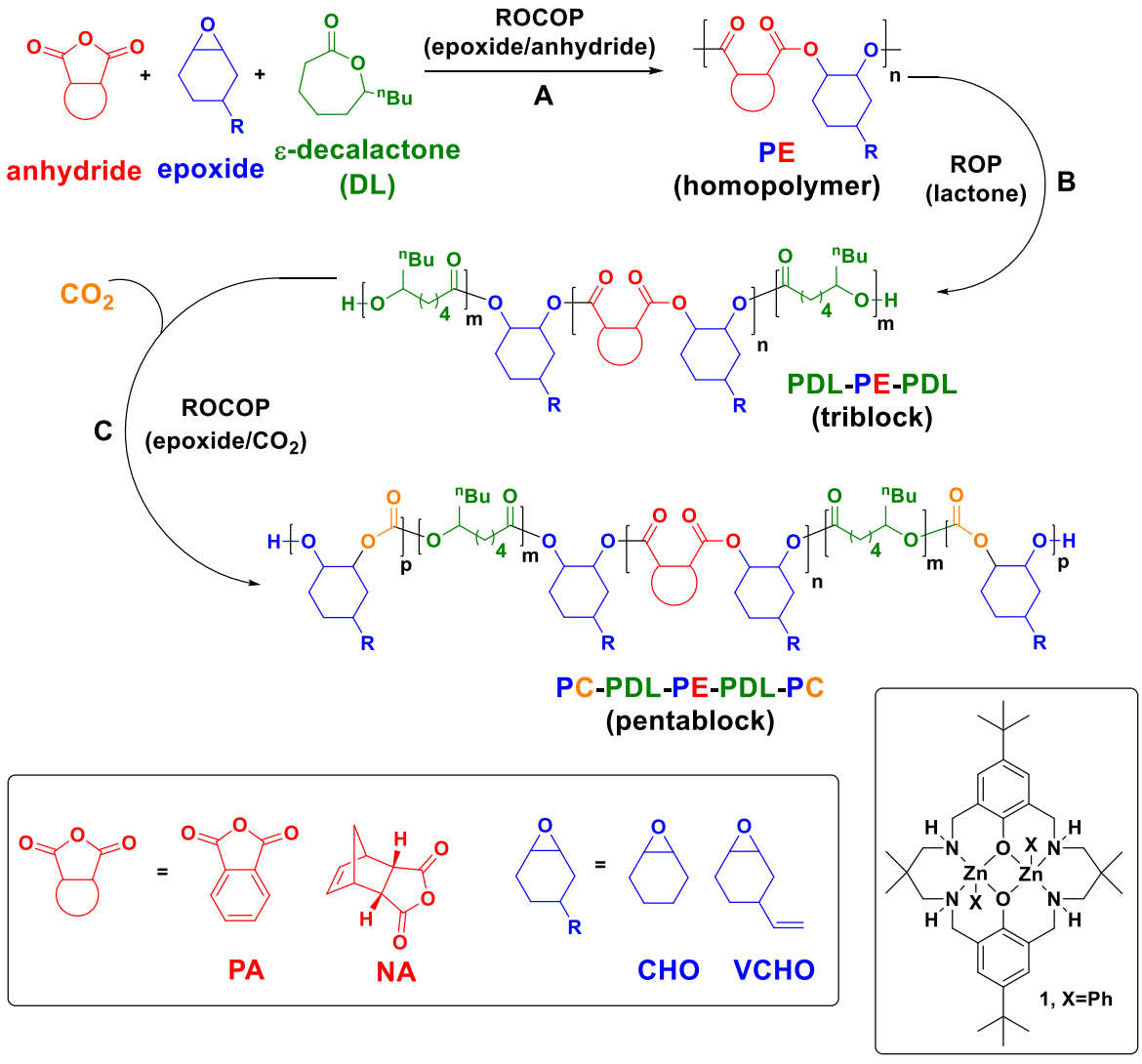


Figure 2.15 Selected region of $^{31}P\{^{1}H\}$ NMR spectra of hydroxyl polymer end analysis of (top) pentablock copolymer from the polymerization of PA/CHO/DL/CO_2 (middle) pentablock copolymer from the polymerization of NA/CHO/DL/CO_2 (bottom) pentablock copolymer from the polymerization of NA/VCHO/DL/CO_2. The hydroxyl end group assessed is highlighted in red. (in $CDCl_3$)

This polymerization breaks new ground in proceeding with *two switches* between *different polymerization mechanisms*, specifically from epoxide/anhydride ROCOP to lactone ROP, followed by epoxide/CO_2 ROCOP (Scheme 2.4).



Scheme 2.4. Four monomer selective polymerization, using [LZn_2Ph_2] (**1**) /1,2-cyclohexanediol (CHD) catalytic system.

2.5. **Mechanistic hypothesis**

In all reactions, epoxide/anhydride ROCOP always occurs first. This selectivity is proposed to arise from the zeroth order rate dependence on the insertion of anhydride and CO_2 into the zinc-alkoxide intermediate (Fig. 2.16).[20, 23] The result obtained in this experimental study is consistent with the previous DFT investigation.[13] It is worth noting that the DFT study also highlighted the relative linkage stability as well as the overall barrier in controlling selectivity; the zinc-carboxylate/carbonate intermediates (anhydride/CO_2 insertion) are significantly more stable than the alternative zinc-alkoxide (lactone insertion).[13] However, the possibility of back-biting from the zinc alkoxide intermediate was not examined in the theoretical study. Experimentally, the back-biting side reaction prevented the pentablock polymer formation and an alternative monomer addition order was needed. The result of this study highlights the importance of considering side reactions, especially when utilising catalysts showing lower propagation rates for polymerization.

Overall, this study experimentally demonstrates the chemistry of the zinc-chain end group which controls the monomer selectivity, linking the three different polymerizations and controlling monomer discrimination.

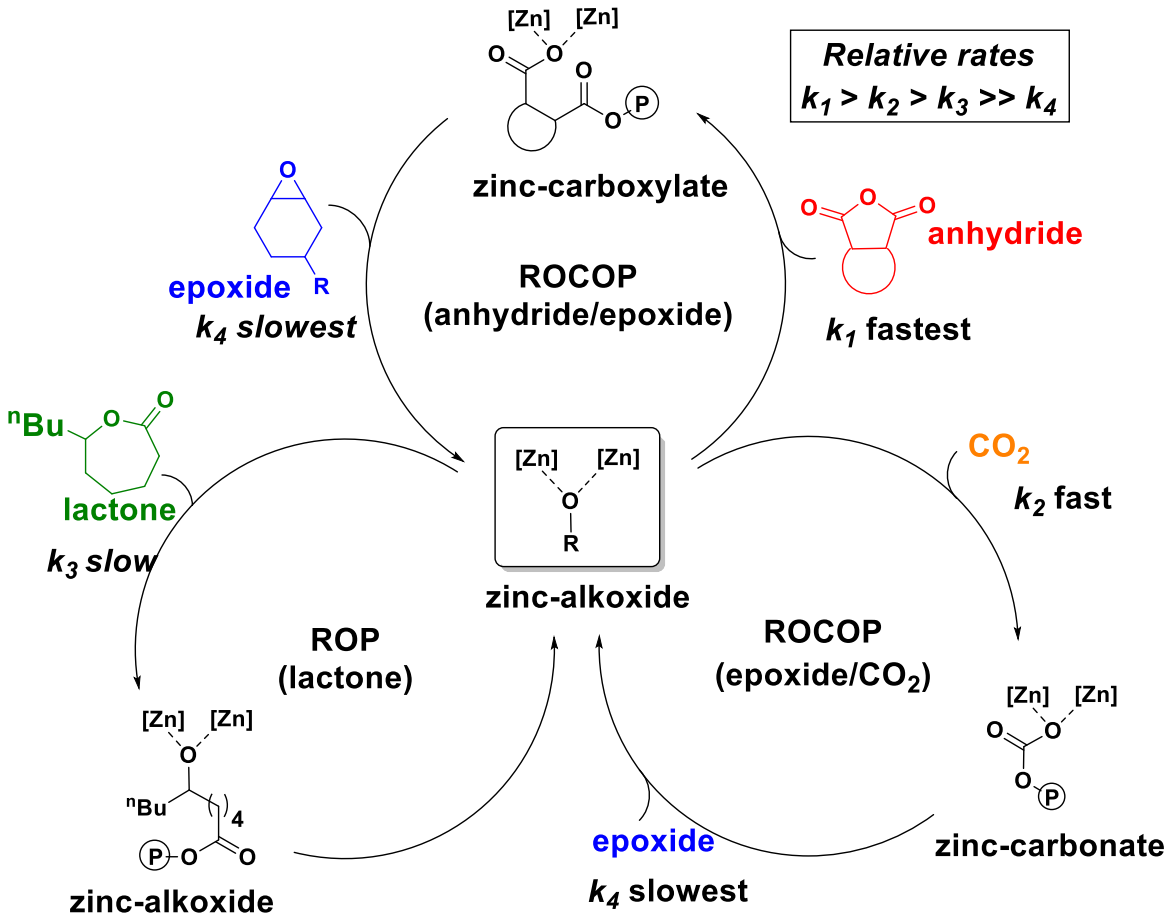
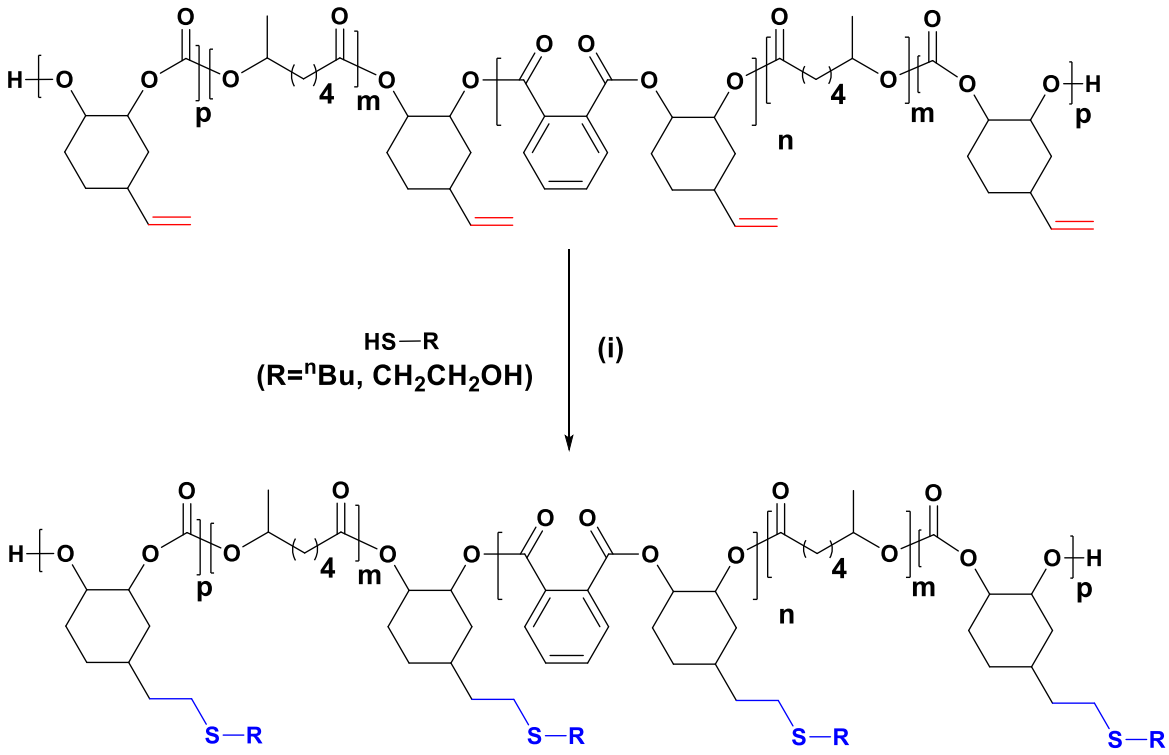


Figure 2.16. Proposed mechanisms occurring during polymerization of anhydride, epoxide, lactone and CO_2, highlighting the central role for the zinc alkoxide intermediate (P = growing polymer chain).

2.6. **Post-polymerization modification**

Several of the pentablock copolymers contain alkene groups that were post-functionalized to install different side chains. Generally, functionalized lactones are difficult to synthesize and polymerize which has limited investigation of functionalized, degradable polyesters.[24] Recently, ROCOP was used to prepare various alkene substituted polyesters and polycarbonates that were later efficiently reacted without compromising the polymer backbone.[17, 25-29] Here, the well-known thiol-ene reaction is applied to install alkane or hydroxy-alkane substituents.[30] UV-initiated reactions were performed on pentablock **P2** using either 1-butanethiol or 2-mercaptoethanol (Scheme 2.5).



Scheme 2.5. Thiol-ene functionalization of the pentablock copolymers. (i) 2,2-Dimethoxy-2-phenylacetophenone (DMPA, photo initiator)/alkene/thiol reagent = 1/2.5/10, UV, 2 h, 25 °C, $CDCl_3$.

The reactions reached complete conversion within 2 h, as shown by ^{1}H NMR spectroscopy (Fig. 2.17). The double bond resonances are consumed during the reaction (5.76 and 5.01-5.09 ppm), whilst all the other resonances remain unchanged. New resonances confirmed attachment of the butyl thioether (2.51 ppm) or the hydroxyl ethyl thioether groups (3.72, 2.71, 2.55 ppm).

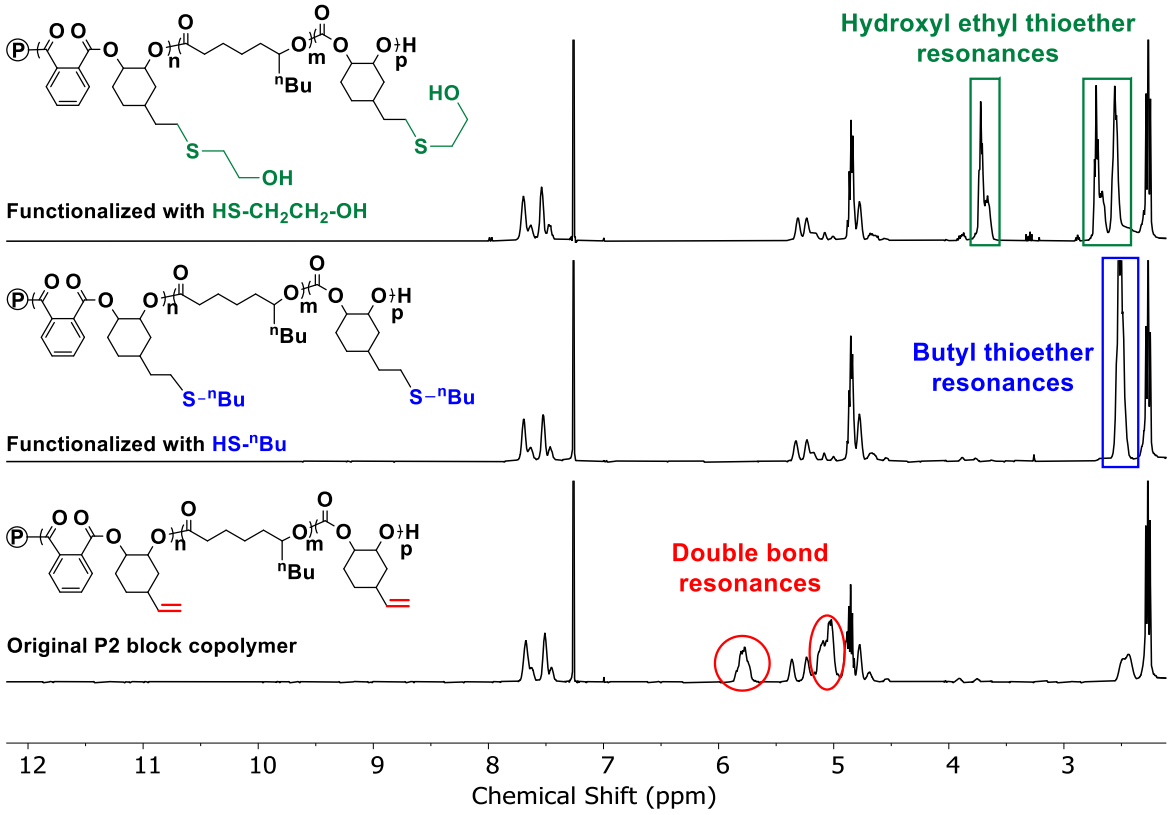


Figure 2.17 ^{1}H NMR spectra showing the changes in NMR resonances on the **P2** pentablock copolymer before and after thiol-ene post-polymerization functionalization. New resonances after functionalization is displayed in blue and green (in $CDCl_3$).

The functionalized polymers show slightly higher molar masses compared to the starting pentablocks with retention of monomodal, narrow dispersity (Fig. 2.18); these findings suggest the polymer backbone remained intact. The pentablock copolymers **P3** and **P4** were also successfully reacted to produce analogous functionalized polymers (Table S1, Fig. S26-S29 in the Appendix). In the case of **P4**, both internal and terminal double bonds reacted with the thiol reagent.

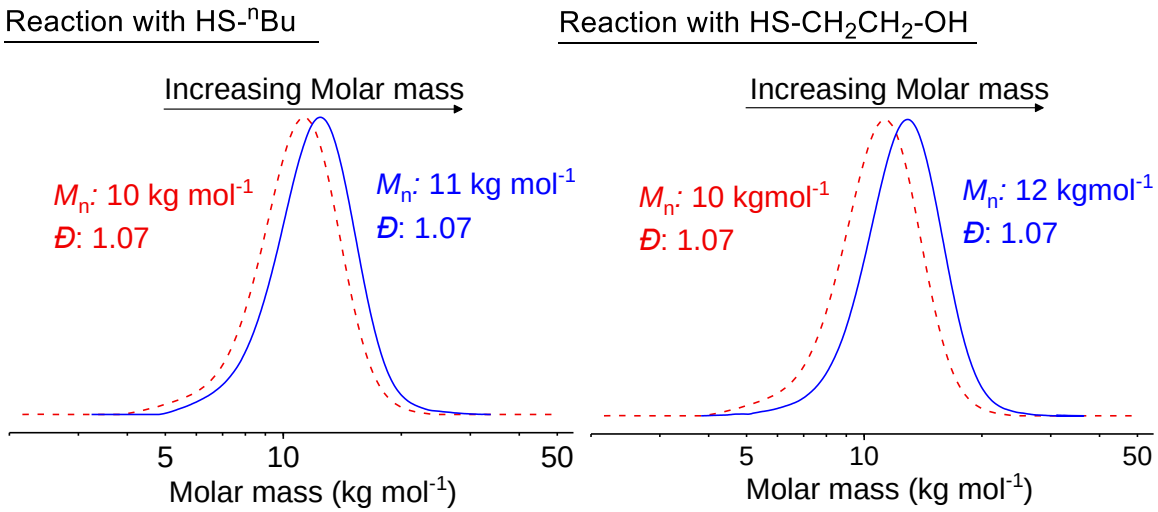


Figure 2.18. SEC analyses of the thiol-ene functionalization of the pentablock copolymer **P2**. Dashed red and solid blue lines illustrate the molar mass distributions before and after reaction, respectively.

Preliminary assessment of pentablock copolymers' thermal properties indicates a single T_g for all polymers, suggesting amorphous structures with partially miscible blocks (See Appendix, Table S2). The block miscibility is tentatively attributed to the lower overall molar masses, since the propensity to undergo phase separation is directly correlated to degree of polymerization. Interestingly, the T_g was easily varied over the range -35 to 20 °C. Moreover, the T_g can be further adjusted by side chain

functionalization: addition of hydroxyl alkyl side-chains increases the T_g (typically >20 °C) compared to the precursor, presumably due to hydrogen bonding.[31] For instance, functionalising **P2** with 1-butanethiol reduced the T_g by 10 °C, whereas the use of mercaptoethanol increased the T_g by 31 °C (Fig. 2.19).

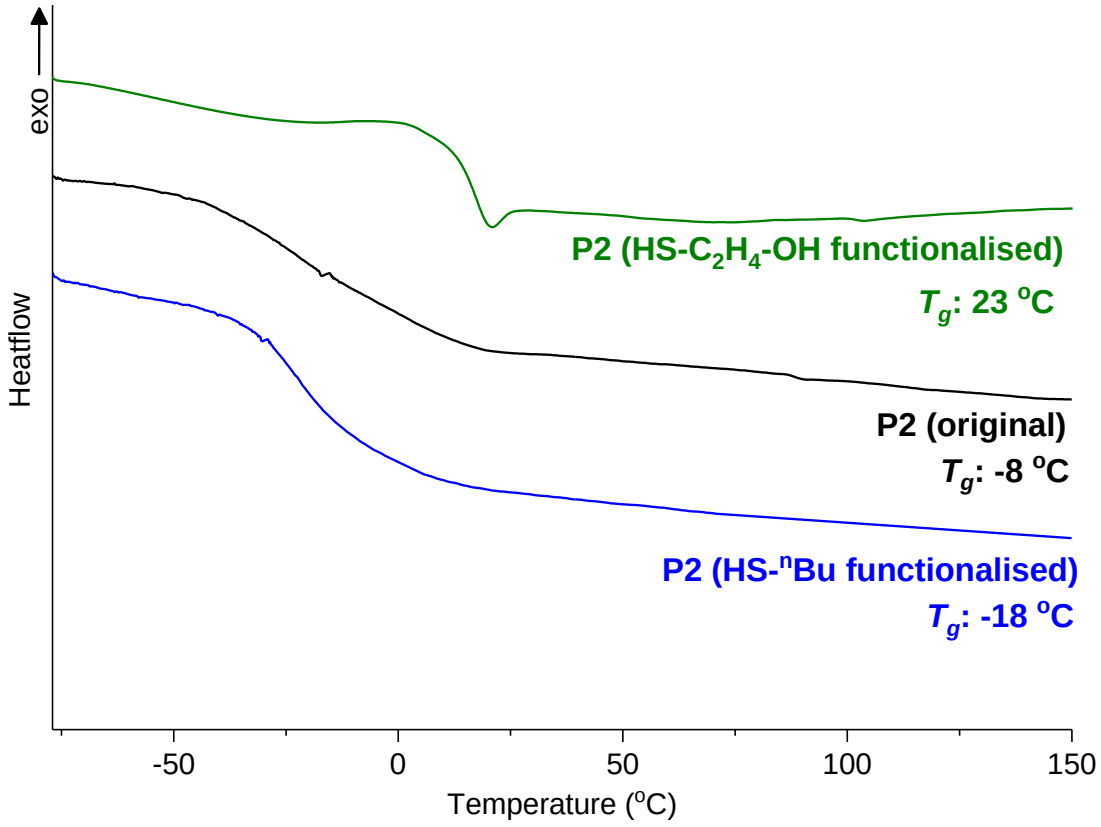
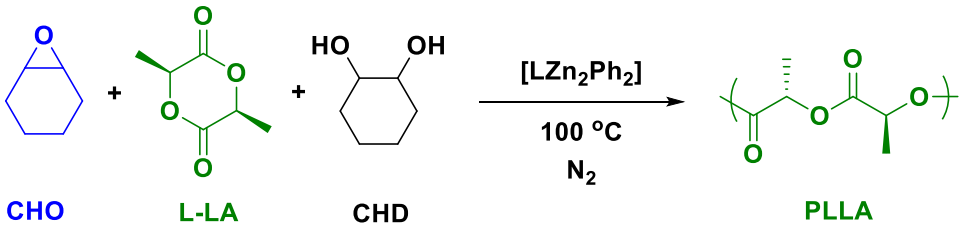


Figure 2.19 DSC thermograph of the original **P2** block copolymer (Black) and functionalised polymers using 1-butanethiol (blue) and 2-mercaptoethanol (green).

The pentablocks' controllable, low T_g, low molar masses and hydroxyl-telechelic structures indicate they are suited for further development as polyols. Recently, polycarbonate polyols, produced using carbon dioxide ROCOP, are being commercially investigated for polyurethane manufacture; these new pentablocks significantly expand the range of carbon dioxide containing polyols.[32]

2.7. **Initial studies using lactide**

Polylactide (PLA) is an important sustainable polymer industrially produced on the 10 thousand tonnes per year scale and used in various applications.[33] PLA can be synthesised through the ROP of lactide (LA).[34] As such, it is of interest to investigate whether LA can be incorporated into the 'Switch' catalysis methodology.



Scheme 2.6 ROP of L-LA using [LZn_2Ph_2]/CHD catalyst system (CHO used as the solvent).

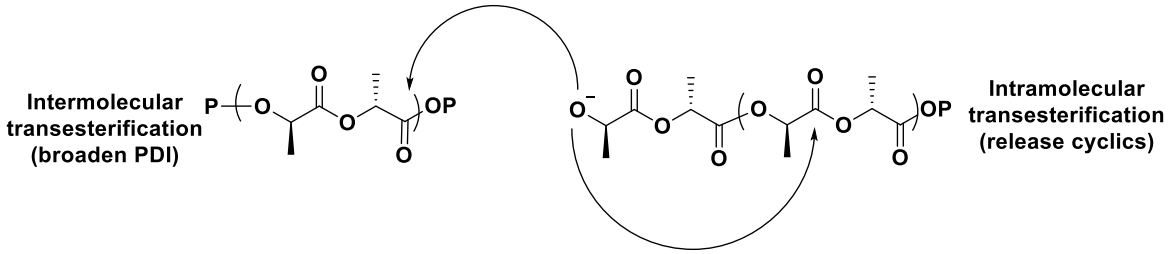
The ROP of (L-lactide) L-LA in neat CHO was performed using **1** as the catalyst and CHD as the initiator/chain transfer agent to form poly(L-lactide) (PLLA) (scheme 2.5 and Table 2.2). L-LA was utilized instead of *rac*-LA to simplify ^{1}H NMR spectroscopy analyses. Furthermore, CHO was utilized as the solvent to mimic conditions required for switch catalysis using multiple monomers.

Table 2.2 ROP of L-LA using **1**/CHD

#	CHD/L-LA/CHO	Time (h)	Conv. (%)[a]	TOF (h^{-1})[b]	M_n (kg mol^{-1}) [$Đ$][c]
1	2/200/1000	0.33	98	593	5.2 [1.54]
2	2/200/1000	0.66	98	297	4.2 [1.98]
3	4/200/1000	0.33	95	576	6.2 [1.52]
4	2/200/2000	0.33	48	291	9.8 [1.03], 2.8 [1.31]

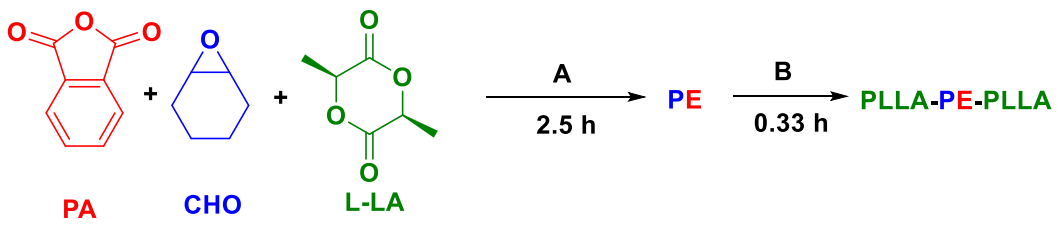
[a]Obtained from ^{1}H NMR spectroscopy [b]Calculated from molar monomer conversion per mole of catalyst per hour [c]Measured by SEC, calibrated with polystyrene.

The polymerization proceeded with high rates (TOF >590 h^{-1}) (Table 3.2, entry 1). However, control was lacking as large dispersity values were observed at high monomer conversions (Đ > 1.5). Monomer purity is not deemed to be a major contributor to the high dispersity, as a doubling of CHD loading did not alter the *Đ* (Table 2.2, entry 1 & 3). Rather, transesterification is likely to be responsible for the high dispersity. Transesterification of polyesters can occur in an intermolecular (with neighboring chains) or in an intramolecular (with itself) manner (Scheme 2.6).[35] The former leads to a broadening of the dispersity and the latter would result in release of cyclic species. Extended reaction time for the ROP of L-LA (beyond full conversion) led to an increase in dispersity and slight reduction in molecular weight; both features are characteristic of transesterification (with possible backbiting) (Table 2.2, entry 1 & 2).



Scheme 2.7 Intermolecular and intramolecular transesterification of PLA

Nevertheless, two separate terpolymerizations were attempted to determine the monomer selectivity. First, the terpolymerization of PA, CHO and L-LA was performed (Scheme 2.7 & Table 2.3).



Scheme 2.8 Terpolymerization of PA/CHO/L-LA; reaction conditions: [LZn_2Ph_2]/CHD/PA/L-LA/CHO = 1/4/50/200/1000, 100 °C, N_2

Table 2.3 Terpolymerization of PA/CHO/L-LA

Stage	Polymerization process	Conversion (%)[a]		TOF (h^{-1})[b]	M_n ($kgmol^{-1}$) [$Đ$][c]
		PA	L-LA		
A	ROCOP of PA/CHO	100	0	20	1.3 [1.08]
B	ROP of L-LA	100	94	570	3.4 [1.69]

[a]conversions obtained from ^{1}H NMR spectra on aliquots taken from polymerisation mixture. [b]TOFs calculated based on number of mol of monomer converted per mol of catalyst per hour. [c]M_n and $Đ$ measured by SEC (calibrated using polystyrene standards). PA and L-LA denotes phthalic anhydride and L-lactide respectively.

A TOF of 20 h^{-1} was observed for the ROCOP of PA/CHO, a comparable rate to previous results**.** In contrast, **1** was very active for the ROP of L-LA (TOF: 570 h^{-1}). Aliquots were removed at key intervals to monitor the reaction progress using ^{1}H NMR spectroscopy and SEC. Mesitylene was used as an internal standard for accurate conversion calculations. The first aliquot showed an ^{1}H NMR spectra with the consumption of PA (8.02 and 7.90 ppm) with the concurrent formation of polyester (PE) (7.66 and 7.50 ppm) (Fig. 2.20). The formation of PLLA (5.14 ppm) was only

observed once all the PA had been consumed. Thus, confirming a switch in polymerization mechanism from the ROCOP of PA/CHO (stage A) to the ROP of L-LA (stage B).

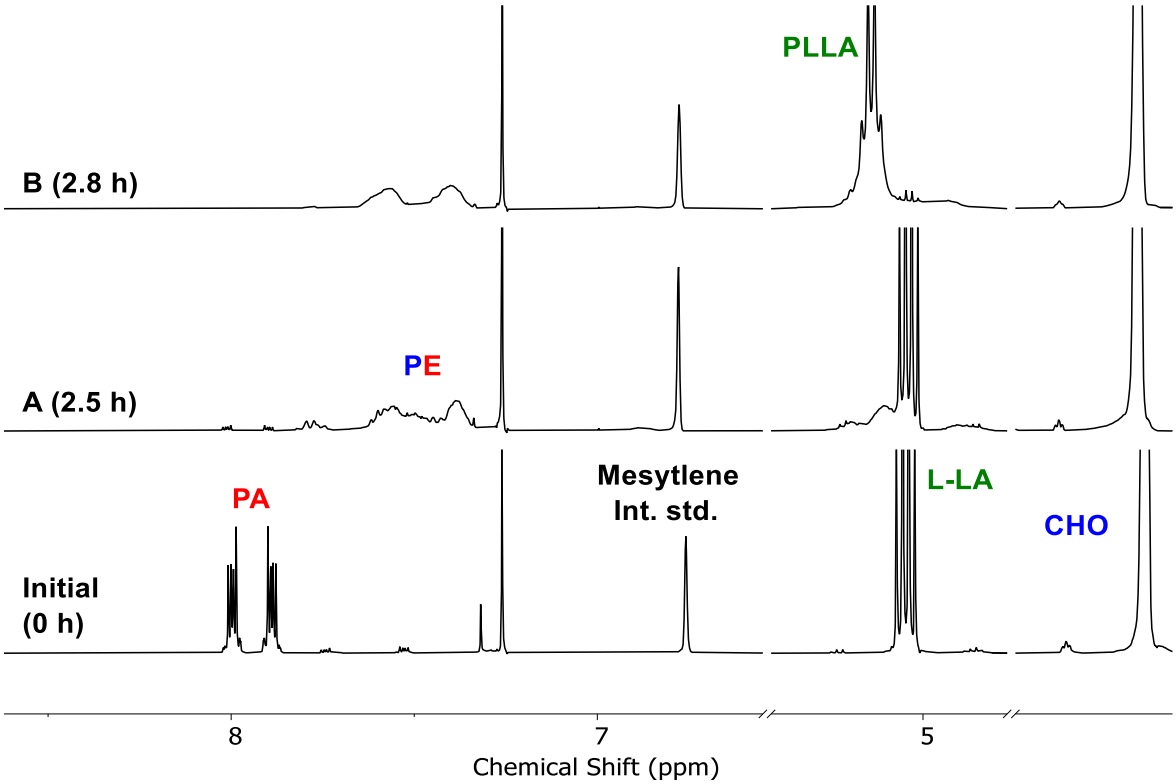


Figure 2.20 Selected region of ^{1}H NMR spectra illustrating changes in various resonances during stages **A** (ROCOP of anhydride/epoxide) and **B** (ROP of lactide) of the terpolymerization using PA/L-LA/CHO as monomer feedstock (in $CDCl_3$).

The SEC revealed an increase in molar mass as the polymerization progressed (Fig. 2.21). However, the increase in molar mass does not amount to the expected theoretical molar mass based on monomer conversion (94% conversion amounts to a weight of 7.2 $kgmol^{-1}$). An increase in polydispersity from 1.08 to 1.69 was also

observed. These observations suggest the later stage of the polymerization was plagued by transesterification.

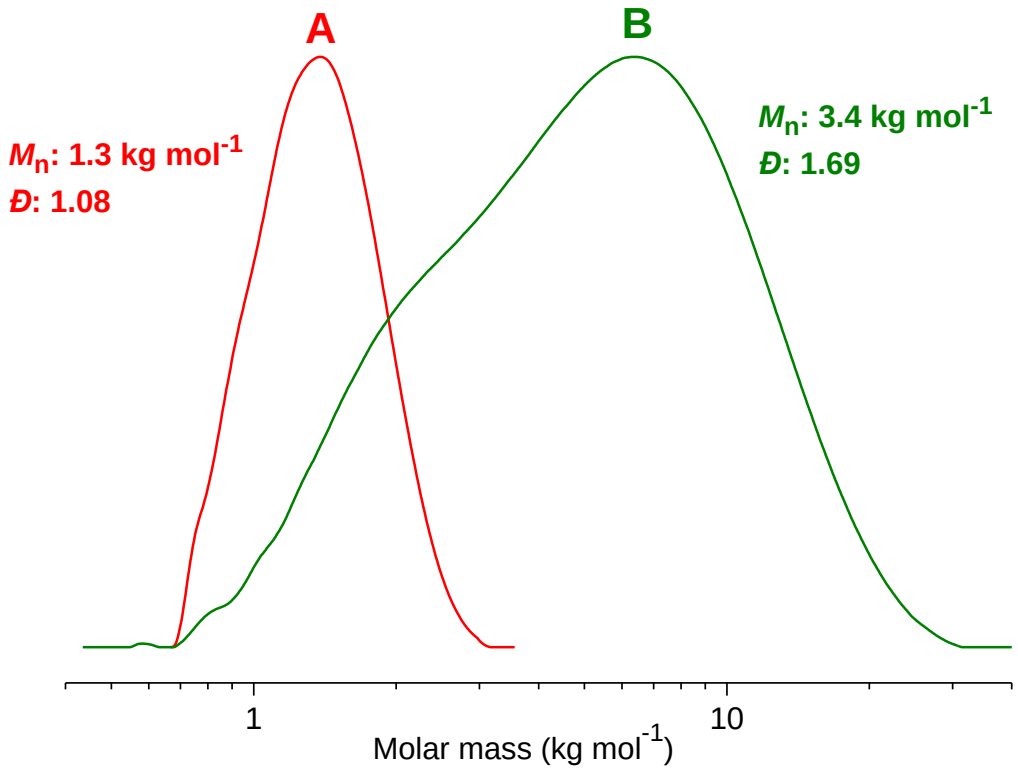
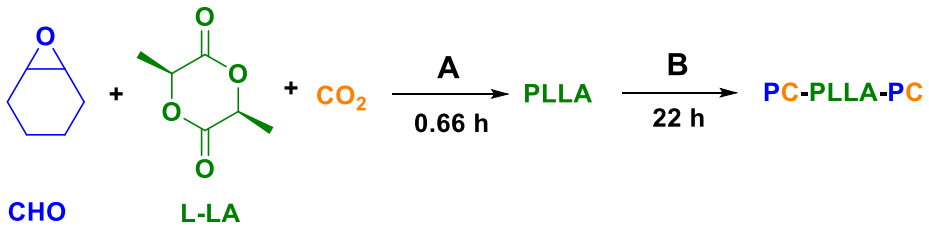


Figure 2.21 SEC traces illustrating the changes in M_n and $Đ$ as the polymerization progresses through stages A (ROCOP of anhydride/epoxide) and B (ROP of lactide) of the terpolymerization using PA/L-LA/CHO as monomer feedstock (calibrated using narrow dispersity polystyrene standards).

The terpolymerization of L-LA/CHO/CO_2 was also carried out in order to ascertain the difference in monomer selectivity and to investigate whether the presence of CO_2 may alleviate the problematic side-reactions (Scheme 2.8 & Table 2.4).



Scheme 2.9 Terpolymerization of CHO/L-LA/CO_2; reaction conditions: [LZn_2Ph_2]/CHD/L-LA/CHO = 1/4/200/1000, 100 °C, N_2

Table 2.4 Terpolymerization of L-LA/CHO/CO_2

Stage	Polymerization process	Conversion (%)[a]		TOF (h^{-1})[b]	M_n ($kgmol^{-1}$) [$Đ$][c]
		CHO	L-LA		
A	ROP of L-LA	0	94	284	10.4 [1.30]
B	ROCOP of CO_2/CHO	45	100	20	4.1 [1.70]

[a]conversions obtained from ^1H NMR spectra on aliquots taken from polymerisation mixture. [b]TOFs calculated based on number of mol of monomer converted per mol of catalyst per hour. [c]M_n and Đ measured by SEC (calibrated using polystyrene standards). CHO and L-LA denotes cyclohexene oxide and L-lactide respectively

A TOF of 284 h^{-1} was observed for the ROP of L-LA under a CO_2 atmosphere. This rate was much slower than that observed under an N_2 atmosphere, presumably due to competing CO_2 insertion. The polymerization was monitored by regular removal of aliquots for analysis by ^1H NMR spectroscopy (mesitylene as an internal standard) and SEC. Initially, the consumption of L-LA (5.04 ppm) occurred together with the simultaneous formation of PLLA (5.14 ppm) (Fig. 2.22). The formation of the PC (4.65 ppm) from the ROCOP of CO_2/CHO was only observed after the full consumption of the L-LA. This result indicates a reversal of the typically observed selectivity between the ROP of cyclic esters and ROCOP of CO_2/epoxide using **1**. It suggests that the rate of LA

insertion into the zinc alkoxide intermediate is faster than the rate of CO_2 insertion or that the linkage formed is more stable.

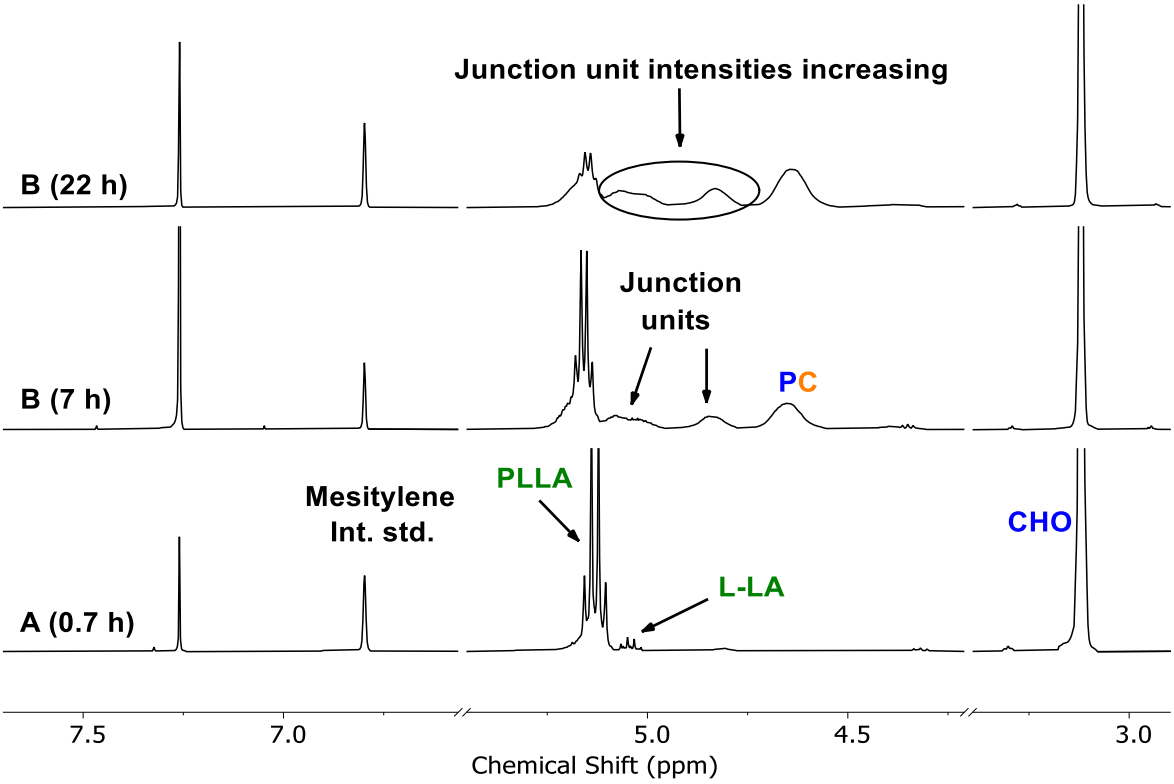


Figure 2.22 Selected region of ^{1}H NMR spectra illustrating changes in various resonances during stages A (ROP of Lactide) and B (ROCOP of epoxide/CO_2) of the terpolymerization using L-LA/CHO/CO2 as monomer feedstock (in $CDCl_3$)

The SEC analysis at the end of stage **A** revealed a molar mass of 10.4 kgmol^{-1} with an acceptable polydispersity ($Đ$ = 1.30) (Fig. 2.23). However, the SEC trace for the aliquots obtained during the ROCOP of CO_2/CHO illustrated a decrease in molar mass and an increase in dispersity (Fig. 2.23). A closer examination of the ^{1}H NMR spectrum of the final aliquot illustrated an increase in the junction unit (5.07 and 4.84 ppm) intensity, indicative of extensive transesterification.

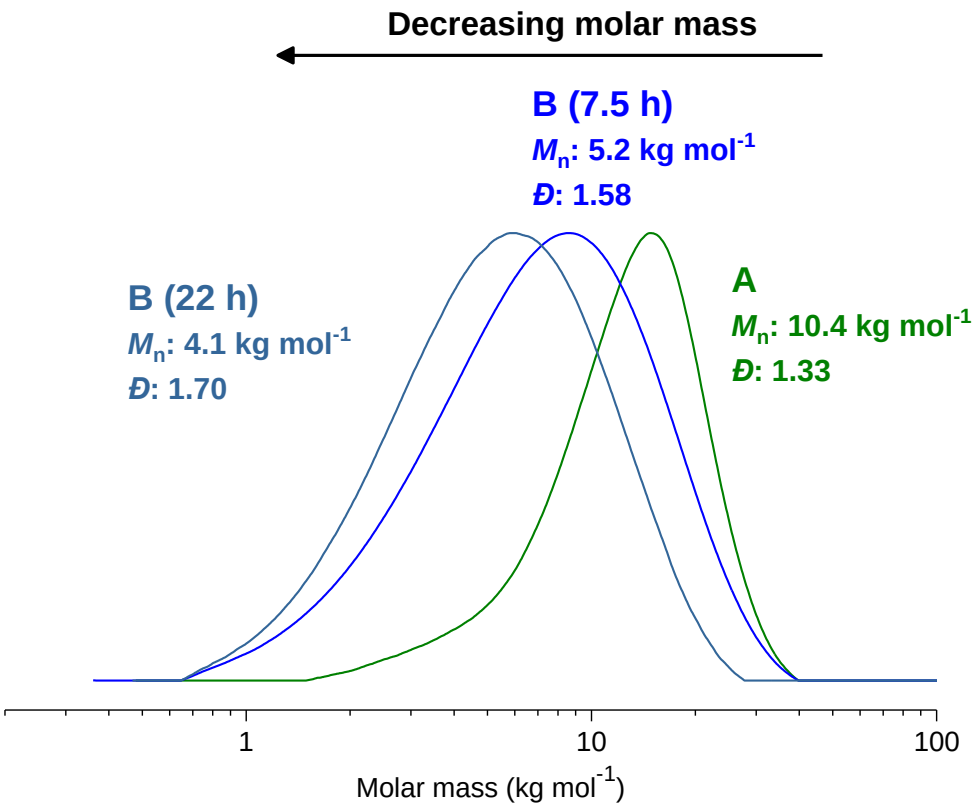


Figure 2.23 SEC traces illustrating the decrease of M_n and increase in $Đ$ as the polymerization progresses through stages **A** (ROP of lactide) and **B** (ROCOP of CO_2/epoxide) in the terpolymerization of L-LA/CO_2/CHO (calibrated using narrow dispersity polystyrene standards).

2.8. **Summary & Future work**

In summary, switchable catalysis is demonstrated using mixtures of four monomers to selectively produce pentablock copolymers. The method applies a single catalyst in one pot to yield hydroxyl-telechelic pentablocks. Fundamentally, the catalyst accesses three different polymerization cycles and switches mechanism twice. Overall, the work demonstrates the high selectivity and complexity of block structures that can be delivered using switchable catalysis. More generally, it should be applicable to other catalysts and monomer combinations. Applications for the new pentablock polyols in areas such as semi-renewable coatings, cross-linked resins and polyurethane manufacture are recommended.[36] Finally, the switchable catalysis is expected to enable variation in polymer composition, block volume fraction and molar mass producing new thermoplastic elastomers, toughened plastics and even functionalized medical materials.

The use of lactide in related switch catalysis showed a reversal in the monomer insertion order between lactide and CO_2. However, the formation of block polymer was hindered by the tendency of **1** to transesterify PLA. If the reaction conditions or catalyst selection for LA ROP could be optimised, a one pot switch catalysis to prepare pentablocks may be achieved.

Future work should target more active catalysts, particularly for the ROCOP processes to enable higher molecular weight pentablocks. Such usage would support the formation of higher molar mass multiblock polymers and facilitate better phase separation. Whilst the nature of the phase separation process and the phase diagram for diblock and triblock copolymers are fairly well researched and understood[37-42],

pentablock copolymers remain as novel materials that necessitate study on the their phase separation behaviour. Such examination would allow for a better understanding of these materials and their possible applications.

2.9. **References**

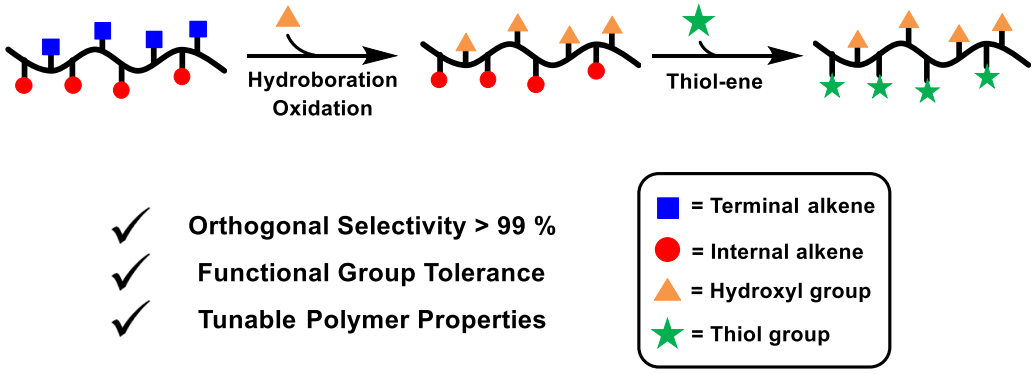
1. Zhu, Y. Q.; Romain, C.; Williams, C. K., Sustainable polymers from renewable resources. *Nature* **2016,** *540*, 354-362.
2. Longo, J. M.; Sanford, M. J.; Coates, G. W., Ring-Opening Copolymerization of Epoxides and Cyclic Anhydrides with Discrete Metal Complexes: Structure-Property Relationships. *Chem. Rev.* **2016,** *116*, 15167-15197.
3. Paul, S.; Zhu, Y. Q.; Romain, C.; Brooks, R.; Saini, P. K.; Williams, C. K., Ring-opening copolymerization (ROCOP): synthesis and properties of polyesters and polycarbonates. *Chem. Commun.* **2015,** *51*, 6459-6479.
4. Guillaume, S. M.; Kirillov, E.; Sarazin, Y.; Carpentier, J. F., Beyond Stereoselectivity, Switchable Catalysis: Some of the Last Frontier Challenges in Ring-Opening Polymerization of Cyclic Esters. *Chem. - Eur. J.* **2015,** *21*, 7988-8003.
5. Jeske, R. C.; Rowley, J. M.; Coates, G. W., Pre-rate-determining selectivity in the terpolymerization of epoxides, cyclic anhydrides, and CO2: A one-step route to diblock copolymers. *Angew. Chem. Int. Ed.* **2008,** *47*, 6041-6044.
6. Broderick, E. M.; Guo, N.; Vogel, C. S.; Xu, C. L.; Sutter, J.; Miller, J. T.; Meyer, K.; Mehrkhodavandi, P.; Diaconescu, P. L., Redox Control of a Ring-Opening Polymerization Catalyst. *J. Am. Chem. Soc.* **2011,** *133*, 9278-9281.
7. Aida, T.; Sanuki, K.; Inoue, S., Well-Controlled Polymerization by Metalloporphyrin - Synthesis of Copolymer with Alternating Sequence and Regulated Molecular-Weight from Cyclic Acid Anhydride and Epoxide Catalyzed by the System of Aluminum Porphyrin Coupled with Quaternary Organic Salt. *Macromolecules* **1985,** *18*, 1049-1055.
8. Kroger, M.; Folli, C.; Walter, O.; Doring, M., Alternating copolymerization of carbon dioxide and cyclohexene oxide and their terpolymerization with lactide catalyzed by zinc complexes of N,N ligands. *Adv. Synth. Catal.* **2006,** *348*, 1908-1918.
9. Romain, C.; Williams, C. K., Chemoselective Polymerization Control: From Mixed-Monomer Feedstock to Copolymers. *Angew. Chem. Int. Ed.* **2014,** *53*, 1607-1610.
10. Wu, G. P.; Darensbourg, D. J.; Lu, X. B., Tandem Metal-Coordination Copolymerization and Organocatalytic Ring-Opening Polymerization via Water To Synthesize Diblock Copolymers of Styrene Oxide/CO2 and Lactide. *J. Am. Chem. Soc.* **2012,** *134*, 17739-17745.
11. Darensbourg, D. J.; Wu, G. P., A One-Pot Synthesis of a Triblock Copolymer from Propylene Oxide/Carbon Dioxide and Lactide: Intermediacy of Polyol Initiators. *Angew. Chem. Int. Ed.* **2013,** *52*, 10602-10606.
12. Paul, S.; Romain, C.; Shaw, J.; Williams, C. K., Sequence Selective Polymerization Catalysis: A New Route to ABA Block Copoly(ester-b-carbonate-b-ester). *Macromolecules* **2015,** *48*, 6047-6056.
13. Romain, C.; Zhu, Y. Q.; Dingwall, P.; Paul, S.; Rzepa, H. S.; Buchard, A.; Williams, C. K., Chemoselective Polymerizations from Mixtures of Epoxide, Lactone, Anhydride, and Carbon Dioxide. *J. Am. Chem. Soc.* **2016,** *138*, 4120-4131.
14. Zhu, Y.; Romain, C.; Williams, C. K., Selective Polymerization Catalysis: Controlling the Metal Chain End Group to Prepare Block Copolyesters. *J. Am. Chem. Soc.* **2015,** *137*, 12179-12182.
15. Zhu, Y.; Radlauer, M. R.; Schneiderman, D. K.; Shaffer, M. S. P.; Hillmyer, M. A.; Williams, C. K., Multiblock Polyesters Demonstrating High Elasticity and Shape Memory Effects. *Macromolecules* **2018,** *51*, 2466-2475.
16. Romain, C.; Garden, J. A.; Trott, G.; Buchard, A.; White, A. J. P.; Williams, C. K., Di-Zinc-Aryl Complexes: CO2 Insertions and Applications in Polymerisation Catalysis. *Chem. - Eur. J.* **2017,** *23*, 7367-7376.

17. Sanford, M. J.; Van Zee, N. J.; Coates, G. W., Reversible-deactivation anionic alternating ring-opening copolymerization of epoxides and cyclic anhydrides: access to orthogonally functionalizable multiblock aliphatic polyesters. *Chem. Sci.* **2018,** *9*, 134-142.
18. Van Zee, N. J.; Coates, G. W., Alternating Copolymerization of Propylene Oxide with Biorenewable Terpene-Based Cyclic Anhydrides: A Sustainable Route to Aliphatic Polyesters with High Glass Transition Temperatures. *Angew. Chem. Int. Ed.* **2015,** *54*, 2665-2668.
19. Saini, P. K.; Fiorani, G.; Mathers, R. T.; Williams, C. K., Zinc versus Magnesium: Orthogonal Catalyst Reactivity in Selective Polymerizations of Epoxides, Bio-derived Anhydrides and Carbon Dioxide. *Chem. - Eur. J.* **2017,** *23*, 4260-4265.
20. Jutz, F.; Buchard, A.; Kember, M. R.; Fredriksen, S. B.; Williams, C. K., Mechanistic Investigation and Reaction Kinetics of the Low-Pressure Copolymerization of Cyclohexene Oxide and Carbon Dioxide Catalyzed by a Dizinc Complex. *J. Am. Chem. Soc.* **2011,** *133*, 17395-17405.
21. Zhu, Y. Q.; Romain, C.; Poirier, V.; Williams, C. K., Influences of a Dizinc Catalyst and Bifunctional Chain Transfer Agents on the Polymer Architecture in the Ring-Opening Polymerization of epsilon-Caprolactone. *Macromolecules* **2015,** *48*, 2407-2416.
22. Stosser, T.; Chen, T. T. D.; Zhu, Y.; Williams, C. K., 'Switch' catalysis: from monomer mixtures to sequence-controlled block copolymers. *Philos. Trans. Royal Soc. A* **2018,** *376*.
23. Saini, P. K.; Romain, C.; Zhu, Y. Q.; Williams, C. K., Di-magnesium and zinc catalysts for the copolymerization of phthalic anhydride and cyclohexene oxide. *Polym. Chem.* **2014,** *5*, 6068-6075.
24. Schneiderman, D. K.; Hillmyer, M. A., Aliphatic Polyester Block Polymer Design. *Macromolecules* **2016,** *49*, 2419-2428.
25. Darensbourg, D. J.; Tsai, F. T., Postpolymerization Functionalization of Copolymers Produced from Carbon Dioxide and 2-Vinyloxirane: Amphiphilic/Water-Soluble CO2-Based Polycarbonates. *Macromolecules* **2014,** *47*, 3806-3813.
26. Darensbourg, D. J.; Chung, W. C.; Arp, C. J.; Tsai, F. T.; Kyran, S. J., Copolymerization and Cycloaddition Products Derived from Coupling Reactions of 1,2-Epoxy-4-cyclohexene and Carbon Dioxide. Postpolymerization Functionalization via Thiol-Ene Click Reactions. *Macromolecules* **2014,** *47*, 7347-7353.
27. Li, C. L.; van Berkel, S.; Sablong, R. J.; Koning, C. E., Post-functionalization of fully biobased poly(limonene carbonate)s: Synthesis, characterization and coating evaluation. *Eur. Polym. J.* **2016,** *85*, 466-477.
28. Hauenstein, O.; Agarwal, S.; Greiner, A., Bio-based polycarbonate as synthetic toolbox. *Nat. Commun.* **2016,** *7*.
29. Han, B.; Zhang, L.; Liu, B. Y.; Dong, X. F.; Kim, I.; Duan, Z. Y.; Theato, P., Controllable Synthesis of Stereoregular Polyesters by Organocatalytic Alternating Copolymerizations of Cyclohexene Oxide and Norbornene Anhydrides. *Macromolecules* **2015,** *48*, 3431-3437.
30. Hoyle, C. E.; Bowman, C. N., Thiol–Ene Click Chemistry. *Angew. Chem. Int. Ed.* **2010,** *49*, 1540-1573.
31. Cho, S.; Heo, G. S.; Khan, S.; Gonzalez, A. M.; Elsabahy, M.; Wooley, K. L., Functionalizable Hydrophilic Polycarbonate, Poly(5-methyl-5-(2-hydroxypropyl)aminocarbonyl-1,3-dioxan-2-one), Designed as a Degradable Alternative for PHPMA and PEG. *Macromolecules* **2015,** *48*, 8797-8805.
32. von der Assen, N.; Bardow, A., Life cycle assessment of polyols for polyurethane production using CO2 as feedstock: insights from an industrial case study. *Green Chem.* **2014,** *16*, 3272-3280.

33. Hillmyer, M. A.; Tolman, W. B., Aliphatic Polyester Block Polymers: Renewable, Degradable, and Sustainable. *Acc. Chem. Res.* **2014,** *47*, 2390-2396.
34. Myers, D.; White, A. J. P.; Forsyth, C. M.; Bown, M.; Williams, C. K., Phosphasalen Indium Complexes Showing High Rates and Isoselectivities in rac-Lactide Polymerizations. *Angew. Chem. Int. Ed.* **2017,** *56*, 5277-5282.
35. Van Zee, N. J.; Sanford, M. J.; Coates, G. W., Electronic Effects of Aluminum Complexes in the Copolymerization of Propylene Oxide with Tricyclic Anhydrides: Access to Well-Defined, Functionalizable Aliphatic Polyesters. *J. Am. Chem. Soc.* **2016,** *138*, 2755-2761.
36. Stosser, T.; Li, C. L.; Unruangsri, J.; Saini, P. K.; Sablong, R. J.; Meier, M. A. R.; Williams, C. K.; Koning, C., Bio-derived polymers for coating applications: comparing poly(limonene carbonate) and poly (cyclohexadiene carbonate). *Polym. Chem.* **2017,** *8*, 6099-6105.
37. Bailer, J.; Feth, S.; Bretschneider, F. A.; Rosenfeldt, S.; Drechsler, M.; Abetz, V.; Schmalz, H.; Greiner, A., Synthesis and self-assembly of biobased poly(limonene carbonate)-block-poly(cyclohexene carbonate) diblock copolymers prepared by sequential ring-opening copolymerization. *Green Chem.* **2019**.
38. Jang, J.; Park, H.; Jeong, H.; Mo, E.; Kim, Y.; Yuk, J. S.; Choi, S. Q.; Kim, Y. W.; Shin, J., Thermoset elastomers covalently crosslinked by hard nanodomains of triblock copolymers derived from carvomenthide and lactide: tunable strength and hydrolytic degradability. *Polym. Chem.* **2019,** *10*, 1245-1257.
39. Schneiderman, D. K.; Hill, E. M.; Martello, M. T.; Hillmyer, M. A., Poly(lactide)-block-poly(epsilon-caprolactone-co-epsilon-decalactone)-block-poly(lactide) copolymer elastomers. *Polym. Chem.* **2015,** *6*, 3641-3651.
40. Stuparu, M. C.; Khan, A.; Hawker, C. J., Phase separation of supramolecular and dynamic block copolymers. *Polym. Chem.* **2012,** *3*, 3033-3044.
41. Yuan, R. C.; Fan, S.; Wu, D. Q.; Wang, X. L.; Yu, J. Y.; Chen, L. J.; Li, F. X., Facile synthesis of polyamide 6 (PA6)-based thermoplastic elastomers with a well-defined microphase separation structure by melt polymerization. *Polym. Chem.* **2018,** *9*, 1327-1336.
42. Bates, F. S., Polymer-Polymer Phase-Behavior. *Science* **1991,** *251*, 898-905.

Chapter 3

Orthogonal Functionalization of Alternating Polyesters: Selective Patterning of $(AB)_n$ Sequences



A series of AB alternating polyesters are orthogonally patterned to install two different functionalities at regular intervals along the backbone and with high precision.

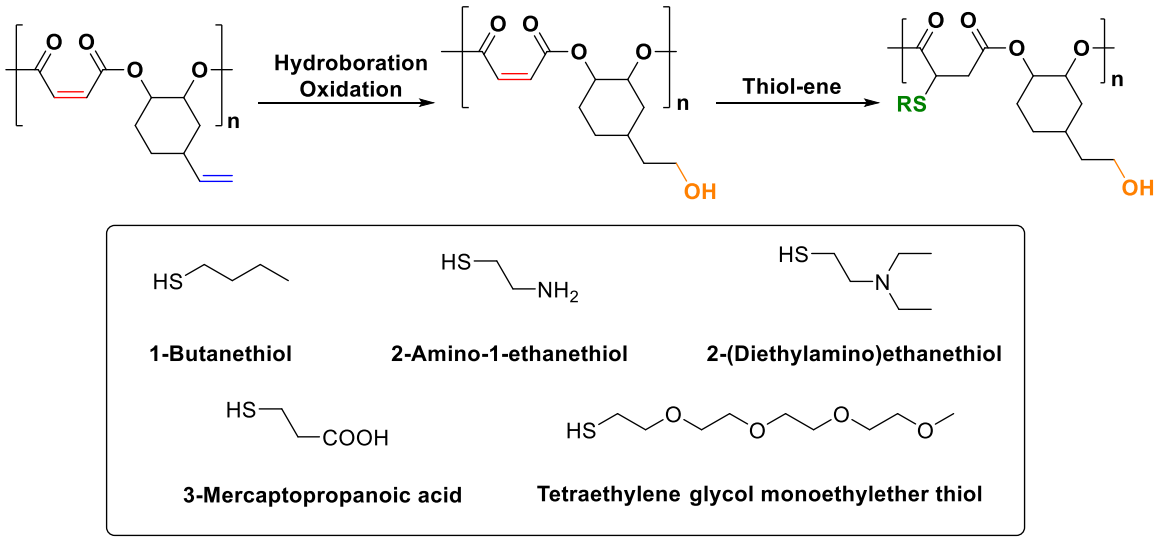
3.1. **Introduction**

The selective placement of functional side chains on a polymer backbone is a key target in polymer chemistry as these materials have been shown to display unprecedented spatial orientation that can lead to novel properties such as self-assembly.[1-2] In particular, orthogonal methodologies that can afford polymers with multiple functionalities remains as one of the key challenges today.[3] Precisely functionalized polyesters are currently very rare as they are generally more challenging to prepare.[4-7] As such, facile orthogonal post-functionalization methods that are widely applicable would greatly accelerate the synthesis of functional polyesters and expand the range of novel materials that can be prepared.

Alkene hydroboration-oxidation is an efficient means to install hydroxyl substituents. It is an interesting reaction in the context of orthogonal post-polymerization functionalization of polyesters as it is compatible with ester linkages, as demonstrated by its use in post-polymerization of functionalized polyhydroxyalkanoates.[8-12] Furthermore, Brown *et al*. showed that the hydroboration of vinyl (terminal) alkenes exhibited a rate enhancement of up to three orders of magnitude when compared to disubstituted (internal) alkenes using bulky boron containing reagents.[13-15] Thus, it is reasoned that polyesters with terminal and internal alkene functionalities would also display a difference in the alkene hydroboration rate and react faster at the terminal C=C double bonds. The hydroborated intermediary species can then be oxidized to afford hydroxyl substituents whilst leaving the internal alkene unaffected and available for further transformations. It is proposed that hydroboration oxidation applied to polymers where there is precise positioning of

terminal alkene substituents, such as in AB sequence alternating polyesters made from ROCOP could enable precisely functionalized AB polyesters.

Previously, Dr. Ni Yi demonstrated the successful synthesis of a dual-functional polyester based on maleic anhydride (MA) and vinyl cyclohexene oxide (VCHO).[16] The procedure applies the polyester precursor prepared by ROCOP, which features internal and vinyl alkene groups. Next, a novel sequential post-polymerization functionalization method involves first a hydroboration-oxidation and thiol-ene reaction, using a range of different thiols (Scheme 3.1). This work is the first proof of principle that an alternating functionalized AB polymer is feasible. Nonetheless, it is very important to establish whether this method is generally applicable to other polymers.



Scheme 3.1 Dual-functionalized polyester synthesis through sequential hydroboration-oxidation and thiol-ene coupling reactions (as demonstrated by Dr. Ni Yi).

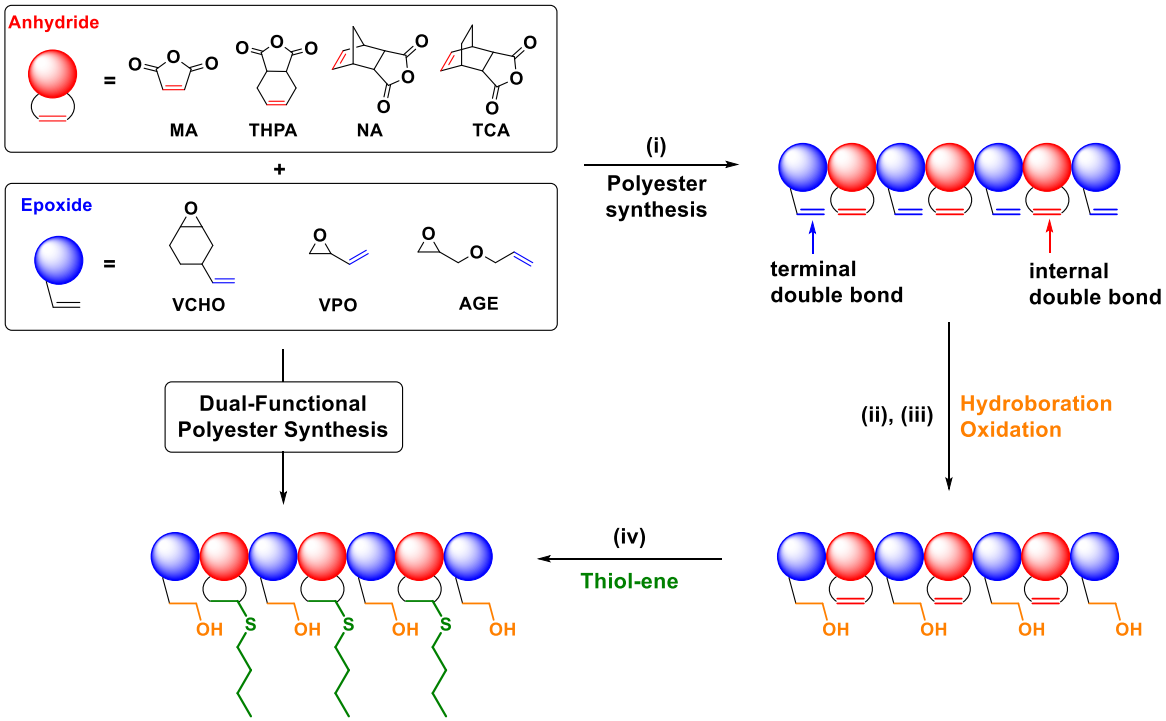
3.2. **Aims**

An orthogonal post-polymerization functionalization methodology that can be used to install two distinct functionalities on to polyesters needs to be proven for a range of polyesters (Scheme 3.2). To achieve this aim, there are three objectives to accomplish:

First, a range of alternating polyesters with AB-alternating internal and terminal C=C double bonds need to be synthesized. Epoxides and anhydrides featuring alkene functionalities will be used in ROCOP reactions, fortunately many of these monomers are commercially available. Monocyclic, bicyclic and tricyclic anhydrides will be employed to test their affects on reaction selectivity.

Second, the alkene hydroboration selectivity will be monitored using *in*-situ ^{1}H NMR spectroscopy to establish that the terminal alkene reacts preferentially for all polyester samples, leaving the internal alkene unreacted. 9-Borabicyclo[3.3.1]nonane (9-BBN), a sterically hindered borane reagent, will be employed in order to maximize the selectivity for the terminal alkene. Following the hydroboration, an oxidation step will be employed to afford hydroxyl-functionalised polyesters (with internal alkenes intact).

Finally, the hydroxyl-functionalized polyesters will be further reacted at the internal alkene group, using thiol-ene coupling reactions, to obtain dual-functional polyesters. In particular, hydrophobic alkyl chains are of interest as polymers with alternating hydrophobic/hydrophilic groups have been shown to self-assemble in solution to form new nanostructures.[17-18]



Scheme 3.2 Selective synthesis of orthogonal functionalization of dual-functional alternating polyesters Reagents and Conditions: (i) : [SalcyCrCl]/PPNCl/1,2-Cyclohexane diol (CHD)/anhydride/epoxide = 1/1/10/100/120, 60 °C, $[anhydride]_0$ = 5 M in toluene. (ii): $[alkene]_0$/[9-BBN] = 1/1.5, 9-BBN, 1.5 h, 25 °C, $[_{alkene}]_0$ = 0.03 M in THF. (iii): $[alkene]_0$/[mCPBA] = 1/5.1, mCPBA, 2 h; 25 °C. (iv): [DMPA]/$[alkene]_0$/[thiol] = 1/2.5/10, DMPA, thiol, DMSO, UV irradiation at 365 nm (10W), 2 h, $[alkene]_0$ = 0.25 M.

3.3. **Polyester synthesis**

A series of 9 alternating polyesters (**P5 – P13**) were synthesized through ROCOP of alkene functionalized epoxides and anhydrides (Fig. 3.1). The epoxides (vinyl-cyclohexene oxide (VCHO), vinyl-propylene oxide (VPO) and allyl glycidyl ether (AGE)) all feature terminal alkene groups, whilst all the anhydrides feature internal alkenes either in maleic anhydride (MA), tetrahydro phthalic anhydride (THPA), norbonene anhydride (NA) or a tricyclic anhydride (TCA).

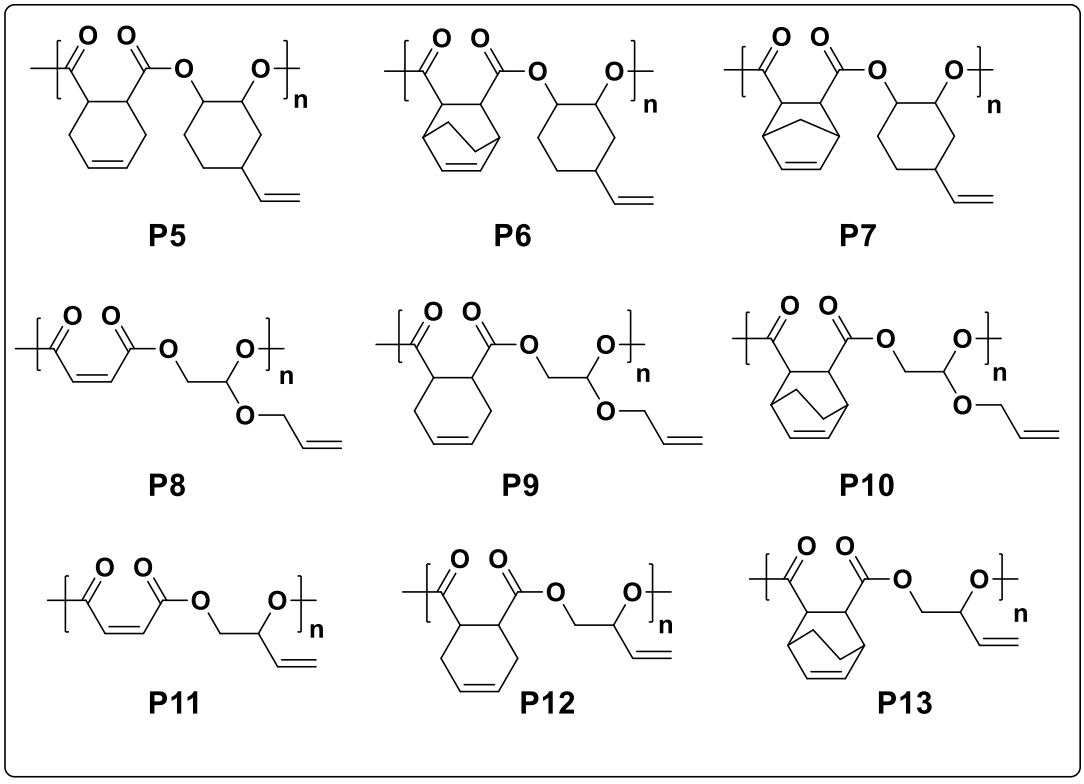


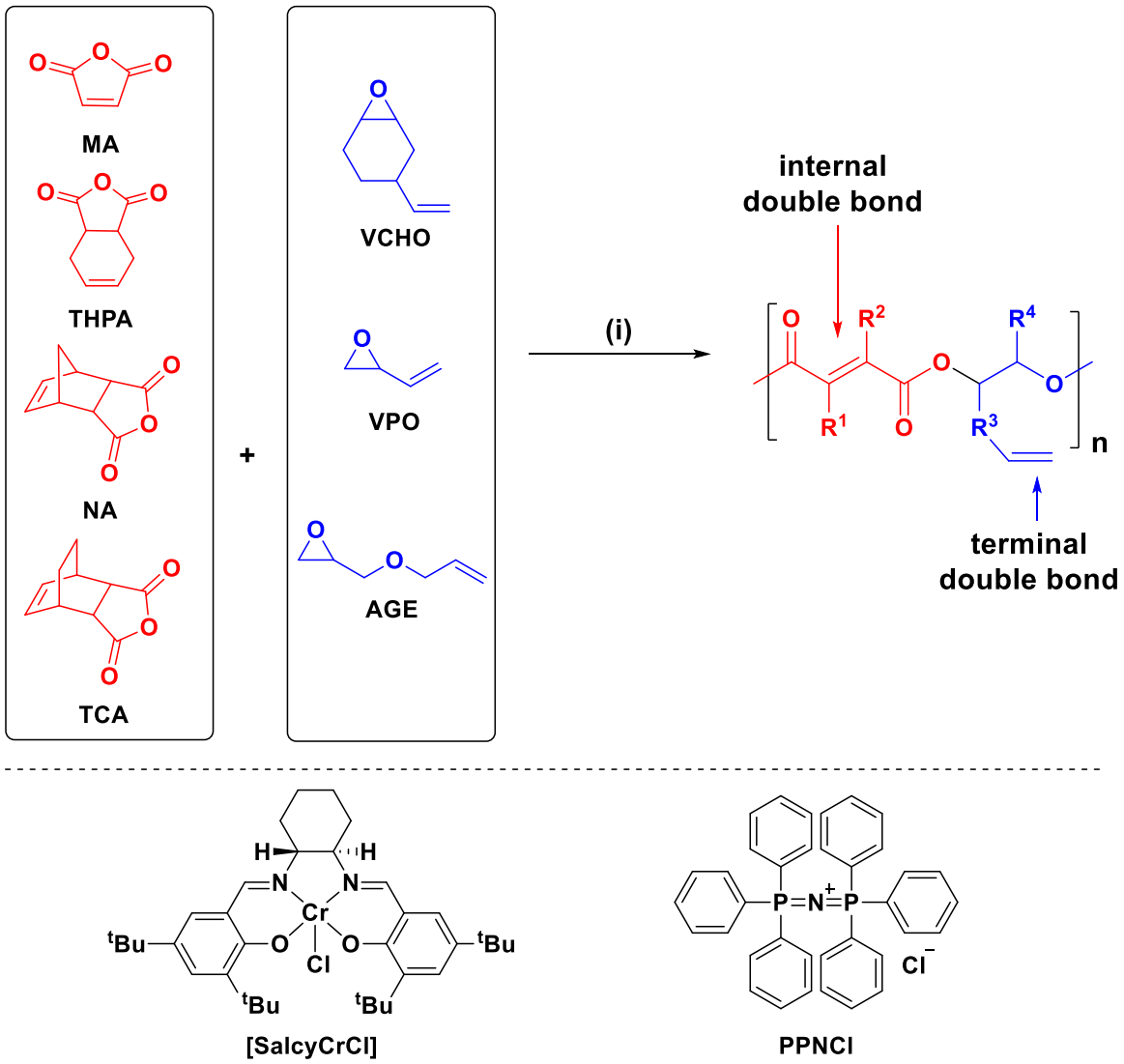
Figure 3.1 Structures of the alternating polyesters **P5 – P13**, all featuring internal and terminal alkene functionalities.

The ROCOP reactions were catalysed by a Cr(III) complex, [SalcyCrCl], in combination with an equimolar quantity of bis(triphenylphosphine)iminium chloride (PPNCl) (Scheme 3.3, see Experimental section for detailed experimental protocols, Table 3.1). This catalyst system was selected due to its good activity, substrate scope and selectivity.[19-21] The catalyst system also results in living polymerizations and is amenable to the use of chain transfer agents. 1,2-Cyclohexanediol (CHD) is added as the chain transfer agent (10 molar equivalents CHD vs. [SalcyCrCl]) to control the polymer composition and ensure formation of monomodal molar mass distributions of hydroxyl telechelic chains (Table 3.1). [22-23]

Table 3.1. Composition and Properties of **P5**-**P13**.

#	Epoxide	Anhydride	Time (h)	Conv. (%)[a]	M_n (kg mol^{-1}) [$Đ$][b]	T_g (^{o}C)[c]
P5	VCHO	THPA	15	80	2.9 [1.11]	80
P6	VCHO	TCA	15	>99	5.6 [1.16]	117
P7	VCHO	NA	18	>99	3.3 [1.14]	107
P8	VPO	MA	46	80	1.5 [1.30]	-27
P9	VPO	THPA	33	90	3.3 [1.18]	14
P10	VPO	TCA	19	>99	2.9 [1.18]	56
P11	AGE	MA	12	>99	4.9 [1.13]	-28
P12	AGE	THPA	6.0	>99	3.2 [1.18]	1
P13	AGE	TCA	3.5	>99	3.6 [1.14]	23

Polymerization conditions: 60 °C, molar ratio: [SalcyCrCl]/PPNCl/CHD/anhydride/epoxide = 1/1/10/100/120, [anhydride] = 5M in toluene. [a]conversions were obtained from ^{1}H NMR spectra [b]M_n and $Đ$ were measured by SEC (THF as eluent, 1 mL/min, 30 °C) calibrated using polystyrene standards. [c]T_g were obtained from DSC (third heating cycle)



Scheme 3.3 ROCOP of epoxide/anhydride using [SalcyCrCl] and PPNCl. (i): [SalcyCrCl], PPNCl, 60 °C, toluene, molar ratio: [SalcyCrCl]/PPNCl/CHD/anhydride/epoxide = 1/1/10/100/120, [anhydride] = 5 M.

The polymerizations were conducted at 60 °C with a molar ratio of [SalcyCrCl]/PPNCl/CHD/anhydride/epoxide = 1/1/10/100/120 in toluene (5M in anhydride). Whilst the polymerizations proceeded at different rates, high conversions were achieved for all 9 alternating polyesters (≥ 80%) (Table 3.1).

Reactions involving VPO and/or MA were noticeably slower due to the lower reactivity of these monomers, perhaps resulting from the reduced ring strain. The crude polyesters were isolated by adding the reaction solution, diluted with methylene chloride, dropwise into hexane. The purified samples were then characterized using various NMR techniques, SEC and DSC. The series **P5** – **P13** all have lower molecular mass values (M_n < 6 kg mol^{-1}) but are all produced with narrow disparities and with monomodal molecular weight distribution. The polymers are all amorphous and show T_g values from -27 – 117 °C, depending on the monomers used (Table 3.1). Considering the ^{1}H NMR spectrum of **P5** as a representative example (Fig. 3.2), only signals for an alternating polyester structure, with no ether linkages was observed. This was evidenced by a lack of signals at 3.50 ppm and the spectrum clearly shows both the internal and terminal alkenes, at 5.80 (peak 'M') and 5.65ppm (peak 'E' and 'F'), respectively.

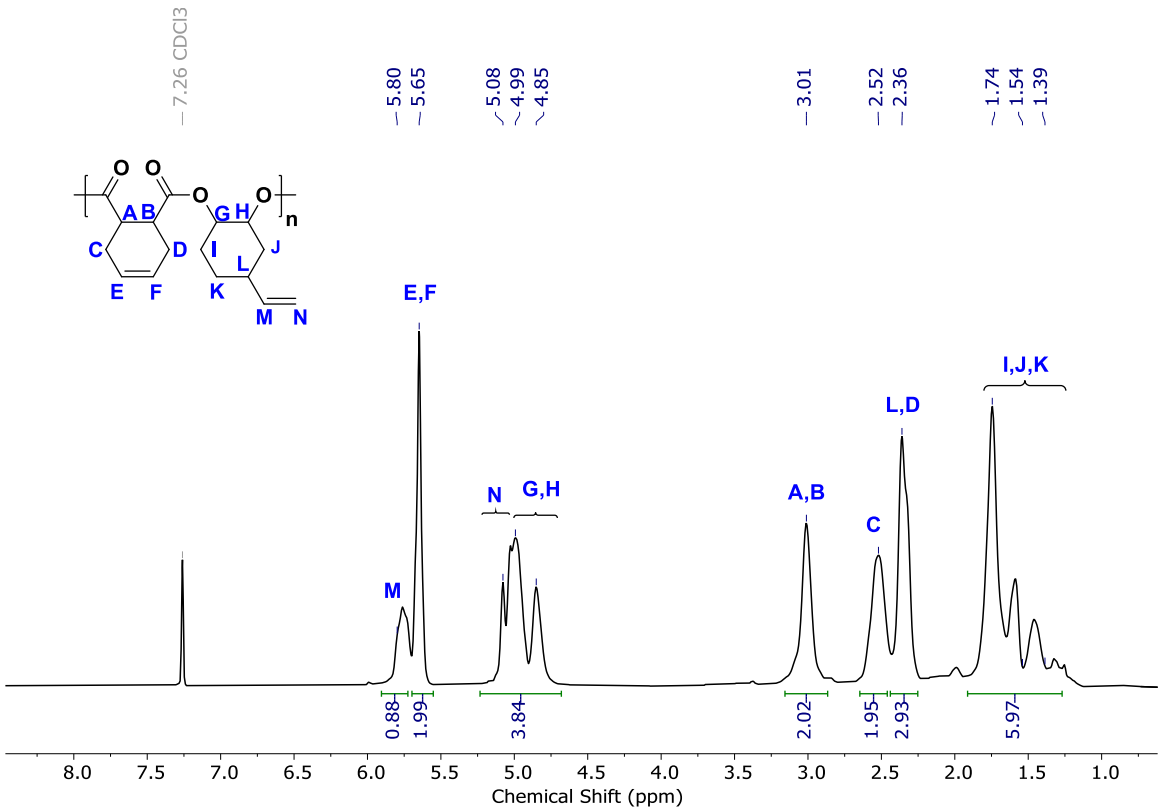


Figure 3.2 ^{1}H NMR spectrum of polymer **P5** ($CDCl_3$, 500.0 MHz, 298 K).

In each case, the ^{1}H NMR spectrum was assigned using a combination of the relative integrals and from the ^{1}H-^{1}H correlations in the 2D COSY NMR spectrum (Fig. 3.3). For instance, the most downfield signal at 5.80 ppm is consistent with an alkene proton region and has a relative integral of 1. This chemical shift also corresponds closely to a signal observed for the VCHO methine proton. Thus, this peak is most likely the methine proton in the terminal alkene (peak 'M' in Fig. 3.2). The 2D COSY NMR shows peak 'M' coupling with a multiplet at 4.99 - 5.08 which suggests the multiplet is assigned to methylene terminal alkene proton (peak 'N' in Fig. 3.2 & correlations highlighted in blue in Fig. 3.3). Peak 'M' also shows a correlation with the peak at 2.36 ppm. This lower chemical shift peak is assigned to a methine proton attached to the

cyclohexane of VCHO (peak 'L' in Fig. 3.2). Furthermore, peak 'L' is correlated with the resonance at 1.74 ppm, which is likely to be peak 'J' or 'K'.

The resonance at 3.01 ppm has a relative integral of 2 and its chemical shift is consistent with an ester signal, which suggests this peak may be either peak 'A + B' or peak 'G + H'. The 2D COSY NMR shows that the resonance at 3.01 ppm couples to resonances at 2.52 and 2.36 ppm (highlighted in green in Fig. 3.3) but does not couple with any signals below 2 ppm. Based on this 2D COSY data, the peak at 3.01 ppm is assigned to protons 'A + B'. This result suggests that the peaks at 2.52 and 2.36 ppm are likely to be peaks 'C + D'. The relative integrals for these peaks are also consistent with this assignment.

The broad peak from 4.85 - 5.99 ppm correlates with resonances below 2 ppm (highlighted in orange in Fig. 3.3), which suggests it is due to methine protons on the VCHO unit (peaks 'G' and 'H'). The peak has a relative integral of 4 which is also in line with the assignment (2 proton due to peaks 'G and 'H' and 2 protons from peak 'N'). Finally, the peak at 5.65 ppm, with a relative integral of 2, is assigned to the internal alkene group (peaks 'E' and 'F' in Fig. 3.2). The ^{1}H NMR spectra for polyesters **P6 – P13** can be found in the Appendix (Fig. S30 – S37).

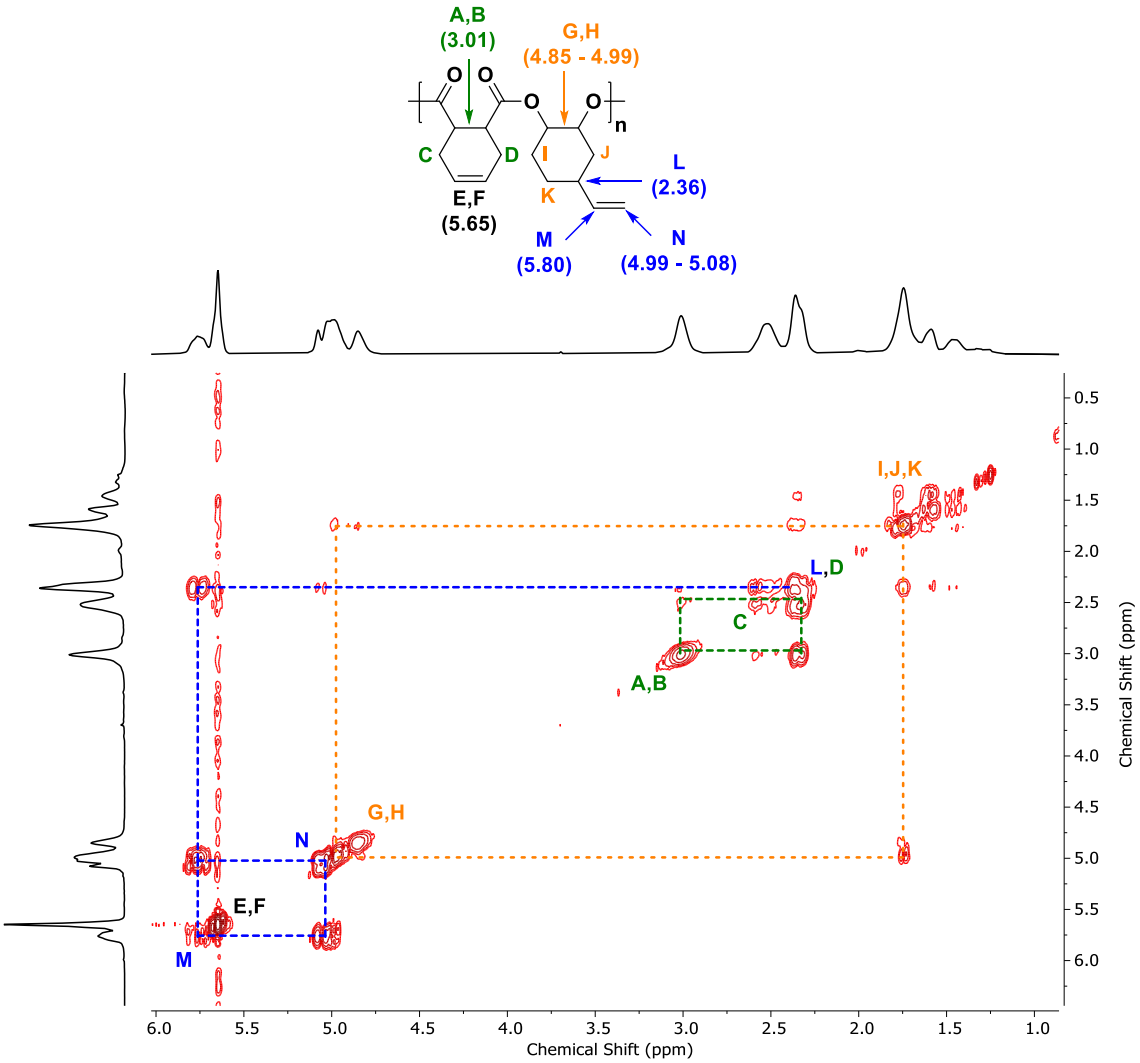


Figure 3.3 ^{1}H-^{1}H COSY NMR spectrum of polymer **P5**. ($CDCl_3$, 500.0 MHz, 298 K). Important chemical shifts are listed in brackets.

The ^{13}C NMR spectrum of **P5** also shows resonances assigned to the maleate and vinyl carbon environments at 141.8 and 130.2 ppm, respectively (Fig. 3.4). Furthermore, the single carbonyl resonance at 172.1 ppm (peaks 'O' and 'P') suggests there is minimal transesterification.

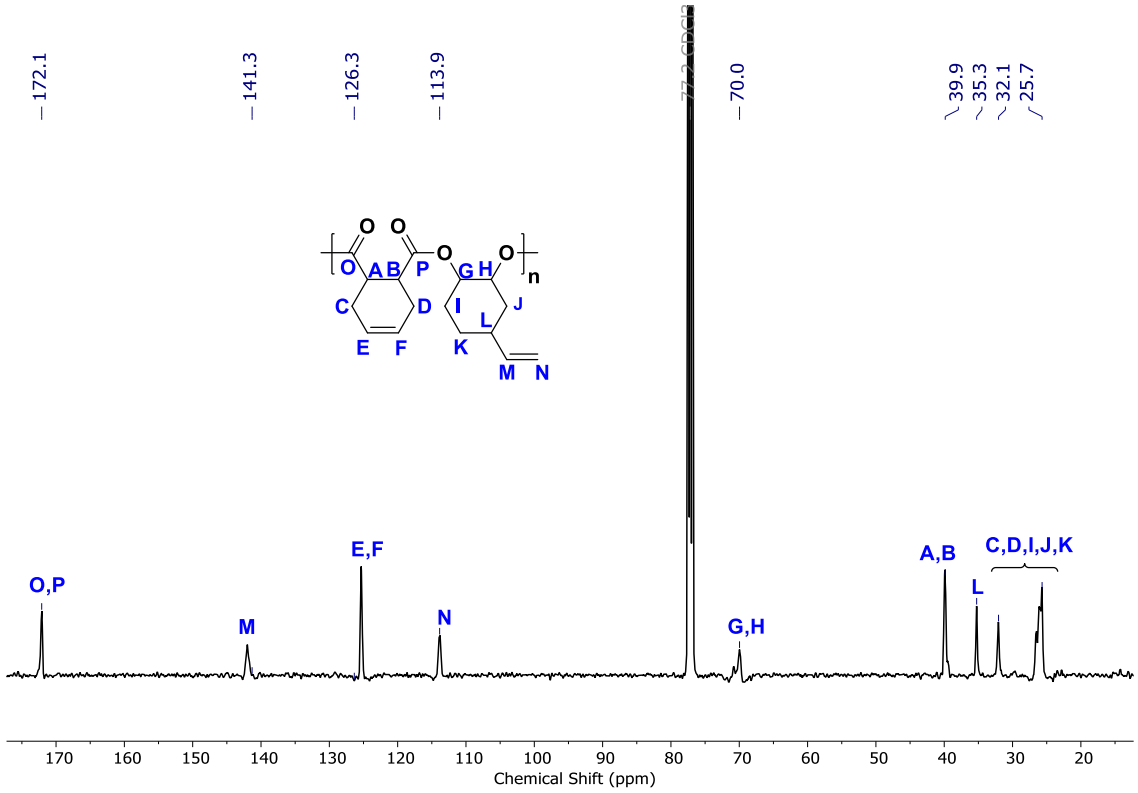


Figure 3.4 $^{13}C\{^{1}H\}$ NMR spectrum of **P5** ($CDCl_3$, 500.0 MHz, 298 K).

The $^{13}C\{^{1}H\}$ NMR spectrum was assigned using 2D ^{1}H-^{13}C HSQC NMR spectroscopy (Fig. 3.5). For instance, the resonance at 141.3 ppm correlates with a resonance at 5.80 ppm in the ^{1}H NMR spectrum assigned to peak 'M'. In a similar fashion, resonances at 126.3, 113.9 and 39.9 ppm are assigned to peaks 'E + F', 'N' and 'A + B' respectively. The resonance at 70.0 ppm is correlated with the broad peak from 4.85 – 4.99 ppm in the ^{1}H NMR spectrum. This is consistent with the protons being attached to carbon atoms in very similar environments. The broad resonance at 2.36 ppm correlates with two carbon environments, suggesting it is due to two overlapping proton environments, assigned to protons 'L' and 'C + D'. The $^{13}C\{^{1}H\}$ NMR spectra for polyesters **P5** – **P13** can be found in the Appendix section (Fig. S38 – S45).

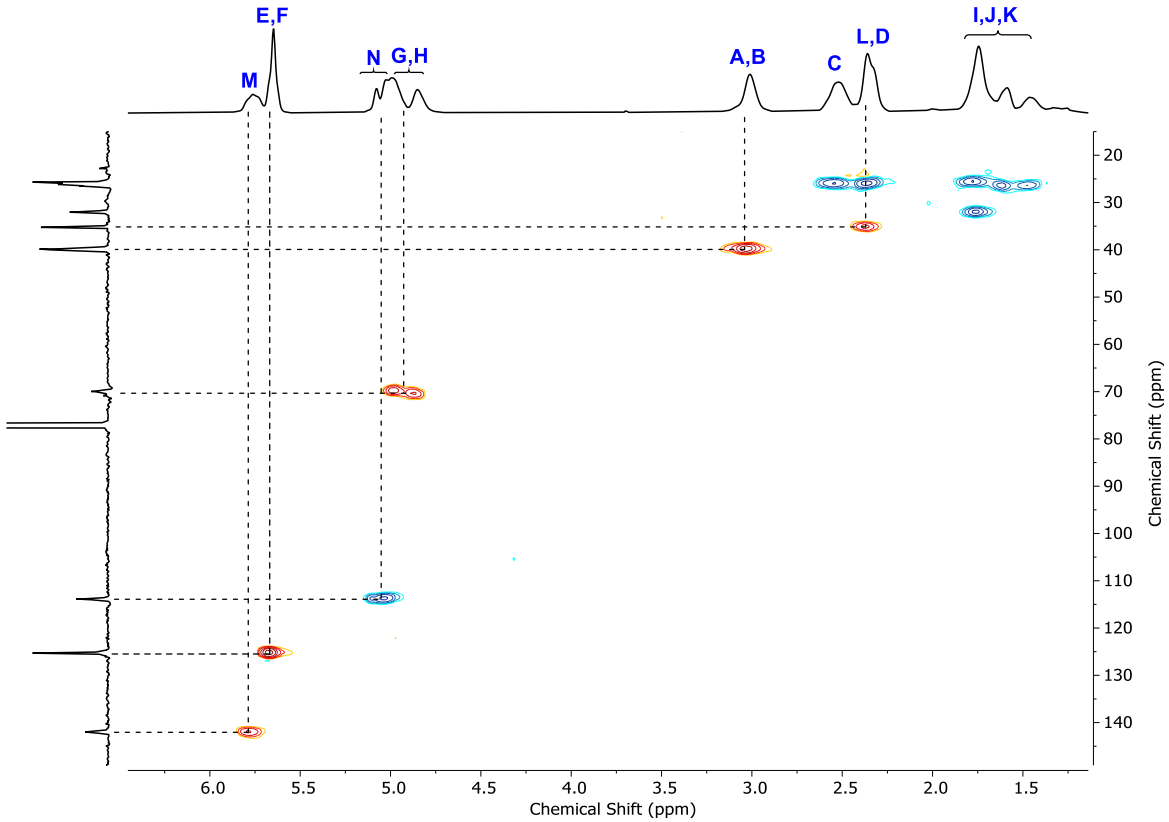
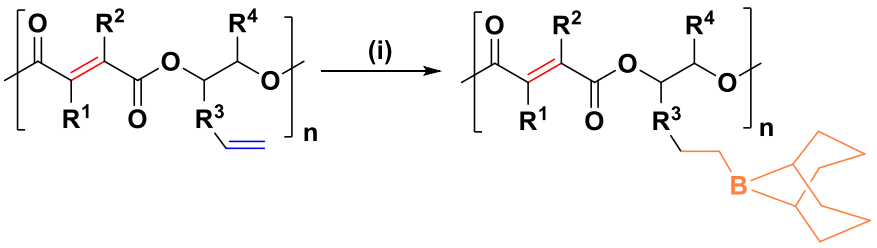


Figure 3.5 ^{13}C-^{1}H HSQC NMR spectrum of **P5** ($CDCl_3$, 500.0 MHz, 298 K).

3.4. **Hydroboration-oxidation of polyesters**

The dual functionalization of polyesters depends upon being able to selectively functionalize the terminal alkene through a hydroboration reaction. As such, for each polymer the extent of this alkene selectivity in the hydroboration reaction was conducted using *in-situ* ^{1}H NMR spectroscopy (Scheme 3.4).



Scheme 3.4 Hydroboration of polyetsers monitored *in-situ* ^{1}H NMR spectroscopy to investigate the internal/terminal alkene selectivity. (i): 9-BBN dimer ([alkene]/[9-BBN] = 1/1.5), 1.5 h, 25 °C, $CDCl_3$ $[alkene]_o$ = 0.03 M, mesitylene used as internal standard.

The reactions were all monitored at 25 °C with relative integrals compared against an internal standard (mesitylene). 9-Borabicyclo(3.3.1)nonane (9-BBN) ([alkene]/[9-BBN] = 1/1.5) was selected as the borane reagent due to its steric hindrance which should increase alkene selectivity.[13, 15] The reactions proceeded with higher selectivity for all but one of the polyesters. For instance, **P5**'s reaction with 9-BBN resulted in the complete consumption of the terminal alkene resonance at 5.80 ppm within 2 h (Fig. 3.6). During this time, the internal alkene resonance at 5.65 ppm remained unchanged.

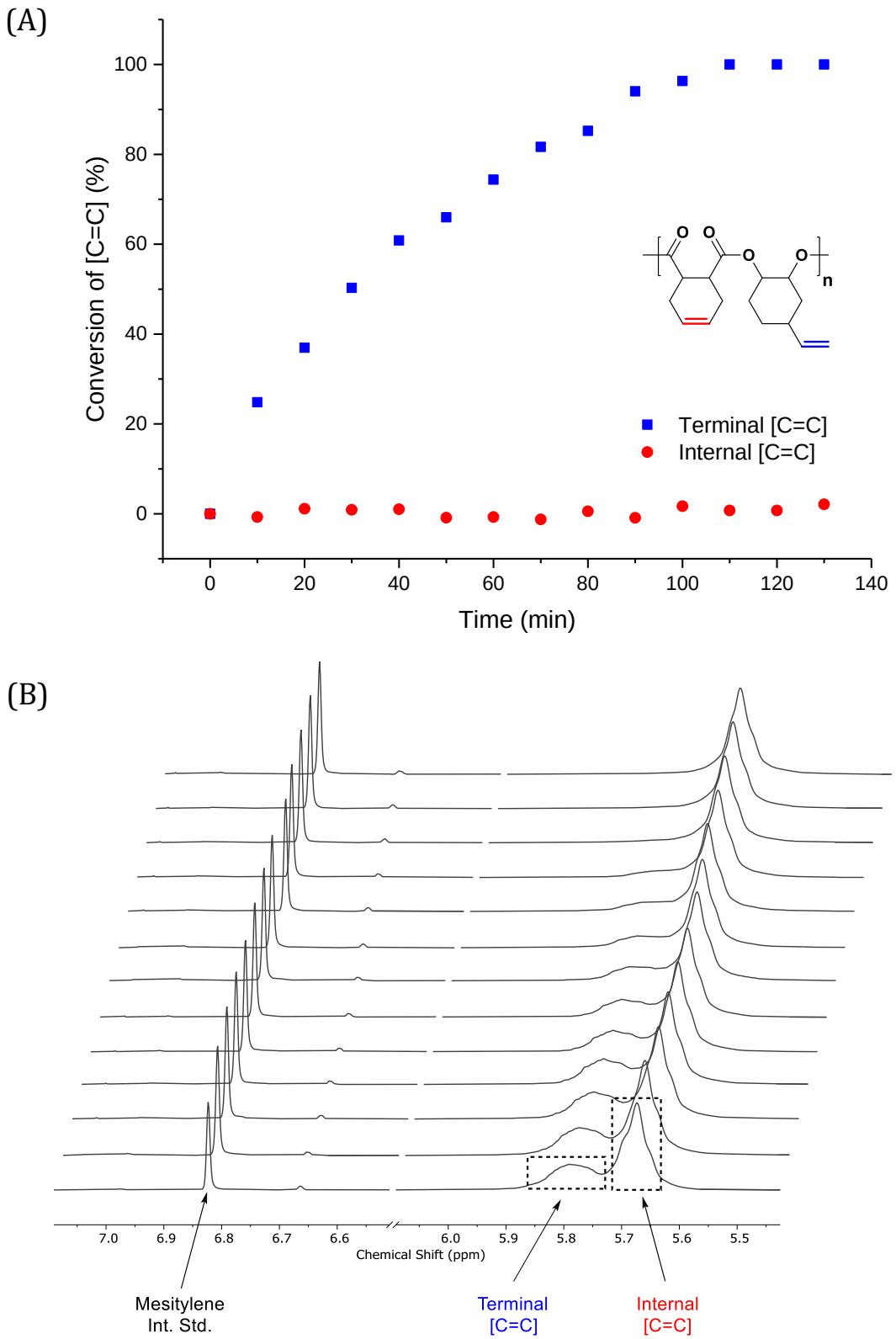


Figure 3.6 (A) Percentage conversion of the two different alkene groups (internal = blue circles and terminal = red squares) vs. time during the hydroboration reaction of **P5** (B) stacked NMR spectra (in $CDCl_3$, mesitylene as internal standard).

The observed selectivity is precisely in line with the earlier alkene hydroboration kinetic investigation which showed that vinyl groups typically react with 9-BBN around 1000 times faster than cyclo-alkenes.[13, 15] A plot of $\ln([C=C]_0/[C=C])$ *vs.* time showed a linear fit, indicative of a first-order dependence of the rate on the concentration of terminal alkene groups. This first order dependence is consistent with the previously proposed hydroboration mechanism (Fig. 3.7).[15]

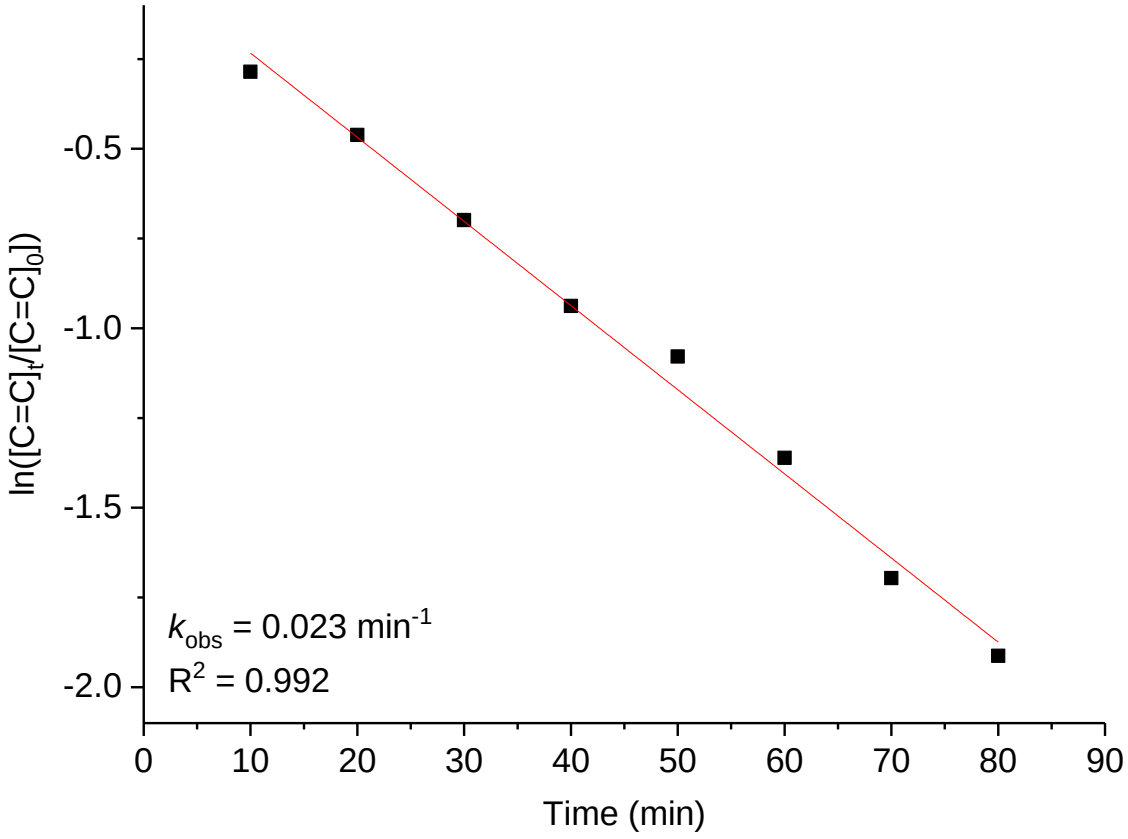


Figure 3.7 Plot of $\ln([C=C]_0/[C=C]_t)$ vs time of terminal alkene groups. Rate = $k[C=C]^1[9\text{-BBN}]^x$, $k_{obs} = k[9\text{-BBN}]^x$.

Whilst the majority of the polyesters investigated showed quantitative terminal alkene selectivity, **P7** does not show this selectivity. When **P7** was subjected to hydroboration with 9-BBN, the *in-situ* ^{1}H NMR spectroscopy experiments suggested that both the internal and terminal alkenes react, albeit at a faster rate for the terminal alkenes (Fig. 3.8).

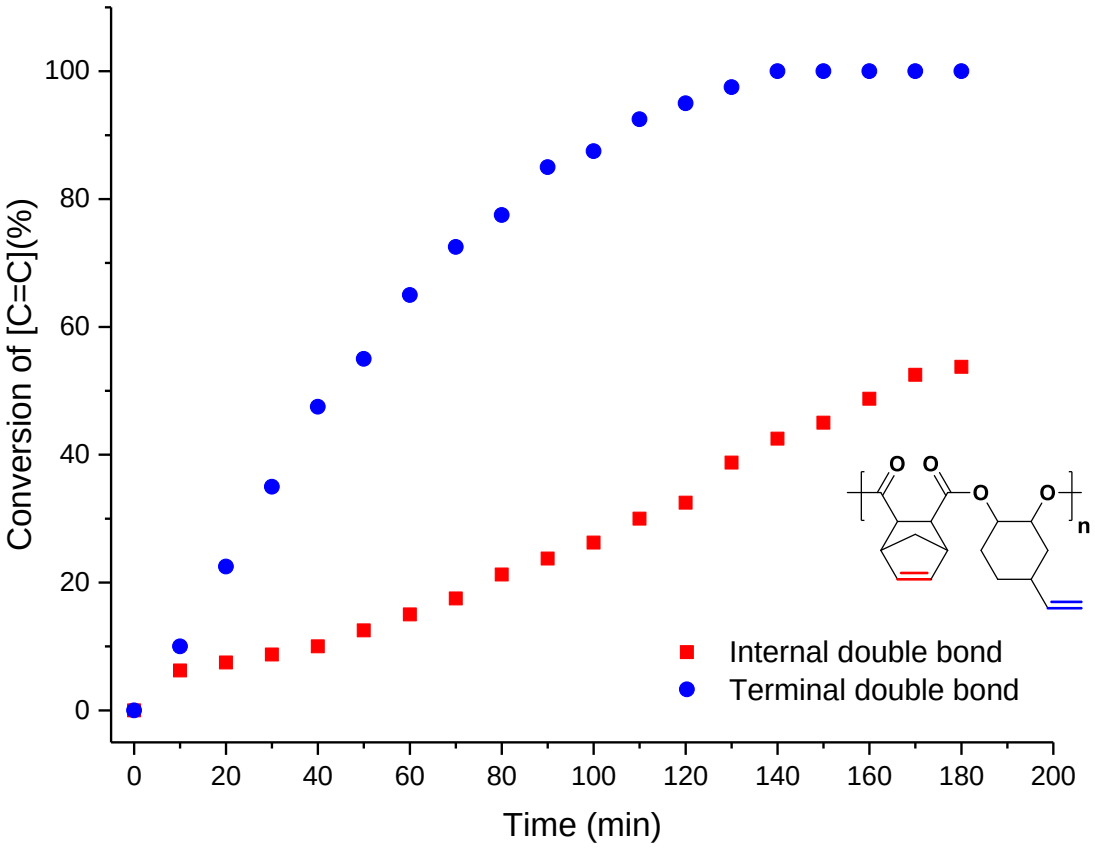
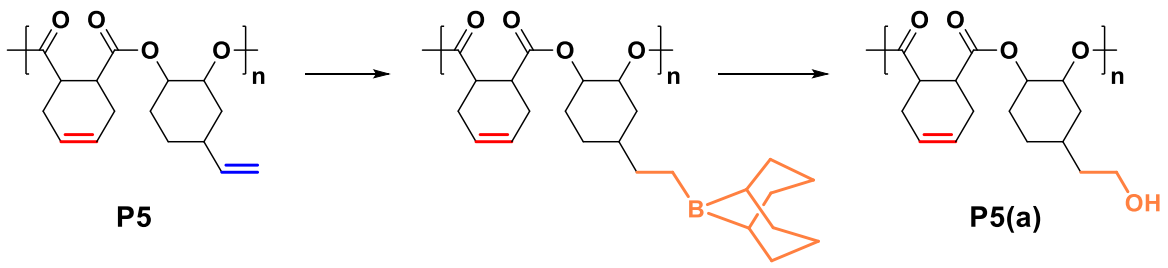


Figure 3.8 Percentage conversion of the two different alkene groups (internal = blue circles and terminal = red squares) vs. time during the hydroboration reaction of **P7**.

A potential reason for this observation may be the enhanced reactivity of the internal alkene unit brought about by the strained norbornene unit. The addition reaction would be expected to reduce the steric strain consistent with this notion is the finding that inverse electron demand Diels-Alder reactions have only been reported using a norborenene unit.[24-25] Notwithstanding the failure for **P7**, the remaining 8 alternating polyesters (**P5-6** and **P8-13**) all show the desired selectivity (see the Appendix for the kinetic plots for the other polyesters, Fig. S46 – S52).

The hydroborated polymers were next reacted with the oxidant, meta-chloroperoxybenzoic acid (mCPBA), to produce a polyester which features alternating primary hydroxyl substituents (ethyl alcohol substituents) (Scheme 3.5).



Scheme 3.5 One-pot hydroboration-oxidation reaction to convert the polyester **P1** terminal alkenes to alternating hydroxyl groups. (i): 9-BBN dimer, 1.5 h, 25 °C, THF (ii): mCPBA, 2 h, 25 °C, THF, molar ratio: $[alkene]_o/[9\text{-}BBN]/[mCPBA] = 1/1.5/5.1$), $[alkene]_o = 0.03$ M in THF.

Using **P5(a)** as an example, ^1H NMR spectrum shows the complete disappearance of signals assigned to the terminal alkene groups and the presence of only the alkene resonances corresponding to the internal double bond (peak 'E' and 'F' in Fig. 3.9).

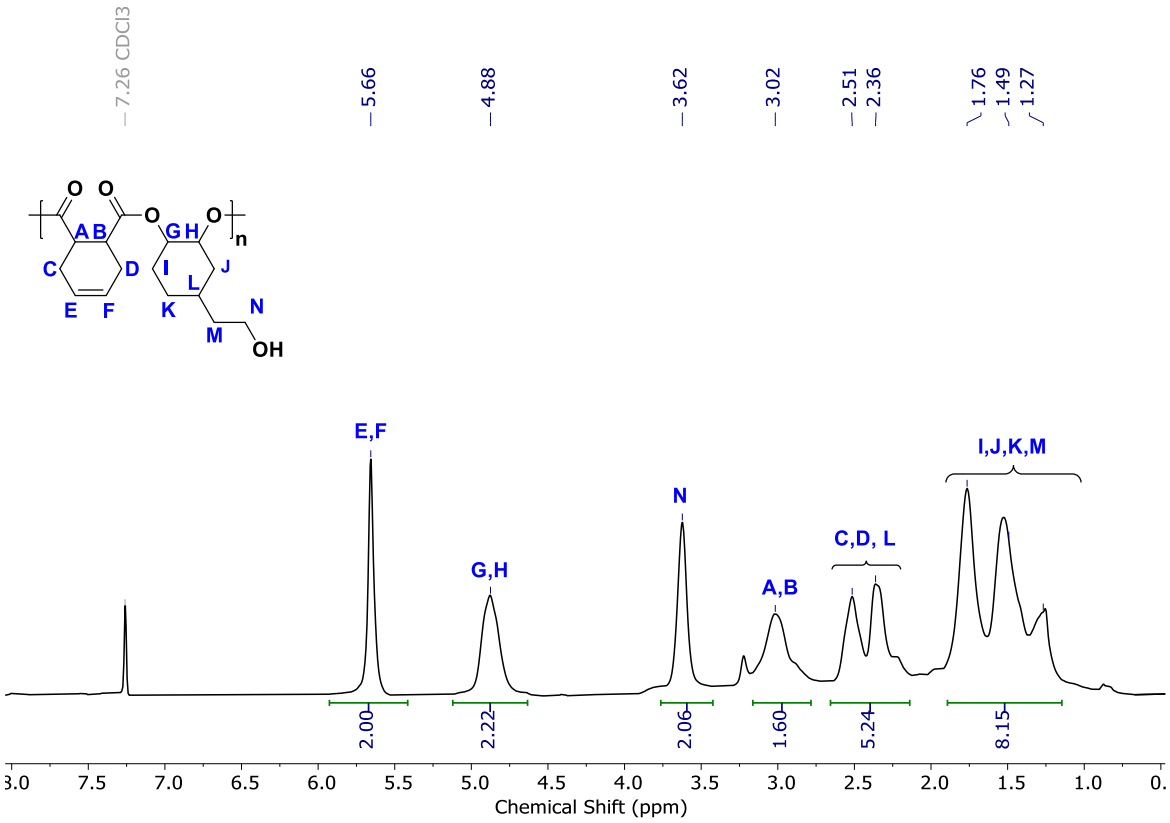


Figure 3.9 ^{1}H NMR spectrum of **P5(a)** ($CDCl_3$, 500 MHz, 298 K).

A new signal is observed in the hydroxyl region at 3.62 ppm and this peak is assigned to the methylene protons adjacent to the hydroxyl group (protons 'N' in Fig. 3.9). Importantly, the resonance at 4.88 ppm, assigned to the methine protons adjacent to the polyester (peak 'G' and 'H' in Fig. 3.9), retains the same relative integral, which confirms that the polymer backbone is not subject to side-reactions in the presence of the oxidant. The successful alternating functionalization of **P5(a)** is also supported by the SEC data which shows a single monomodal peak at slightly higher molar mass (4.4 kg mol^{-1}) than **P5** but with the same narrow dispersity ($Đ$ = 1.14) (Table 3.2).

The alkene-to-hydroxyl transformation was successfully generalized to the whole series of polyesters **P6** – **P13** (excluding **P7**). In most cases, it was highly selective and

resulted in quantitative conversion of the primary alkene groups as indicated by a range of characterization techniques, including ^{1}H NMR, SEC and DSC (Table 3.2). In the case of **P4** and **P7**, selective hydroboration was clearly indicated using *in-situ* ^{1}H NMR spectroscopy (see Appendix, Fig. S53 – S57) but the isolation of these hydroxylated polymers was hampered by their high water solubility.

Table 3.2 Characterization Data for Hydroxyl-functionalized polyesters **P5(a) – P13(a)**.

#	Epoxide	Anhydride	M_n[a]	$Đ$ [a]	T_g [b]
P5(a)	VCHO	THPA	2.6	1.12	106
P6(a)	VCHO	CHMA	5.6	1.18	133
P9(a)[*]	VPO	THPA	3.0	1.31	55
P10(a)	VPO	CHMA	4.2	1.11	75
P12(a)[*]	AGE	THPA	3.8	1.19	28
P13(a)[*]	AGE	CHMA	5.6	1.15	41

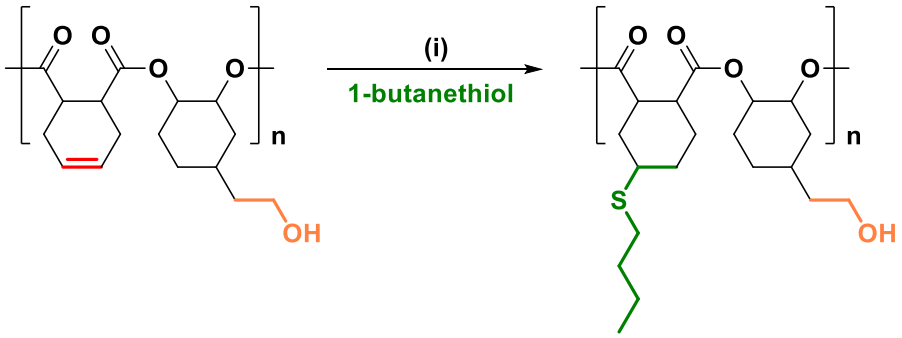
[a]M_n and $Đ$ were measured by SEC (THF as eluent, 1 mL/min, 30 °C) calibrated using PMMA standards.[*]M_n and $Đ$ were measured by SEC using DMF as eluent (D with 0.075 wt% LiBr, 1 mL/min, 30 °C) due to solubility issues [b]T_g were obtained from DSC (third heating cycle)

3.5. **Dual-functionalization of alternating polyesters**

With a successful means to 'pattern' the polymer and install hydroxyl substituents on alternating sites, the next challenge was to react the remaining internal-alkene monomers to install a second functional group.

Previously, Dr. Ni Yi showed that a range of different dual functional polyesters were possible by further reacting the hydroxylated polymer with various thiol reagents.[16] It was discovered that installing alternating hydroxyl and butyl thiol ethers in an AB pattern led to self-assembly of the polymer. Currently, homopolymer self-assembly is rather rare and the exact mechanism for chain interaction is not well understood.[18, 26] One hypothesis for the observed self-assembly may be a balance between the hydrophobicity and hydrophilicity of the polymer bought about by the alkyl chain and hydroxyl groups respectively.

To demonstrate the generality of the orthogonal post-polymerisation functionalization method, selected hydroxylated polyesters were further functionalized using thiol-ene coupling reactions. 1-Butanethiol was chosen as the model thiol reagent so as to target dual-functional polyesters with alternating hydrophobic and hydrophilic groups and further investigate homopolymer self-assembly. For instance, **P5(a)** was further reacted with 1-butanethiol, using a UV-initiated thiol-ene process, to afford a new $(AB)_n$ alternating and orthogonally functionalized polyester, **P5(b)** (Scheme 3.6).



Scheme 3.6 Photo-initiated thiol-ene reactions to transform the hydroxyl-functionalized alternating polyesters into orthogonally functionalized (AB)n Polyesters. (i): DMPA, 1-butanethiol, DMSO, irradiated under UV (365 nm, 10W) for 2 h, molar ratio: [DMPA]/[alkene]$_0$/[thiol] = 1/2.5/10, [alkene]$_0$ = 0.25 M in DMSO

The ^{1}H NMR spectrum of **P5(b)** showed the complete disappearance of the internal double bond signal at 5.65 ppm. Furthermore, a new signal at 0.90 ppm is assigned to the butyl side-chain substituents (Fig. 3.10).

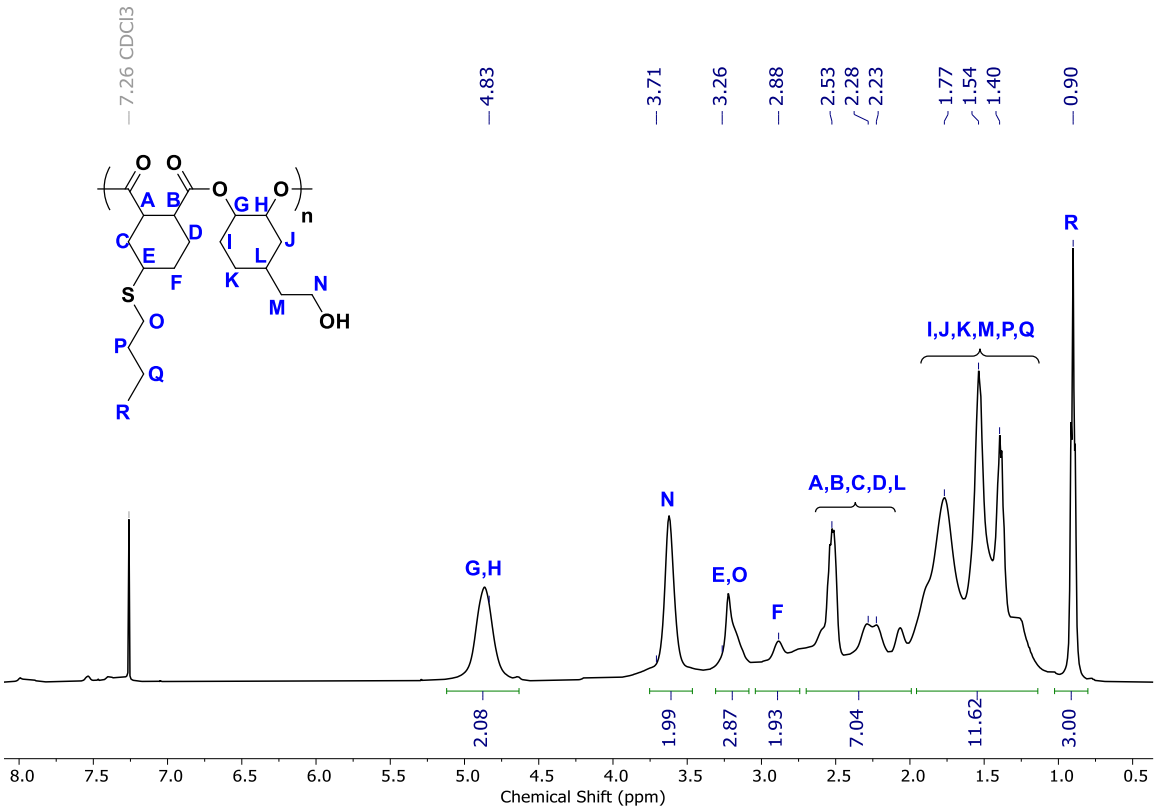


Figure 3.10 ^{1}H NMR spectrum of **P5(b)** ($CDCl_3$, 500.0 MHz, 298 K).

The functionalization is clearly apparent by analysing the stacked ^{1}H NMR spectra of **P5**, **P5(a)** and **P5(b)** (Fig. 3.11). The hydroboration-oxidation functionalization transformed **P5** to **P5(a)** and the ^{1}H NMR spectra (Fig. 3.11, bottom and middle spectra) shows the complete depletion of the terminal alkene signal (peak 'B' in Fig. 3.11) and appearance of signal due to the methylene protons (protons 'D' in Fig. 3.11, bottom and middle spectra).

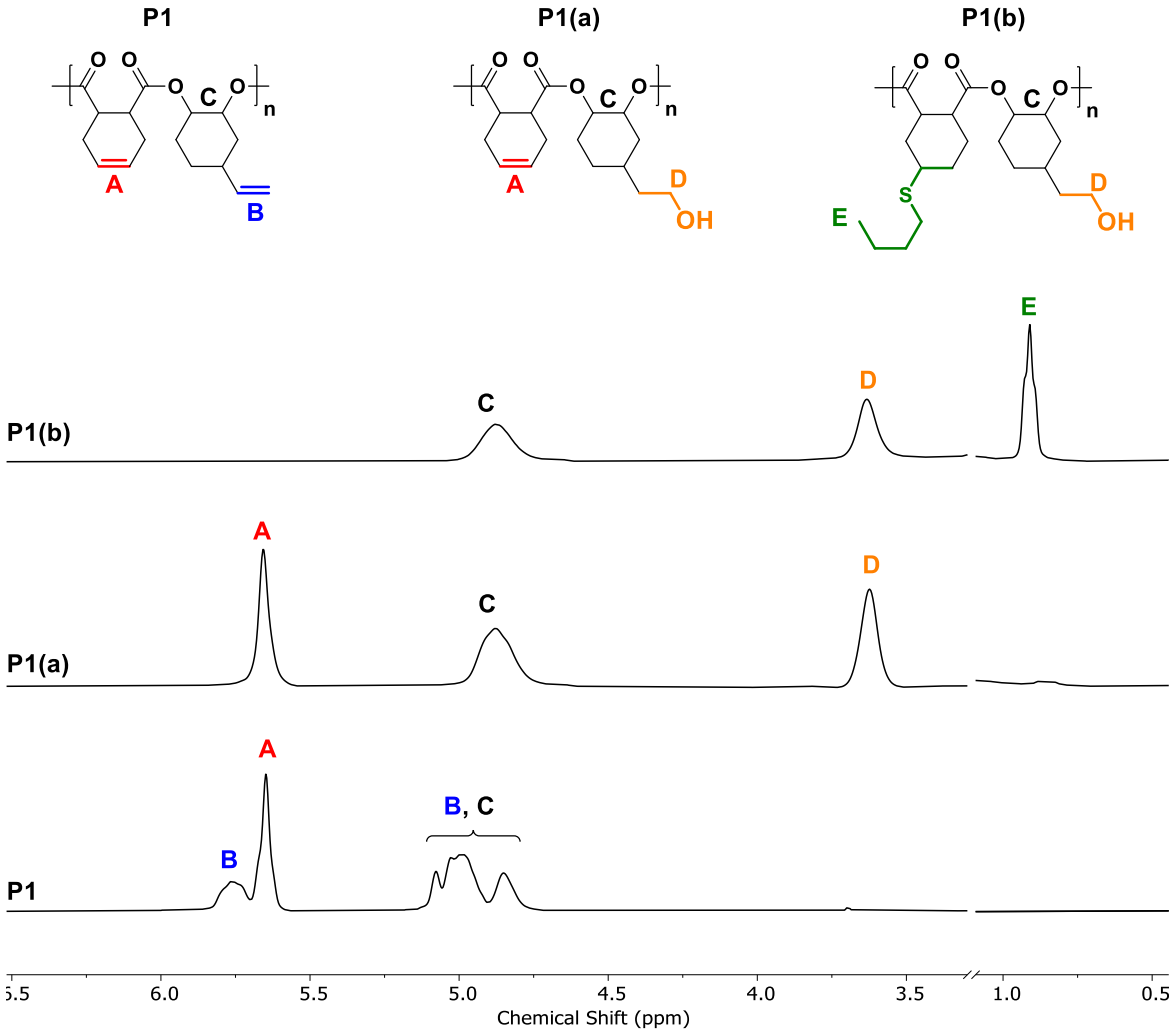


Figure 3.11 Selected regions of the ^{1}H NMR spectra showing the changes in proton resonances of (purified) polymers after functionalization steps (in $CDCl_3$).

The thiol-ene modification transforms the remaining internal alkene functionality in **P5(a)** (proton 'A' in Fig. 3.11) and installs a new butyl thiolether group in **P5(b)** (peak 'E' in Fig. 3.11). It is worth nothing that throughout the functionalization process, the polyester backbone signals remain unchanged which indicates that the polymer is stable to the reaction conditions (proton 'C' in Fig. 3.11).

The SEC traces obtained using THF as eluent, initially show a reduction in M_n upon transforming **P5** to **P5(a)**, before displaying a slight increase in molar mass when forming **P5(b)** (Table 3.3). The slight changes to molar mass values are likely due to different interactions between the polymers and the SEC column (i.e. not a true reduction in molar mass). Such effects have been seen previously by other researchers working with hydroxyl functional polymers.[27] Indeed, a consistent increase in molar mass values, with retention of narrow dispersities, were observed when the samples were analyzed using a SEC employing DMF as the eluent (with 0.075 wt% LiBr) (Table 4.3). For instance, an increase in M_n from 2.4 kg mol^{-1} to 4.5 kg mol^{-1} was seen when **P5** was functionalized to **P5(a)** and a further increased to 5.6 kg mol^{-1} for **P5(b)** (Table 3.3). Furthermore, the constant increase in molar mass was accompanied by a retention of narrow monomodal dispersity ($Đ \sim 1.2$) that suggests a quantitative transformation at each stage and lack of any degradation/side-reactions (Fig. 3.12).

The orthogonal functionalization method was also applied to **P6** to obtain a hydrophilic/phobic dual functional polyester, **P6(b)** (see Appendix for ^{1}H NMR spectra and SEC traces, Fig. S58 – S59).

Table 3.3 SEC characterization data (in THF and DMF) for **P5** and **P6**.

#	**THF GPC** (M_n (kg mol^{-1}) [$Đ$])[1]			**DMF GPC** (M_n (kg mol^{-1}) [$Đ$])[2]		
	Precursor	Hydroxyl functionalized (a)	Dual-functionalized (b)	Precursor	Hydroxyl functionalized (a)	Dual-functionalized (b)
P5	2.9 [1.21]	2.2 [1.22]	4.0 [1.24]	2.4 [1.20]	4.5 [1.27]	5.6 [1.27]
P6	6.0 [1.16]	5.6 [1.18]	6.2 [1.13]	4.4 [1.13]	5.8 [1.26]	7.0 [1.24]

[1]measured using SEC (THF as eluent, 1 mL/min, 30 °C) calibrated using PS standards. [2]Measured using SEC (DMF as eluent with 0.075 wt% LiBr, 1 mL/min, 30 °C) calibrated using PMMA standards.

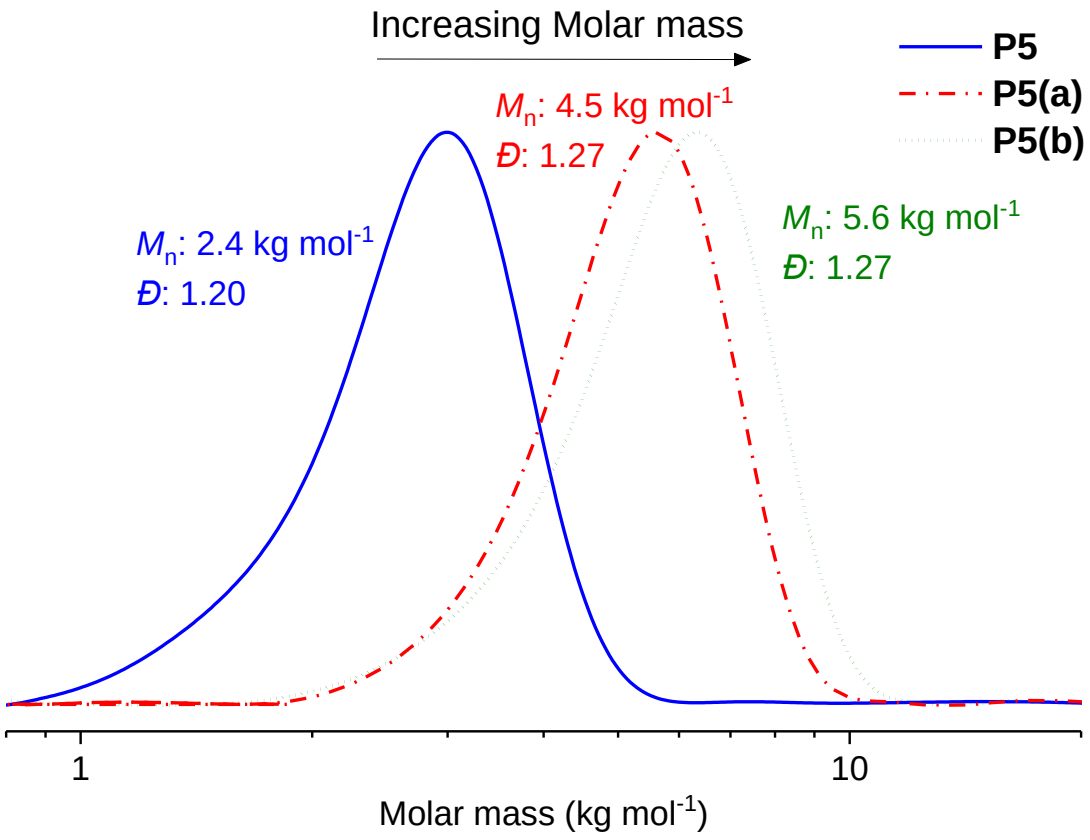
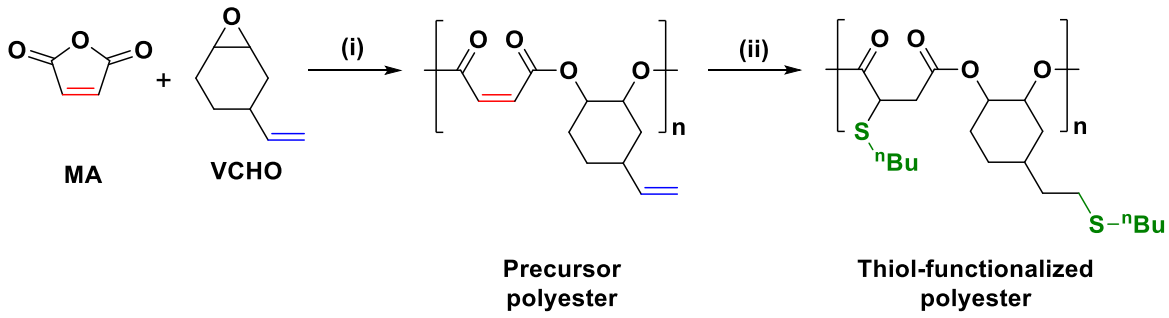


Figure 3.12 SEC (in DMF) showing an increase in molar mass after functionalization, in each case with retention of monomodal distributions and narrow dispersity.

To emphasize the power of this orthogonal functionalization strategy, the control reaction between a polyester synthesized using VCHO and maleic anhydride (to mimic the polyester first tested by Dr. Ni Yi) and a thiol reagent (1-butanethiol) was conducted (Scheme 3.7).



Scheme 3.7 Thiol-ene control reaction using polyester from the ROCOP of MA and VCHO. (i): [SalcyCrCl], PPNCl, 60 °C, toluene, molar ratio: [SalcyCrCl]/PPNCl/CHD/ anhydride/epoxide = 1/1/10/100/120, [anhydride] = 5 M. (ii) DMPA, 1-butanethiol, DMSO, irradiated under UV (365 nm, 10W) for 2 h, molar ratio: [DMPA]/[alkene]$_0$/[thiol] = 1/2.5/10, [alkene]$_0$ = 0.25 M in DMSO.

Using otherwise identical reaction conditions, the thiol-ene functionalization resulted in an increase in the molar mass and retention of narrow dispersities ($Đ \leq 1.17$) indicative of a successful transformation (Fig. 3.13). However, comparing the ^{1}H NMR spectra of the precursor and the thiol-functionalized polyester, the complete reaction of all the alkene groups (both vinyl and maleate) and placement of butyl thioethers on every repeat unit was observed (Fig. 3.14). Thus, to selectively pattern the polymers requires both hydroboration/oxidation *and* thiol-ene reactions in the correct order.

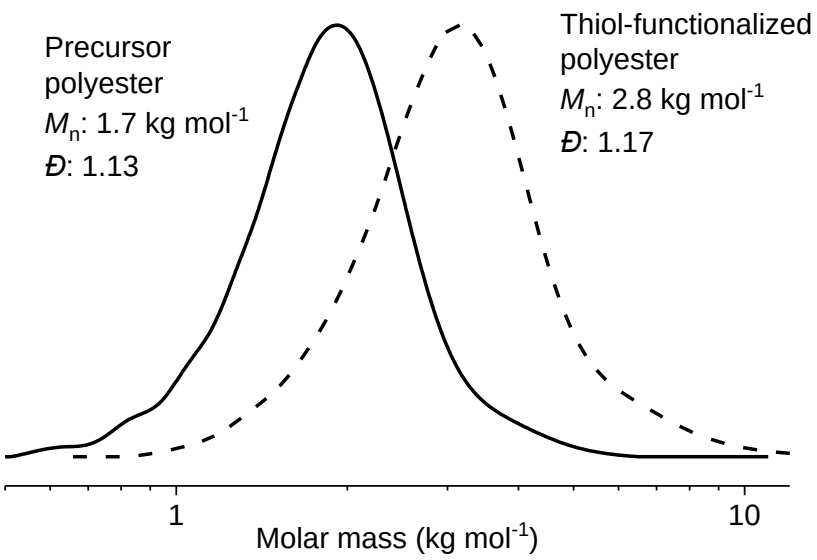


Figure 3.13 SEC traces (in THF) illustrating a successful coupling in the control reaction.

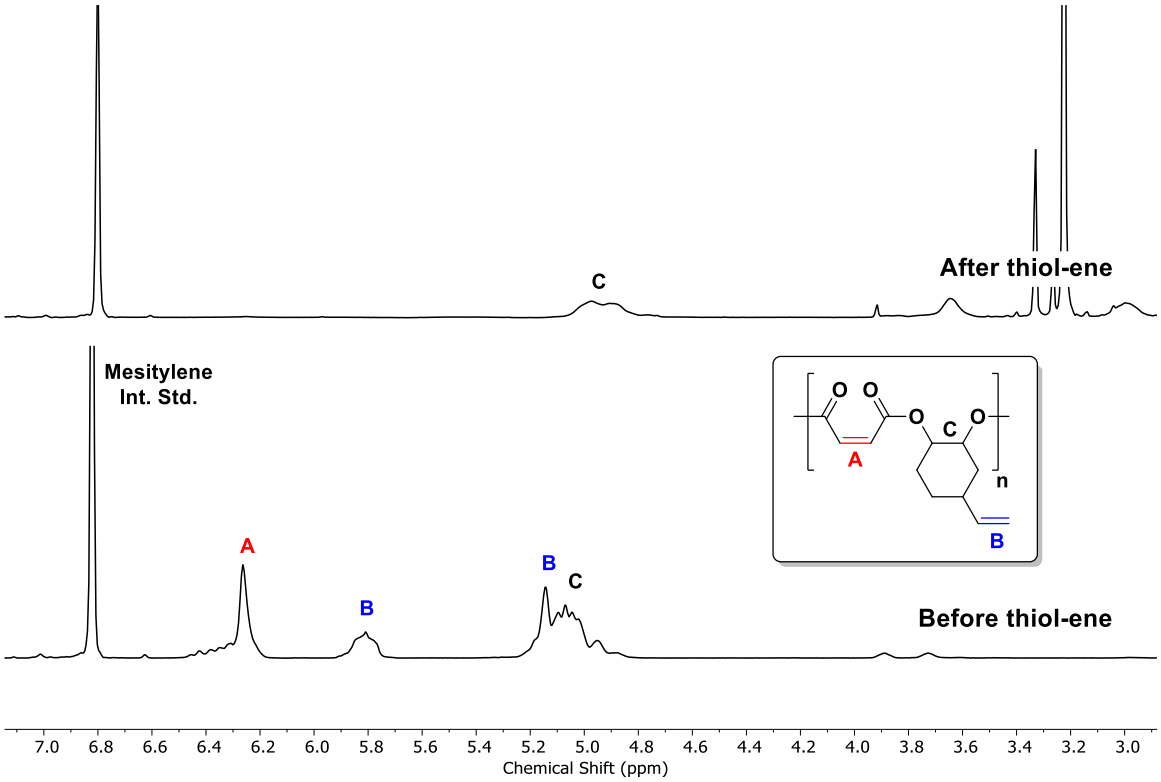


Figure 3.14 ^{1}H NMR data illustrating the unselective UV-initiated thiol-ene reactions. (Bottom) before application of thiol-ene reaction. (Top) after the thiol-ene reaction (mesitylene as internal standard).

3.6. **Thermal properties of dual-functional polyesters**

All the polymers are amorphous as only glass transitions are observed in the DSC (i.e. no melting transitions). Furthermore, the addition of the hydroxyl functional groups generally increases the glass transition temperatures compared to the precursor polyesters (Table 4.4 & Table 4.5). For instance, **P5(a)** has a T_g of 106 °C, which is 28 °C higher than its precursor **P5**. The increase in T_g is attributed to inter-/intra-chain hydrogen bonding, a phenomenon which is common in biopolymers and has been observed for other hydroxyl-functionalized polymers.[28-29]

Table 3.4 Glass transition temperatures for dual-functionalized polyesters

Epoxide	**Anhydride**	Precursor Polyester		OH-functionalized polyester		Dual-functional Polyester	
		#	$\boldsymbol{T_g}$[a]	**#**	$\boldsymbol{T_g}$[a]	**#**	$\boldsymbol{T_g}$[a]
VCHO	THPA	**P5**	80	**P5(a)**	106	**P5(b)**	78
VCHO	CHMA	**P6**	129	**P6(a)**	140	**P6(b)**	123

[a]T_g were obtained from DSC (third heating cycle)

Table 3.5 Glass transition temperatures for hydroxyl-functionalized polyesters

Epoxide	**Anhydride**	Precursor Polyester		OH-functionalized polyester	
		#	$\boldsymbol{T_g}$[a]	**#**	$\boldsymbol{T_g}$[a]
VPO	THPA	**P9**	14	**P9(a)**	55
VPO	CHMA	**P10**	56	**P10(a)**	75
AGE	THPA	**P12**	1	**P12(a)**	28
AGE	CHMA	**P13**	23	**P13(a)**	41

[a]T_g were obtained from DSC (third heating cycle)

Installment of the butyl thiol-ether group reduced the T_g to 80 °C (Fig. 3.15). This is likely due to an increased hydrodynamic volume as the alkyl chains impede polymer packing.

The T_g for polyesters derived from VCHO and TCA (i.e. **P6**, **P6(a)** and **P6(b)**) were all well above 100 °C (See Appendix, Fig. S60). The introduction of the bulky tricyclic anhydride likely reduced the polyesters backbone flexibility and increased the glass transition temperature. Nevertheless, a similar trend for the T_g was observed for the series of polyesters, with an increase from **P6** to **P6(a)** and reduction when the butyl thiol ether groups were added (Table 3.4).

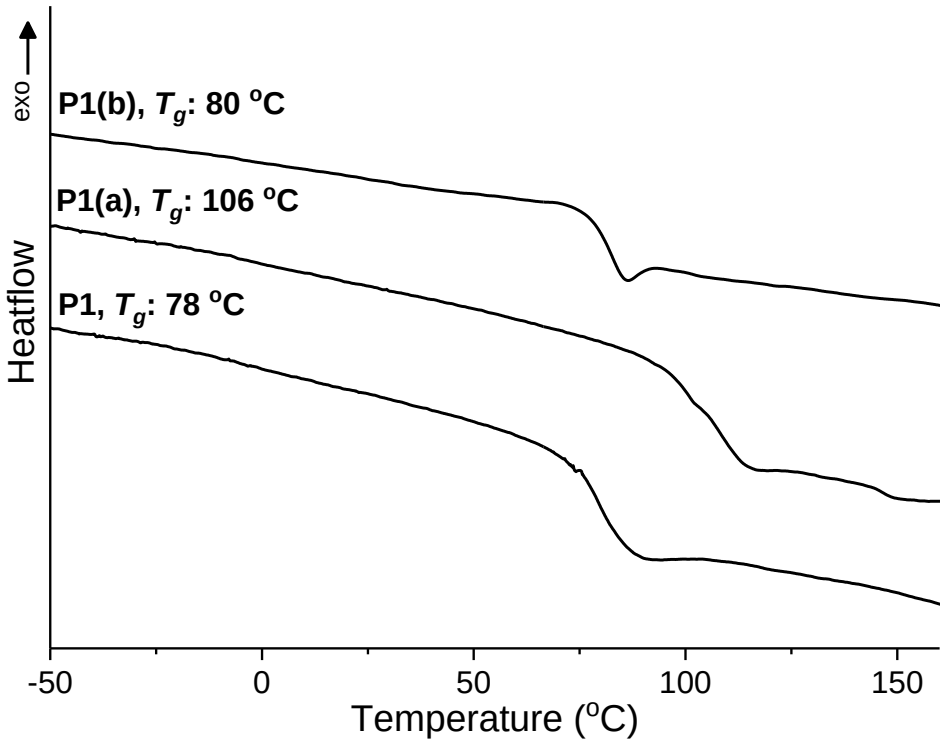


Figure 3.15 DSC thermograms of **P5**, **P5(a)** and **P5(b)** showing an increase in T_g after the hydroboration-oxidation and a decrease after the further instalment of butyl thiolether groups.

3.7. **Alternating homopolymer self-assembly**

A guiding principle for polymer self-assembly is that chains should feature domains of hydrophobic and hydrophilic substituents. Most polymer self-assembled nanostructures form from amphiphilic block polymers featuring hydrophobic and hydrophilic blocks.[30-31] In contrast, there are only limited examples of alternating polymer self-assembly and most of these are based on non-degradable polyacrylate backbones.[17, 26, 32-37]

Dr. Yi had previously observed that the dual-functional polyester derived from VCHO and MA, featuring alternating hydroxyl and butyl thiol ether groups, self-assembled in aqueous media. Since the polymer has a potentially degradable ester backbone, it may be suited for potential uses, such as drug delivery applications. As such, it is important to investigate whether this effect is general or specific to that backbone/substituent pattern.

P5(b) and **P6(b),** both featuring the same alternating hydroxyl and butyl substituents, were first dissolved in THF (~1 mL), in separate vials, followed by drop-wise addition of an equal volume of deionized water, with vigorous stirring to induce self-assembly. The THF was then removed, *via* dialysis prior to characterization of the resultant particles. Dynamic light scattering (DLS) and TEM measurements both confirmed the formation of stable self-assembled nanostructures in water. DLS analysis of the samples in water shows **P5(b)** and **P6(b)** form nanostructure with hydrodynamic diameters of 381.0 ± 1.8 nm (PDI: 0.21) and 302.7 ± 2.0 nm, respectively (Fig. 3.19 (A)). The DLS data show a low cumulant fit error (<0.005) and the raw

correlation data have flat baselines which reinforces the reliability of the measurements.

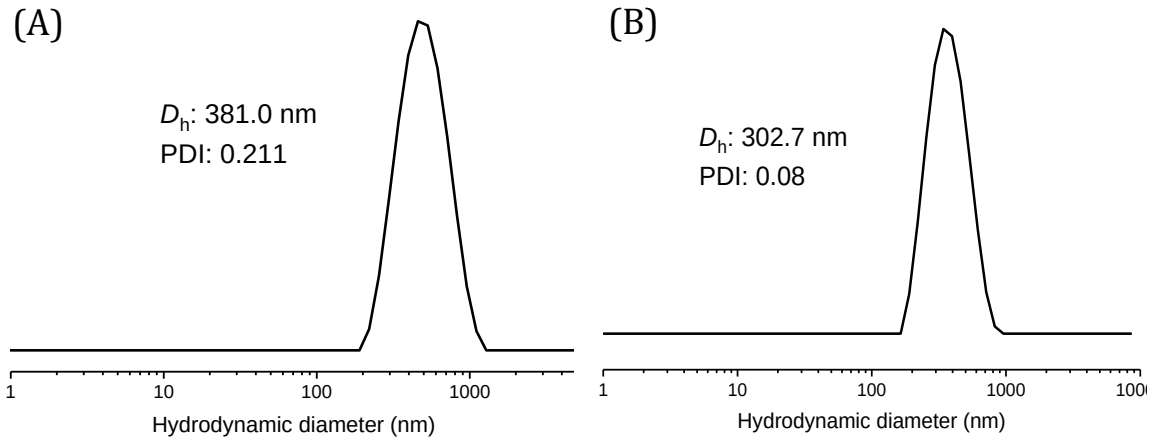


Figure 3.16 (A) DLS data collected from an aqueous solution of **P5(b)** (A) and **P6(b)** (B) (10 mgmL-1).

Transmission electron microscopy (TEM) analysis (performed by Ms Tianyi Chen, Department of Chemistry, University of Oxford) reveals that **P5(b)** and **P6(b)** both formed spherical nanoparticles with similar diameters to those obtained by DLS (ca. 300 nm and ca. 250 nm for **P5(b)** and **P6(b)**, respectively) (Fig. 3.21 & 4.22). The slight discrepancy in nanoparticle sizes, determined by DLS and TEM, is tentatively proposed to result from some dehydration of the nanoparticles during TEM analysis and is consistent with previous reports of alternating polymer self-assemblies.[17, 32]

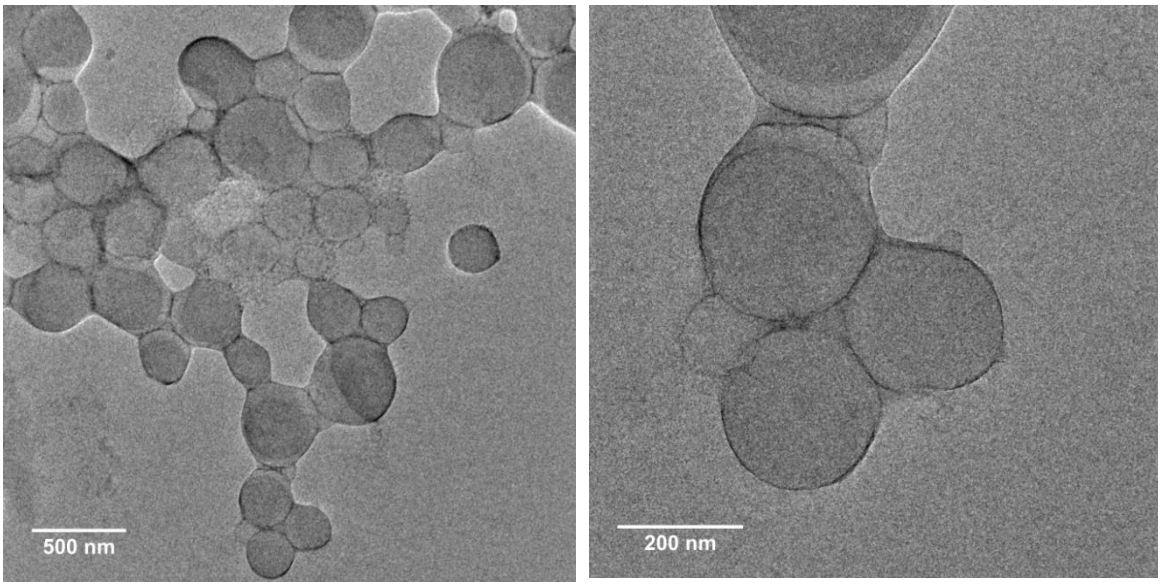


Figure 3.17 TEM images for the structure of the homopolymer micelle from **P5(b)**. Measurements performed by Ms. Tianyi Chen (Department of Chemistry, University of Oxford).

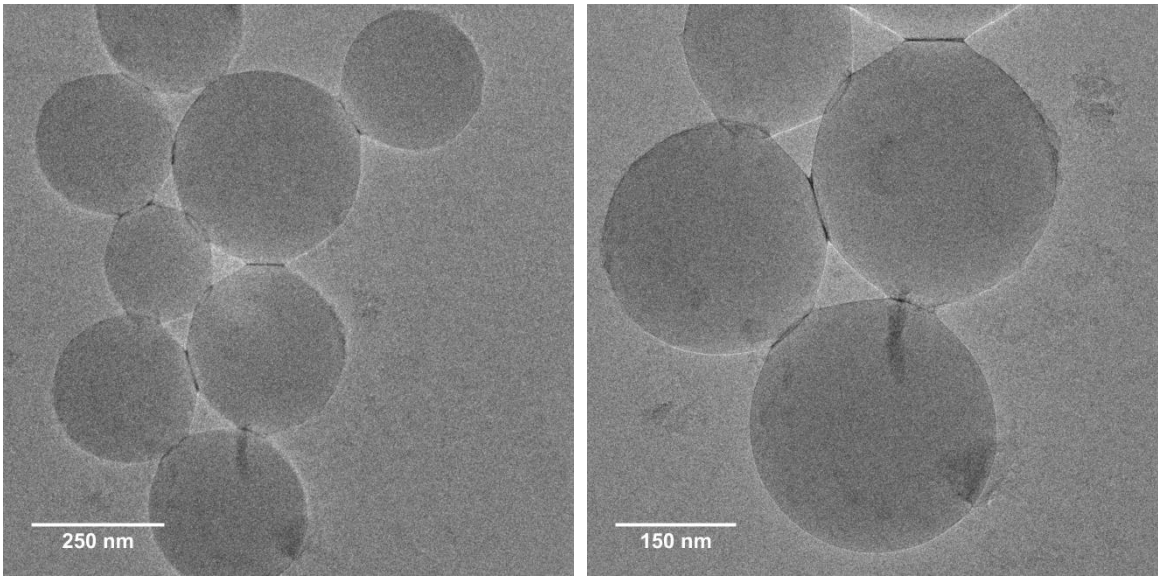


Figure 3.18 TEM images for the structure of the homopolymer micelle from **P6(b).** Measurements performed by Ms. Tianyi Chen (Department of Chemistry, University of Oxford).

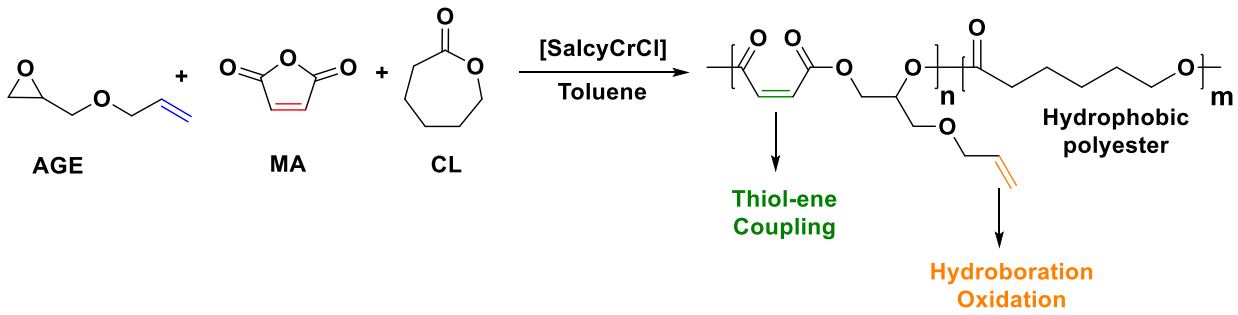
The TEM images also show a lack of clear hydrophilic/hydrophobic boundary regions suggesting that single chains may adopt conformations that maximise the density of polar hydroxyl substituents on the outside of the self-assembled structures and, thus, solvation effects drive self-assembly.[17, 36, 38] Future investigations should continue to explore the self-assembled structures of these alternating and degradable polymers.

3.8. **Summary & Future work**

In summary, a series of orthogonally functionalized alternating polyesters were prepared by exploiting the high AB monomer sequence selectivity of epoxide/anhydride ring-opening copolymerization. Starting from polyesters featuring alternating terminal and internal alkene substituents, a hydroboration-oxidation reaction allows for selective and quantitative conversion of the vinyl substituents into hydroxyl groups, leaving the adjacent internal alkenes unreacted. Taking two hydroxyl-functionalized polyesters as representative examples, the remaining internal alkene substituents were selectively and quantitatively transformed into butyl thioether groups. These dual-functional polyesters self-assemble in aqueous solution to form spherical nanostructures, as shown with DLS and TEM characterization. Overall, the results demonstrate a generally applicable, scalable and efficient means to deliver different AB alternating functionalized polyesters. These functionalized AB polyesters are an important addition to the sustainable polymer palette and are particularly attractive as they allow for straightforward tuning of polymer properties such as glass transition temperatures.

Investigation into the adjacency, cooperativity and multi-valent effects of the substituents should be explored in the future. Precision placement of hydroxyl substituents is expected to significantly influence both hydrolysis and biodegradation rates, particularly those dependent on serine proteases. In the future, such polyesters, sequentially patterned with hydrophilic, -phobic and ionisable groups, could be useful as bio-inspired antimicrobials, cell penetrating but degradable polymers and to improve upon the properties of biodegradable plastics.

As future work, the sequential post-polymerization functionalization method should also be demonstrated in block polymers. Amphiphilic block copolyesters can be easily synthesised by switchable catalysis whereby a combination of lactone, epoxide and anhydride are selectively enchained (See Chapter 2). The new orthogonal post-polymerization modifications described in this chapter should be applied to those block polymer. For instance, a combination of caprolactone (CL), AGE and MA could be used to synthesise block polymers (Scheme 3.8).

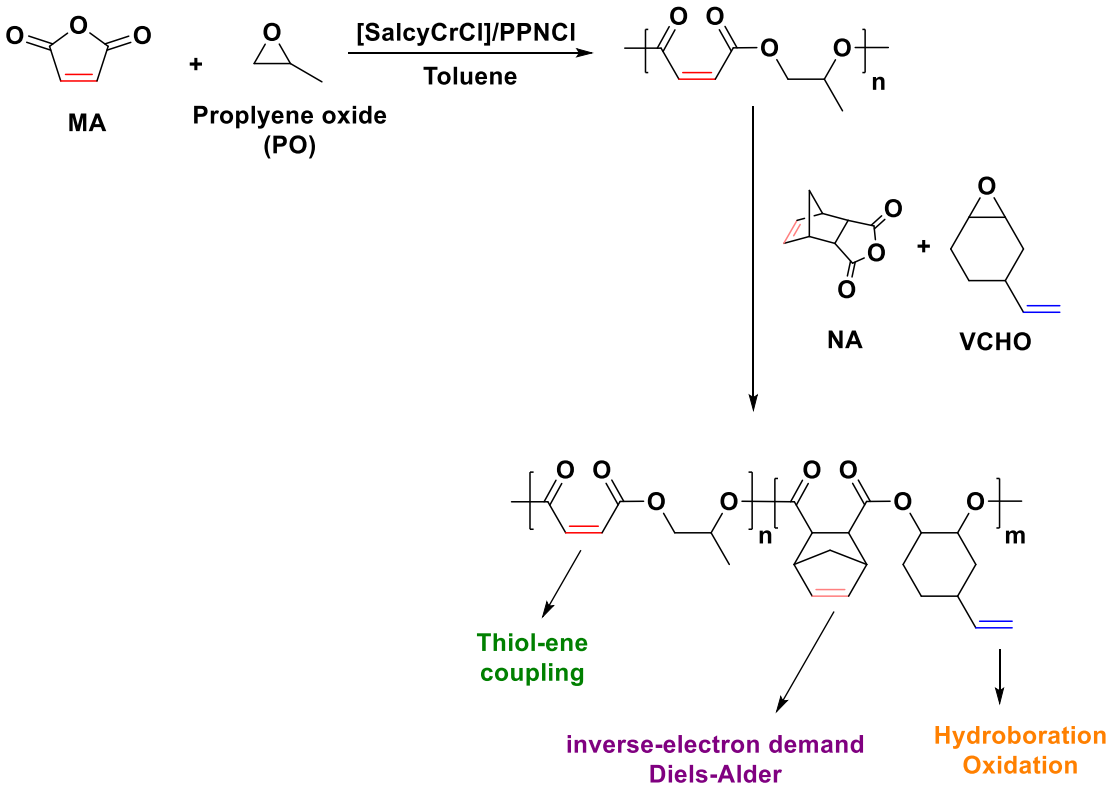


Scheme 3.8. Block copolyester synthesis *via* switchable catalysis and sites for selective functionalization

The orthogonal hydroboration-oxidation and thiol-ene reaction could then be applied to the block polymer to form useful amphiphilic materials. Those targets could be prepared through the instalment of hydroxyl groups and zwitterionic groups. Such materials could be useful in applications such as drug delivery systems or anti-fouling surfaces.

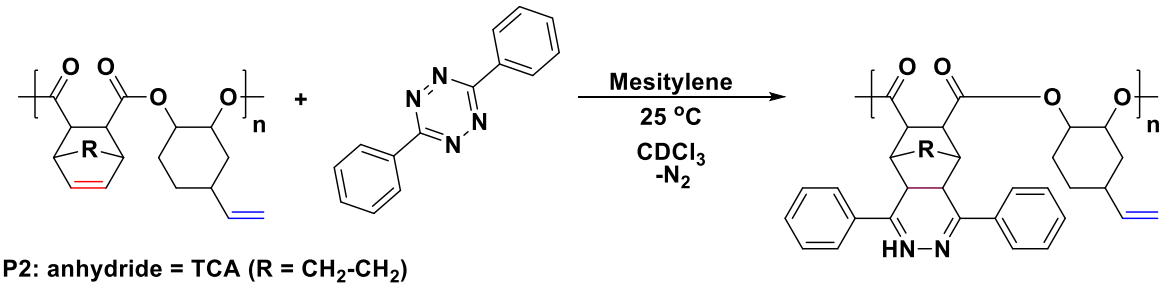
The addition of a second block could allow for further functionality. As described in Section 3.4, the norbornene moiety appears to be unusually reactive, due to its

highly strained nature. Moreover, this functionality is unique in undergoing the inverse-electron demand Diels-Alder reactions (iEDDA), e.g. using tetrazine as the functionalization reagent.[24-25] Block copolymers could be designed to include internal alkenes, terminal alkenes and norbornene moieties (Scheme 3.9).



Scheme 3.9 Block copolymer formation to include 3 post-polymerization functionalization sites *via* sequential ROCOP.

Ensuring a high selectivity in the iEDDA reaction between the 3 possible alkenes would be paramount in ensuring successful placement of different functional groups. To assess this approach, preliminary *in-situ* ^{1}H NMR studies were conducted using **P6** and **P7** with 3,6-diphenyl-1,2,4,5-tetrazine as the model tetrazine (scheme 3.10)



Scheme 3.10. *In-situ* ^{1}H NMR studies of iEDDA using **P2** and **P3** with 3,6-Diphenyl-1,2,4,5-tetrazine (in $CDCl_3$ and Mesitylene used as internal standard).

Initial results suggest that neither the internal nor terminal alkene groups from the TCA nor VCHO groups reacted with the tetrazine after 3 days (Fig. 3.19(A)). Interestingly, the internal alkene integrals ,from the NA unit, can be seen to decrease slowly (~50% conversion after 2 days) and suggests that it had reacted (Fig. 3.19(B)). This data is encouraging as it suggests selective functionalization, additional investigation should be carried out to drive full conversion of the NA groups and to establish the polymer backbone remains intact e.g. using SEC and NMR spectroscopic analyses.

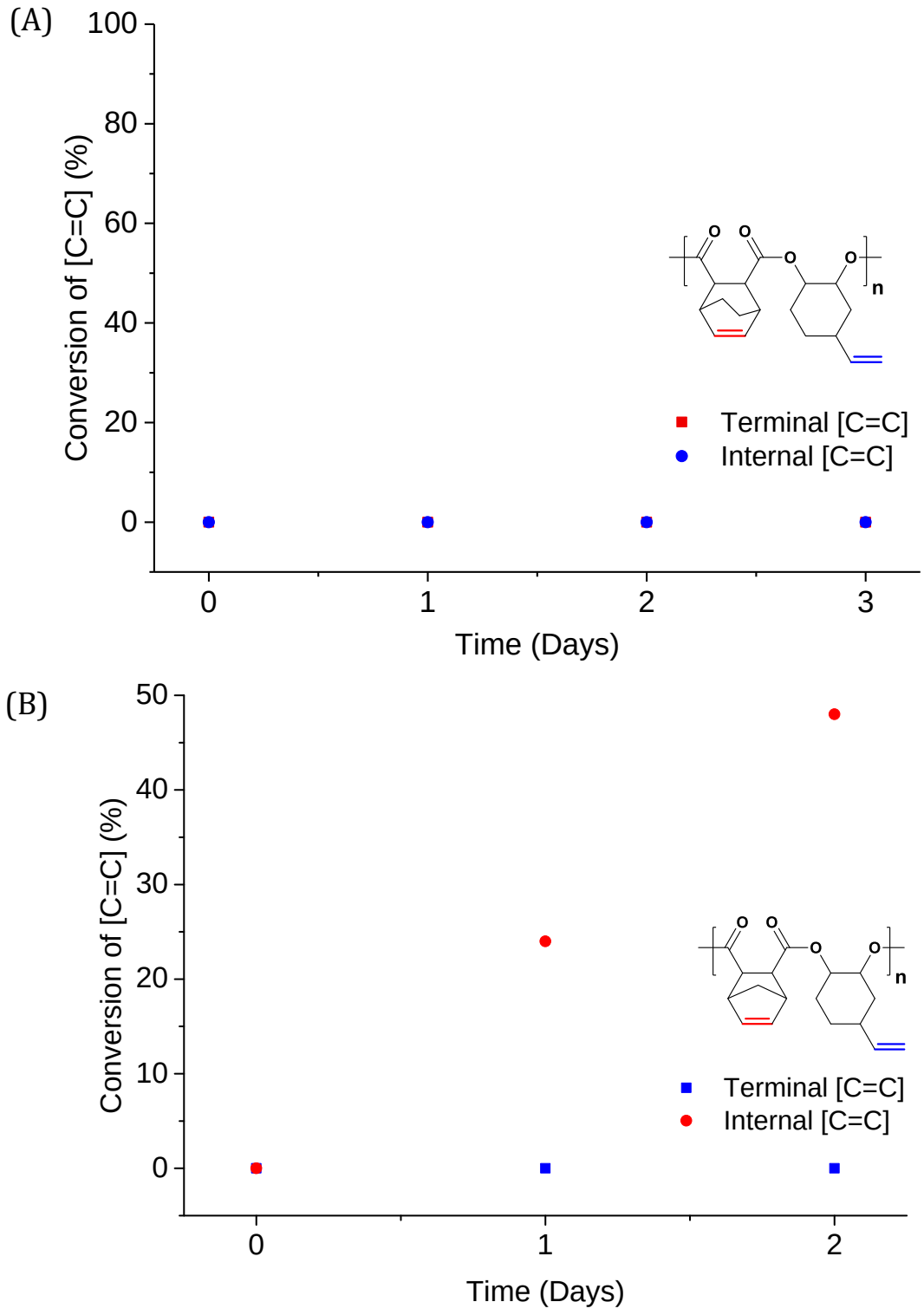


Figure 3.19. Percentage conversion of the two different alkene groups (internal = blue circles and terminal = red squaers) vs. time during the iEDDA reaction with tetrazine of **P6** (A) and **P7**(B).

3.9. **References**

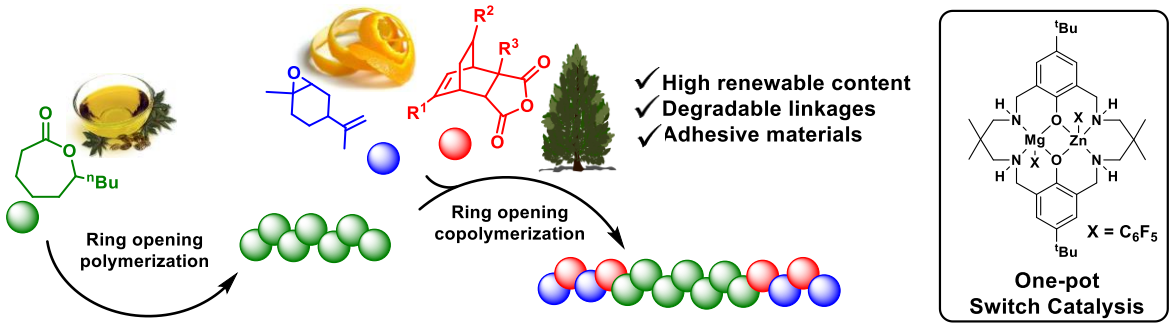
1. Lutz, J. F.; Lehn, J. M.; Meijer, E. W.; Matyjaszewski, K., From precision polymers to complex materials and systems. *Nat. Rev. Mater.* **2016,** *1*.
2. Altintas, O.; Barner-Kowollik, C., Single-Chain Folding of Synthetic Polymers: A Critical Update. *Macromol. Chem. Phys.* **2016,** *37*, 29-46.
3. Blasco, E.; Sims, M. B.; Goldmann, A. S.; Sumerlin, B. S.; Barner-Kowollik, C., 50th Anniversary Perspective: Polymer Functionalization. *Macromolecules* **2017,** *50*, 5215-5252.
4. Kramer, J. W.; Treitler, D. S.; Dunn, E. W.; Castro, P. M.; Roisnel, T.; Thomas, C. M.; Coates, G. W., Polymerization of Enantiopure Monomers Using Syndiospecific Catalysts: A New Approach To Sequence Control in Polymer Synthesis. *J. Am. Chem. Soc.* **2009,** *131*, 16042-16044.
5. Ligny, R.; Hanninen, M. M.; Guillaume, S. M.; Carpentier, J. F., Highly Syndiotactic or Isotactic Polyhydroxyalkanoates by Ligand-Controlled Yttrium-Catalyzed Stereoselective Ring-Opening Polymerization of Functional Racemic beta-Lactones. *Angew. Chem. Int. Ed.* **2017,** *56*, 10388-10393.
6. Sun, Y. Y.; Jia, Z. W.; Chen, C. J.; Cong, Y.; Mao, X. Y.; Wu, J. C., Alternating Sequence Controlled Copolymer Synthesis of alpha-Hydroxy Acids via Syndioselective Ring-Opening Polymerization of O-Carboxyanhydrides Using Zirconium/Hafnium Alkoxide Initiators. *J. Am. Chem. Soc.* **2017,** *139*, 10723-10732.
7. Sanford, M. J.; Van Zee, N. J.; Coates, G. W., Reversible-deactivation anionic alternating ring-opening copolymerization of epoxides and cyclic anhydrides: access to orthogonally functionalizable multiblock aliphatic polyesters. *Chem. Sci.* **2018,** *9*, 134-142.
8. Herz, K.; Imbrich, D. A.; Unold, J.; Xu, G. J.; Speiser, M.; Buchmeiser, M. R., Functional ROMP-Derived Poly(cyclopentene)s. *Macromol. Chem. Phys.* **2013,** *214*, 1522-1527.
9. Guillaume, C.; Ajellal, N.; Carpentier, J. F.; Guillaume, S. M., Boron-Functionalized Poly(3-hydroxybutyrate)s from Hydroboration of Poly(allyl-beta-hydroxyalkanoate)s: Synthesis and Insights into the Microstructure. *J. Polym. Sci. Part A, Polym. Chem* **2011,** *49*, 907-917.
10. Tanaka, R.; Kasai, Y.; Shinzawa, M.; Cai, Z. G.; Nakayama, Y.; Shiono, T., Synthesis of a Multiblock Copolymer of cis-1,4Polybutadiene and Poly(3-buten-1-ol). *Macromol. Chem. Phys.* **2014,** *215*, 888-892.
11. Ajellal, N.; Thomas, C. M.; Carpentier, J. F., Functional Syndiotactic Poly(beta-hydroxyalkanoate)s via Stereoselective Ring-Opening Copolymerization of rac-beta-Butyrolactone and rac-Allyl-beta-Butyrolactone. *J. Polym. Sci Part A, Polym. Chem.* **2009,** *47*, 3177-3189.
12. Grayson, S. M.; Frechet, J. M. J., Synthesis and surface functionalization of aliphatic polyether dendrons. *J. Am. Chem. Soc.* **2000,** *122*, 10335-10344.
13. Brown, H. C.; Chandrasekharan, J.; Nelson, D. J., Hydroboration Kinetics .10. Kinetics, Mechanism, and Selectivity for Hydroboration of Representative Alkenes with Borinane. *J. Am. Chem. Soc.* **1984,** *106*, 3768-3771.
14. Brown, H. C.; Wang, K. K.; Scouten, C. G., Hydroboration Kinetics - Unusual Kinetics for the Reaction of 9-Borabicyclo[3.3.1]Nonane with Representative Alkenes. *Proc. Natl. Acad. Sci. U. S. A.* **1980,** *77*, 698-702.
15. Brown, H. C.; Wang, K. K.; Scouten, C. G., Hydroboration Kinetics - Unusual Kinetics for the Reaction of 9-Borabicyclo[3.3.1]Nonane with Representative Alkenes. *Proc. Natl. Acad. Sci. U.S.A.* **1980,** *77*, 698-702.

16. Yi, N. Synthesis and Post-polymerisation Modification of Degradable Polymers Based on Polycarbonates/Polyesters Prepared Using Ring-opening Copolymerisation. University of Oxford, Oxford, UK, 2018.
17. Zhu, Y. Q.; Liu, L.; Du, J. Z., Probing into Homopolymer Self-Assembly: How Does Hydrogen Bonding Influence Morphology? *Macromolecules* **2013,** *46*, 194-203.
18. Xu, Q.; Li, S.; Yu, C.; Zhou, Y., Self-assembly of Amphiphilic Alternating Copolymers. *Chem. - Eur. J.* **2018,** *0*.
19. DiCiccio, A. M.; Coates, G. W., Ring-Opening Copolymerization of Maleic Anhydride with Epoxides: A Chain-Growth Approach to Unsaturated Polyesters. *J. Am. Chem. Soc.* **2011,** *133*, 10724-10727.
20. Longo, J. M.; Sanford, M. J.; Coates, G. W., Ring-Opening Copolymerization of Epoxides and Cyclic Anhydrides with Discrete Metal Complexes: Structure-Property Relationships. *Chem. Rev.* **2016,** *116*, 15167-15197.
21. Stößer, T.; Williams, C. K., Selective Polymerization Catalysis from Monomer Mixtures: Using a Commercial Cr‐Salen Catalyst To Access ABA Block Polyesters. *Angew. Chem. Int. Ed.* **2018,** *57*, 6337-6341.
22. Stößer, T.; Mulryan, D.; Williams, C. K., Switch Catalysis To Deliver Multi-Block Polyesters from Mixtures of Propene Oxide, Lactide, and Phthalic Anhydride. *Angew. Chem. Int. Ed.* **2018,** *57*, 16893-16897.
23. Stosser, T.; Williams, C. K., Selective Polymerization Catalysis from Monomer Mixtures: Using a Commercial Cr-Salen Catalyst To Access ABA Block Polyesters. *Angew. Chem. Int. Ed.* **2018,** *57*, 6337-6341.
24. Hansell, C. F.; Espeel, P.; Stamenovic, M. M.; Barker, I. A.; Dove, A. P.; Du Prez, F. E.; O'Reilly, R. K., Additive-Free Clicking for Polymer Functionalization and Coupling by Tetrazine-Norbornene Chemistry. *J. Am. Chem. Soc.* **2011,** *133*, 13828-13831.
25. Williams, R. J.; Barker, I. A.; O'Reilly, R. K.; Dove, A. P., Orthogonal Modification of Norbornene-Functional Degradable Polymers. *ACS Macro Lett.* **2012,** *1*, 1285-1290.
26. Du, J. Z.; Willcock, H.; Patterson, J. P.; Portman, I.; O'Reilly, R. K., Self-Assembly of Hydrophilic Homopolymers: A Matter of RAFT End Groups. *Small* **2011,** *7*, 2070-2080.
27. Schaefer, M.; Hanik, N.; Kilbinger, A. F. M., ROMP Copolymers for Orthogonal Click Functionalizations. *Macromolecules* **2012,** *45*, 6807-6818.
28. Scharfenberg, M.; Hofmann, S.; Preis, J.; Hilf, J.; Frey, H., Rigid Hyperbranched Polycarbonate Polyols from CO2 and Cyclohexene-Based Epoxides. *Macromolecules* **2017,** *50*, 6088-6097.
29. Schubert, C.; Osterwinter, C.; Tonhauser, C.; Schomer, M.; Wilms, D.; Frey, H.; Friedrich, C., Can Hyperbranched Polymers Entangle? Effect of Hydrogen Bonding on Entanglement Transition and Thermorheological Properties of Hyperbranched Polyglycerol Melts. *Macromolecules* **2016,** *49*, 8722-8737.
30. Blanazs, A.; Armes, S. P.; Ryan, A. J., Self-Assembled Block Copolymer Aggregates: From Micelles to Vesicles and their Biological Applications. *Macromol. Rapid. Comm.* **2009,** *30*, 267-277.
31. Mai, Y. Y.; Eisenberg, A., Self-assembly of block copolymers. *Chem. Soc. Rev.* **2012,** *41*, 5969-5985.
32. Kubo, T.; Bentz, K. C.; Powell, K. C.; Figg, C. A.; Swartz, J. L.; Tansky, M.; Chauhan, A.; Savin, D. A.; Sumerlin, B. S., Modular and rapid access to amphiphilic homopolymers via successive chemoselective post-polymerization modification. *Polym. Chem.* **2017,** *8*, 6028-6032.
33. Jiang, X.; Feng, C.; Lu, G. L.; Huang, X. Y., Thermoresponsive Homopolymer Tunable by pH and CO2. *ACS Macro Lett.* **2014,** *3*, 1121-1125.
34. Basu, S.; Vutukuri, D. R.; Shyamroy, S.; Sandanaraj, B. S.; Thayumanavan, S., Invertible amphiphilic homopolymers. *J. Am. Chem. Soc.* **2004,** *126*, 9890-9891.

35. Savariar, E. N.; Aathimanikandan, S. V.; Thayumanavan, S., Supramolecular assemblies from amphiphilic homopolymers: Testing the scope. *J. Am. Chem. Soc.* **2006,** *128*, 16224-16230.
36. Arumugam, S.; Vutukuri, D. R.; Thayumanavan, S.; Ramamurthy, V., Amphiphilic homopolymer as a reaction medium in water: Product selectivity within polymeric nanopockets. *J. Am. Chem. Soc.* **2005,** *127*, 13200-13206.
37. Xu, Q. S.; Li, S. L.; Yu, C. Y.; Zhou, Y. F., Self-assembly of Amphiphilic Alternating Copolymers. *Chem.-Eur. J.* **2019,** *25*, 4255-4264.
38. Zhang, J.; Liu, K. L.; Mullen, K.; Yin, M. Z., Self-assemblies of amphiphilic homopolymers: synthesis, morphology studies and biomedical applications. *Chem. Commun.* **2015,** *51*, 11541-11555.

Chapter 4

Bio-Derived Degradable Block Copolymers as Pressure-Sensitive Adhesives



Well-defined bio-based triblock copolymers are prepared using a mixture of renewable monomers in one-pot using a homogenous catalyst. These materials show excellent adhesive properties and are easily degradable under acidic conditions.

4.1. Introduction

Pressure-sensitive adhesives (PSAs) are a class of viscoelastic materials that represent the fastest growing product in the adhesives market with applications spanning the packaging, medical, automotive and electric industries.[1-2] Typically, PSAs are formulated using ABA-type styrenic triblock copolymers (SBCs), where A and B consist of high T_g styrene hard blocks and low T_g butadiene or isoprene-based soft blocks, respectively, mixed with additives such as tackifier resins, plasticizers and stabilizers.[2-4] Problems associated with SBCs' dependence on depleting petroleum sources and its non-degradable nature have motivated research into renewable and degradable polymers. [5-8] Aliphatic polyesters are promising options as they contain degradable linkages and are often prepared from bio-renewable monomers.[9-11] As such, polyesters may be used to replace traditional SBC-based adhesives if they can display peel adhesion that matches current commercial products.

In 2011, Hillmyer & Tolman and co-workers utilized the ring opening polymerization (ROP) of renewable (-)menthone and lactide to prepare ABA-type triblock copolymers, which when mixed with tackifiers, resulted in moderate adhesive properties (peel adhesion = 3.2 N cm^{-1}).[12] In 2015, the researchers attempted to improve the peel adhesion by employing a two-step method consisting of (-)menthone ROP followed by radical polymerization of an alkene substituted lactone to add more suitable hard blocks. [13] This method afforded triblock copolymers with superior PSA qualities (peel adhesion = 9.9 N cm^{-1}) at the expense of non-degradable blocks. Shin and co-workers attempted a one-pot two-step ROP of ε-decalactone (DL, derived from castor oil) and lactide to prepare triblocks for PSAs.[14] Whilst this method utilized

renewable monomers and retained fully degradable ester linkages, the block copolymer required additives and offered moderate adhesive properties (peel adhesion = 2.6 N cm^{-1}).[14] These results suggested polylactide (PLA) may not be the most optimal polyester for use as the hard segment as not only can it not offer sufficient tack to the material but also its low T_g (50-60 °C) limits its usage range. As such, there is a need to investigate fully degradable triblock copolyesters that display high peel adhesion (> 5 N cm^{-1}).

An alternative method to the lactone ROP previously used is through the ring opening copolymerization (ROCOP) of epoxides and cyclic anhydrides.[15] This method has advantages due to the highly controlled nature of the synthesis and the variety of structures and properties accessible through altering either of the two monomers. Polyesters made from ROCOP with higher T_g (> 60°C) commonly employ cyclohexene oxide (CHO) or propylene oxide (PO) as the epoxide and phthalic anhydride (PA) as the anhydride.[15] However, these monomers are typically derived from petroleum sources and thus the resultant polyester cannot be considered as renewable. Nevertheless, it is worth noting that there are reports suggesting these monomers can be derived from agricultural waste and plant oil which may be applicable in the future (See Appendix for industrial and potential renewable routes to monomers).[16-21]

In the attempts to prepare polyesters with higher renewable content, Coates and co-workers have combined a range of different tricyclic anhydride (TCAs) derived from terpenes/sugar-based sources,[22] together with either PO or CHO to prepare a range of polyesters.[23-24] On the other hand, Kleij and co-workers have replaced CHO/PO with different terpene-based epoxides, including the commercially available

limonene oxide (LO), which can undergo ROCOP with aromatic based anhydrides such as PA to afford polyesters with high T_g.[25] In particular, LO is increasingly becoming an important monomer as it can be derived from fully bio-based sources.[25-30]

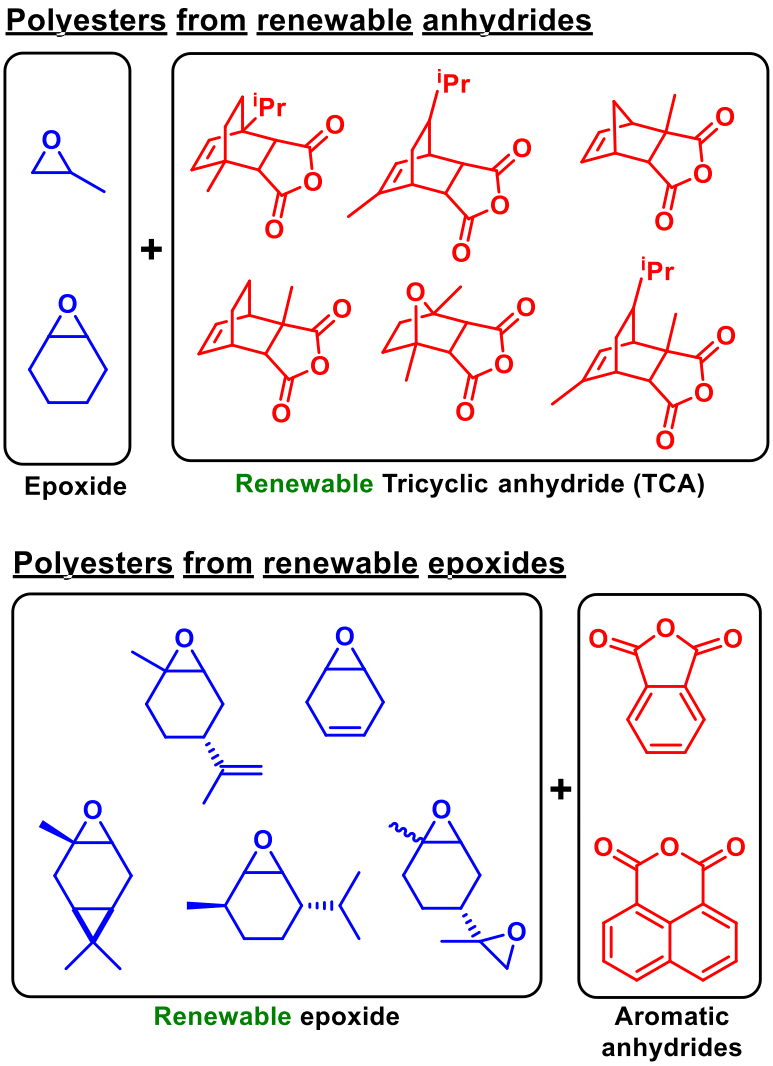


Figure 4.1 Literature examples of polyesters synthesised through ROCOP utilizing either renewable anhydrides (TOP)[23-24] or epoxides (Bottom).[25]

4.2. **Aims**

New fully renewable and degradable triblock copolymers are to be synthesised and tested for their potential as PSAs with high peel adhesion. To accomplish this there are three objectives to achieve:

First, suitable fully-renewable hard block polyesters (PE) are to be investigated. As mentioned in Section 4.1, ROCOP is a useful method for synthesising polyesters with higher T_g, but currently no fully renewable (i.e. 100%) ROCOP-derived polyesters exist. To enhance the renewable content of the ROCOP polyesters, both renewable epoxides and anhydrides will be utilized. By using monomers with rigid rings, the resulting polyesters are likely to have higher T_g. For example, by combining LO with TCAs, the resultant polyester may be able to reach a theoretical renewable content of 100% (based on weight of the monomers used). To make these polyesters, it will be necessary to find a suitable catalyst and once a successful system is established a systematic series of materials will be targeted.

Second, the 'hard' ROCOP-based polyesters, with higher T_g, need to be combined with low T_g 'soft' polyesters, made from ROP of DL, ideally this will be achieved using a one pot strategy. To make the target ABA-type 'hard-soft-hard' triblock copolyesters the synthetic strategy will be to employ a bifunctional initiator, such as 1,4-benzenedimethanol (BDM), together with a catalyst capable of switching between the two different polymerization cycles (ROP and ROCOP) (Fig. 4.2). The formation of the block polymer structures will be examined using a range of techniques, including NMR spectroscopy and SEC analysis.

Third, the triblock copolymers' thermal and mechanical properties are to be examined using a combination of thermal gravimetric analysis (TGA), differential scanning calorimetry (DSC) and dynamic mechanical thermal analysis (DMTA). Furthermore, their potential as new PSA will studied using the ISO standardised 180° peel test on steel substrates.

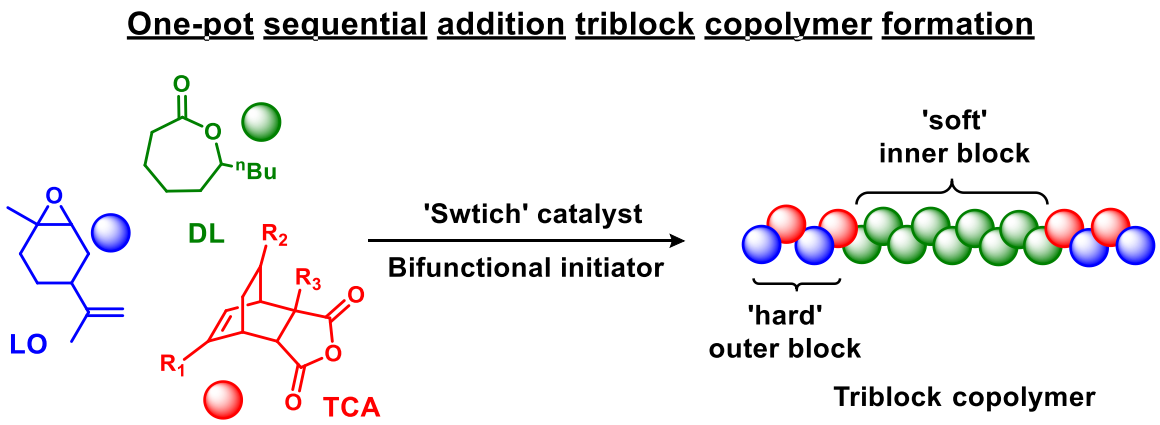
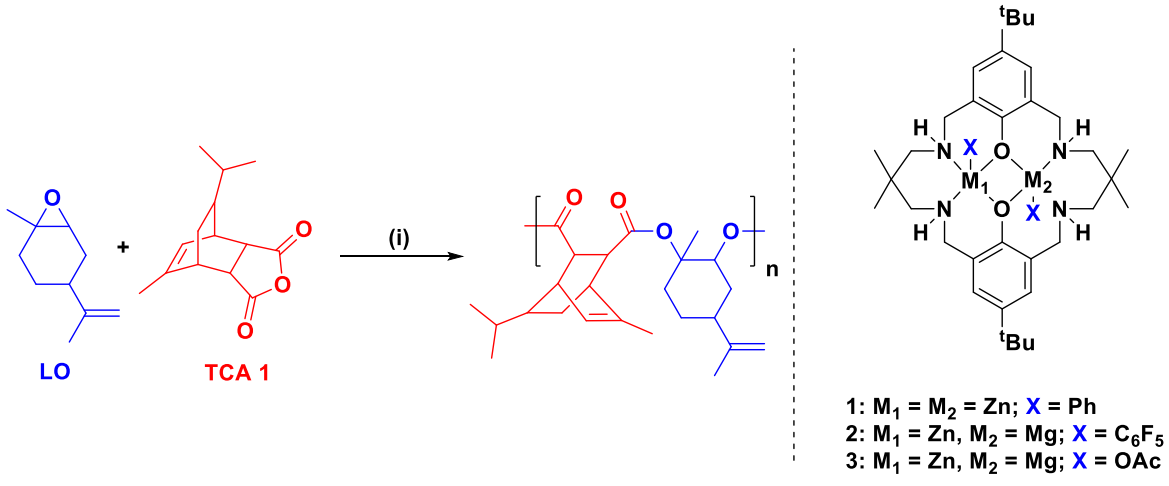


Figure 4.2 One post synthesis for triblock copolymers using a combination of LO, DL and TCA with a 'switch' catalyst and bifunctional initiator.

4.3. **Hard block polyester through ROCOP**

The first step in establishing plausible routes to hard block polyesters (PE) made from LO and TCA is to determine a suitable catalyst for the ROCOP reaction. The recently reported heterodinuclear Zn/Mg catalyst, [LMgZn(C_6F_5)$_2$], **2**, was chosen for two reasons (See Appendix for ^{1}H and ^{13}C NMR spectra of the complex, Figs. S61 – S62). First, the heterodinuclear nature of the catalyst results in faster polymerization rates compared to its homodinuclear counterpart such as [LZn_2Ph_2], **1**, used in Chapter 3.[31] This was particularly important as both the epoxide (LO) and anhydride (TCA) are sterically hindered and is slow to polymerize. For instance, in the reaction between LO and TCA 1 (Scheme 4.1), no conversion was observed after 48 h with [LZn_2Ph_2] (**1**) /BDM at 140 °C (Table 4.1, Entry 1). In contrast, when **2** was utilized, the ROCOP proceeded to full conversion (>99 %) after 22 h under the same conditions (Table 4.1, entry 3). It is worth noting that the reaction is also feasible at 120 °C, albeit the expected slower rates (Table 4.1, entry 2).



Scheme 4.1 ROCOP of LO with TCA 1 using various dinuclear catalysts **1**, **2**, and **3**. (i): Molar ratio: [cat.]/[BDM]/[TCA 1]/[LO] = 1/4/100/300, 120-140 °C, 22-48 h.

Table 4.1 ROCOP of LO with TCA 1 using various dinuclear catalysts **1**, **2**, and **3**.

#	Catalyst	Temp (°C)	Time (h)	Conv. (%)[a]	Polyester Selec. (%)[b]	M_n (kg mol^{-1}) [$Đ$][c]
1	**1**	140	48	0	-	-
2	**2**	120	46	>99	>99	6.2 [1.18]
3	**2**	140	22	>99	>99	6.3 [1.19]
4	**3**	140	22	>99	>99	4.2 [1.10], 1.8 [1.11]

Reaction conditions: [catalyst]/[BDM]/TCA 1/ BDM = 1/4/100/300, 120 or 140 °C. [a]Conversions obtained from ^{1}H NMR spectra by comparing the monomer and polymer peaks at 5.62 ppm and 5.70-5.72 ppm, respectively. [b]Polyester selectivity obtained from ^{1}H NMR spectra by comparing the polyester and polyether peaks at 5.70-5.72 ppm and 3.30-3.60 ppm, respectively. [c]M_n and $Đ$ measured by SEC (THE as eluent, 1 mL/min, 30 °C, calibrated using polystyrene standards).

Furthermore, **2** has non-initiating co-ligands (C_6F_5) which react in situ with BDM to yield only α,ω-dihydroxyl telechelic polymer chains which are needed to produce ABA-block polymers. This high selectivity is important as catalysts containing initiating co-ligands (e.g. acetates (OAc) in [LMgZn(OAc)$_2$], **3**) yield a mixture of α,ω-dihydroxyl telechelic and α-acetate-ω-hydroxyl polymer chains.[32-33] The two different types of chains can be distinguished using SEC analysis. For instance, the polymer formed using **2** shows a monomodal peak with a molar mass of 6.3 kg mol^{-1} and a dispersity of 1.19 (Table 4.1, Entry 3 and Fig. 5.3 red solid line). This suggests that the polymer has a single type of end-group. In contrast, when **3** was used a bimodal peak is observed which is consistent with two different polymer end groups (Table 4.1, Entry 4 and Fig. 4.3 (black dashed line)). One of the peaks has a molar mass of 4.2 kg mol^{-1} and the other has around half the molar mass. The bimodal distribution most likely arose from the mixture of initiators (the bifunctional BDM and monofunctional acetate) present in the reaction. The presence of multiple initiators also leads to lower

overall molar mass. Furthermore, any further block copolymer formation on the bimodality mixture would result in a blend of ABA and AB block copolymers, which would affect the final product properties. As the eventual target would be ABA-type block polymers, the **2**/BDM catalyst system is chosen in order to obtain solely telechelic polymer chains and to maximize the molar mass obtained.

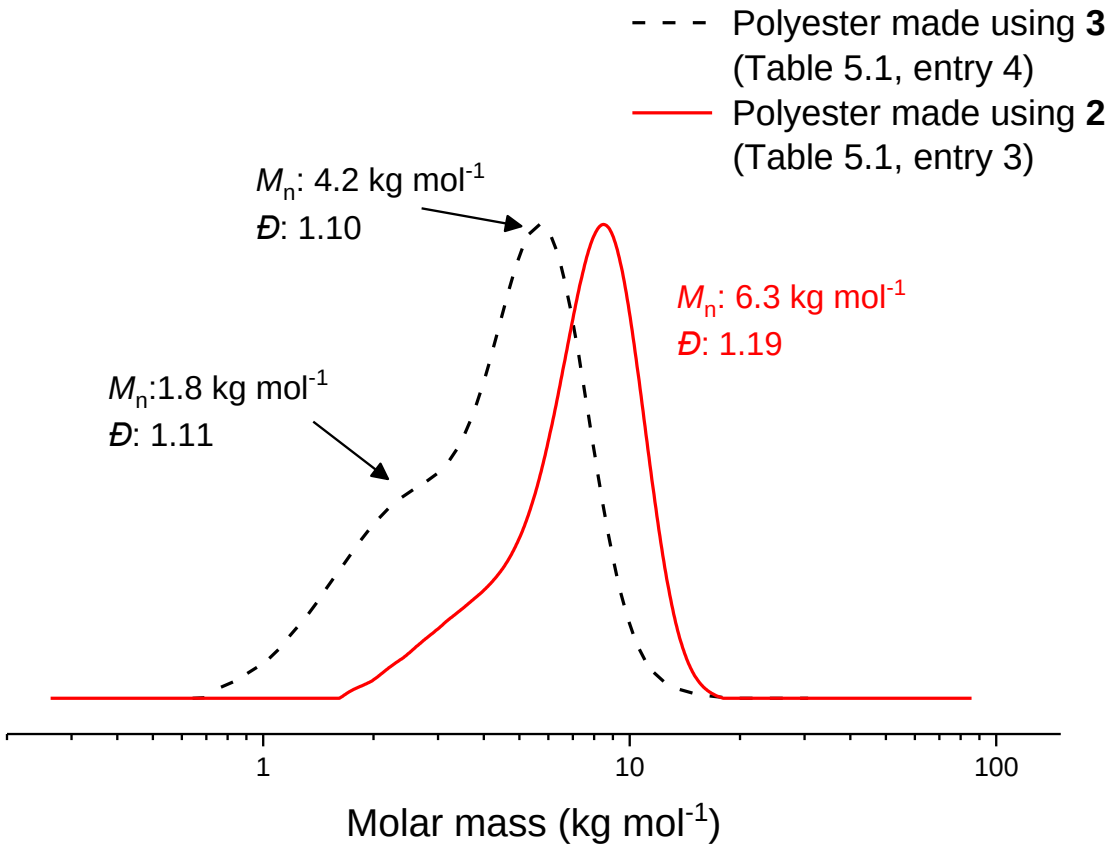
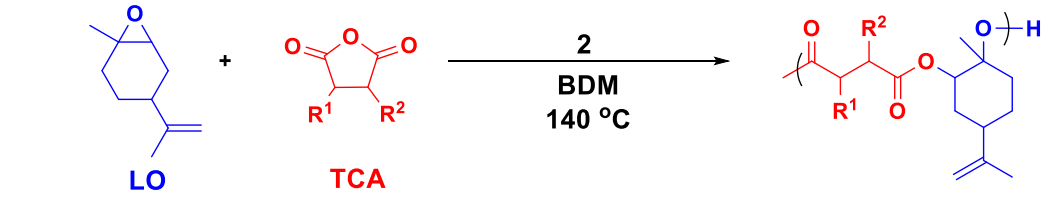
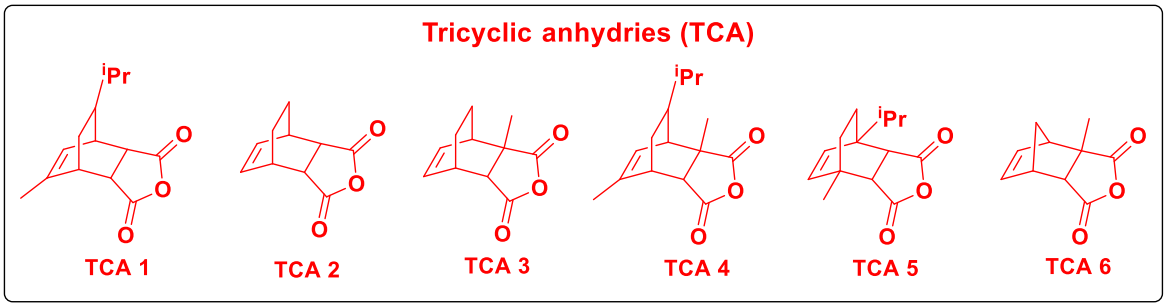


Figure 4.3 SEC curve comparison between the polymer product made using catalyst **2** and **3**.

Six different TCAs with varying renewable potential were examined to test for their compatibility in the ROCOP with LO at 140 °C using **2** and BDM as the catalyst and initiator, respectively (Table 4.2).

Table 4.2 ROCOP of LO and TCAs





#	TCA	Time (h)	Conv. (%)[c]	Selec. (%)[d]	M_n (kg mol^{-1})[e]	$Đ$[e]	T_g (°C)[f]	$T_{d,5}$ (°C)[g]
1	TCA 1	22	>99	>99	6.3	1.19	93	259
2[a]	TCA 1	14	>99	>99	7.0	1.18	92	258
3[b]	TCA 1	34	0	-	-	-	-	-
4	TCA 2	11	>99	>99	5.4	1.19	102	266
5	TCA 3	53	>99	>99	5.9	1.15	82	264
6	TCA 4	75	>99	>99	5.3	1.18	88	260
7	TCA 5	110	>99	>99	2.9	1.40	N/A	N/A
8	TCA 6	34	0	-	-	-	-	-

Reaction conditions: [**1**]/[BDM]/[TCA]/[LO] = 1/4/100/300, 140 °C. [a]*trans*-limonene oxide used. [b]*cis*-limonene oxide used. [c]Conversions obtained from ^{1}H NMR spectra (See Appendix for specific peaks). [d]Selectivity of polyester vs. polyether, determined from ^{1}H NMR spectra by comparing main chain signals to signals in the polyether region (3.3-3.6 ppm). [e]M_n and $Đ$ measured by SEC (THF as eluent, 1 mL/min, 30 °C, calibrated using polystyrene standards). [f]Determined by DSC (from 3rd heating cycle). [g]Decomposition temperature (at 5% decomposed mass) determined by TGA.

The result suggests that TCA 1-5 can be polymerized with LO using the **2**/BDM catalyst system (Table 4.2, entry 1, 4-7). No anhydride conversion was seen for ROCOP of LO with TCA 6 after 34 h at 140 °C (Table 4.2, entry 8). An examination of the ^{1}H NMR spectrum of the reaction product suggests TCA 6 had degraded. This may be due to the higher ring strain of the norbornene moiety in TCA 6 and indicates TCA 6 is not stable under the reaction conditions. Whilst full conversion can be observed in the ROCOP between LO and TCA 5, the reaction takes over 100 h and the resulting polymer has half the molar mass compared to those obtained using TCA 1 – 4 with higher dispersity ($Đ$ = 1.40).

The ROCOP rate depends on the anhydride steric hindrance, specifically upon the number and position of the substituents present. For instance, TCA 1 has methyl and isopropyl substituents compared to unsubstituted TCA 2. However, the latter required doubled the reaction time to reach full conversion compared to the former (Table 4.1, Entry 1 and 4). Moreover, while TCA 1 and 5 both have additional methyl and isopropyl substituents, the former is 5 times faster (Table 4.1, Entry 1 and 7). Thus, the closer the substituents are to the anhydride unit, the slower the reaction rate. This effect is perhaps most apparent when comparing the rates for TCA 1 and TCA 3. Whilst TCA 1 has an additional isopropyl group compared to TCA 3, its rate is twice that of TCA 3 (Table 4.2, Entry 1 and 5).

The influence of LO stereochemistry on the ROCOP was examined. Although full conversion was observed for LO/TCA 1 ROCOP, no conversion was observed when *cis*-LO was used (Note: commercial LO has a *trans*/*cis* diastereoisomer ratio of 60:40) (Table 4.2, Entry 1 and 3). Using *trans*-LO resulted in ~40% faster rate compared to

the reaction using the *cis*/*trans* mixture (Table 4.2, Entry 1 and 2). As the ROCOP rate is expected to be first order in epoxide concentration,[15, 34] the catalyst system is expected to react fastest with the *trans*-LO, in most cases, *cis*-LO is not polymerized (remain as the solvent). In this work, our goal was to use the mixture of *cis* and *trans*-LO as it is the most abundant raw material.

The ROCOP of LO with TCA 1-4 reached full anhydride conversion (>99 %) with molar masses between 5 – 7 kg mol^{-1} and narrow dispersities ($Đ \leq 1.19$) (Table 4.2, Entry 1, 4 – 6). These reactions are the first examples of LO/TCA ROCOP and no control reactions were performed to investigate the polymerization. The ROCOP of LO/TCA 1 was monitored by regular removal of aliquots for analysis by ^{1}H NMR spectroscopy and SEC to obtain conversion, M_n and dispersity data. The linear plot of M_n vs. monomer conversion shows that the polymerization is controlled and that the number of chains remaining constant (Fig. 4.4). Stacked SEC traces, from aliquots with 5 % to 95 % conversion, all showed monomodal peaks with low dispersities ($Đ \leq 1.19$) and a consistent linear increase in molar mass (Fig. 4.5).

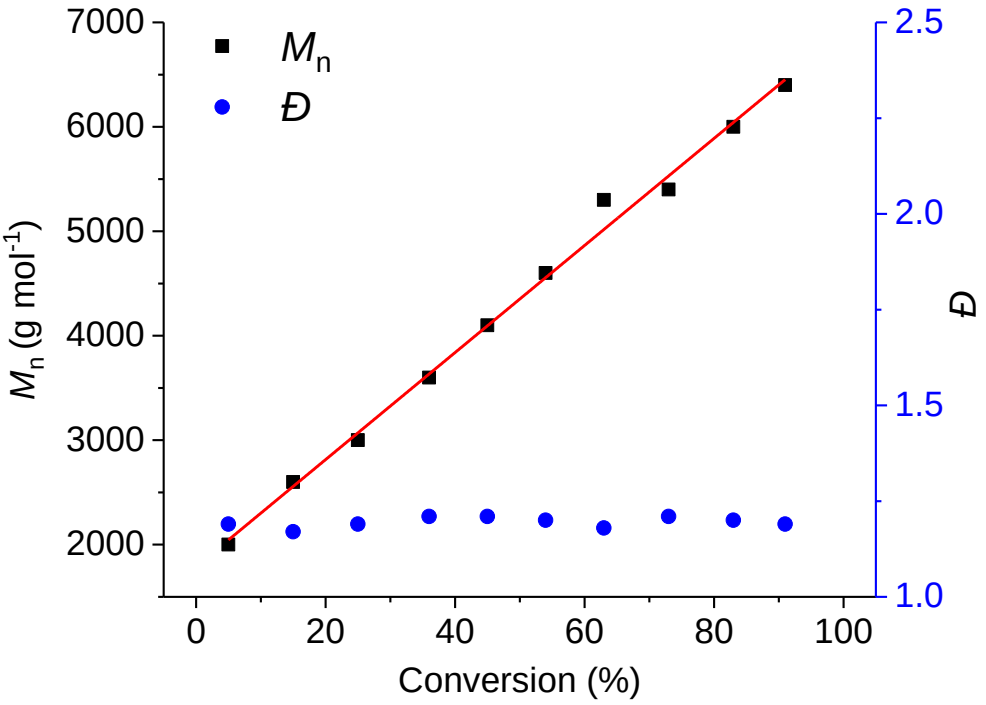


Figure 4.4 M_n and $Đ$ vs. conversion for the ROCOP of LO/TCA 1

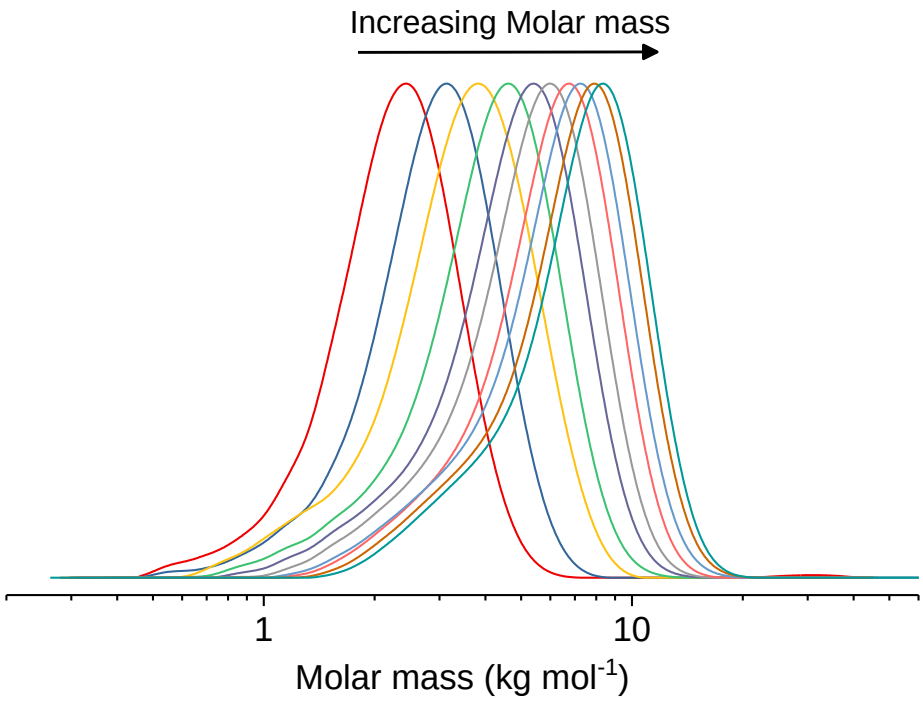


Figure 4.5 SEC traces of aliquots obtained in thee ROCOP of LO/TCA 1 (between 5% and 90% conv.)

The linear plot of TCA 1 conversion (%) *vs.* time is indicative of zeroth order kinetics for the anhydride (Fig. 4.6). This observation suggests that the anhydride insertion is pre-rate limiting which is similar to previous reports of epoxide/anhydride ROCOP.[15, 34-36]

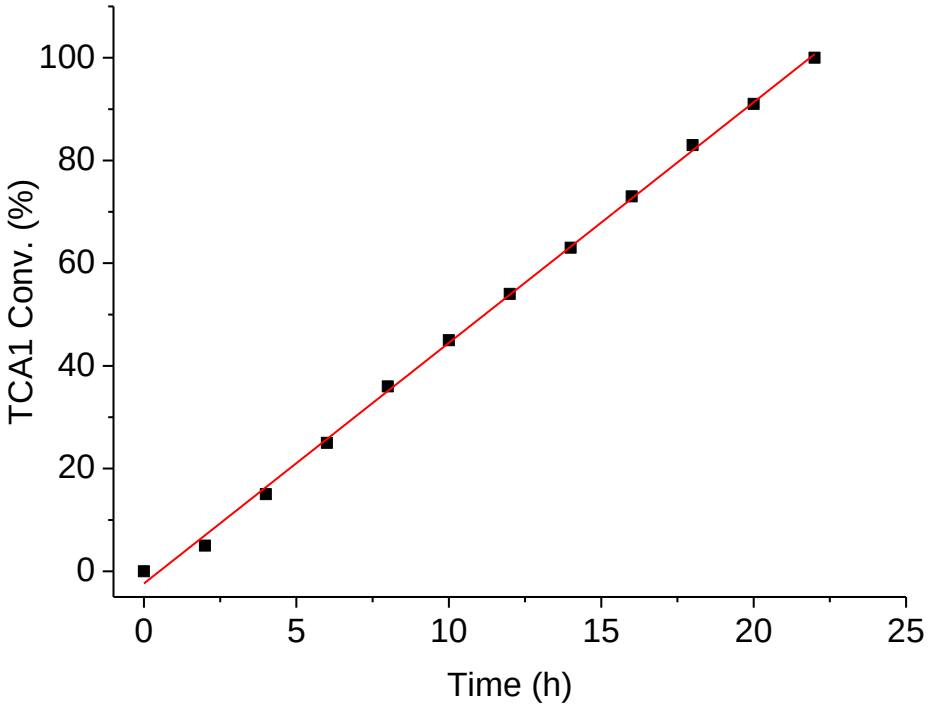


Figure 4.6 Conversion % vs. time for the ROCOP of LO/TCA 1.

The crude samples were purified by precipitation of a DCM solution of the polymer into methanol and the purified polyester was characterized by NMR spectroscopy and MALDI-ToF analysis. The ^{1}H NMR spectroscopy of the purified polyester indicated the chains are highly alternating as no ether linkages, at 3.30-3.60 ppm, were observable (Fig. 4.7). (See Appendix for the ^{1}H NMR spectra for the polyesters formed using TCA 2 – 4, Fig S63 – S65)

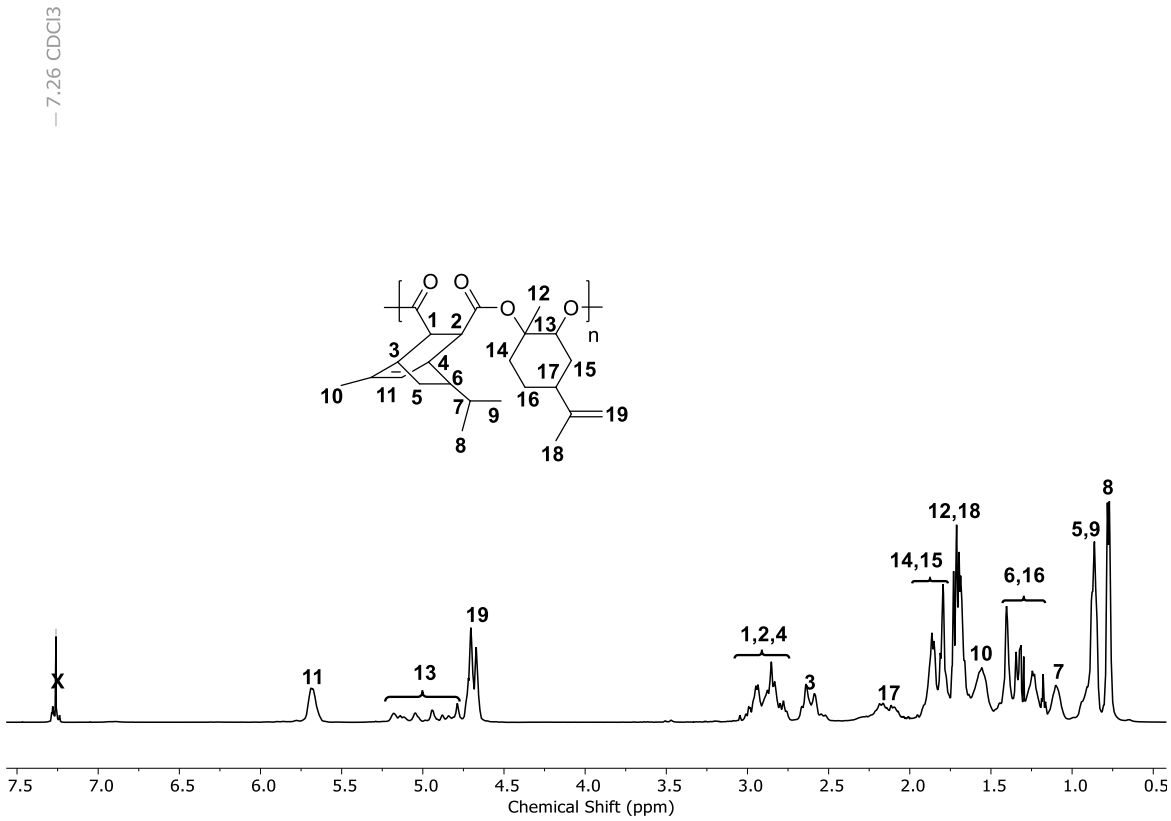


Figure 4.7 ^{1}H NMR of the polyester from the ROCOP of LO/TCA 1 ($CDCl_3$, 500.0 MHz, 298K).

Interestingly, the polyester LO methine proton was observed as a multiplet (4.78 - 5.18 ppm), which is a feature different to previous polymers utilizing LO. [25, 37] The HSQC NMR spectrum confirms these peaks correlate to carbon atoms in very similar environments, thus suggesting these peaks are likely the due the same proton. The multiplets are proposed to be due to regio-irregularity in the ROCOP process.

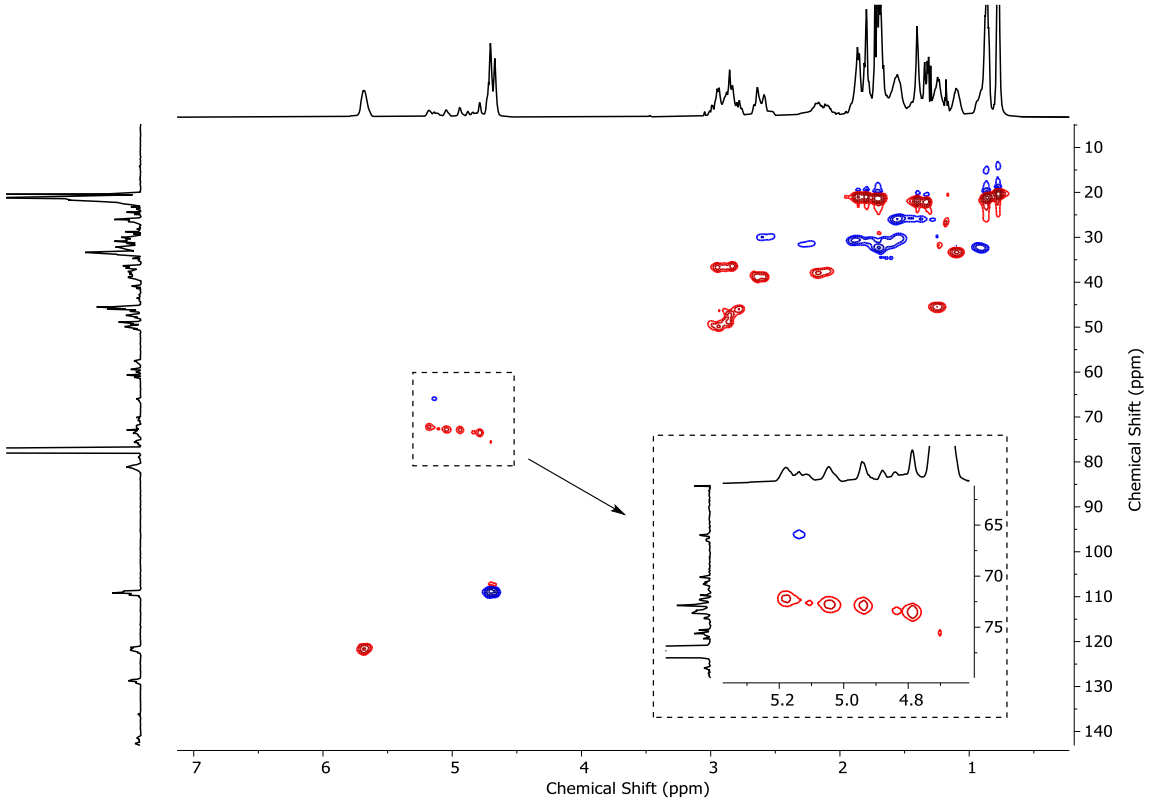


Figure 4.8 ^{1}H-^{13}C HSQC NMR spectrum of the polyester from the ROCOP of LO/TCA 1 in $CDCl_3$. Insert: selected expanded region illustrating multiplet splitting between 4.78-5.18 ppm correlating to very similar carbon environments.

MALDI-ToF analysis show two series of chains, each with a spacing of 386 *m/z* consistent with the expected repeat unit (Fig. 4.9). One series is assigned to chains initiated by BDM (α,ω-hydroxyl telechelic chains). The other minor population is assigned to cyclic polymers and these may have formed by transesterification side reactions. This was unexpected as **2** and its related macrocyclic-based catalysts (including **1** and **3**) had not previously produced cyclic polyesters in epoxide/anhydride ROCOP. [31-33]

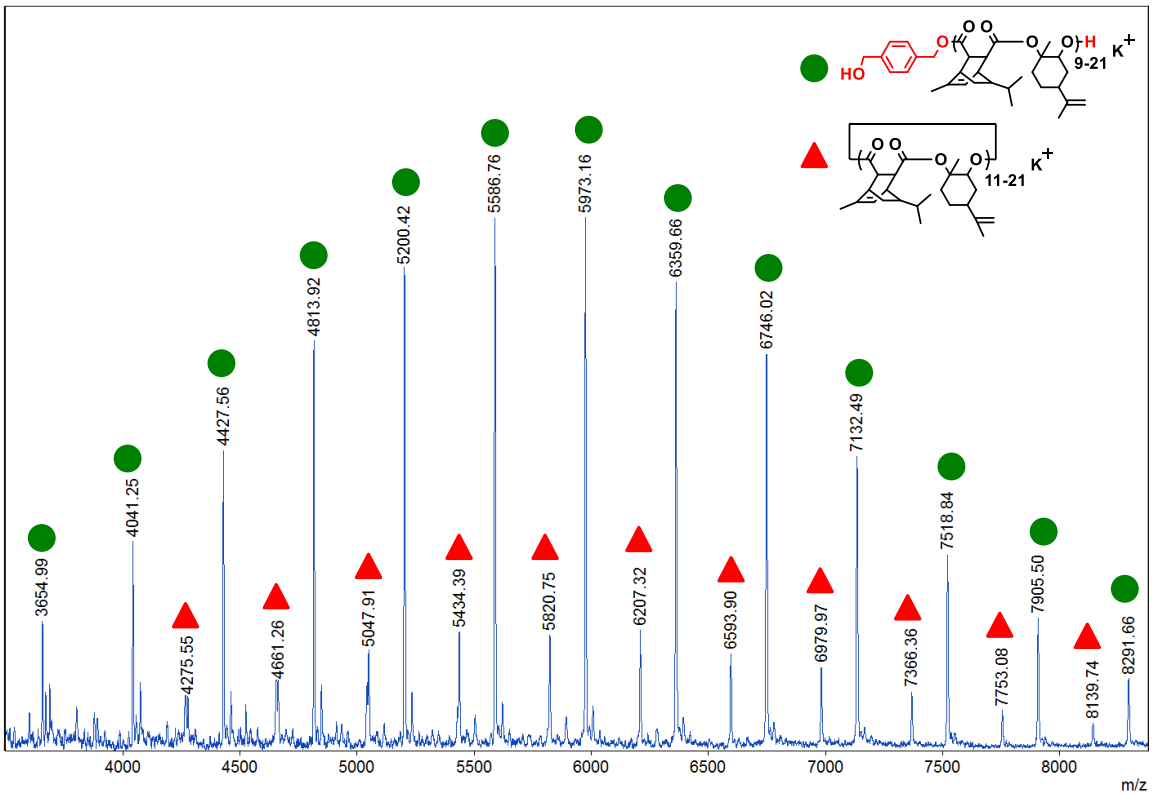


Figure 4.9 Representative MALDI-ToF of the polyester from the ROCOP of LO/TCA 1.

To investigate whether transesterification had occurred, the ROCOP of LO/TCA 1 at full conversion was deliberately heated at 140 °C for an extended period of time (7 days). The subsequent SEC trace showed no further transesterification as *Đ* remained ≤ 1.19 and no major changes in molar mass were seen (Fig. 4.10). The steric hindrance afforded by both monomers should hinder transesterification and the formation of cyclic polymers is inhibited. Thus, the cyclic polymers is tentatively attributed to a minor degree of transesterification (not observable by changes in the SEC traces).

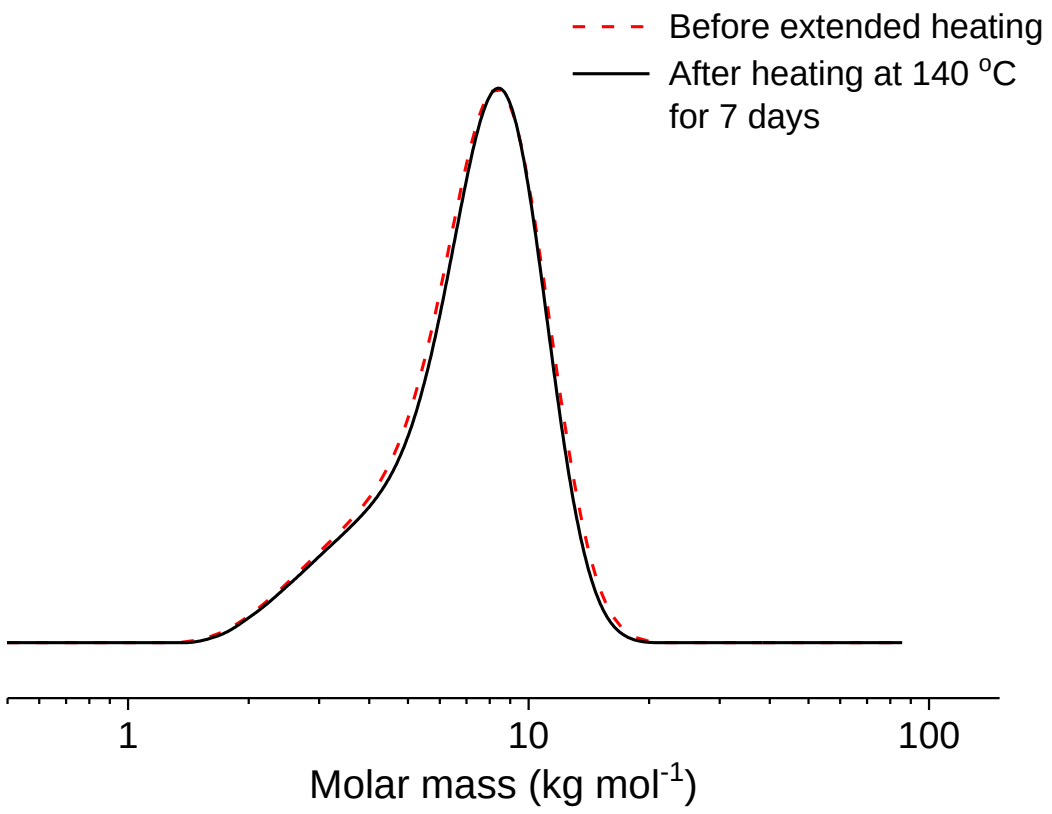


Figure 4.10 SEC trace comparison between before and after deliberate heating at 140 °C for 7 days for the ROCOP of LO/TCA 1.

A theoretical wt% renewable content for the polyesters was determined (Fig. 4.11). As mentioned, most ROCOP polyesters are made from either PO or CHO and PA which are currently derived from the petrochemicals propylene, benzene and o-xylene, respectively.[16, 18, 20] There are potential synthetic routes from renewable precursors (albeit with multiple steps) and these routes may be applicable in the future. For instance, PA may be obtained from the Diels-Alder reaction between maleic anhydride and furan.[19] Both of compounds can be obtained from cellulose through heat/acid treatments, dehydration, decarbonylation and oxidation reactions.[19, 38] PO may be obtained from propylene glycol, which is formed by the hydrolysis and subsequent

hydrogenation of glycerol (from triglycerides).[17] CHO may be obtained from the partial oxidation and subsequent hydrogenation of 1,4-cyclohexadiene, obtainable from the metathesis of plant oils.[39] In contrast, LO is clearly a renewable monomer as it is derived from the epoxidation of limonene, which is a biorenewable precursor obtained from waste citrus peels (yield: ~1 % by mass which is considered quite high as typical essential oil extraction has yields between 1-0.01 %) .[40] The TCAs are obtained through Diels-Alder reactions between dienes and maleic/citraconic anhydride. TCA 2 and 3 are derived from 1,3-cyclohexadiene,[24] which is produced from petrochemical benzene (i.e. it is not a renewable source).[41-43] Nevertheless, potential renewable routes to this diene from plant oils have been reported.[39] On the other hand, α-phellandrene, used in the synthesis of TCA 1 and 4, is a terpene (i.e. renewable precursor).[23] Maleic anhydride is used to make TCA 1 and 2 and is currently synthesised through the oxidation of n-butane,[44] but there are several routes from cellulose.[19, 38] Citraconic anhydride, used in the synthesis of TCA 3 and 4, is derived from itaconic acid.[23] Itaconic acid is produced by carbohydrate fermentation .[45-46] As such, it has been listed by the U.S. Department of Energy as one of the Top 12 chemicals derived from biomass.[45] Thus, by combining LO with various TCAs, polyesters with high theoretical renewable contents, including up to 100%, were synthesised (see the Appendix for schemes of the monomer synthesis).

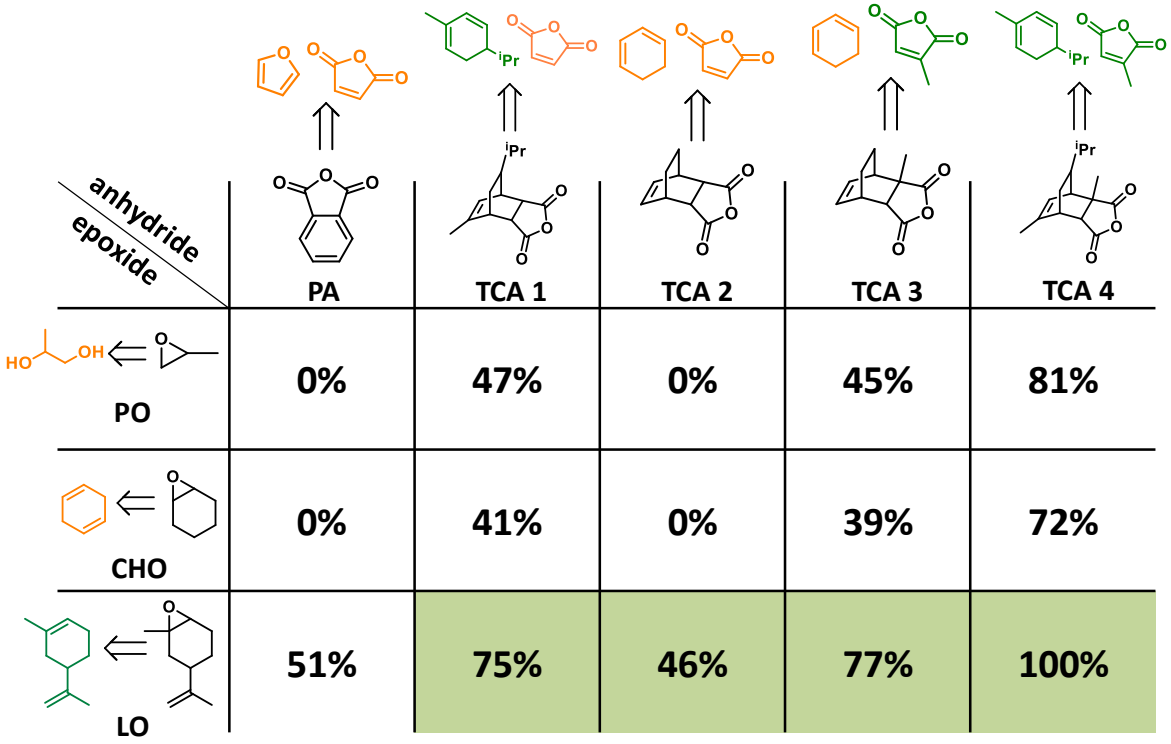


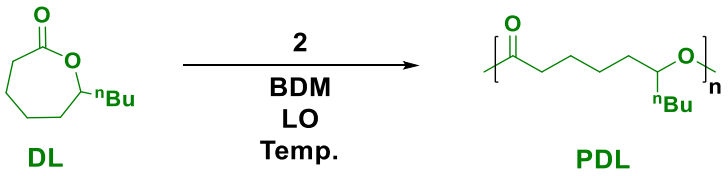
Figure 4.11 Assessed theoretical renewable content of polyesters from different epoxide/anhydride ROCOP (based on mass of monomers used). PO, CHO and PA are used in previous work (non-shaded boxes). Green shaded areas indicate newly synthesised polyesters. Orange and green structures indicate potentially renewable and fully renewable precursors for the epoxides and anhydrides (see Appendix for full monomer synthesis routes).

None of the polyesters displayed melting points (T_m), suggesting they are all amorphous. TGA analysis shows these PE have good thermal stability, with $T_{d,5}$ values between 258 – 266 °C. The T_g of the resulting polyesters ranged from 82 - 102 °C (Table 4.2). The polyester from unsubstituted TCA 2 resulted in highest T_g, consistent with similar polyesters.[47] These new biorenewable polyesters all display higher T_g values than alternative renewable polymers like PLA.

4.4. Soft block polyester through ROP

The 'soft' block polyester, poly(ε-decalactone) (PDL) was synthesized through DL ROP, using **2**/BDM, under a range of monomer ratios and temperatures (Table 4.3).

Table 4.3 ROP of DL



#	[2]/[BDM]/[DL]/[LO]	Temp (°C)	Time (min)	Conv. (%)[a]	TOF (h^{-1})[b]	M_n (kg mol^{-1})[c]	$Đ$[c]
1	1/4/500/500	25	15	25	500	7.5	1.08
2	1/4/500/500	40	5	25	1500	7.2	1.11
3	1/4/1000/1000	60	5	38	4560	22.9	1.08
4	1/4/1000/1000	80	5	57	6840	31.0	1.11
5	1/4/1000/1000	80	7	74	6340	37.6	1.32

[a]Conversions obtained from ^{1}H NMR spectra by comparing the monomer and polymer peaks at 4.15 ppm and 4.85 ppm, respectively. [b]Turn over frequency (TOF) is calculated based on number of mol of monomer converted/mol of catalyst/time. [c]M_n and $Đ$ measured by SEC (THF as eluent, 1 mL/min, 30 °C, calibrated using polystyrene standards).

The **2**/BDM catalyst system is highly active for the DL ROP, at 80 °C the TOF exceeds 6,800 h^{-1} (Table 4.3, entry 1 and 4). In addition, high molar mass PDL (M_n > 30 kg mol^{-1}) was prepared in a highly controlled manner ($Đ$ ≤ 1.11).

However, at DL conversion >60% transesterification side reactions do occur which was observed by increases in the dispersities ($Đ$ = 1.32) (Table 4.3, Entry 5). At higher conversions, DL concentration decreases significantly. As the ROP kinetics are typically first order in the monomer, this is expected to cause a decrease in the ROP rate. As such, the rate of transesterification may become competitive with propagation (Fig. 4.12). Overall, the results indicate that the DL ROP conversion using **2,** at a given monomer concentration, should be kept around 50-60% in order to circumvent any transesterification side reactions.

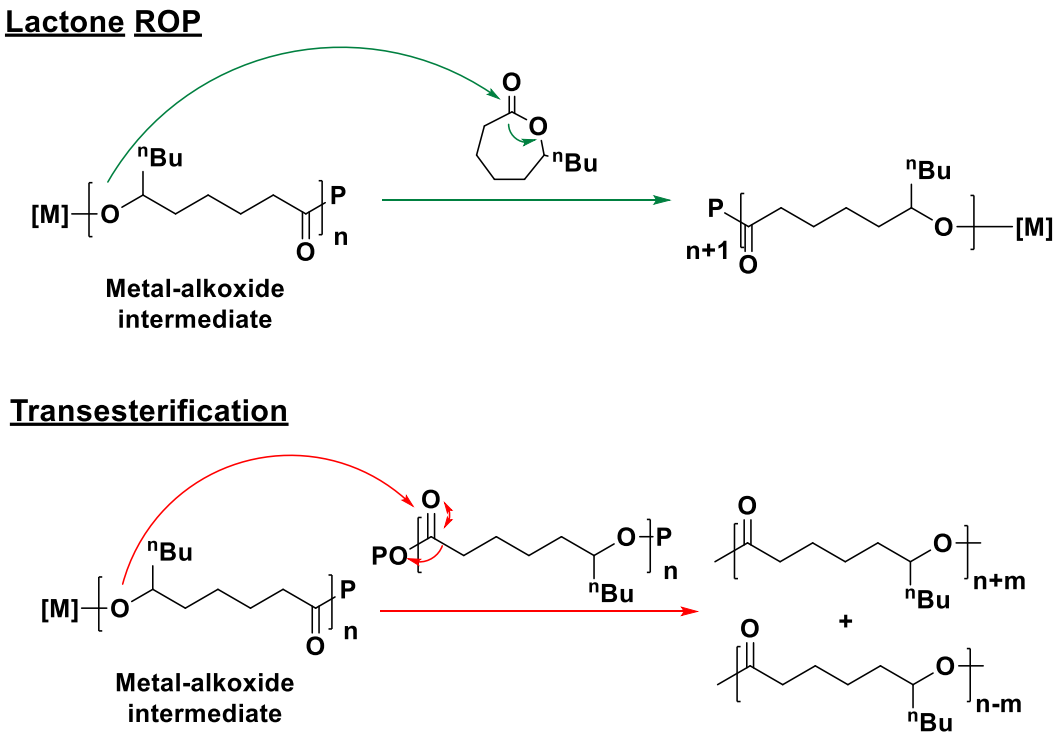
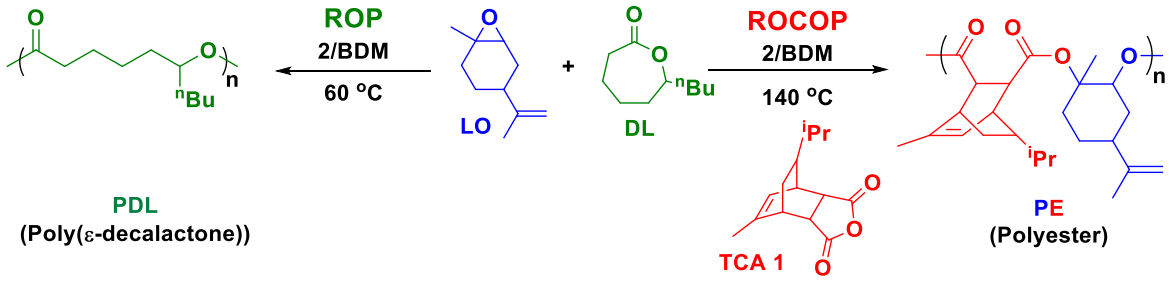


Figure 4.12 Illustration of the DL ROP and transesterification mechanisms. The latter may have become competitive at high DL conversion as the monomer concentration drops (note: P = polymer chain. n and m indicate number of repeat units and n≠ m and n > m).

4.5. **Triblock copolymer formation: Selectivity study**

Typical block polymer adhesives have an ABA-triblock structure with a '*hard-soft-hard*' block configuration, where the *soft* block provides the surface contact with the substrates, while the *hard* block provide resistance to shear.[12, 48] Previous work has shown that 'Switch Catalysis' (switching between ROP and ROCOP cycles using a single catalyst) provides an efficient route to block polymers obviating intermediate isolation and purification steps.[33, 49-51] These studies suggested that epoxide/anhydride ROCOP was faster (and thermodynamically favoured) than lactone ROP. Thus, mixtures of anhydride, epoxide and lactone would be expected to yield BAB-structure (with ROP polyester on the outside). To make the desired ABA structures, a sequential addition strategy was utilized with DL ROP occurring first followed by LO/TCA.

The same 'Switch' mechanism occurs between ROP and ROCOP and this addition strategy allows for high control of block composition (wt%) and molar mass. To establish the feasibility of the approach with sterically hindered anhydrides and epoxides, a selectivity study was conducted where the DL ROP was first carried out using **2**/BDM catalyst system at 60 °C to form PDL (Scheme 4.2, LHS). Once the desired conversion was reached (50-60% to limit PDL transesterification), TCA 1, the 'switch' reagent, was added and the catalyst changed from ROP to LO/TCA ROCOP (Scheme 4.2, RHS). To accelerate rates, the temperature was increased to 140 °C.



Scheme 4.2 Selectivity study using **2**/BDM catalyst system. (LHS) ROP of DL at 60 °C (RHS) ROCOP of LO/TCA 1 at 140 °C.

The reaction was monitored by periodic aliquot collection and the results revealed an immediate switch in polymerization mechanism when the TCA was added (Fig. 4.13).

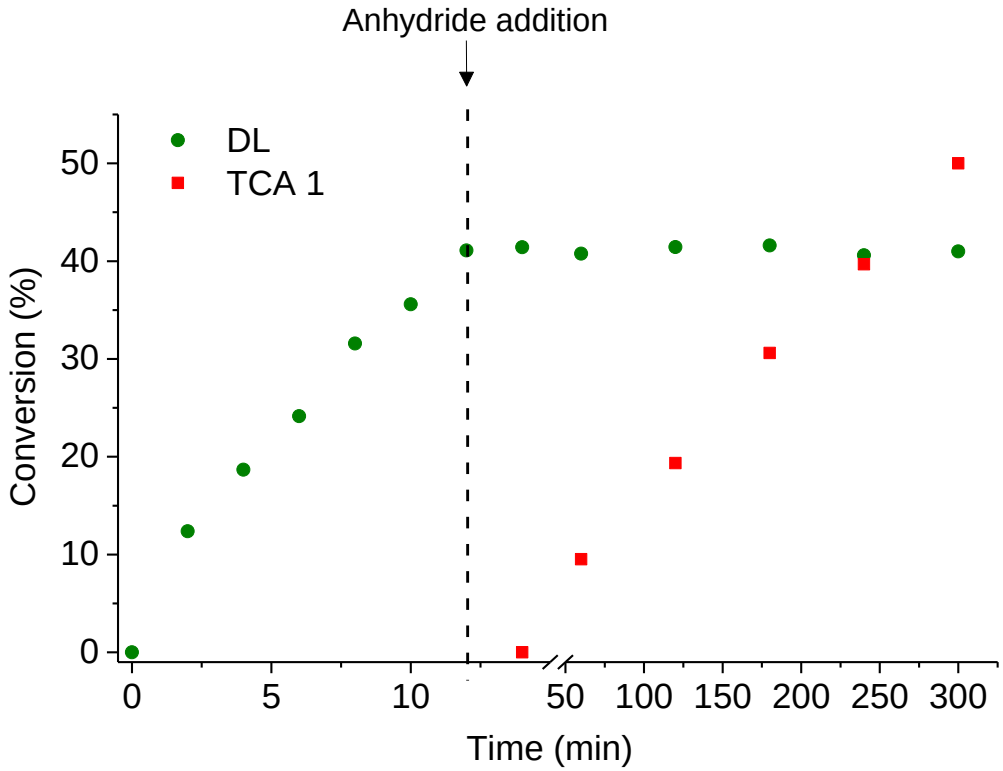


Figure 4.13 Conversion vs. time plot for the ROP of DL and ROCOP of LO/TCA 1.

The results showed that the insertion of anhydride is favoured over lactone into the common metal alkoxide intermediate. This observation agrees with previously reported switch catalysis and is likely to be due to both faster rates of anhydride insertion and formation of more stable metal carboxylate linkages (Fig. 4.14).[49]

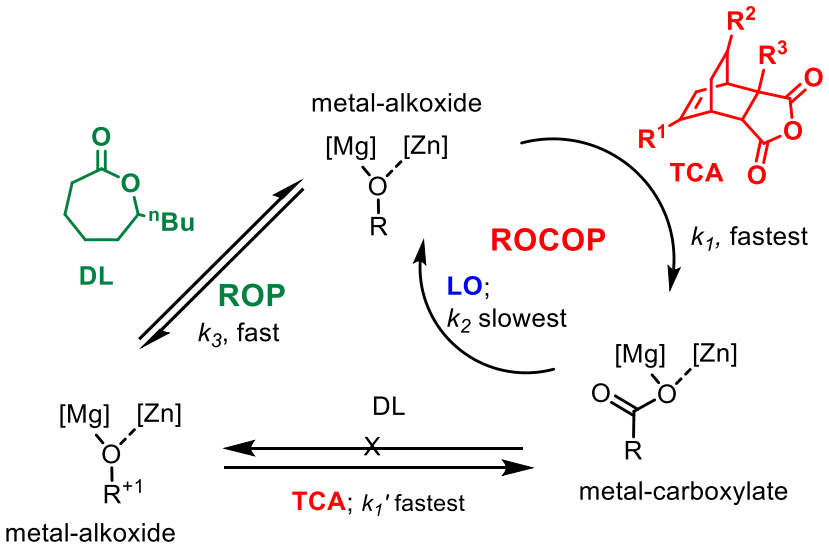
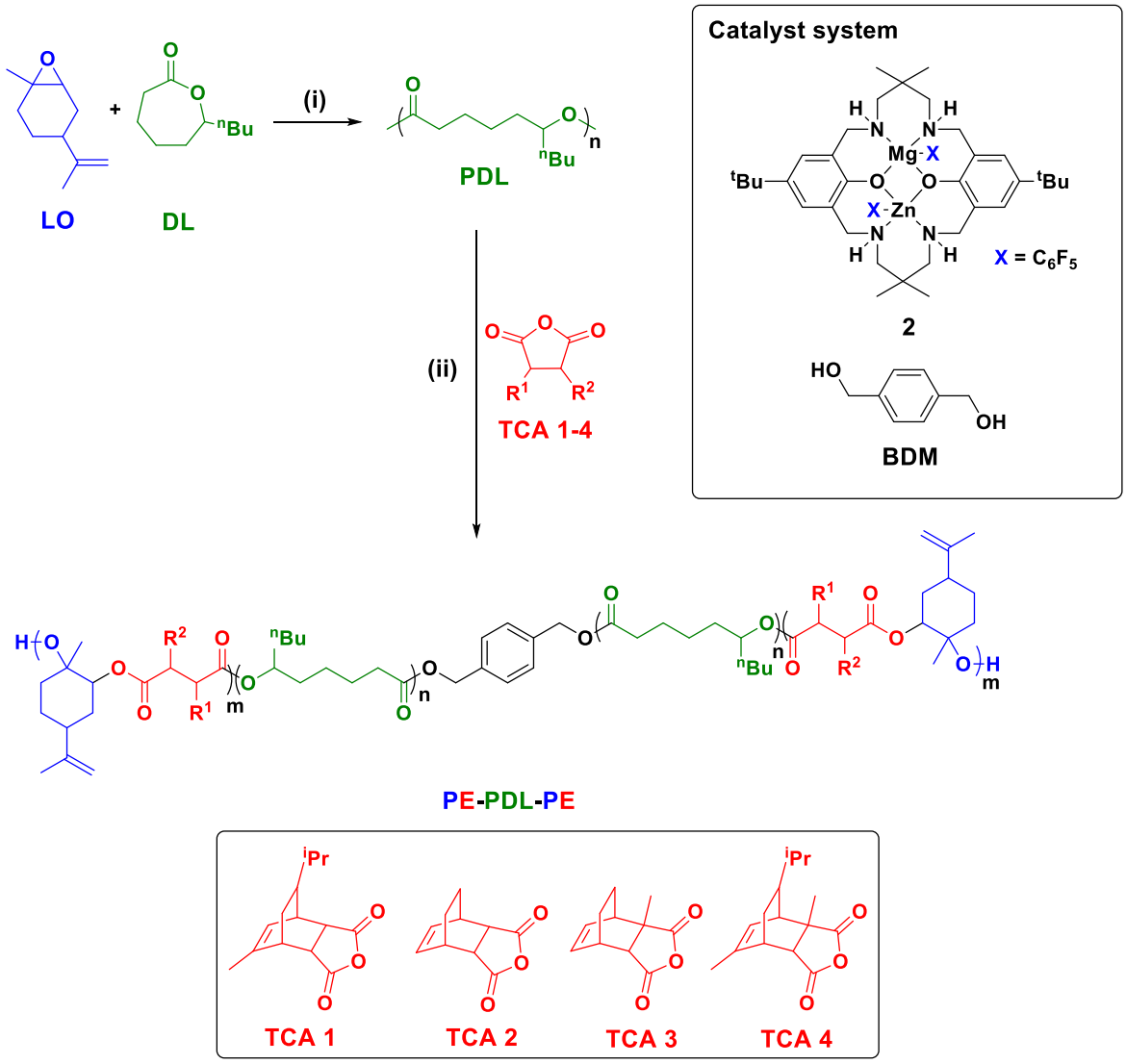


Figure 4.14 Proposed mechanism for ROCOP of LO/TCA and ROP of DL using a single catalyst

4.6. **Triblock copolymer formation: Material preparation**

A series of high renewable content polyesters were made from DL, LO and TCAs using the sequential addition 'method (Scheme 4.3).



Scheme 4.3 ABA-triblock polymer synthesis *via* a sequential addition strategy using **2**/BDM catalyst system with DL, LO and TCA 1-4 as monomers. (i): [1]/[BDM]/[DL]/[LO] = 1/4/800-1200/2000, 60 °C, 4-7 min. (ii): [TCA] = 1/75-225, 140 °C, 32-138 h (for exact molar ratios and reaction times please see Appendix).

Seven ABA-triblock polymers (**P14 – P20**) were made and the series showed systematic variation in the hard block weight% (wt%$_{Hard}$) and the type of TCAs (Table 4.4). By adjusting the monomer concentration and reaction times, the wt%$_{Hard}$ was easily varied from ~20% to ~50% (Table 4.4, Entry 1-4). The molar masses were measured using ^{1}H NMR spectroscopy and SEC and both methods showed close agreement with the theoretical M_n of ~40 kg mol^{-1}.

Table 4.4 One pot ABA-triblock copolymer

#	TCA used	$M_{n,\,NMR}$ (kg mol^{-1})[a]			Wt%$_{Hard}$[b]	$M_{n,\,SEC}$ (kg mol^{-1}) [$Đ$][c]		T_g (°C)[d]	Renewable content (%)[e]
		PDL	PE	Triblock		PDL	Triblock		
P14	TCA 1	29.3	7.7	37.0	21	34.3 [1.09]	39.1 [1.08]	-44, 72	95
P15	TCA 1	25.2	10.8	36.0	30	31.8 [1.09]	40.2 [1.07]	-40, 70	93
P16	TCA 1	22.5	15.5	37.9	41	28.8 [1.09]	40.9 [1.07]	-31, 79	90
P17	TCA 1	17.7	17.0	34.7	49	26.2 [1.08]	34.7 [1.06]	-21, 103	88
P18	TCA 2	23.8	16.5	40.4	41	34.3 [1.08]	45.3 [1.05]	-34, 79	78
P19	TCA 3	21.8	15.2	36.9	41	28.0 [1.07]	38.2 [1.05]	-31, 81	91
P20	TCA 4	21.8	14.4	36.2	40	27.7 [1.08]	38.1 [1.10]	-30, 70	100

Reaction conditions: (i): [1]/[BDM]/[DL]/[LO] = 1/4/800-1200/2000, 60 °C, 4-7 min. (ii): [TCA] = 1/75-225, 140 °C, 32-138 h (for exact molar ratios and reaction times please see Appendix). [a]M_n obtained from ^{1}H NMR spectra by comparing the PDL and PE peaks at 4.85 ppm and 5.7-6.0 ppm, respectively. [b]Hard block weight %, obtained from ^{1}H NMR spectra. [c]M_n and $Đ$ measured by SEC (THE as eluent, 1 mL/min, 30 °C, calibrated using polystyrene standards). [d]glass transition temperature obtain from a combination of DSC (third cycle of heating) and DMTA (from tan(δ)). [e]Theoretical renewable content calculated based on mass and amount of each monomer present in the block copolymer (weight%) (See Appendix for explanations on renewable content of each monomer).

The purified triblock polymers were obtained by precipitation of the reaction mixture into methanol (three times). The polymers were analysed using a range of NMR spectroscopy techniques and SEC. Following this, the material thermal and mechanical properties were analysed using DSC, TGA and DMTA (*via* an oscillatory rheometer). For instance, the ^{1}H NMR spectrum of the polymer formed from DL, LO and TCA 1 (**P16**, Table 4.4, Entry 3) shows peaks corresponding to both PDL and PE blocks (Fig. 4.15).

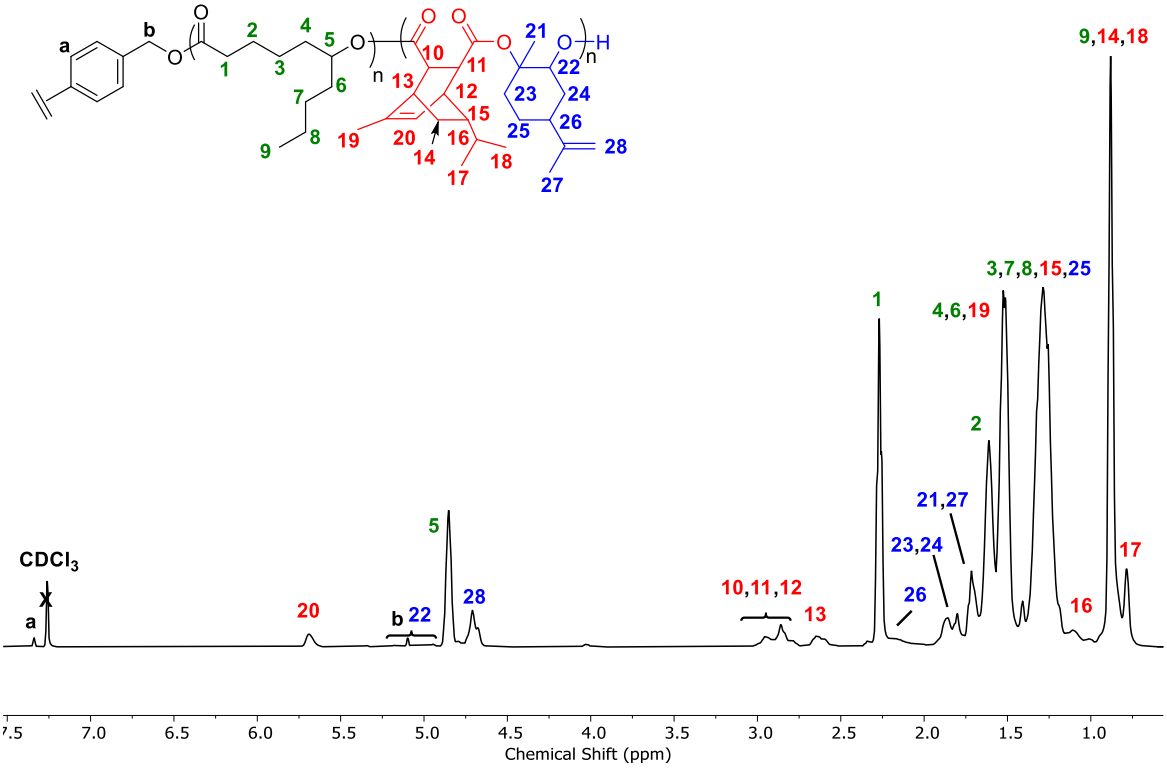


Figure 4.15 ^{1}H NMR spectrum of **P16** (Table 4.4, Entry 3) ($CDCl_3$, 500.0 MHz, 298K).

One of the methods to establish block polymer formation is by identifying the block junction units in the NMR spectrum. These junction unit peaks often show slightly different chemical shifts compared to the equivalent main chain resonances due to change in the adjacent unit. These junction units are typically observed from 3 - 5 ppm and can be identified using 2D COSY NMR spectroscopy where correlations with main chain signals are apparent. For example, the 2D COSY NMR spectrum for **P16**, shows two peaks at 4.03 ppm and 4.21 ppm that both couple to the PDL main chain signals (Fig. 4.16 and Fig. 4.17).

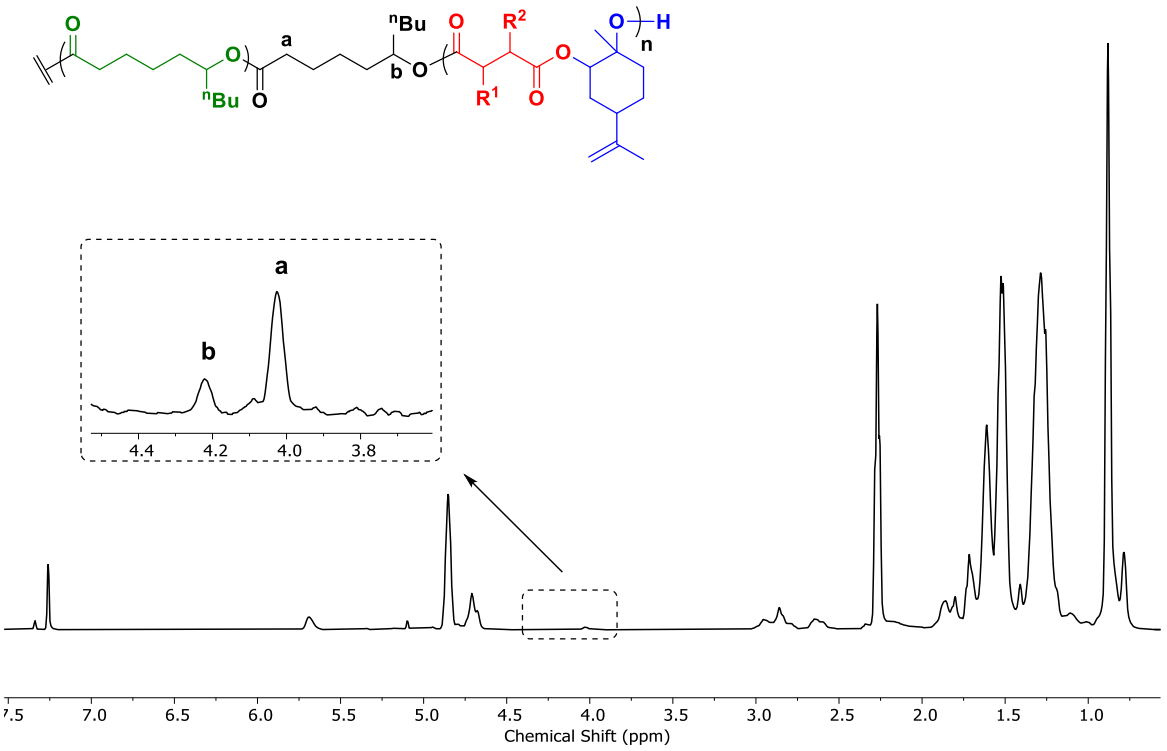


Figure 4.16 ^{1}H NMR spectrum of a block polymer illustrating junction units signals (**a** and **b**) ($CDCl_3$, 500.0 MHz, 298K).

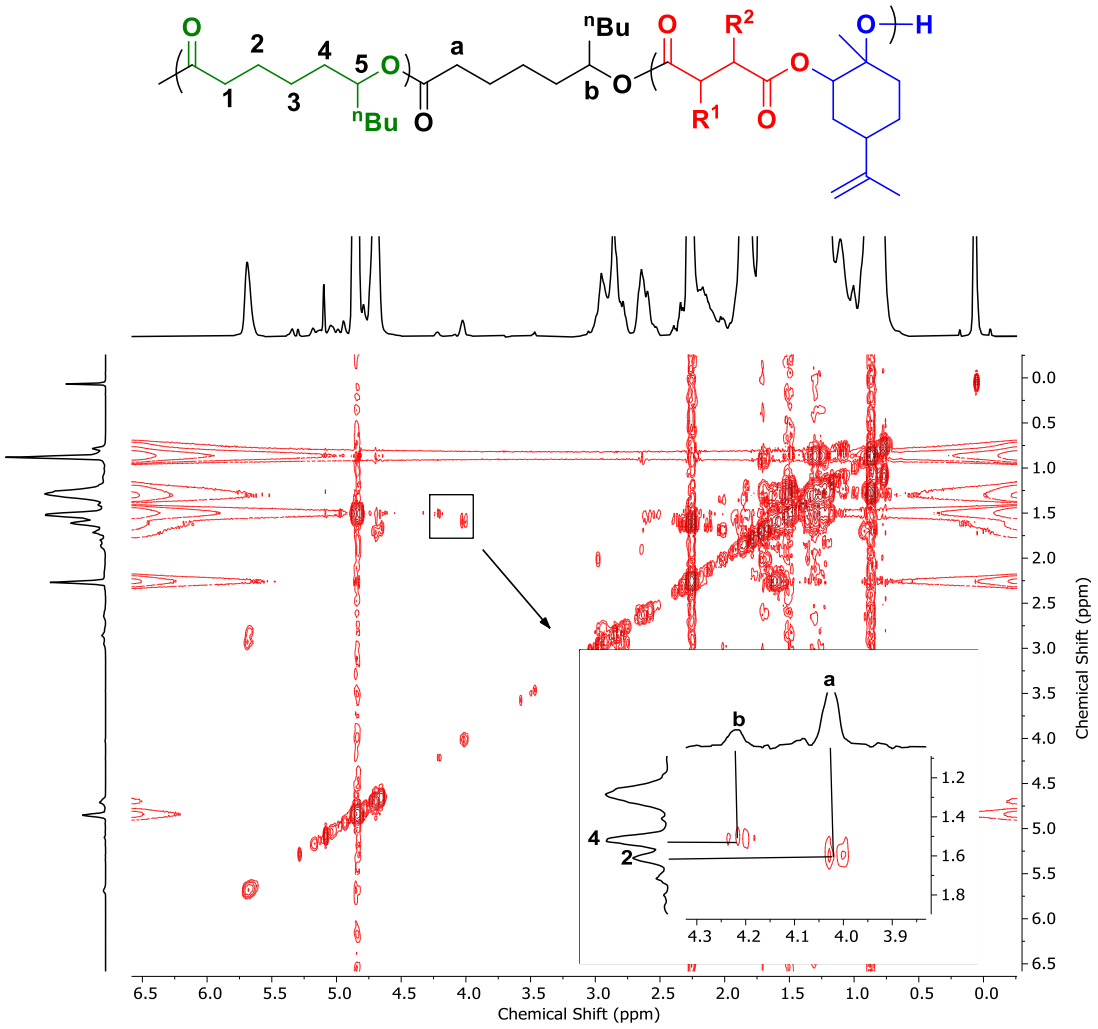


Figure 4.17 COSY NMR spectrum of **P16** (Table 4.4, entry 3) in $CDCl_3$. Insert: Expanded region showing correlation between the junction unit and the main chain resonances.

The COSY NMR spectrum shows the peak at 4.03 ppm (peak 'a' in Fig. 4.17) couples with resonances due to the protons in the PDL main chain (peak '2' in Fig. 4.17). Similarly, the peak at 4.21 ppm (peak 'b' in Fig. 4.17) couples to resonances assigned to protons in a different methylene PDL main chain environment (peak '4' in Fig. 4.17). It is worth noting that peaks 'a' and 'b' are not due to the protons at position '1' and '5', as these show peaks at different chemical shifts. Furthermore, peaks 'a' and 'b' only

appear in the block polymer ^{1}H NMR spectrum and are not observed in the ^{1}H NMR spectrum of PDL, i.e. these peaks are due to new junction units in the block polymer.

$^{31}P\{^{1}H\}$ NMR spectroscopy end group analysis is an effective method for identifying protic end groups.[52] The $^{31}P\{^{1}H\}$ NMR spectrum for **P16** displays only the ROCOP end groups (Fig. 4.18).

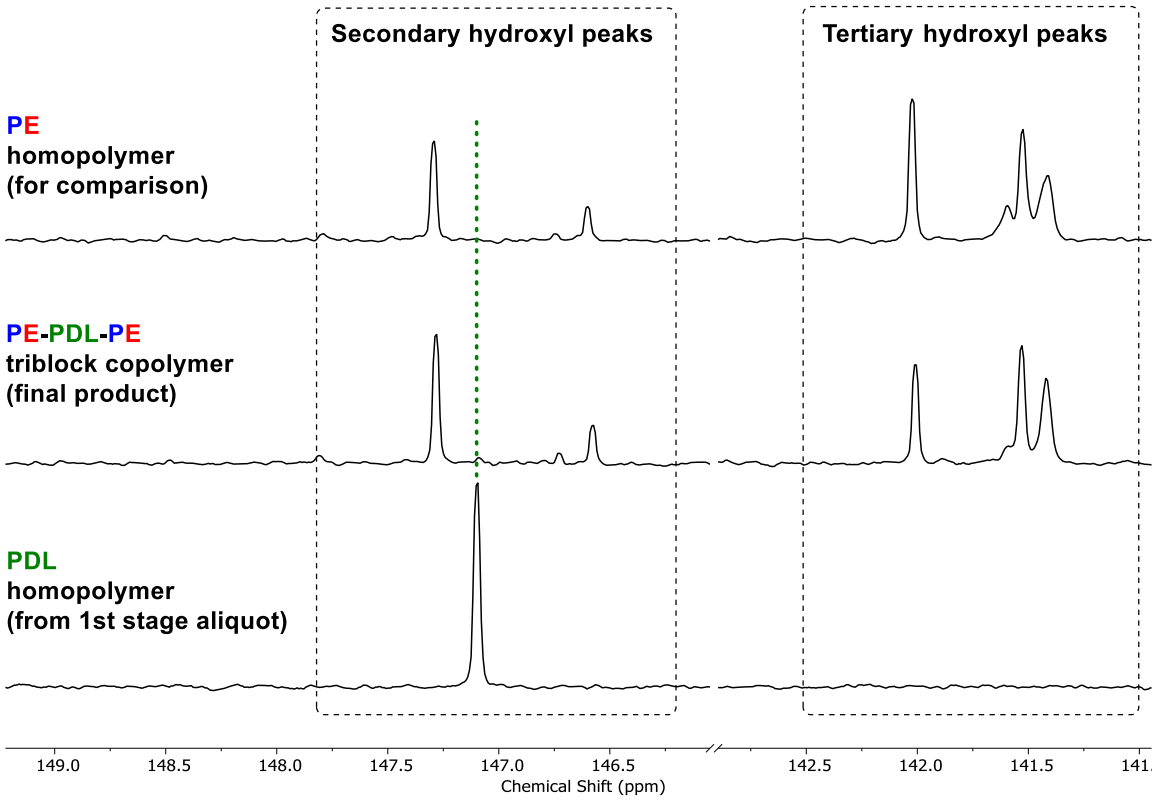


Figure 4.18 Selected region of $^{31}P\{^{1}H\}$ NMR spectra of **P16**, PE from LO/TCA 1 ROCOP and PDL hydroxyl polymers in $CDCl_3$.

The $^{31}P\{^{1}H\}$ NMR spectrum of an aliquot from the PDL stage shows the characteristic hydroxyl end group at 147.1 ppm, assigned using pure PDL (Fig. 4.18, bottom spectrum). After the ROCOP, the PDL hydroxyl end group disappears and two sets of peaks, at 147.3-146.6 ppm and 142.0-141.4 ppm, appear and these are identical to those observed for the homopolymer from the LO/TCA 1 ROCOP (Fig. 4.18, middle and top spectra). The chemical shifts of theses peaks are indicative of secondary and tertiary hydroxyl groups, respectively.[52] These end groups arise from a lack of regioselectivity in the LO and TCA opening reactions causing differing chemical shifts at the diad and triad level (Fig. 4.19). In polymer analysis, it is common that relative stereochemistry is observed at the diad and triad levels.[53]

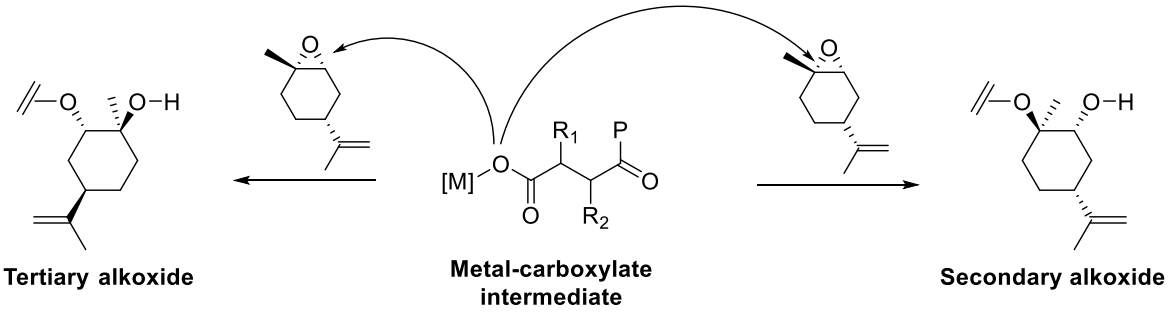


Figure 4.19 Illustration of the reactions to form different LO end groups (P denotes polymer chain).

The ^{1}H DOSY NMR spectrum shows a single diffusion coefficient for all resonances, suggesting block formation for **P16** (Fig. 4.20 (Top)). The DOSY NMR of a blend of the corresponding homopolymers shows two different diffusion coefficients (Fig. 4.20 (Bottom)).

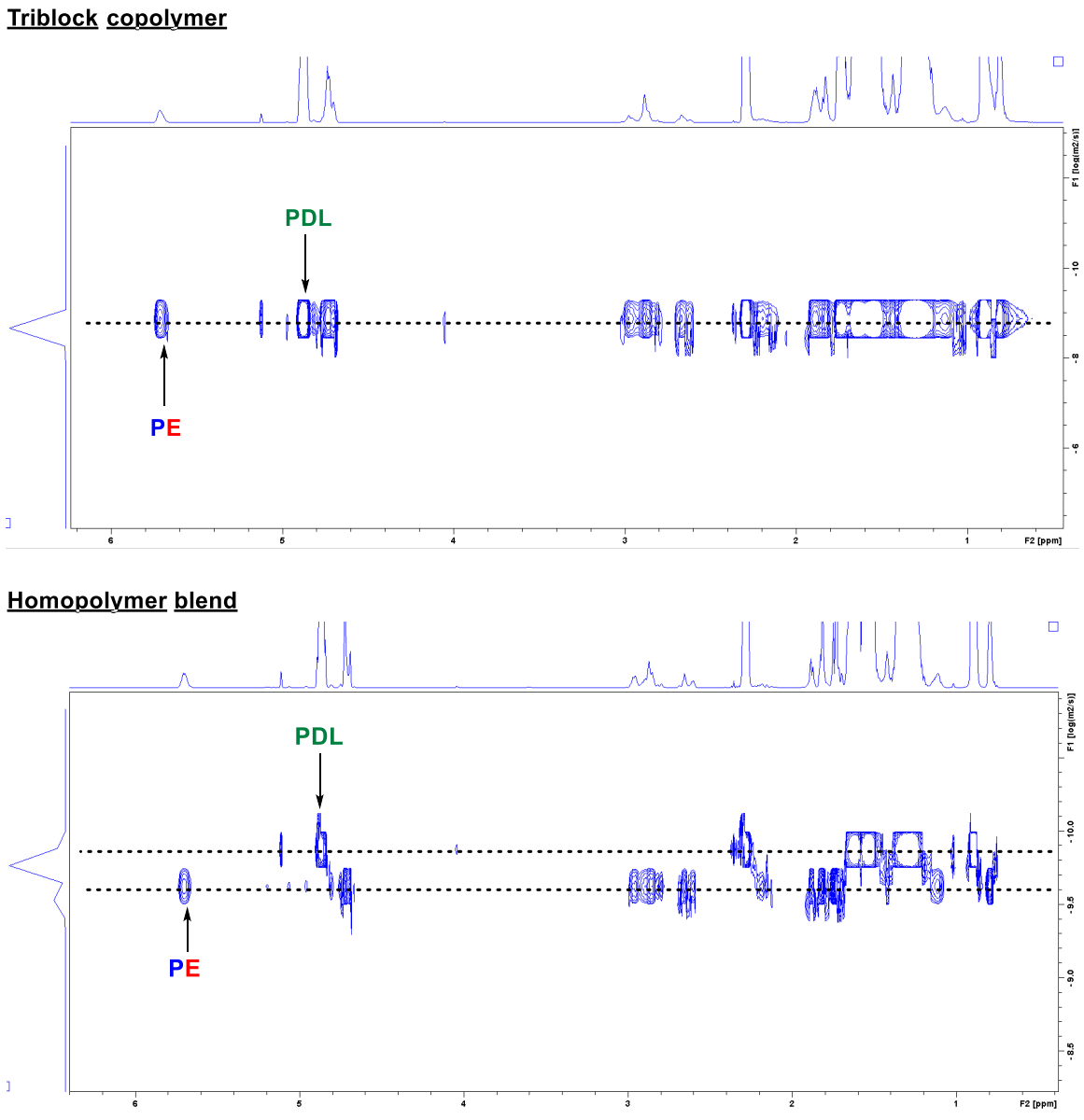


Figure 4.20 ^{1}H DOSY NMR spectra of **P16** with a single diffusion coefficient (Top) and the homopolymer blend, at equivalent molar masses, showing two diffusion coefficients (Bottom) ($CDCl_3$).

The high polymerization control is indicated by a clear increase in molar mass and retention of narrow dispersity values as the polymerization progresses. For instance, SEC analysis of **P16** shows a final molar mass of ~ 41 kg mol^{-1}. It shows an increase in M_n of ~ 12 kg mol^{-1} between the ROP and ROCOP stages (Fig. 4.21). The dispersity remains narrow throughout the reaction ($Đ$ ≤1.09) which is indicative of high polymerization control (Fig. 4.21).

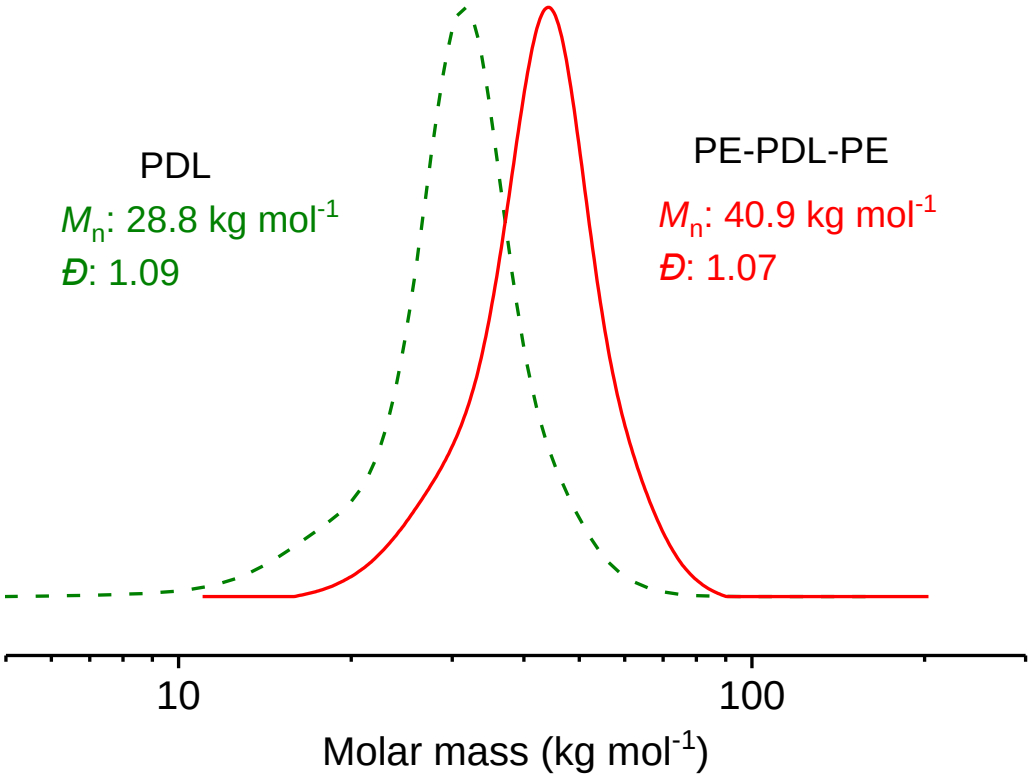


Figure 4.21 SEC traces illustrating an increase molar mass with retention of very narrow Đ (in THF at 30 °C, calibrated using polystyrene standards) for **P16**.

TGA analyses shows $T_{d,5}$ values for the block polymers ranging from 260 – 270 °C, and relatively reasonable thermal stability. Examining **P16**, TGA shows a two-step degradation with weight loss % corresponding the two block segments (Fig. 4.22). The first step corresponds with the decomposition of the *'hard'* block PE from the ROCOP of LO/TCA 1 which has a onset thermal degradation temperature of around 264 °C. The second step belongs to the PDL segment with an onset degradation temperature of 325 °C.

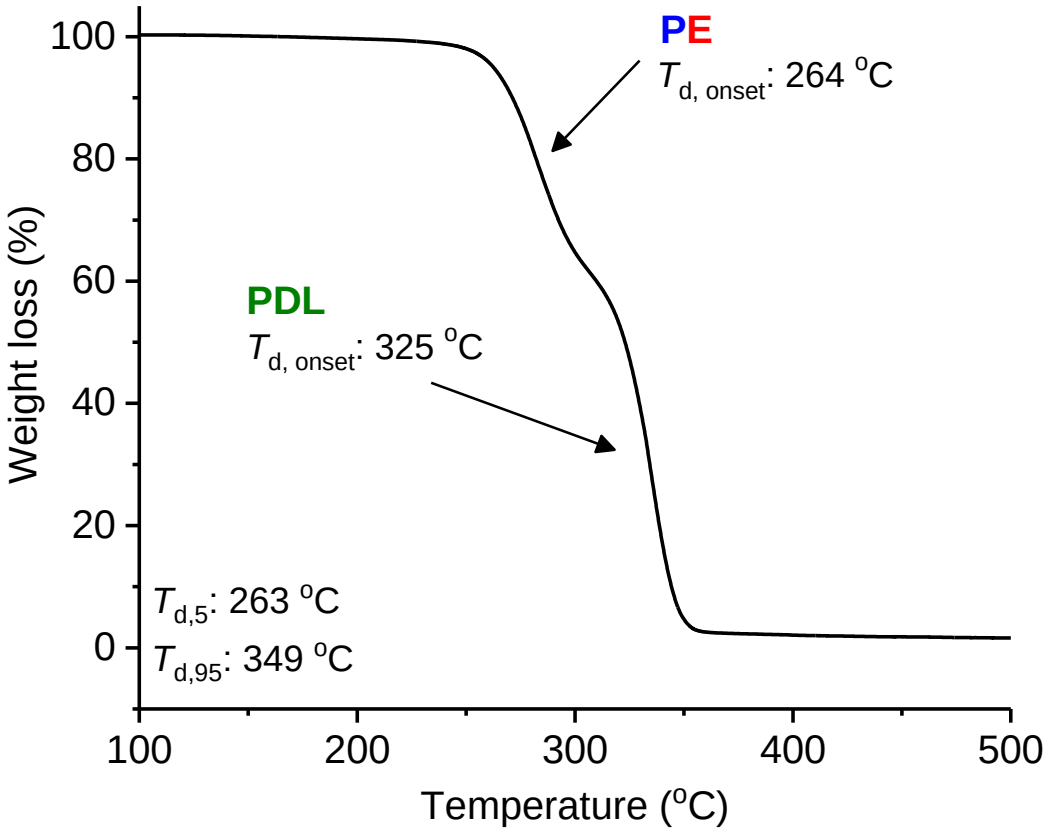


Figure 4.22 TGA curve of **P16** showing a two-step thermal degradation process.

Furthermore, a first derivative plot of the TGA data was obtained by differentiating the weight loss (%) vs. temperature. This allows the different thermal degradation steps to be more clearly distinguished. For instance, two distinct peaks, corresponding to the thermal decomposition for PE and PDL are identified in the first derivative plot for **P16** (Fig. 4.23). The minima represent the thermal decomposition temperature at the degradation inflection point, $T_{d,\,inf}$, which is another measure for the thermal degradation temperature of the material.

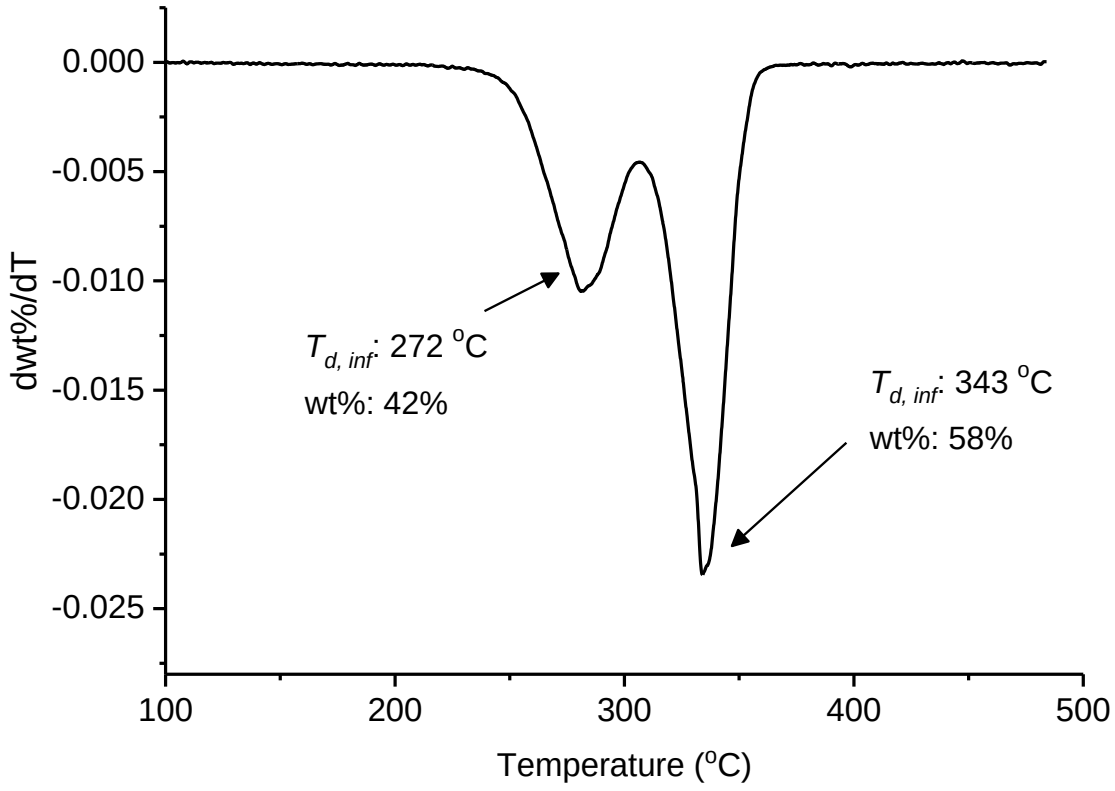


Figure 4.23 First derivative TGA curve for of **P16**.

Lastly, a rough estimate of the weight% of each block can be obtained by integrating the area under each peak. The first derivative plot suggests the *hard* block PE consists roughly 42% of the overall weight (Fig. 4.23), which is consistent with the 41 wt% obtained from NMR spectroscopy.

The T_g of the materials were measured using DSC, and typical thermographs show a single glass transition at low temperatures (< -20 °C). For instance, **P16** has a single transition at -31 °C (Fig. 4.24).

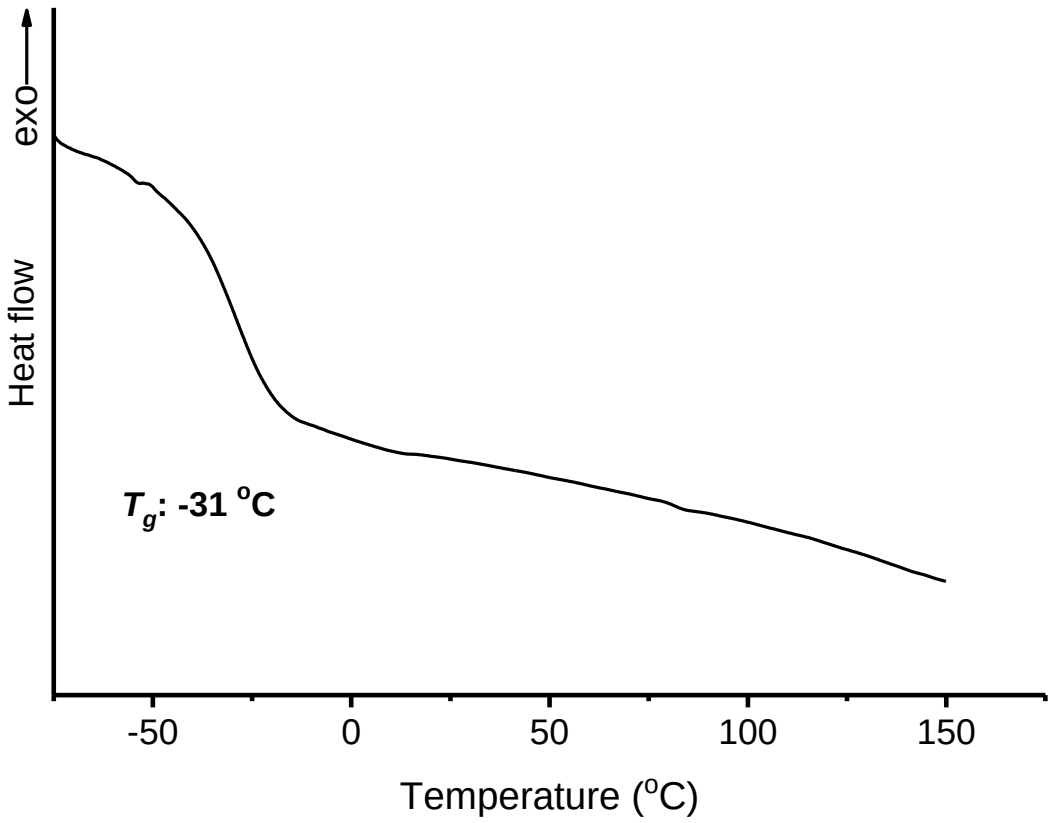


Figure 4.24 DSC thermograph of **P16** (third cycle).

In considering the two segments used in the triblock copolymers, the *soft* PDL block has a T_g of around -50 °C [32-33] and the *hard* PE block typically have T_g > 80 °C. If the blocks are fully phase separated, two glass transitions should be observed at the same temperatures as the constituent. Conversely, if the blocks are fully miscible, one transition should be observed at a temperature corresponding to that obtained from the Fox equation (rule of mixtures). For instance, fully miscible DL/LO/TCA 1 triblock (41 $wt\%_{Hard}$) is predicted to show a T_g of -7 °C. As the obtained T_g was -31 °C, it can be hypothesised that the blocks are only partially miscible (i.e. there are domains of PDL or PE). It should be noted that the lack of an observable upper T_g, for the *hard* block, is a common feature to other polyesters from epoxides/lactones/anhydrides.[32-33, 50] To determine the upper T_g, a more sensitive technique, such as those based on mechanical properties could be applied.

Following thermal analysis of the materials, their mechanical properties were measured using DMTA *via* oscillatory rheology, which measures the sample's shear storage, *G'*, and loss modulus, *G''*, under stress. The measurements were conducted under two modes: (1) constant oscillatory frequency with variable temperature and (2) variable oscillatory frequency at constant temperature (25 °C). Under the constant frequency and variable temperature mode, the change in *G'* and *G''* were measured for an oscillatory frequency of 1 Hz over a temperature range of 25 °C to 150 °C. The storage and loss modulus *vs*. temperature plot shows the triblock copolymers have a viscous dominated profile. Where *G''* is always larger than its *G'* (Fig. 4.25).

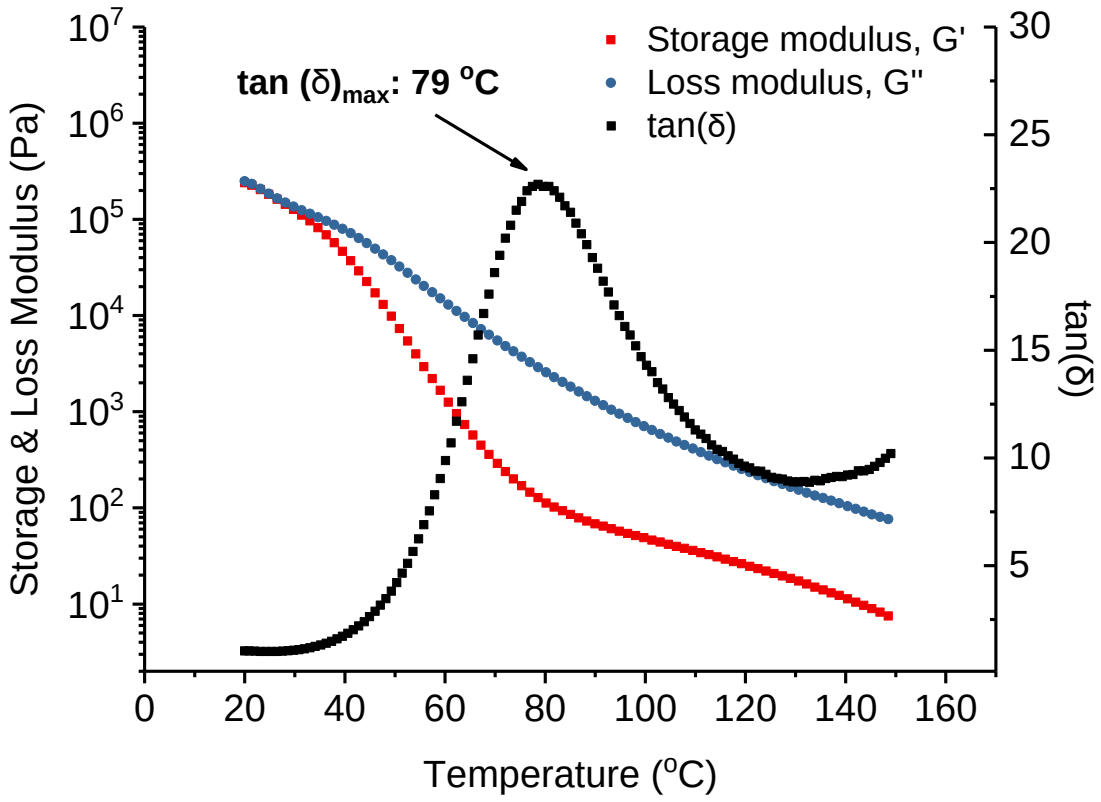


Figure 4.25. Storage and loss modulus and tan(δ) vs. temperature plot of **P16**.

As the temperature increase, the storage modulus decrease consistent with a reduction in the materials' elasticity. Tan(δ) represents the loss factor and is described by the ratio of G''/G'. A peak in Tan(δ) would, thus, suggest a major change in the material's structure, e.g. a glass transition. For DL/LO/TCA 1 triblock, a peak in Tan(δ) is observed at 79 °C consistent with the expected upper T_g (Fig. 4.25). Thus, by combining the data from DMTA and DSC, both T_g values are determined for the triblock polymers and the data indicates partial block phase separation.

In the constant temperature (25 °C) variable frequency mode, the materials change in *G'* and *G''* in response to different frequency stimuli is investigated. As the frequency increases, both the material's storage and loss moduli increase (Fig. 4.26).

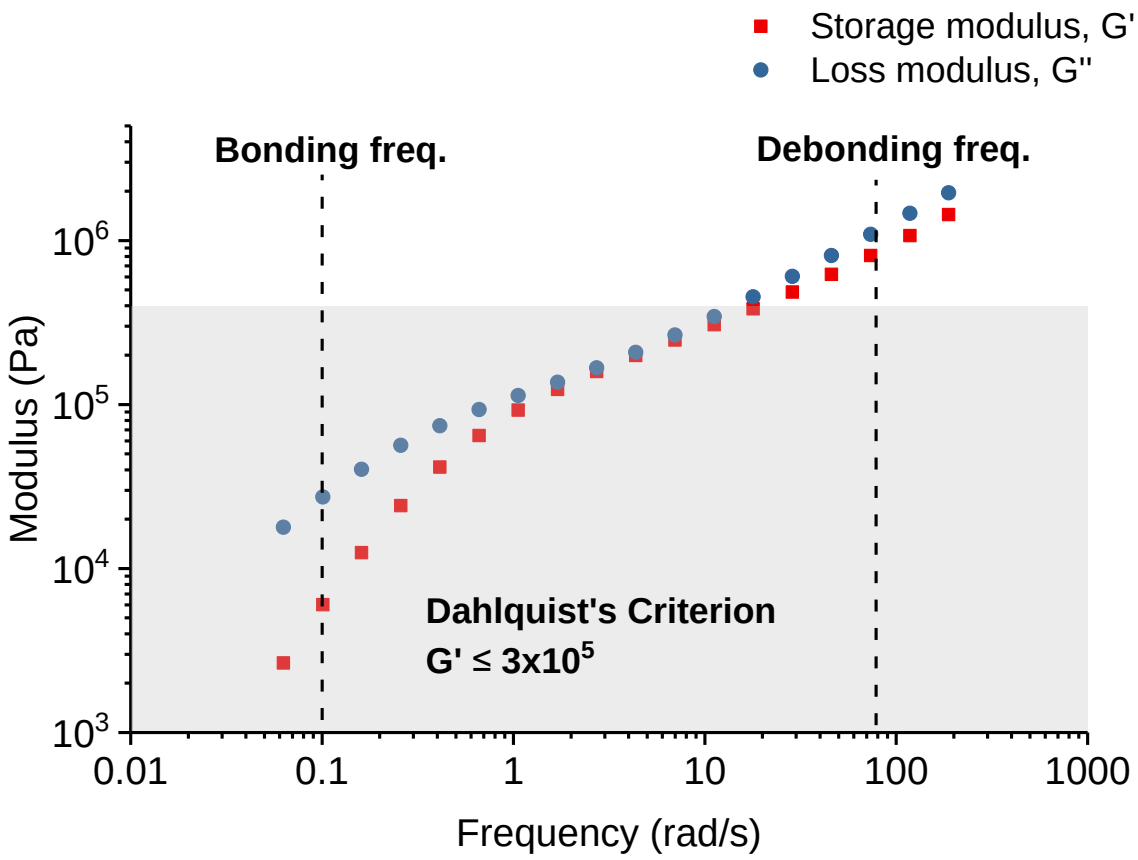


Figure 4.26 Plot of storage and loss moduli vs. frequency for **P16**.

For adhesives, the bonding and debonding frequencies are particularly important as these mimic the shear experienced by the material during the adhesive application and removal, respectively.[2] Typically for these polymers, the bonding and debonding frequencies are 0.1 and 100 rad/s.[54] Furthermore, at the bonding frequency, the *G*' value should be below the Dahlquist's criterion (*G*' ≤ 3 x 10^5 Pa) so as to promote effective wetting between the substrate and adhesive.[12, 14, 54] PDL on its own should show a low storage modulus that is below the Dahlquist's criterion. However, in the copolymers, the *hard* block is needed to offer resistance to shear, but causes increases to *G*'. In many cases of block polymer adhesives, the *hard* block used (e.g. polystyrene) increases the storage modulus too much and tackifers are needed to return *G'* to below the Dahlquist value.[2, 7, 48] Thus, a balance between the material's ability to wet a surface and its resistance to shear (from the *hard* block) needs to be achieved for it to function as an effective adhesive. Interestingly, the modulus *vs.* frequency plot for the DL/LO/TCA 1 triblock (**P16**) shows that the bonding frequency (6 x 10^3 Pa) is below the Dahlquist's criterion without the need for any tackifer (Fig. 4.26).

Overall, a range of different TCA incorporating triblocks were evaluated as PSA. The block polymers were prepared using the methods described and fully characterized (See Appendix, Fig. S66 – S101). It is relevant to note that because DL is bio-based, [14] by selecting the TCA to be bio-based, it is possible to target fully renewably sourced block polymers.

4.7. **Adhesion property testing**

The pressure sensitive adhesive behaviour of the block polymers was investigated using a 180° peel test. This test was conducted using 5 µm thick polyethylene terephthalate (PET) sheets (Mylar®) and polished stainless steel plates at room temperature (according to ISO 29862:2018) (Fig. 4.27). A 30 wt% DCM solution of the adhesive (weight ratio of DCM/triblock polymer = 3/7) was prepared and then applied to the PET film using a wound wire rod (K-bars), so as to achieve a wet film with thickness of ~ 80 µm. The samples were then dried overnight in a vacuum oven and pressed on to the steel sheets using a 500 g weight before undergoing the peel test.

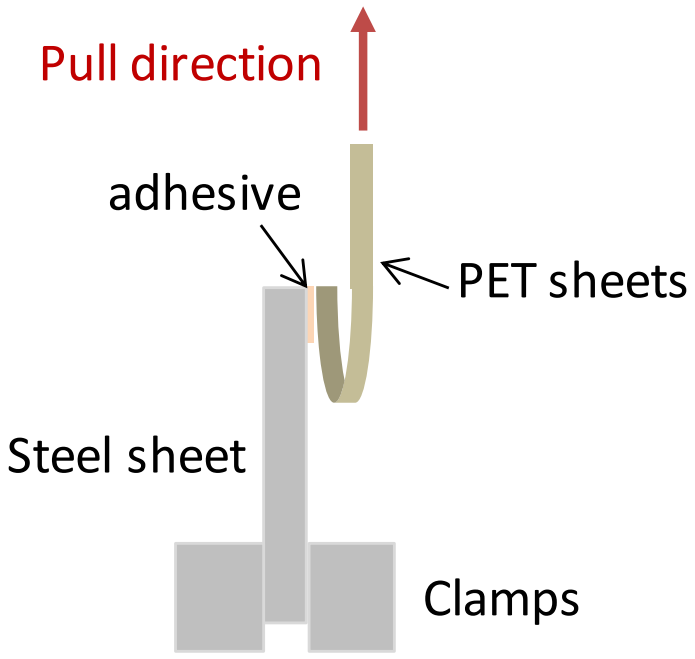


Figure 4.27 Schematic diagram illustrating the 180 ° Peel test apparatus.

Using the triblock from DL/LO/TCA 1 as an example (**P14** – **P17**), at a constant molar mass of ~40 kg mol^{-1}, an increase in hard block content from 21 – 41 % improved the peel adhesion from 0.1 N cm^{-1} to 10.8±0.4 N cm^{-1} (Fig. 4.28). This improvement may be due to the increasing physical crosslink density achieved as the content of hard domains increases, leading to better mechanical strength.

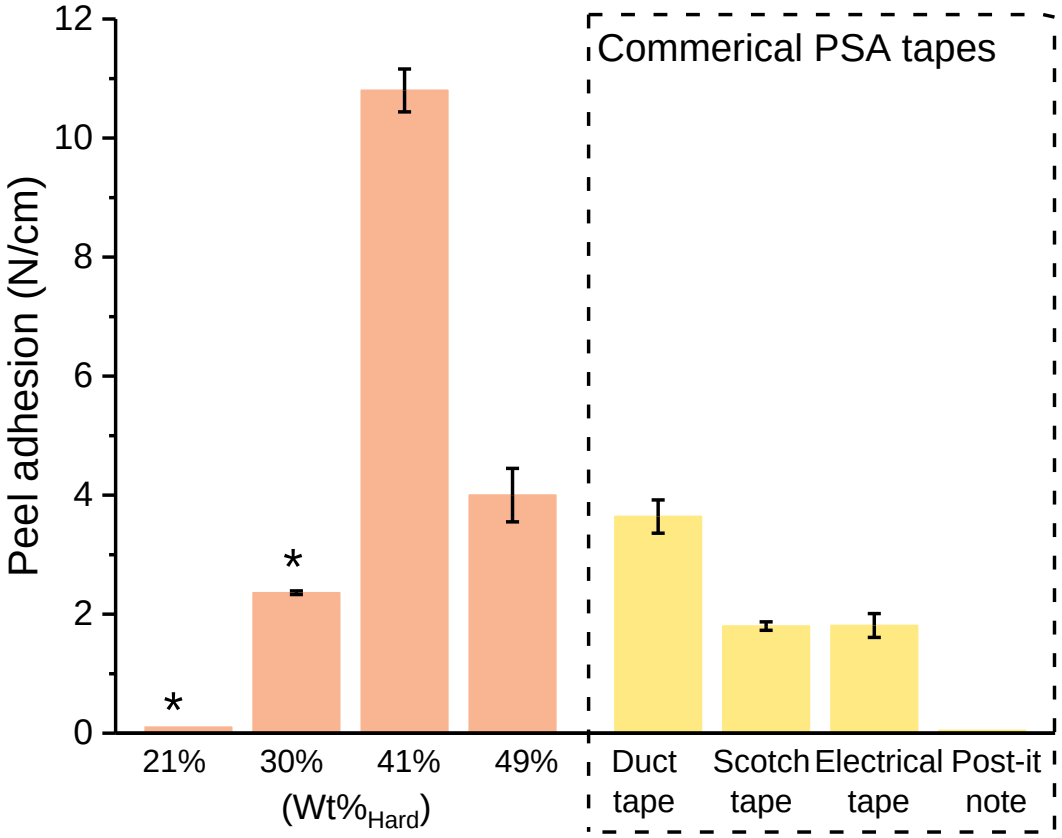


Figure 4.28 180° Peel adhesion test results comparison between DL/LO/TCA 1 triblock samples (~40 kg mol^{-1}) of varying hard block weight % and commercial samples. Data in yellow show the results for commercial PSA PSA tapes (* indicates a cohesive mode of failure). Error is the standard deviation of 3 repeat experiments.

There is an optimum hard block content since the sample with 49% showed lower peel adhesion (4.0 N cm^{-1}), possibly due to its reduced ability to bond to the substrate. As such, it can be concluded that a balance between the amount of *hard* and *soft* block that needs to be struck in order to obtain the best adhesive material and it may also correlate with phase separated microstructures. In comparing the performance with commercial samples **P14**, **P15** and **P16** (21, 30 and 49 wt%, respectively) showed similar peel strength to Post-it notes, Scotch tape and Duct tape, respectively. The 41 % sample (**P16**) showed a peel adhesion that is almost three times that of Duct tape (Fig. 4.28). Moreover, the desired adhesive mode of failure (i.e. without any residue) was displayed by samples with >40 $wt\%_{Hard}$ (Fig. 4.29). At lower wt%, the reduced mechanical strength results in cohesive failure for the samples.

(A) Adhesive failure (no residue) (B) Cohesive failure (residue left over)

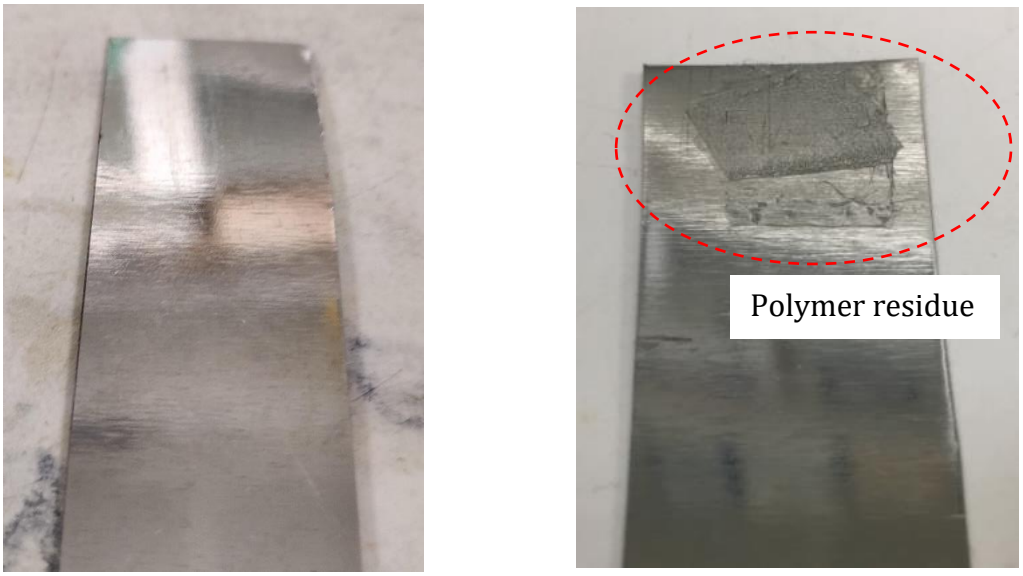


Figure 4.29. Stainless steel substrate photograph post-peel test show the difference between (A) an adhesive mode of failure with no polymer residue left over and (B) a cohesive mode of failure with visible polymer residue on the substrate.

Comparing a series of polymers incorporating different TCAs, at 40 wt% hard block, afforded PSAs with similar peel adhesions ranging from 8.1 – 13.1 N cm^{-1} and all samples show adhesive failure (Fig. 4.30). In comparison with literature renewable triblock adhesives, these polymers show better adhesive performance around 4-5 times (Fig. 4.30, see Fig. S102 in the Appendix for structures of these polymers).[7, 14] Furthermore, the literature polymers typically require the addition of tackifiers. The acrylic/ester based PSA has a similar peel adhesion to the series of DL/LO/TCA, but acrylic polymers cannot be easily or fully degraded.[13] In contrast, the triblock of PDL and PE are expected to be degraded with acid/bases to small molecules – providing a future recycle option.

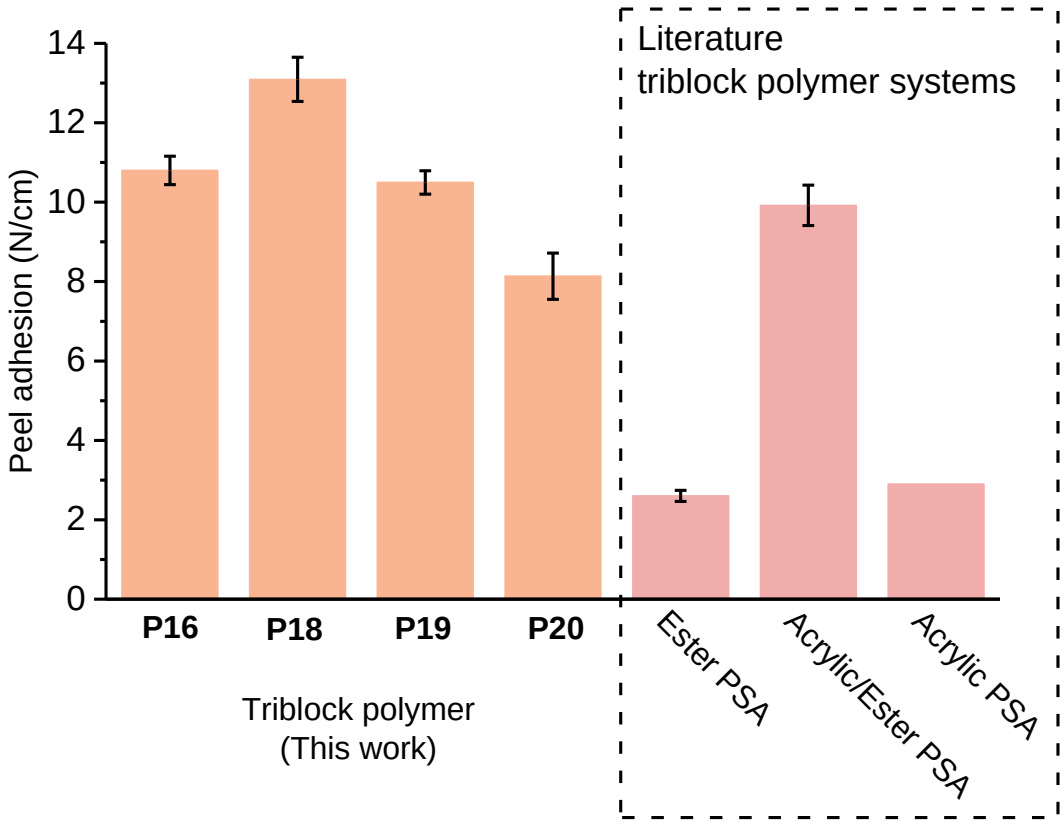


Figure 4.30 180° Peel adhesion test results for the series of polymers from DL/LO and TCA 1-4 (~40 kg mol^{-1} and ~40% weight hard block, **P16** and **P18 – P20**) and literature renewable triblock polymer systems.[7, 13-14]

The fundamental viscoelastic properties of the block polymers and their PSA application potential were analyzed from the shear storage and loss moduli at the bonding and debonding frequencies. Cheng and co-workers proposed a quadrant system, based on a G' vs. G'' plot, to describe potential adhesive application types (Fig. 4.31).[54] For a particular sample, a viscoelastic window (constructed by plotting G' and G'' at the bonding/debonding frequencies) is mapped on to the G' vs. G'' plot. The region in which the window lies provides qualitative assessment of its possible adhesive application.[54]

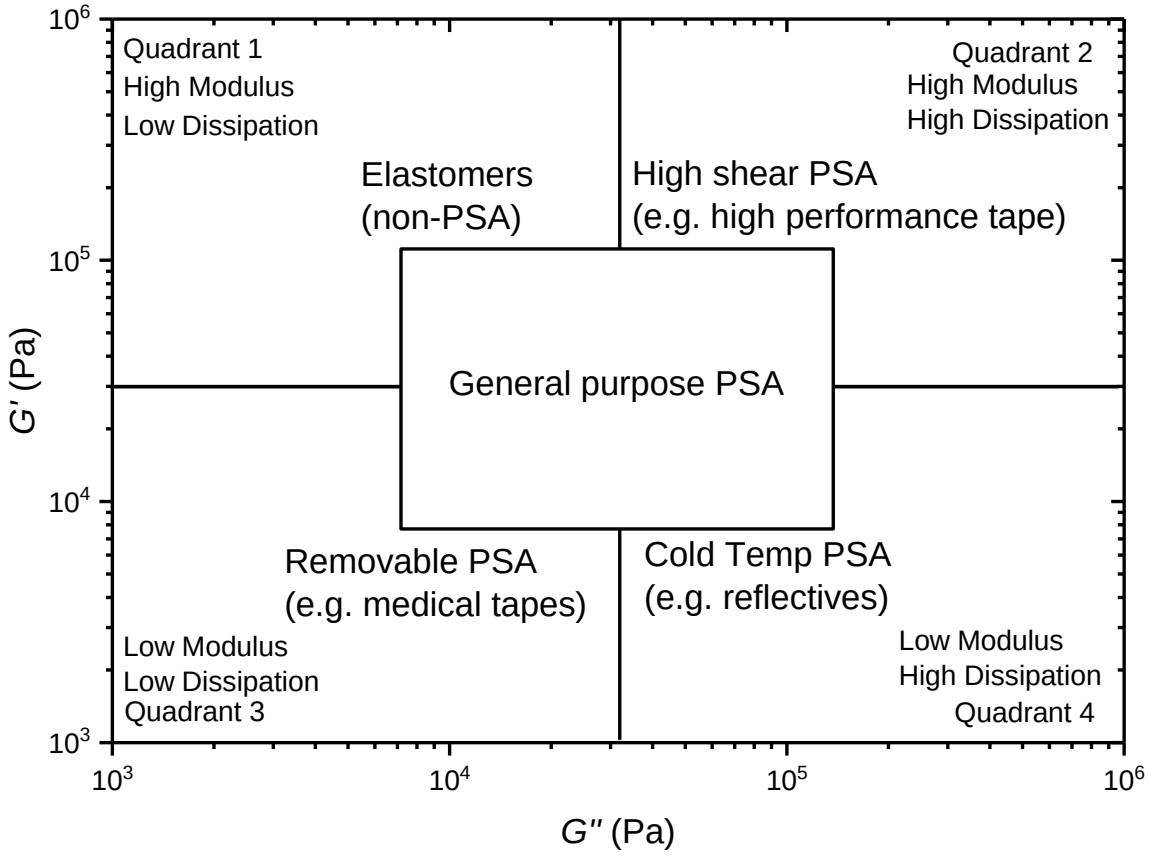


Figure 4.31 Schematic of G' vs. G'' plot used for illustrating an adhesive's potential application.

For instance, the DL/LO/TCA 1 triblock polymer with 41 wt%$_{Hard}$ (**P16**) and 30 wt%$_{Hard}$ (**P15**) have viscoelastic windows suggesting they are suitable as general purpose PSA (Fig. 4.32). Triblock with 41 wt%$_{Hard}$ (and higher mechanical strength) is better matched as high shear PSA and the 30 wt%$_{Hard}$ sample is more suited as a removable PSA. The cohesive failure of the 30 wt%$_{Hard}$ sample would be disadvantageous for any applications as a removable PSA and this issue could be tackled by increasing the overall molar mass and allow the PDL segments to achieve maximum entanglement.

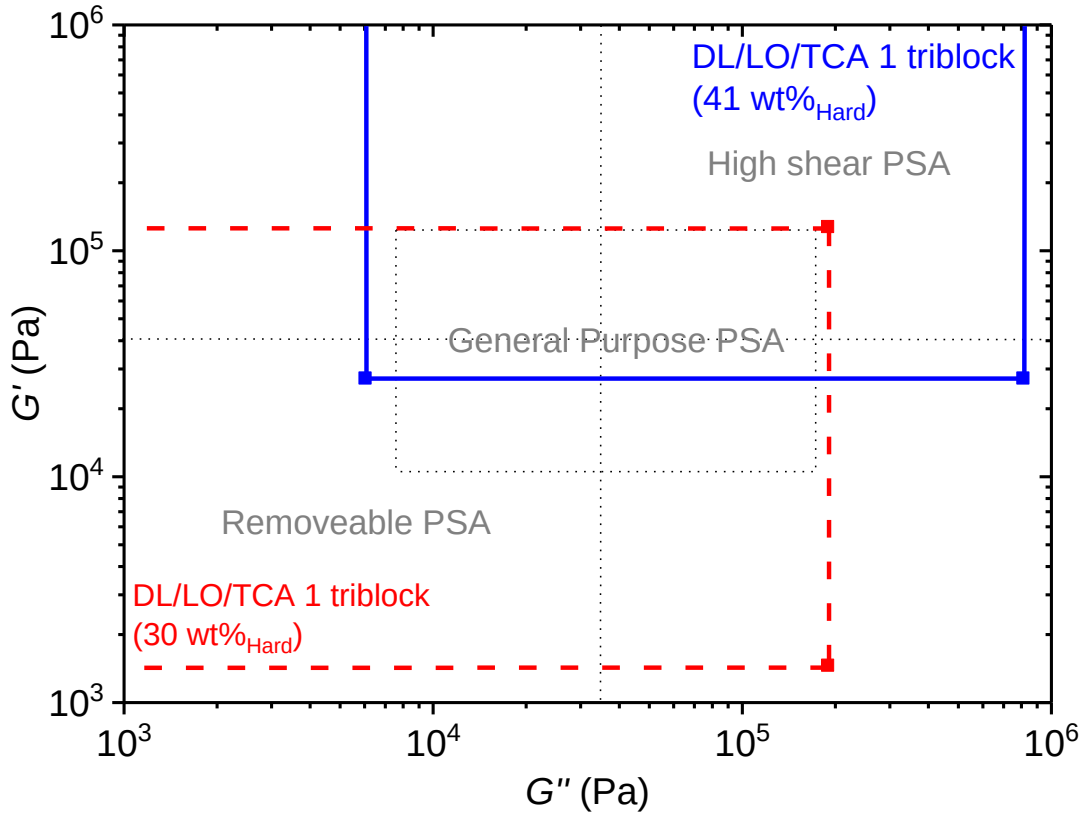


Figure 4.32 Viscoelastic windows for DL/LO/TCA 1 triblock polymer with 41 and 30 wt%$_{Hard}$.

4.8. **Triblock polymer degradation**

Whilst traditional styrene block copolymers are not susceptible to degradation, block polyesters can be hydrolyzed under a range of conditions. **P16** was subjected to acid-catalyzed degradation at 60 °C. Under concentrated acidic conditions (*p*-toluenesulfonic acid in wet THF (1M)), the polymer molecular weight rapidly reduces and the degradation shows a half-life of around 20 min. The data can be fitted to obtain a k_{obs} of 0.0123 s^{-1} (See Appendix for plot, Fig. S103).

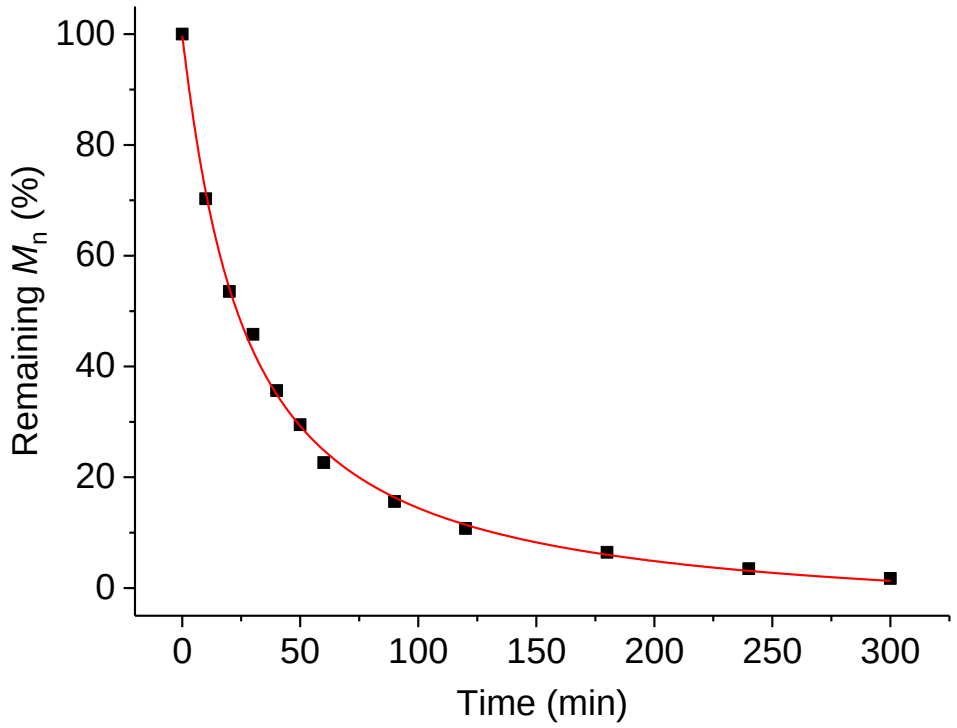


Figure 4.33 Acid degradation of DL/LO/TCA 1 triblock polymer with (41 $wt\%_{Hard}$), using *p*-toluenesulfonic acid (1M in wet THF at 60 °C).

Samples were removed regularly for SEC analysis and the molar mass decreased from 41 kg mol^{-1} to ~ 700 g mol^{-1} in line with near complete degradation of the block copolyester (>98%) in 5 h (Fig. 4.34). The polydispersity of the molecular mass distribution also drastically increased. This indicates a random chain degradation mechanism instead of a chain end reaction. The random scission is consistent with other acid-catalysed polyester hydrolyses.[55]

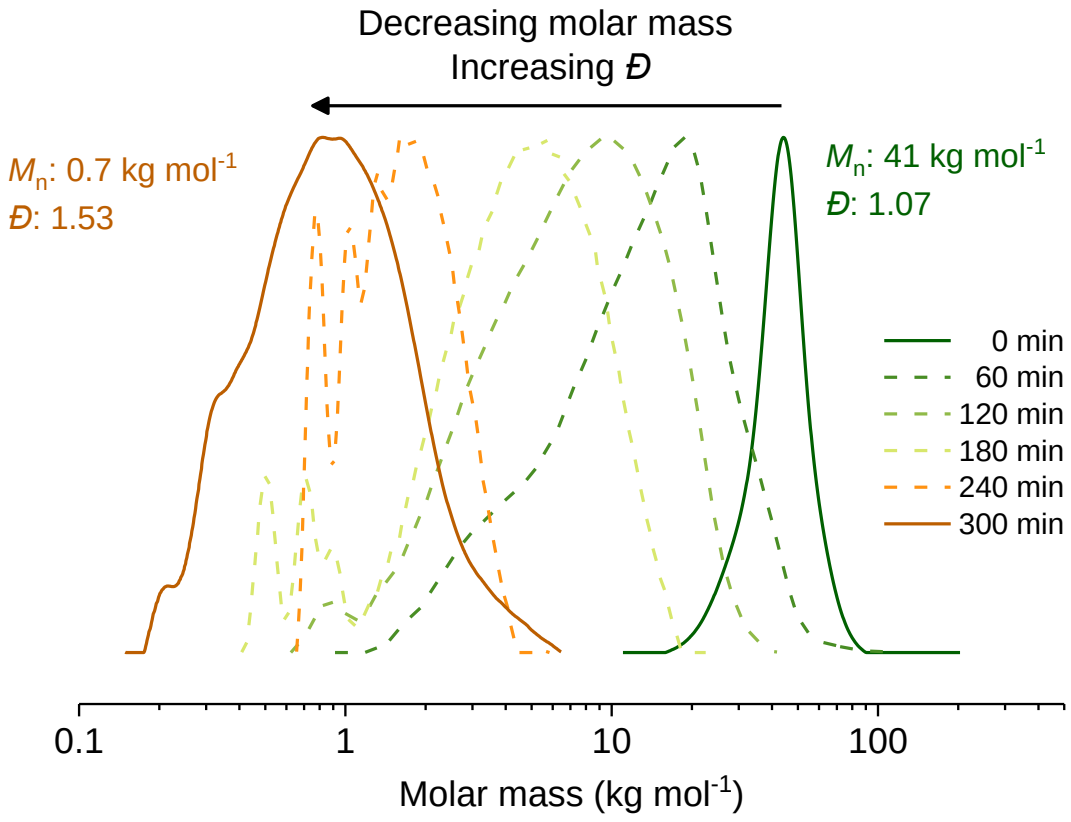


Figure 4.34 Stacked SEC traces for the acid degradation test on trblock polymer from DL/LO/TCA 1 with 41 wt%$_{Hard}$ (1M in THF, 60 °C).

4.9. **Summary & Future work**

New biorenewable polyesters produced from the ROCOP of LO and four different TCA were prepared. Using a sequential addition strategy, seven different *hard-soft-hard* triblock copolyesters (up to 100% renewable content) were synthesized in a highly controlled manner with predictable molar masses and very narrow dispersities ($Đ \leq 1.10$). The block polymer synthesis and materials were characterized using a range of techniques, including SEC, identification of junction units using 2D NMR spectroscopy, investigation of block attachment using ^{1}H DOSY NMR and end group analysis using ^{31}P{^{1}H} NMR spectroscopy. A systematic series of polymers were prepared showing a molar mass of 40 kg mol^{-1} and with variable *hard* block content, from 20 - 50 wt%. The sample with ~40 wt% hard block showed the best peel adhesion. The materials are suitable for various PSA applications as identified through viscoelastic property evaluation. The block polyesters degrade, under acidic conditions (1M, 60°C), showing >98% mass loss within 5 h. These new polymers might be particularly useful when applied together with natural materials like wood or thermoplastics as all components (including the adhesives applied) would be fully degradable. This study focused on applications as PSA but these renewable block polyesters should also be investigated in other fields, such as thermoplastic elastomers and biomedical applications.

There are two potential direction for future research: (1) investigate other bio-based monomers for the synthesis of renewable polymers. (2) Improve material properties through post-polymerization modification and/or changes in polymer architecture. This Chapter used LO with a range of TCAs, a natural extension would be

to test other epoxides. For instance, cyclohexadiene oxide (CHDO), carene oxide (CAO), menthene oxide (MEO) and α-pinene oxide (αPO) all have precedent in ROCOP reactions (Fig. 4.35).[21, 25, 40] Carvone oxide (CVO) has previously been used in the synthesis of cyclic carbonates but it's applicability in ROCOP has not been examined and would also be an interesting candidate.[56] Its use in ROCOP may be possible given its structural similarity to LO.

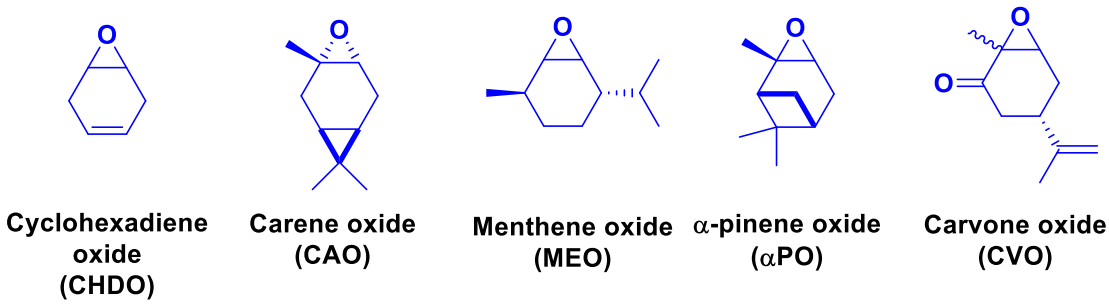


Figure 4.35 Bio-based epoxides for use in the synthesis of renewable polyesters.

The low T_g of PDL allows it to act as a *soft* block, but other lactones may also be explored. For instance, poly(menthide) which is obtained from the ROP of the menthide lactone (derived from peppermint) is widely used by Hillmyer and co-workers (Fig. 4.36).[57] It has a T_g of around -25 °C and has been shown to be an effective *soft* block in combination with PLA.[12-13, 57]

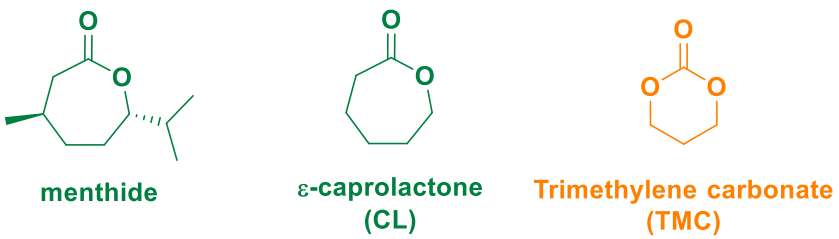


Figure 4.36 Possible candidates for use as monomer for the *soft* block

One drawback of DL is its high price (~ £90/100 mL) and the lack of large scale industrial production. A cheaper alternative is ε-caprolactone (CL) (Fig. 4.36). Poly(ε-caprolactone) (PCL) is a semi-crystalline polymer which prevents its use as a *soft* block. A possible solution may be to random copolymers of PCL/PDL to inhibit PCL crystlization. Previous work has shown that random enchainment of DL/CL = 30/70 can be used effectively as a *soft* block.[58] Analogously, PCL can be copolymerized with trimethylene carbonate (TMC), in a CL/TMC = 90/10 ratio, to achieve similar effects.[59] Although TMC is also a specialty chemical with high cost.

There are two immediate strategies for improving the material properties. The first is through post-polymerization functionalization as LO and the TCAs both possess alkene substituents. Using efficient reactions e.g. thiol-ene coupling or hydroboration-oxidation (see Chapter 3), it should be straight forward to add additional functionalities on to the polymer backbone. For instance, installation of hydroxyl groups often leads to higher T_g values due to hydrogen bonding networks toughening the polymers (Fig. 4.37).[60] By using substituents which increase χ (Flory-Higgins interaction parameter), it is also possible to induce phase separation at lower degrees of polymerization and thereby increase shear resistance.

Another method to alter the polymer properties would be to access different polymer architectures.[61-62] For instance, mechanical properties have been shown to improve if the structure is changed from an AB linear to a 6-armed star polymer. Improvement occurs because the 'core' of the star acts in a similar way to physical cross links.[61] The most efficient method to access multi-armed polymer architectures would be through multifunctional initiators. For instance, tris(hydrodylmethyl)ethane,

pentaerythritol or dipentaerythritol can be used as initiators to obtain three-arm, four-arm or six-arm star polymers respectively (Fig. 4.38). Any improvements to mechanical properties would result in better adhesive resistance to shear.

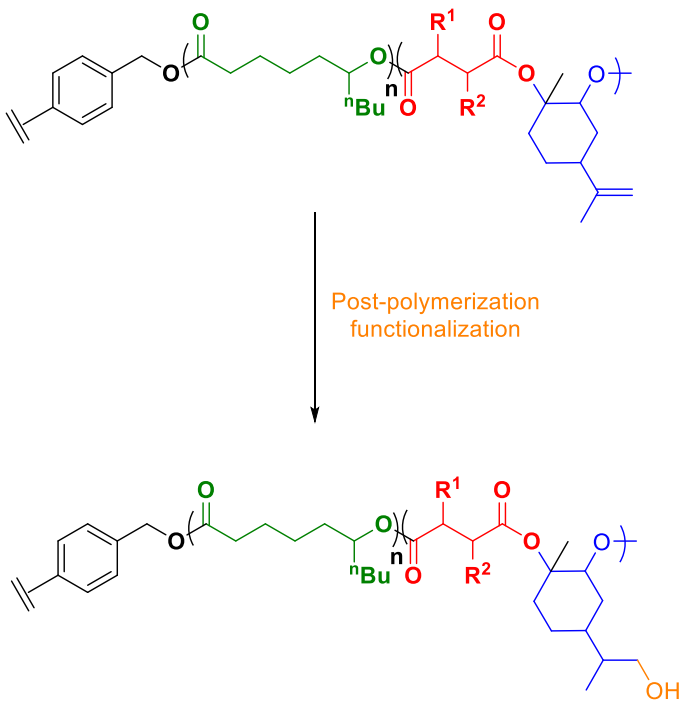


Figure 4.37 Post-polymerization functionalization to install functional groups on to the triblock copolymer to improve properties.

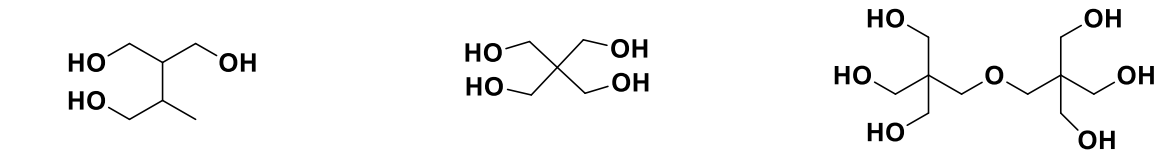


Figure 4.38 Possible multi-arm initiators to use for different polymer architectures.

4.10. **References**

1. Khan, I.; Poh, B. T., Natural Rubber-Based Pressure-Sensitive Adhesives: A Review. *J. Polym. Environ.* **2011,** *19*, 793-811.
2. Benedek, I., *Pressure-Sensitive Adhesives and Applications*. 2nd ed.; Marcel Dekker: 2004.
3. Tse, M. F., Studies of Triblock Copolymer Tackifying Resin Interactions by Viscoelasticity and Adhesive Performance. *J. Adhes. Sci. Technol.* **1989,** *3*, 551-570.
4. Kraus, G.; Rollmann, K. W.; Gruver, J. T., Dynamic Properties of a Model Reinforced Elastomer . Styrene-Butadiene Reinforced with Polystyrene. *Macromolecules* **1970,** *3*, 92-96.
5. Ragauskas, A. J.; Williams, C. K.; Davison, B. H.; Britovsek, G.; Cairney, J.; Eckert, C. A.; Frederick, W. J.; Hallett, J. P.; Leak, D. J.; Liotta, C. L.; Mielenz, J. R.; Murphy, R.; Templer, R.; Tschaplinski, T., The path forward for biofuels and biomaterials. *Science* **2006,** *311*, 484-489.
6. Gandini, A., The irruption of polymers from renewable resources on the scene of macromolecular science and technology. *Green Chem.* **2011,** *13*, 1061-1083.
7. Gallagher, J. J.; Hillmyer, M. A.; Reineke, T. M., Acrylic Triblock Copolymers Incorporating Isosorbide for Pressure Sensitive Adhesives. *ACS Sustainable Chem. Eng.* **2016,** *4*, 3379-3387.
8. Beharaj, A.; Ekladious, I.; Grinstaff, M. W., Poly(Alkyl Glycidate Carbonate)s as Degradable Pressure-Sensitive Adhesives. *Angew. Chem. Int. Ed.* **2019,** *58*, 1407-1411.
9. Mecking, S., Nature or petrochemistry? Biologically degradable materials. *Angew. Chem. Int. Ed.* **2004,** *43*, 1078-1085.
10. Williams, C. K., Synthesis of functionalized biodegradable polyesters. *Chem. Soc. Rev.* **2007,** *36*, 1573-1580.
11. Gross, R. A.; Kalra, B., Biodegradable polymers for the environment. *Science* **2002,** *297*, 803-807.
12. Shin, J.; Martello, M. T.; Shrestha, M.; Wissinger, J. E.; Tolman, W. B.; Hillmyer, M. A., Pressure-Sensitive Adhesives from Renewable Triblock Copolymers. *Macromolecules* **2011,** *44*, 87-94.
13. Ding, K. Y.; John, A.; Shin, J.; Lee, Y.; Quinn, T.; Tolman, W. B.; Hillmyer, M. A., High-Performance Pressure-Sensitive Adhesives from Renewable Triblock Copolymers. *Biomacromolecules* **2015,** *16*, 2537-2539.
14. Lee, S.; Lee, K.; Kim, Y. W.; Shin, J., Preparation and Characterization of a Renewable Pressure-Sensitive Adhesive System Derived from epsilon-Decalactone, L-Lactide, Epoxidized Soybean Oil, and Rosin Ester. *ACS Sustainable Chem. Eng.* **2015,** *3*, 2309-2320.
15. Longo, J. M.; Sanford, M. J.; Coates, G. W., Ring-Opening Copolymerization of Epoxides and Cyclic Anhydrides with Discrete Metal Complexes: Structure-Property Relationships. *Chem. Rev.* **2016,** *116*, 15167-15197.
16. Nijhuis, T. A.; Makkee, M.; Moulijn, J. A.; Weckhuysen, B. M., The production of propene oxide: Catalytic processes and recent developments. *Ind. Eng. Chem. Res.* **2006,** *45*, 3447-3459.
17. Yu, Z. X.; Xu, L.; Wei, Y. X.; Wang, Y. L.; He, Y. L.; Xia, Q. H.; Zhang, X. Z.; Liu, Z. M., A new route for the synthesis of propylene oxide from bio-glycerol derivated propylene glycol. *Chem. Commun.* **2009,** 3934-3936.
18. Dias, C. R.; Portela, M. F.; GalanFereres, M.; Banares, M. A.; Granados, M. L.; Pena, M. A.; Fierro, J. L. G., Selective oxidation of o-xylene to phthalic anhydride on V2O5 supported on TiO2-coated SiO2. *Catal. Lett.* **1997,** *43*, 117-121.
19. Mahmoud, E.; Watson, D. A.; Lobo, R. F., Renewable production of phthalic anhydride from biomass-derived furan and maleic anhydride. *Green Chem.* **2014,** *16*, 167-175.

20. Ouyang, X.; Ian Zones, S.; Katz, A. S. Highly active, selective, accessible, and robust zeolitic Sn-baeyer-villiger oxidation catalyst. US9687830B2, June 27, 2017.
21. Winkler, M.; Romain, C.; Meier, M. A. R.; Williams, C. K., Renewable polycarbonates and polyesters from 1,4-cyclohexadiene. *Green Chem.* **2015,** *17*, 300-306.
22. Dakshinamoorthy, D.; Weinstock, A. K.; Damodaran, K.; Iwig, D. F.; Mathers, R. T., Diglycerol-Based Polyesters: Melt Polymerization with Hydrophobic Anhydrides. *ChemSusChem* **2014,** *7*, 2923-2929.
23. Sanford, M. J.; Carrodeguas, L. P.; Van Zee, N. J.; Kleij, A. W.; Coates, G. W., Alternating Copolymerization of Propylene Oxide and Cyclohexene Oxide with Tricyclic Anhydrides: Access to Partially Renewable Aliphatic Polyesters with High Glass Transition Temperatures. *Macromolecules* **2016,** *49*, 6394-6400.
24. Van Zee, N. J.; Coates, G. W., Alternating Copolymerization of Propylene Oxide with Biorenewable Terpene-Based Cyclic Anhydrides: A Sustainable Route to Aliphatic Polyesters with High Glass Transition Temperatures. *Angew. Chem. Int. Ed.* **2015,** *54*, 2665-2668.
25. Carrodeguas, L. P.; Martin, C.; Kleij, A. W., Semiaromatic Polyesters Derived from Renewable Terpene Oxides with High Glass Transitions. *Macromolecules* **2017,** *50*, 5337-5345.
26. Carrodeguas, L. P.; Gonzalez-Fabra, J.; Castro-Gomez, F.; Bo, C.; Kleij, A. W., Al-III-Catalysed Formation of Poly(limonene)carbonate: DFT Analysis of the Origin of Stereoregularity. *Chem. - Eur. J.* **2015,** *21*, 6115-6122.
27. Zhu, Y. Q.; Romain, C.; Williams, C. K., Sustainable polymers from renewable resources. *Nature* **2016,** *540*, 354-362.
28. Hauenstein, O.; Agarwal, S.; Greiner, A., Bio-based polycarbonate as synthetic toolbox. *Nat. Commun.* **2016,** *7*.
29. Robert, C.; de Montigny, F.; Thomas, C. M., Tandem synthesis of alternating polyesters from renewable resources. *Nat. Commun.* **2011,** *2*, 586.
30. Bailer, J.; Feth, S.; Bretschneider, F.; Rosenfeldt, S.; Drechsler, M.; Abetz, V.; Schmalz, H.; Greiner, A., Synthesis and self-assembly of biobased poly(limonene carbonate)-block-poly(cyclohexene carbonate) diblock copolymers prepared by sequential ring-opening copolymerization. *Green Chem.* **2019,** *21*, 2266-2272.
31. Garden, J. A.; Saini, P. K.; Williams, C. K., Greater than the Sum of Its Parts: A Heterodinuclear Polymerization Catalyst. *J. Am. Chem. Soc.* **2015,** *137*, 15078-15081.
32. Chen, T. T. D.; Zhu, Y. Q.; Williams, C. K., Pentablock Copolymer from Tetracomponent Monomer Mixture Using a Switchable Dizinc Catalyst. *Macromolecules* **2018,** *51*, 5346-5351.
33. Zhu, Y.; Romain, C.; Williams, C. K., Selective Polymerization Catalysis: Controlling the Metal Chain End Group to Prepare Block Copolyesters. *J. Am. Chem. Soc.* **2015,** *137*, 12179-12182.
34. Paul, S.; Zhu, Y. Q.; Romain, C.; Brooks, R.; Saini, P. K.; Williams, C. K., Ring-opening copolymerization (ROCOP): synthesis and properties of polyesters and polycarbonates. *Chem. Commun.* **2015,** *51*, 6459-6479.
35. Nejad, E. H.; van Melis, C. G. W.; Vermeer, T. J.; Koning, C. E.; Duchateau, R., Alternating Ring-Opening Polymerization of Cyclohexene Oxide and Anhydrides: Effect of Catalyst, Cocatalyst, and Anhydride Structure. *Macromolecules* **2012,** *45*, 1770-1776.
36. Sanford, M. J.; Van Zee, N. J.; Coates, G. W., Reversible-deactivation anionic alternating ring-opening copolymerization of epoxides and cyclic anhydrides: access to orthogonally functionalizable multiblock aliphatic polyesters. *Chem. Sci.* **2018,** *9*, 134-142.

37. Saini, P. K.; Fiorani, G.; Mathers, R. T.; Williams, C. K., Zinc versus Magnesium: Orthogonal Catalyst Reactivity in Selective Polymerizations of Epoxides, Bio-derived Anhydrides and Carbon Dioxide. *Chem. - Eur. J.* **2017,** *23*, 4260-4265.
38. Giarola, S.; Romain, C.; Williams, C. K.; Hallett, J. P.; Shah, N., Techno-economic assessment of the production of phthalic anhydride from corn stover. *Chem. Eng. Res. Des.* **2016,** *107*, 181-194.
39. Mathers, R. T.; Shreve, M. J.; Meyler, E.; Damodaran, K.; Iwig, D. F.; Kelley, D. J., Synthesis and Polymerization of Renewable 1,3-Cyclohexadiene Using Metathesis, Isomerization, and Cascade Reactions with Late-metal Catalysts. *Macromol. Rapid. Comm.* **2011,** *32*, 1338-1342.
40. Poland, S. J.; Darensbourg, D. J., A quest for polycarbonates provided via sustainable epoxide/CO2 copolymerization processes. *Green Chem.* **2017,** *19*, 4990-5011.
41. Weisz, A.; Mandelbaum, A., Dehydrobromination of 1,2-Dibromocyclohexane and Related-Compounds by Lithium-Chloride in Hexamethylphosphoric Triamide - an Improved Synthesis of 1,3-Cyclohexadiene and Some Deuterium-Labeled Analogs. *J. Org. Chem.* **1984,** *49*, 2648-2650.
42. Kato, T.; Ichinose, I., Cyclization of Polyenes .32. Selective Bromination of Polyenes by 2,4,4,6-Tetrabromocyclohexa-2,5-Dienone. *J. Chem. Soc., Perkin Trans. 1* **1980,** 1051-1056.
43. Konishi, M. Method for producing cycloolefin and production apparatus thereof. US20110130600A1, June 2, 2011.
44. Taheri, H.; Dickinson, C. D.; Jacobson, P. A. Flow reactors for chemical conversions with heterogeneous catalysts. US 2009/0043114A1, February 12, 2009.
45. Hajian, H.; Yusoff, W. M. W., Itaconic Acid Production by Microorganisms: A Review. *Curr. Res. J. Biol. Sci.* **2015,** *7*, 37-42.
46. Sheldon, R. A., Green and sustainable manufacture of chemicals from biomass: state of the art. *Green Chem.* **2014,** *16*, 950-963.
47. Yu, X.; Jia, J.; Xu, S.; Lao, K. U.; Sanford, M. J.; Ramakrishnan, R. K.; Nazarenko, S. I.; Hoye, T. R.; Coates, G. W.; DiStasio, R. A., Jr., Unraveling substituent effects on the glass transition temperatures of biorenewable polyesters. *Nat. Commun.* **2018,** *9*, 2880.
48. Comyn, J., Adhesion Science. The Royal Society of Chemistry: Cambridge, UK, 1997.
49. Romain, C.; Zhu, Y. Q.; Dingwall, P.; Paul, S.; Rzepa, H. S.; Buchard, A.; Williams, C. K., Chemoselective Polymerizations from Mixtures of Epoxide, Lactone, Anhydride, and Carbon Dioxide. *J. Am. Chem. Soc.* **2016,** *138*, 4120-4131.
50. Stößer, T.; Mulryan, D.; Williams, C. K., Switch Catalysis To Deliver Multi-Block Polyesters from Mixtures of Propene Oxide, Lactide, and Phthalic Anhydride. *Angew. Chem. Int. Ed.* **2018,** *57*, 16893-16897.
51. Stosser, T.; Chen, T. T. D.; Zhu, Y.; Williams, C. K., 'Switch' catalysis: from monomer mixtures to sequence-controlled block copolymers. *Philos. Trans. Royal Soc. A* **2018,** *376*.
52. Spyros, A.; Argyropoulos, D. S.; Marchessault, R. H., A study of poly(hydroxyalkanoate)s by quantitative P-31 NMR spectroscopy: Molecular weight and chain cleavage. *Macromolecules* **1997,** *30*, 327-329.
53. Ramey, K. C., Nmr Study of Poly(Methyl Methacrylate) - Diads and Triads and Tetrads and Pentads. *J. Polym. Sci. Poly. Lett.* **1967,** *5*, 859-&.
54. Chang, E. P., Viscoelastic Windows of Pressure-Sensitive Adhesives. *J. Adhesion* **1991,** *34*, 189-200.
55. Kobayashi, S.; Uyama, H.; Takamoto, T., Lipase-catalyzed degradation of polyesters in organic solvents, a new methodology of polymer recycling using enzyme as catalyst. *Biomacromolecules* **2000,** *1*, 3-5.

56. Fiorani, G.; Stuck, M.; Martin, C.; Belmonte, M. M.; Martin, E.; Escudero-Adan, E. C.; Kleij, A. W., Catalytic Coupling of Carbon Dioxide with Terpene Scaffolds: Access to Challenging Bio-Based Organic Carbonates. *ChemSusChem* **2016,** *9*, 1304-1311.
57. Hillmyer, M. A.; Tolman, W. B., Aliphatic Polyester Block Polymers: Renewable, Degradable, and Sustainable. *Acc. Chem. Res.* **2014,** *47*, 2390-2396.
58. Schneiderman, D. K.; Hill, E. M.; Martello, M. T.; Hillmyer, M. A., Poly(lactide)-block-poly(epsilon-caprolactone-co-epsilon-decalactone)-block-poly(lactide) copolymer elastomers. *Polym. Chem.* **2015,** *6*, 3641-3651.
59. Bergfelt, A.; Lacey, M. J.; Hedman, J.; Sangeland, C.; Brandell, D.; Bowden, T., epsilon-Caprolactone-based solid polymer electrolytes for lithium-ion batteries: synthesis, electrochemical characterization and mechanical stabilization by block copolymerization. *RSC Adv.* **2018,** *8*, 16716-16725.
60. Yi, N.; Chen, T. T. D.; Unruangsri, J.; Zhu, Y.; Williams, C. K., Orthogonal functionalization of alternating polyesters: selective patterning of (AB)n sequences. *Chem. Sci.* **2019,** *10*, 9974-9980.
61. Burns, A. B.; Register, R. A., Mechanical Properties of Star Block Polymer Thermoplastic Elastomers with Glassy and Crystalline End Blocks. *Macromolecules* **2016,** *49*, 9521-9530.
62. Lutz, J. F.; Lehn, J. M.; Meijer, E. W.; Matyjaszewski, K., From precision polymers to complex materials and systems. *Nat. Rev. Mater.* **2016,** *1*, 16024.

Chapter 5

Perspective and Future Work

5.1. ‘Switch’ catalysis and sustainable polymers

Whilst ‘Switch’ catalysis has progressed rapidly in the last 5 years, there are still many elements of the methodology that can be explored in order to increase its effectiveness and wider applicability. ‘Switch’ catalysis can be organized into three different layers of research: (1) the fundamentals of ‘switch’ catalysis (2) mechanistic complexity (3) advanced architectural control (Fig. 5.1).

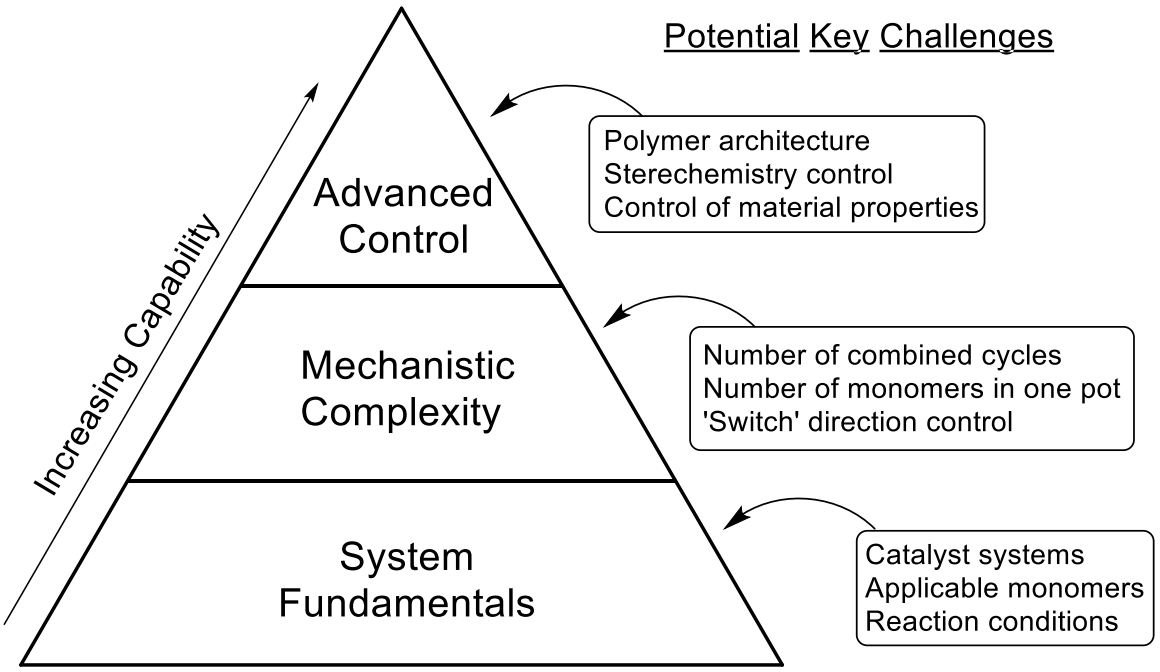


Figure 5.1 Three layered view of ‘Switch’ catalysis research.

The segment focuses on different challenges. For instance, the system fundamentals layer focuses on investigating catalysts for ‘Switch’ catalysis, the applicable monomers as well as the conditions required for the various systems. A major challenge would be to produce high molar mass polymers (ca. 100 kg mol^{-1}) which necessitates examination of possible catalyst systems and appropriate

conditions. The middle layer investigates the wider mechanistic challenges such as increasing the number of catalytic cycles/monomers that can be incorporated in a one pot reaction and the ability to control the direction of the 'Switch' and hence sequence selectivity with the ability to generate multi-block polymers. Finally, Advanced Control should have an emphasis on building a desired polymer architecture based on 'Switch' principles built up. Key challenges include the formation of stereospecific blocks or blocks deviating from the traditional linear structures such as star or graft block polymer. Such materials have been shown to have enhanced physical properties and is expected to display complex morphologies.[1] 'Switch' catalysis as a concept has been developed. [2-11] However, its utility is not yet realized and further research should bes to enhance the capability of 'Switch' catalysis.

The monomers that have been published in 'Switch' catalysis include oxygenated monomers such as epoxides, anhydrides and lactones. To enhance the wider applicability of the method, other monomers susceptible to ROP should be targeted (Fig. 5.2). The ROP of trimethlyene carbonate (TMC) and its derivatives have been researched extensively using organocatalysts as well as metal-based complexes.[12-13] These monomers are highly relevant in biomedical applications, offer another route to polycarbonates and should be a primary target for future 'Switch' catalysis systems.[14] Nitrogen containing monomers, such as lactams have been shown to undergo ROP using a variety of acids or bases to form polyamide.[15] Polyamides have a variety of uses that range from biomedical to industrial applications.[16-17] Furthermore, block poly(amide-*b*-butadiene) and block poly(amide-*b*-ether) have been shown to display useful elastomeric properties and would be good target for future 'Switch' catalysis strategies.[18] Cyclic carbamates have been shown to undergo ROP using bases.[19-20] Such

processes would offer a route to polyurethanes, which is typically only accessed through use of toxic isocynate.[20] Sulphur containing monomers such as thiolactones have been shown to undergo ROP using Tin(II) Octanoate and organocatalysts such as 1,8-Diazabicyclo[5.4.0]undec-7-ene (DBU) and thus may prove to be interesting in 'Switch' systems.[21-22] Finally, ROP of cyclic siloxanes have been achieved using bases to afford polysiloxanes.[23] These materials are of particular interest as they are highly incompatible with many different polymers (i.e. block polymers with polysiloxane typically possess high Flory-Huggins parameter, χ) and thus increases their propensity to phase-separate.[24-25] Furthermore, polydimethylsiloxane (PDMS) has been shown to be a useful coating matieral (with a T_g of -125 °C)[26] but lacks mechanical strength.[27] Block polymers incorporating PDMS and hard blocks such as CHO/CO_2 polycarbonate could afford useful materials with a wide operating window (e.g. -125 °C to 100 °C).

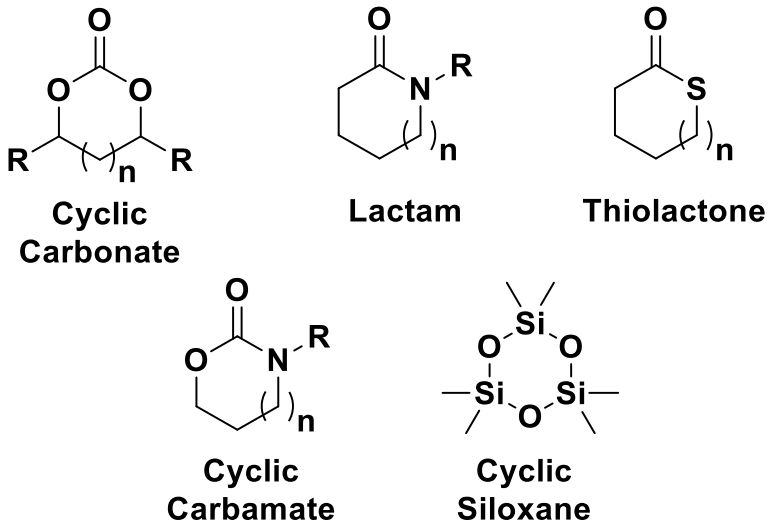


Figure 5.2 Selection of possible candidate monomers for 'Switch' catalysis

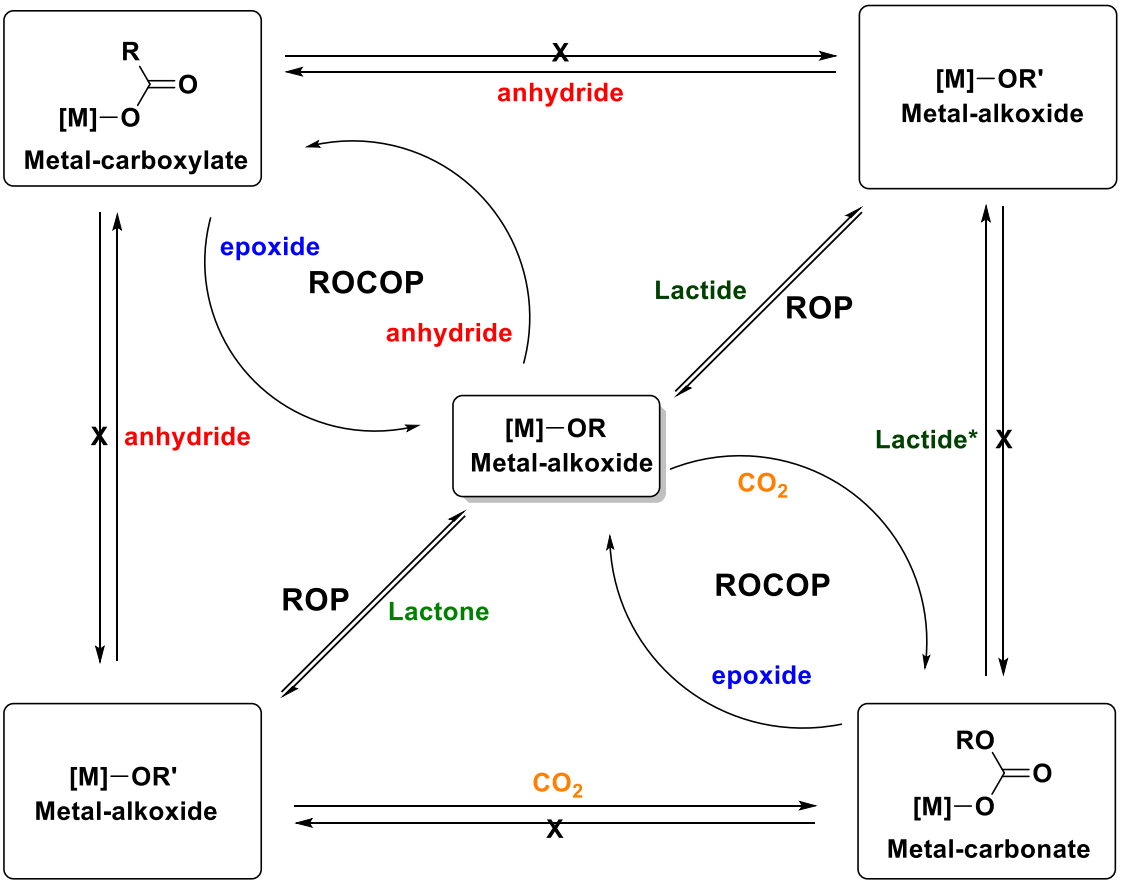
Currently, 'Switch' catalysis utilising CO_2 as a feedstock has only been shown for two catalysts.[2, 6] CO_2 has many benefits including being abundant, inexpensive and

non-toxic.[28] As such, it is worthwhile to expand both the number of catalysts that can carry out 'Switch' catalysis and monomer mixtures involving CO_2. For instance, it would be useful to prepare well-defined block polymers through 'Switch' catalysis strategies using industrially relevant monomer mixtures such as PO/CO_2/LA with organocatalysts.

A possible direction for potential future 'Switch' catalysts would be to improve the sustainability of its usage. Two important elements that can be improved include the sourcing of the catalyst as well as its recyclability. Ideal metal-based 'Switch' catalysts should employ metals that are inexpensive and abundant (such as group 1&2 elements). The use of heterogeneous catalysts would improve the recyclability of the catalyst and is worth exploring. Possible heterogeneous 'Switch' catalyst candidates include zinc glutarate derivatives as well as metal organic frameworks (MOFs). The former has been widely studied for their production of polypropylene carbonate and has also been shown to carry out the ROP of CL.[29-30] MOFs have been shown to conduct ROP of CL and LA.[31] Finally, the use of enzymes as 'Switch' catalysts may also be worth exploring due to their sustainability and biocompatibility. Enzymes have been shown to conduct ROP of various lactones as well as the ROCOP of epoxide/anhydrides.[32-33]

To improve the mechanistic complexity of 'Switch' catalysis, the number of monomers and cycles encompassed in a one-pot reaction can be increased. Such an extension further enhances the complexity of the 'Switch' mechanism. Part of this thesis improved the complexity of the 'Switch' catalysis from the typical use of 3 monomers and 2 cycles to 4 monomers and 3 cycles using epoxide, anhydride, CO_2 and lactone. Preliminary work with epoxide, CO_2 and lactide (LA) indicated that the latter

inserts preferentially into the metal alkoxide, possibly due to stronger chelating effects with the catalyst. As such, it may be possible to extend the complexity of the 'Switch' catalysis using a monomer mixture consisting of 5 monomers, namely epoxide, anhydride, CO_2, lactone and LA with the incorporation of 4 polymerization cycles (Fig. 5.3).



(Insertion rate: anhydride > lactide > CO_2 > lactone)

Figure 5.3 Proposed selectivity mechanism for a 5 monomer (epoxide, anhydride, lactide, CO_2 and lactone) 'Switch' polymerization (* *via* a metal-alkoxide intermediate after epoxide insertion).

By using a bifunctional initiator, ABCDCBA-type heptablock polymers can be prepared. Furthermore, the usage of LA has an added benefit of employing an

industrially relevant monomer.[34] To retain/improve the industrial relevance of the method, particular targets for the 5 monomer 'Switch' polymerization would encompass other industrially relevant monomers such as PO, PA and commercially available lactones. Potential catalyst systems include the [Salphen^{F}AlCl]/PPNCl, organocatalysts (phosphazene, ^{t}BuP$_1$) or BDI-Zn catalysts as these have been shown to conduct the ring-opening polymerization (ROP) of LA in a controlled manner.[7-8, 35]

'Switch' catalysis has received a strong foundation with the introduction of many catalytic systems and different types of applicable monomers. Nevertheless, there is still room for improvement. Expansion of the fundamental 'toolkit' should focus on investigating new types of monomer classes as well as other new catalysts that may excel in terms of wider monomer scope, milder reaction conditions or enhanced recyclability.

5.2. **Post-polymerization modification and applications**

The progress of post-polymerization modification of polyesters and polycarbonates should focus on two areas. The first area entails exploration of additional reactions and functional groups that can be installed. The method should preferentially install functionalities in a selective manner as to allow for more than one functionality to be furnished on the polymer backbone. Such strategies would allow for the preparation of polymers that have multiple functionalities and give access to high value materials.

For instance, the selectivity of the mCPBA epoxidation can be exploited. mCPBA meditated epoxidation typically requires an electron rich alkene. When applied to the polyester synthesised from the ROCOP of MA and VCHO, it is expected that the epoxidation will solely occur on the terminal alkene. The singly epoxidated polyester can then be employed for further functionalization. Possible options include preparing brush polymers by using the epoxide as an initiating group and installation of additional functionalities via reaction with nuclophiles such as amines and alcohols (Fig. 5.4).

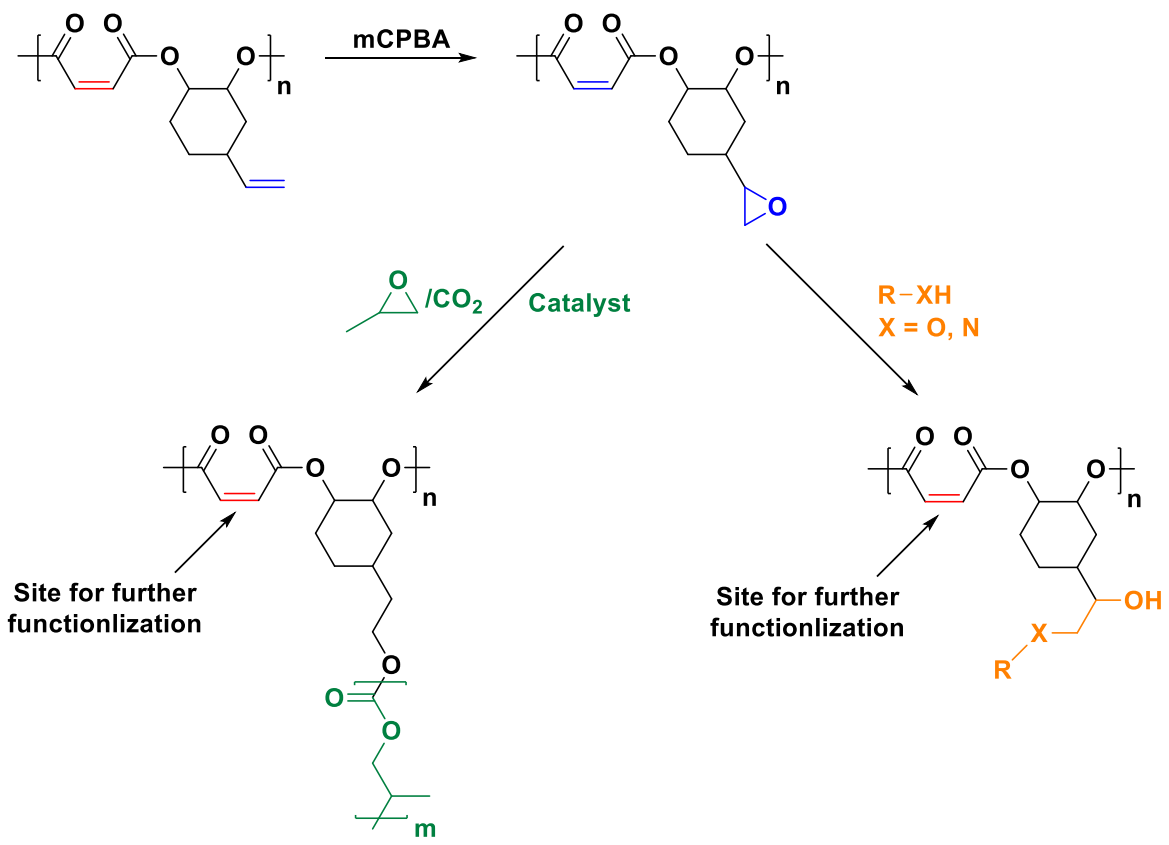


Figure 5.4 Potential new sequential post-polymerization modification methods.

The second area involves investigating applications for the established post-polymerization modification methods. For instance, the inclusion of hydrophilic hydroxyl groups in precise locations may improve the hydrolysis of polyesters and warrants further examination. If the presence of hydroxyl groups are proven to have an effective on the degradation rates of polymers, post-polymerization modification methods that install hydroxyl groups on to polyesters, such as the newly introduced hydroboration-oxidation, can be applied to commercially relevant polymers such as polylactide (PLA). Whilst PLA has been widely described as biodegradable, the process often requires high temperatures (> 60 °C) and extended time periods (90 days).[36]

Indeed, at lower temperatures of 35 °C, the biodegradation process can take up to 160 days to reach ~40% degradation.[37]

The hydrolysis of PLA has been described to be dependent on the amount of absorbed water.[38] As such, the introduction of hydroxyl groups is expected to enhance the degradation potential. By employing 'Switch' catalysis methodologies, periodic injections of epoxide/anhydride during the ROP of lactide and subsequent hydroboration-oxidation would allow for the preparation of PLA with interspersed hydroxyl functionalized polyesters (Fig. 5.5).

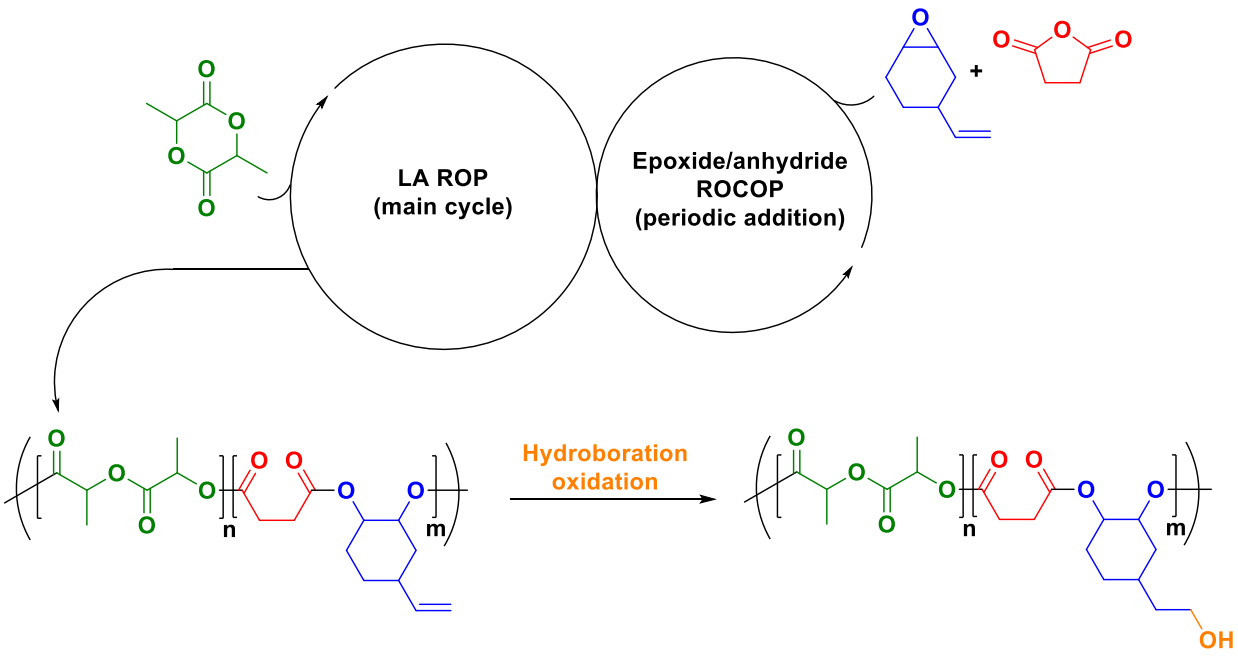


Figure 5.5. Potential procedure for preparing PLA with interspersed hydroxyl functionalized polyesters (note: n >> m).

5.3. **References**

1. Polymeropoulos, G.; Zapsas, G.; Ntetsikas, K.; Bilalis, P.; Gnanou, Y.; Hadjichristidis, N., 50th Anniversary Perspective: Polymers with Complex Architectures. *Macromolecules* **2017,** *50*, 1253-1290.
2. Romain, C.; Williams, C. K., Chemoselective Polymerization Control: From Mixed-Monomer Feedstock to Copolymers. *Angew. Chem. Int. Ed.* **2014,** *53*, 1607-1610.
3. Paul, S.; Romain, C.; Shaw, J.; Williams, C. K., Sequence Selective Polymerization Catalysis: A New Route to ABA Block Copoly(ester-b-carbonate-b-ester). *Macromolecules* **2015,** *48*, 6047-6056.
4. Zhu, Y.; Romain, C.; Williams, C. K., Selective Polymerization Catalysis: Controlling the Metal Chain End Group to Prepare Block Copolyesters. *J. Am. Chem. Soc.* **2015,** *137*, 12179-12182.
5. Romain, C.; Zhu, Y. Q.; Dingwall, P.; Paul, S.; Rzepa, H. S.; Buchard, A.; Williams, C. K., Chemoselective Polymerizations from Mixtures of Epoxide, Lactone, Anhydride, and Carbon Dioxide. *J. Am. Chem. Soc.* **2016,** *138*, 4120-4131.
6. Kernbichl, S.; Reiter, M.; Adams, F.; Vagin, S.; Rieger, B., CO_2-Controlled One-Pot Synthesis of AB, ABA Block, and Statistical Terpolymers from beta-Butyrolactone, Epoxides, and CO2. *J. Am. Chem. Soc.* **2017,** *139*, 6787-6790.
7. Ji, H.-Y.; Wang, B.; Pan, L.; Li, Y.-S., One-Step Access to Sequence-Controlled Block Copolymers by Self-Switchable Organocatalytic Multicomponent Polymerization. *Angew. Chem. Int. Ed.* **2018,** *57*, 16888-16892.
8. Stößer, T.; Mulryan, D.; Williams, C. K., Switch Catalysis To Deliver Multi-Block Polyesters from Mixtures of Propene Oxide, Lactide, and Phthalic Anhydride. *Angew. Chem. Int. Ed.* **2018,** *57*, 16893-16897.
9. Stosser, T.; Williams, C. K., Selective Polymerization Catalysis from Monomer Mixtures: Using a Commercial Cr-Salen Catalyst To Access ABA Block Polyesters. *Angew. Chem. Int. Ed.* **2018,** *57*, 6337-6341.
10. Kernbichl, S.; Reiter, M.; Mock, J.; Rieger, B., Terpolymerization of β-Butyrolactone, Epoxides, and CO2: Chemoselective CO2-Switch and Its Impact on Kinetics and Material Properties. *Macromolecules* **2019,** *52*, 8476-8483.
11. Stosser, T.; Sulley, G. S.; Gregory, G. L.; Williams, C. K., Easy access to oxygenated block polymers via switchable catalysis. *Nat. Commun.* **2019,** *10*, 2668.
12. Gregory, G. L.; Lopez-Vidal, E. M.; Buchard, A., Polymers from sugars: cyclic monomer synthesis, ring-opening polymerisation, material properties and applications. *Chem. Commun.* **2017,** *53*, 2198-2217.
13. Becker, G.; Wurm, F. R., Functional biodegradable polymers via ring-opening polymerization of monomers without protective groups. *Chem. Soc. Rev.* **2018,** *47*, 7739-7782.
14. Thomas, A. W.; Dove, A. P., Postpolymerization Modifications of Alkene-Functional Polycarbonates for the Development of Advanced Materials Biomaterials. *Macromol. Biosci.* **2016,** *16*, 1762-1775.
15. Sebenda, J., Lactam Polymerization. *J Macromol Sci Chem* **1972,** *A 6*, 1145-1199.
16. Sibikin, I.; Karger-Kocsis, J., Toward industrial use of anionically activated lactam polymers: Past, present and future. *Advanced Industrial and Engineering Polymer Research* **2018,** *1*, 48-60.
17. Zhang, J.; Kissounko, D. A.; Lee, S. E.; Gellman, S. H.; Stahl, S. S., Access to Poly-β-Peptides with Functionalized Side Chains and End Groups via Controlled Ring-Opening Polymerization of β-Lactams. *J. Am. Chem. Soc.* **2009,** *131*, 1589-1597.

18. Dubois, P.; Coulembier, O.; Raquez, J.-M., *Handbook of Ring-Opening Polymerization*. Wiley-VCH: 2009.
19. Zhang, D. P.; Zhang, Y.; Fan, Y. J.; Rager, M. N.; Guerineau, V.; Bouteiller, L.; Li, M. H.; Thomas, C. M., Polymerization of Cyclic Carbamates: A Practical Route to Aliphatic Polyurethanes. *Macromolecules* **2019,** *52*, 2719-2724.
20. Suzuki, M.; Yoshida, S.; Shiraga, K.; Saegusa, T., New Ring-Opening Polymerization via a π-Allylpalladium Complex. 5. Multibranching Polymerization of Cyclic Carbamate To Produce Hyperbranched Dendritic Polyamine. *Macromolecules* **1998,** *31*, 1716-1719.
21. Sanda, F.; Jirakanjana, D.; Hitomi, M.; Endo, T., Anionic ring-opening polymerization of epsilon-thionocaprolactone. *Macromolecules* **1999,** *32*, 8010-8014.
22. Langlais, M.; Coutelier, O.; Moins, S.; De Winter, J.; Coulembier, O.; Destarac, M., Scope and limitations of ring-opening copolymerization of trimethylene carbonate with substituted gamma-thiolactones. *Polym. Chem.* **2018,** *9*, 2769-2774.
23. Chojnowski, J., Kinetically controlled siloxane ring-opening polymerization. *Journal of Inorganic and Organometallic Polymers* **1991,** *1*, 299-323.
24. Sinturel, C.; Bates, F. S.; Hillmyer, M. A., High χ–Low N Block Polymers: How Far Can We Go? *ACS Macro Lett.* **2015,** *4*, 1044-1050.
25. Azuma, K.; Sun, J.; Choo, Y.; Rokhlenko, Y.; Dwyer, J. H.; Schweitzer, B.; Hayakawa, T.; Osuji, C. O.; Gopalan, P., Self-Assembly of an Ultrahigh-χ Block Copolymer with Versatile Etch Selectivity. *Macromolecules* **2018,** *51*, 6460-6467.
26. Bosq, N.; Guigo, N.; Persello, J.; Sbirrazzuoli, N., Melt and glass crystallization of PDMS and PDMS silica nanocomposites. *Phys Chem Chem Phys* **2014,** *16*, 7830-7840.
27. Pan, F.; Altenried, S.; Liu, M.; Hegemann, D.; Bülbül, E.; Moeller, J.; Schmahl, W. W.; Maniura-Weber, K.; Ren, Q., A nanolayer coating on polydimethylsiloxane surfaces enables a mechanistic study of bacterial adhesion influenced by material surface physicochemistry. *Materials Horizons* **2020,** *7*, 93-103.
28. Kamphuis, A. J.; Picchioni, F.; Pescarmona, P. P., CO2-fixation into cyclic and polymeric carbonates: principles and applications. *Green Chem.* **2019,** *21*, 406-448.
29. Hwang, Y.; Jung, J.; Ree, M.; Kim, H., Terpolymerization of CO2 with Propylene Oxide and ε-Caprolactone Using Zinc Glutarate Catalyst. *Macromolecules* **2003,** *36*, 8210-8212.
30. Marbach, J.; Höfer, T.; Bornholdt, N.; Luinstra, G. A., Catalytic Chain Transfer Copolymerization of Propylene Oxide and CO2 using Zinc Glutarate Catalyst. *ChemistryOpen* **2019,** *8*, 828-839.
31. Chuck, C. J.; Davidson, M. G.; Jones, M. D.; Kociok-Köhn, G.; Lunn, M. D.; Wu, S., Air-Stable Titanium Alkoxide Based Metal−Organic Framework as an Initiator for Ring-Opening Polymerization of Cyclic Esters. *Inorg. Chem.* **2006,** *45*, 6595-6597.
32. Albertsson, A.-C.; Srivastava, R. K., Recent developments in enzyme-catalyzed ring-opening polymerization. *Adv Drug Deliver Rev* **2008,** *60*, 1077-1093.
33. Soeda, Y.; Okamoto, T.; Toshima, K.; Matsumura, S., Enzymatic Ring-Opening Polymerization of Oxiranes and Dicarboxylic Anhydrides. *Macromol. Biosci.* **2002,** *2*, 429-436.
34. Shen, L.; Worrell, E.; Patel, M., Present and future development in plastics from biomass. *Biofuel. Bioprod. Bior.* **2010,** *4*, 25-40.
35. Chamberlain, B. M.; Cheng, M.; Moore, D. R.; Ovitt, T. M.; Lobkovsky, E. B.; Coates, G. W., Polymerization of lactide with zinc and magnesium beta-diiminate complexes: Stereocontrol and mechanism. *J. Am. Chem. Soc.* **2001,** *123*, 3229-3238.
36. Boonmee, C.; Kositanont, C.; Leejarkpai, T., Degradation of Poly(Lactic Acid) under Simulated Landfill Conditions. *Environ. Nat. Resour. J.* **2016,** *14*, 1-9.
37. Kolstad, J. J.; Vink, E. T. H.; De Wilde, B.; Debeer, L., Assessment of anaerobic degradation of Ingeo™ polylactides under accelerated landfill conditions. *Polym. Degrad. Stabil.* **2012,** *97*, 1131-1141.

38. Schliecker, G.; Schmidt, C.; Fuchs, S.; Kissel, T., Characterization of a homologous series of d,l-lactic acid oligomers; a mechanistic study on the degradation kinetics in vitro. *Biomaterials* **2003,** *24*, 3835-3844.

Chapter 6

Experimental

6.1. General Comments

All solvents and reagents were obtained from commercial sources (Sigma Aldrich) unless stated otherwise. [SalenCr(III)Cl] and metal precursors were purchased from Strem Chemicals. The synthesis of [H_2L] macrocyclic ligand, was carried out in air and performed according to literature procedures.[1] Monomer purification and subsequent polymerizations were carried out under inert conditions using standard Schlenk line techniques and a nitrogen-filled glovebox. Common organic solvents were obtained from an SPS system degassed by bubbling nitrogen or freeze-pump-thaw before being stored over 3 Å molecular sieves under a nitrogen atmosphere.

Purification of epoxides. Cyclohexene oxide (CHO) was dried by stirring over CaH_2 followed by fractional distillation at 130 °C and kept under nitrogen atmosphere. 4-Vinyl-1-cyclohexene 1,2-epoxide (VCHO) was dried by stirring over CaH_2 followed by fractional distillation at 80 °C under reduced pressure and kept under nitrogen atmosphere. Limonene oxide (LO) was purified by first stirring over NaH followed by addition of MeI and fractional distillation at 40 °C (1 mbar). This procedure was repeated twice more (three distillations in total) then kept under a nitrogen atmosphere. ε All other epoxides were dried over CaH_2 followed by fractional distillation and kept under nitrogen atmosphere.

Purification of lactones. ε-decalactone (DL) had been dried over CaH_2, distilled under reduced pressure and kept under a nitrogen atmosphere. Lactide (LA) was recrystallised from anhydrous toluene and sublimed three times.

Purification of anhydrides. Phthalic anhydride (PA) was purified by first dissolving in benzene. The filtrate was then collected and the solvent was removed under reduced

pressure followed by recrystallization from $CHCl_3$ and sublimed. Maleic anhydride (MA) was purified by recrystallization from $CHCl_3$ followed by sublimation. All other anhydrides were purification by sublimation up to three times. The tricyclic anhydrides (TCAs) were synthesised and purified based on modified literature procedures.[2] TCAs (a1-a3) were purified by crystallization in methanol (TCA-a1) or 80:20 hexanes: ethyl acetate (TCA-a2 and TCA-a3) followed by double sublimation at 100 °C. TCA-a4 was purified by column chromatography with 90:10 hexanes: ethyl acetate (three times) then dried under vacuum overnight to yield a colorless oil.

Purification of chain transfer agents. 1,2-cyclohexanediol (CHD) had been recrystallised from ethyl acetate and kept under nitrogen. 1,4-Benzenedimethanol (BDM) had been recrystallised from toluene three times and kept under nitrogen.

6.2. **Techniques**

NMR Spectroscopy. All NMR spectroscopy were obtained using a Bruker AV 400 instrument and processed using either MestReNova or Bruker TopSpin software packages.

Size Exclusion Chromatography (SEC). SEC data was obtained using a Shimadzu LC-20AD instrument with two Mixed Bed PSS SDV linear S columns in series and HPLC grade THF as the eluent flowing at 1.0 mL/min at 30 °C and monodisperse polystyrene standard was used for calibration. All samples were dissolved in HPLC grade THF and filtered before analysis.

Elemental Analysis (EA). EA was performed by Mr. Stephen Boyer at London Metropolitan University, North Campus, Holland Road, London, N7.

Matrix-Assisted Laser Desorption/Ionization – Time of Flight Mass Spectrometry Mass Spectrosocpy (MALDI-ToF MS). MALDI-ToF MS was performed using a Micromass MALDI micro MX spectrometer. Potassium trifluoroacetate (KTFA) was used as the ionising agent. Dithranol was used as the matrix for polycarbonates and poly(caprolactone). Trans-2-[3-(4-tert-butylphenyl)-2-methyl-2-propenylidene] malononitrile (DCTB) was used as the matrix for all other polyesters. The polymer, the matrix and the ionising agent were dissolved in THF separately at a concentration of 10 mg·mL-1 and mixed at a loading of 1: 1: 1. The mixed solution was spotted on a stainless steel MALDI plate repeatedly (3 times) and left to dry for 16 h. All the spectra were recorded using reflectron mode and analysed using mmass software.

Attenuated Total Reflection – Infrared Spectroscopy (ATR-IR). IR spectra were recorded on a Perkin Elmer Spectrum 100 (FT-IR) with an AT-IR crystal. All measurements were performed in the reflection mode at a resolution of 4 cm^{-1}. For *in-situ* ATR-IR, a Mettler-Toledo ReactIR 4000 spectrometer equipped with a silver halide DiComp probe was employed. The data was processed with in-build baseline correction software.

Differential Scanning Calometry (DSC). The thermal properties were measured using DSC3+ (Mettler Toledo, Ltd). A sealed empty crucible was used as a reference, and the DSC was calibrated using indium. Samples were heated from 25 °C to 150 °C, at a rate of 10 °C/min, under N_2 flow (80 ml/min), and were kept at 150 °C for 2 min to erase the thermal history. Subsequently, the samples were cooled to -80 °C, at a rate of 10 ^oC/min, and kept at -80 °C·min^{-1} for a further 2 mins, followed by a heating procedure from -80 °C to 150 °C, at a rate of 10 °C/min. Each sample was run for three heating–cooling cycles. The glass transition temperatures (T_g) reported are taken from the third heating.

Thermal Gravimetric Analysis (TGA). TGA was measured using a TGA/DSC 1 system (Mettler-Toledo Ltd). Samples were heated from 25 °C to 500 °C, at a rate of 5 °C/min, under N2 flow (100 cm3/min).

Dynamic Mechanical Analysis (DMA). Viscoelastic properties were measured using an Anton Paar Physica MCR 301 rheometer. Temperature sweep tests were performed at a constant shear strain of 0.5% and a frequency of 1 Hz from 20 °C to 150 °C at 2 °C/min. Frequency sweep tests were performed at a constant shear strain of 0.5% from 0.01 Hz to 30 Hz at 25 °C.

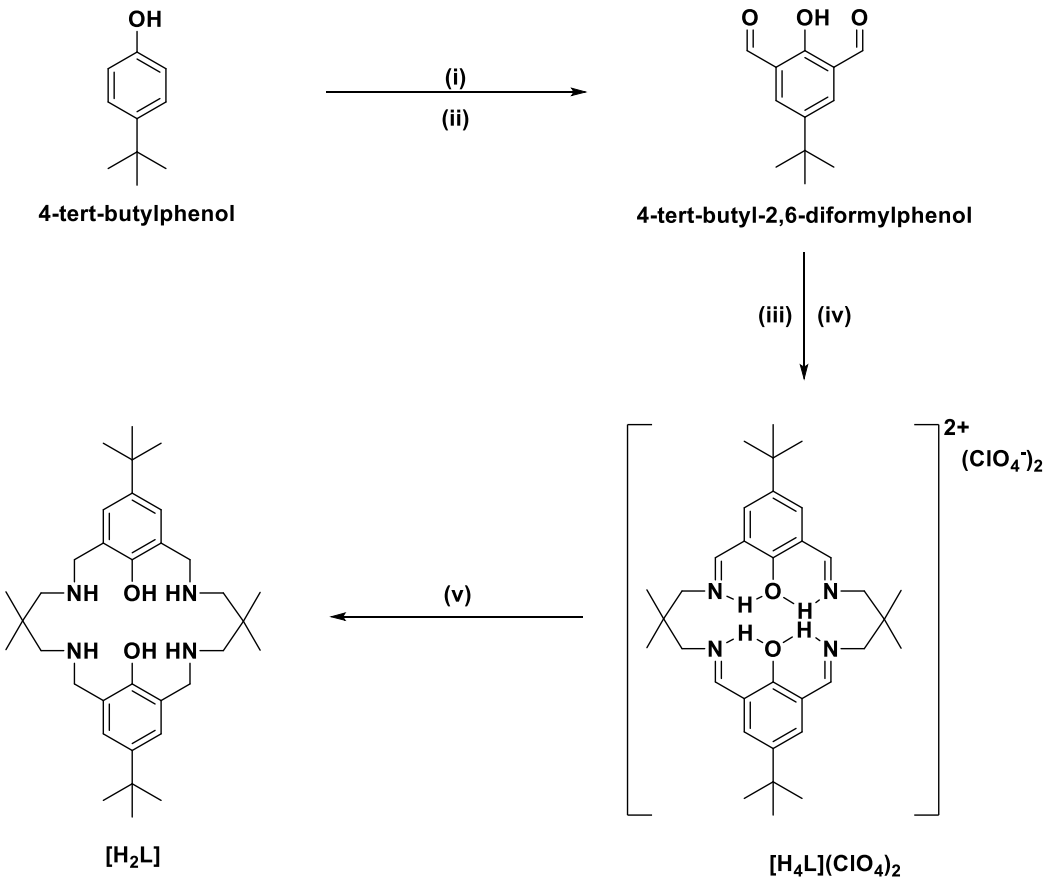
180 °C Peel Test. The 180 ° Peel test was performed according to ASTM D3000 standard testing methods using a Shimadzu EZ-LX Universal Testing Instrument at a peeling rate of 305 mm/min. The adhesive material was placed on a PET sheet (0.5 inch width) and adhered to a polished stainless steel test panel with a constant pressure provided by a 4.5 lb weight. The average peel force was collected and reported from three samples.

Dynamic Light Scattering (DLS). The DLS measurements were conducted using a Zetasizer Nano series instrument (Malvern Instrument Zen 1600). The scattering angle was set at 173 ° and all the aqueous aggregate solutions were put into disposable PMMA cuvettes for analysis.

Transmission Electron Microscopy (TEM). Amorphous carbon-coated copper TEM grids (Agar Scientific) were plasma glow-discharged for 15 s to generate a hydrophilic surface. Individual samples (2-4 μL) were placed onto the freshly discharged grids for 5 mins, before being blotted with a filter paper to remove excess solutions. Uranium acetate (0.5 w/v %) was used to stain the sample by placing onto the sample-loaded grids for 5 mins and then removing the excessive staining solution. The grids were dried in fume hood overnight prior to characterization. TEM images were obtained by Tianyi Chen on JEOL 3000F scanning transmission electron microscope, equipped with an Oxford X-Max 80 SDD EDX detector, at an operating voltage of 200 kV.

6.3. **Experimental Procedures**

Ligand synthesis



Scheme 6.1. Three-step synthesis of $[H_2L]$ macrocyclic ligand: (i) Hexamethylenetetramine (HMTA) (2 equiv), Trifluoroacetic acid (TFA) (10 equiv), 125 °C, 17 h (ii) 3M HCl, 100 °C, 50% yield (iii) $NaClO_4$ (4 equiv), acetic acid (2 equiv), 2,2-dimethyl-1,3-propanediene (1 equiv), MeOH, 70 °C, 1 h, 70% yield (iv) 25 °C, 16 h (v) $NaBH_4$ (30 equiv), MeOH, 0 °C, 72% yield.

Synthesis of 4-tert-Butyl-2,6-diformylphenol

4-*Tert*-butylphenol (20.6 g, 137.1 mmol), hexamethylenetetramine (38.4 g, 273.9 mmol) and TFA (104 mL, 1358 mmol) were placed in a round-bottom flask with stirring to yield a bright yellow solution that was refluxed at 125 °C for 17 h to obtain a darkened solution. Using a Dean-Stark condenser, the solution was further refluxed for 4 h at 150 °C. The reaction mixture was cooled to 100 °C and charged with 3M HCl (400 mL). The resulting mixture was refluxed for a further 40 min at 100 °C. Precipitation was observed after cooling to -10°C for 10 h. The precipitate was filtered, washed with cold (−78 °C) MeOH and dried to yield yellow crystals (14.56 g, 55%).

^{1}H NMR (400 MHz, $CDCl_3$, 298 K): δ(ppm) = 11.48 (s, 1H, -OH), 10.25 (s, 2H, CHO), 7.98 (s, 2H, Ar-H), 1.36 (s, 9H, CH_3)

Synthesis of $[H_4Ln](ClO_4)_2$

4-*Tert*-Butyl-2,6-diformylphenol (5.0 g, 24 mmol), $NaClO_4$ (11.87 g, 96.9 mmol), acetic acid (2.7 mL, 48.5 mmol) and MeOH (120 mL) was added to a round-bottom flask and heated to 70 °C with stirring. After the solution started to boil, 2,2-dimethyl-1,3-propanediene (2.9 mL, 24.2 mmol) in MeOH (60 mL) was added dropwise to obtain an orange/red solution. The mixture was refluxed at 75 °C for 1 h and left to stand for 16 h. The resultant precipitate was filtered and washed with cold (-78 °C) MeOH and dried to yield orange crystals (6.39 g, 70%).

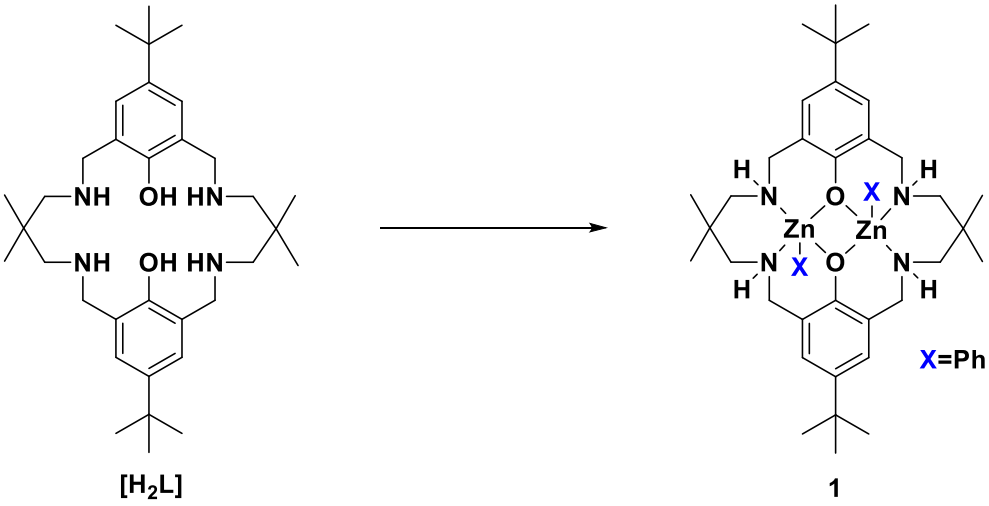
^{1}H NMR (400 MHz, DMSO-d_6, 298 K): δ(ppm) = 13.58 (br s, 4H, NH/OH), 8.68 (d, 4H, N=CH), 7.65 (s, 4H, ar-H), 3.88 (2, 8H, CH_2), 1.28 (s, 12H, CH_3), 1.14 (s, 18H, CH_3).

Synthesis of H_2L

$[H_4Ln](ClO_4)_2$ (5.0 g, 6.7 mmol) and MeOH (500 mL) were added to a round-bottom flask to obtain a red/orange solution. The solution was cooled to 0 °C before the slow addition of $NaBH_4$ (7.58 g, 200 mmol) to yield a colourless solution. The solution was left stirring at room temperature for 1 h before water was added until precipitation was observed (400 mL). The resultant suspension was left standing for 10 h before being filtered, washed with water and dried under vacuum, at 40 °C, to yield a white solid. The precipitate was crystallised from MeOH to yield white crystals (2.56 g, 72%).

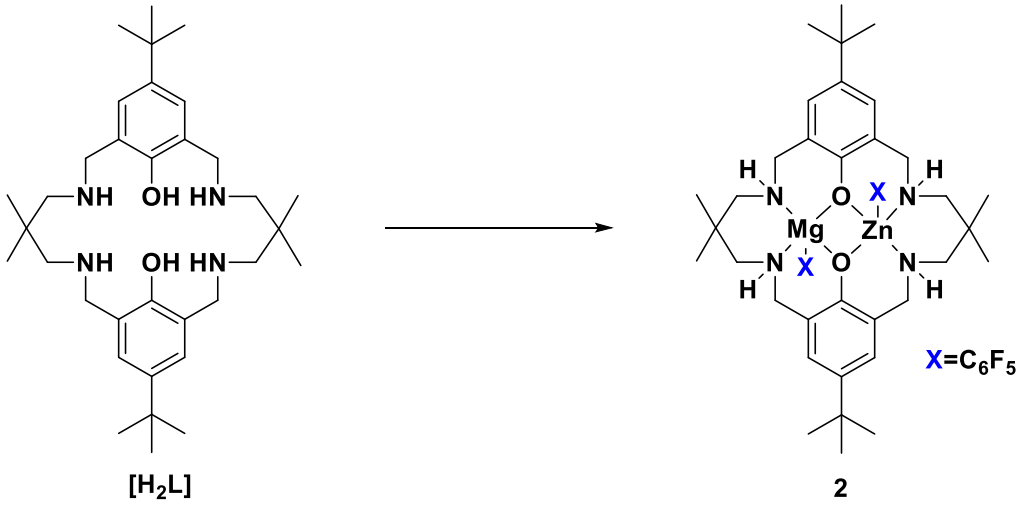
^1H NMR (400 MHz, $CDCl_3$, 298 K): δ(ppm) = 6.93 (s, 4H, Ar-H), 3.73 (s, 8H, CH_2), 2.52 (s, 8H, CH_2), 1.25 (s, 18H, CH_3), 1.01 (s, 12H, CH_3). Elemental analysis calcd (%) for H_2L: C, 73.87; H, 10.21; N 10.13; found: C 73.64, H 10.36, N 9.96.

Synthesis of [LZn$_2$(Ph)$_2$] (1)



Under anaerobic conditions, two separate solutions of [H_2L] macrocyclic ligand (0.40 g, 0.7 mmol) in THF (5 mL) and $ZnPh_2$ (0.25 g, 1.2 mmol) in THF (2 mL) were pre-cooled to -40 °C before being added to a glass vial together to obtain a cloudy solution. The mixture stirred for 25 h at 25 °C and filtered to obtain a white solid (0.26 g, 55%). ^{1}H NMR (500MHz, TCE-*d*$_2$, 403 K): δ(ppm) =7.40 (br, 6H, aryl-H) , 7.00 (br, 4H, aryl-H), 5.01-4.29 (br, 4H), 3.37-2.46 (br, 16H), 1.35 (br, ^{t}Bu, 6H), 1.31 (br, 6H, CH_3), 1.05 (br, 6H, CH_3). ^{13}C{H} (500MHz, TCE-*d*$_2$, 403 K): δ(ppm) = 138.5 ($C_{quat,}$ aryl), 128.1 (Ph), 128.0 (C_{quat}, aryl), 123.8 (C_{quat}, aryl), 63.5 (CH_2), 56.7 (CH_2), 33.4 and 33.3 (C_{quat}, *t*Bu and C_{qaut}, CMe_2), 31.4 (tBu), 27.9 (CH_3), 21.4 (CH_3). Elemental analysis calcd (%) for [LZn$_2$(Ph)$_2$]: C 66.10, H 7.72, N 6.70; found C 65.94, H 7.63, N 6.78.

Synthesis of [LMgZn(C_6F_5)$_2$] (2)



Under inert conditions, the [H_2L] macrocyclic ligand (500 mg, 0.90 mmol) and magnesium bis(hexamethyldisilazide) (Mg(N($SiMe_3$)$_2$)$_2$)(312 mg, 0.90 mmol) were stirred in anhydrous THF (10 mL) at 25 °C for 1 h. A solution of bis(pentafluorophenyl) zinc (361 mg, 0.90mmol), in anhydrous THF (5 mL), was then added dropwise to the ligand/$MgHMDS_2$ mixture which was stirred overnight at 25 °C to afford a cloudy orange solution. The solvent was filtered and washed with pentane (2 x 20 mL) to yield a white solid (0.72 mg, 81%). ^{1}H NMR (400 MHz, $CDCl_3$, 298 K) δ(ppm): 6.81 (d, 2H, J=3 Hz), 6.75 (d, 2H, J=3 Hz), 4.36 (t, 2H, J=13 Hz), 4.30 (t, 2H, J=13 Hz), 3.38 (d, 2H, J=14 Hz), 3.24 (d, 2H, J=13 Hz), 3.08 (t, 2H, J=13 Hz), 3.01 (t, 2H, J=13 Hz) 2.77-2.62 (m, 6H), 2.10-2.02 (m, 2H), 1.26 (s, 3H), 1.20 (s, 18H), 1.16 (s, 3H), 1.06-1.00 (m, 6H). ^{13}C{^{1}H} (125 MHz, $CDCl_3$, 298 K) δ(ppm): 159.4, 137.3, 126.5, 124.7, 122.2.5, 62.7, 61.9, 58.0, 56.1, 34.4, 33.6, 31.7, 28.5 – 20.3. Elemental analysis: Calcd for $C_{46}H_{54}F_{10}MgN_4O_2Zn$ (%): C 56.69, H 5.58, N 5.75. Found: C 56.55, H 5.61, N 5.68.

End group analysis by $^{31}P\{^{1}H\}$ NMR spectroscopy

Literature procedure for hydroxyl end group analysis by $^{31}P\{^{1}H\}$ NMR spectroscopy was followed.[3] A mixture of stock solution (40 µL), excess 2-chloro-4,4,5,5-tetramethyl dioxaphospholane (40 µL) and polymer sample (20 mg) was added to a NMR tube and shaken. The mixture was allowed to react for 6 h before measurement. The stock solution consists of Bisphenol A (400 mg) and of $Cr(acac)_3$ (5.5 mg) in pyridine (10 mL).

Ring-opening polymerization of ε-DL

Under anaerobic conditions, CHO (1.2 mL, 11.9 mmol), $[LZn_2(Ph)_2]$ (0.01 g, 0.01 mmol), CHD (5.6 mg, 0.04 mmol) and ε-DL (0.42 mL, 2.4 mmol) were placed in a vial and heated to 100 °C with stirring for 1.25 h. After the desired reaction time, the solution became viscous and the mixture was exposed to air to quench the polymerization. The crude sample was analysed by ^{1}H NMR spectroscopy. SEC analysis (THF as eluent, 1 mL/min, 30 °C) of the crude polymer was carried out following removal of excess CHO under reduced pressure. The polymer was purified by precipitation of a DCM solution (<1 g/mL) into MeOH (50 mL) at -78 °C.

Exemplar ring-opening copolymerization of epoxide and CO_2

Under anaerobic conditions, the chosen epoxide, $[LZn_2(Ph)_2]$ (0.01 g, 0.01 mmol) and CHD (5.6 mg, 0.04 mmol) were added into a Schlenk tube (molar ratio: cat./CHD/epoxide = 1/4/1000). The Schlenk tube was refilled with CO_2 (1 bar) via three vacuum/CO_2 cycles and allowed to react at 80 °C with stirring. Thereafter, the mixture was exposed to air to quench the polymerization. The crude sample was analysed by ^{1}H NMR spectroscopy. SEC analysis (THF as eluent, 1 mL/min, 30 °C) of

the crude polymer was carried out following removal of excess CHO under reduced pressure. The polymer was purified by precipitation of a DCM solution (<1 g/mL) into MeOH (50 mL).

Exemplar ring opening copolymerization of epoxides/anhydride

In a glovebox, [SalenCr(III)Cl] catalyst (10.0 mg, 16.0 μmol), Bis(triphenylphosphoranylidene)ammonium chloride (PPNCl) (9.0 mg, 16 μmol), cyclohexene diol (18.0 mg, 0.2 mmol), anhydride (1.6 mmol) and epoxide (1.90 mmol) were dissolved in toluene (2.0 mL) placed in a Schlenk tube (molar ratio: **1**/PPNCl/CHD/anhydride/epoxide = 1/1/10/100/120). The reaction mixture was stirred at 60 °C for a predetermined time period. The volatiles were removed *in vacuo*. The crude polymer was dissolved in THF, filtered through an Amberlyst-15 column (to remove Cr(III) catalyst and PPNCl) and purified by repetitive precipitation from hexane (3 x 100 mL). The purified polymer was then collected was then dried *in vacuo*.

Exemplar four monomer polymerization

Under anaerobic conditions, the selected epoxide, [$LZn_2(Ph)_2$] (0.01 g, 0.01 mmol), CHD (5.6 mg, 0.04 mmol), DL (0.42 mL, 2.4 mmol) and the selected anhydride were added to a Schlenk tube charged with a stirring bar (molar ratio: cat./CHD/anhydride/lactone/epoxide = 1/4/50/200/1000). Under N_2, the mixture allowed to react at 100 °C for a desired amount of time. CO_2 was then added via three vacuum/CO_2 gas feed cycles and left to react further. The reaction was monitored using *in situ* ATR-IR and by taking aliquots for ^{1}H NMR spectroscopy and SEC analysis (THF as eluent, 1 mL/min, 30 °C) at key intervals. The polymer was purified by precipitation of a DCM solution (<1 g/mL) into MeOH (50 mL).

Exemplar thiol-ene post-polymerization functionalization

Under anaerobic conditions, the pentablock copolymer (100 mg), the chosen thiol reagent and dimethoxy-2-phenylacetophenone (DMPA) was added to a vial (molar ratio: DMPA/[C=C]/thiol reagent = 1/2.5/10) with $CDCl_3$ (0.5 mL). The mixture was allowed to react at 25 °C under UV radiation for 2 h with stirring. Excess thiol was initially removed under vacuum. Residual thiol was removed by dissolving the functionalized polymer in DCM (<1 g/mL) and precipitating into diethyl ether (50 mL). The diethyl ether was decanted and the polymer was dried under vacuum before being analysed by NMR spectroscopy and SEC (THF as eluent, 1 mL/min, 30 °C).

Hydroboration-oxidation of polyesters

To a solution of the polyester (0.60 mmol) in THF (20 mL), was added a solution of 9-borabicyclo(3.3.1)nonane (9-BBN) dimer (2.41 g, 9.90 mmol) in THF (20.0 mL). After stirring the reaction mixture for 2 h at 25 ^{o}C, 0.1 mL of pure methanol was added to react with any 9-BBN left after hydroboration. The oxidation of the hydroborated polymer was carried out in the same Schlenk flask by adding meta-chloroperoxybenzoic acid (mCPBA) (11.62 g, 0.07 mol) at 0 °C under an inert atmosphere. The relative molar ratio of $[C=C]_0/[9\text{-BBN}]_0/[m\text{- CPBA}]_0$ was 1/1.5/5.1. After stirring the solution mixture at 25 °C for 2 h, a methanol/water (10:1 v/v, 10 mL) mixture was added dropwise. The volatiles were removed under reduced pressure to ~2 mL. The product was precipitated from a 1 M $NaHCO_3$ aqueous solution (500 mL), washed with water and dried *in vacuo* for 72 h.

NMR scale reaction between polyester and 9-BBN.

To a solution of the polyester (0.008 mmol) (in $CDCl_3$ (0.30 mL) in an NMR tube, equipped with a J. Young Teflon valve, was added a solution of 9-BBN dimer (0.02 g,

0.088 mmol) in $CDCl_3$ (0.30 mL) at 25 °C. The reaction was monitored for 2 h using ^1H NMR spectroscopy with mesitylene as an internal standard.

Exemplar terpolymerization of DL, LO and TCA

Under anaerobic conditions, LO (3.3 mL, 20.6 mmol), **1** (10.0 mg, 0.01 mmol), BDM (5.6 mg, 0.04 mmol) and DL were added to a vial charged with a stirring bar and allowed to react at 60 °C for a desired amount of time. After an aliquot was taken, the selected TCA was added and the mixture was allowed to react further at 140 °C until complete conversion of the anhydride (see table for molar ratios). Thereafter, the mixture was exposed to air to quench the polymerization. ^1H NMR spectroscopy and SEC analysis (THF as eluent, 1 mL/min, 30 °C) were performed at key intervals. The polymer was purified by precipitation of a DCM solution (<1 g/mL) into MeOH (50 mL) three times.

Sample	TCA used	[DL]	[TCA]	DL conv. (%)	TCA conv. (%)	ROP time (min)	ROCOP time (h)
1	TCA 2	1200	75	65	>99	8	32
2	TCA 2	1000	125	58	>99	6	48
3	TCA 2	1000	175	52	>99	6	67
4	TCA 2	800	225	58	>99	5	88
5	TCA 1	1000	175	50	>99	6	49
6	TCA 3	1000	175	50	>99	6	108
7	TCA 4	1000	175	50	>99	6	138

Molar ratio: [cat.]/[BDM]/[LO] = 1/4/2000 please see table for molar ratios for the individual samples

Degradation experiments

A modified literature procedure was followed.[4] **P16** (50 mg) was dissolved in THF (3 mL) before adding *p*TSA.H_2O (5 mg, 0.03 mmol) and heating with stirring to 60 °C in a vial. Progress was monitored by SEC analysis of aliquots taken at various time points.

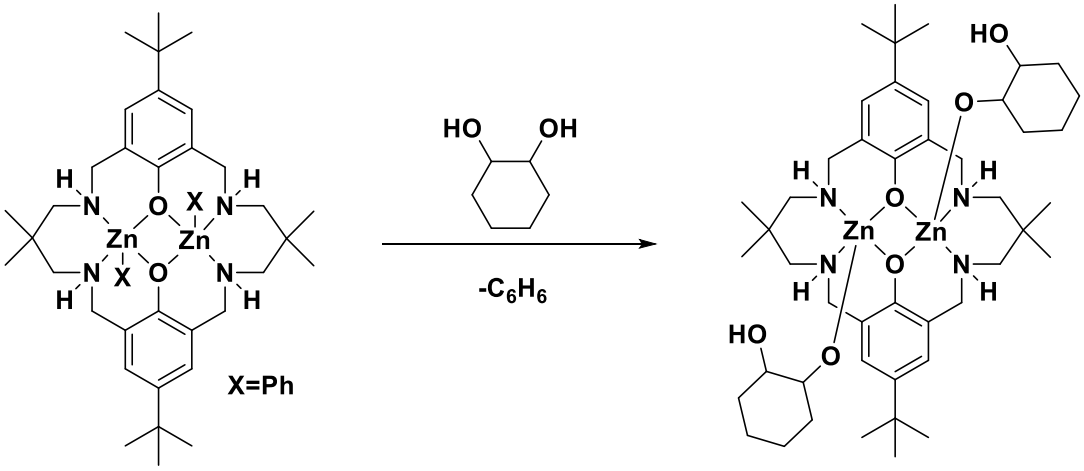
6.4. **References**

1. Kember, M. R.; Knight, P. D.; Reung, P. T. R.; Williams, C. K., Highly Active Dizinc Catalyst for the Copolymerization of Carbon Dioxide and Cyclohexene Oxide at One Atmosphere Pressure. *Angew. Chem. Int. Ed.* **2009,** *48*, 931-933.
2. Sanford, M. J.; Carrodeguas, L. P.; Van Zee, N. J.; Kleij, A. W.; Coates, G. W., Alternating Copolymerization of Propylene Oxide and Cyclohexene Oxide with Tricyclic Anhydrides: Access to Partially Renewable Aliphatic Polyesters with High Glass Transition Temperatures. *Macromolecules* **2016,** *49*, 6394-6400.
3. Spyros, A.; Argyropoulos, D. S.; Marchessault, R. H., A study of poly(hydroxyalkanoate)s by quantitative P-31 NMR spectroscopy: Molecular weight and chain cleavage. *Macromolecules* **1997,** *30*, 327-329.
4. Kobayashi, S.; Uyama, H.; Takamoto, T., Lipase-catalyzed degradation of polyesters in organic solvents, a new methodology of polymer recycling using enzyme as catalyst. *Biomacromolecules* **2000,** *1*, 3-5.

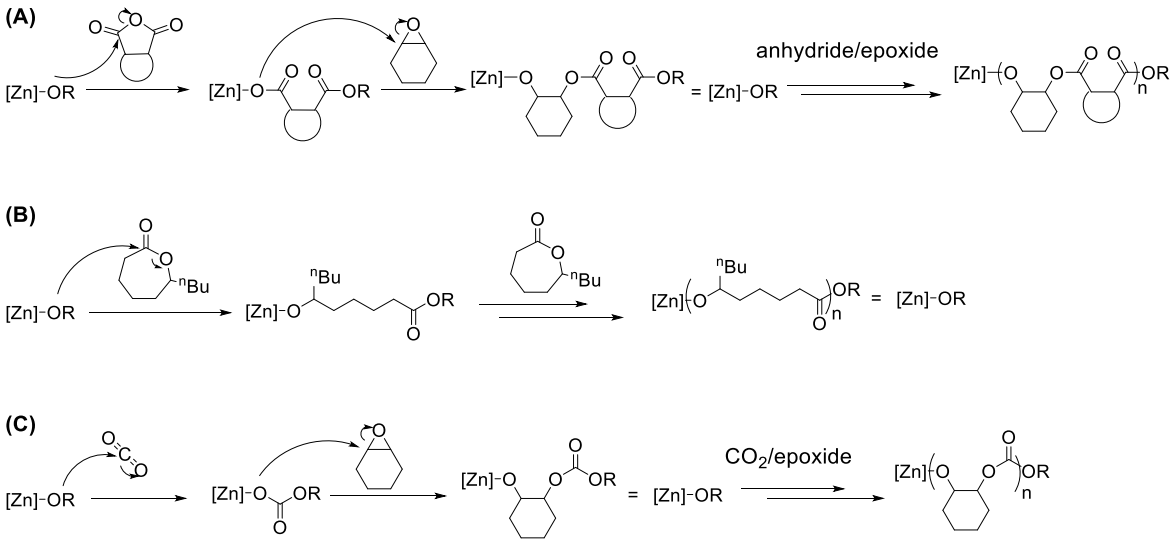
Chapter 7

Appendices

7.1. **Chapter 2**



Scheme S1. *In situ* activation of the catalyst from reaction between **1** and cyclohexandiol (CHD).



Scheme S2. Propagation mechanism for (A) ROCOP of anhydride/epoxide (B) ROP of lactone and (C) ROCOP of CO_2/epoxide.

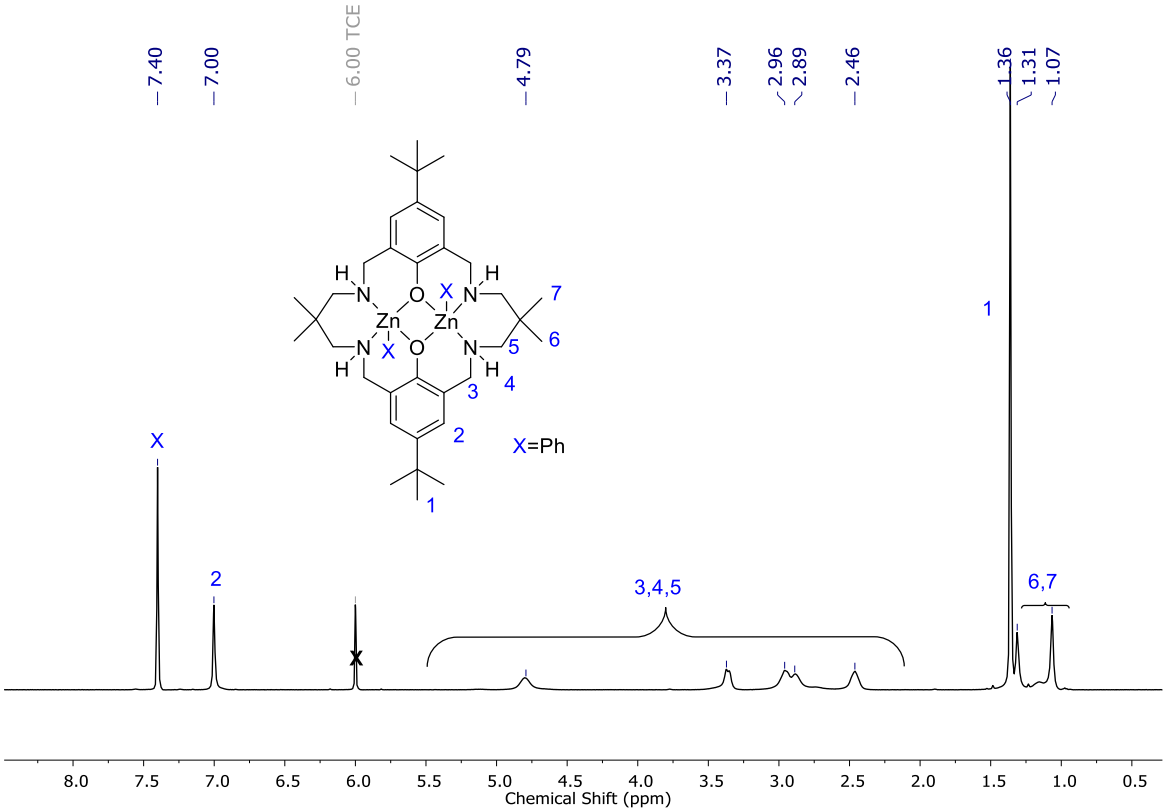


Figure S1. ^{1}H NMR spectrum of [LZn_2Ph_2], **1**, in TCE-d_2 at 403 K.

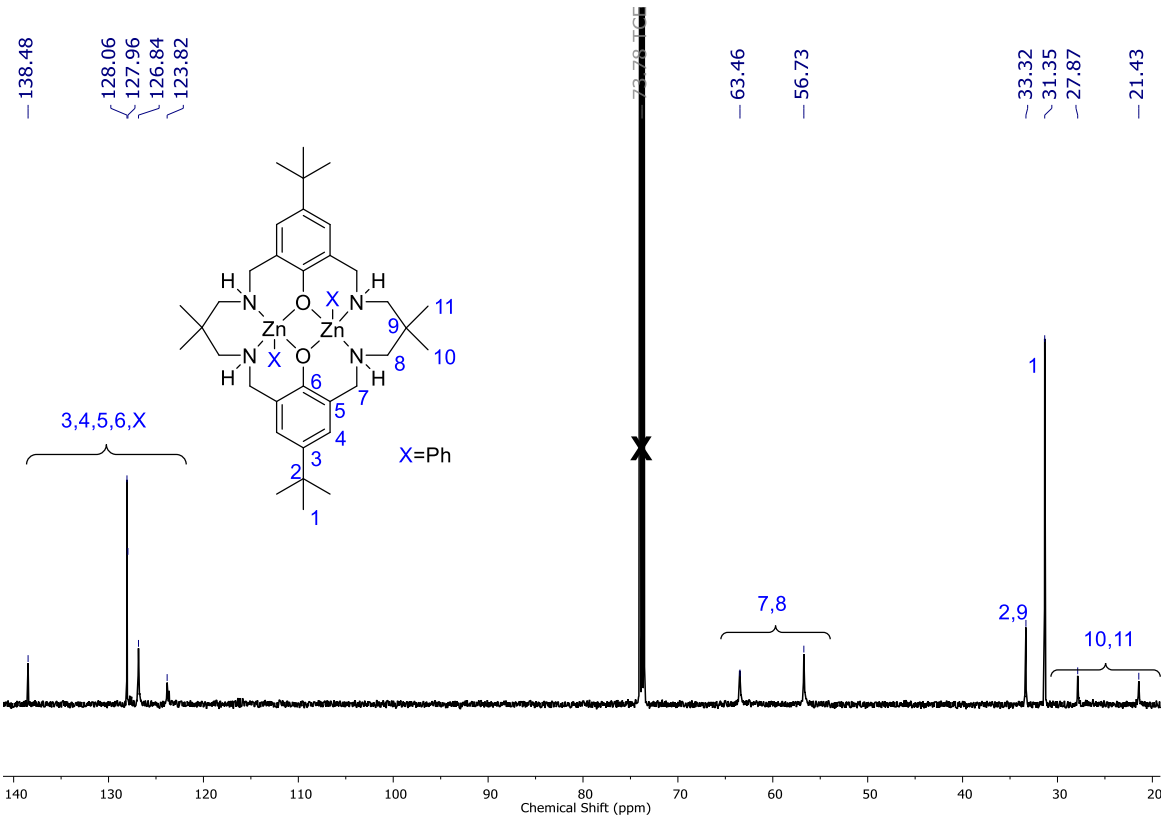


Figure S2. ^{13}C{^{1}H} NMR spectrum of [LZn_2Ph_2], **1**, in TCE-d_2 at 403 K.

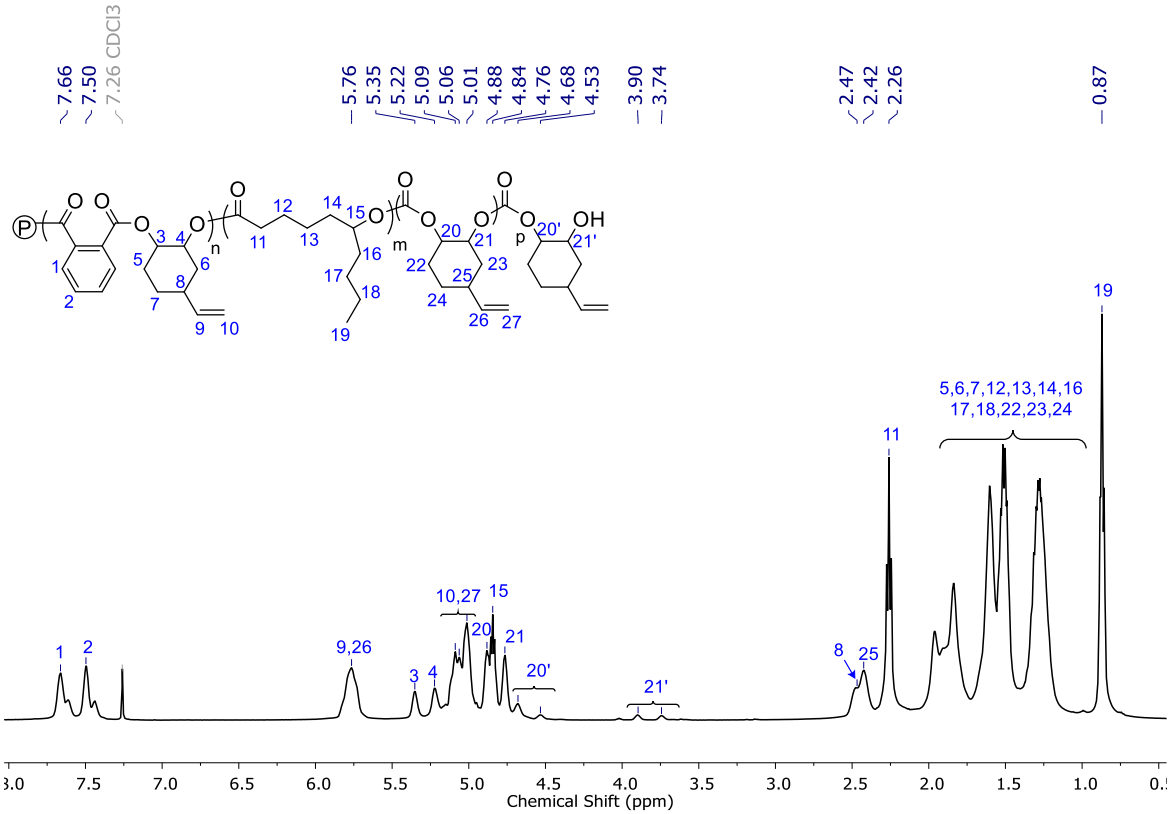


Figure S3. ^{1}H NMR spectrum of pentablock polymer from polymerization of PA/VCHO/DL/CO_2.

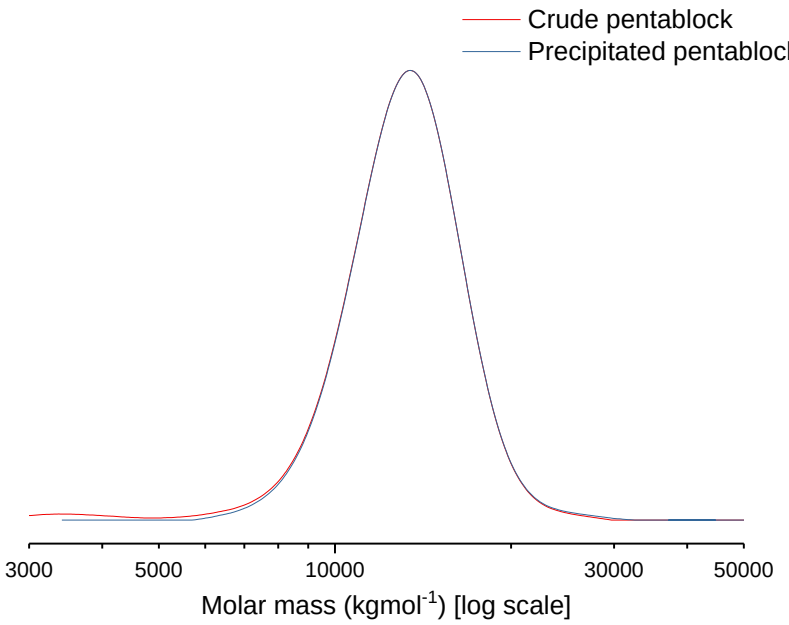


Figure S4. SEC of pentablock from polymerization of PA/VCHO/DL/CO_2 before and after precipitation (no changes in composition is detected)

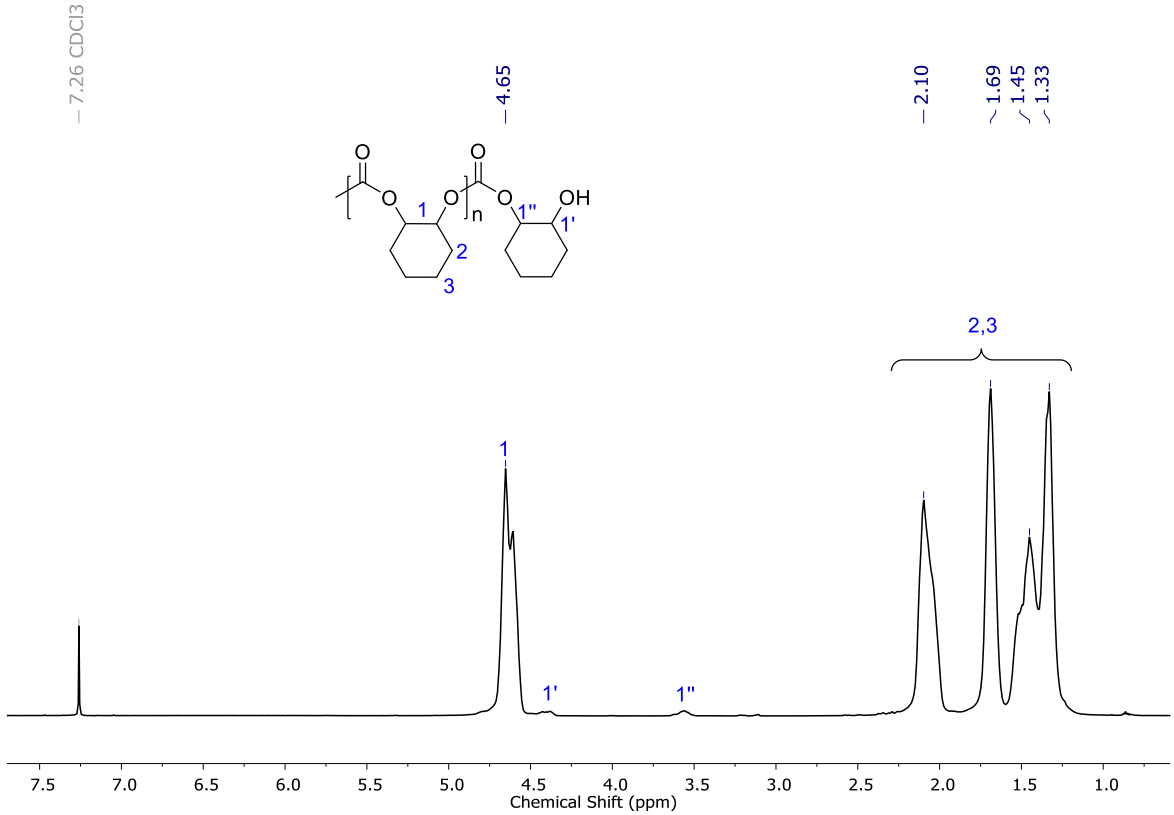


Figure S5. ^{1}H NMR spectrum of PCHC homopolymer polymer (in $CDCl_3$).

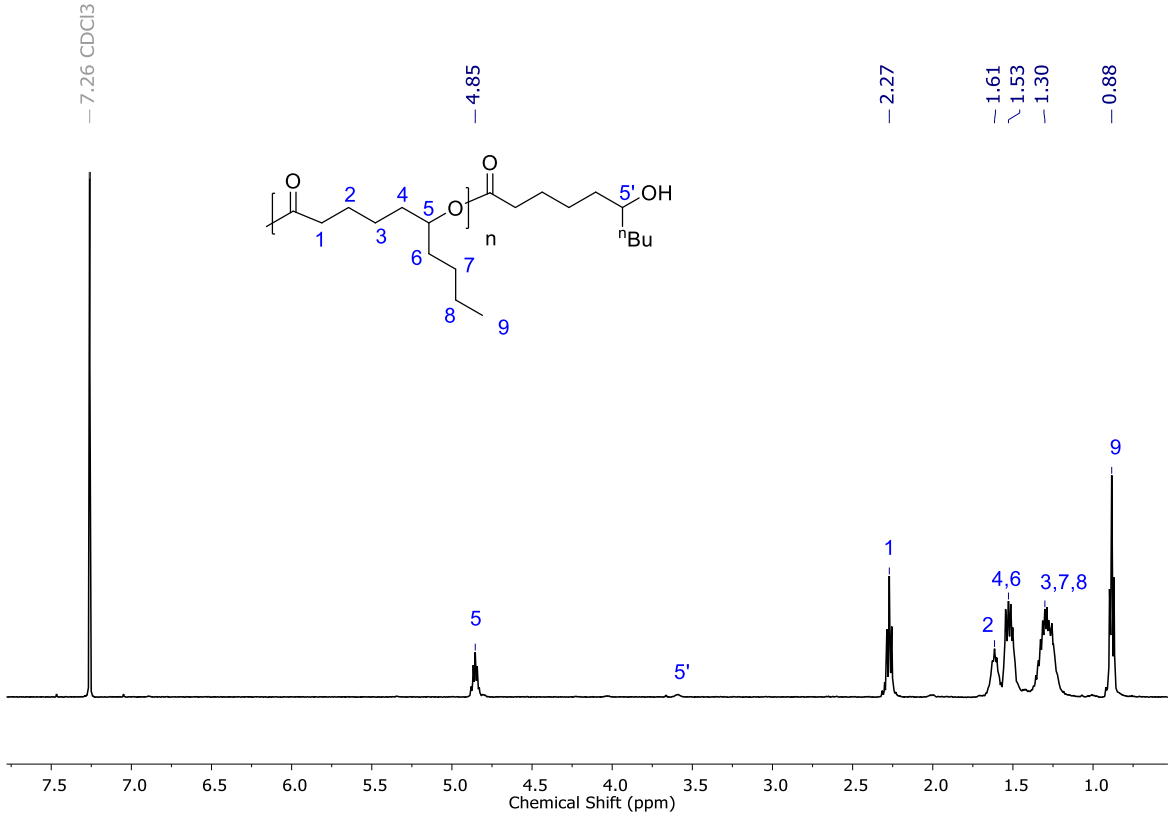


Figure S6. 1H NMR spectrum of PDL homopolymer polymer (in CDCl3).

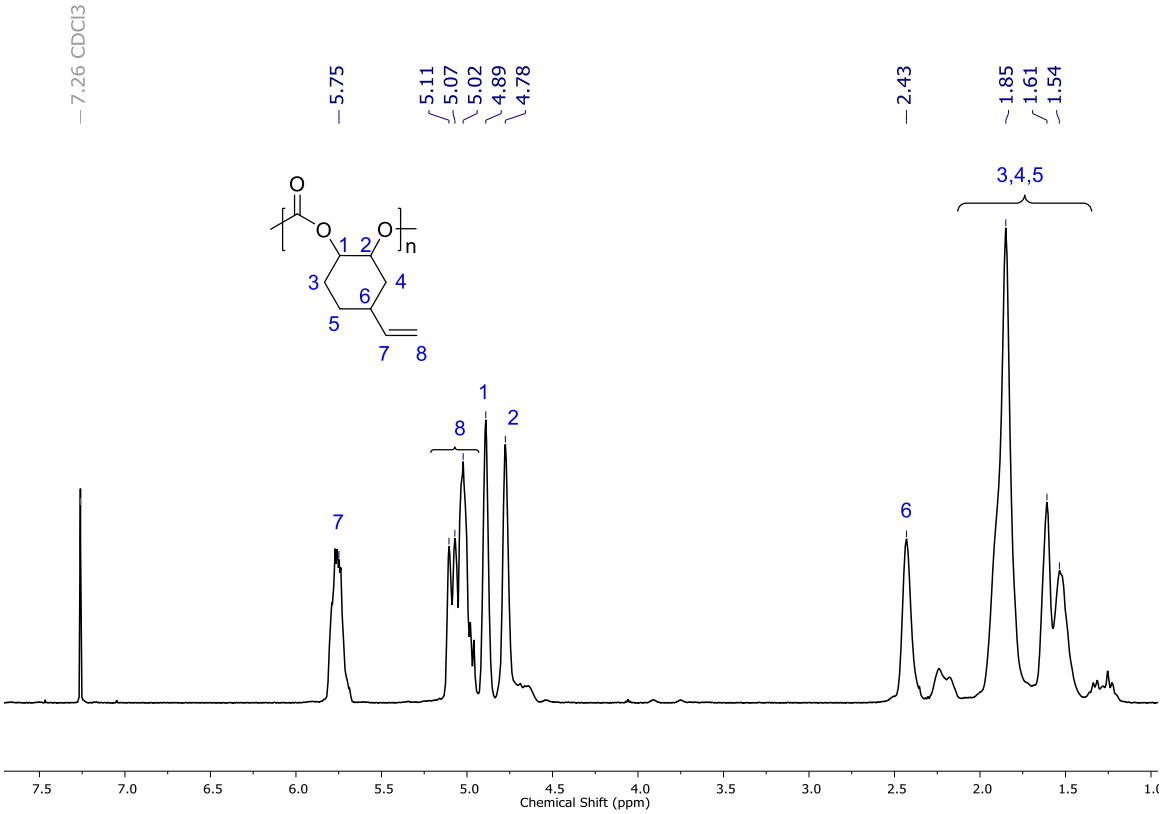


Figure S7. ^{1}H NMR spectrum of PVCHC homopolymer polymer (in $CDCl_3$).

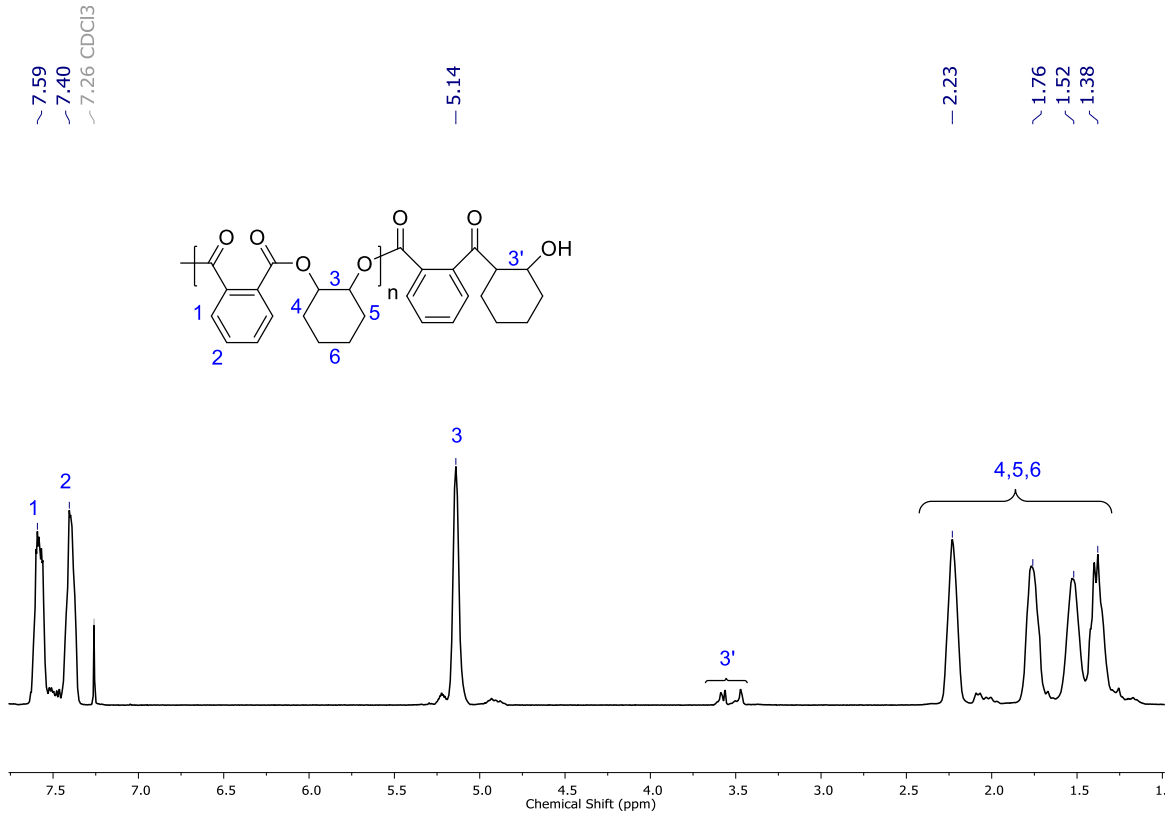


Figure S8. ^{1}H NMR spectrum of PCHPE homopolymer polymer (in $CDCl_3$).

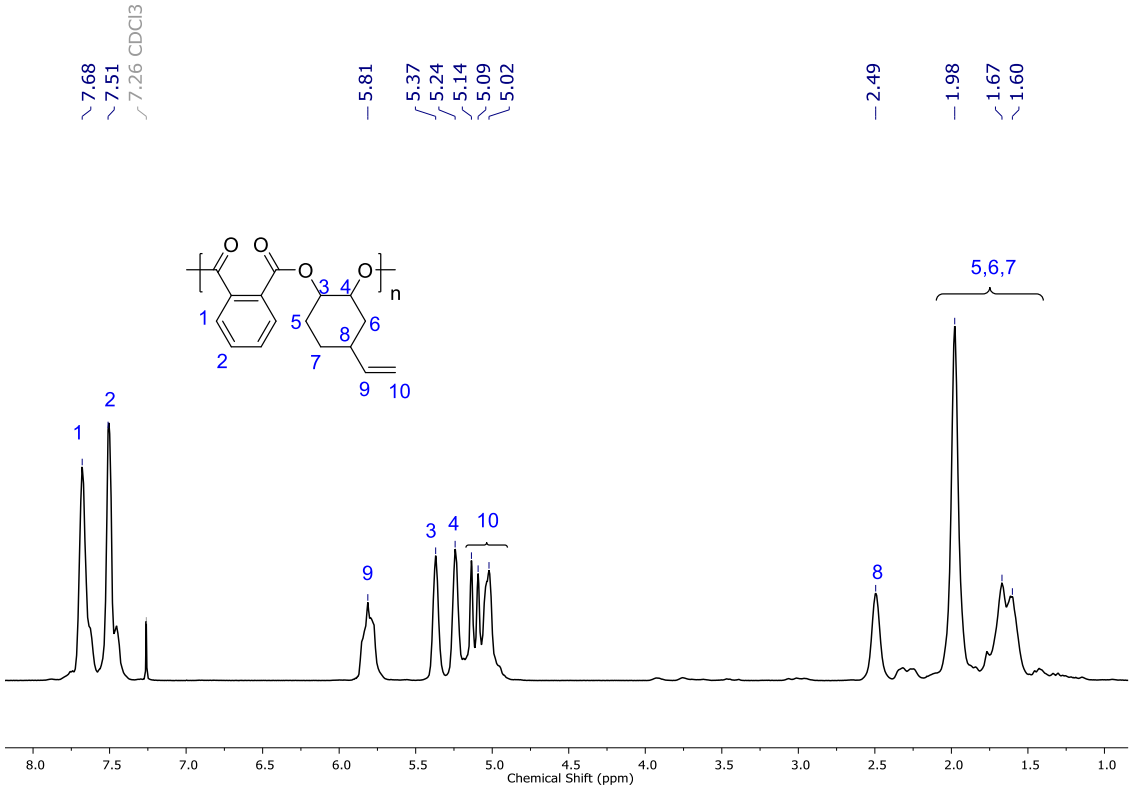


Figure S9. 1H NMR spectrum of PVCHPE homopolymer polymer (in CDCl3).

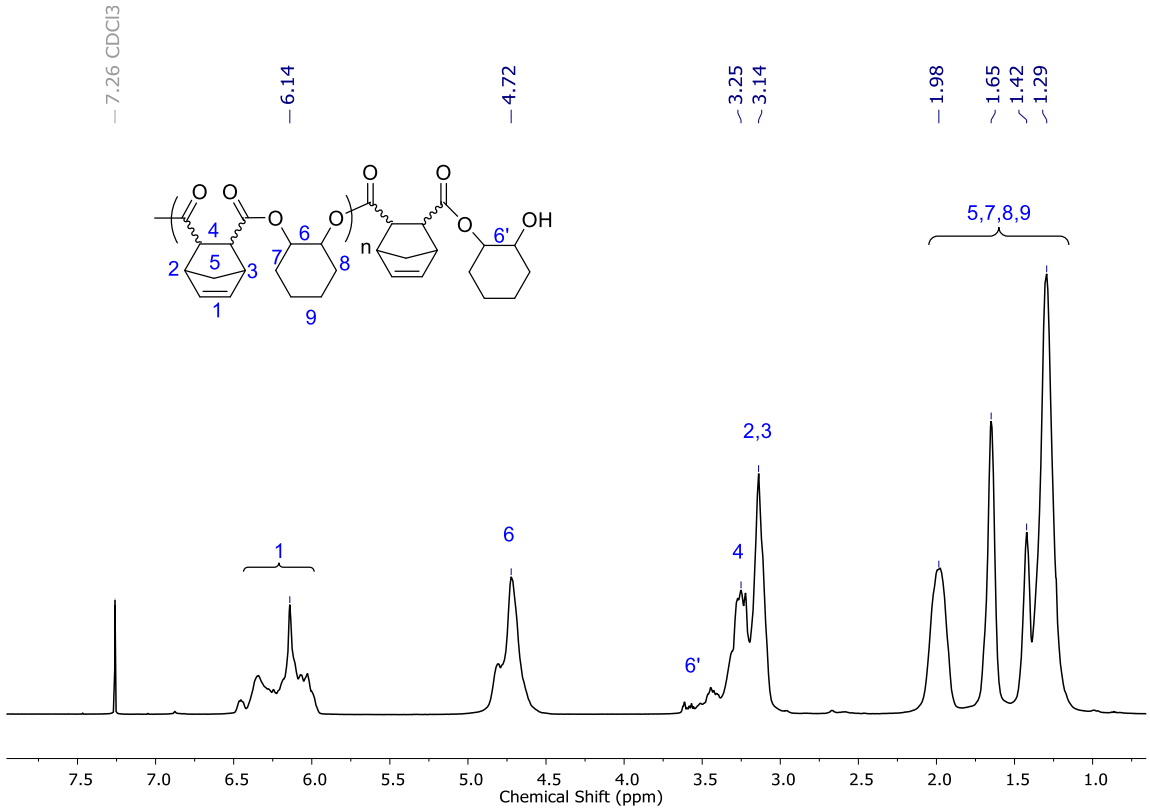


Figure S10. 1H NMR spectrum of PCHNE homopolymer polymer (in CDCl3).

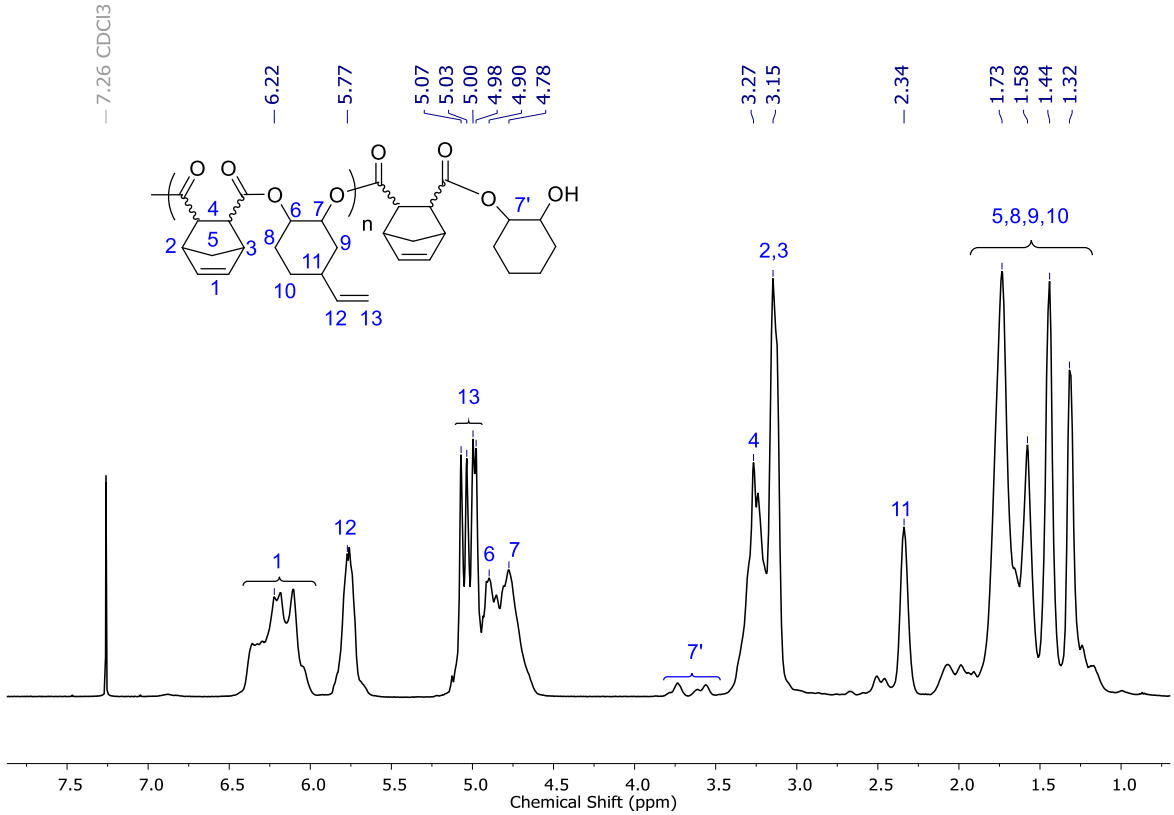


Figure S11. 1H NMR spectrum of PVCHNE homopolymer polymer (in CDCl3).

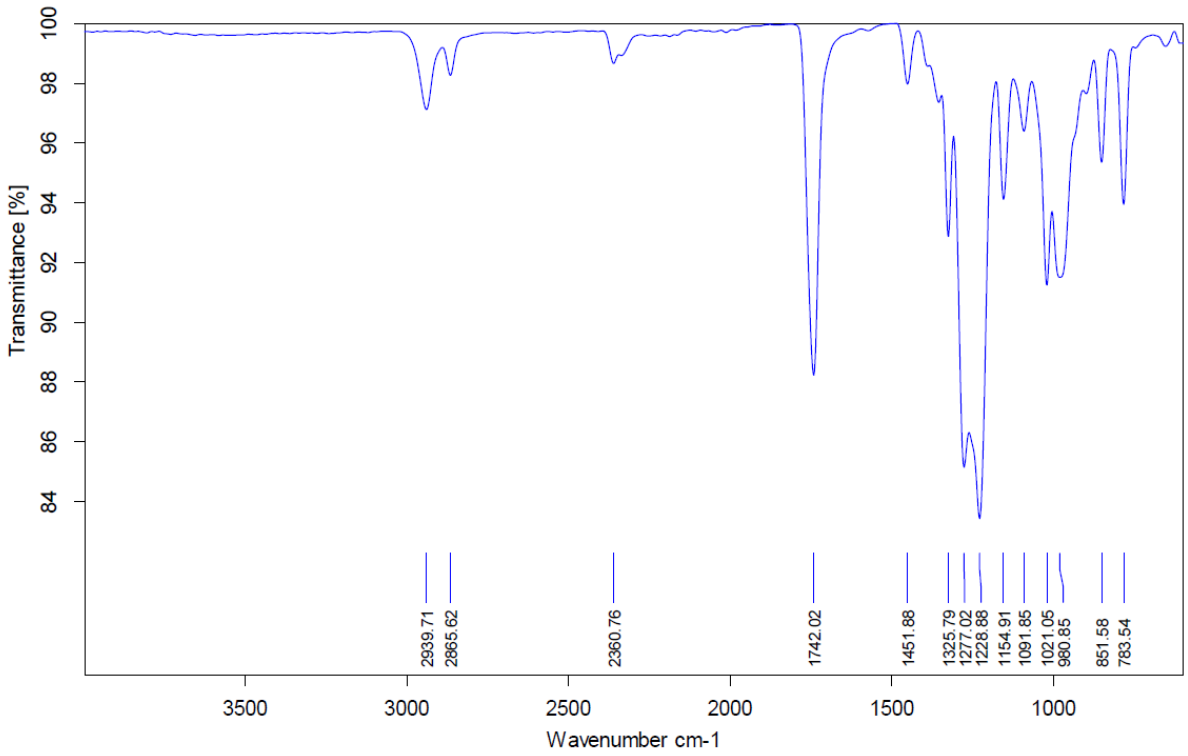


Figure S12. ATR-IR spectrum of PCHC homopolymer polymer

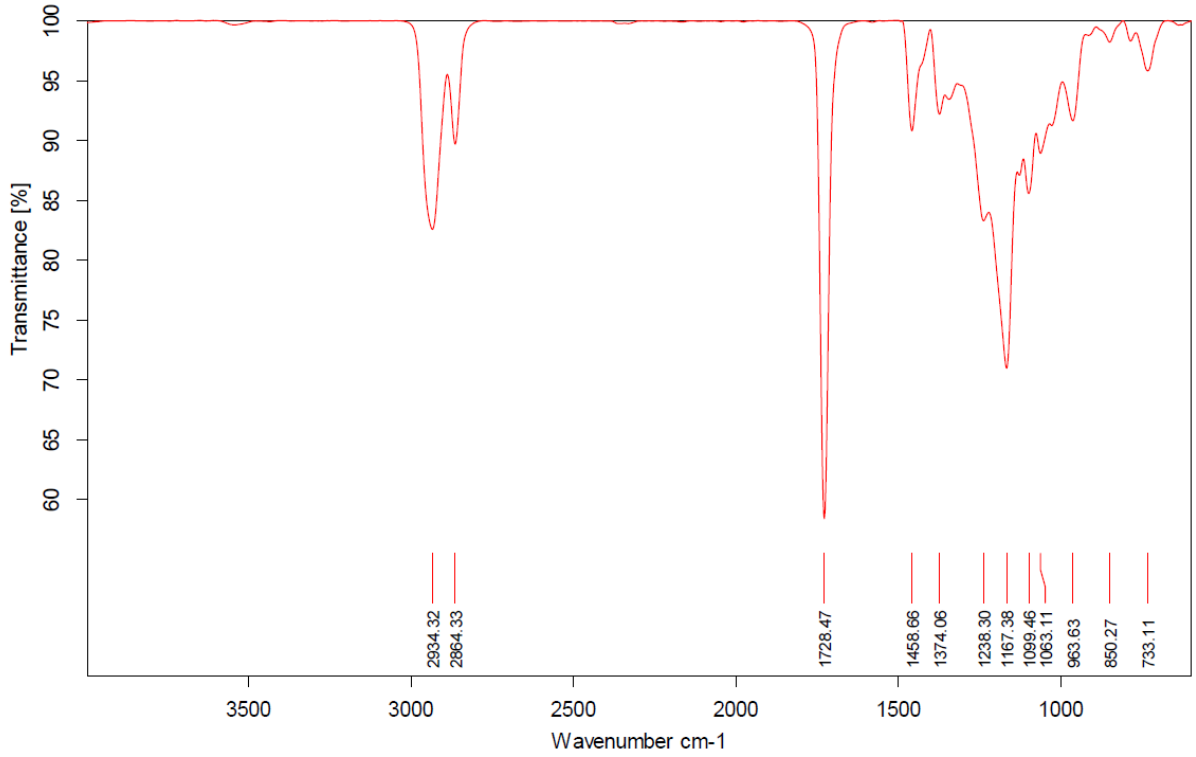


Figure S13. ATR-IR spectrum of PDL homopolymer polymer

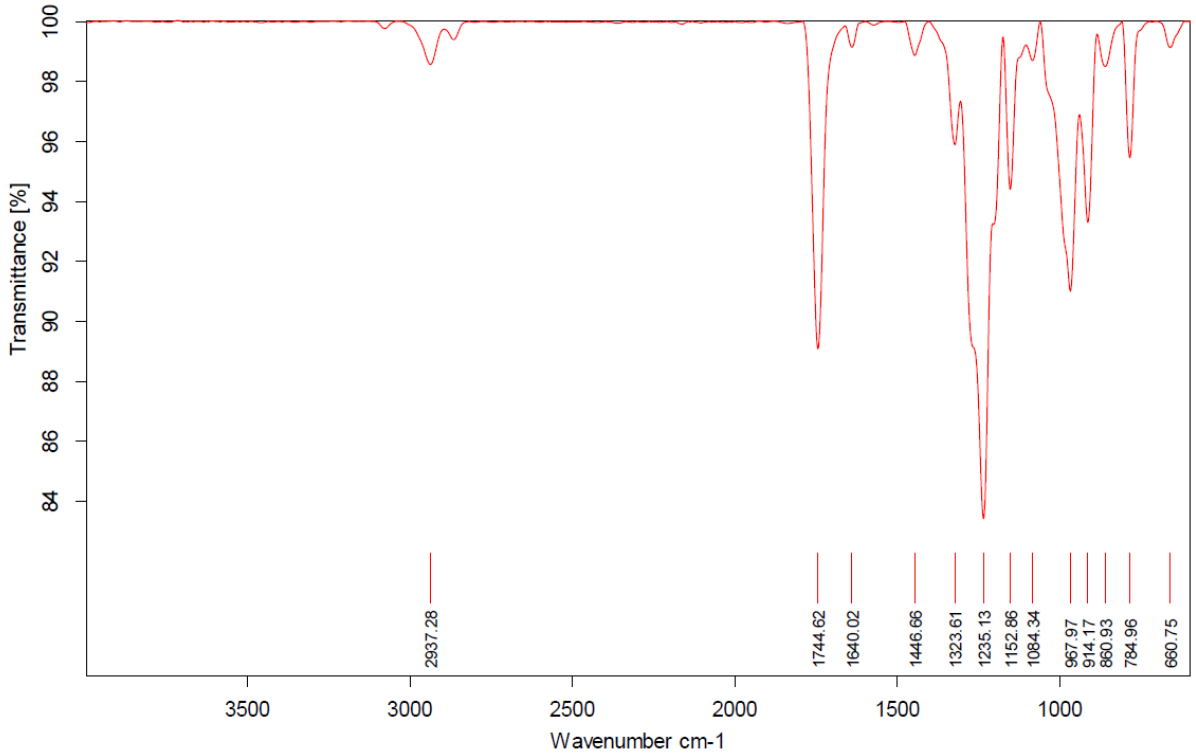


Figure S14. ATR-IR spectrum of PVCHC homopolymer polymer

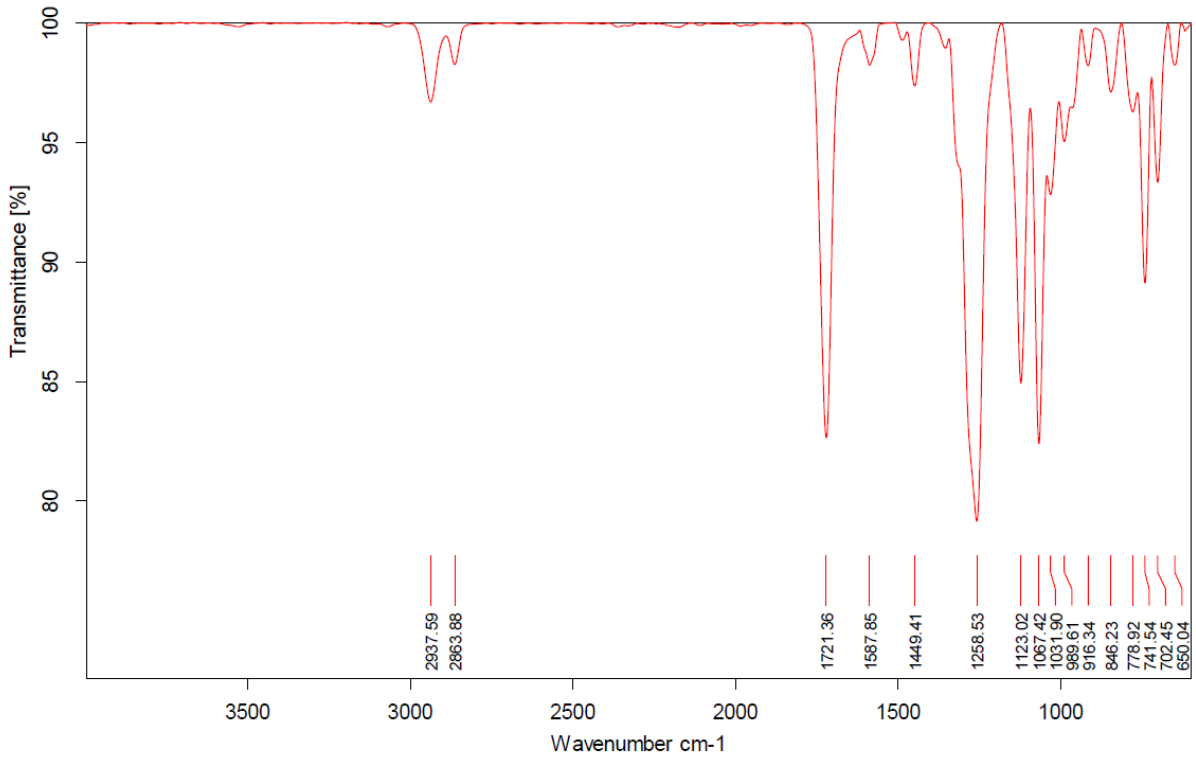


Figure S15. ATR-IR spectrum of PCHPE homopolymer polymer.

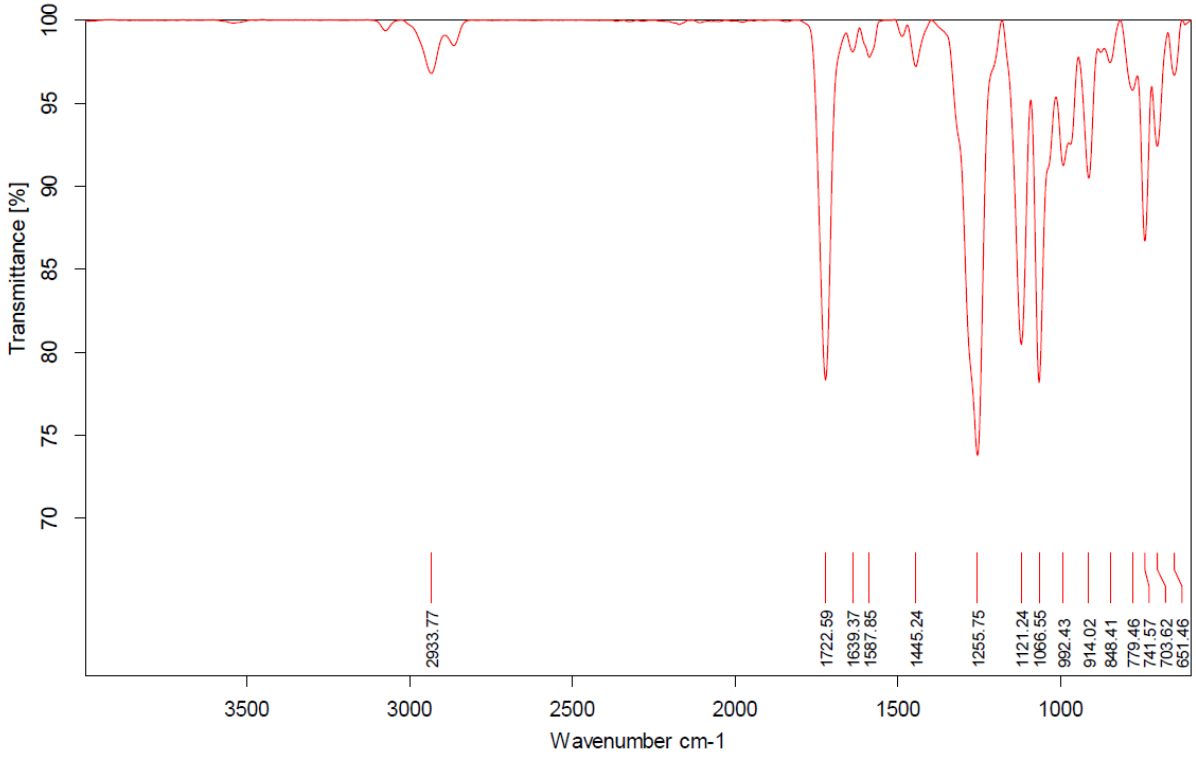


Figure S16. ATR-IR spectrum of PVCHPE homopolymer polymer.

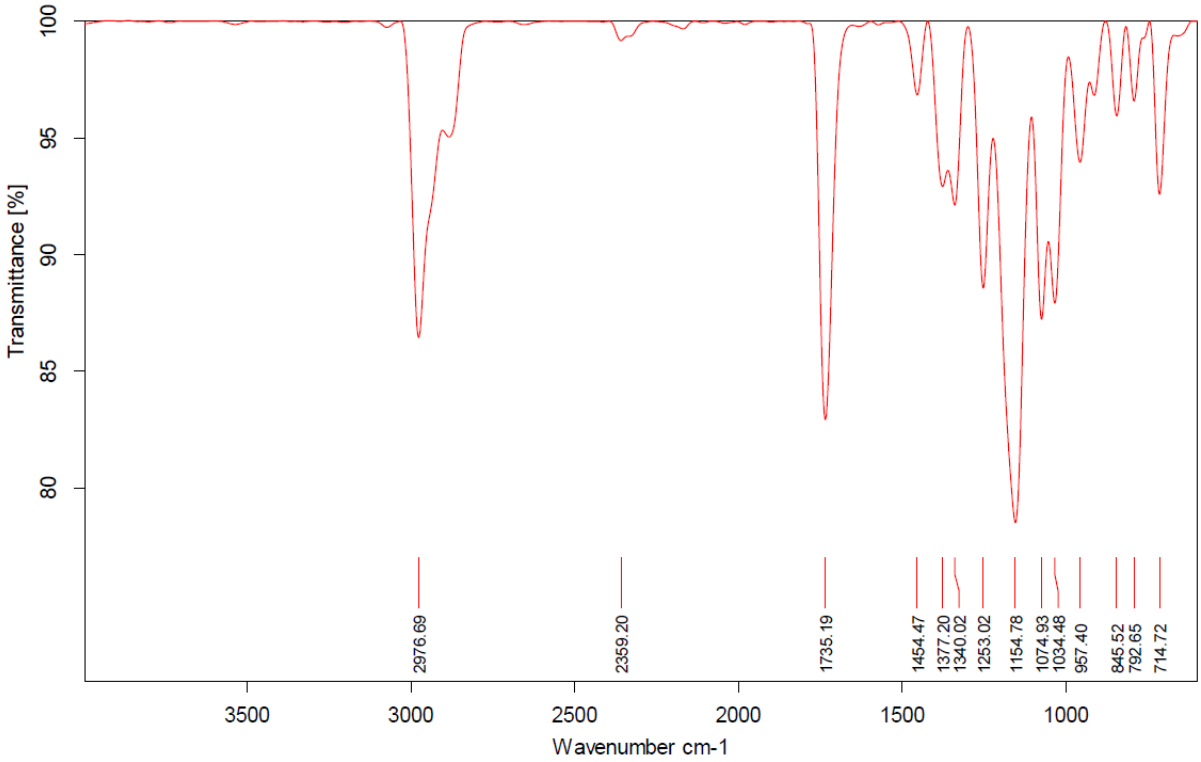


Figure S17. ATR-IR spectrum of PCHNE homopolymer polymer.

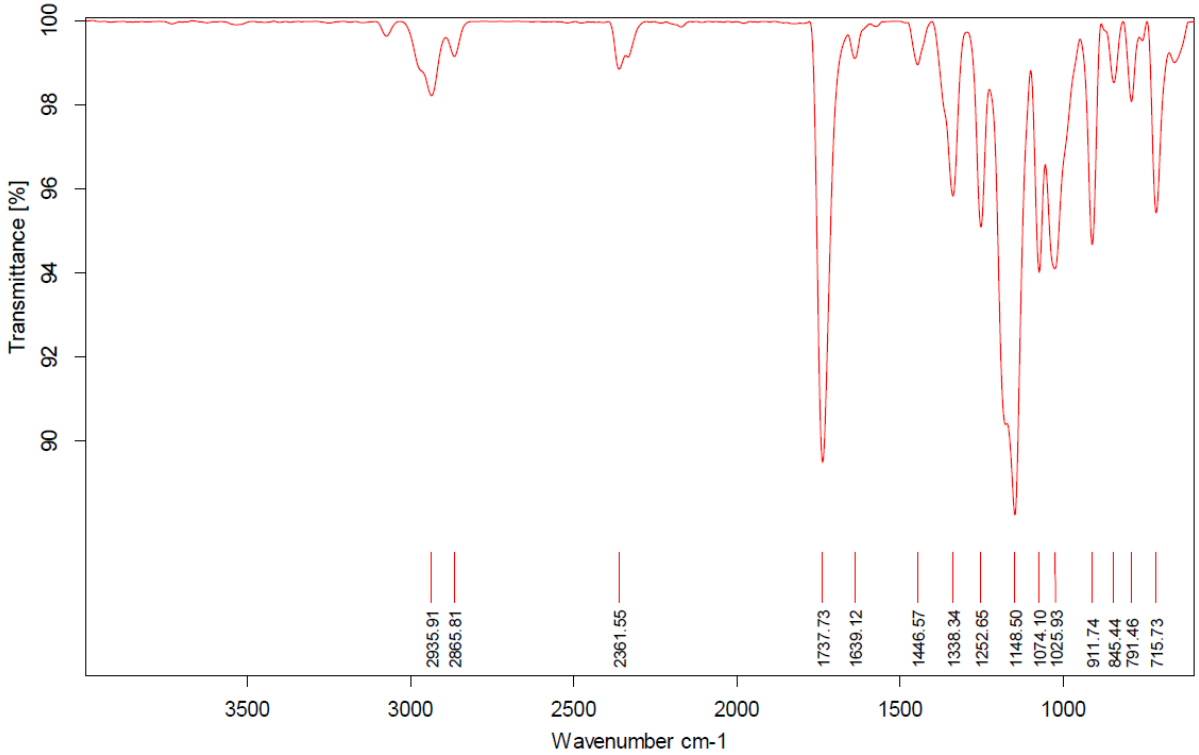


Figure S18. ATR-IR spectrum of PVCHNE homopolymer polymer.

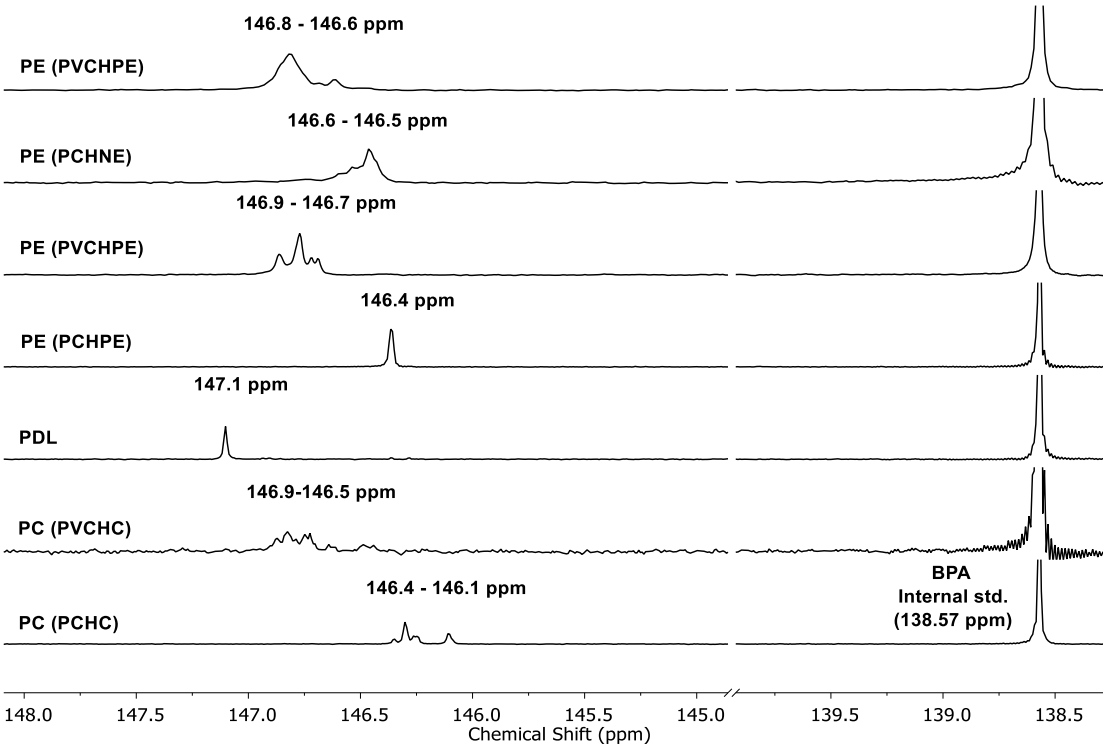


Figure S19. Selected region of $^{31}P\{^{1}H\}$ NMR spectra of hydroxyl polymer end group analysis on various homopolymers. Bisphenol A (BPA) is added as an internal standard (in $CDCl_3$).

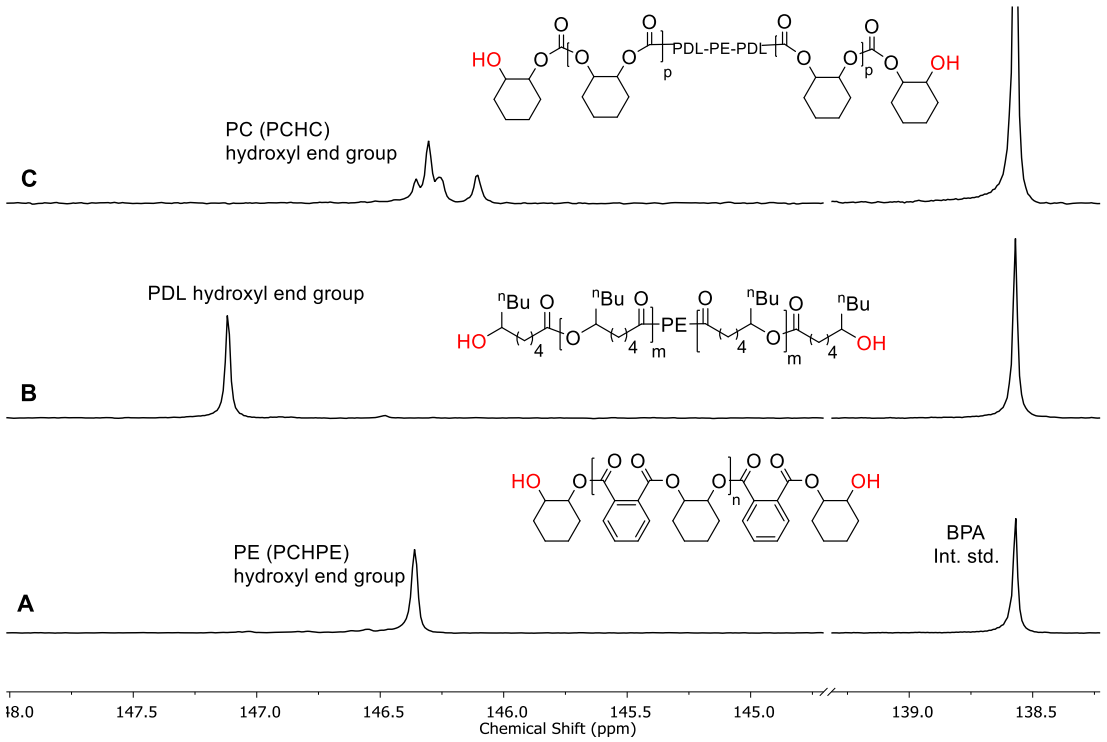


Figure S20. $^{31}P\{^{1}H\}$ NMR spectra of end analysis on the polymerization of PA/CHO/DL/CO_2. PE (PCHPE), PDL and PC (PCHC) end groups can be observed at 146.4, 147.1 and 146.4-146.1 ppm respectively. Bisphenol A (BPA) is added as an internal standard (in $CDCl_3$).

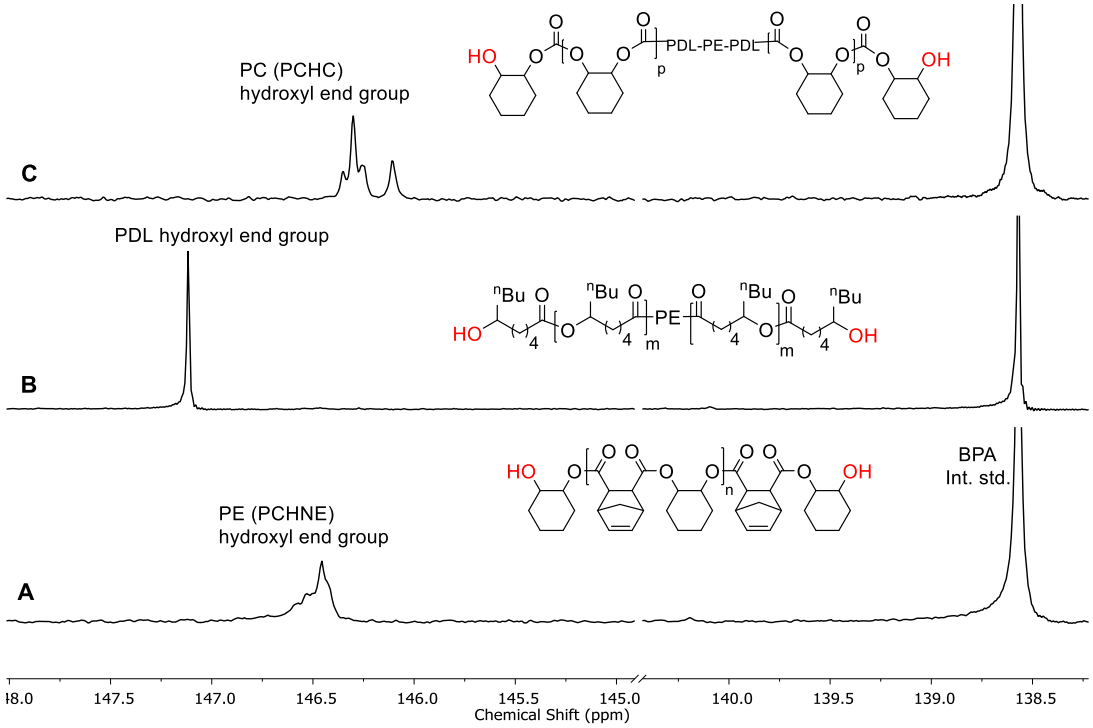


Figure S21. $^{31}P\{^{1}H\}$ NMR spectra of end group analysis on the polymerization of NA/CHO/DL/CO_2. PE (PCHNE), PDL and PC (PCHC) end groups can be observed at 146.6-146.5, 147.1 and 146.4-146.1 ppm respectively. BPAis added as an internal standard (in $CDCl_3$).

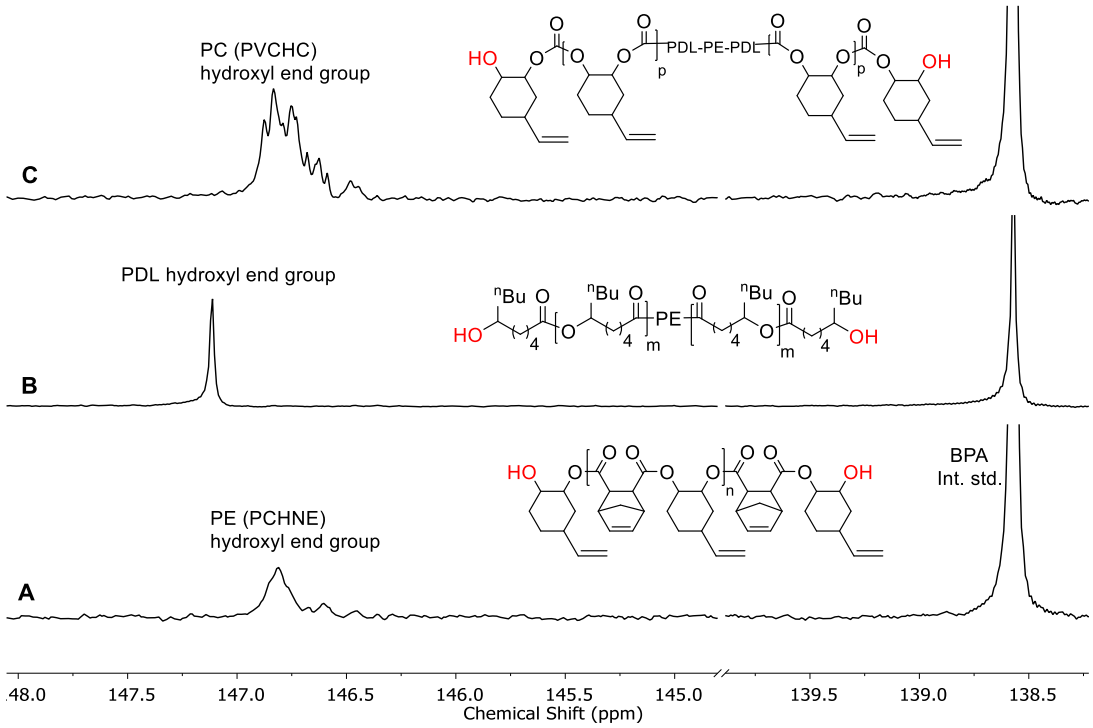


Figure S22. $^{31}P\{^{1}H\}$ NMR spectra of end group analysis on the polymerization of NA/VCHO/DL/CO_2. PE (PVCHNE), PDL and PC (PVCHC) end groups can be observed at 146.8-146.6, 147.1 and 146.9-146.5 ppm respectively. BPA is added as an internal standard (in $CDCl_3$).

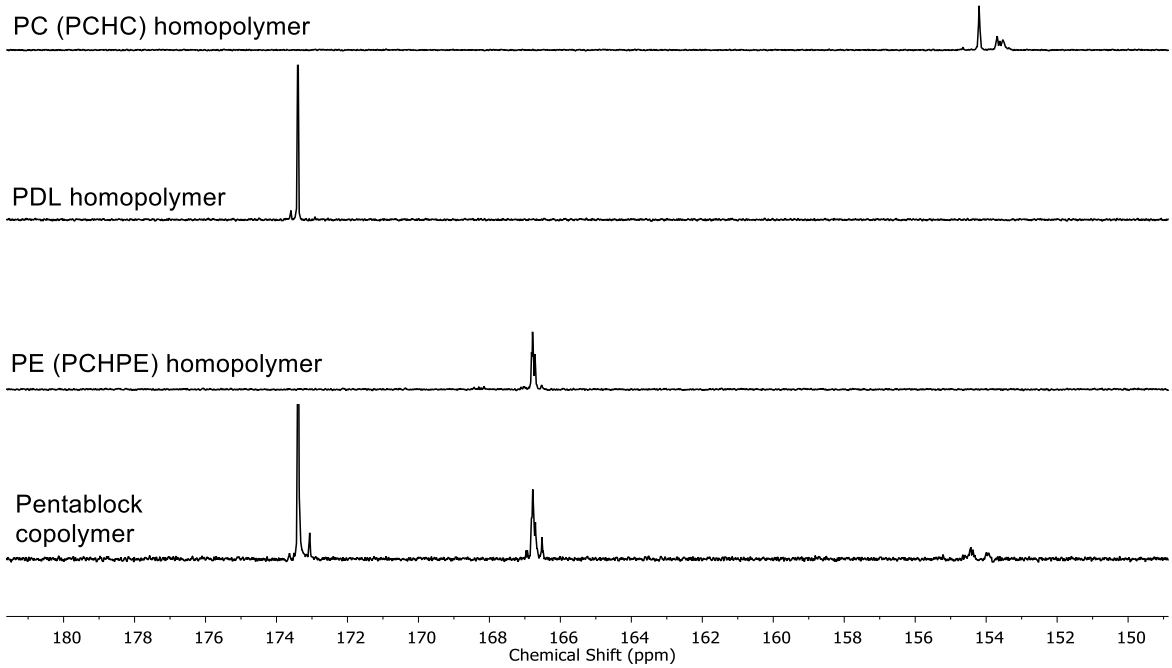


Figure S23. Carbonyl region of $^{13}C\{^{1}H\}$ NMR spectra of pentablock copolymer from the polymerization of PA/CHO/DL/CO_2 and PE(PCHPE), PDL and PC (PVCHC) homopolymers. Carbonyl resonances for PCHPE (PE), PDL and PCHC (PC) blocks at 166.8-166.5 ppm, 173.4 ppm and 154.4-153.9 ppm respectively (in $CDCl_3$).

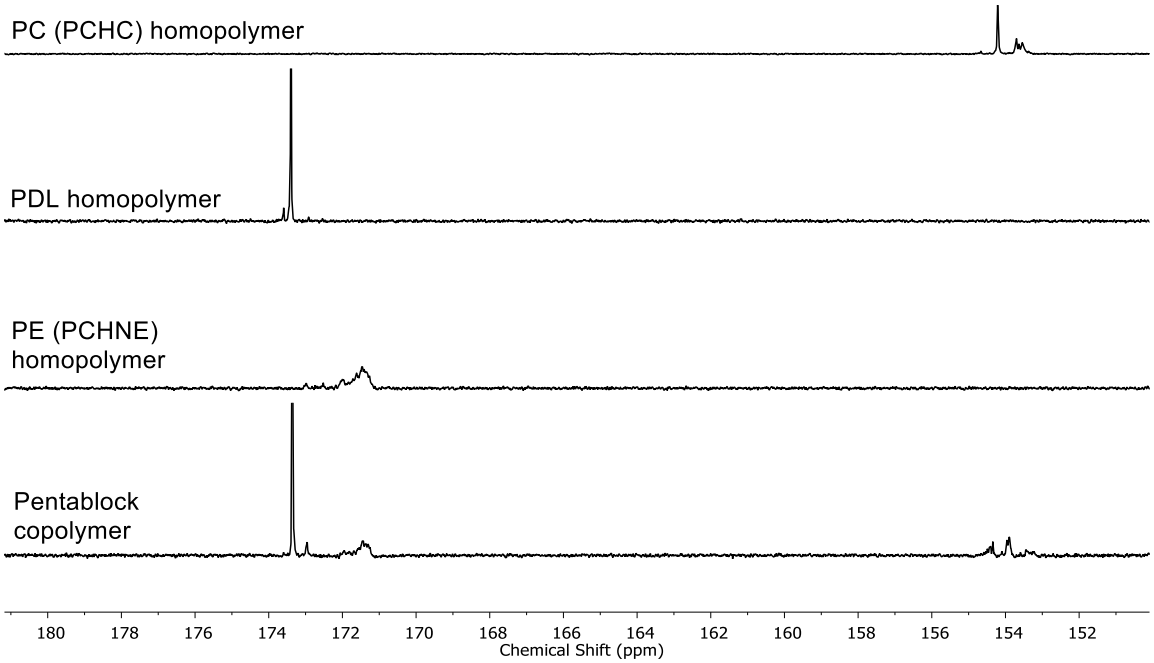


Figure S24. Carbonyl region of $^{13}C\{^{1}H\}$ NMR spectra of pentablock copolymer from the polymerization of NA/CHO/DL/CO_2 and PE(PCHNE), PDL and PC (PCHC) homopolymers. Carbonyl resonances for PCHPE (PE), PDL and PVCHC (PC) blocks at 172.0-171.2 ppm, 173.4 ppm and 154.4-153.9 ppm respectively (in $CDCl_3$).

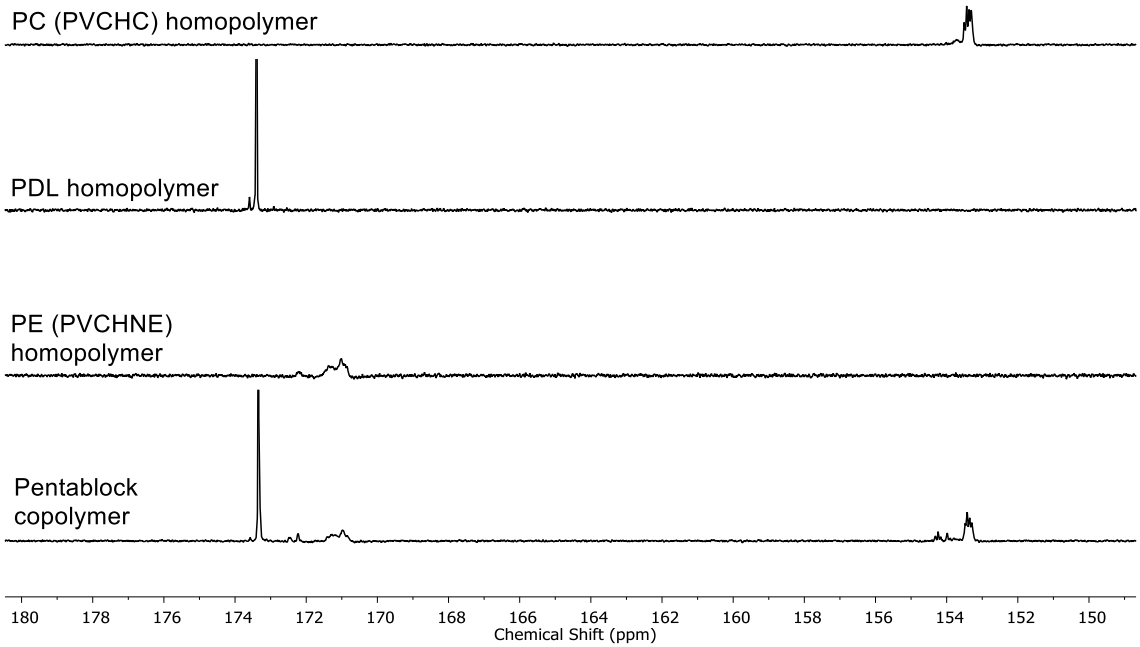


Figure S25. Carbonyl region of $^{13}C\{^{1}H\}$ NMR spectra of pentablock copolymer from the polymerization of NA/VCHO/DL/CO_2 and PE(PVCHNE), PDL and PC (VPCHC) homopolymers. Carbonyl resonances for PVCHPE (PE), PDL and PVCHC (PC) blocks at 171.4-170.8 ppm, 173.4 ppm and 154.4-153.2 ppm respectively (in $CDCl_3$).

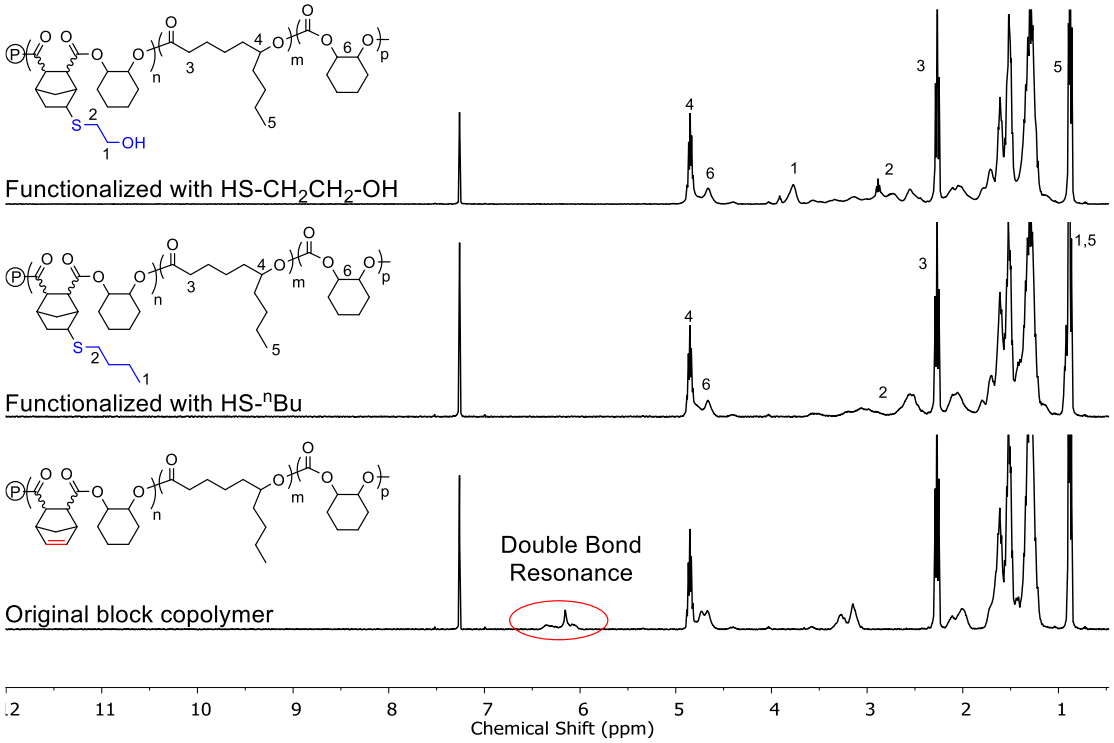


Figure S26. ^{1}H NMR spectra showing the changes in NMR resonances on the PCHC-*b*-PDL-*b*-PCHNE-*b*-PDL-*b*-PCHC pentablock copolymer before and after *thiol*-ene post-polymerization functionalization (in $CDCl_3$).

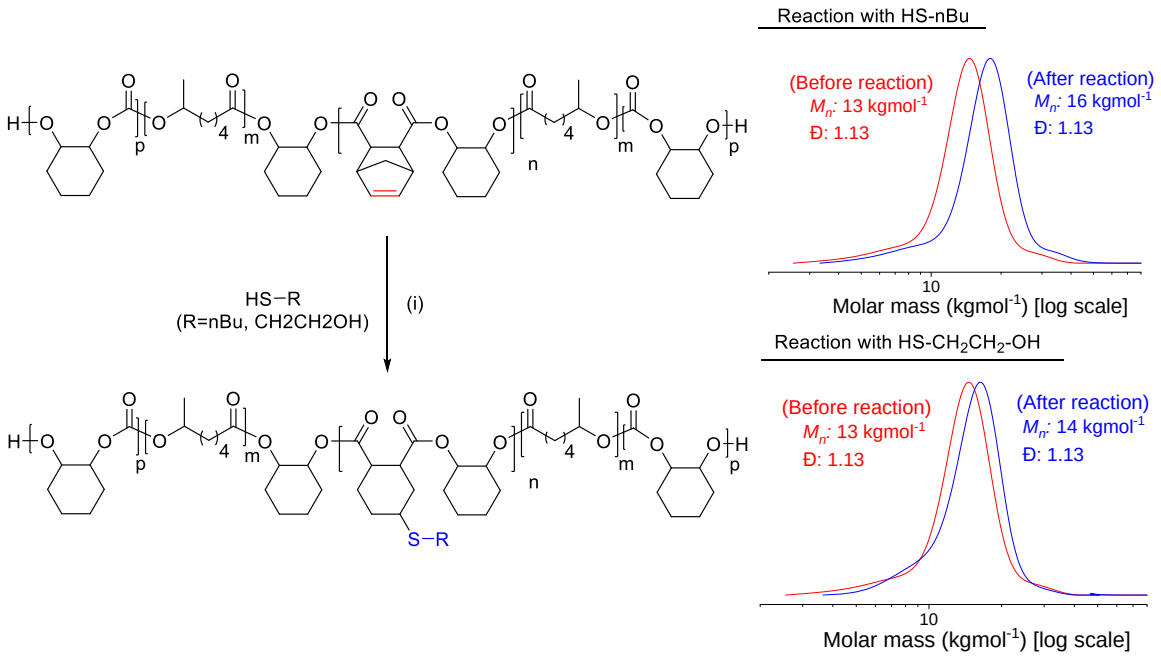


Figure S27. SEC of Thiol-ene post-polymerization functionalization of PCHC-*b*-PDL-*b*-PCHNE-*b*-PDL-*b*-PCHC pentablock polymer (THF as eluent, calibrated using PS standards).

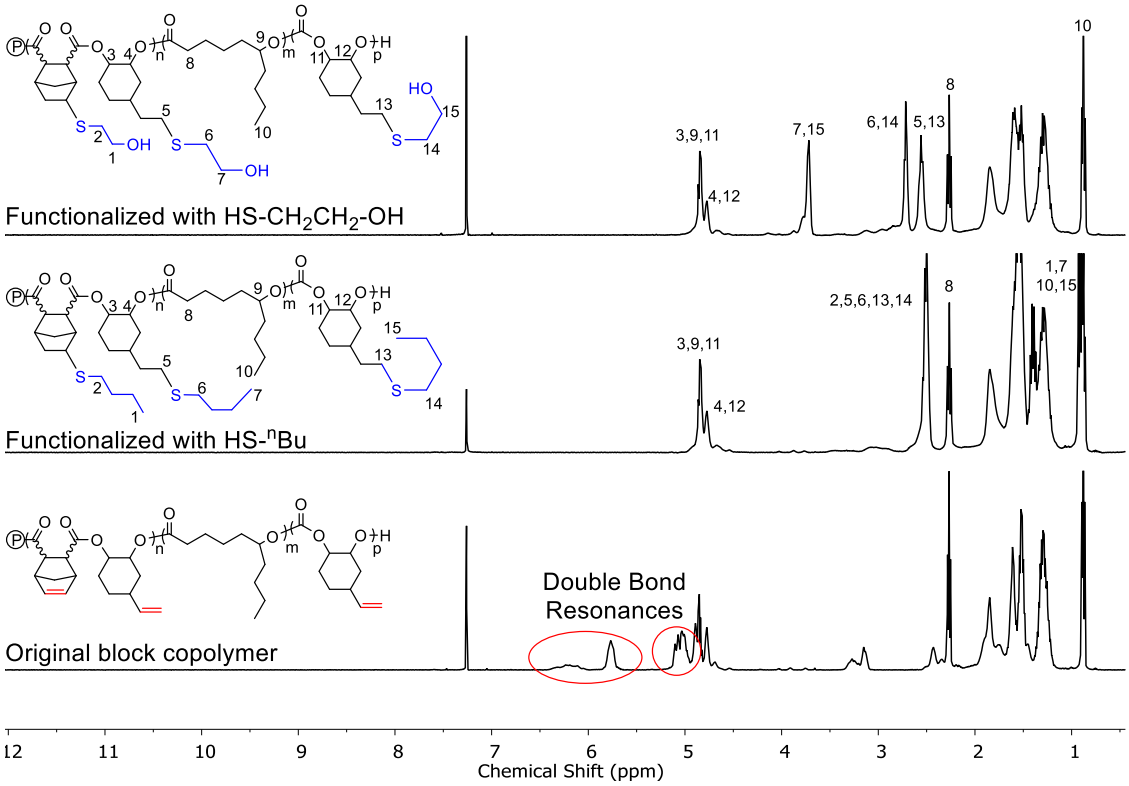


Figure S28. ^{1}H NMR spectra showing the changes in NMR resonances on the PVCHC-*b*-PDL-*b*-PVCHNE-*b*-PDL-*b*-PVCHC pentablock copolymer before and after *thiol*-ene post-polymerization functionalization (in $CDCl_3$).

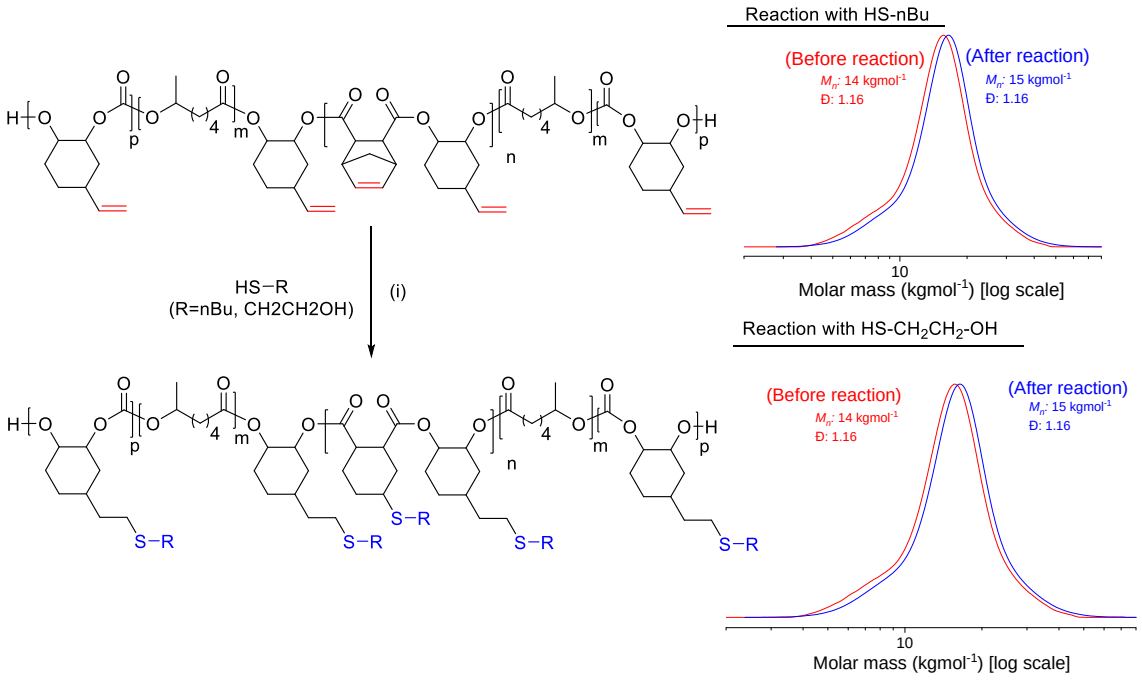


Figure S29. SEC of Thiol-ene post-polymerization functionalization of PVCHC-*b*-PDL-*b*-PVCHNE-*b*-PDL-*b*-PVCHC pentablock polymer (THF as eluent, calibrated using PS standards).

Table S1. Post-polymerization functionalization of pentablock copolymers with unsaturated moieties

Monomer Combination	Functionalization thiol-reagent used	M_n/kgmol^{-1} ($Đ$)[a]
PA/VCHO/DL/CO_2	Original block copolymer	10 (1.07)
	HS-^{n}Bu	12 (1.06)
	HS-CH_2CH_2OH	11 (1.06)
NA/CHO/DL/CO_2	Original block copolymer	13 (1.13)
	HS-^{n}Bu	16 (1.13)
	HS-CH_2CH_2OH	14 (1.13)
NA/VCHO/DL/CO_2	Original block copolymer	14 (1.16)
	HS-^{n}Bu	15 (1.16)
	HS-CH_2CH_2OH	15 (1.16)

[a]M_n and Đ measured by SEC (calibrated using polystyrene standards).

Table S2. T_g of various block copolymers

Block copolymer	wt% PE[c]	wt% PDL[c]	wt% PC[c]	T_g/°C[d]
PCHC-b-PDL-b-PCHNE-b-PDL-b-PCHC	18	67	15	-35
PCHC-b-PDL-b-PCHPE-b-PDL-*b*-PCHC	23	64	13	-28
PCHC-b-PDL-b-PCHNE-b-PDL-*b*-PCHC	19	53	28	-24
PVCHC-b-PDL-b-PVCHNE-b-PDL-b-PVCHC	12	49	39	-21
PVCHC-b-PDL-b-PVCHNE-b-PDL-b-PVCHC[a]	14	45	41	-18
PCHC-b-PDL-b-PCHNE-b-PDL-b-PCHC[a]	18	67	15	-17
PVCHC-b-PDL-b-PVCHNE-b-PDL-b-PVCHC	14	45	41	-15
PVCHC-b-PDL-b-PVCHPE-b-PDL-b-PVCHC[a]	23	51	26	-15
PVCHC-b-PDL-b-PVCHPE-b-PDL-b-PVCHC	20	49	31	-10
PVCHC-b-PDL-b-PVCHPE-b-PDL-b-PVCHC	23	51	26	-8
PVCHC-b-PDL-b-PVCHPE-b-PDL-b-PVCHC[b]	23	51	26	13
PCHC-b-PDL-b-PCHNE-b-PDL-b-PCHC[b]	18	67	15	15
PVCHC-b-PDL-b-PVCHNE-b-PDL-b-PVCHC[b]	14	45	41	20

[a]Block polymer functionalized with 1-butanethiol. [b]Block copolymer functionalized with 2-mercapoethanol. [c]wt% obtained from ^{1}H NMR spectra. [d]T_g obtained from DSC (second heating cycle)

7.2. **Chapter 3**

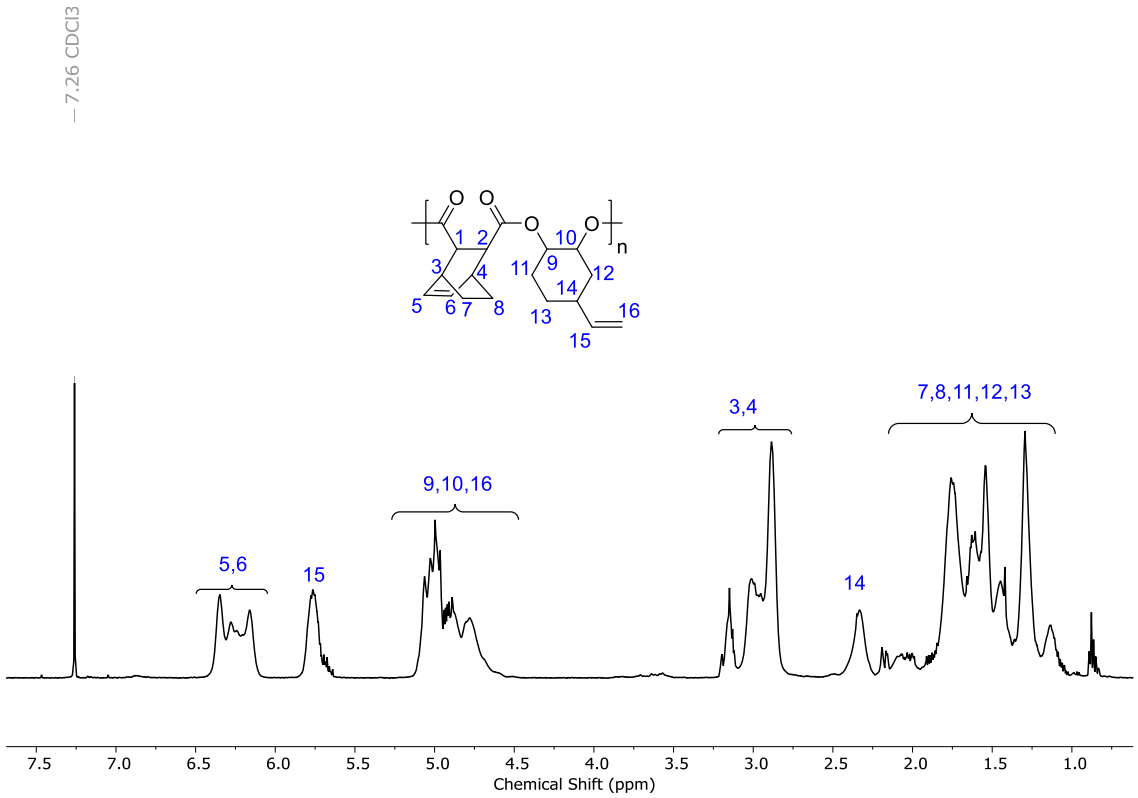


Figure S30. ^{1}H NMR spectrum of polymer **P6** ($CDCl_3$, 500.0 MHz, 298 K).

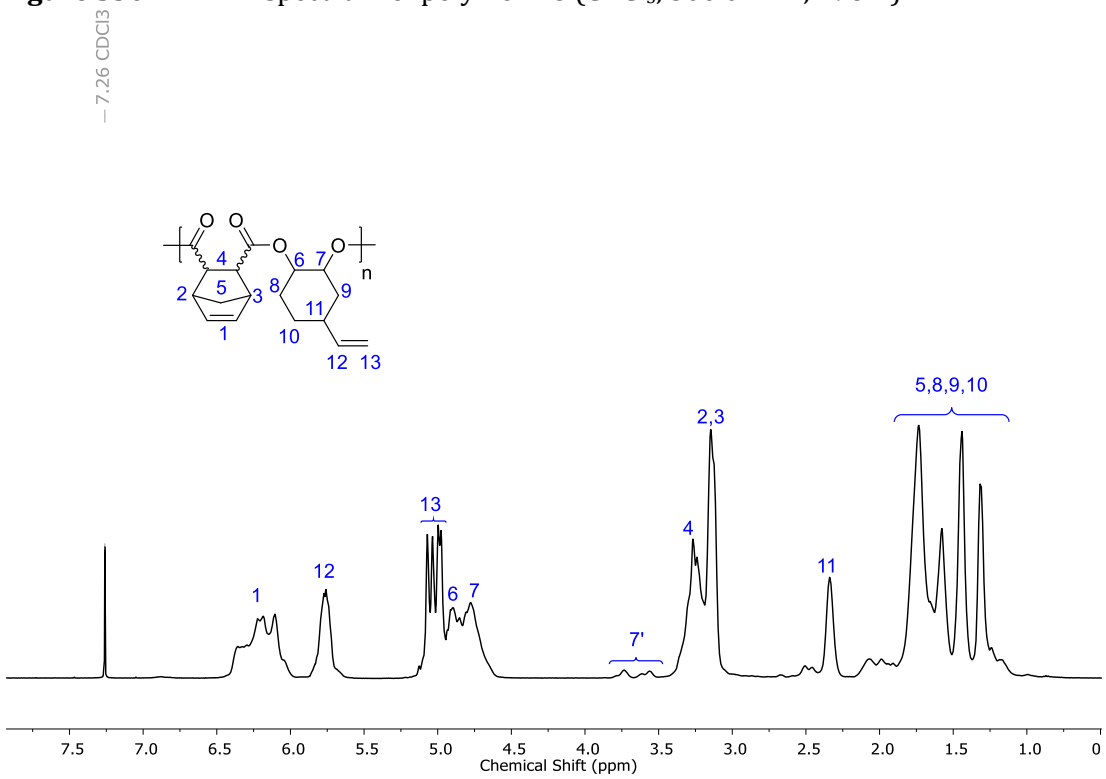


Figure S31. ^{1}H NMR spectrum of polymer **P7** ($CDCl_3$, 500.0 MHz, 298 K).

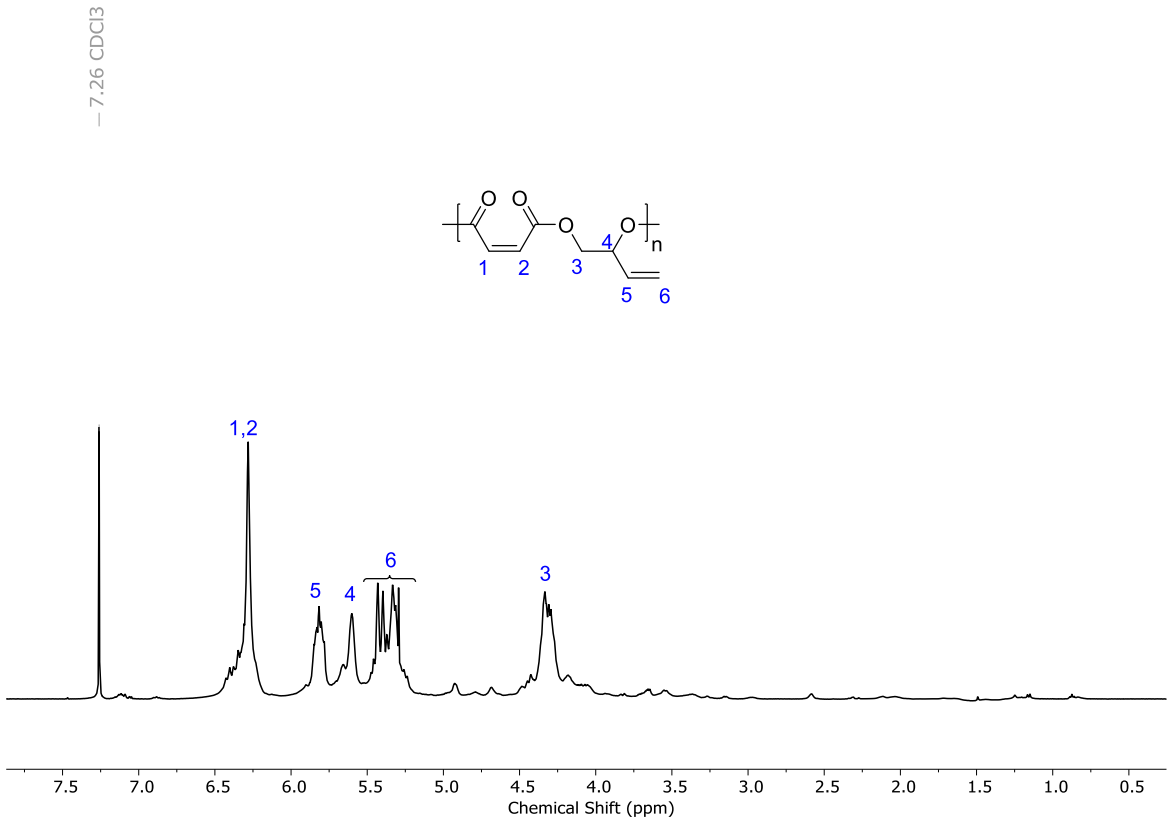


Figure S32. ^{1}H NMR spectrum of polymer **P8** ($CDCl_3$, 500.0 MHz, 298 K).

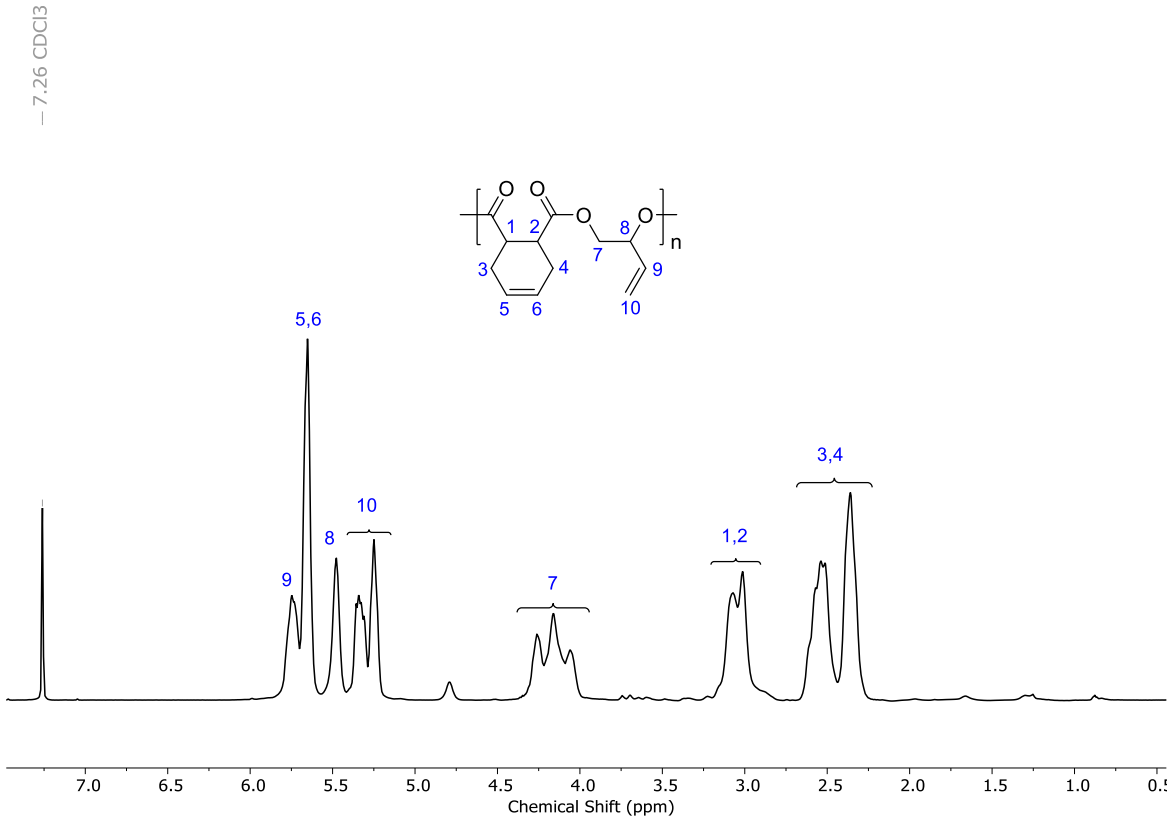


Figure S33. ^{1}H NMR spectrum of polymer **P9** ($CDCl_3$, 500.0 MHz, 298 K).

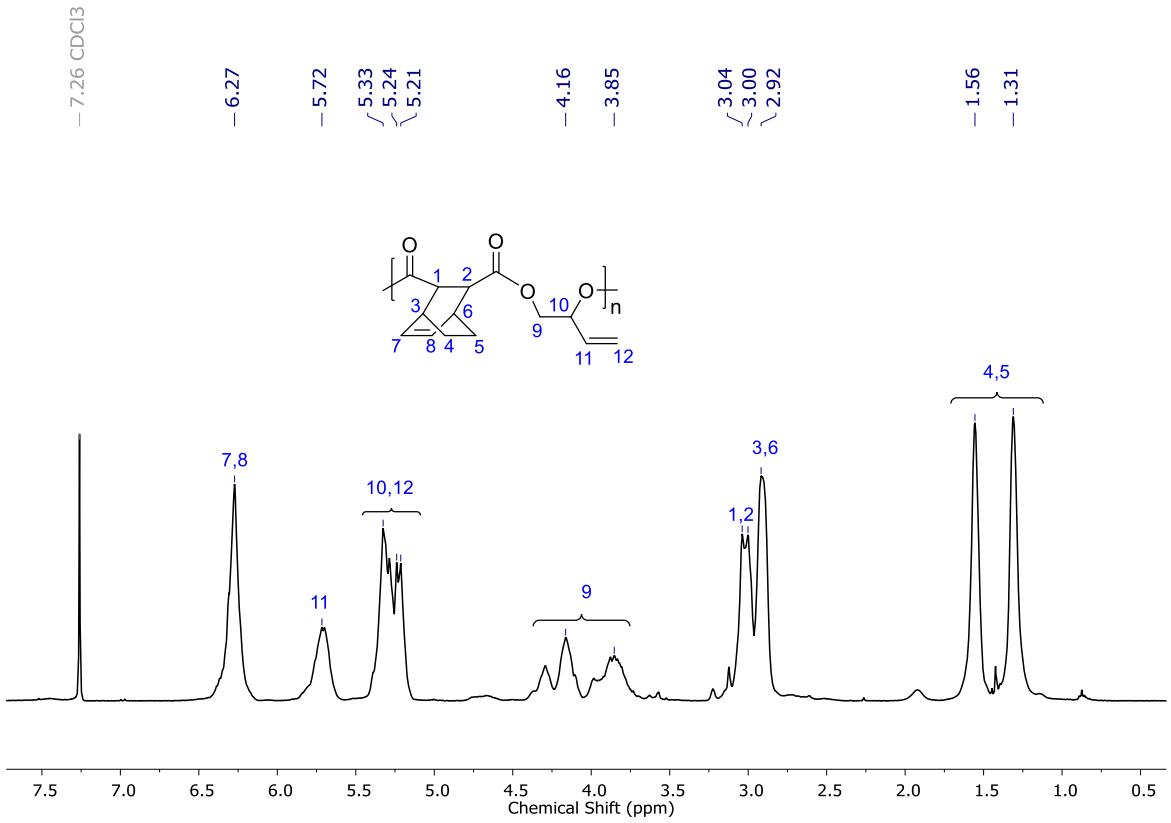


Figure S34. ^{1}H NMR spectrum of polymer **P10** ($CDCl_3$, 500.0 MHz, 298 K).

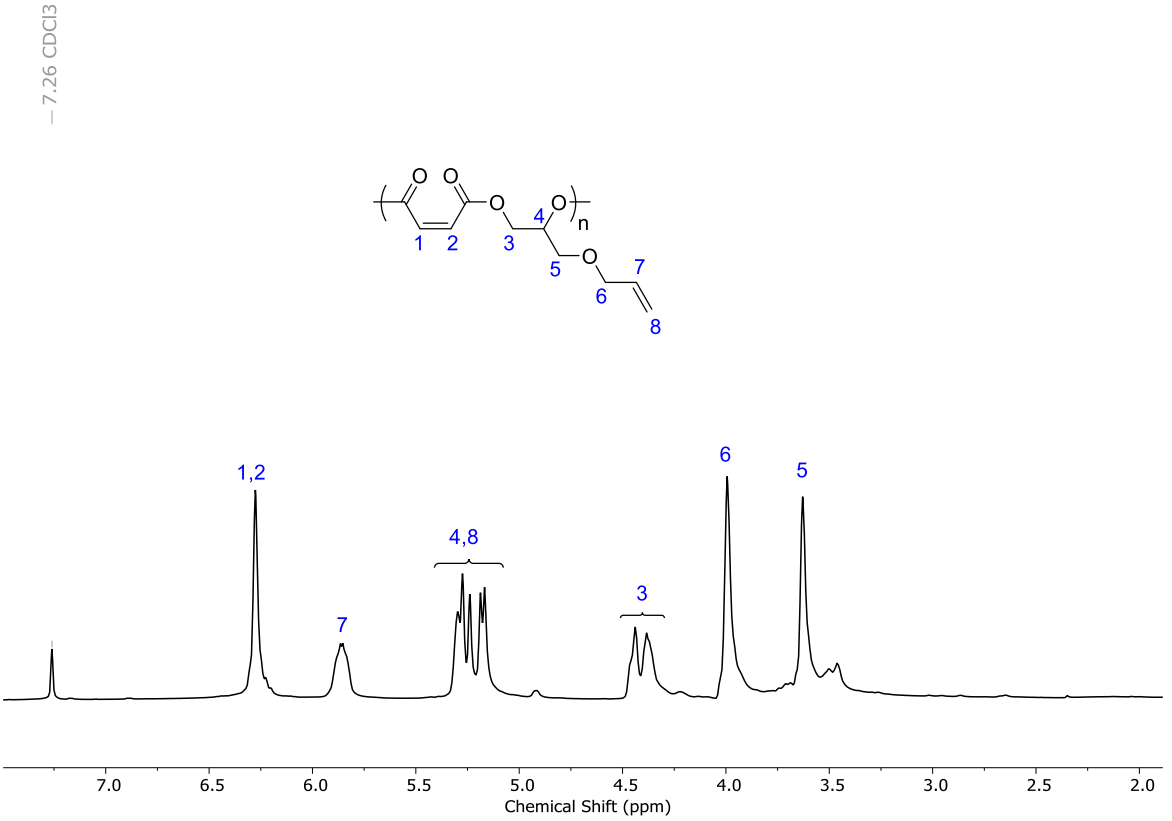


Figure S35. ^{1}H NMR spectrum of polymer **P11** ($CDCl_3$, 500.0 MHz, 298 K).

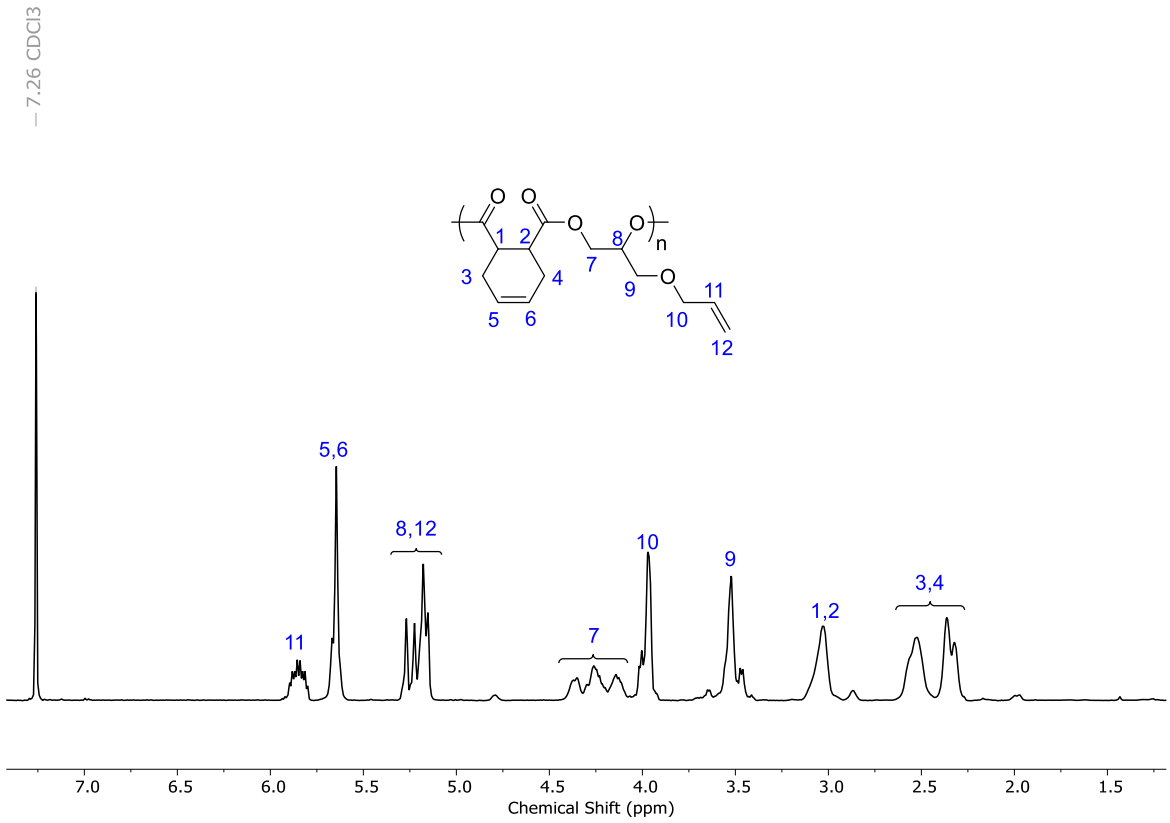


Figure S36. ^{1}H NMR spectrum of polymer **P12** ($CDCl_3$, 500.0 MHz, 298 K).

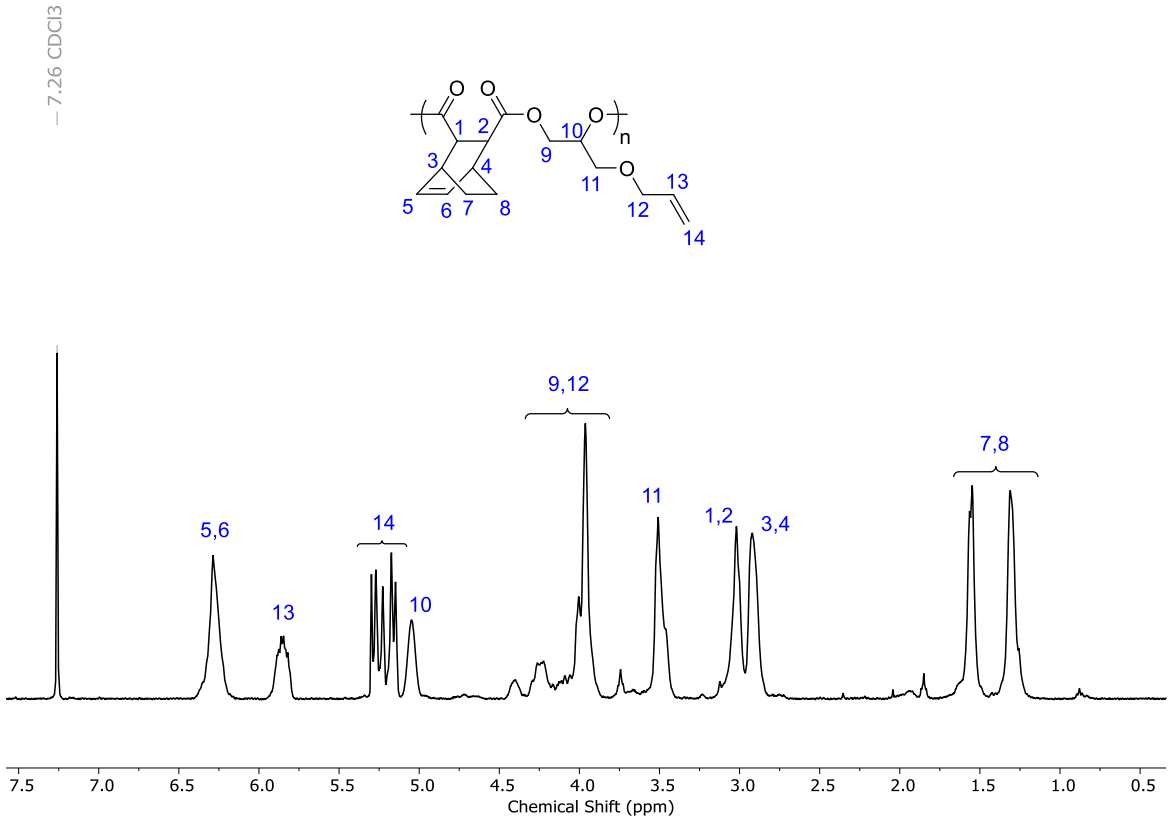


Figure S37. ^{1}H NMR spectrum of polymer **P13** ($CDCl_3$, 500.0 MHz, 298 K).

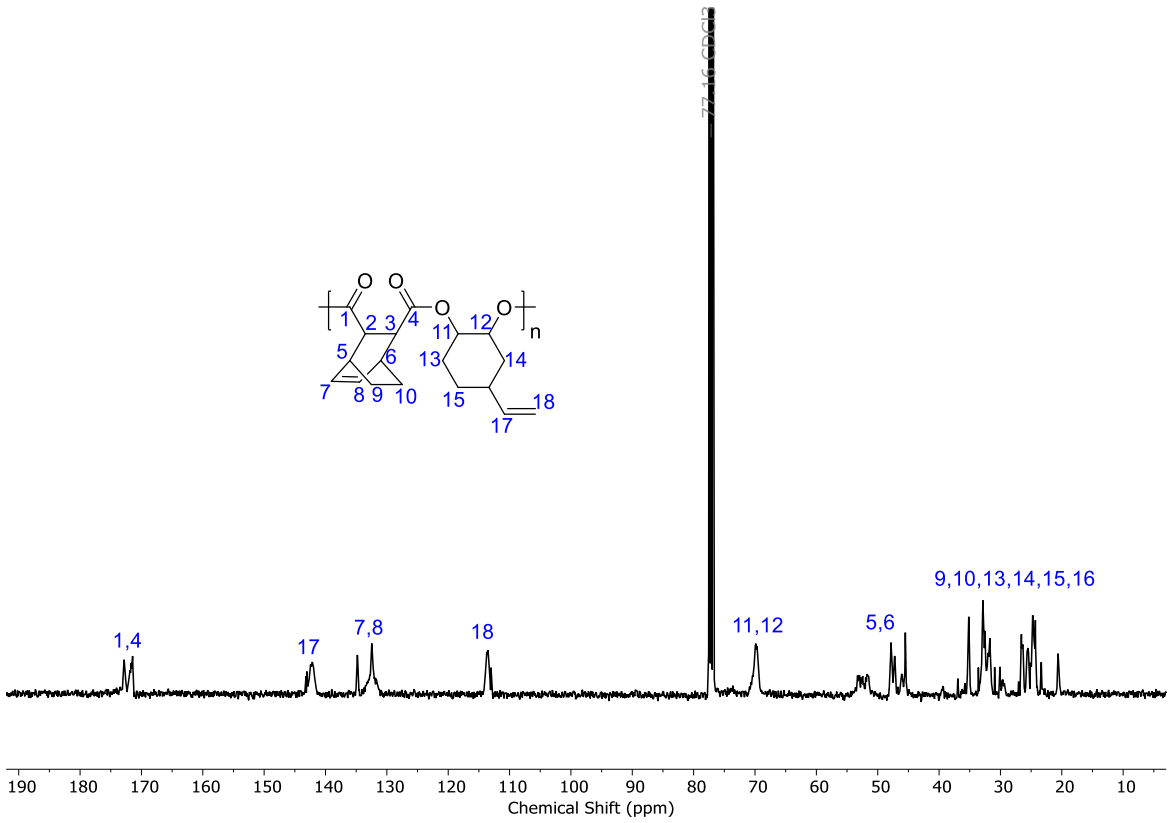


Figure S38. $^{13}C\{^{1}H\}$ NMR spectrum of **P6** ($CDCl_3$, 500.0 MHz, 298 K).

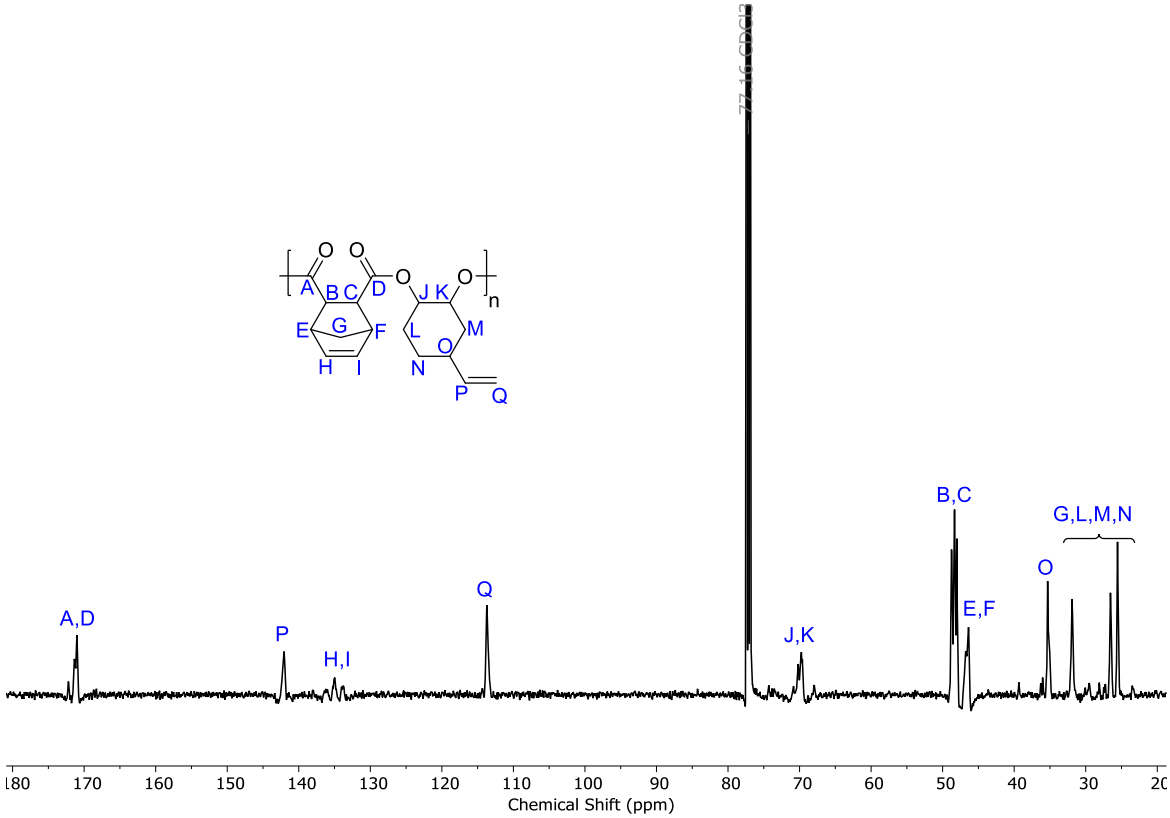


Figure S39. $^{13}C\{^{1}H\}$ NMR spectrum of **P7** ($CDCl_3$, 500.0 MHz, 298 K).

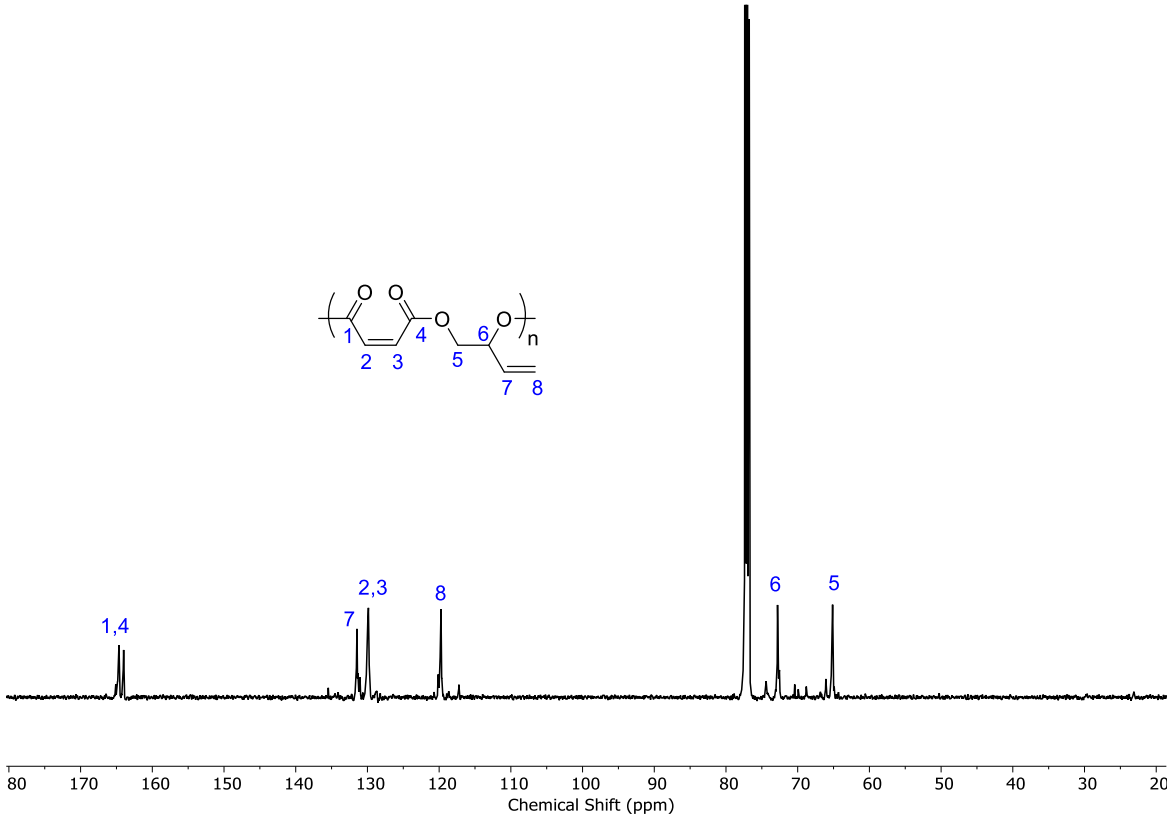


Figure S40. $^{13}C\{^{1}H\}$ NMR spectrum of **P8** ($CDCl_3$, 500.0 MHz, 298 K).

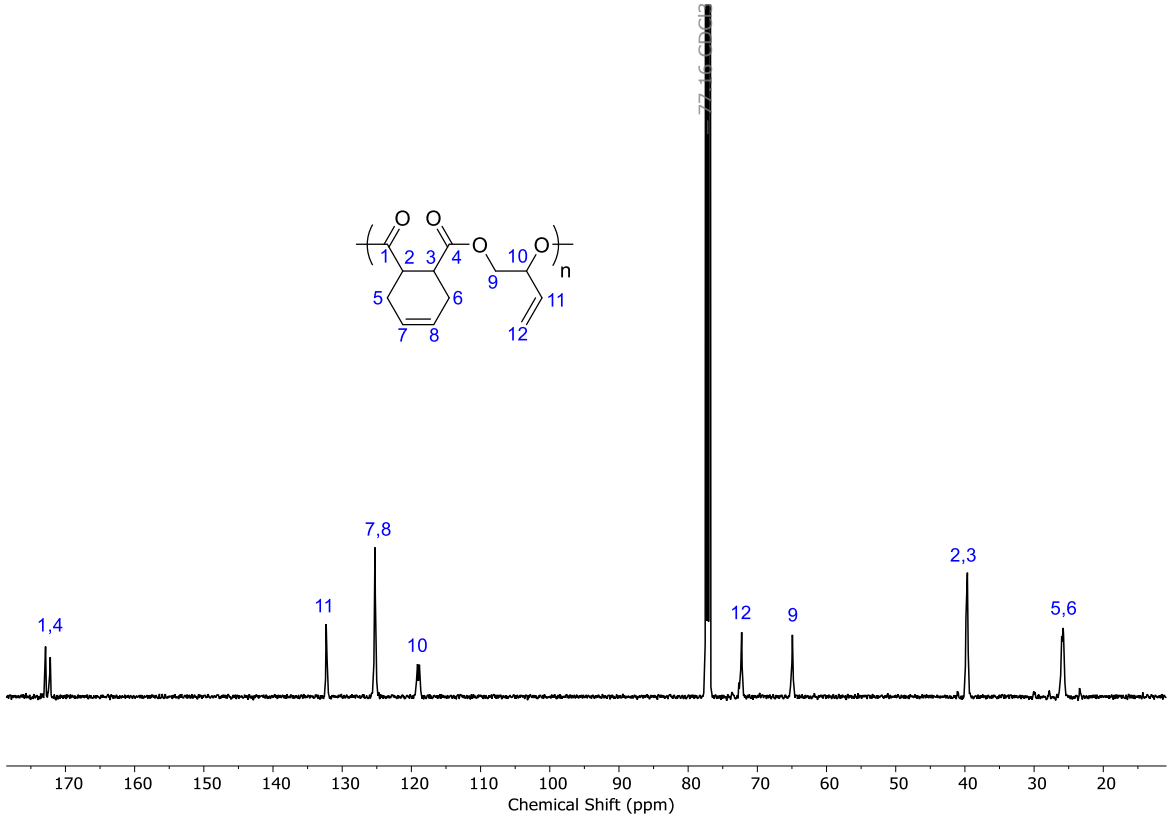


Figure S41. $^{13}C\{^{1}H\}$ NMR spectrum of **P9** ($CDCl_3$, 500.0 MHz, 298 K).

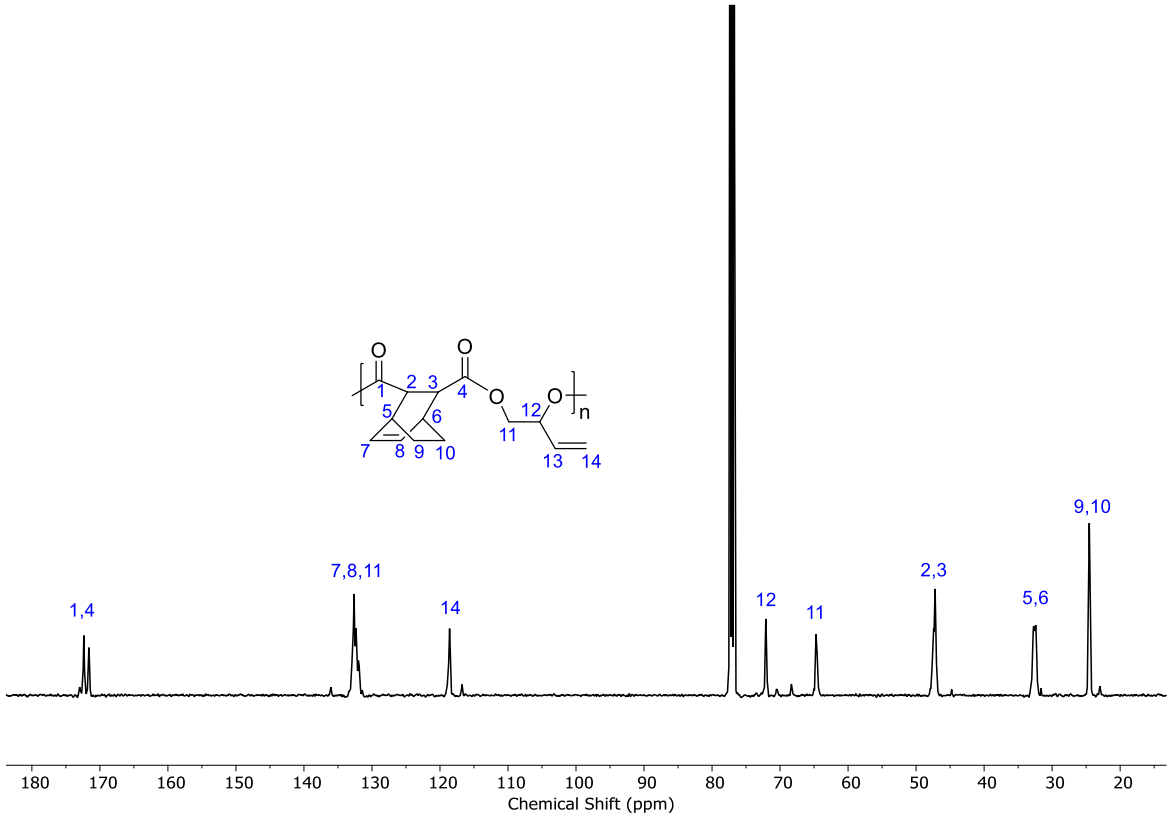


Figure S42. $^{13}C\{^{1}H\}$ NMR spectrum of **P10** ($CDCl_3$, 500.0 MHz, 298 K).

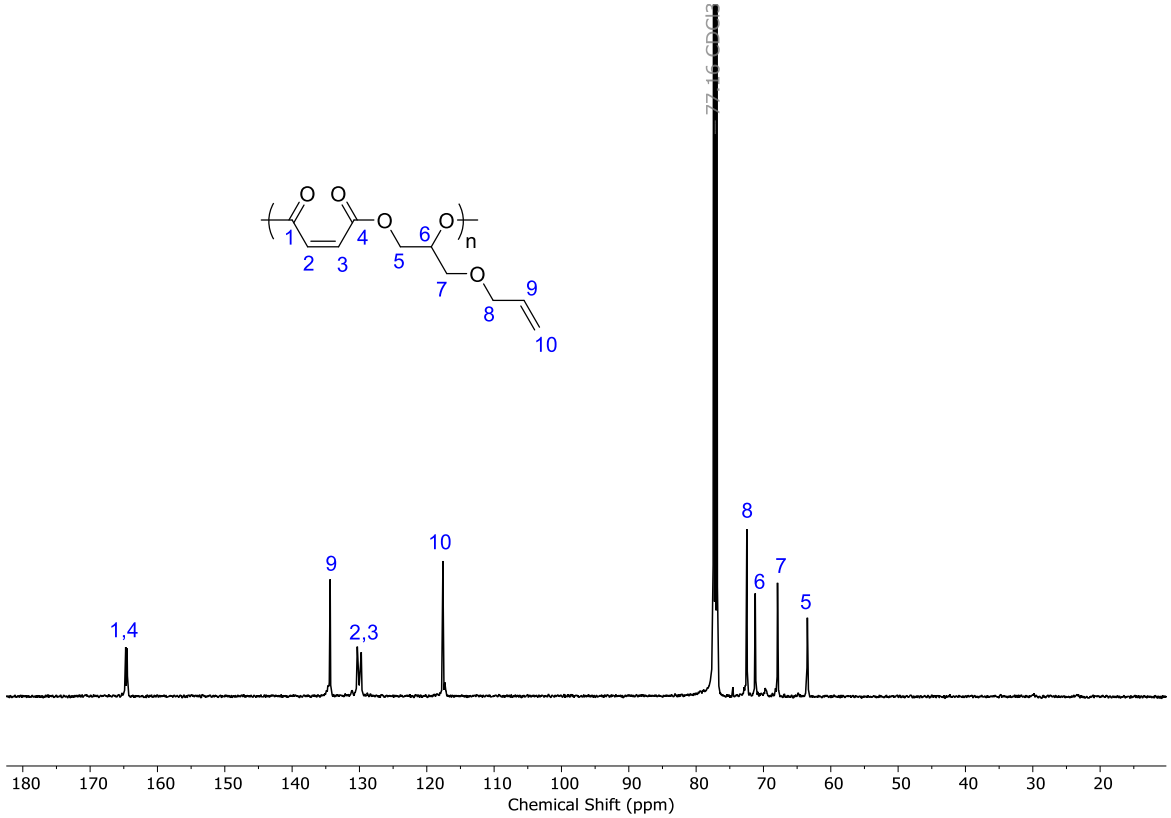


Figure S43. $^{13}C\{^{1}H\}$ NMR spectrum of **P11** ($CDCl_3$, 500.0 MHz, 298 K).

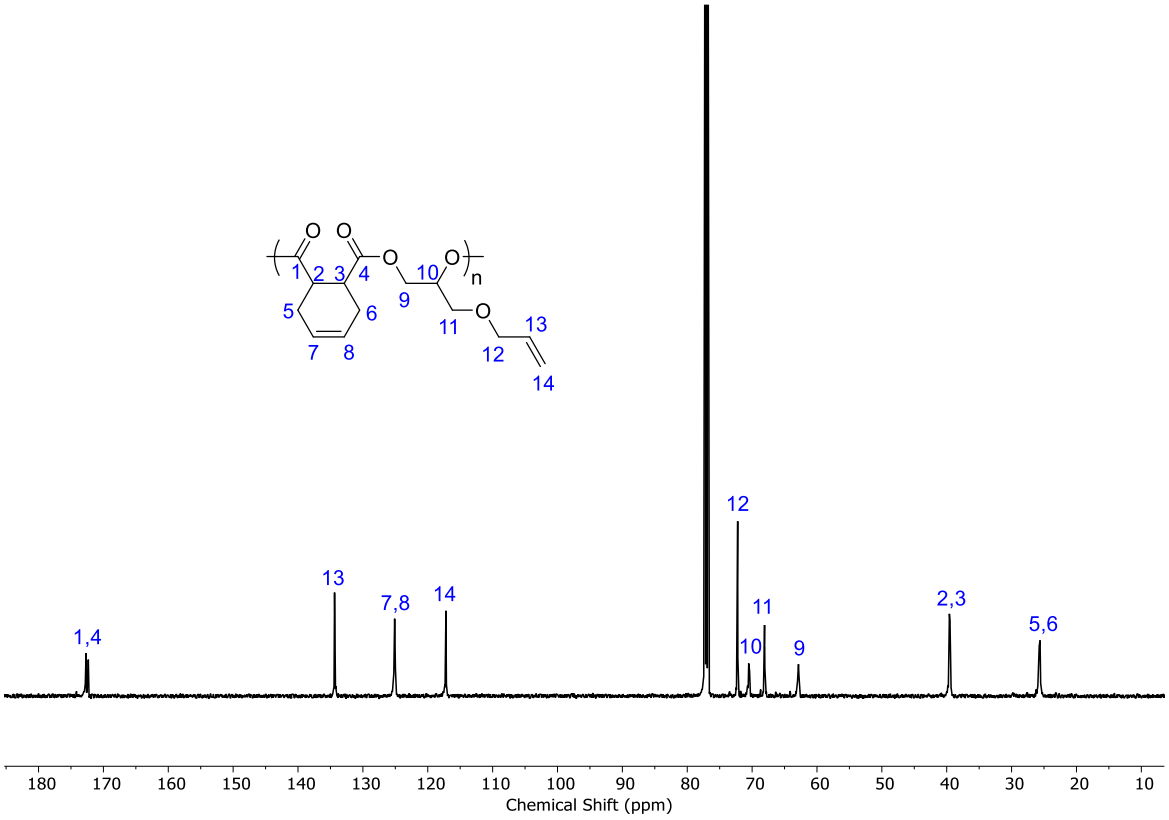


Figure S44. $^{13}C\{^{1}H\}$ NMR spectrum of **P12** ($CDCl_3$, 500.0 MHz, 298 K).

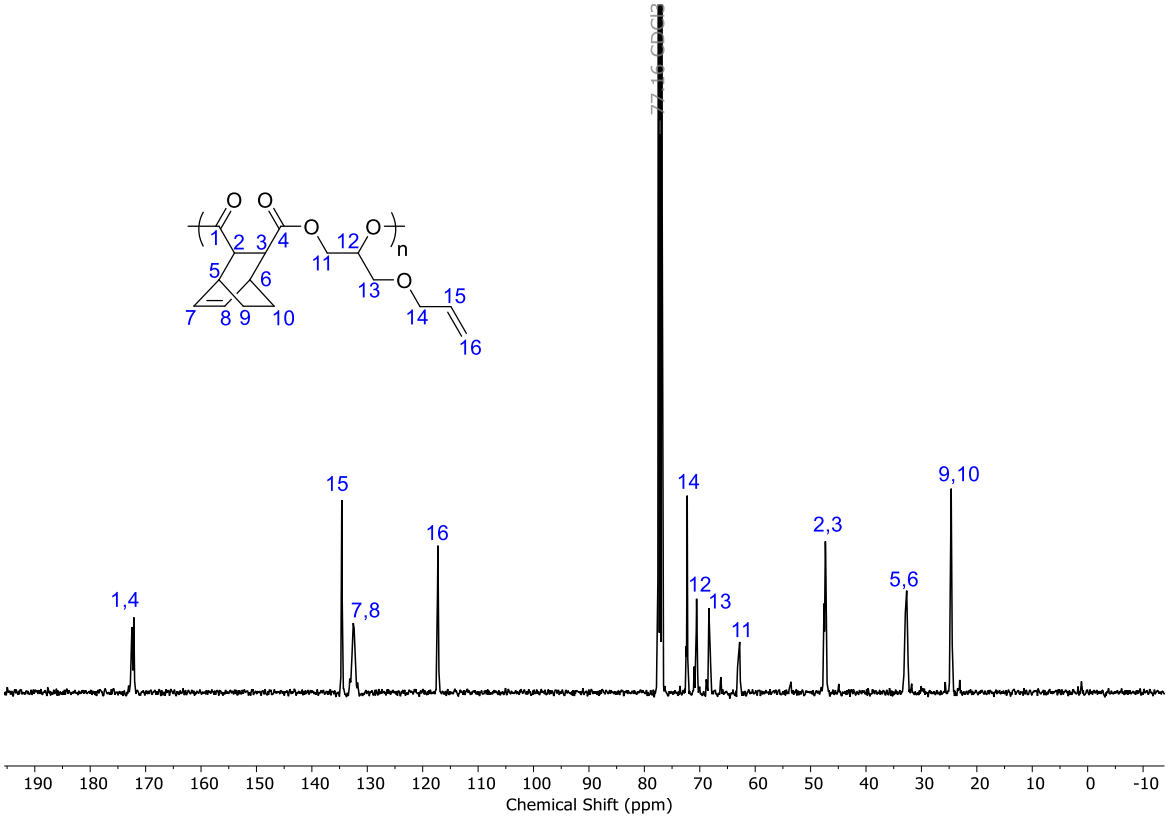


Figure S45. $^{13}C\{^{1}H\}$ NMR spectrum of **P13** ($CDCl_3$, 500.0 MHz, 298 K).

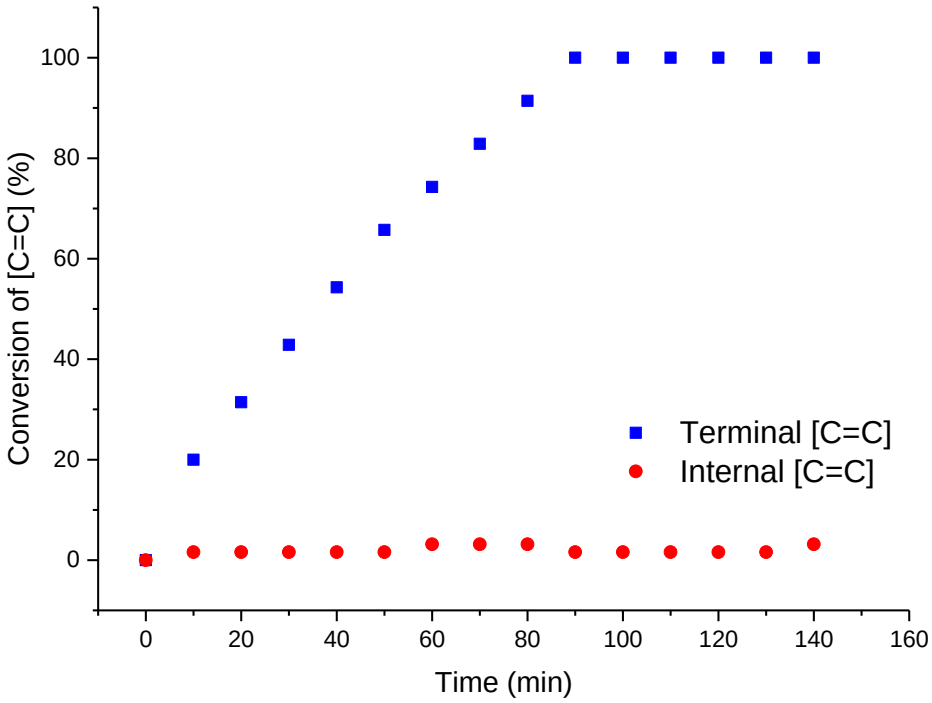


Figure S46. Percentage conversion of the two different alkene groups (internal = blue circles and terminal = red squares) vs. time during the hydroboration reaction of **P6**.

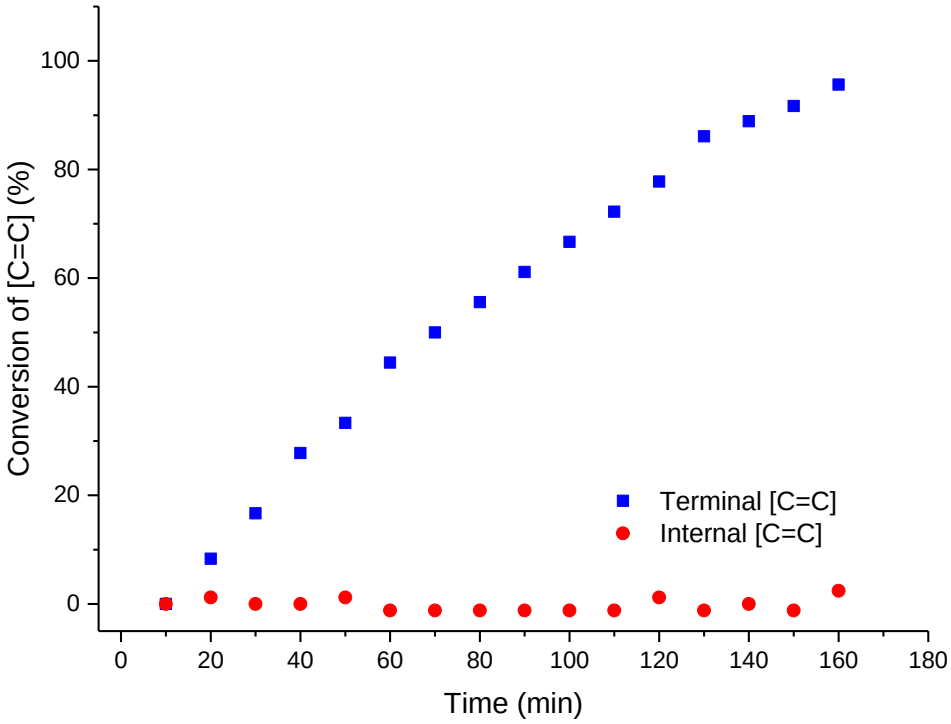


Figure S47. Percentage conversion of the two different alkene groups (internal = blue circles and terminal = red squares) vs. time during the hydroboration reaction of **P8**.

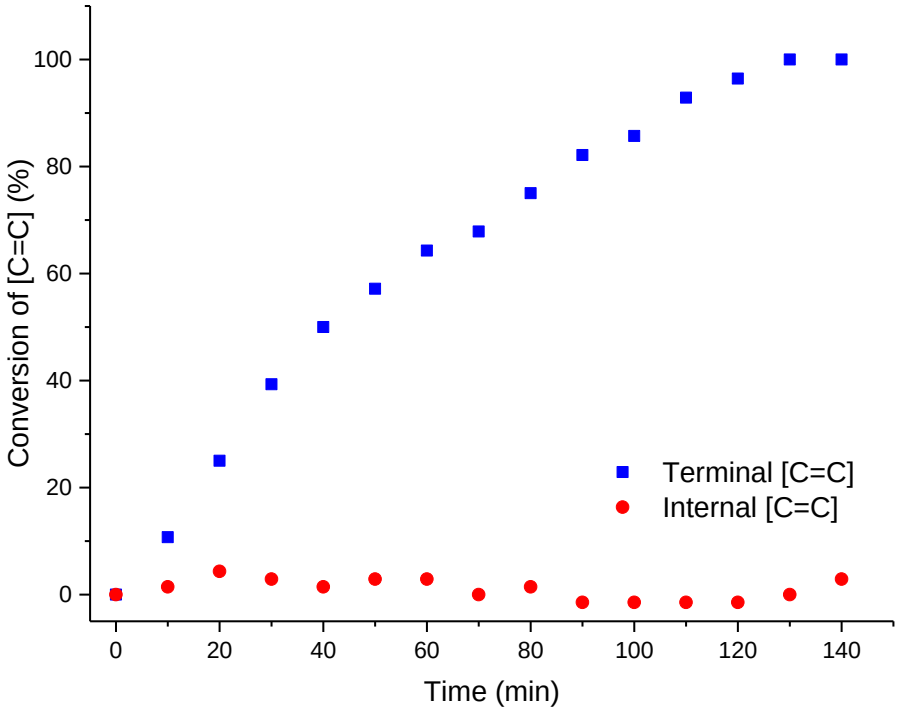


Figure S48. Percentage conversion of the two different alkene groups (internal = blue circles and terminal = red squares) vs. time during the hydroboration reaction of **P9**.

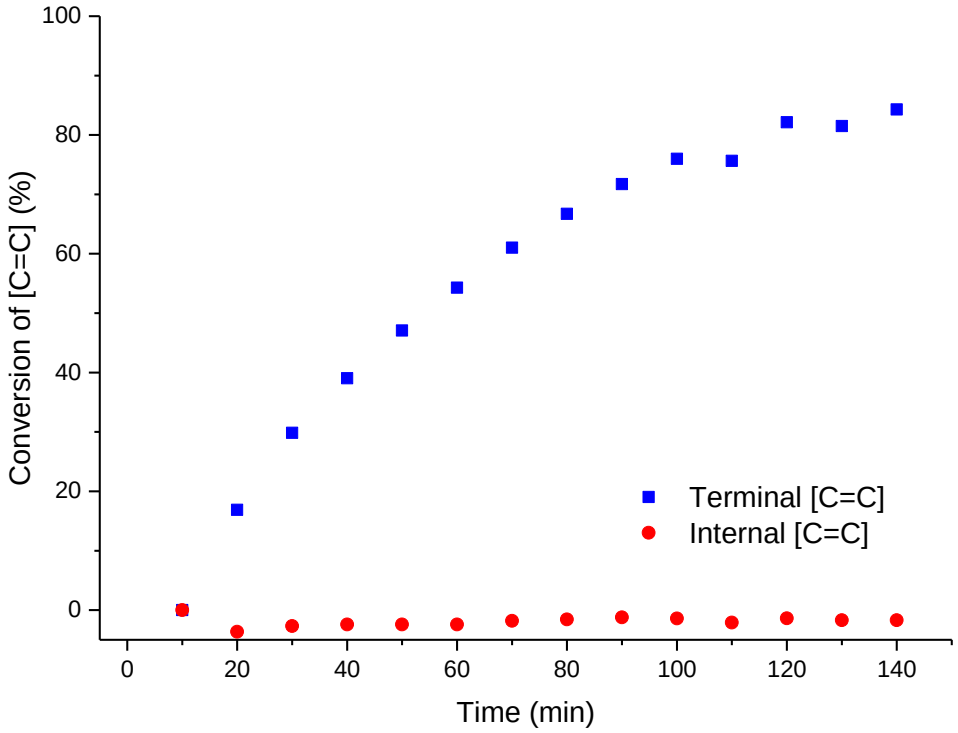


Figure S49. Percentage conversion of the two different alkene groups (internal = blue circles and terminal = red squares) vs. time during the hydroboration reaction of **P10**.

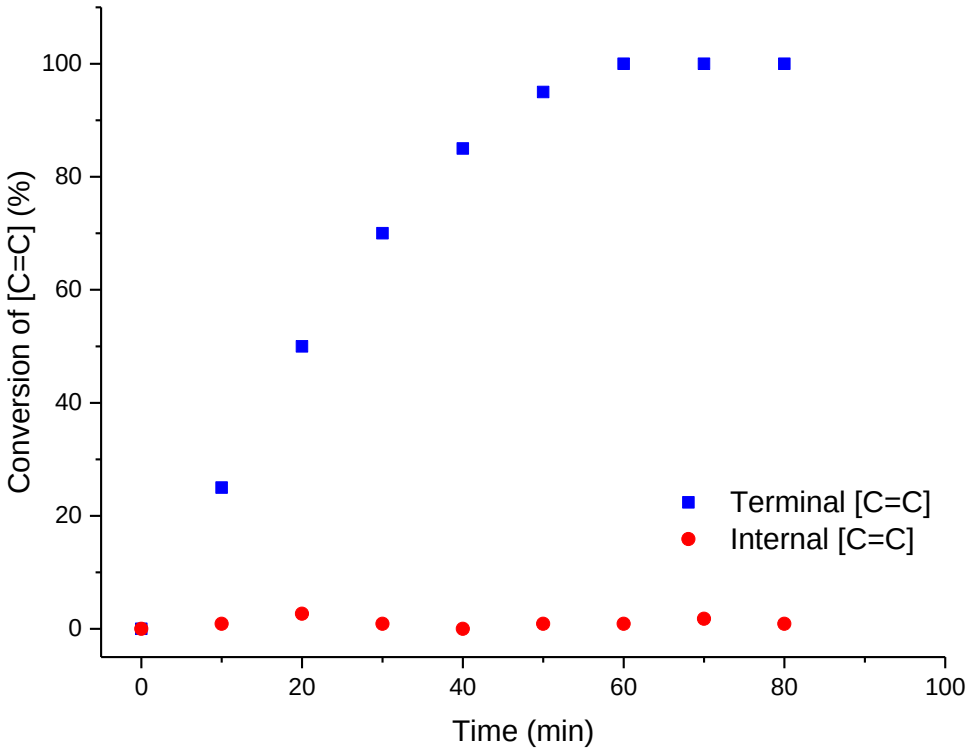


Figure S50. Percentage conversion of the two different alkene groups (internal = blue circles and terminal = red squares) vs. time during the hydroboration reaction of **P11**.

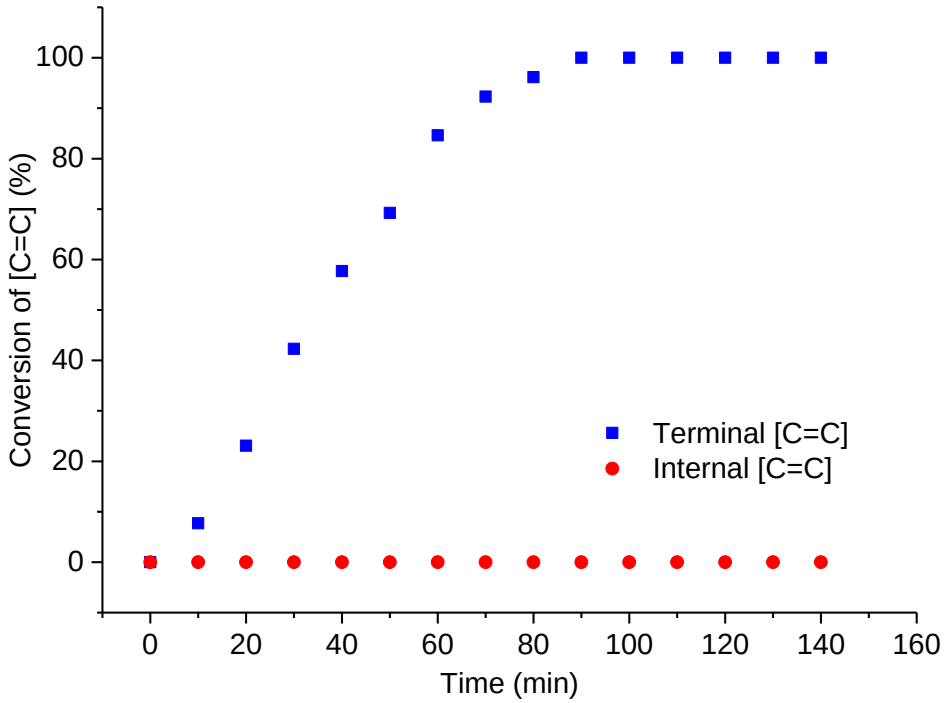


Figure S51. Percentage conversion of the two different alkene groups (internal = blue circles and terminal = red squares) vs. time during the hydroboration reaction of **P12**.

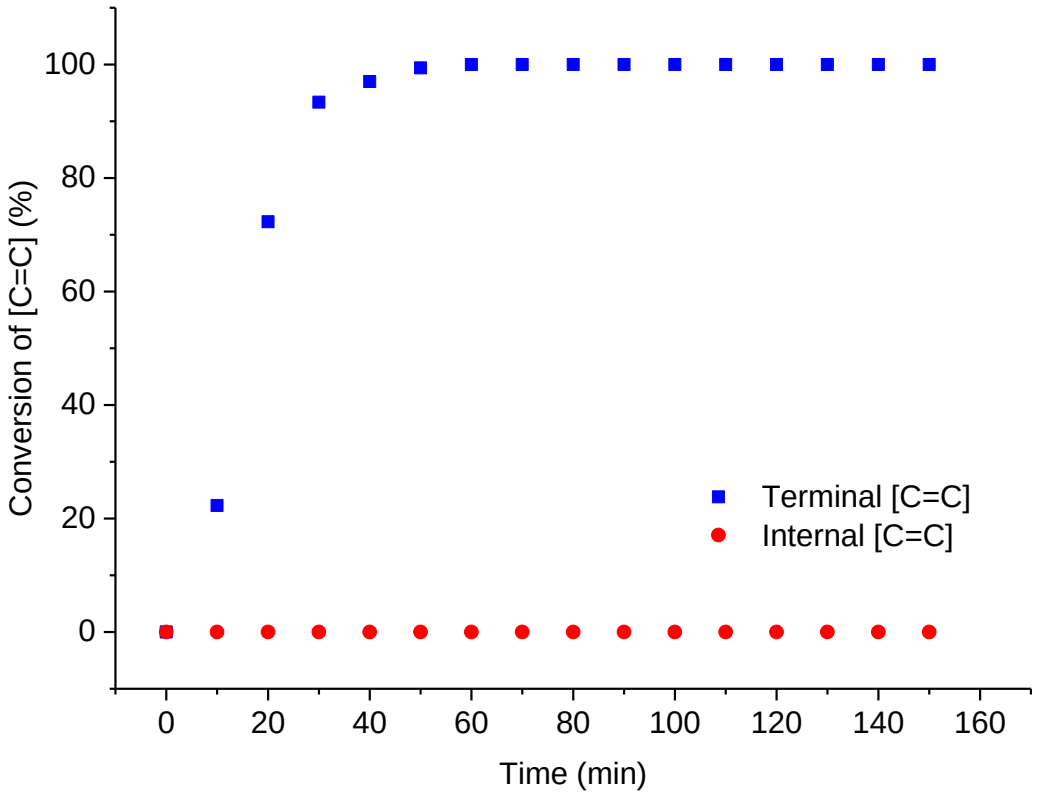


Figure S52. Percentage conversion of the two different alkene groups (internal = blue circles and terminal = red squares) vs. time during the hydroboration reaction of **P13**.

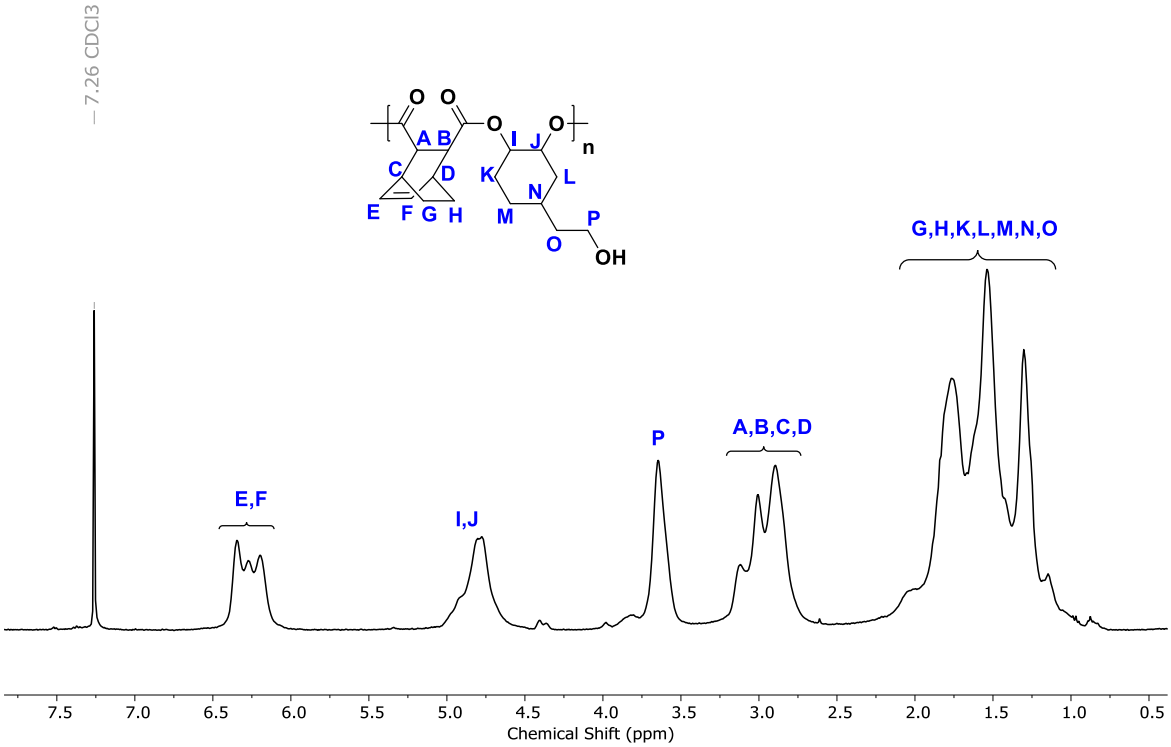


Figure S53. ^{1}H NMR spectrum of **P6(a)** ($CDCl_3$, 400 MHz, 298 K).

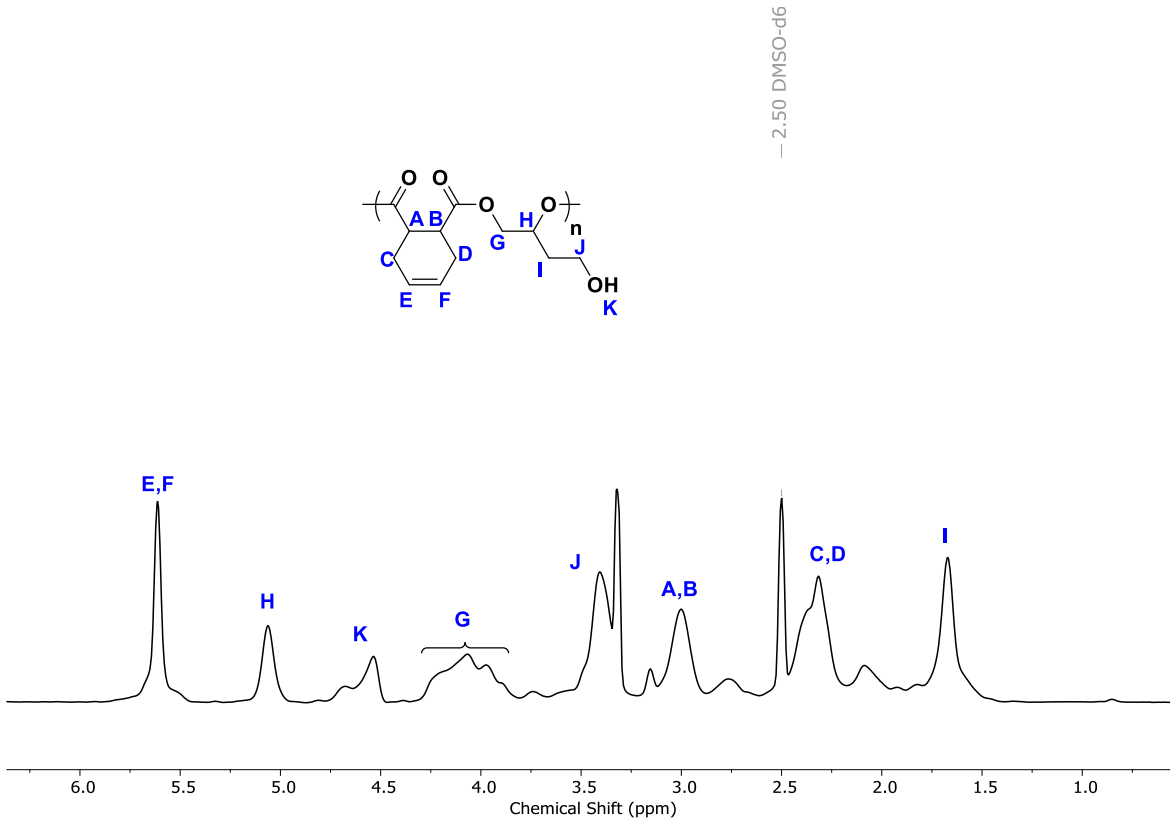


Figure S54. ^{1}H NMR spectrum of **P9(a)** ($CDCl_3$, 400 MHz, 298 K).

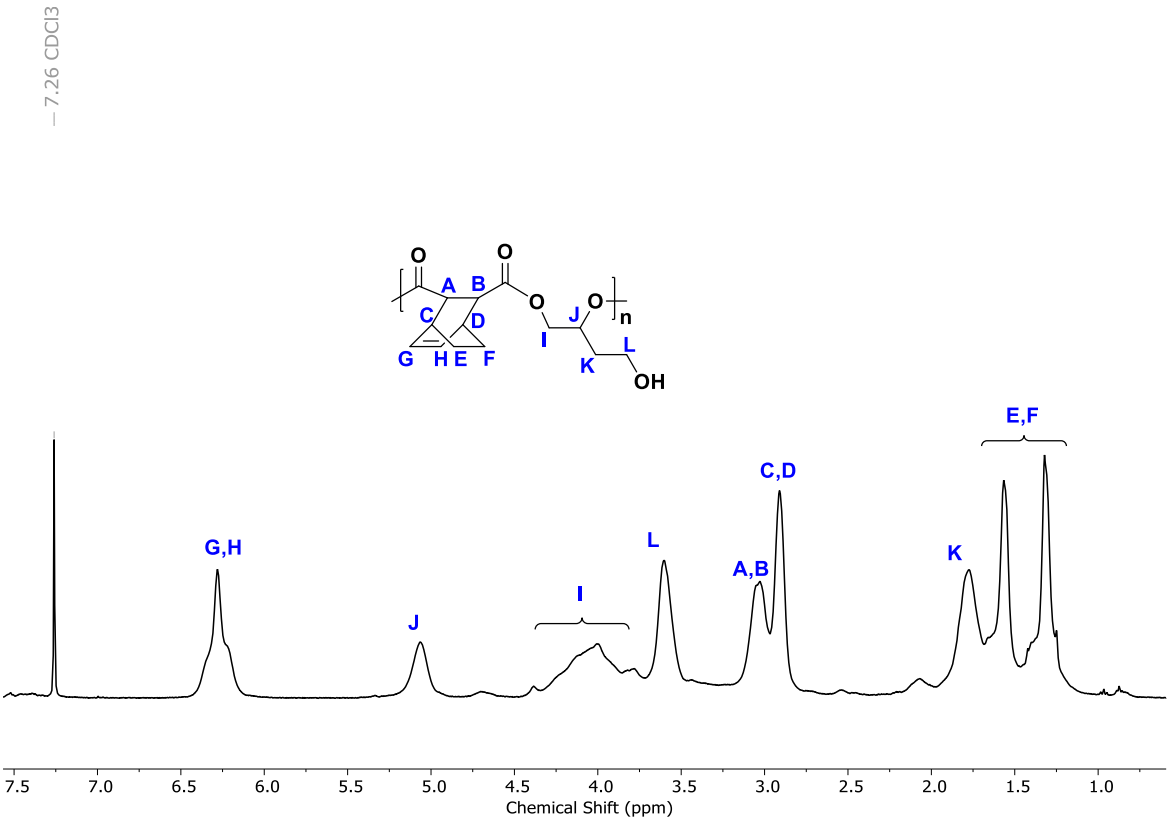


Figure S55. ^{1}H NMR spectrum of **P10(a)** ($CDCl_3$, 400 MHz, 298 K).

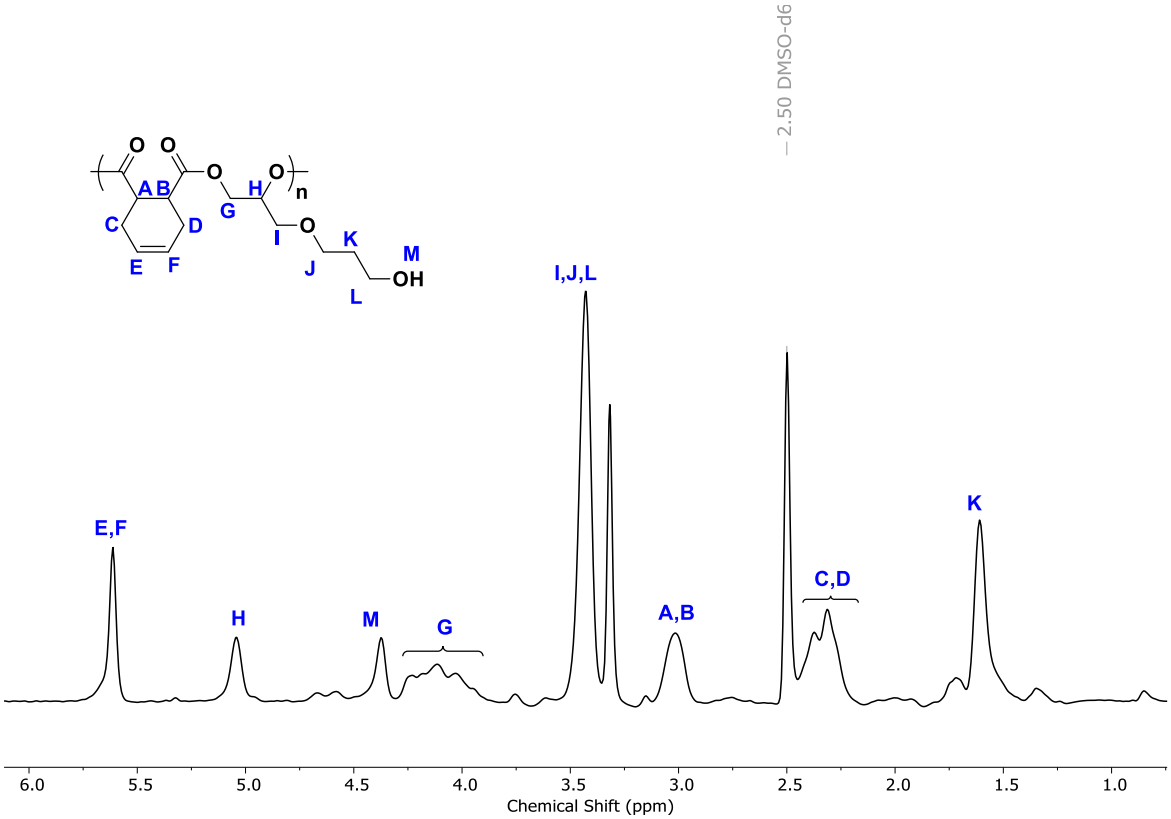


Figure S56. ^{1}H NMR spectrum of **P12(a)** ($CDCl_3$, 400 MHz, 298 K).

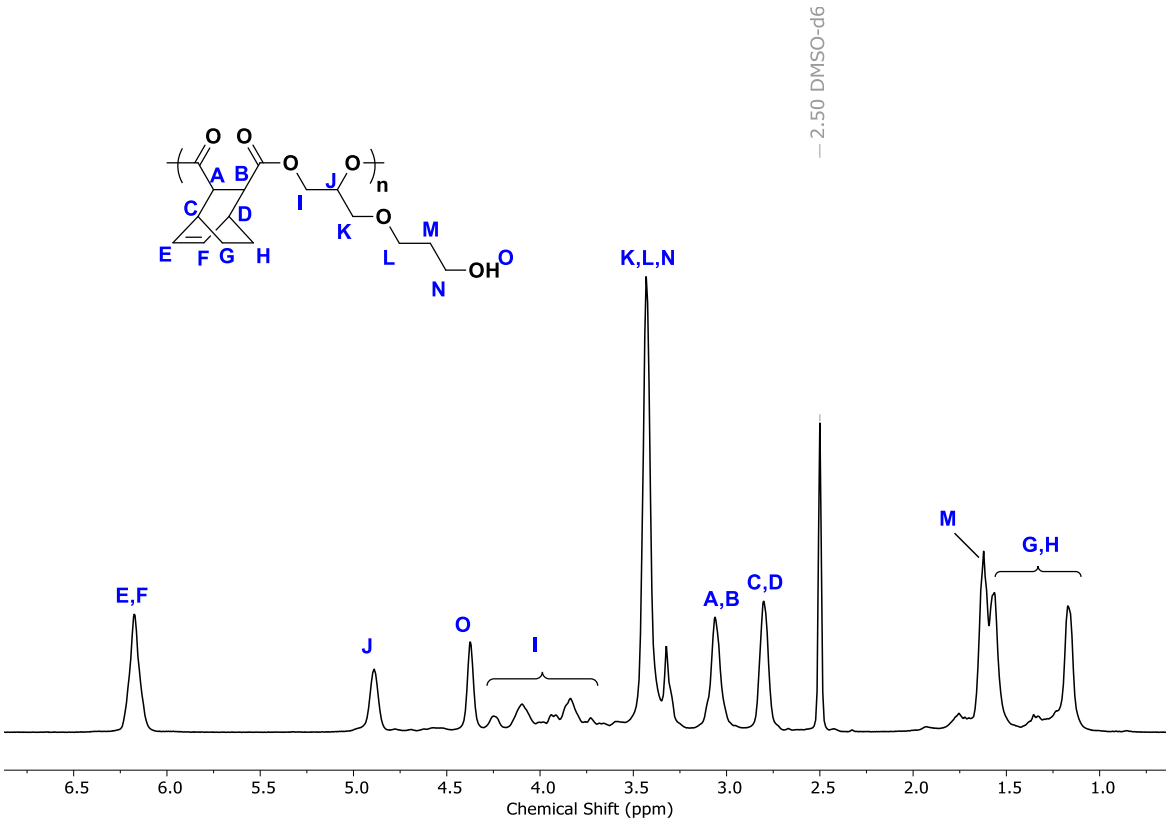


Figure S57. ^{1}H NMR spectrum of **P13(a)** ($CDCl_3$, 400 MHz, 298 K).

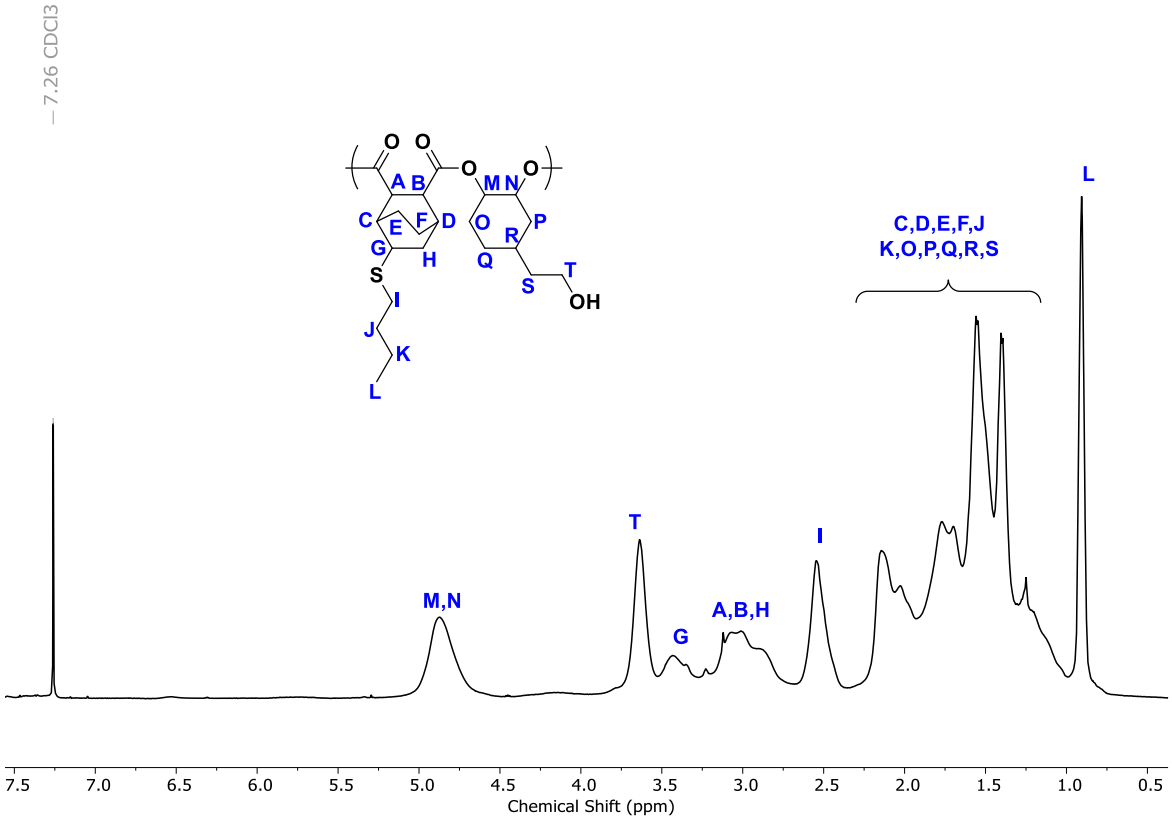


Figure S58. ^{1}H NMR spectrum of **P6(b)** ($CDCl_3$, 400 MHz, 298 K).

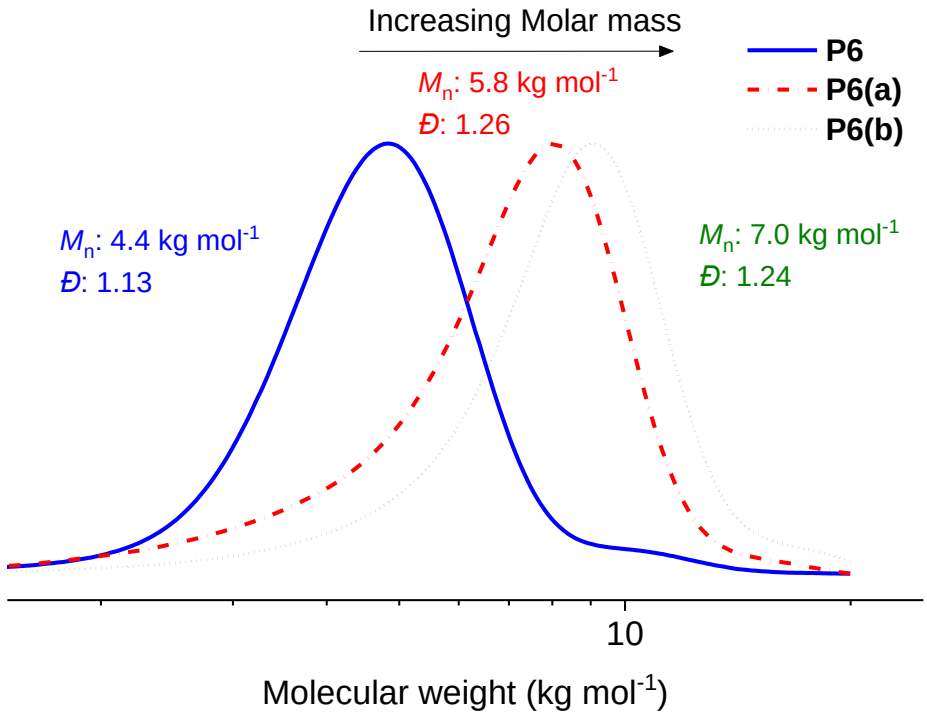


Figure S59. SEC (in DMF) showing an increase in molar mass after functionalization, in each case with retention of monomodal distributions and narrow dispersity for **P6**, **P6(a)** and **P6(b).**

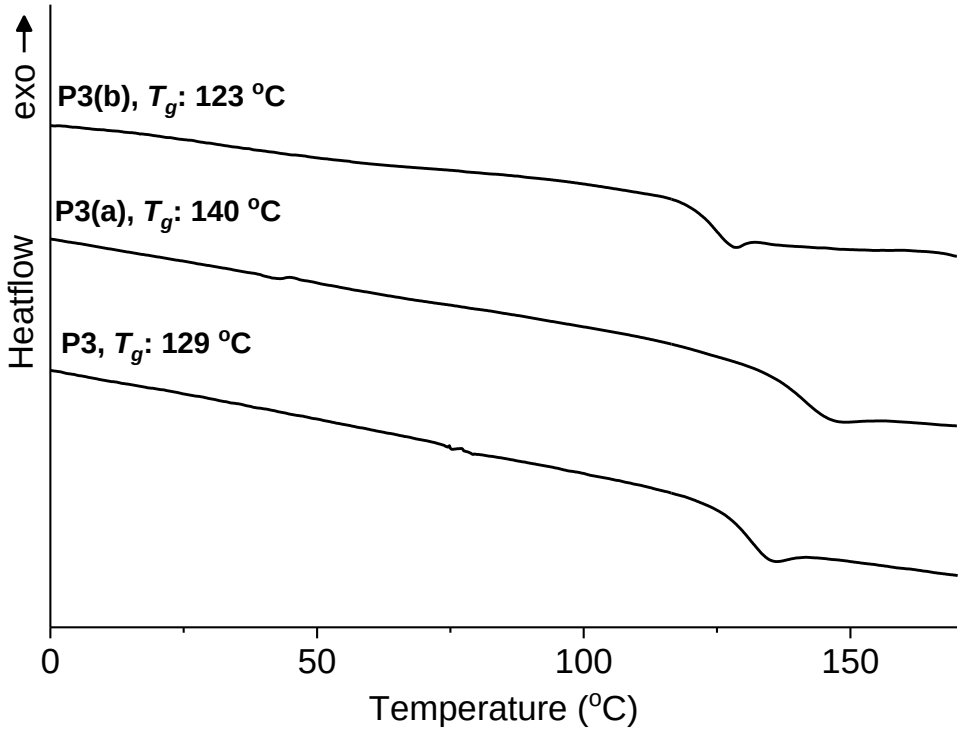


Figure S60. DSC thermograms of **P6**, **P6(a)** and **P6(b)** showing an increase in T_g after the hydroboration-oxidation and a decrease after the further instalment of butyl thiolether groups.

7.3. Chapter 4

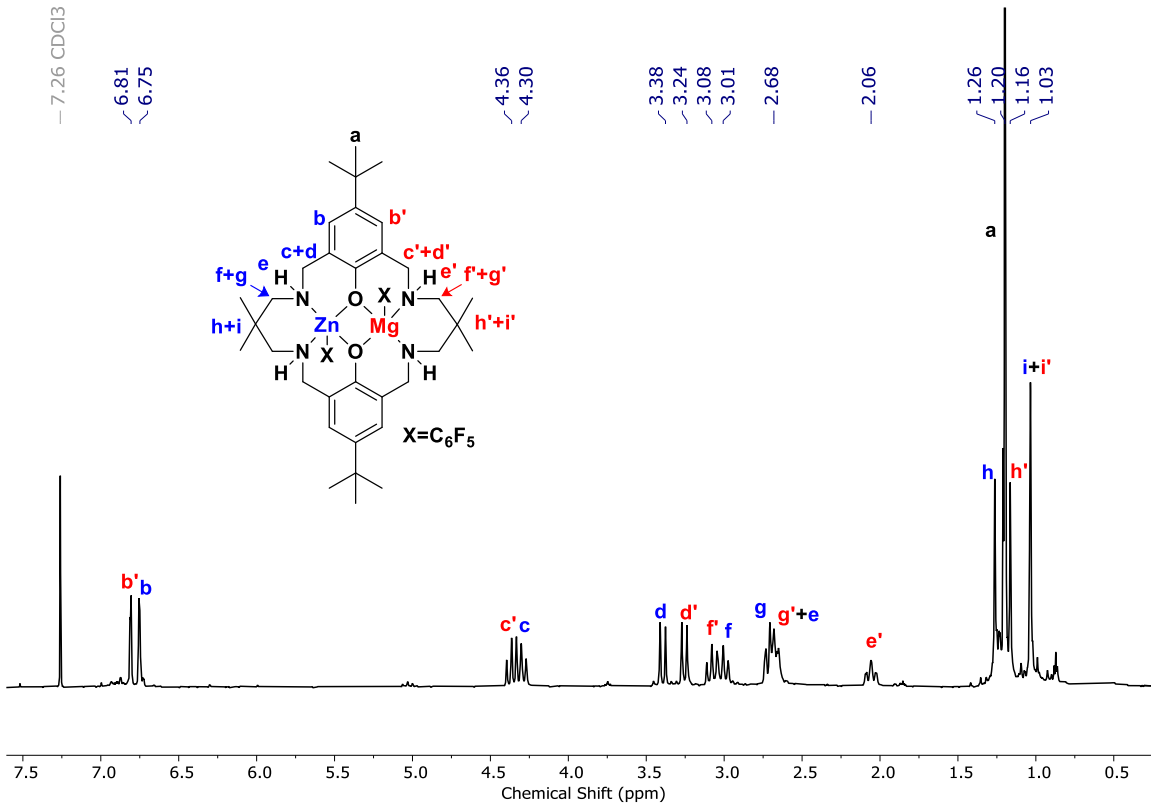


Figure S61. ^{1}H NMR spectrum of $[LMgZn(C_6F_5)_2]$(in $CDCl_3$ at 298 K)

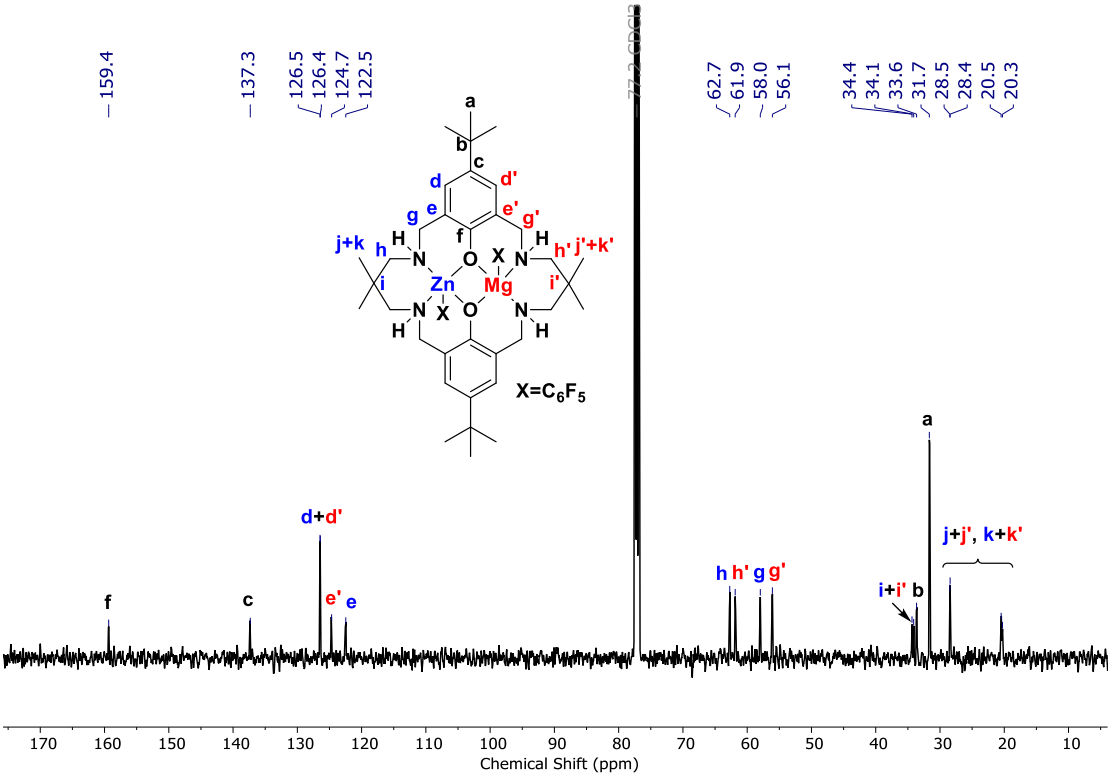


Figure S62. $^{13}C\{^{1}H\}$ NMR spectrum of $[LMgZn(C_6F_5)_2]$(in $CDCl_3$ at 298 K)

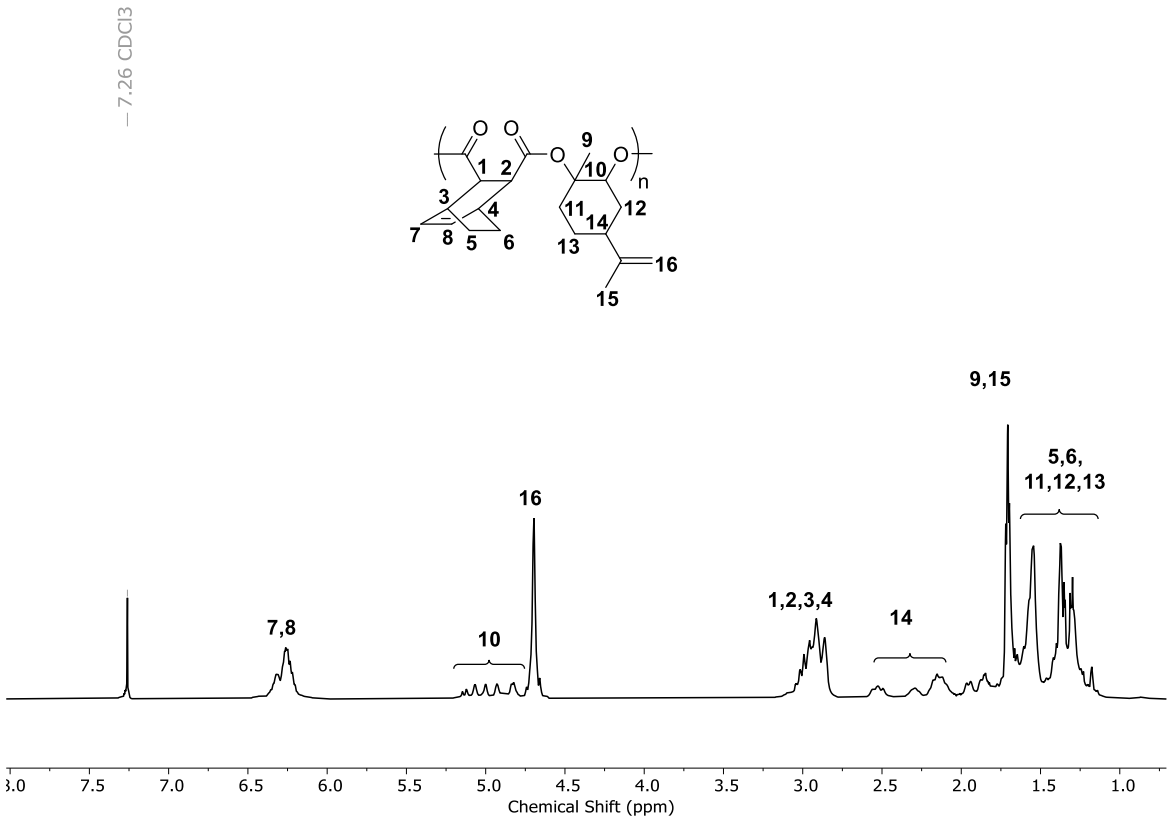


Figure S63. ^{1}H NMR of the polyester from the ROCOP of LO/TCA 2 ($CDCl_3$, at 298K).

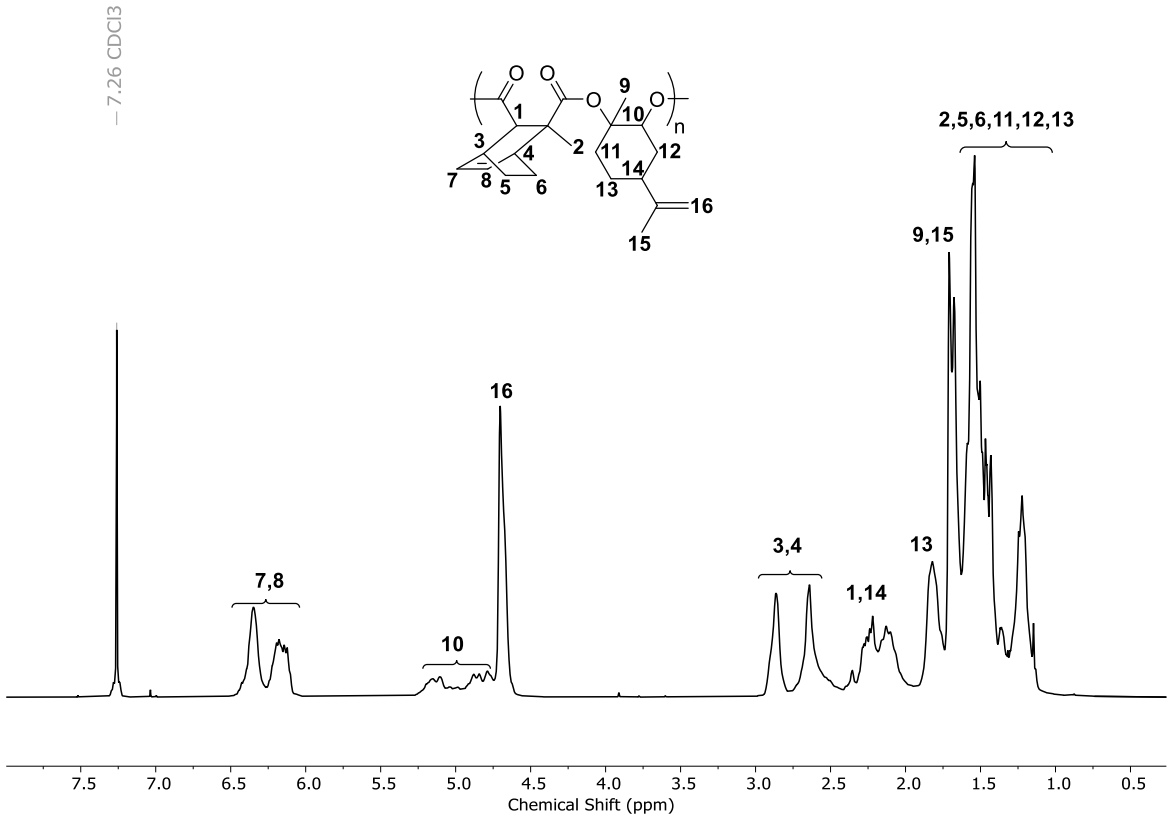


Figure S64. ^{1}H NMR of the polyester from the ROCOP of LO/TCA 3 ($CDCl_3$, at 298K).

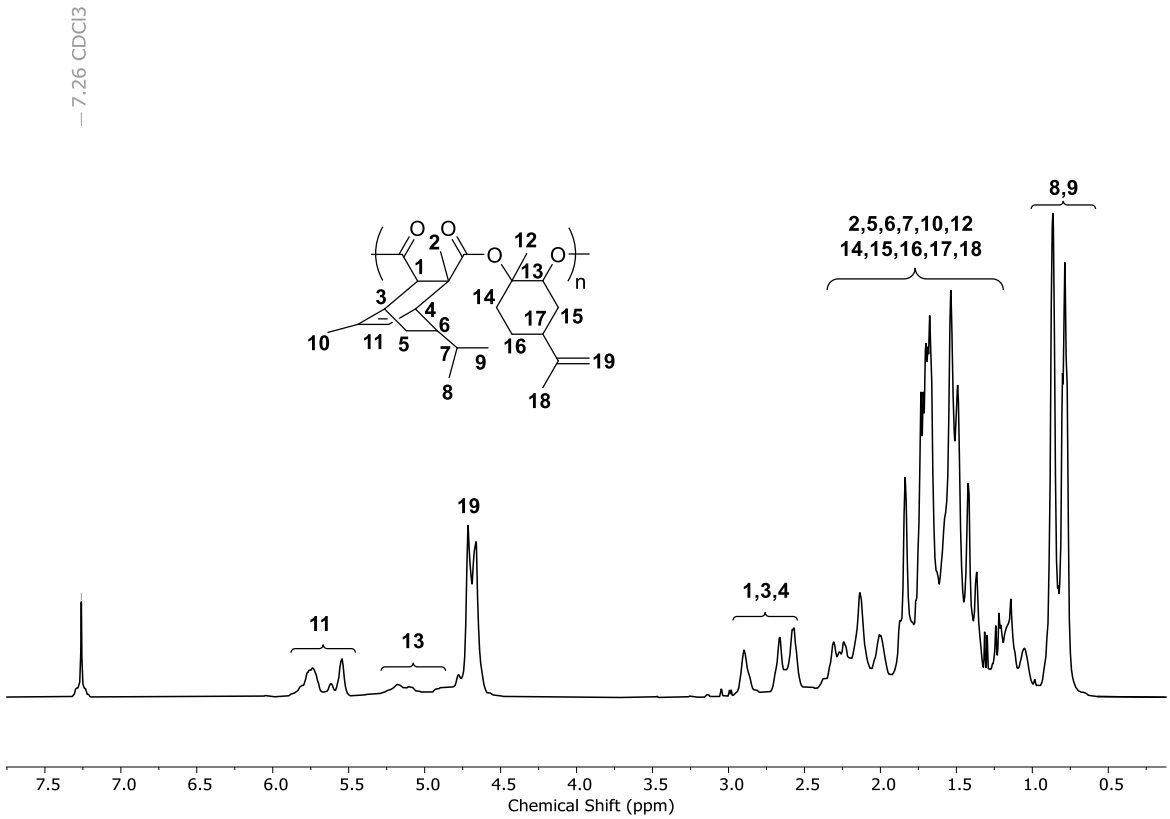


Figure S65. ^{1}H NMR of the polyester from the ROCOP of LO/TCA 4 ($CDCl_3$, at 298K).

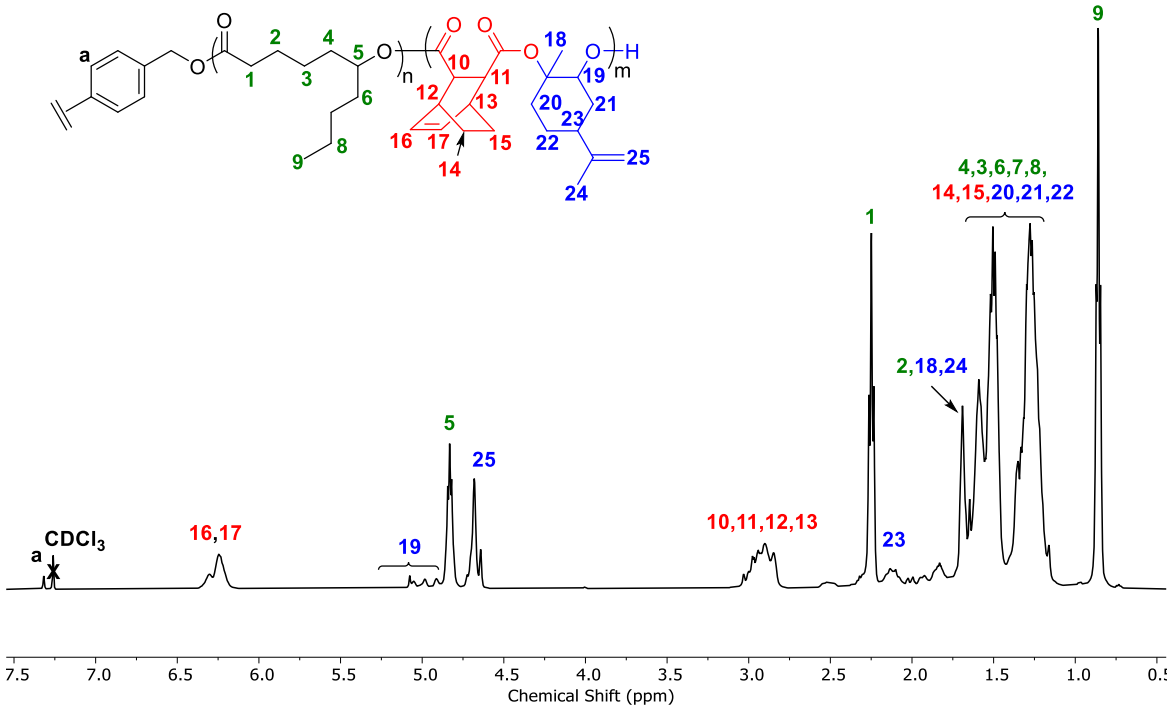


Figure S66. ^{1}H NMR spectrum of **P18** ($CDCl_3$, 500.0 MHz, 298K).

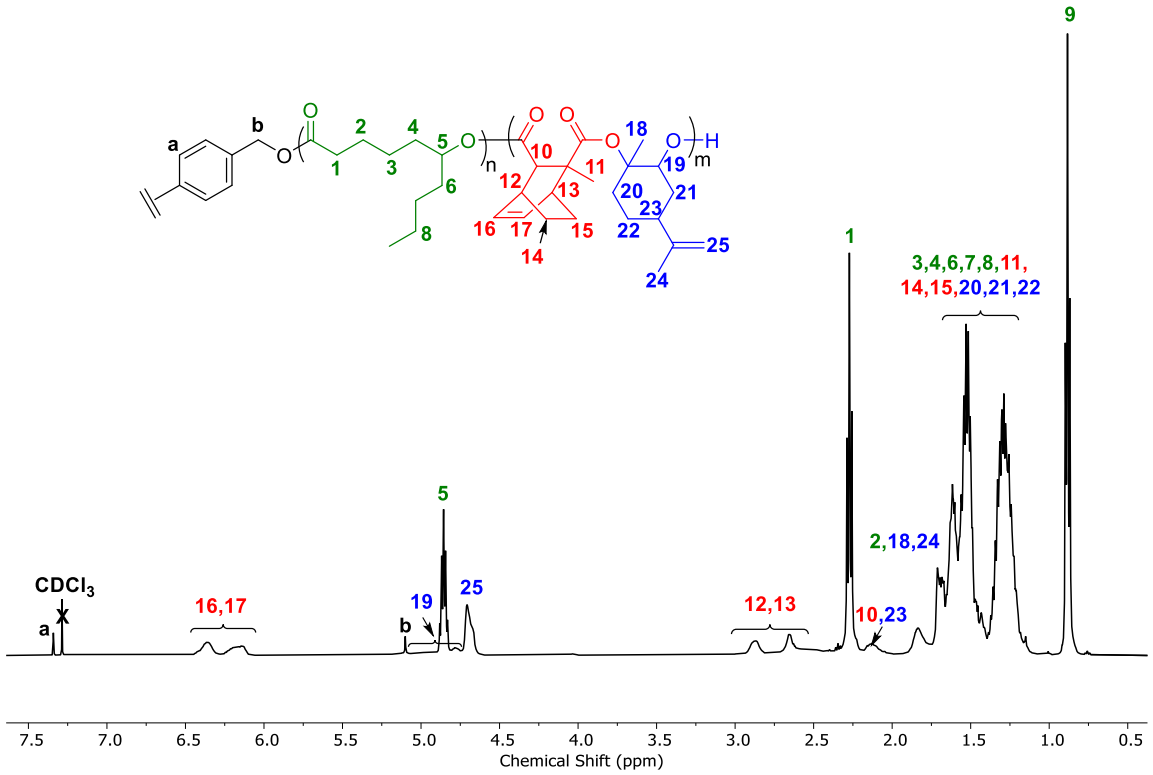


Figure S67. ^{1}H NMR spectrum of **P19** ($CDCl_3$, 500.0 MHz, 298K).

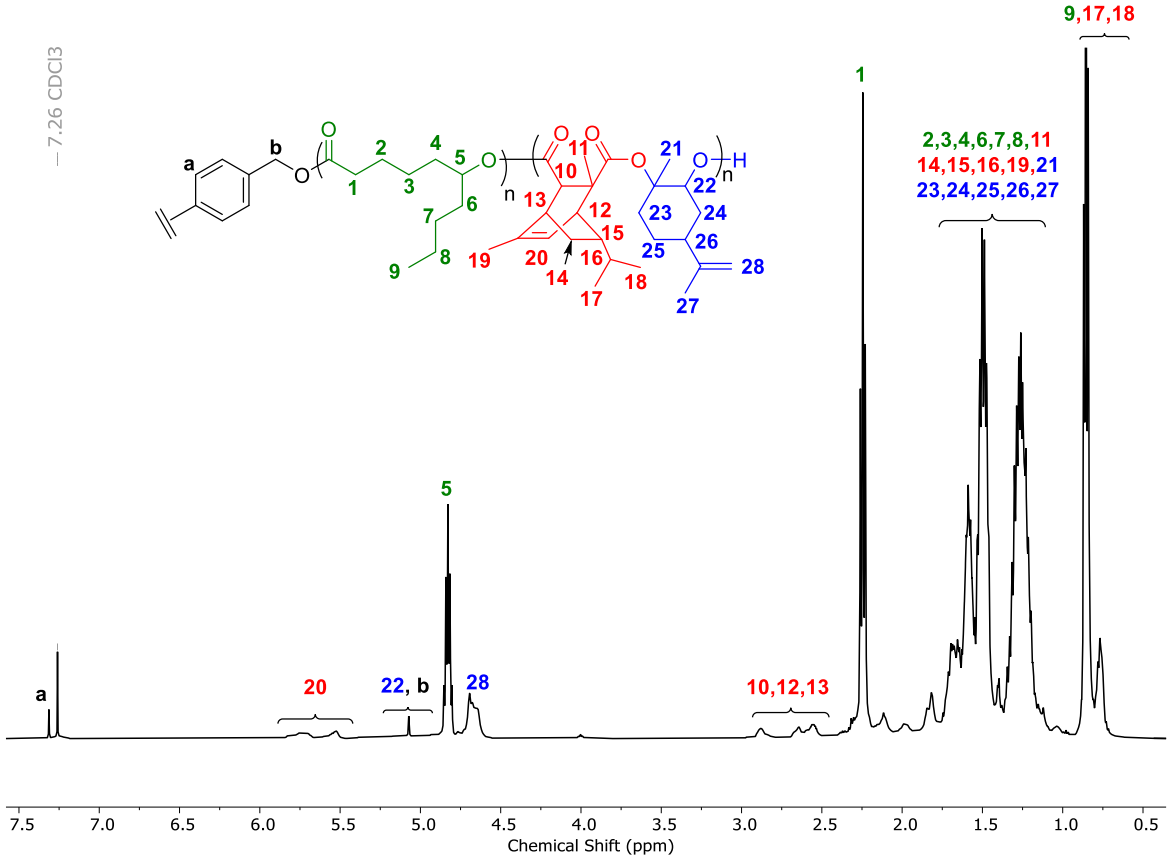


Figure S68. ^{1}H NMR spectrum of **P20** ($CDCl_3$, 500.0 MHz, 298K).

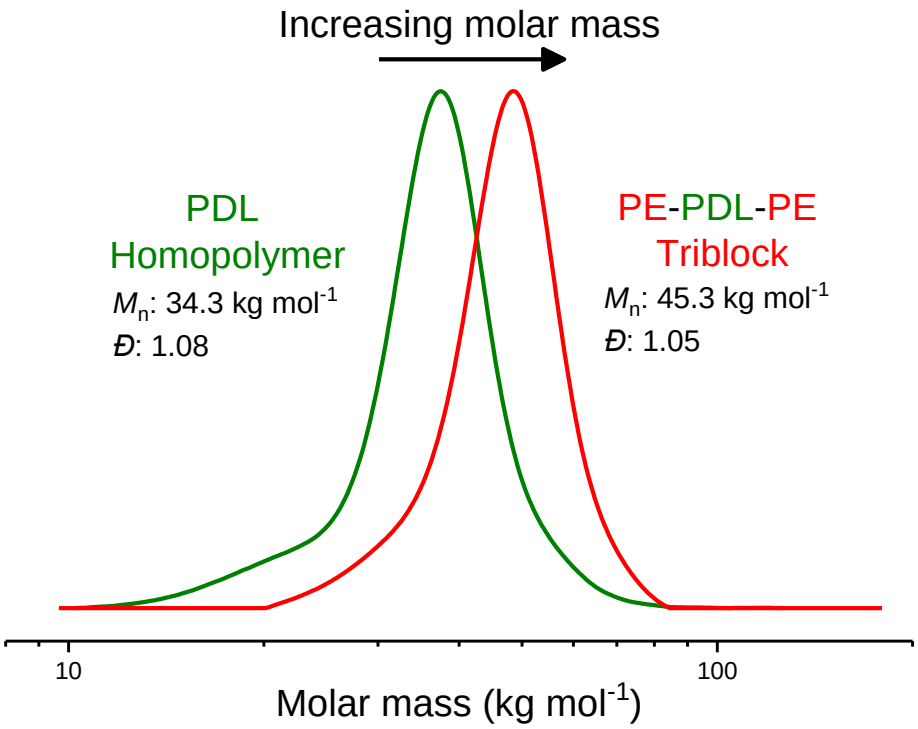


Figure S69. SEC traces illustrating an increase molar mass with retention of very narrow Đ (in THF at 30 °C, calibrated using polystyrene standards) for **P18**.

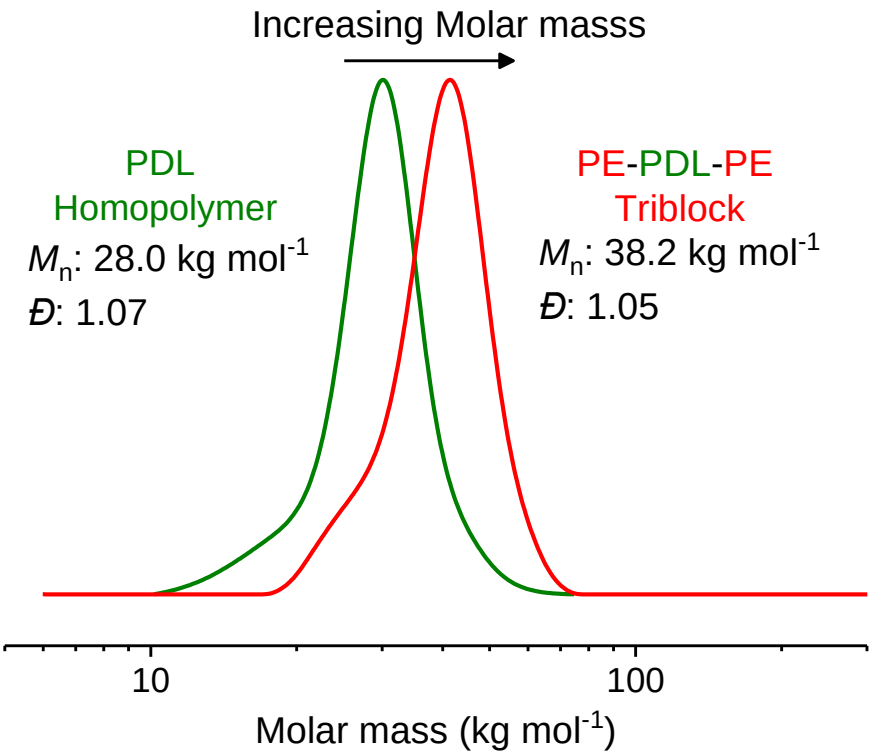


Figure S70. SEC traces illustrating an increase molar mass with retention of very narrow Đ (in THF at 30 °C, calibrated using polystyrene standards) for **P19**.

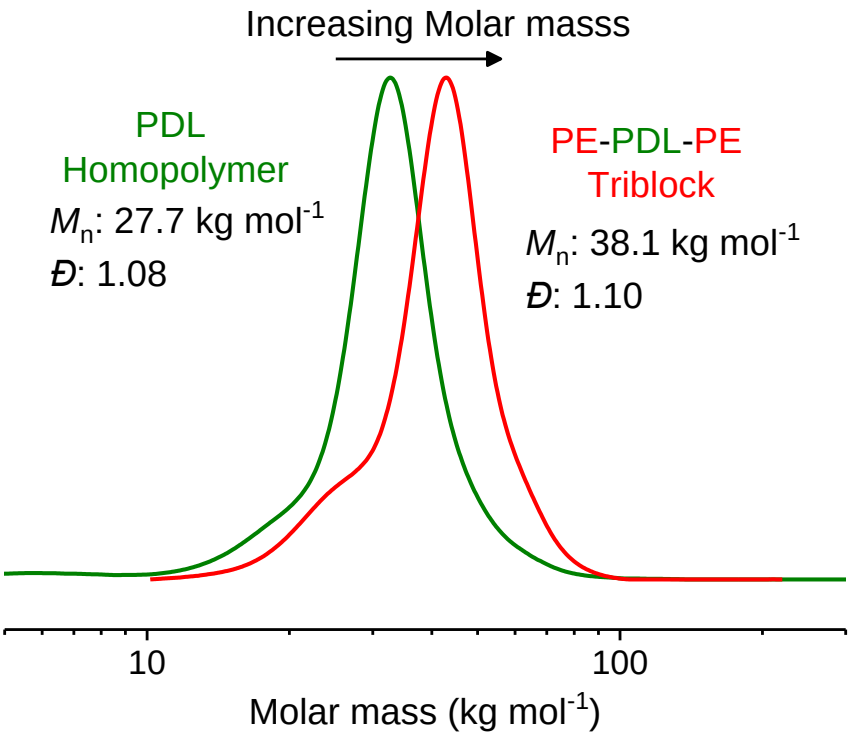


Figure S71. SEC traces illustrating an increase molar mass with retention of very narrow Đ (in THF at 30 °C, calibrated using polystyrene standards) for **P20**.

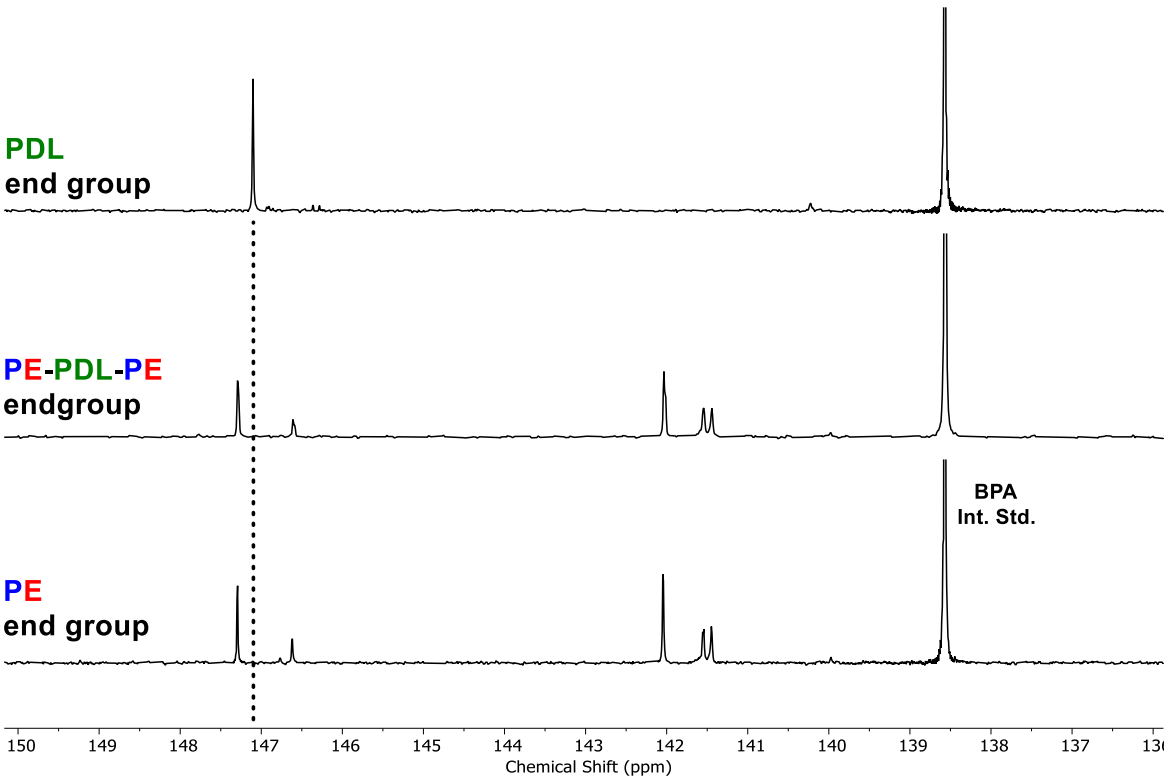


Figure S72. $^{31}P\{^{1}H\}$ NMR spectra of **P18**, PE from LO/TCA 2 ROCOP and PDL hydroxyl polymers (in $CDCl_3$).

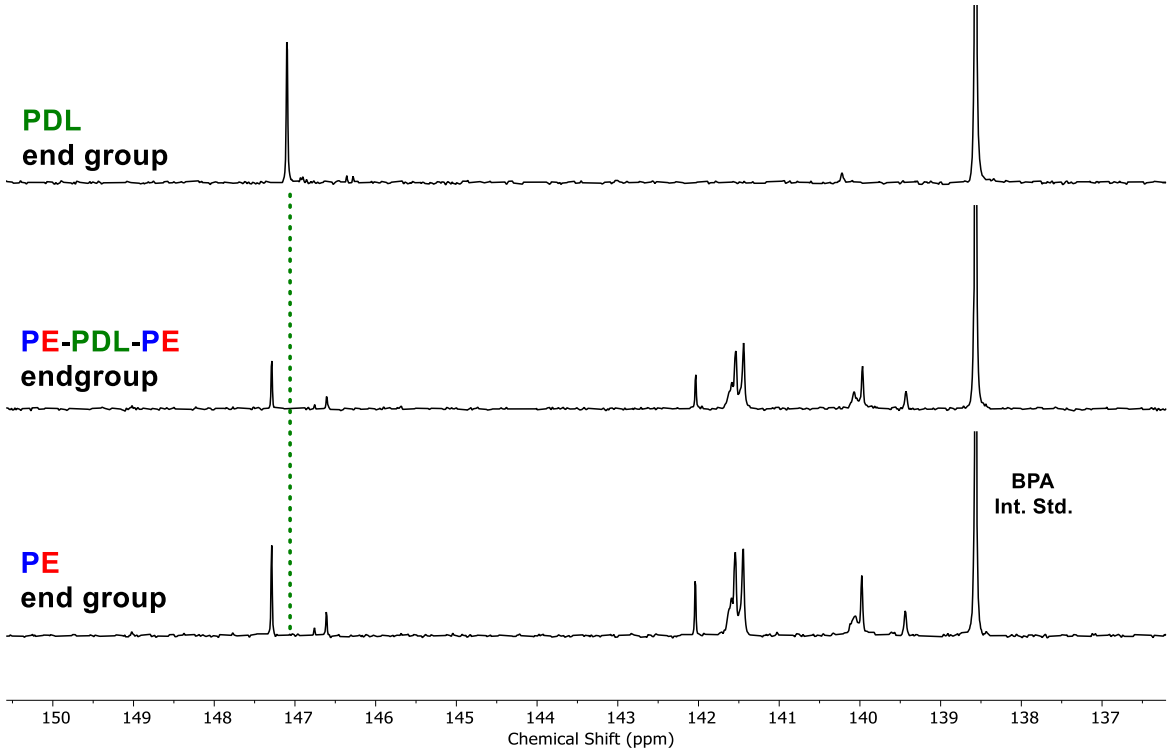


Figure S73. $^{31}P\{^{1}H\}$ NMR spectra of **P19**, PE from LO/TCA 3 ROCOP and PDL hydroxyl polymers (in $CDCl_3$).

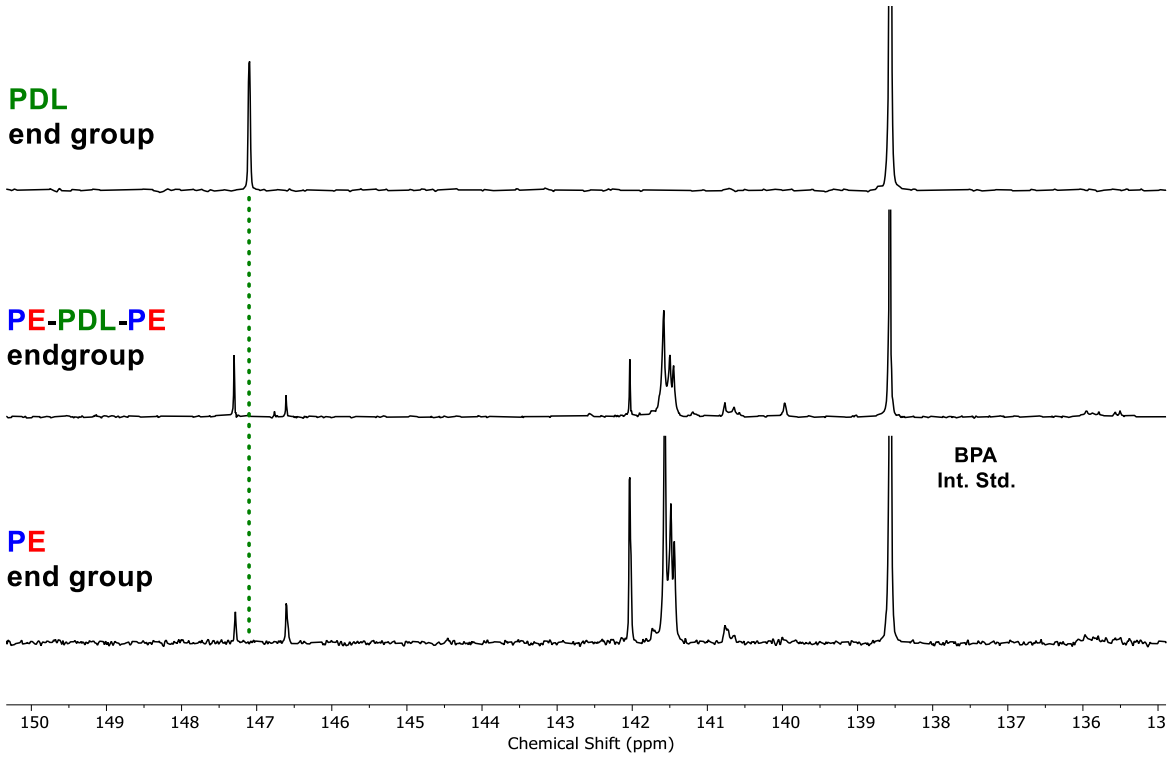


Figure S74. $^{31}P\{^{1}H\}$ NMR spectra of **P20**, PE from LO/TCA 4 ROCOP and PDL hydroxyl polymers (in $CDCl_3$).

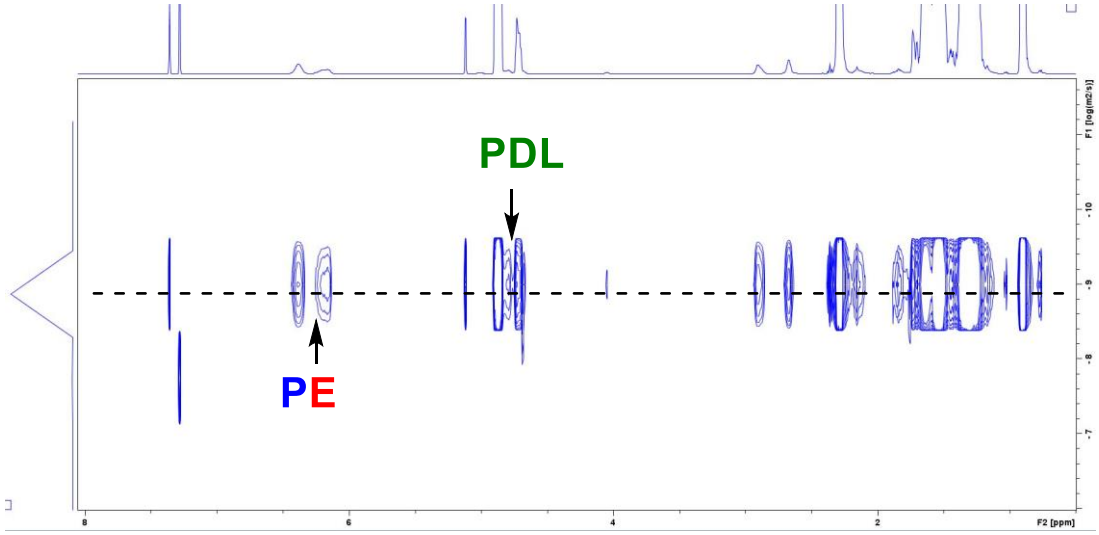


Figure S75. ^{1}H DOSY NMR spectra of **P18** with a single diffusion coefficient (in $CDCl_3$).

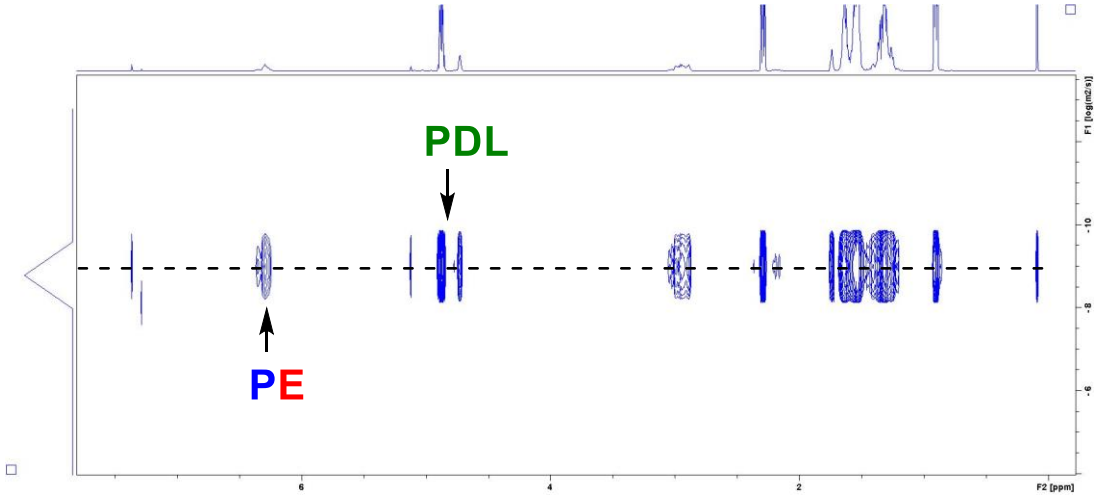


Figure S76. ^{1}H DOSY NMR spectra of **P19** with a single diffusion coefficient (in $CDCl_3$).

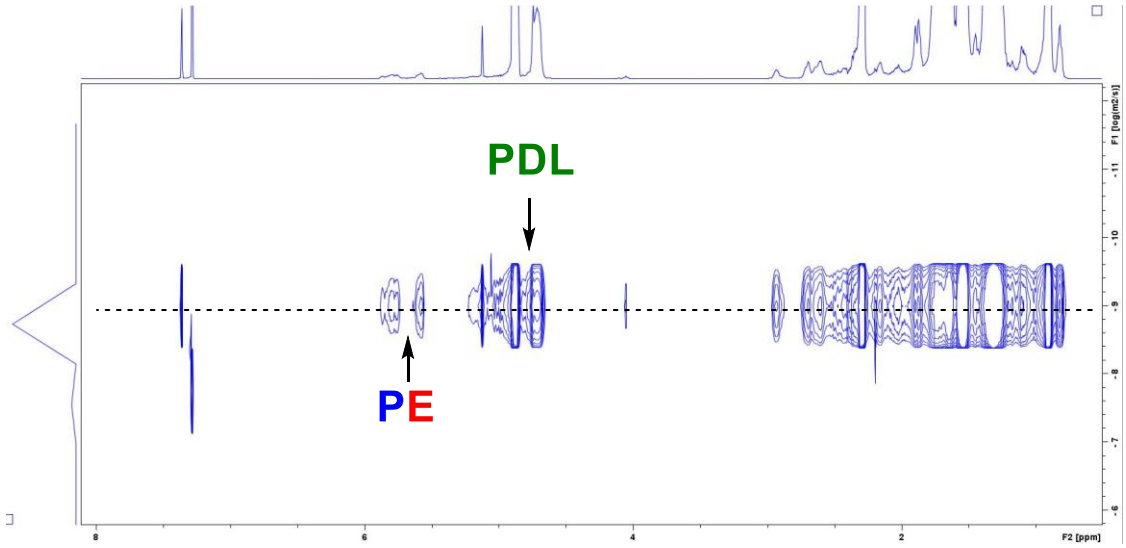


Figure S77. ^{1}H DOSY NMR spectra of **P20** with a single diffusion coefficient (in $CDCl_3$).

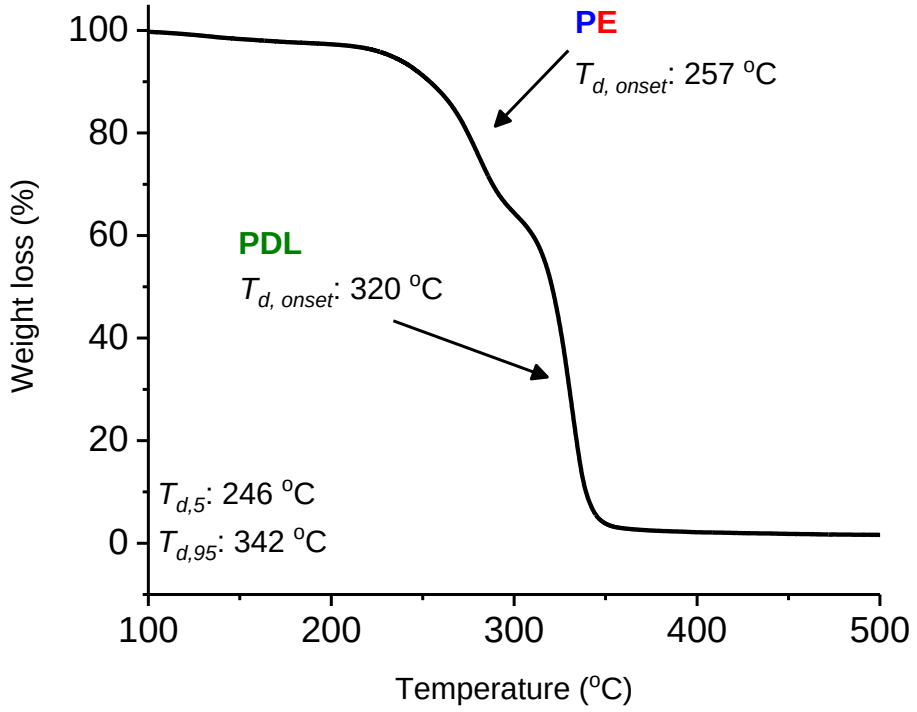


Figure S78. TGA curve of **P18** showing a two-step thermal degradation process.

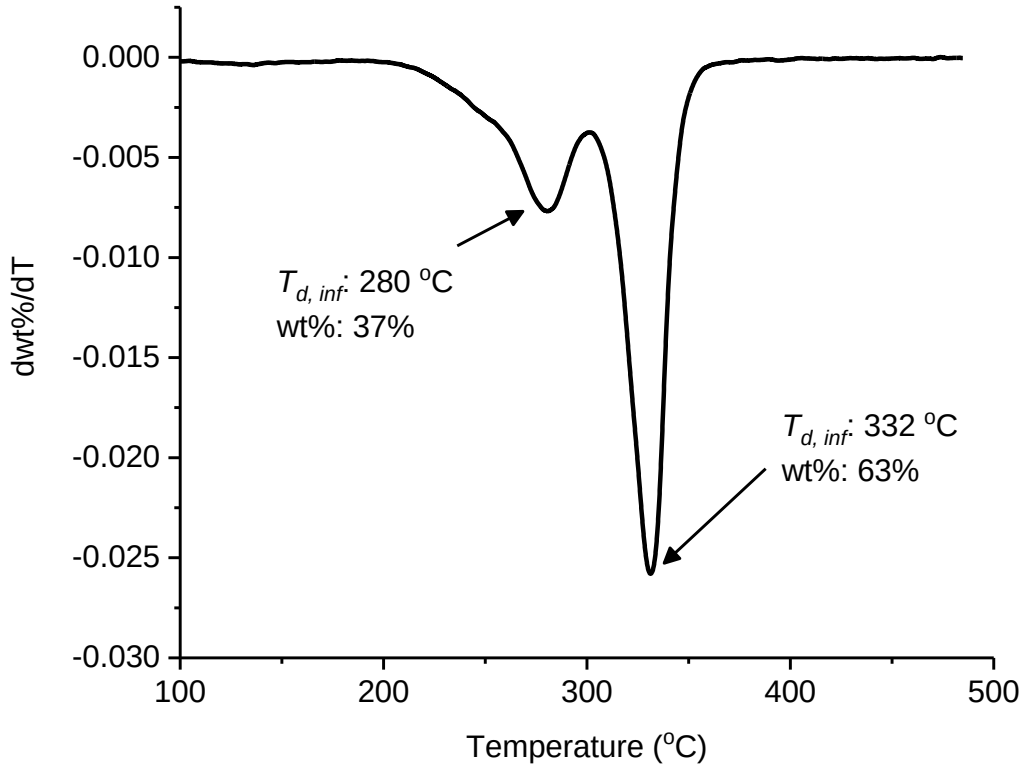


Figure S79. First derivative TGA curve for of **P18**.

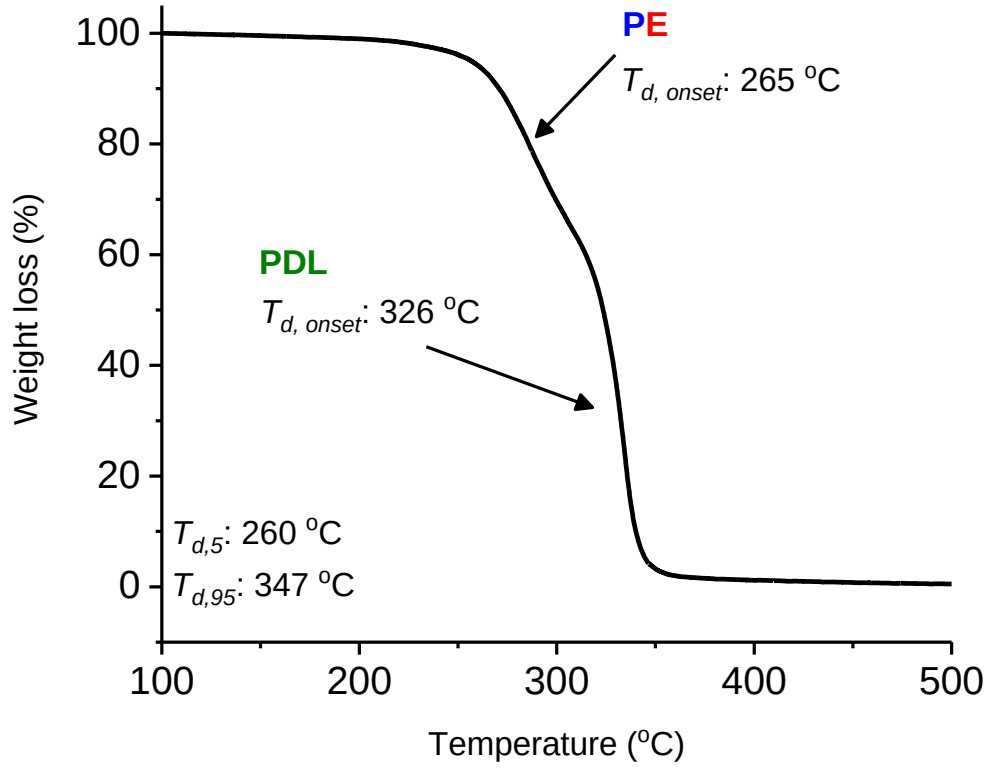


Figure S80. TGA curve of **P19** showing a two-step thermal degradation process.

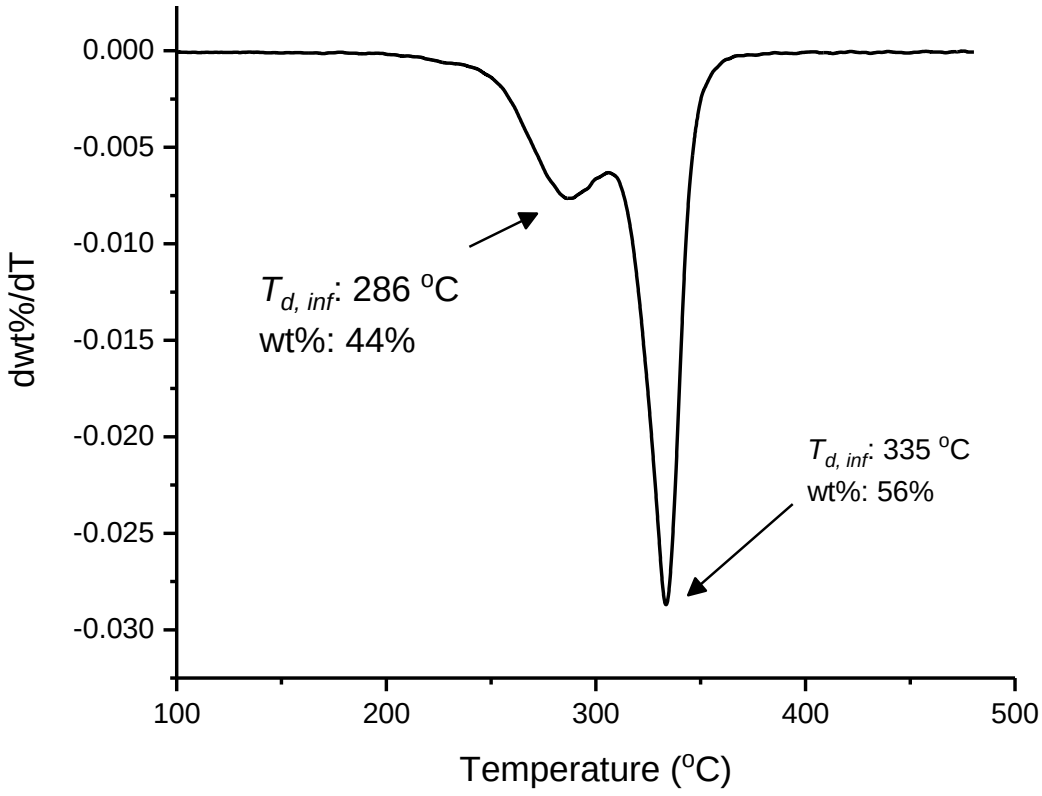


Figure S81. First derivative TGA curve for of **P19**.

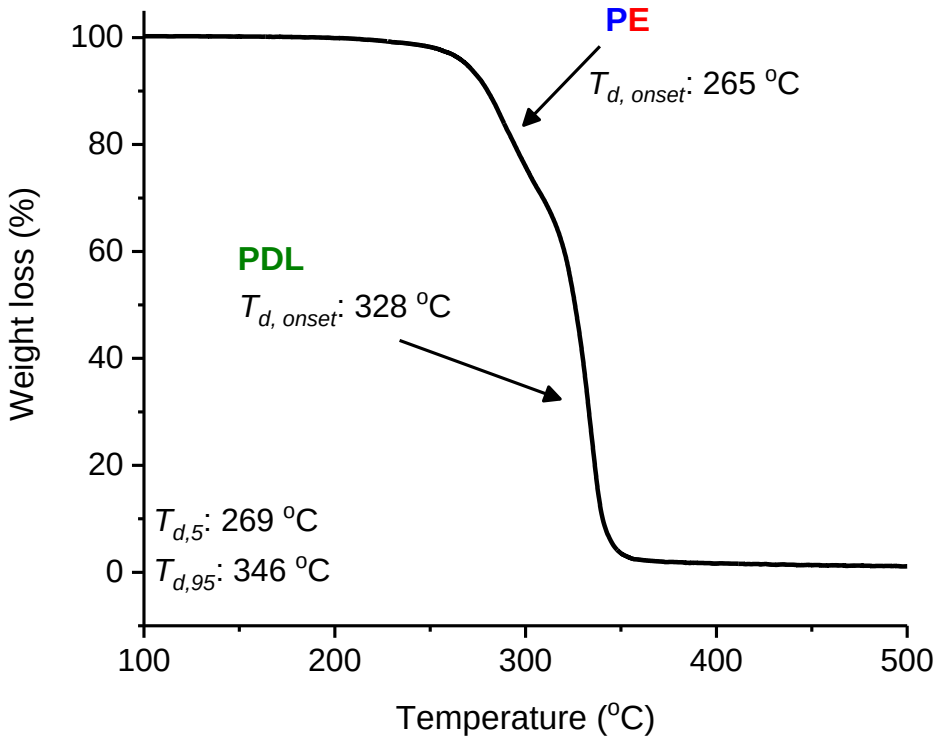


Figure S82. TGA curve of **P20** showing a two-step thermal degradation process.

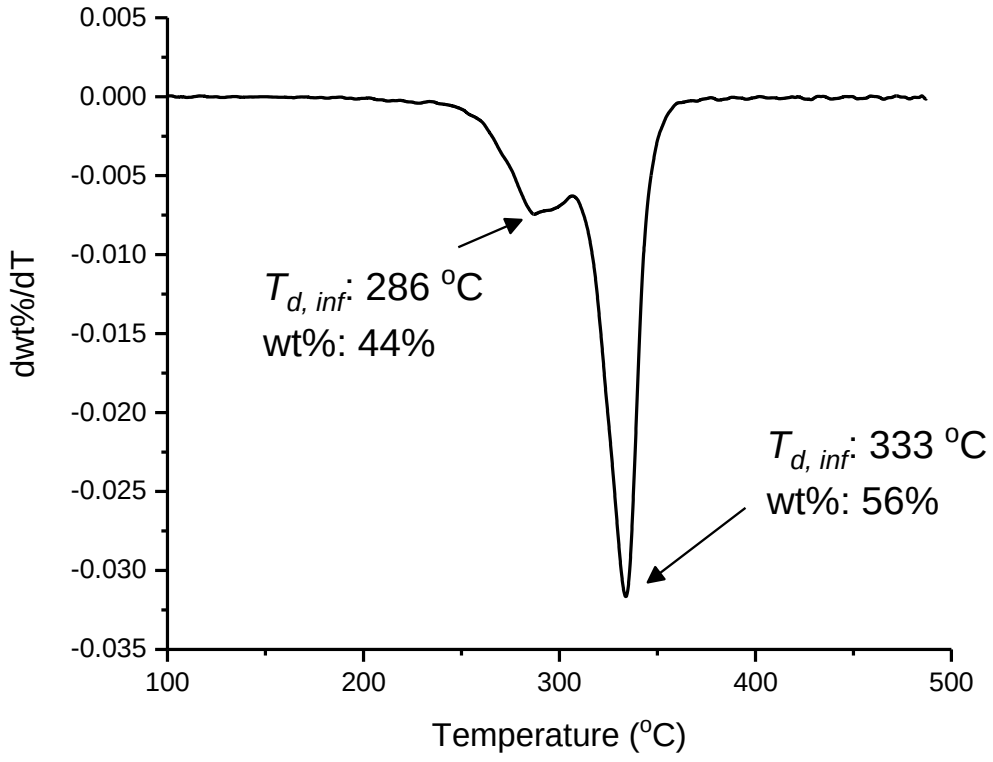


Figure S83. First derivative TGA curve for of **P20**.

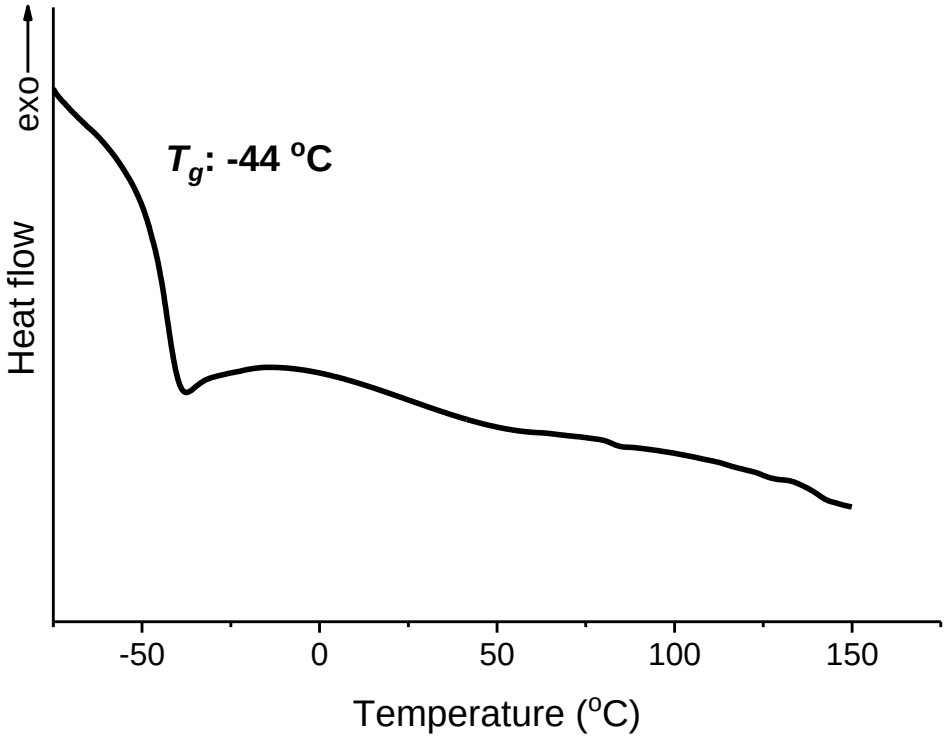


Figure S84. DSC thermograph of **P14** (third cycle).

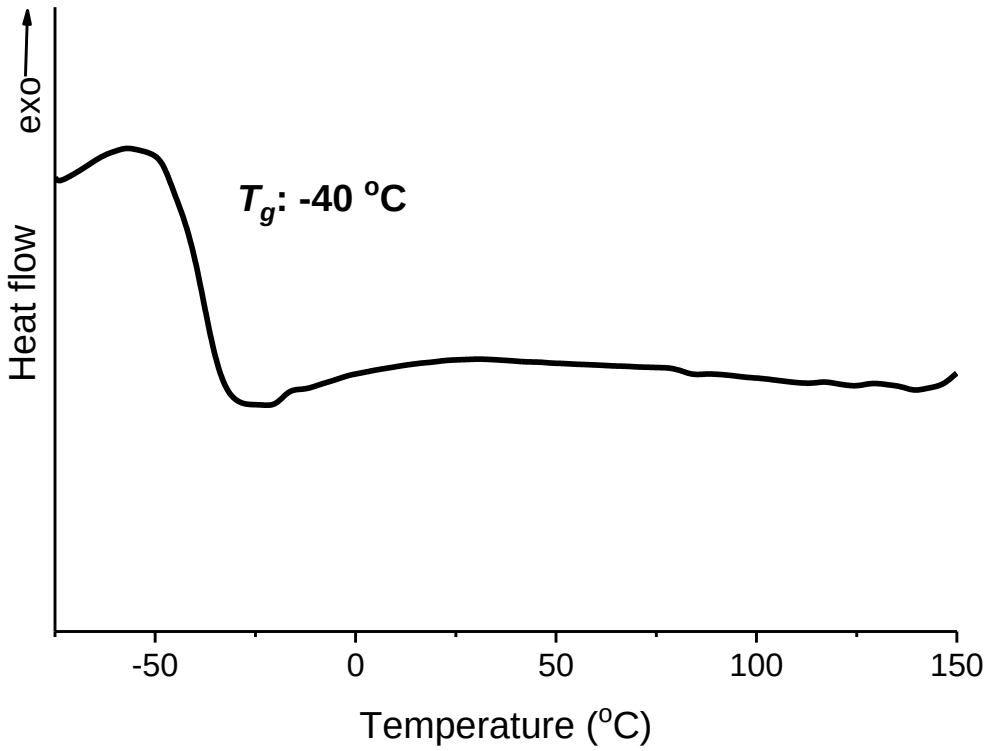


Figure S85. DSC thermograph of **P15** (third cycle).

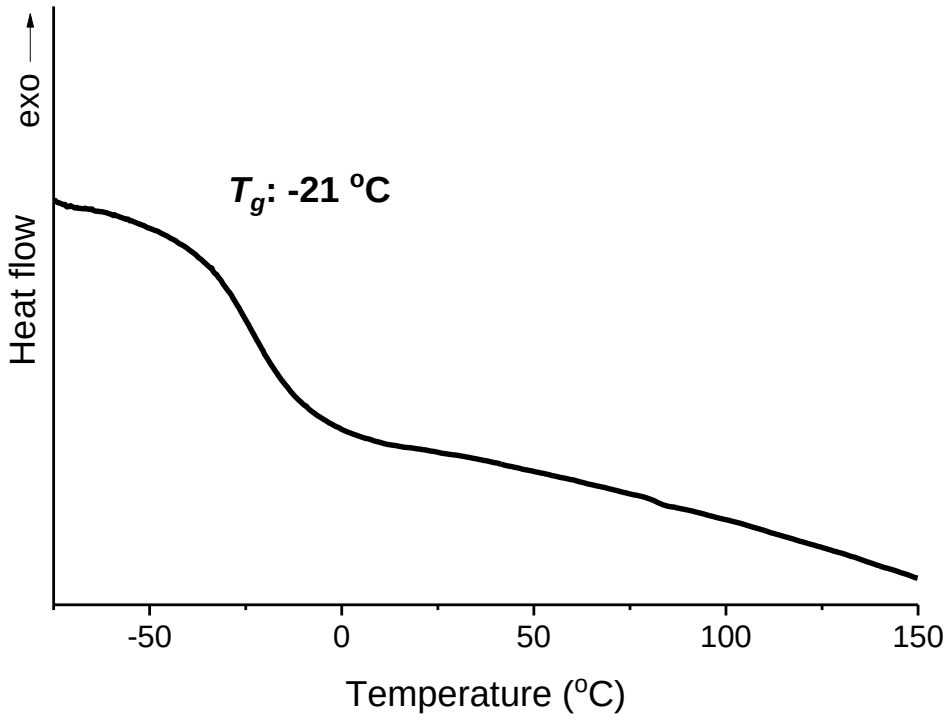


Figure S86. DSC thermograph of **P17** (third cycle).

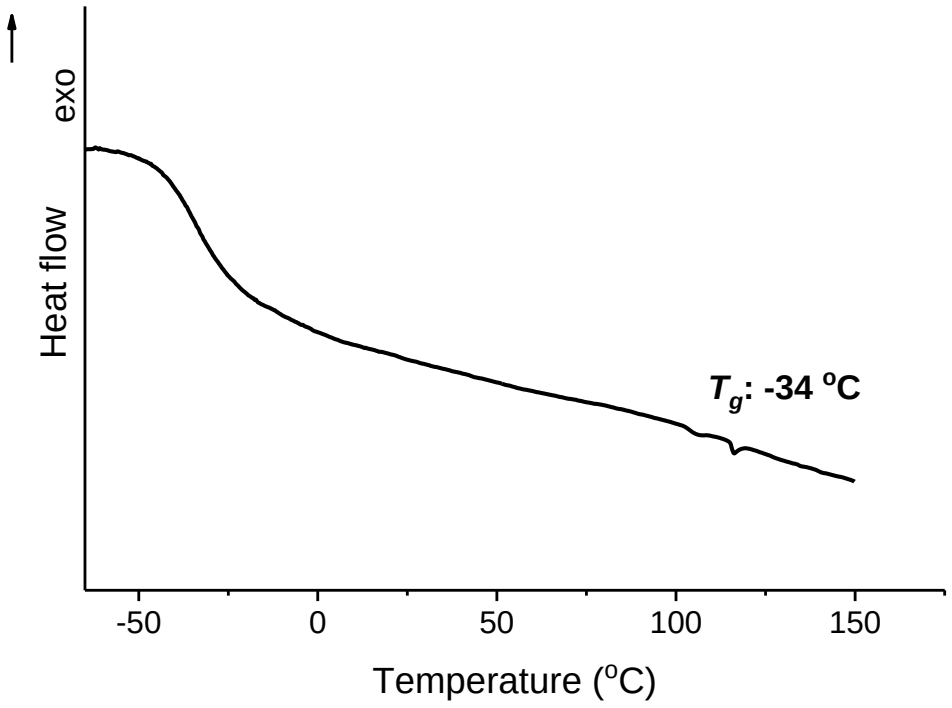


Figure S87. DSC thermograph of **P18** (third cycle).

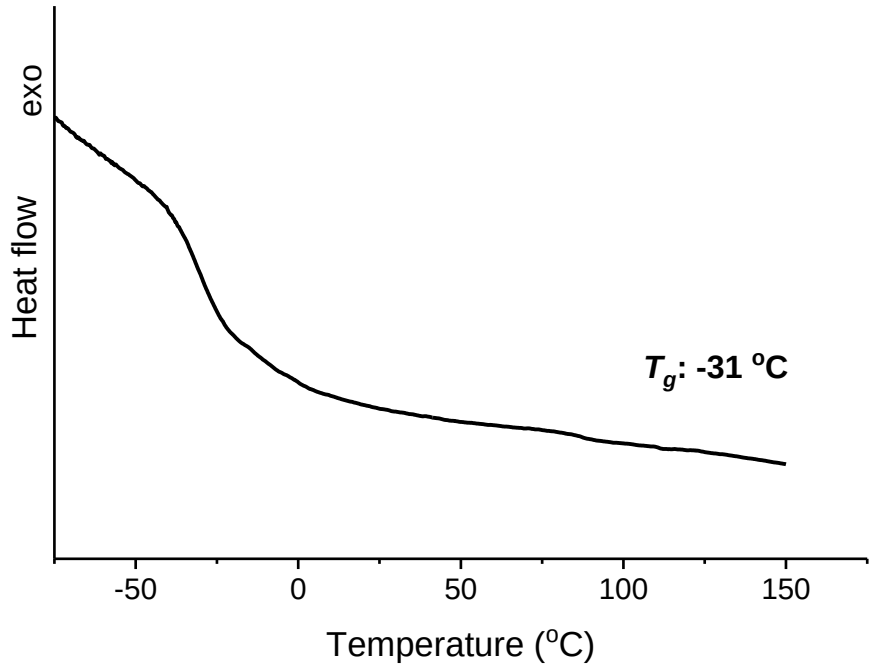


Figure S88. DSC thermograph of **P19** (third cycle).

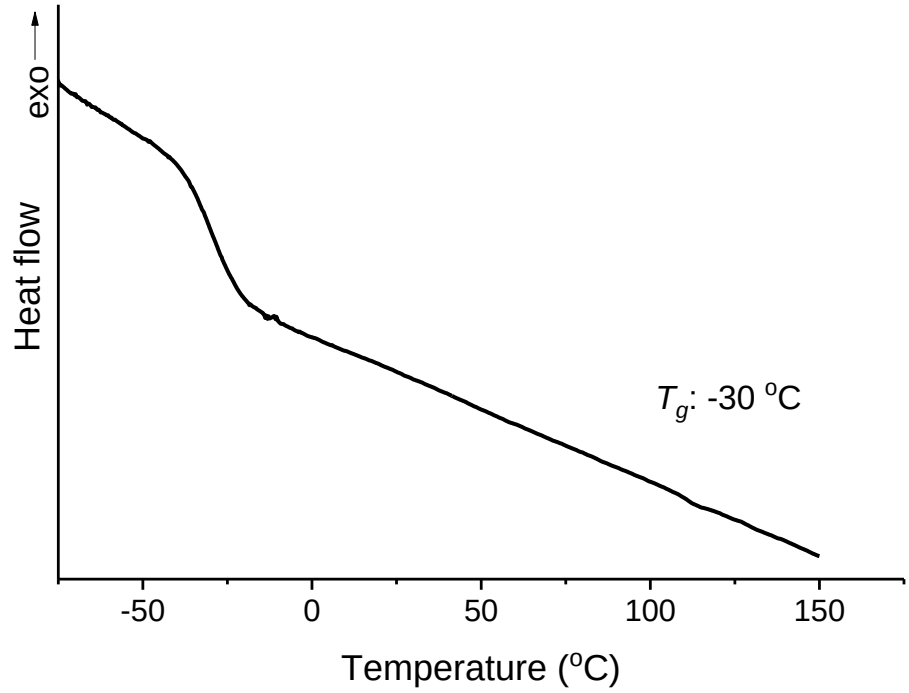


Figure S89. DSC thermograph of **P20** (third cycle).

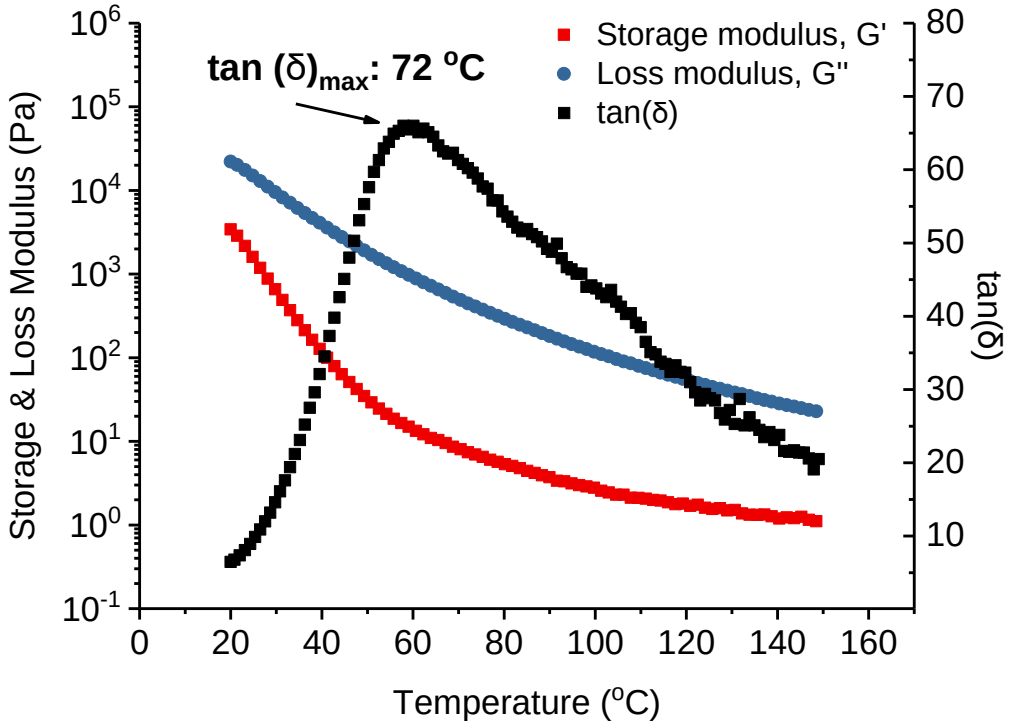


Figure S90. Storage and loss modulus and tan(δ) vs. temperature plot of **P14**.

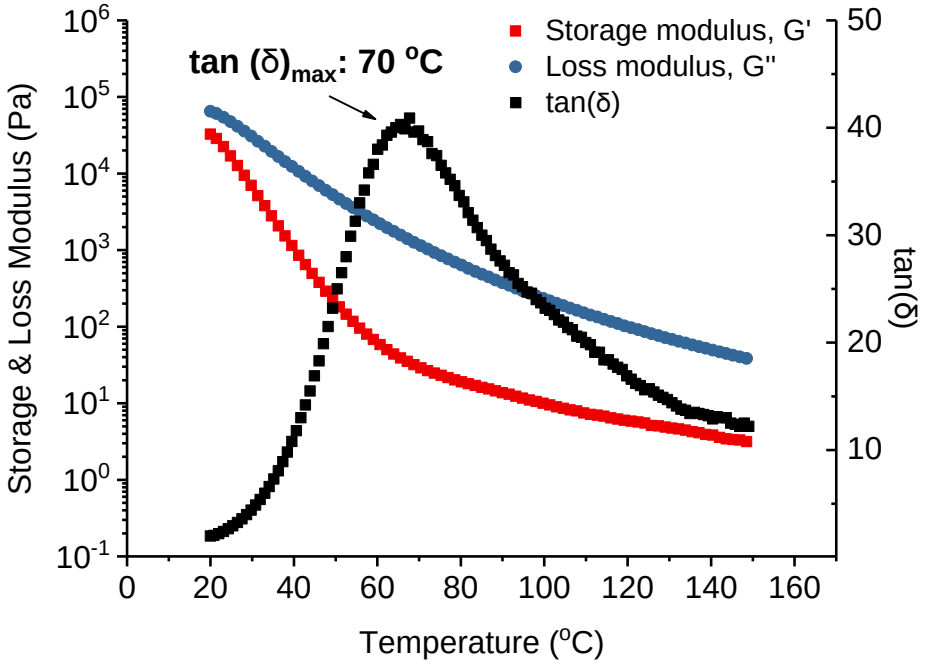


Figure S91. Storage and loss modulus and tan(δ) vs. temperature plot of **P15**.

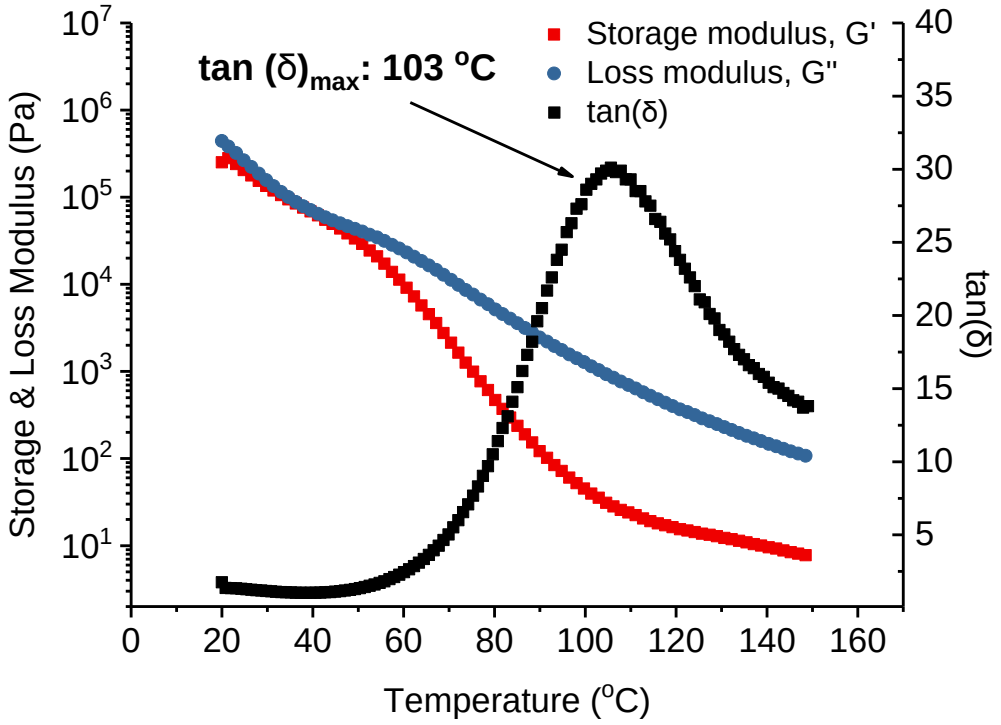


Figure S92. Storage and loss modulus and tan(δ) vs. temperature plot of **P17**.

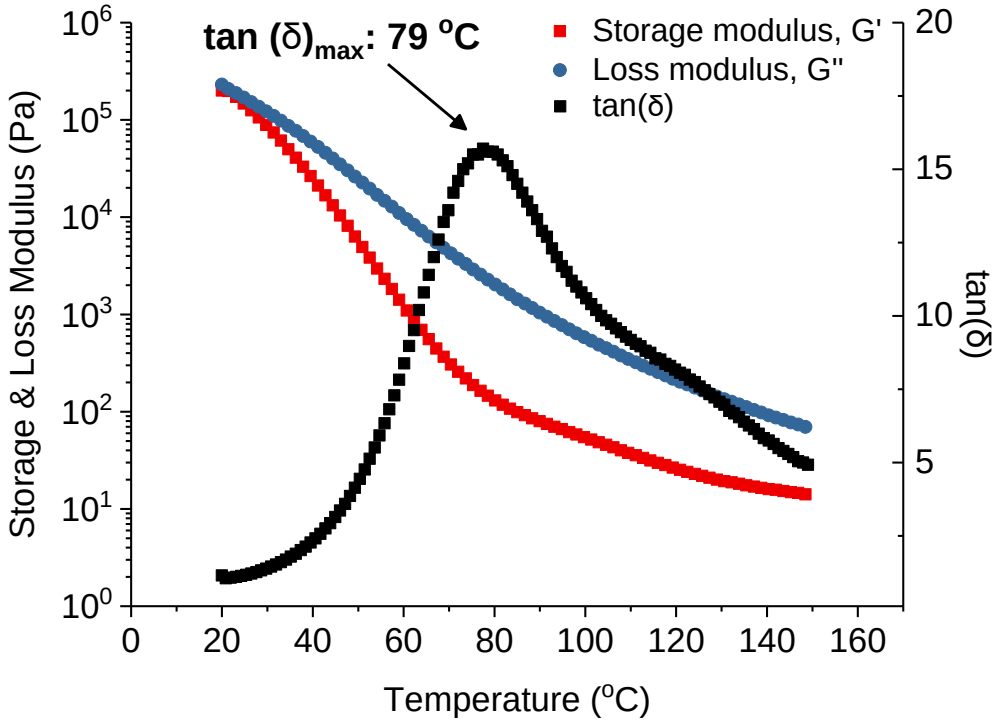


Figure S93. Storage and loss modulus and tan(δ) vs. temperature plot of **P18**

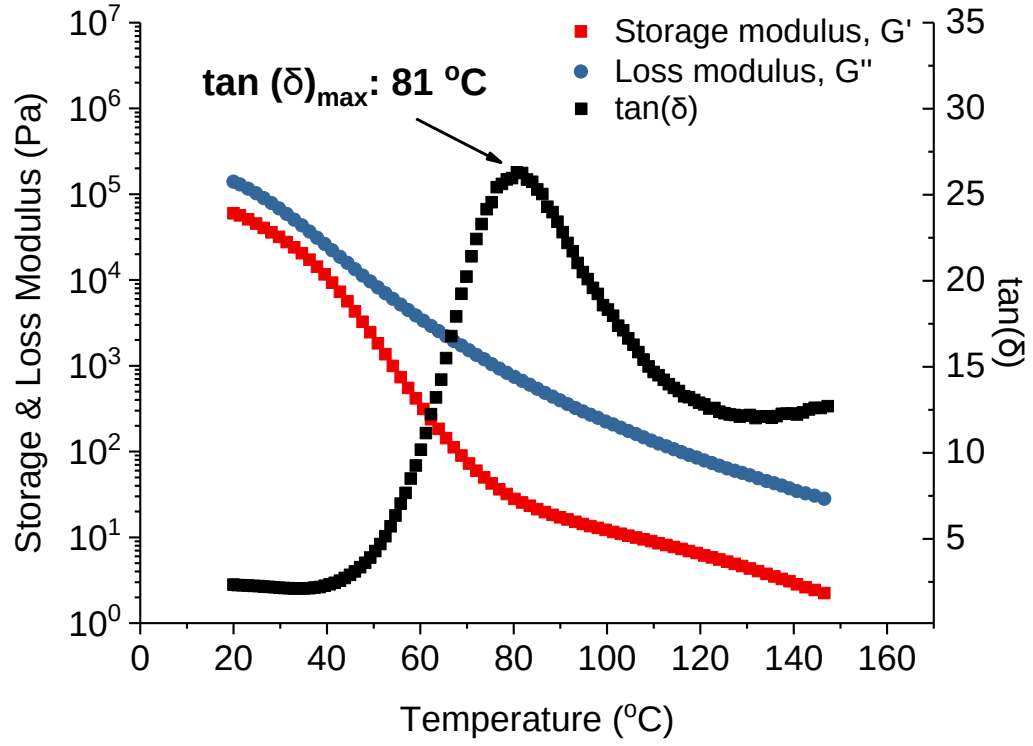


Figure S94. Storage and loss modulus and tan(δ) vs. temperature plot of **P19**

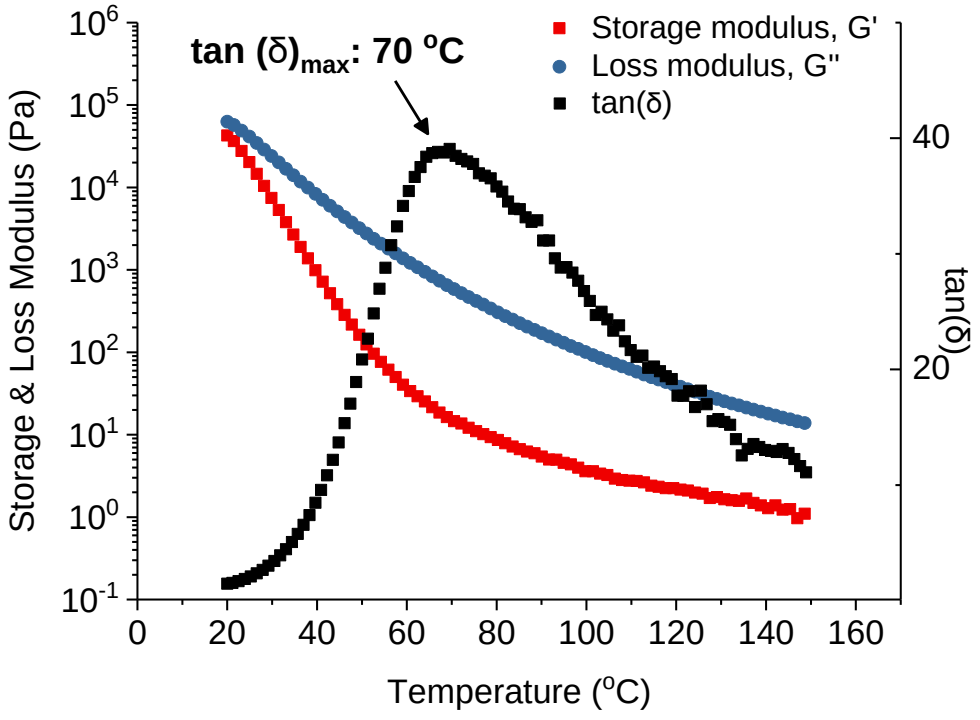


Figure S95. Storage and loss modulus and tan(δ) vs. temperature plot of **P20**

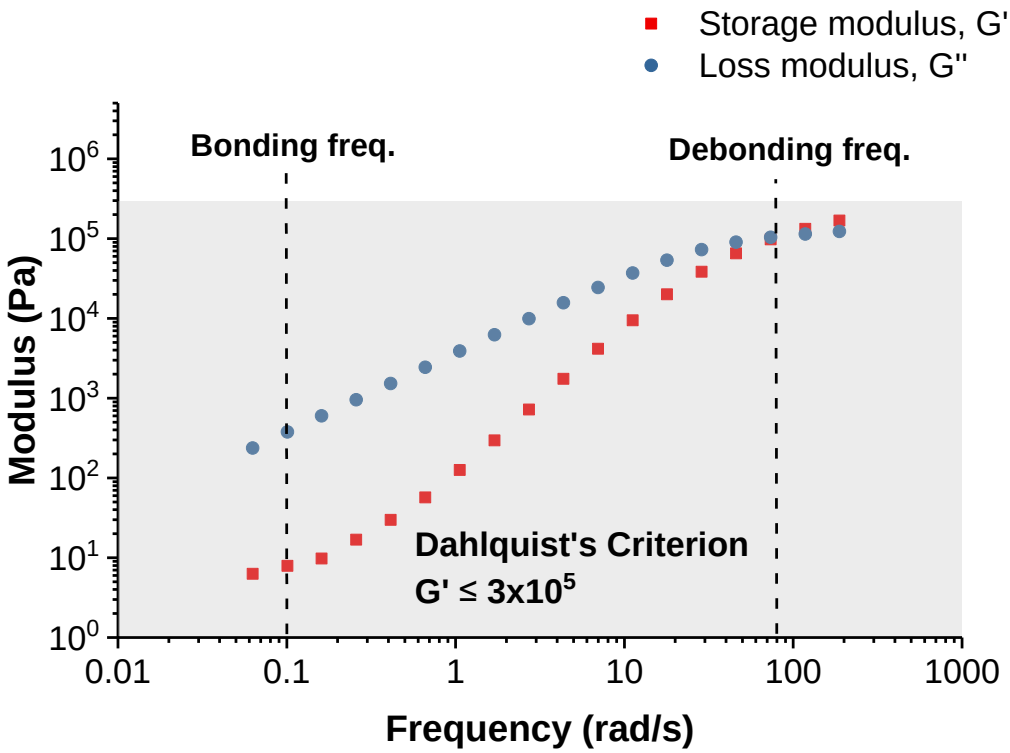


Figure S96. Plot of storage and loss moduli vs. frequency for **P14**.

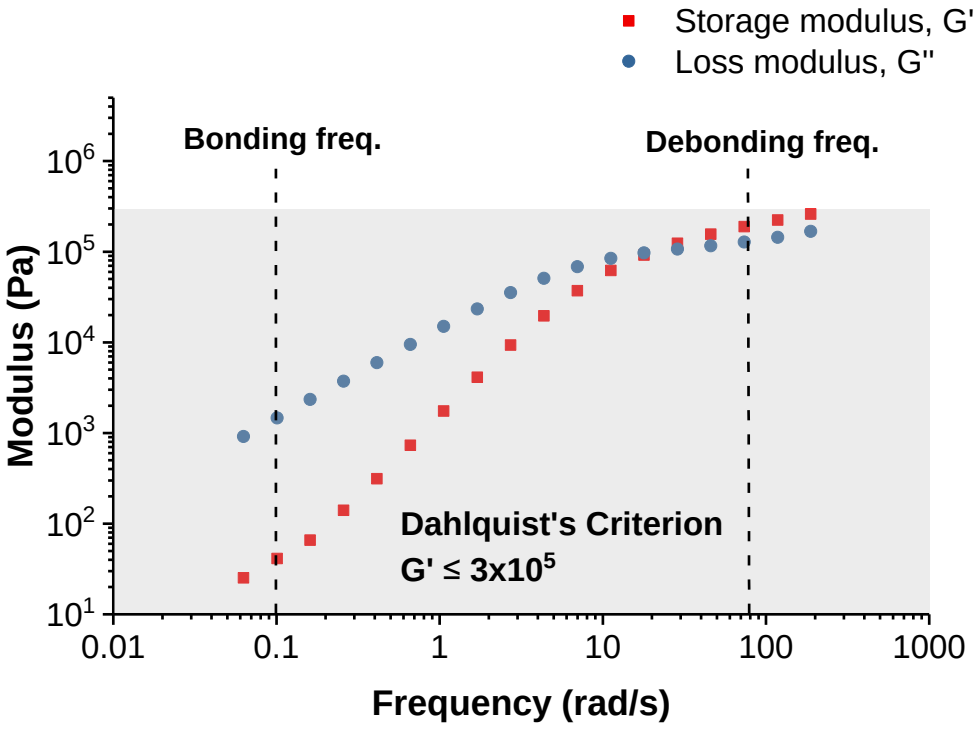


Figure S97. Plot of storage and loss moduli vs. frequency for **P15**.

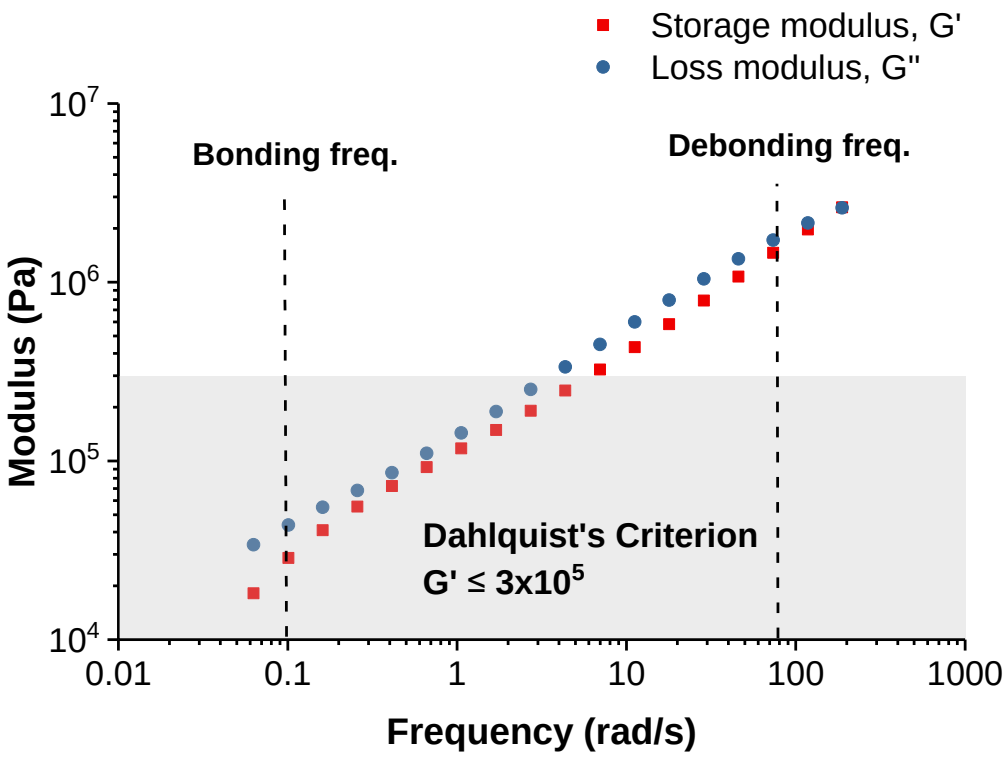


Figure S98. Plot of storage and loss moduli vs. frequency for **P17**.

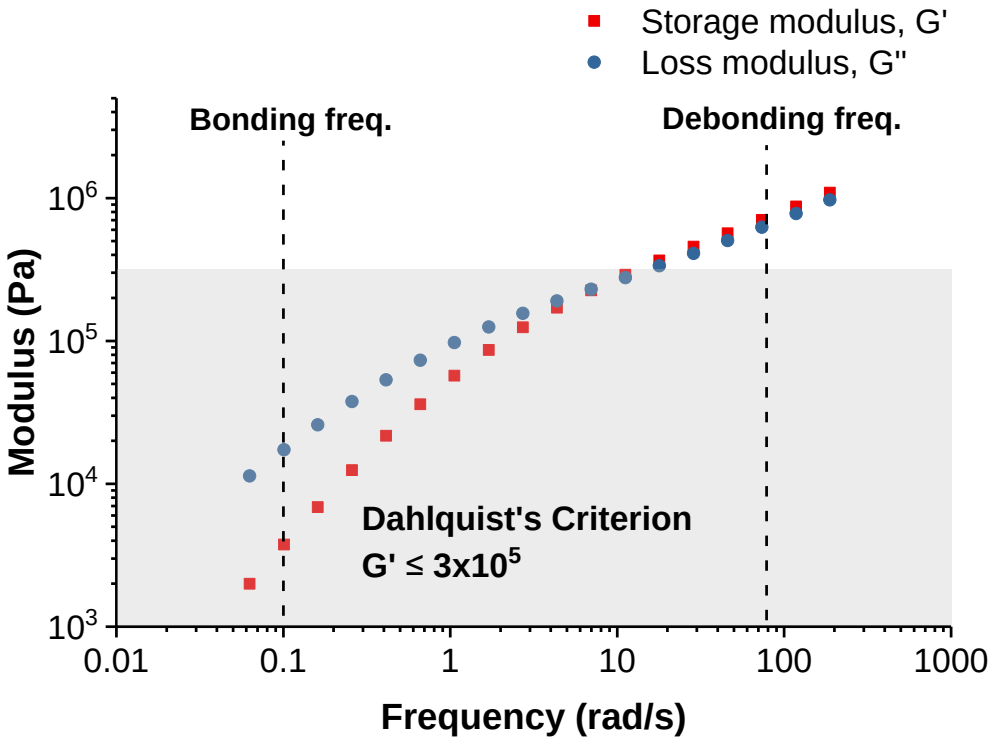


Figure S99. Plot of storage and loss moduli vs. frequency for **P18**.

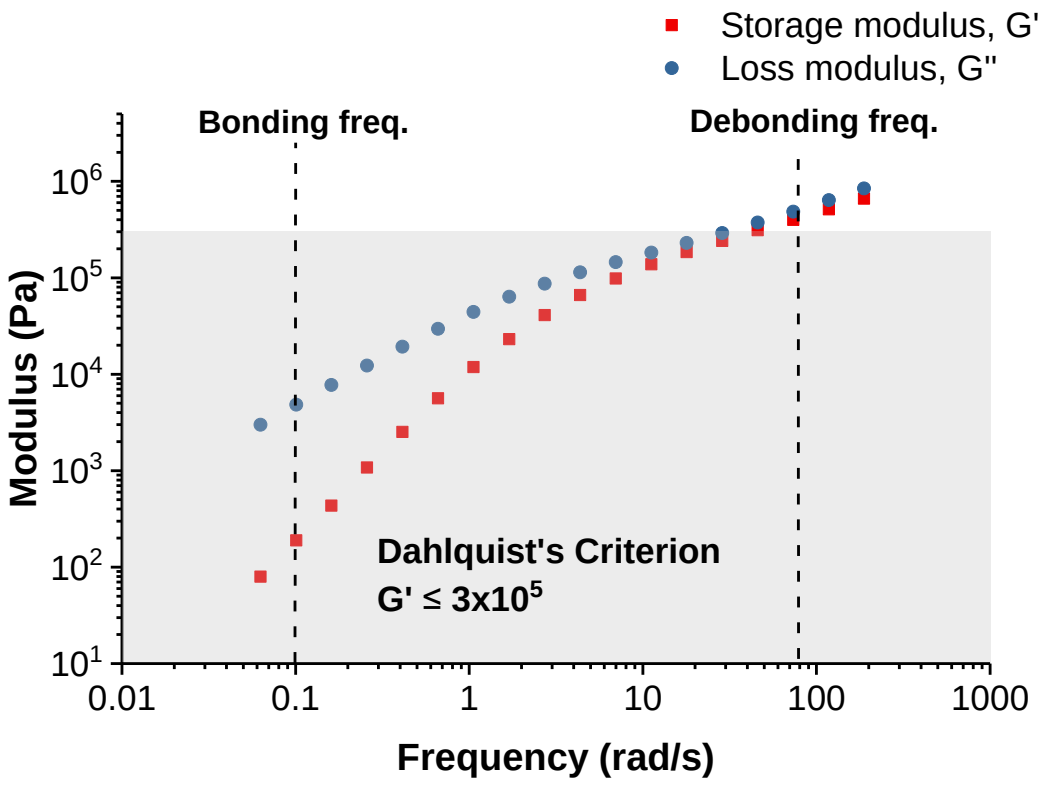


Figure S100. Plot of storage and loss moduli vs. frequency for **P19**.

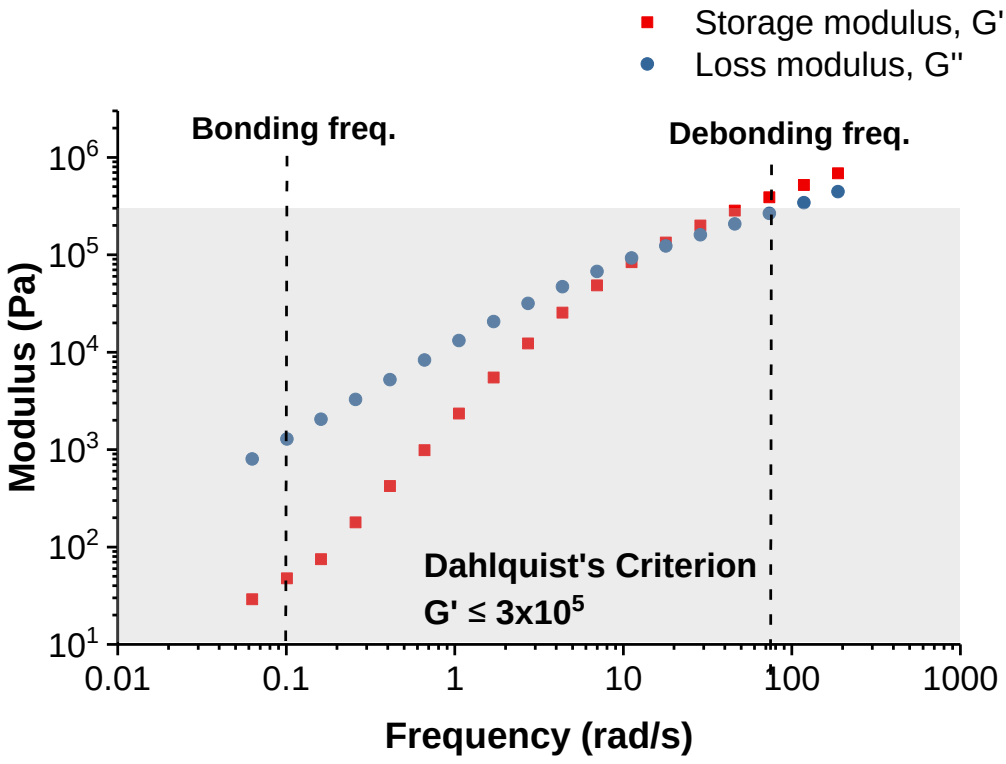


Figure S101. Plot of storage and loss moduli vs. frequency for **P20.**

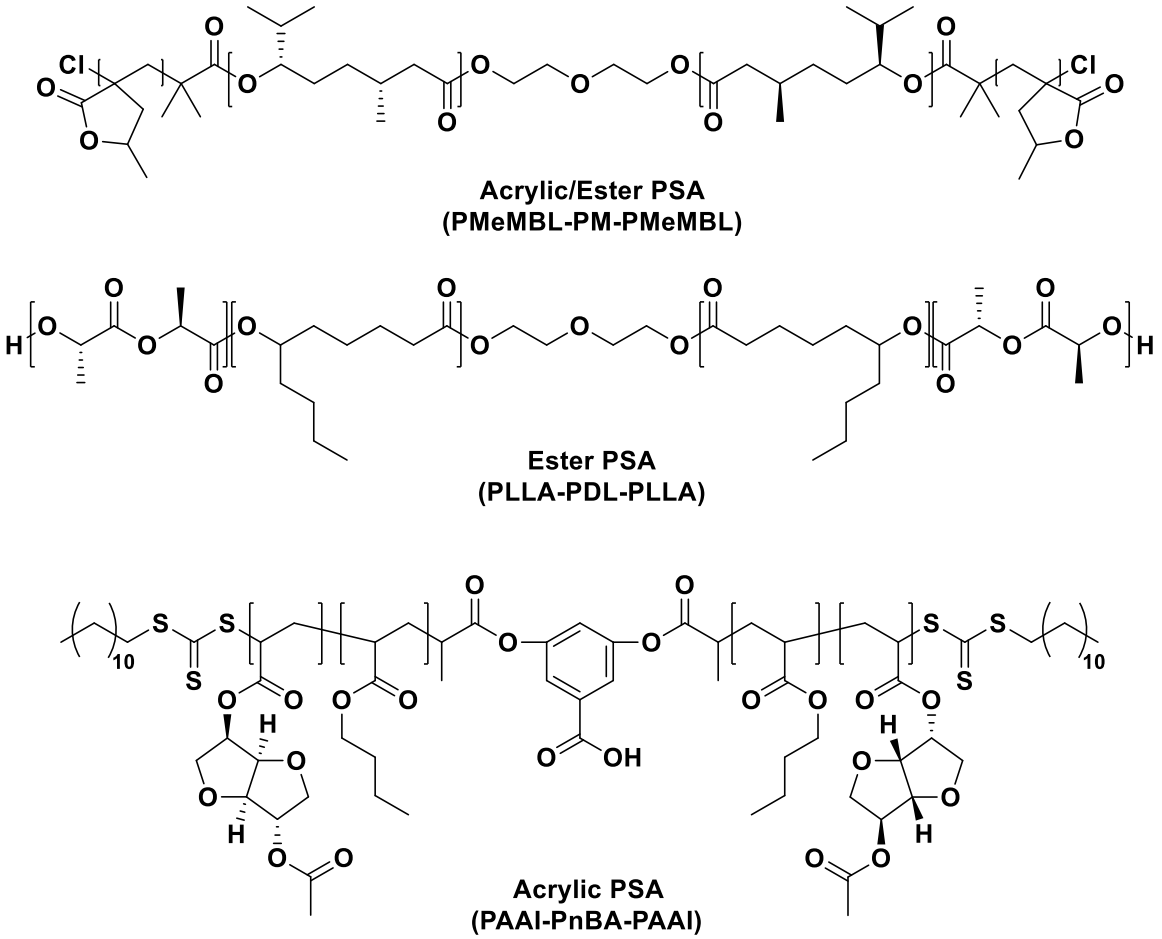


Figure S102. Literature examples of triblock polymer-based PSA

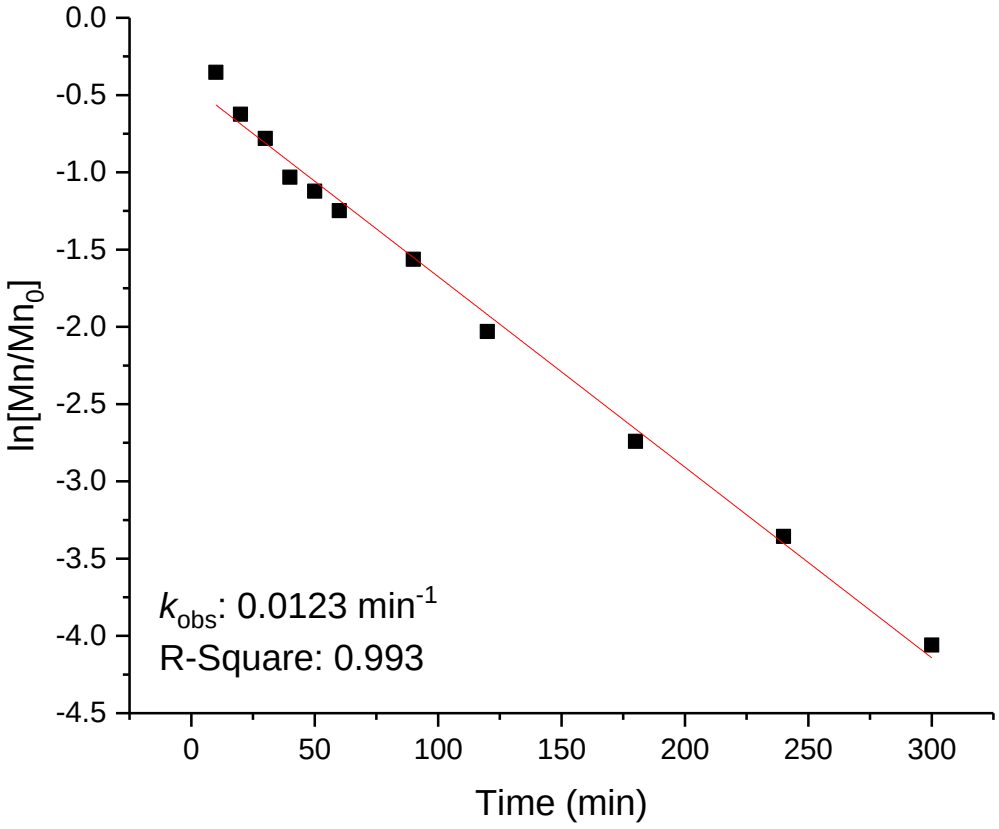


Figure S103. Plot of $\ln(M_n/M_{n0})$ vs time.

7.4. **Chapter 6**

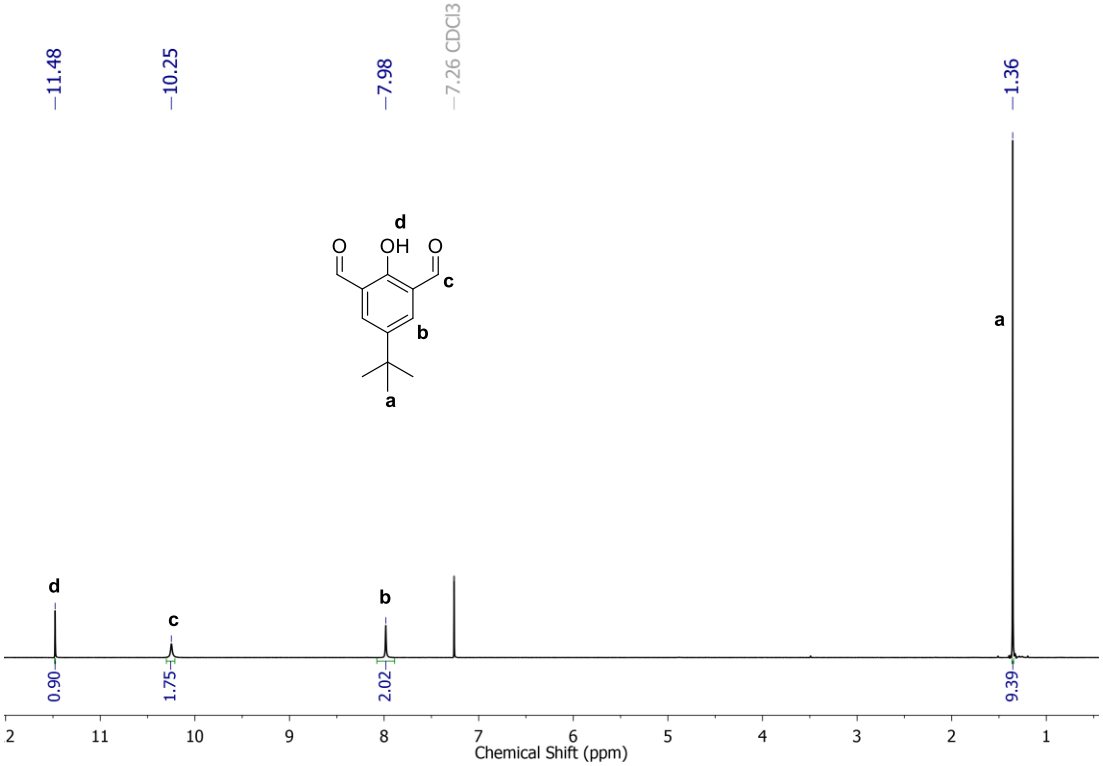


Figure S104. ^{1}H NMR spectrum of 4-tert-butyl-2,6-diformylphenol at 298 K in $CDCl_3$

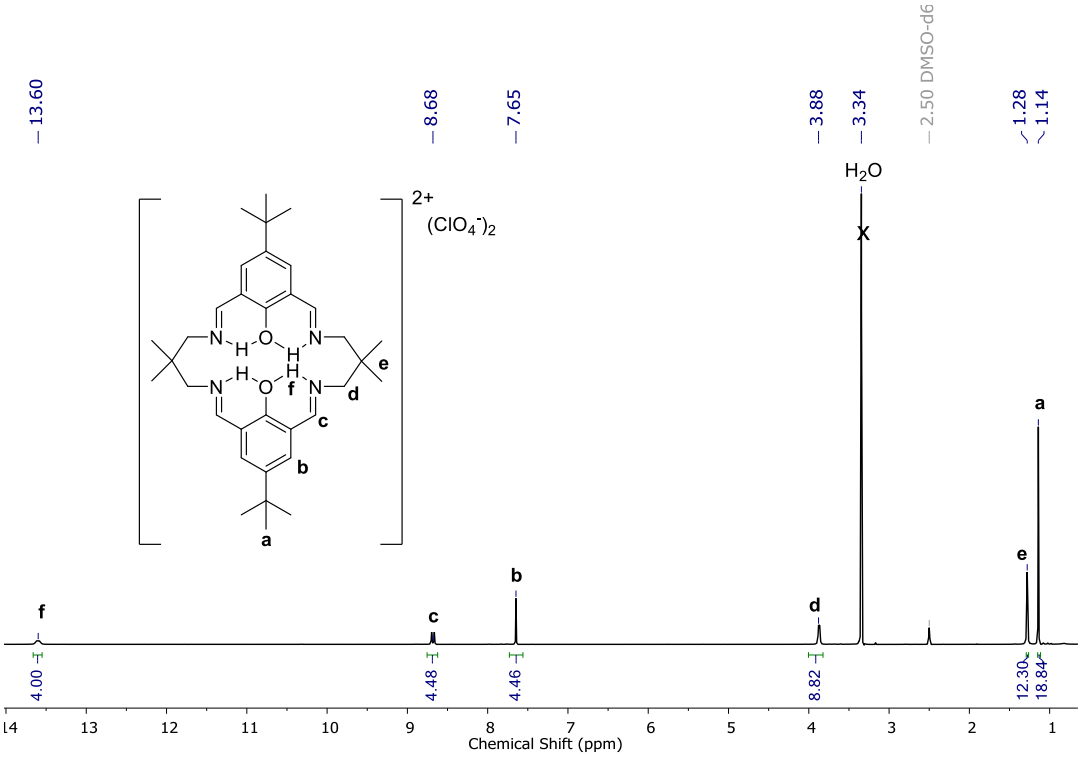
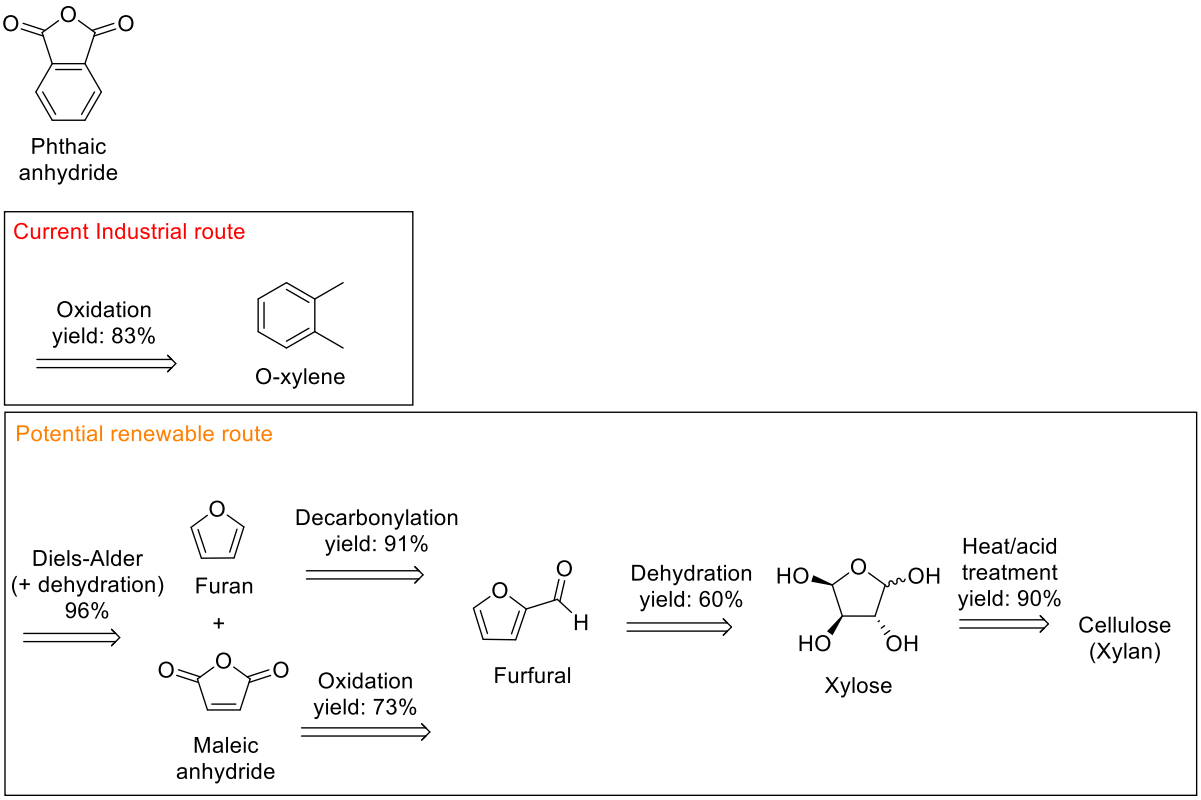
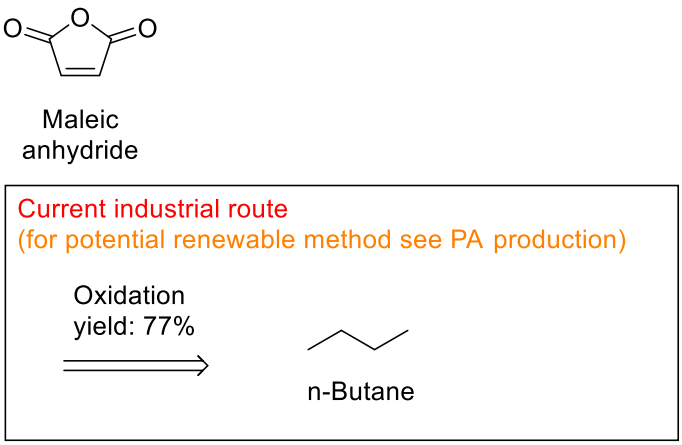


Figure S105. ^{1}H NMR spectrum of $[H_4L](ClO_4)_2$ at 298 K in DMSO-d_6

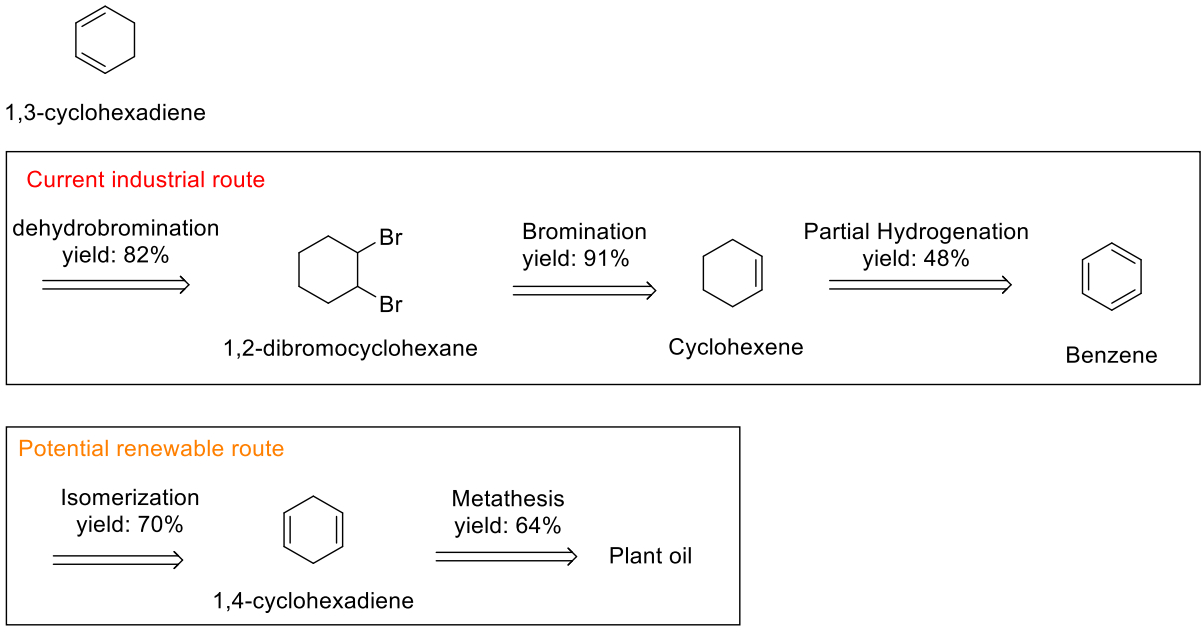
7.5. Synthetic routes to monomers



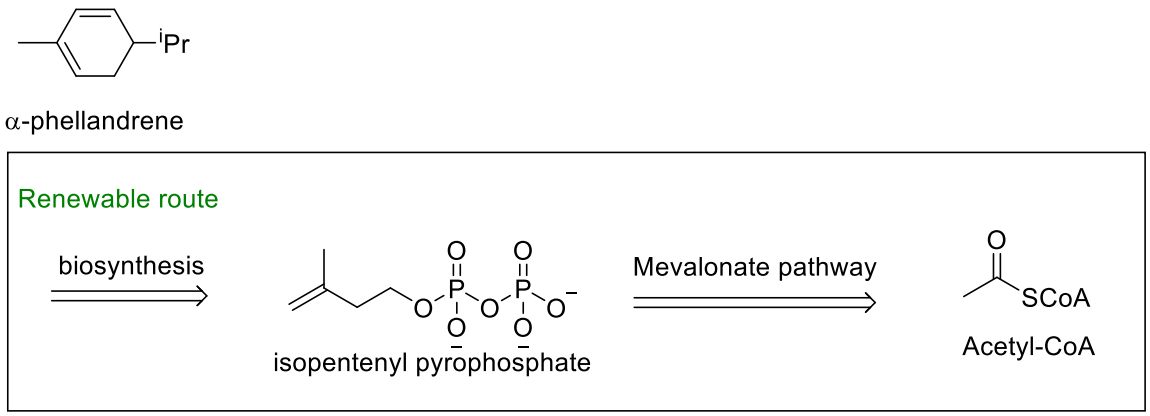
Scheme S3. Industrial and potential renewable routes to phthalic anhydride.[1-3]



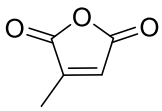
Scheme S4. Industrial and potential renewable routes to maleic anhydride.[4]



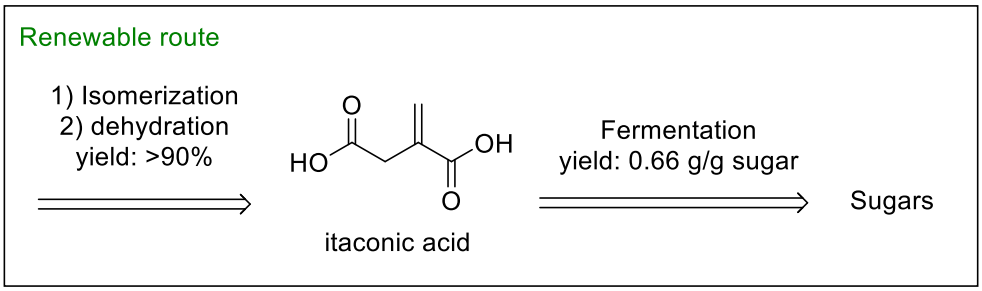
Scheme S5. Industrial and potential renewable routes to 1,3-cyclohexadiene.[5-8]



Scheme S6. Renewable routes to α-phellandrene.[9]



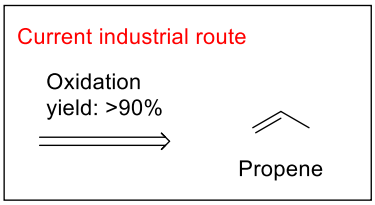
Citraconic anhydride

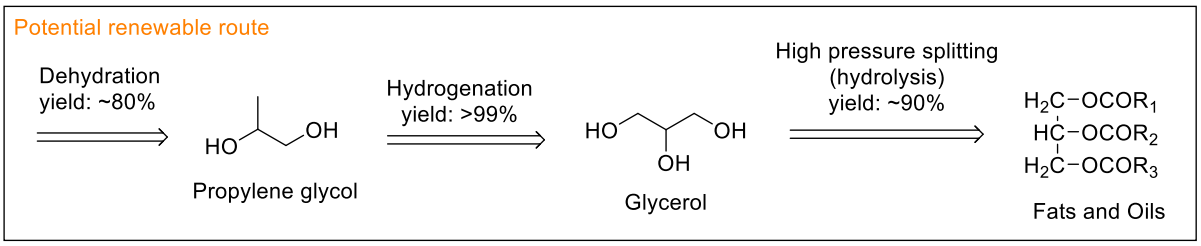


Scheme S7. Renewable routes to citraconic anhydride.[9-10]

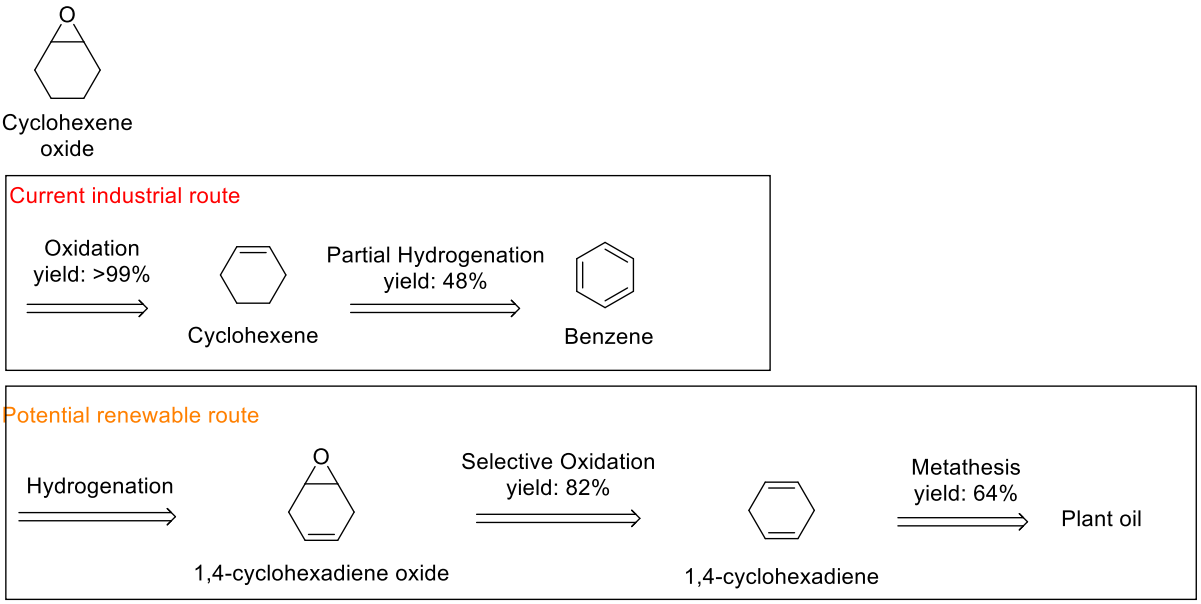


Propylene oxide

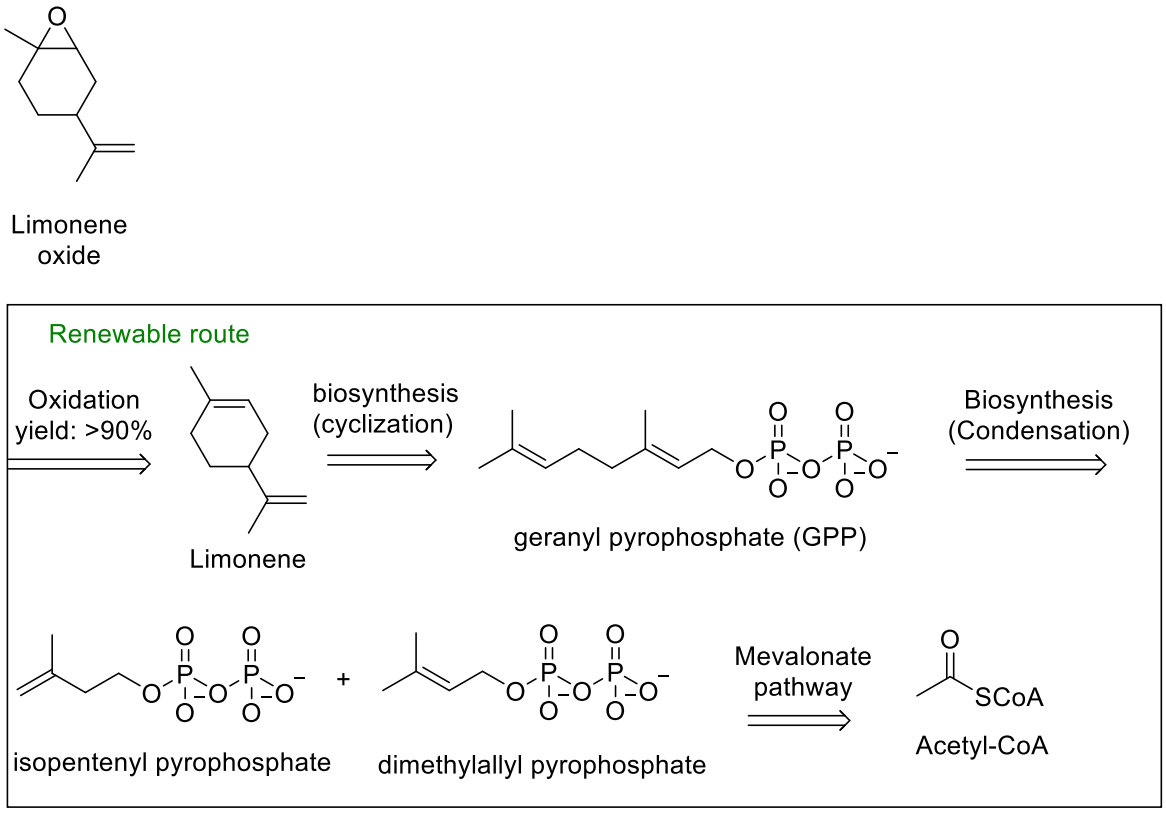




Scheme S8. Industrial and potential renewable routes to propylene oxide.[11-12]



Scheme S9. Industrial and potential renewable routes to cyclohexene oxide.[13-14]



Scheme S10. Renewable routes to limonene oxide.[15-16]

7.6. References

1. Dias, C. R.; Portela, M. F.; GalanFereres, M.; Banares, M. A.; Granados, M. L.; Pena, M. A.; Fierro, J. L. G., Selective oxidation of o-xylene to phthalic anhydride on V2O5 supported on TiO2-coated SiO2. *Catal. Lett.* **1997,** *43*, 117-121.
2. Mahmoud, E.; Watson, D. A.; Lobo, R. F., Renewable production of phthalic anhydride from biomass-derived furan and maleic anhydride. *Green Chem.* **2014,** *16*, 167-175.
3. Giarola, S.; Romain, C.; Williams, C. K.; Hallett, J. P.; Shah, N., Techno-economic assessment of the production of phthalic anhydride from corn stover. *Chem. Eng. Res. Des.* **2016,** *107*, 181-194.
4. Taheri, H.; Dickinson, C. D.; Jacobson, P. A. Flow reactors for chemical conversions with heterogeneous catalysts. US 2009/0043114A1, February 12, 2009.
5. Konishi, M. Method for producing cycloolefin and production apparatus thereof. US20110130600A1, June 2, 2011.
6. Kato, T.; Ichinose, I., Cyclization of Polyenes .32. Selective Bromination of Polyenes by 2,4,4,6-Tetrabromocyclohexa-2,5-Dienone. *J. Chem. Soc., Perkin Trans. 1* **1980,** 1051-1056.
7. Weisz, A.; Mandelbaum, A., Dehydrobromination of 1,2-Dibromocyclohexane and Related-Compounds by Lithium-Chloride in Hexamethylphosphoric Triamide - an Improved Synthesis of 1,3-Cyclohexadiene and Some Deuterium-Labeled Analogs. *J. Org. Chem.* **1984,** *49*, 2648-2650.
8. Mathers, R. T.; Shreve, M. J.; Meyler, E.; Damodaran, K.; Iwig, D. F.; Kelley, D. J., Synthesis and Polymerization of Renewable 1,3-Cyclohexadiene Using Metathesis, Isomerization, and Cascade Reactions with Late-metal Catalysts. *Macromol. Rapid. Comm.* **2011,** *32*, 1338-1342.
9. Sanford, M. J.; Carrodeguas, L. P.; Van Zee, N. J.; Kleij, A. W.; Coates, G. W., Alternating Copolymerization of Propylene Oxide and Cyclohexene Oxide with Tricyclic Anhydrides: Access to Partially Renewable Aliphatic Polyesters with High Glass Transition Temperatures. *Macromolecules* **2016,** *49*, 6394-6400.
10. Saha, B. C.; Kennedy, G. J.; Qureshi, N.; Bowman, M. J., Production of Itaconic Acid from Pentose Sugars by Aspergillus terreus. *Biotechnol Progr* **2017,** *33*, 1059-1067.
11. Nijhuis, T. A.; Makkee, M.; Moulijn, J. A.; Weckhuysen, B. M., The production of propene oxide: Catalytic processes and recent developments. *Ind. Eng. Chem. Res.* **2006,** *45*, 3447-3459.
12. Kong, P. S.; Aroua, M. K.; Daud, W. M. A. W., Conversion of crude and pure glycerol into derivatives: A feasibility evaluation. *Renewable and Sustainable Energy Reviews* **2016,** *63*, 533-555.
13. Ouyang, X.; Ian Zones, S.; Katz, A. S. Highly active, selective, accessible, and robust zeolitic Sn-baeyer-villiger oxidation catalyst. US9687830B2, June 27, 2017.
14. Winkler, M.; Romain, C.; Meier, M. A. R.; Williams, C. K., Renewable polycarbonates and polyesters from 1,4-cyclohexadiene. *Green Chem.* **2015,** *17*, 300-306.
15. Lee, S. Y.; Kim, H. U.; Chae, T. U.; Cho, J. S.; Kim, J. W.; Shin, J. H.; Kim, D. I.; Ko, Y. S.; Jang, W. D.; Jang, Y. S., A comprehensive metabolic map for production of bio-based chemicals. *Nat Catal* **2019,** *2*, 18-33.
16. Davis E.M.; R., C., Cyclization Enzymes in the Biosynthesis of Monoterpenes, Sesquiterpenes, and Diterpenes. In *Topics in Current Chemistry*, Springer: Berlin, 2000; Vol. 209.